RHO-BWI-ST-14

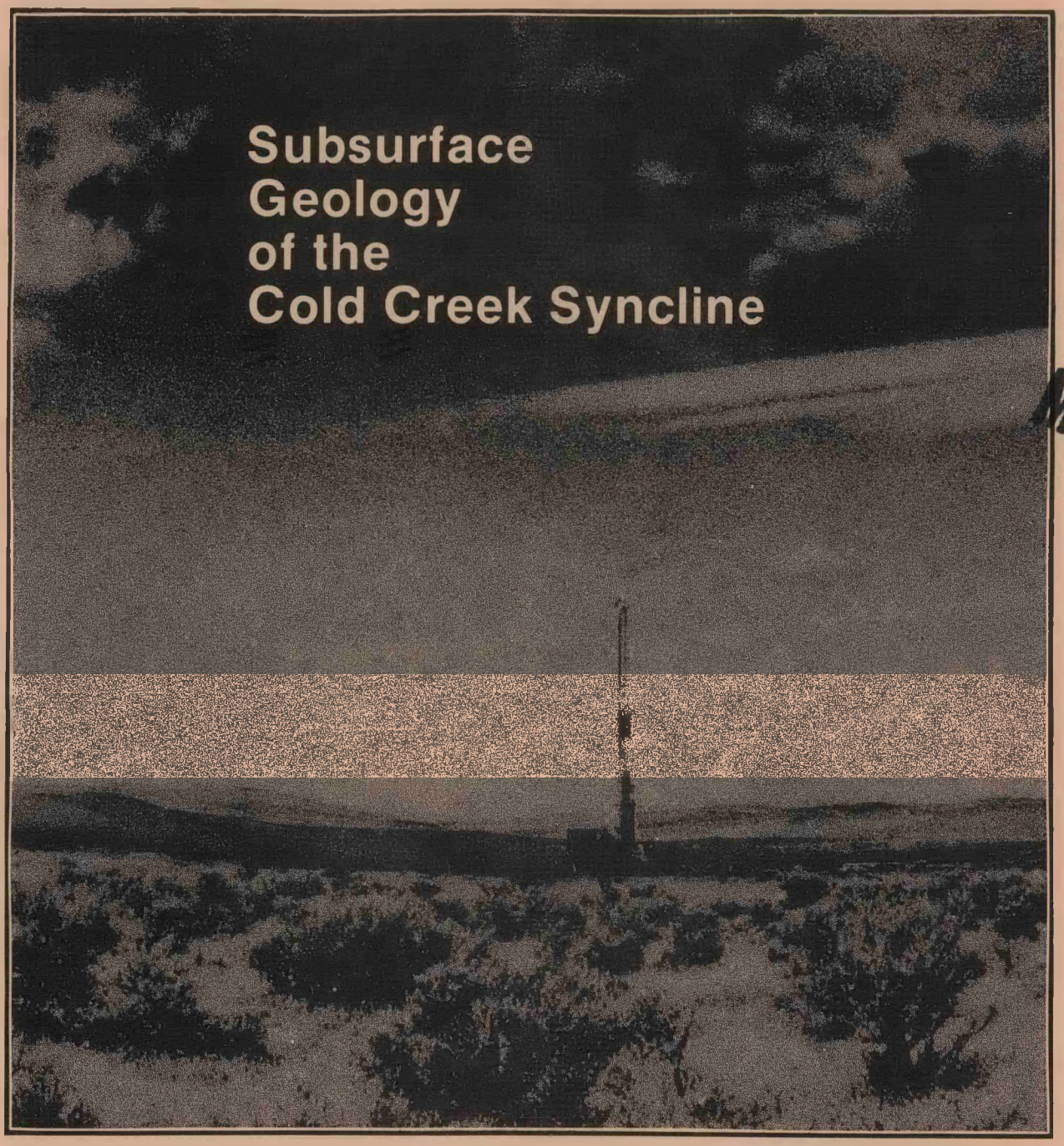

Subsurface Geology of the Cold Creek Syncline

MASTER

Prepared for the United States
Department of Energy
Under Contract DE-AC06-77RL01030

Rockwell International

Rockwell Hanford Operations
Energy Systems Group
Richland, WA 99352

DISTRIBUTION OF THIS DOCUMENT IS UNLIMITED

DISCLAIMER

This report was prepared as an account of work sponsored by an agency of the United States Government. Neither the United States Government nor any agency thereof, nor any of their employees, makes any warranty, express or implied, or assumes any legal liability or responsibility for the accuracy, completeness, or usefulness of any information, apparatus, product, or process disclosed, or represents that its use would not infringe privately owned rights. Reference herein to any specific commercial product, process, or service by trade name, trademark, manufacturer, or otherwise does not necessarily constitute or imply its endorsement, recommendation, or favoring by the United States Government or any agency thereof. The views and opinions of authors expressed herein do not necessarily state or reflect those of the United States Government or any agency thereof.

DISCLAIMER

Portions of this document may be illegible in electronic image products. Images are produced from the best available original document.

Rockwell International
Rockwell Hanford Operations
Energy Systems Group
Richland, WA 99352

DISCLAIMER

This report was prepared as an account of work sponsored by an agency of the United States Government. Neither the United States Government nor any agency thereof, nor any of their employees, makes any warranty, express or implied, or assumes any legal liability or responsibility for the accuracy, completeness, or usefulness of any information, apparatus, product, or process disclosed, or represents that its use would not infringe privately owned rights. Reference herein to any specific commercial product, process, or service by trade name, trademark, manufacturer, or otherwise, does not necessarily constitute or imply its endorsement, recommendation, or favoring by the United States Government or any agency thereof. The views and opinions of authors expressed herein do not necessarily state or reflect those of the United States Government or any agency thereof.

AVAILABLE FROM THE
NATIONAL TECHNICAL INFORMATION SERVICE
SPRINGFIELD, VA. 22161

PRICE: MICROFICHE: $3.50
PAPER COPY: $27.50

DOE Richland, WA

BD-9300-090.1 (R-1-80)

RHO-BWI-ST-14
Distribution Categories
UC-11, -70, and -85

RHO-BWI-ST--14

DE82 007589

SUBSURFACE GEOLOGY OF THE COLD CREEK SYNCLINE

Editors

C. W. Myers
S. M. Price

Graphics

R. W. Cross
W. H. Crowley

July 1981

Prepared for the United States
Department of Energy Under
Contract DE-AC06-77RL01030

Rockwell International

Rockwell Hanford Operations
Energy Systems Group
P.O. Box 800
Richland, Washington 99352

DISTRIBUTION OF THIS DOCUMENT IS UNLIMITED

DOE-Richland, WA

DISTRIBUTION

This report has been distributed according to the category "Environmental Control Technology and Earth Sciences," UC-11, "Nuclear Waste Management," UC-70, and "Spent Fuel Storage," UC-85, as given in the Standard Distribution for Unclassified Scientific and Technical Reports, TID-4500.

EXECUTIVE SUMMARY

Staff

Bedrock beneath the Hanford Site is being evaluated by the Basalt Waste Isolation Project (BWIP) for possible use by the U.S. Department of Energy as a geologic repository for nuclear waste storage. Initial BWIP geologic and hydrologic studies served to determine that the central Hanford Site contains basalt flows with thick, dense interiors that have low porosities and permeabilities. Furthermore, within the Cold Creek syncline, these flows appear to be nearly flat lying across areas in excess of tens of square kilometers. Such flows have been identified as potential repository host rock candidates. The Umtanum flow, which lies from 900 to 1,150 m beneath the surface, is currently considered the leading host rock candidate. Within the west-central Cold Creek syncline, a 47-km^2 area designated as the reference repository location (RRL) is currently considered the leading candidate site.

The specific purpose of this report is to present current knowledge of stratigraphic, lithologic, and structural factors that directly relate to the suitability of the Umtanum flow within the Cold Creek syncline for use as a nuclear waste repository host rock. The BWIP geologic studies have concentrated on factors that might influence groundwater transport of radionuclides from this flow. These factors include: (1) intraflow structures within the interiors of individual lava flows, (2) interflow zones and flow fronts between adjacent lava flows, and (3) bedrock structures. Data have been obtained primarily through coring and geophysical logging of deep boreholes, petrographic, paleomagnetic, and chemical analysis, seismic-reflection, gravity, and magnetic (ground and multilevel airborne) surveys, and surface mapping. Results included in this document comprise baseline data which will be utilized to prepare a Site Characterization Report as specified by the U.S. Nuclear Regulatory Commission.

The Cold Creek syncline is part of the Pasco Basin, one of several structural and topographic basins within the western Columbia Plateau. The western and central parts of the Pasco Basin are located within the Yakima Fold Belt, a structural subprovince of the plateau characterized by east-west-trending, asymmetrical, anticlinal ridges and intervening synclinal valleys. Yakima folds bound the Pasco Basin on the north and south and plunge into the basin from the west. The Cold Creek syncline lies between the Umtanum Ridge-Gable Mountain anticlinal structure on the north and the Yakima Ridge and Rattlesnake Mountain anticlinal structures on the south. Two subtle depressions are present along the troughline of the Cold Creek syncline: (1) Cold Creek Valley depression, located within the area of the RRL; and (2) Wye Barricade depression, located $\sim$25 km to the east. The Cold Creek Valley syncline plunges and dies out to the east in the vicinity of the Wye Barricade depression.

A key aspect of site-identification work has been the delineation of relatively intact volumes of basalt in the Cold Creek syncline area. These relatively intact volumes of bedrock are bounded by known or

inferred geologic structures, excluding intraflow structures. Such structures determine the size and geometry of basalt host rock within which a repository could be constructed, and represent zones of vertically oriented fractures which might affect shallow and deep groundwater flow systems. Based on the results of geophysical surveys and surface and subsurface mapping, the western Cold Creek syncline area is presently interpreted to consist of five, large, relatively intact volumes of bedrock whose boundaries are defined by structures such as first-order anticlines or other known or inferred structures. The interior of the RRL lies within one of these large relatively intact bedrock volumes.

The bedrock of the Cold Creek syncline is comprised of flows belonging to three formations of the Columbia River Basalt Group: (1) Grande Ronde Basalt, (2) Wanapum Basalt, and (3) Saddle Mountains Basalt. The over 2,500 m of Grande Ronde Basalt in the syncline consist of at least 50 flows, one of which is the Umtanum. These flows have an average thickness of 35 m and range in thickness from 4 to 150 m. The Wanapum and Saddle Mountains Basalts within the Cold Creek syncline are comprised of up to 20 flows, with a total maximum thickness of $\sim$700 m. The basalt section is interbedded with sediments of the Ellensburg Formation and is overlain by up to 220 m of the fluvial-lacustrine Miocene-Pliocene Ringold Formation and catastrophic flood deposits of the Pleistocene Hanford formation.

The extent and thickness variations exhibited by basalt flows indicate that the Pasco Basin and Cold Creek syncline were active structural features by at least late Grande Ronde time; rates of uplift and subsidence during the period of late Grande Ronde through Saddle Mountains time are estimated to be <40 m/million years. The steeply inclined flows on anticlinal limbs contain the most extensive faulting and brecciation. Tectonic fractures are, in general, infrequent in the thousands of meters of core drilled in the synclinal areas of the Pasco Basin. The breccia zones that were identified are generally intact and <10 cm thick. Such small tectonic breccia zones and their associated fractures are viewed as typical strain features of folded basalt and should be expected within the limbs of any of the Yakima folds, including the Cold Creek syncline. None of the tectonic breccias identified in core were judged as being associated with large displacements.

The Umtanum flow is found throughout the Pasco Basin; a broad zone of relatively constant thickness ($\sim$64 m) occurs in the central Pasco Basin, including the RRL. In this area, the entablature appears to have a consistent, uniform, glass-rich texture, suggesting few differences in fracture abundance. The entablature also contains secondary minerals as fracture fillings. The high mesostasis abundance in the entablature means that it will alter and, hence, may react with and inhibit the migration of radionuclides more readily than will the colonnade which has a lower mesostasis abundance. The occurrence of fracture fillings of clay (smectite), zeolite (clinoptilolite), and silica acts to reduce the permeability of the basalts, as well as to provide highly sorbtive minerals along potential groundwater pathways.

The sequence of Grande Ronde Basalt flows which overlie the Umtanum flow consists of relatively thick laterally continuous flows intercalated with relatively thin flows, some of which are discontinuous. The thick laterally continuous flows are likely to be hydrologic barriers; whereas, the intervening thin flows with a relatively higher proportion of porous flow top are likely to provide the most transmissive zones. The discontinuous character of some of the thin flows may result in an increase in vertical permeability relative to those parts of the section with thick flows.

Drill core from some Grande Ronde Basalt flows in the Cold Creek syncline area, including the Umtanum, exhibits a type of fracturing known as disking. The degree of disking is variable, with individual disk thicknesses generally ≤ 1.5 cm. The mineralogy and intraflow structures of the Umtanum core have been studied in detail and no correlation with disking is apparent, except that disking does not occur in the flow top. It is concluded that the disking phenomenon probably results from higher horizontal than vertical in situ stresses in basalt.

Overall, the central and eastern parts of the Cold Creek Valley depression which lie within the RRL appear to contain a uniformly thick portion of the Umtanum flow and to be free of potentially adverse bedrock structures relative to other parts of the Cold Creek syncline area and Hanford Site. The structure of the top of basalt and the structure at deeper horizons within this area are interpreted as being nearly flat lying with very gentle dips toward the trough of the Cold Creek syncline and with a slight westward component of dip toward the deepest point of the Cold Creek Valley depression. Additional drilling and geophysical work will be designed to detect and characterize subtle structures which may be present within this depression and to test the predictive capabilities of interpretations outlined in this report.

CONTENTS

TABLES:

CHAPTER 1 - INTRODUCTION

C. W. Myers
S. M. Price

PURPOSE AND SCOPE

The Basalt Waste Isolation Project (BWIP), administered by Rockwell Hanford Operations (Rockwell), is one of the elements of the U.S. Department of Energy's (DOE) National Waste Terminal Storage (NWTS) Program. As such, BWIP is chartered with the responsibility of assessing the basalt beneath DOE's Hanford Site (Fig. 1-1) as a medium for the disposal of nuclear waste. Geologic and hydrologic studies performed by BWIP during the period from 1977 and 1979 are summarized in Myers, Price and others (1979) and Gephart and others (1979a), respectively. These studies served to determine that the central Hanford Site contains basalt flows with thick, dense interiors that have low porosities and permeabilities. Furthermore, within the Cold Creek syncline, these flows appear to be nearly flat lying across areas in excess of tens of square kilometers. Such flows within this area have been identified as potential repository host rock candidates. The Umtanum flow, which lies from 900 to 1,150 m beneath the surface, is currently considered the leading candidate.

For a discussion of the geology of the entire Pasco Basin and the approach used to study this area, the reader is referred to Myers, Price and others (1979); the interpretations to be discussed herein should be considered an update and expansion of those contained in that earlier report. The specific purpose of the present report is to review current knowledge of stratigraphic, lithologic, and structural factors that directly relate to the suitability of the Umtanum flow within the Cold Creek syncline for siting a repository. As such, Chapters 2 through 5 contain discussions of the stratigraphic setting of the Cold Creek syncline and lithologic properties of the Umtanum flow. The remaining three chapters (6, 7, and 8) contain discussions which relate to the bedrock structure of the study area. Borehole and geophysical data pertinent to these discussions are contained in the five appendices. The concluding sections of this chapter are devoted to brief summaries of the geologic setting of the Cold Creek syncline and status of the repository-siting effort. Results included in this document comprise baseline data which will be utilized to prepare the initial Site Characterization Report (NRC, 1981a and b).

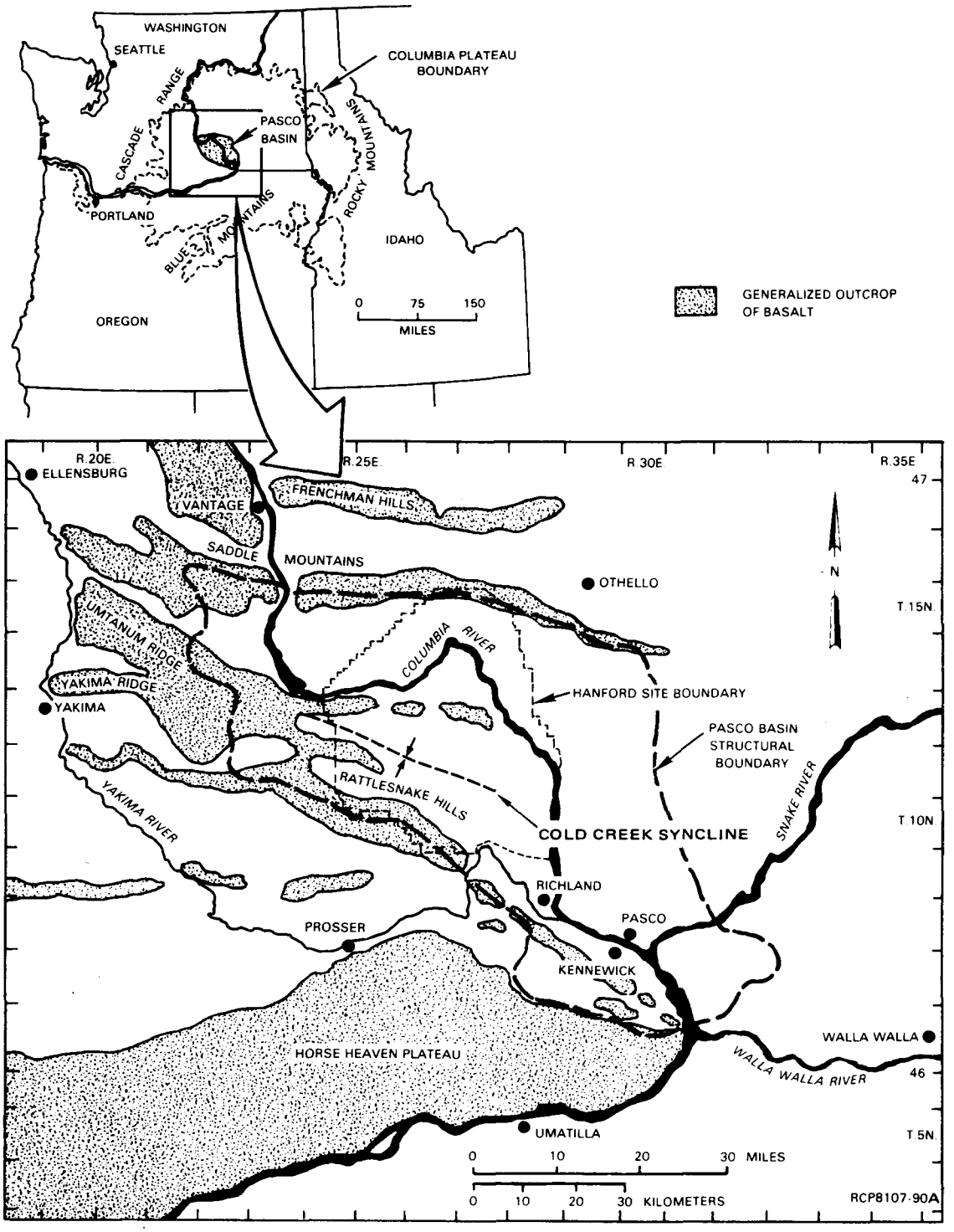

FIGURE 1-1. Location Map, Columbia Plateau, Pasco Basin, Hanford Site.

GENERAL GEOLOGIC SETTING

The Cold Creek syncline is a subdivision of the Pasco Basin, one of several structural and topographic basins within the western Columbia Plateau (Fig. 1-1). The plateau is primarily underlain by a Miocene volcanic sequence termed the Columbia River Basalt Group (Fig. 1-2). Lava flows of this group were erupted from linear vent systems, remnants of which are exposed as dikes primarily in the eastern and southeastern Columbia Plateau (Taubeneck, 1970; Price, 1977). Because of their high fluidity and large volume, the lavas spread considerable distances from their source fissures. In so doing, they covered vast areas, inundated older rocks and structures within the plateau interior, and onlapped highlands around the plateau margin. The thickest flows generally record ponding in pre-basalt valleys, in structurally controlled basins that developed during volcanism, or in narrow canyons previously eroded in older flows, termed intracanyon flows.

The bulk of the Columbia River Basalt Group is comprised of flows which belong to the Yakima Basalt Subgroup (Fig. 1-2). The oldest formation of this subgroup, the Grande Ronde Basalt, was erupted between 16.5 and 14.5 million years before present (mybp). The Grande Ronde Basalt is the most voluminous unit of the group ($\sim$85 vol%) and underlies most of the Columbia Plateau. Grande Ronde Basalt is overlain by Wanapum Basalt. This unit is the secondmost voluminous formation of the group ($\sim$5 vol%) and was erupted between 14.5 and 13.5 mybp. The Saddle Mountains Basalt is the youngest formation of this subgroup, comprises <1 vol% of the group, and was erupted during a period of waning volcanism, 13.5 to 6 mybp (Swanson and others, 1979b).

Flows of the Columbia River Basalt Group are interbedded with and overlain by Miocene-Pliocene epiclastic and volcaniclastic sediments, especially along the margin of the province. Invasive flows, formed when lava "burrowed" into surficial deposits of unconsolidated sediments, are also common. The youngest suprabasalt sedimentary units on the plateau are fluvial, lacustrine, glaciofluvial, and eolian deposits of Pliocene to Holocene age. Much of the plateau surface is dominated by erosional features and sedimentary deposits attributable to Pleistocene catastrophic floods. These floods resulted from the periodic breakup of ice dams impounding glacial lakes along the northern and northeastern margins of the plateau.

In general, the Columbia Plateau can be subdivided into three informal structural subprovinces: (1) Yakima Fold Belt subprovince, (2) Palouse subprovince, and (3) Blue Mountains subprovince (Fig. 1-3). The Yakima Fold Belt subprovince is characterized by east-west-trending, asymmetrical, anticlinal ridges and intervening synclinal valleys. The formation of these folds began as early as late Grande Ronde time. The Palouse subprovince is underlain by basalt flows with a regional dip of $<5^{o}$ to the southwest. The dip is a reflection of regional westward tilting which occurred throughout most of the period of basalt extrusion. The Blue Mountains subprovince is essentially a broad, northeast-trending, anticlinal arch.

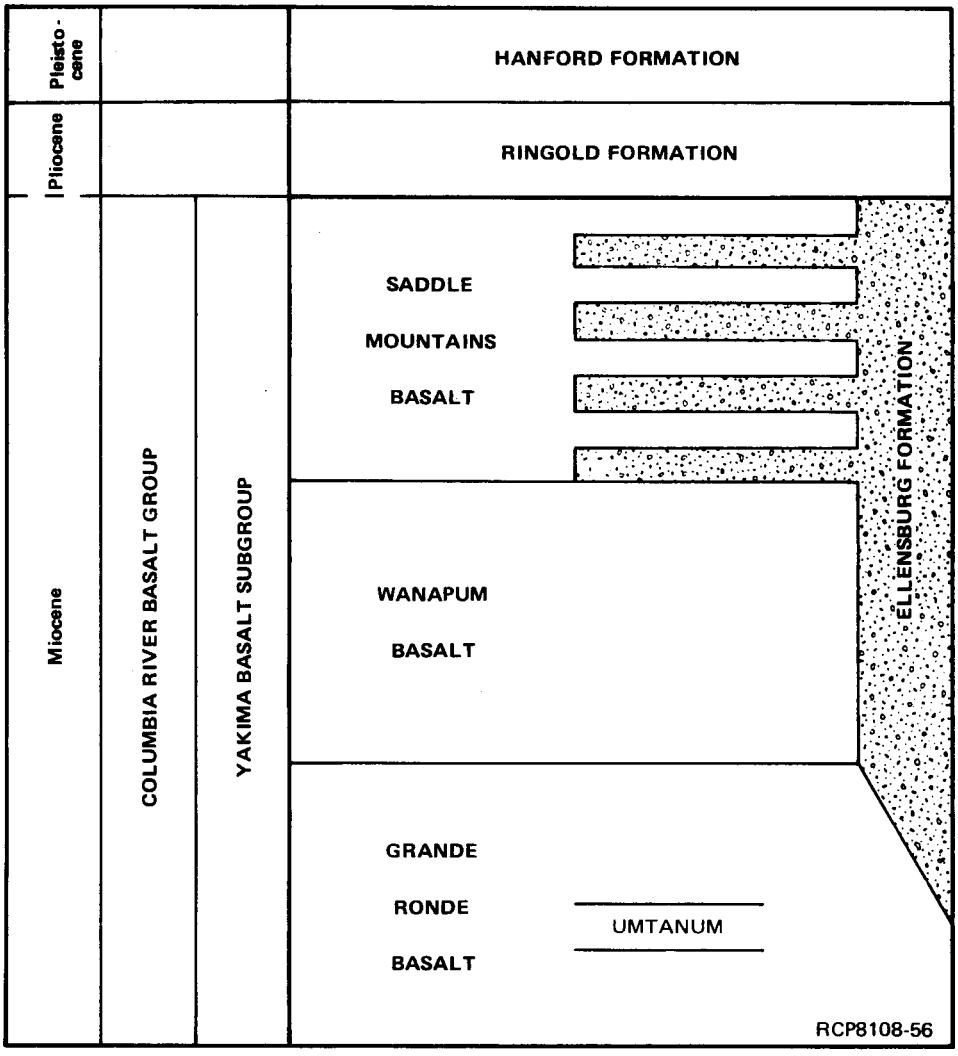

FIGURE 1-2. Stratigraphy of the Columbia River Basalt Group, Yakima Basalt Subgroup, and Intercalated and Suprabasalt Sediments within the Pasco Basin.

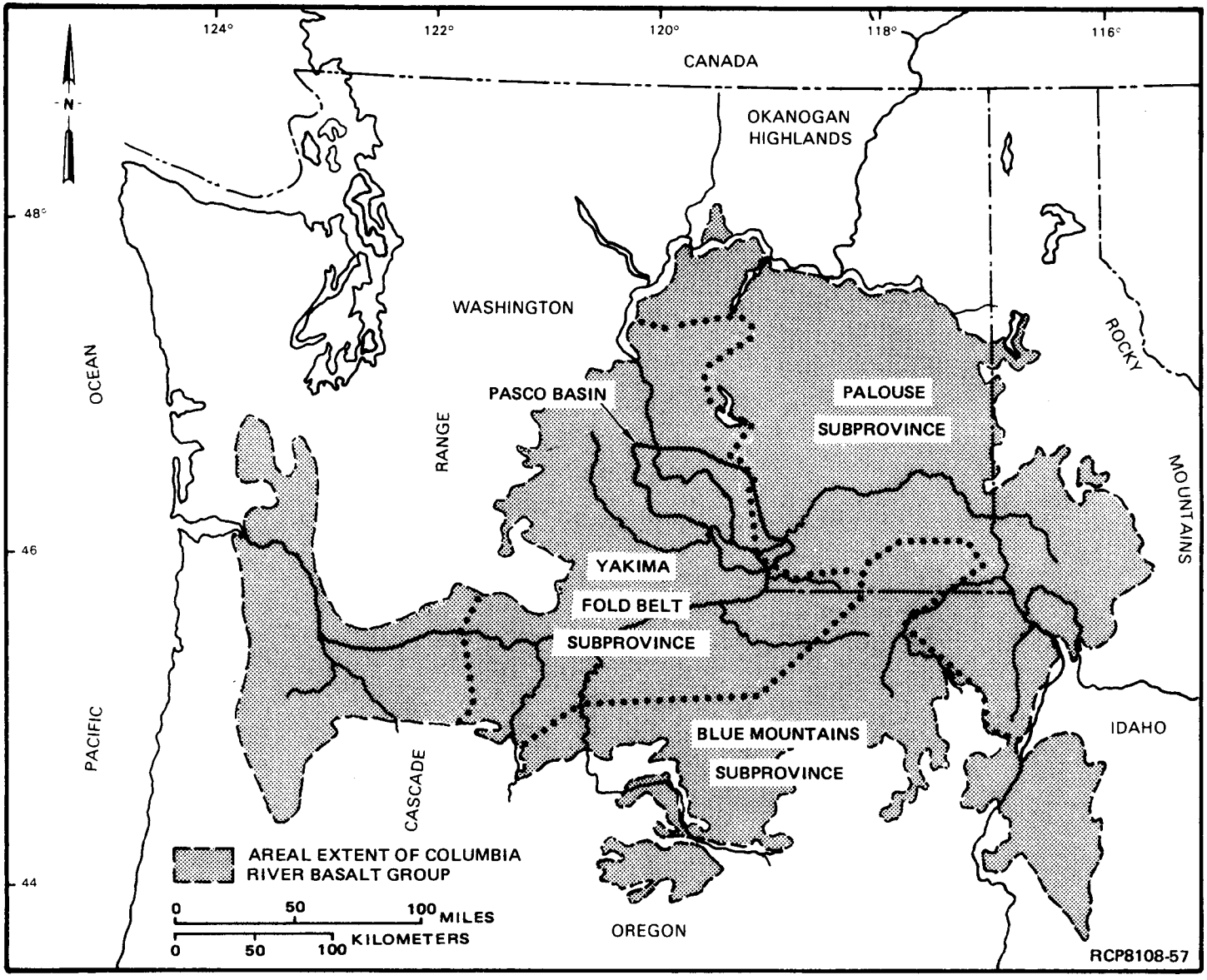

FIGURE 1-3. Informal Structural Subprovinces of the Columbia Plateau.

The Pasco Basin spans the area of transition between the Yakima Fold Belt subprovince and the Palouse subprovince. Yakima folds bound the basin on the north and south and plunge eastward into the basin from the west (Fig. 1-4). Most of the anticlines are asymmetric and have second-order folds in their hinge zones. Their style of deformation changes along strike and their steep flanks are commonly faulted where structural relief is high. Drill holes and geophysical surveys reveal that most subsurface structures in the central Pasco Basin appear to be extensions of the Yakima folds and their associated second-order structures; however, a few subsurface structures might be related to northwest-trending structures that appear to crosscut the east-west-trending Yakima folds.

Synclines between the anticlines are generally broad, open folds that are sediment filled. Major synclines within the Pasco Basin include the Wahluke and Cold Creek synclines. The Wahluke syncline lies between the Saddle Mountains and Umtanum Ridge-Gable Mountain anticlinal structures (Fig. 1-4). The Cold Creek syncline is the relatively low-relief, sediment-filled trough which is bounded by the Umtanum Ridge-Gable Mountain anticlinal structure and the Yakima Ridge and Rattlesnake Mountain anticlinal structures (Fig. 1-4).

The Cold Creek syncline is asymmetrical, with a steeper southern limb and a troughline much nearer the Yakima Ridge structure than the Umtanum Ridge-Gable Mountain structure. The eastern portion of the northern limb has been deformed into a series of northwest-trending folds. The "interior" of the syncline is a broad, open, undulatory structure with two minor depressions.

The bedrock of the Cold Creek syncline is comprised of flows belonging to all three formations of the Yakima Basalt Subgroup. Grande Ronde Basalt in the syncline consists of >2,500 m of basalt, including at least 50 flows. These flows have an average thickness of 34 m and range in thickness from 4 to 150 m. The basalt flows of this formation, which include the Umtanum (Fig. 1-2), are currently considered the most likely candidates for a repository host rock.

The Wanapum and Saddle Mountains Basalts within the Cold Creek syncline are comprised of up to 20 flows with a maximum thickness of ∿700 m. The basalt section is interbedded with sediments of the Ellensburg Formation (Fig. 1-2) and is overlain by up to 220 m of the fluvial-lacustrine, Miocene-Pliocene Ringold Formation and catastrophic flood deposits of the Pleistocene Hanford formation. Holocene eolian deposits of loess and dune sand mantle much of the syncline.

A preliminary assessment of the timing and rate of deformation of the Pasco Basin has been made using available geologic, geodetic, and seismologic data (Reidel and others, 1980; Caggiano and others, 1980). The thickness and distribution of flows indicate that basalt deformation began over 14 million years ago and progressed at a slow rate (<1 mm/yr). Decreasing dip with decreasing age of Pliocene sediments overlying basalt supports the proposed rate. Deformation, once localized, has apparently

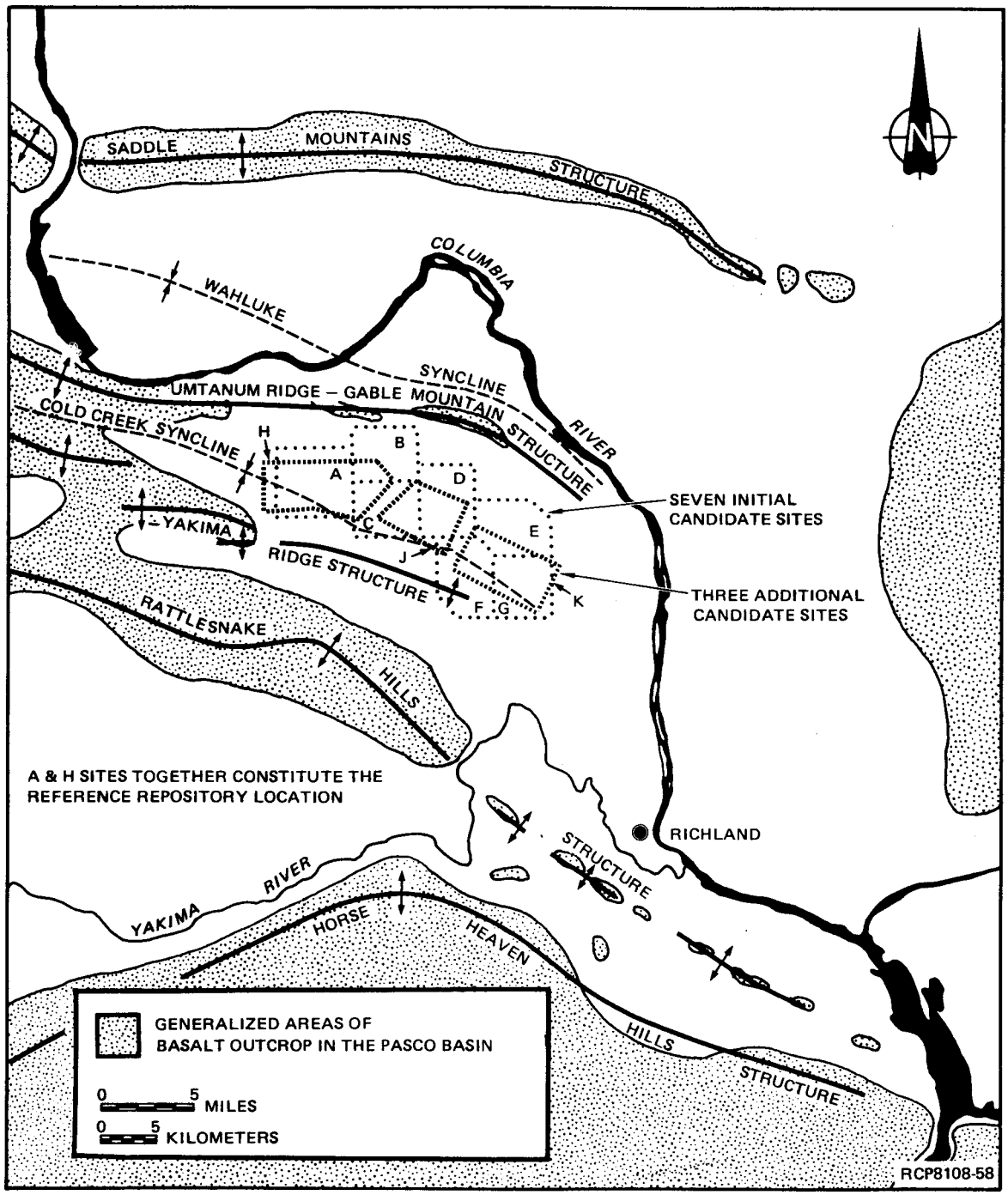

FIGURE 1-4. Location of Candidate Sites in the Cold Creek Syncline.

continued along the same trends and zones of weakness developed in the Miocene, as suggested by horizonal to sub-horizontal attitudes of Pliocene sediments in basins between anticlinal ridges. Historical seismicity indicates that moderate-sized earthquakes (<magnitude 6) are infrequent and separated by periods of relatively low-level, diffuse, stress release. Instrumental records of earthquakes reveal no concentrated stress release along mapped geologic structures or along planar zones. Focal mechanism solutions indicate rupture occurs on steeply dipping planes of varying orientation in volumetrically restricted zones in basalt (i.e., earthquake swarms) and in broad zones below basalt under nearly horizonal, north-south compression. Measurements of strain with trilateration arrays in the Pasco Basin indicate strain of <1 mm/yr. Available data currently support a model of slow, ongoing deformation.

SELECTION OF A REFERENCE REPOSITORY LOCATION WITHIN THE COLD CREEK SYNCLINE

The nationwide NWTS siting process is a stepwise procedure involving several phases, beginning with site screening and ending with site selection (DOE, 1980). All NWTS work is currently in the site-screening phase. Generic site-qualification criteria developed by the Office of Nuclear Waste Isolation (ONWI, 1981) are being used by various components of the NWTS, including BWIP, to help in the screening and site-identification process. To date, the BWIP geologic studies have concentrated on factors that might influence groundwater transport of radionuclides from a candidate host rock, such as the Umtanum flow. These factors include: (1) intraflow structures (discontinuities) within the interiors of individual lava flows, (2) interflow zones and flow fronts between adjacent lava flows, and (3) existing bedrock structures.

In 1979, available geologic and hydrologic information (Myers, Price and others, 1979; Gephart and others, 1979a) was combined with existing information on socioeconomics, land use, and the environment to identify seven initial candidate sites in the Cold Creek syncline area for further investigation (Fig. 1-4) (BWIP Staff, 1980; Woodward-Clyde Consultants, in press). Geologic information obtained subsequent to that presented in Myers, Price and others (1979) was used to identify three additional candidate repository sites (H, J, and K; Fig. 1-4). All candidate sites were evaluated by a committee comprised of personnel from Rockwell and Woodward-Clyde Consultants. One candidate site, the combination of candidate sites A and H (Fig. 1-4), emerged as the highest ranked. This candidate site is currently referred to as the reference repository location (RRL).

Current BWIP plans are to formally recommend to DOE a site for detailed characterization in 1981. The RRL site remains the leading candidate at this time. Information contained in the remainder of this report provides the basis for further review of the geologic qualifications of the A-H site. Consequently, special emphasis has been given in this report to the western part of the Cold Creek syncline where the RRL is located.

CHAPTER 2 - SUPRABASALT SEDIMENTS OF THE COLD CREEK SYNCLINE AREA

A. M. Tallman
J. T. Lillie
K. R. Fecht

INTRODUCTION

This chapter describes the general stratigraphy of the sediments overlying the basalt bedrock in the Cold Creek syncline. Included is a brief discussion of their distribution, lithology, stratigraphy, and age relationships in the Pasco Basin and a more detailed discussion for the western Cold Creek syncline area across the RRL.

The study of these sediments is important to the identification and evaluation of candidate sites for a repository because: (1) Plio-Pleistocene geologic history of the Cold Creek syncline area is recorded in these sediments; (2) physical properties of these sediments, especially their lateral variations, affect the ability of seismic reflection surveys to resolve details of bedrock structure in the underlying basalt; (3) shafts constructed in the RRL will penetrate these sediments and require knowledge of their character; and (4) surface facilities constructed on or in these sediments will require information on their engineering properties.

The post-Columbia River Basalt Group sediments of the Cold Creek syncline are composed of two major units (Fig. 2-1): (1) Ringold Formation, a Miocene-Pliocene fluvial unit with some lacustrine facies; and (2) Pleistocene glaciofluvial sediments, informally termed the Hanford formation. Deposition of the Ringold Formation by ancestral streams flowing through the Pasco Basin started shortly after cessation of basalt flows. Talus and alluvium deposited on the flanks of basaltic ridges during Ringold time are also included in the Ringold Formation. The Hanford formation was deposited by catastrophic floodwaters which inundated the Pasco Basin when ice dams impounding glacial lakes failed in Montana, Idaho, northern Washington, and southern British Columbia. Minor units include the Pleistocene and Holocene talus, colluvium, alluvium, landslide debris and loess, and Holocene dune sand.

PREVIOUS WORK

Investigations of the sediments in the Cold Creek syncline area began during the 1940s during construction of the Hanford Site facilities in the 200 East and 200 West Areas and have continued since then with ongoing construction and groundwater-monitoring investigations (Newcomb and Strand, 1953; Brown, 1959; Newcomb and others, 1972; Liverman, 1975; Routson and Fecht, 1979; Tallman and others, 1979). Additional work was completed by

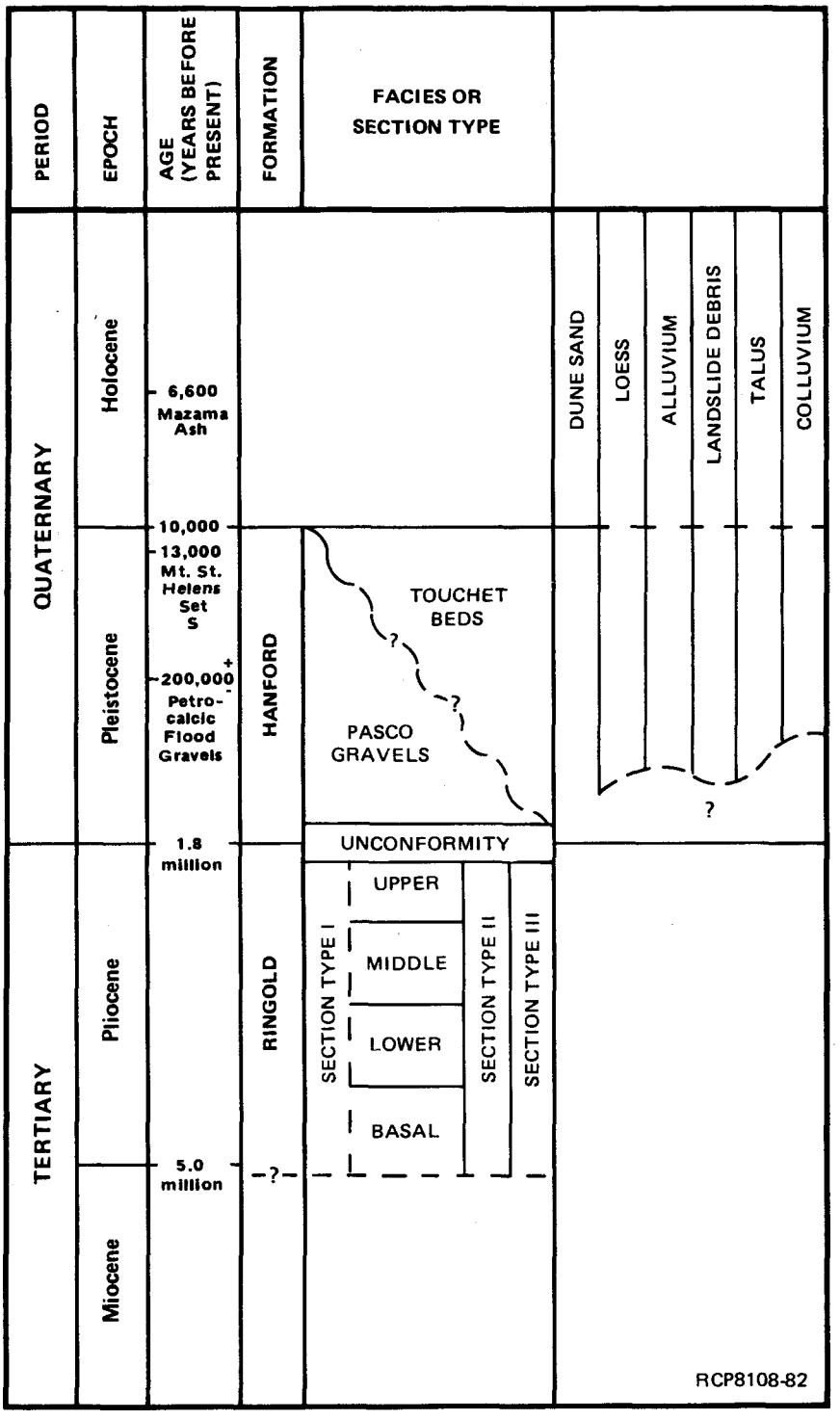

FIGURE 2-1. Sediment Stratigraphic Chart, Pasco Basin, Cold Creek Syncline.

Washington Public Power Supply System, Inc. (WPPSS, 1977, 1981) and recently by Northwest Energy Services Company. A summary of regional and Pasco Basin post-Columbia River basalt geology is presented in Myers, Price and others (1979).

METHODOLOGY

Reconnaissance field mapping (1:62,500) of sediments in the Cold Creek syncline was completed in 1978 (Lillie and others, 1978; Myers, Price and others, 1979) and more detailed field mapping (1:24,000) is currently being done by Rockwell.

Investigations of subsurface sediments in the Cold Creek syncline utilize primarily driller's logs and samples from boreholes. These boreholes were drilled using cable-tool, mud and air rotary, and diamond-coring drilling methods (Fecht and Lillie, in press; also see Appendix A). The quality of driller's logs and sediment samples is variable and is considered in the interpretations presented in this report. Granulometric analyses and calcium carbonate ($CaCO_3$) determinations were completed on sediments from selected boreholes to aid in delineation and correlation of major facies changes within the Hanford and Ringold Formations. Geophysical logs are available for some boreholes, and some areas are covered by geophysical surveys (see Appendix B).

Paleomagnetic analyses of sediments from the Ringold Formation were completed for exposures along the Columbia River and for three core holes on the Hanford Site (Woodward-Clyde Consultants, 1978; Packer and Johnston, 1979). These data are being used to delineate time-stratigraphic units and, in conjunction with fossils, can be used for dating and correlating the Ringold Formation.

GENERAL STRATIGRAPHIC SETTING

RINGOLD FORMATION

The Ringold Formation overlies the Columbia River Basalt Group within most of the Pasco Basin, except where: (1) basalt crops out, (2) glaciofluvial Hanford formation onlaps ridges above the margin of the Ringold Formation, and (3) it has been eroded and Hanford sediments were deposited directly on basalt.

The Ringold Formation within the Pasco Basin has been divided vertically into three textural facies, generally following the divisions of Newcomb (1958): (1) lower Ringold, the "blue clay" facies consisting of silt, clay, sand, and gravel extending upward from the basalt; (2) middle Ringold, conglomerate or gravel facies; and (3) upper Ringold, clay, silt, and sand, with some minor gravel lenses (Brown, 1959). Recent work (Routson and Fecht, 1979; Tallman and others, 1979; Myers, Price and

others, 1979; Brown, 1981) has distinguished a basal unit, the predominantly gravel facies in the bottom portion of lower Ringold, as described by Newcomb (1958) and Brown (1959).

The division of the Ringold Formation into a (1) basal, (2) lower, (3) middle, and (4) upper facies, based primarily on texture, is appropriate for much of the central Pasco Basin. On the edges of the basin, the character of the Ringold Formation differs because of derivation from local sources.

In general, three representative stratigraphic section types can be used to describe the lateral variations of the Ringold Formation in the Pasco Basin (Fig. 2-2). The central portion of the Cold Creek syncline and much of the central Pasco Basin are representative of section type I (the four facies listed above) and illustrated in DH-12 (Fig. 2-3). However, all four textural facies are not present throughout all the section type I area. Much of the upper Ringold is eroded and the lower Ringold pinches out on anticlinal ridges, and in some areas, the basal gravel unit is not present or cannot be distinguished from middle Ringold where the two are in contact. The lateral distribution is shown in Figure 2-2. A more detailed discussion of this section type is presented later in the discussion of the RRL stratigraphy.

Section type II of the Ringold Formation is found north and east of Gable Mountain (Fig. 2-2) and is composed predominantly of silt, sand, and clay as represented in DH-19 (Fig. 2-3). Minor gravel lenses are present, mostly north of Gable Mountain. Sediments of this section are interpreted as floodplain overbank deposits throughout Ringold time. Erosional unconformities and paleosols are present, but there is no evidence of high-energy, main-channel, sedimentation characteristics of the middle and basal Ringold facies in the central basin.

Section type III, the fanglomerate facies (Grolier, 1965), occurs on the flanks of anticlinal ridges and includes the talus, slope wash, and side stream facies which interfinger with the central basin deposits of section types I and II (Fig. 2-2 and 2-3). This facies of the Ringold Formation is composed chiefly of basalt clasts in a matrix of quartz and feldspar or basalt sand. Locally, some openwork, angular, basalt debris is present. It is generally compacted to cemented with silica and/or $CaCO_3$. The unit is the result of mass wastage and runoff on the emerging ridges during the deposition of the other Ringold section types in the lower elevations of the Pasco Basin.

Section types I and II were deposited by a major river system which flowed through the Pasco Basin. The middle Ringold gravel of section type I is present from Sentinel Gap to the west side of Gable Mountain and throughout the central Pasco Basin to Wallula Gap, except where it is locally eroded south of the city of Pasco (Fig. 2-2). The main channel meandered across the Pasco Basin, depositing the time-transgressive middle Ringold gravels and the associated finer grained sediments. Several fluvial cycles are recognized within section type I, but have not been correlated across the basin. The fine-grained sediments of section types I

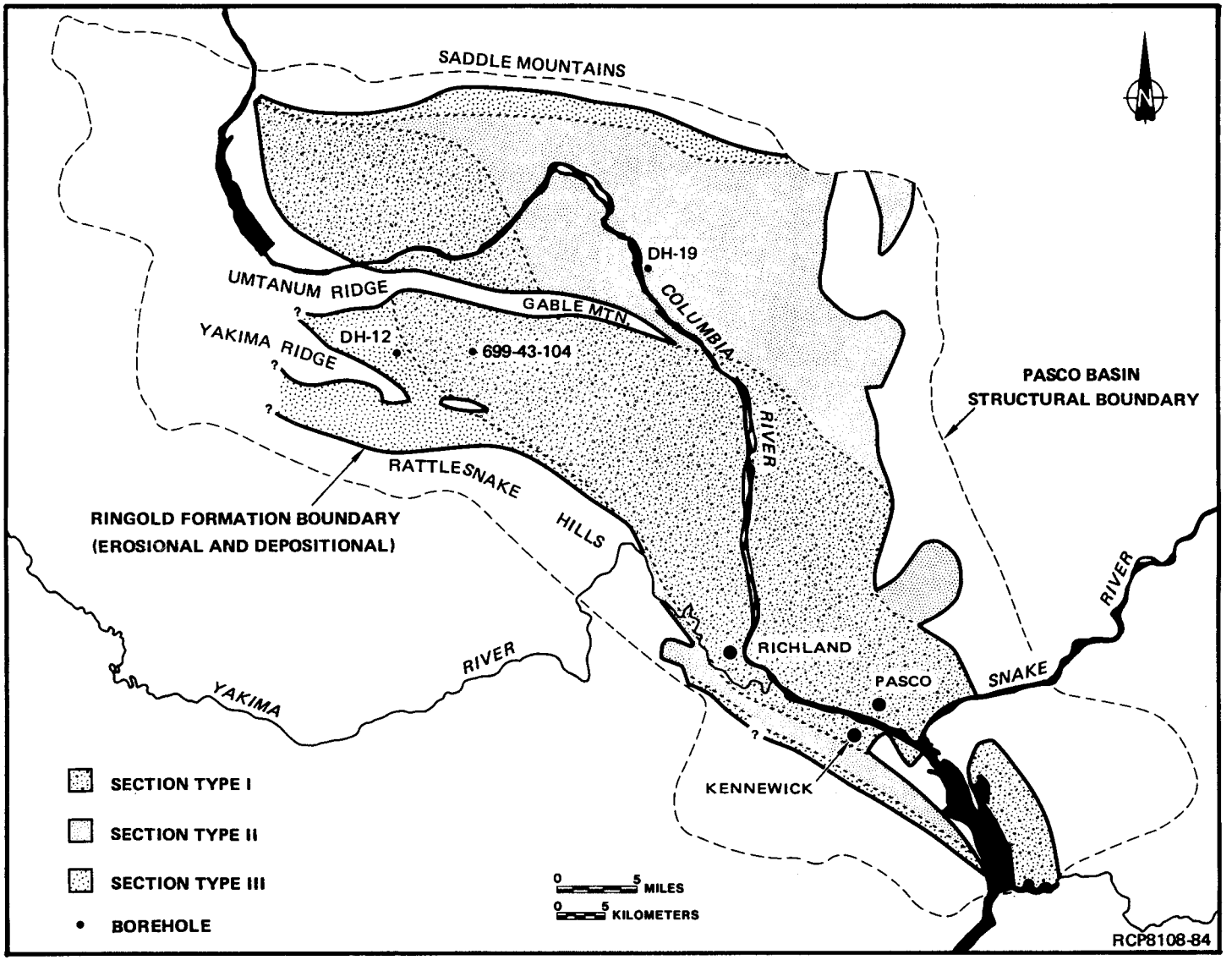

FIGURE 2-2. Distribution of Ringold Section Types.

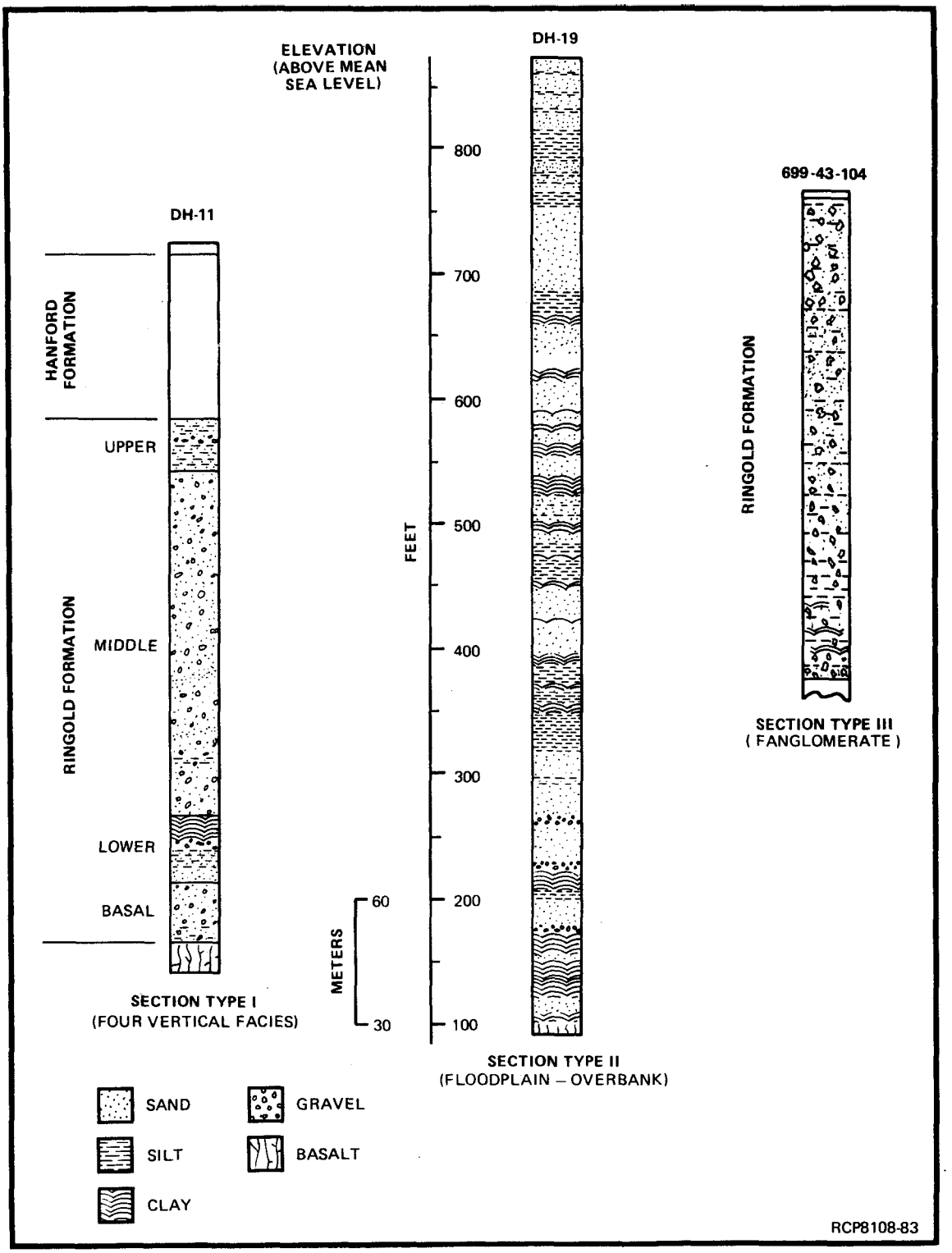

FIGURE 2-3. Ringold Section Types.

and II were deposited as lateral equivalents of the main-stream facies. After the deposition of the upper Ringold of section type I and before the deposition of the Hanford formation, there was a major period of fluvial incision and as much as 150 m of Ringold sediments were eroded across the central portion of the Pasco Basin. The nature of these missing sediments is not known, but the lateral equivalent, the upper Ringold of the White Bluffs, is a fine facies similar to the sand and silt of section type II. Erosional remnants of the upper Ringold are present in the west-central part of the basin. These fine-grained sediments are either the floodplain overbank equivalents of a now eroded channel deposit, or they represent a low-energy, fluvial-lacustrine environment throughout the basin for all of upper Ringold time.

HANFORD FORMATION

The Pasco Basin was inundated by multiple Pleistocene floods when ice dams failed along the glacier margin in northern Montana, Idaho, Washington, and southern British Columbia (Bretz, 1923, 1925; Baker, 1973). An estimated 2,000 km^3 of water from Glacial Lake Missoula surged across eastern Washington (Pardee, 1942), deeply scouring basalt and aggrading thick sequences of subfluvially deposited sediments. The floodwaters were diverted into numerous anastomosing channels which debouched into the Pasco Basin (Baker, 1973; Baker and Nummedal, 1978). Water was temporarily impounded behind the underfit water gap at Wallula, with the resultant temporary lake reaching an elevation of ∿365 m in the Pasco Basin.

The sediments deposited in the Pasco Basin during these flood events are informally referred to as the Hanford formation. The Hanford formation is divided into two textural facies: (1) Pasco Gravels (Brown, 1975) and (2) Touchet Beds (Flint, 1938). The Pasco Gravels (Fig. 2-4) range in texture from boulders to fine sand and represent varied energy environments during flooding. The Touchet Beds (Fig. 2-5) are made up of rhythmically bedded, fine-grained sediments deposited in low-energy, slackwater environments.

Floodwaters entered the Pasco Basin by three routes: (1) through Sentinel Gap, (2) across the northeastern flanks of the Pasco Basin in several well-developed coulees, and (3) down the Snake River (Fig. 2-6). The texture of the Hanford formation varies throughout the Pasco Basin. In general, the Pasco Gravels are coarsest immediately south of Sentinel Gap and south of the Gable Mountain-Gable Butte constriction, where coarse debris was deposited when the floodwaters spread out into the Pasco Basin and deposited a swath of gravels to Wallula Gap. Coarse gravels are also present in the southern Pasco Basin, where floodwaters entered the basin via the Snake River (Brown, 1981; Lindberg and Brown, 1981). The Touchet Beds are generally restricted to higher elevations on the flanks of ridges and up tributary valleys of the Pasco Basin away from the higher energy, main-channel flow.

The number of Pleistocene floods in eastern Washington and the Pasco Basin is not known. Stratigraphic evidence for as many as 12 floods is reported in the Spokane area by Stradling and others (1980). In work done

FIGURE 2-4. Pasco Gravels, Reference Repository Location.

FIGURE 2-5. Touchet Beds, Pasco Basin.

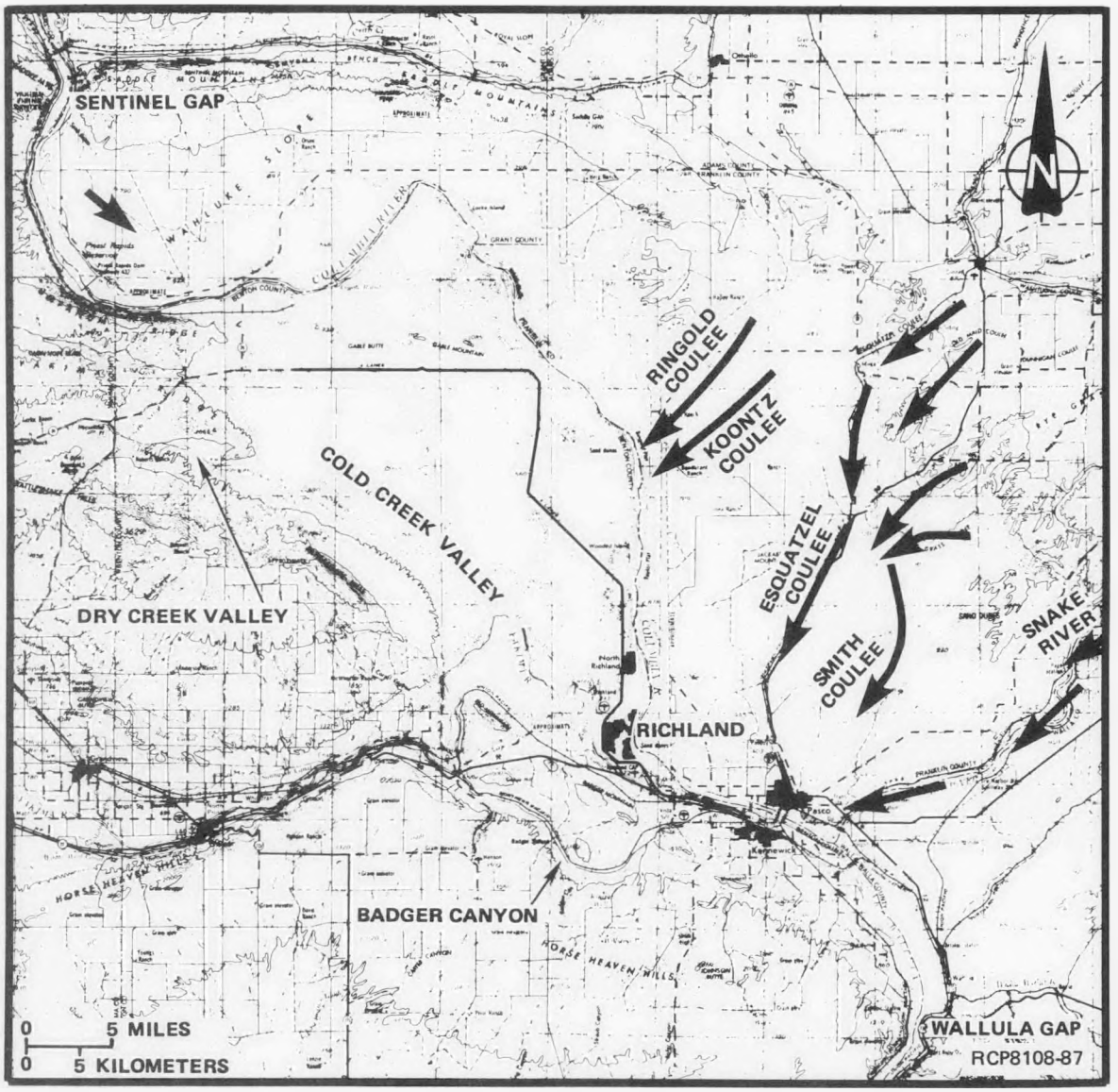

FIGURE 2-6. Floodwater Routes into the Pasco Basin.

for Rockwell, L. G. Hansen reported stratigraphic evidence for at least seven floods in the Columbia River Valley in the northwestern Columbia Plateau. The Touchet Beds in the Walla Walla Valley are interpreted to represent "about 40" individual floods (Waitt, 1980) based on the assumption that each major sedimentary cycle represents one flood. Bjornstad (1980) concluded that these cycles represented energy pulses in one major flood, but he did find evidence for at least two separate floods. Within the Pasco Basin, multiple, graded sequences of Pasco Gravels and Touchet Beds have been observed in boreholes and outcrop. Whether each sequence represents an individual flood or merely changes in the environment during deposition is not known.

Locally, three sedimentary sequences identified in boreholes in the Pasco Basin (Brown, 1981) are interpreted to be three separate flood events. In an excavation in the south-central basin, three main sequences of Hanford sediment are interpreted to represent multiple flood events in the late Pleistocene (Wisconsinan, ~80,000 to 10,000 yr before present). Older gravels in Badger Coulee contain a petrocalcic horizon and are interpreted as pre-Wisconsinan flood sediments. More detailed analysis of borehole samples and exposures is needed to refine the flood history of the Pasco Basin.

Clastic dikes (Fig. 2-7) commonly occur in the Touchet Beds and Pasco Gravels. They are also found in the Ringold and Ellensburg Formations and in basalt. The dikes are generally vertical- to irregular-dipping fissure fillings in the host sediments that are filled with clay-to-gravel sediments. The mechanism for the formation of the clastic dikes is not known, but they have been interpreted not to be related to permafrost, desiccation, or seismic activity (Black, 1979). Most dikes observed appear to be filled from above and display intricate fluvial bedding with evidence for multiple, filling events. The mechanism for opening of the fissure may be related to loading and dewatering during Pleistocene catastrophic flooding (Black, 1979; Baker 1973).

SURFICIAL DEPOSITS

Relatively minor amounts of alluvium, dune sand, loess, talus, colluvium, and landslide debris occur in the Pasco Basin. Most of these deposits are Holocene, but some may be as old as the Pleistocene (Lillie and others, 1978; Myers, Price and others, 1979).

Alluvium occurs in the floodplains of the Yakima and Columbia Rivers and in the Cold Creek and Dry Creek Valleys. Alluvium below the elevation of major Pleistocene catastrophic flooding is Holocene, but ranges from Pleistocene to present above flood level. Some Pleistocene alluvium may be overlain by the Hanford formation.

Dune sand is present throughout much of the Pasco Basin and consists of medium- to fine-grained sand with minor amounts of silt. Active dunes are present in the central Pasco Basin and to the north and east along the

FIGURE 2-7. Clastic Dike in Touchet Beds, Pasco Basin.

Columbia River. Stabilized, longitudinal dunes occur in the south-central portion of the Pasco Basin. Dune sand is chiefly reworked Hanford sediments.

Talus and colluvium are present on ridge flanks. These deposits are primarily Holocene, but are in part Pleistocene at elevations above flood level. Basalt landslide debris is present along anticlinal ridges. Large, partly eroded landslides and landslide complexes are probably Pleistocene or older. Landslides in the Ringold Formation along the White Bluffs are predominantly Holocene; however, some large landslide complexes are overlain by the Pleistocene Hanford formation. Active landsliding on the White Bluffs chiefly is related to increased irrigation on top of the White Bluffs as well as undercutting by the Columbia River.

STRATIGRAPHY OF THE REFERENCE REPOSITORY LOCATION

The Ringold and Hanford formations overlie the Columbia River Basalt Group in the RRL area (Fig. 2-8 and 2-9). Dune sand veneers the Hanford formation in parts of the area.

RINGOLD FORMATION

The Ringold Formation within the RRL is composed of the basal, lower, middle, and upper units (section type I), with some interfingering of the fanglomerate and side-stream facies (section type III) in the western part of the area (Fig. 2-2 and 2-3).

Basal Ringold

The basal Ringold unit overlies the Elephant Mountain Member of the Saddle Mountains Basalt in the RRL and is chiefly a silty, sandy gravel to a gravelly sand that varies in thickness from 0 to >45 m (Fig. 2-8 and 2-9). The bedding structure is not known from available borehole data. Clasts are predominantly basalt, but include quartzite, granitic rocks, metamorphic rocks, and other lithologies from outside the Pasco Basin. The sand fraction is primarily quartz and feldspar. The exotic lithologies indicate a through drainage in the Pasco Basin during deposition of the basal Ringold. The dominance of basalt reflects the influence of the side-stream and fanglomerate debris of section type III and proximity to basalt highs. The unit is commonly well cemented with silica and/or calcite. It is generally thicker in the deepest part of the Cold Creek syncline in the RRL area and is folded with the basalt, suggesting that this unit was deposited during deformation of the Cold Creek syncline (Fig. 2-10). Previous work on the northern flank of the Cold Creek syncline suggested that the unit was generally the same thickness throughout (Routson and Fecht, 1979; Tallman and others, 1979) and that most deformation occurred after deposition.

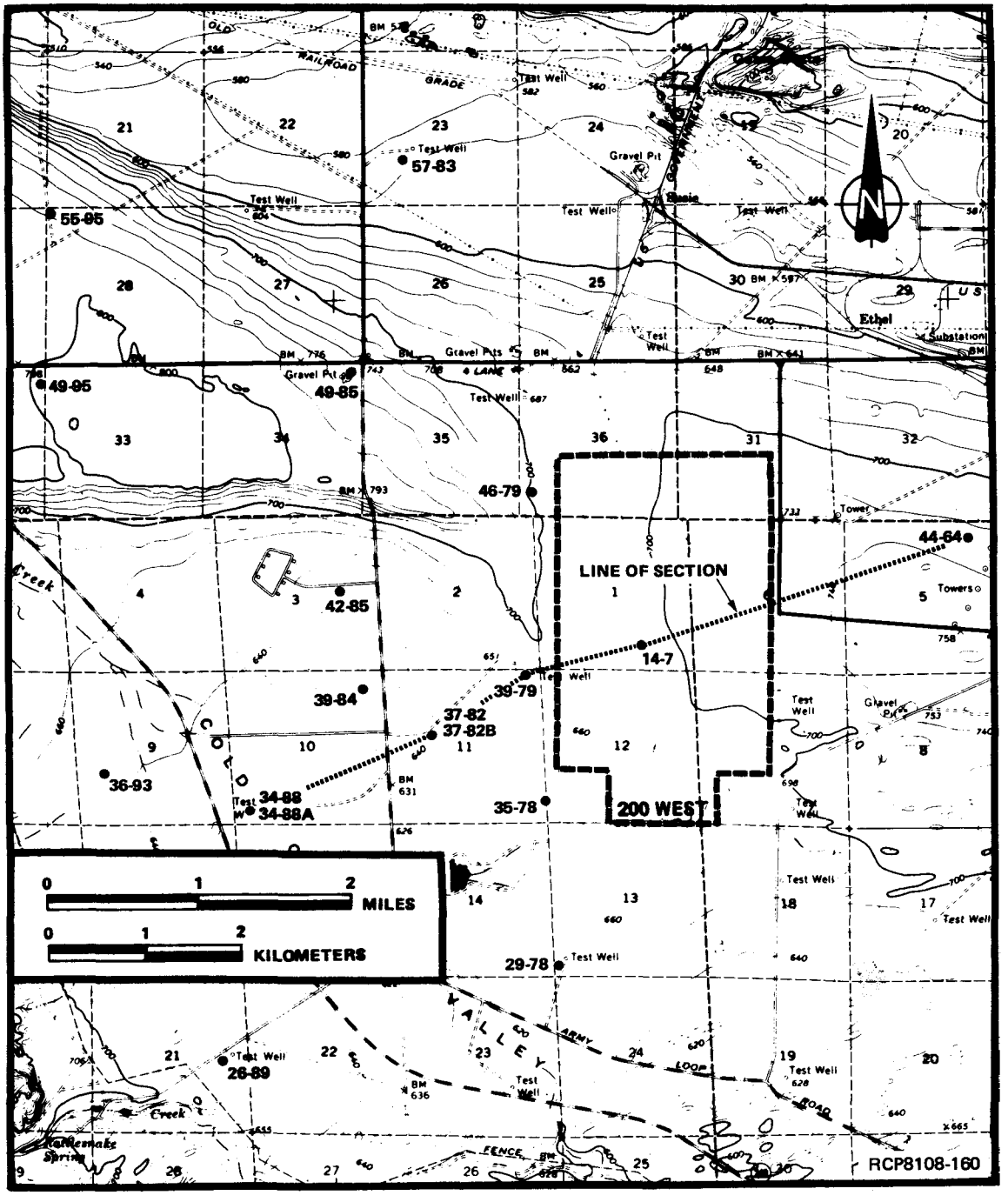

FIGURE 2-8. Index to Location of Fence Diagram Wells and Cross Sections.

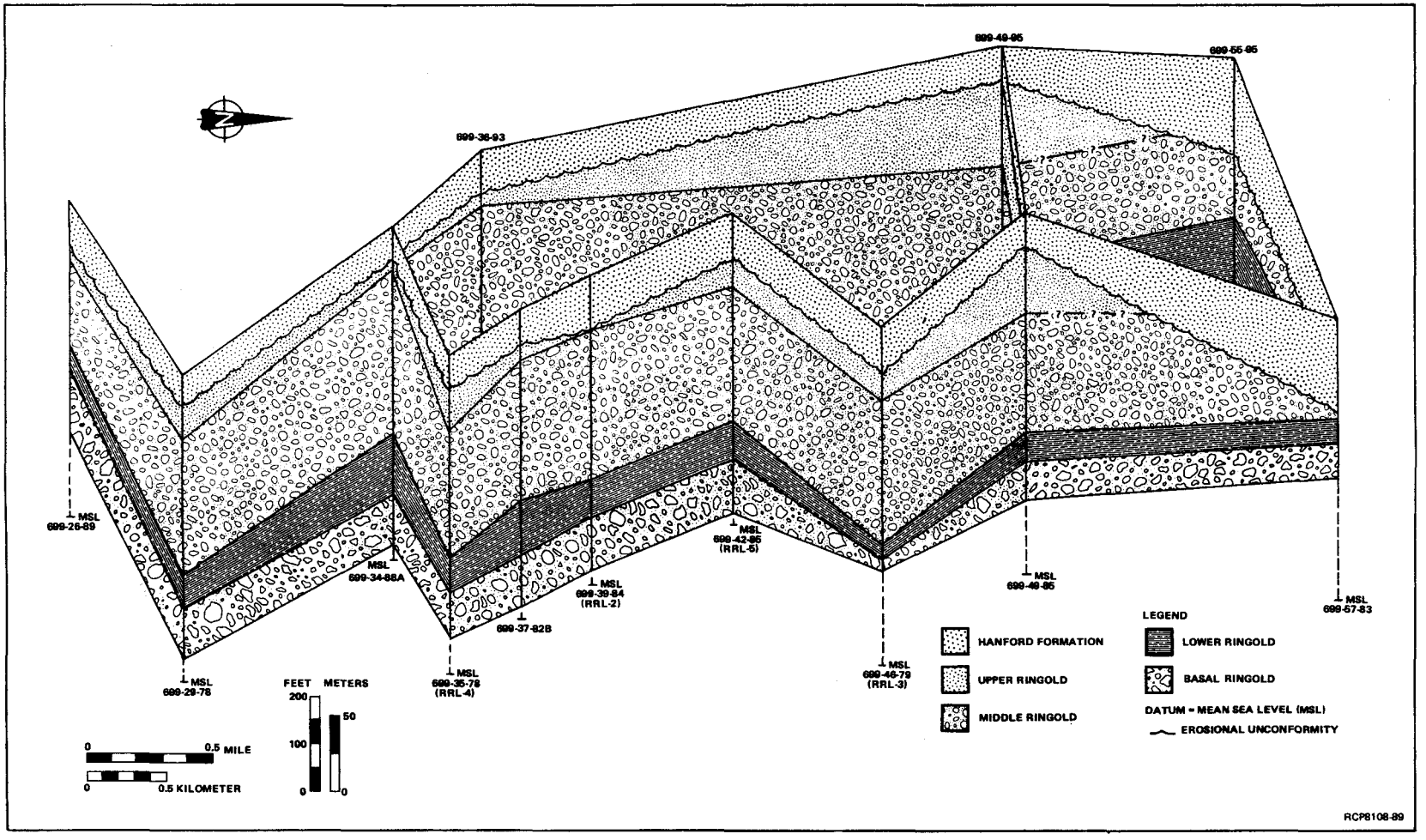

FIGURE 2-9. Fence Diagram, Reference Repository Location.

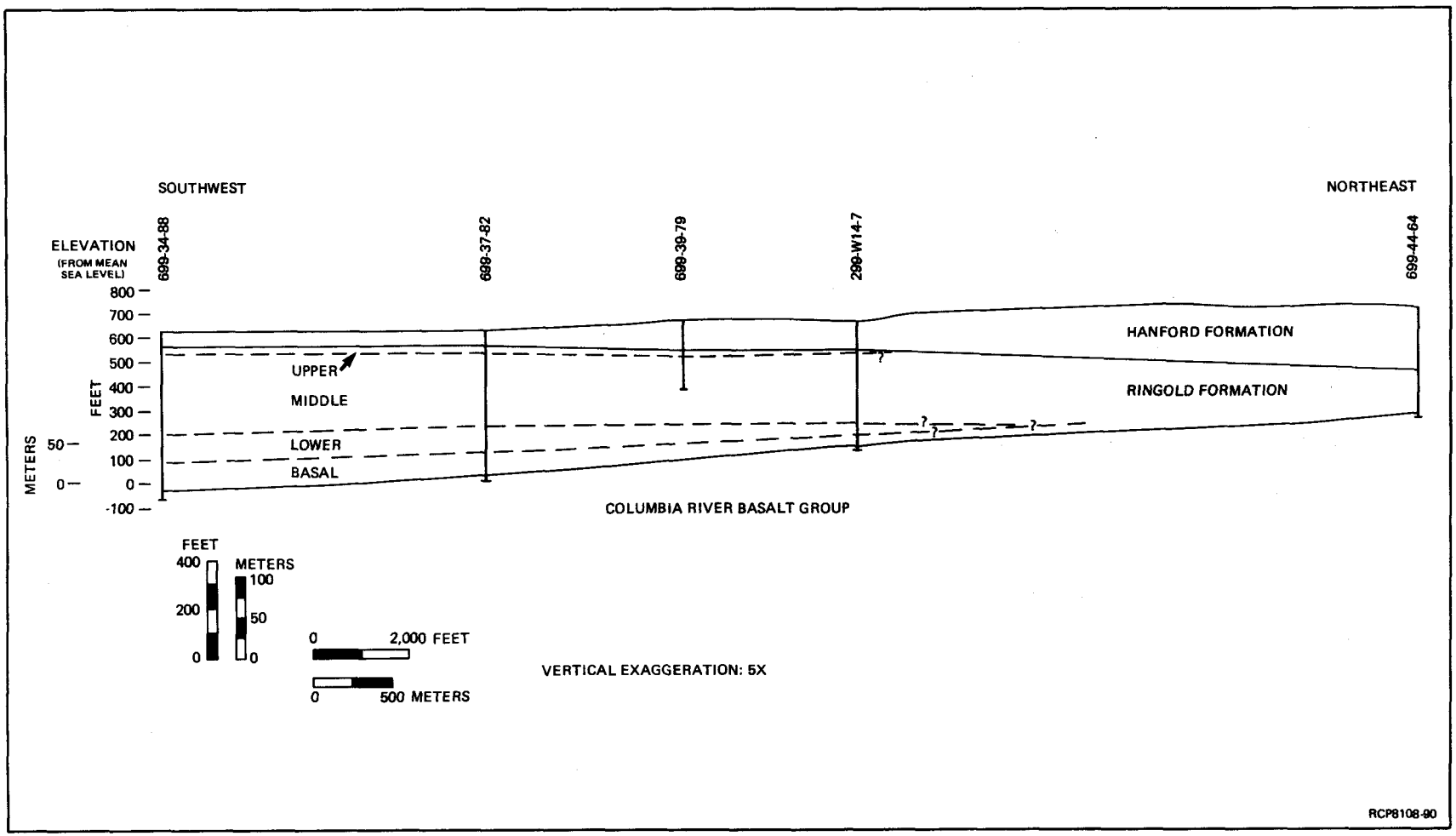

FIGURE 2-10. Structure Cross Section, Reference Repository Location.

The nature of the contact between the basal Ringold and the basalt is not fully understood, but it is assumed that regional drainage was the dominant influence on sediment deposition in the Pasco Basin very soon after the deposition of the last basalt flow (Ice Harbor Member) in the southern Pasco Basin. In the RRL, the Ringold overlies the Elephant Mountain Member, but the sediments differ from the tuffaceous Levey interbed between the Ice Harbor and Elephant Mountain Members in the southern part of the Pasco Basin (Chapter 3). It is, therefore, assumed that most deposition of the highly basaltic Ringold gravels occurred after deposition of the Ice Harbor Member. Upon continued deformation, the main channels were confined primarily to synclinal areas with local slope wash off the synclinal limbs. The unit includes gravel deposited in high-energy, main-channel environments and associated fine sediments from floodplain and local lacustrine environments.

Lower Ringold

A sand, silt, and clay facies with some gravel stringers overlies the basal Ringold gravels throughout the RRL area (Fig. 2-8 and 2-9). This represents a low-energy, fluvial unit with some lacustrine facies; the unit varies in thickness from 5 to 35 m. The unit is thickest in the deepest parts of the syncline, generally thins updip, and pinches out on anticlinal ridges (Fig. 2-10). Fining, upward, sedimentary cycles are observed in grab samples from wells, but the low well density precludes correlating these cycles between wells. In core, the silt-clay fraction is finely laminated to massive (Fig. 2-11).

The sand and silt are composed of quartz, feldspar, and mica with lithic fragments of Columbia River basalt and rocks from outside the Pasco Basin. The sediments are generally compacted with variable induration.

The thinning of the lower Ringold unit on the flanks of the Cold Creek syncline indicates that the unit was deposited during or after deformation of the Cold Creek syncline (Fig. 2-10). During lower Ringold time, the RRL area, as well as most of the Cold Creek syncline, was a region of low-energy deposition. Floodplain deposits are dominant, with some relatively thick sequences of lacustrine deposits. Minor gravel horizons indicate that there was periodic, minor, channel deposition throughout the region. The contact between the basal and lower units is generally gradational, indicating a general decrease in fluvial energy. It is not known whether this low-energy environment is representative of the entire Pasco Basin, with subsequent erosion of the lower Ringold sediments on the anticlinal highs, or is only present in the synclinal areas with coeval, major, channel deposition outside major synclinal areas.

Middle Ringold

The middle gravel facies overlies the lower Ringold and is present throughout the RRL (Fig. 2-9 and 2-10). It consists of pebble-to-cobble gravel with a matrix of sand, silt, and some clay. The unit is up to

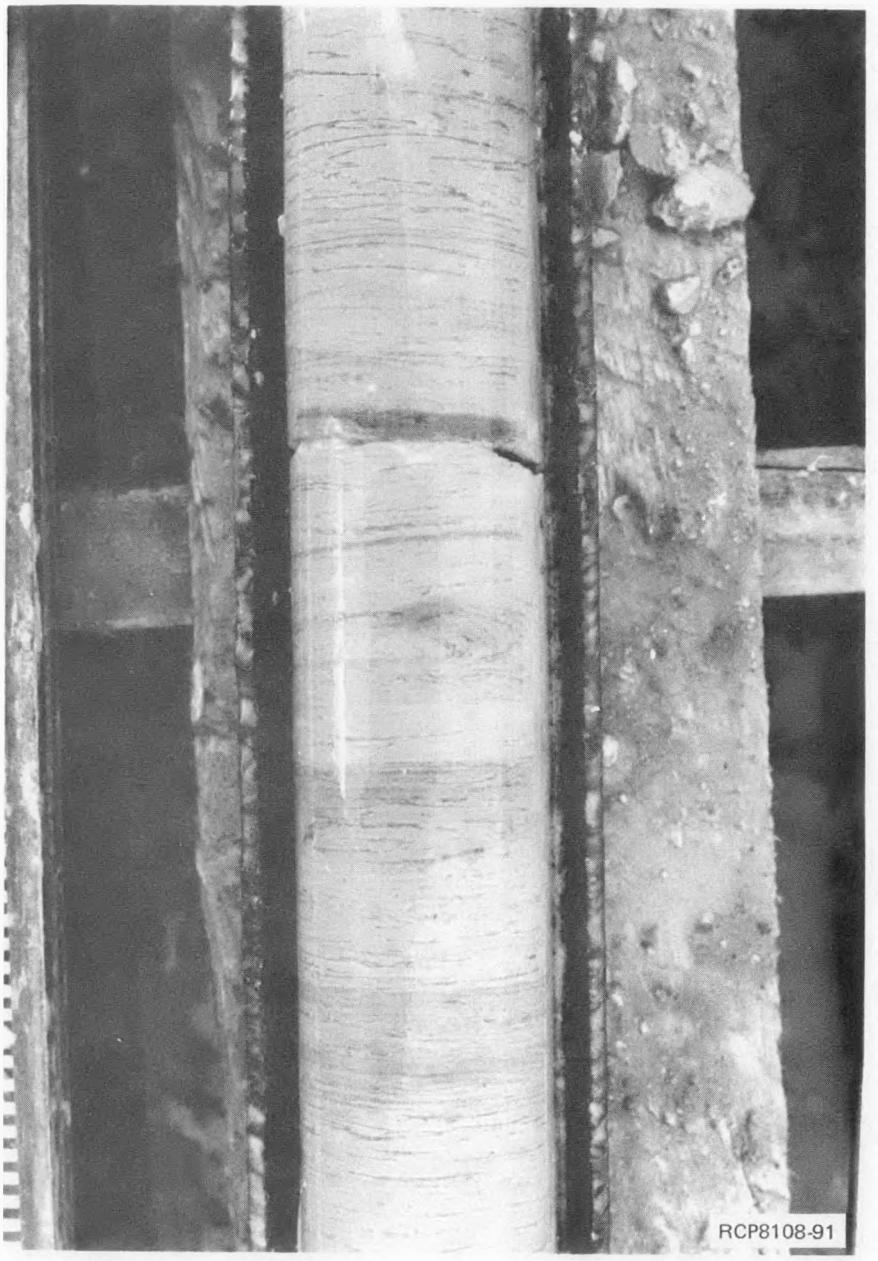

FIGURE 2-11. Lower Ringold Sediments, Borehole DH-19.

100 m thick in the RRL and contains horizons of sand and silt. The gravel is composed of basalt and quartzite with metamorphic, granitic, and porphyritic-volcanic rocks. The sand fraction is predominantly quartz and feldspar, with mica and basalt commonly a significant constituent. The silt and clay fraction is quartz, feldspar, and smectite. The conglomerate observed in cores from the 200 West Area and exposed at the White Bluffs, 30 km east of the RRL, has a massive appearance with minor imbrication of clasts. Cross bedding is common in the sand lenses from cores and at the White Bluffs exposure (Fig. 2-12).

Induration varies from essentially no cementation to well cemented by $CaCO_3$ and/or silica (SiO_2). Much of the well-indurated conglomerate facies is matrix supported (Fig. 2-13).

Openwork, uncemented gravel is occasionally found in core. Limited data within the RRL do not reveal deformation of the middle Ringold (Fig. 2-10), but a general, arcuate, concave, upward contact with the upper Ringold throughout much of the Cold Creek syncline suggests there has been some deformation of the middle Ringold. The variations in thickness are generally related to channels of middle Ringold into the lower Ringold and erosion of the middle Ringold by post-Ringold fluvial activity, primarily Pleistocene flood channels.

The contact with the lower Ringold is generally sharp, indicating an abrupt change in fluvial energy environment. The conglomerate was deposited in a high-energy environment and the particle roundness and exotic lithologies suggest transport over considerable distance. The Ringold Formation has long been considered to be of Columbia River drainage origin (Merriam and Buwalda, 1917). The presence of modern Snake River lithologies indicates an influence of the present Snake River drainage (Tallman and others, 1979; Brown, 1981). Recent studies indicate that lithologies of the modern Clearwater and Salmon River drainages are present in the middle Ringold in the southeastern Pasco Basin (Richman, 1981; Webster and others, in press). This facies is interpreted as main-channel deposition, undoubtedly recording multiple erosional unconformities and sedimentary cycles.

Upper Ringold

The upper Ringold unit is present in parts of the RRL as an erosional remnant overlying the conglomerate facies (Fig. 2-9 and 2-10). The unit is composed of well-sorted sand and silt with minor amounts of clay. Thin horizons of pebble gravel are common. The sand and silt fraction is primarily quartz and feldspar, with locally large amounts of mica and basalt. Quartz, smectite, and mica make up the clay fraction. Caliche horizons are common and usually are present on the upper erosional surface where the unit is moderately to well cemented. The unit generally appears to grade from the silty-sandy-gravel of the middle Ringold facies. The upper surface is erosional throughout the RRL (Fig. 2-9).

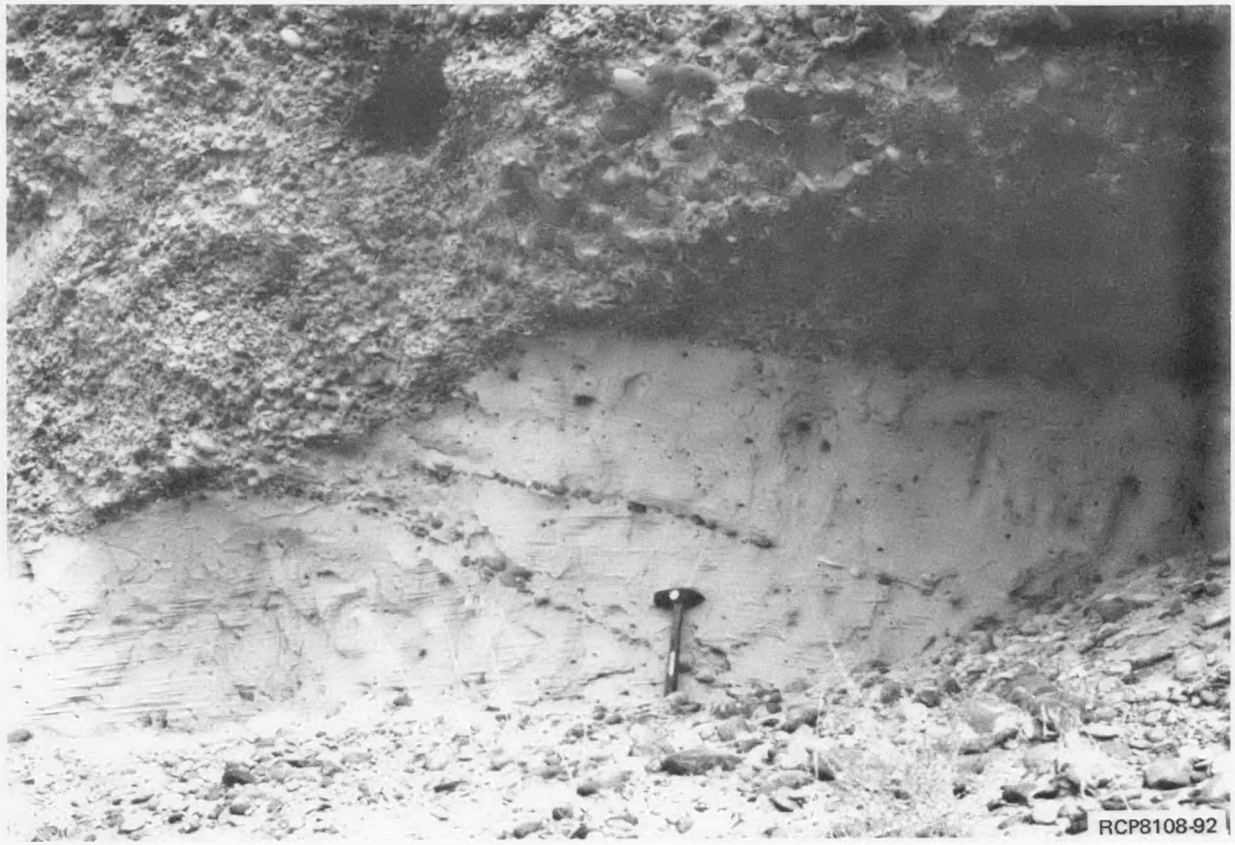

FIGURE 2-12. Cross-Bedded Sand Lens of Middle Ringold, White Bluffs.

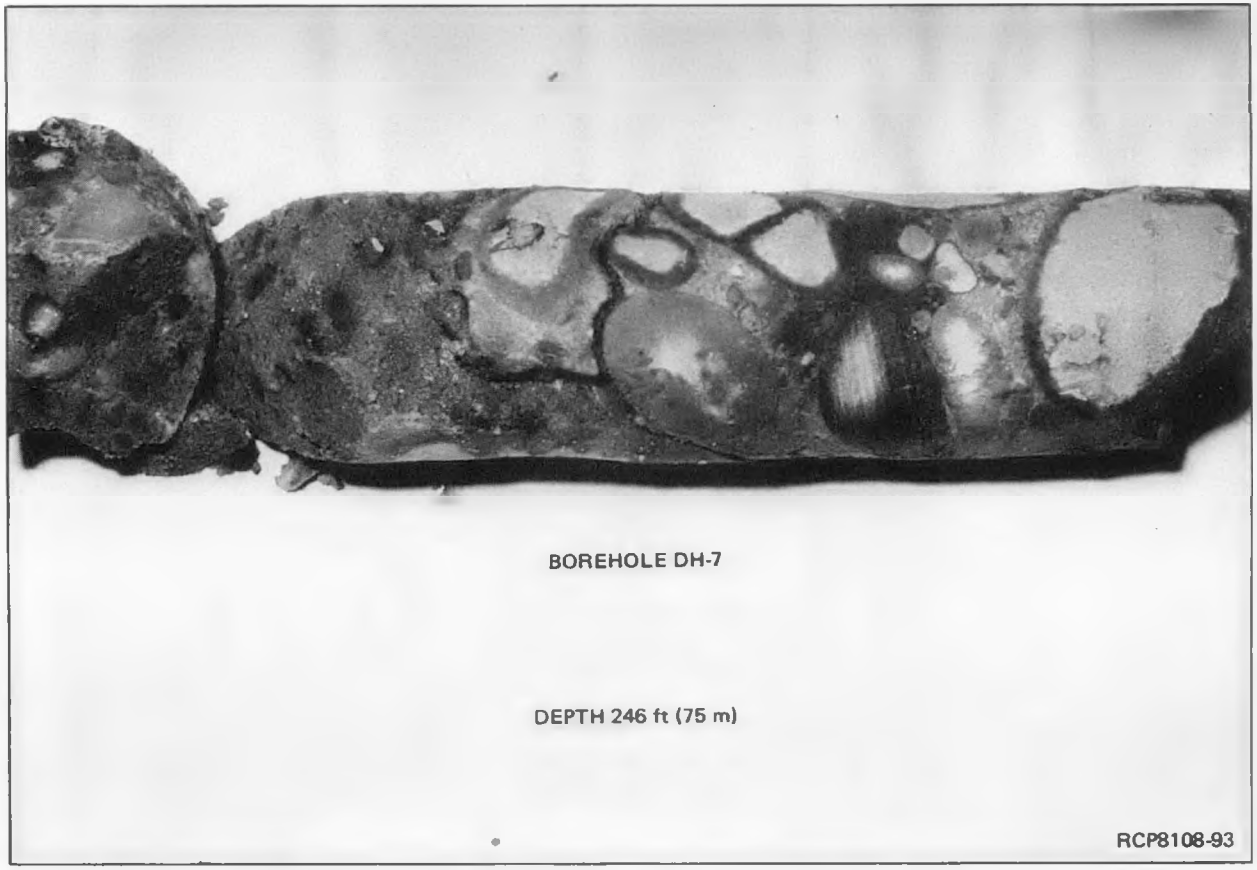

FIGURE 2-13. Matrix-Supported Clast of Middle Ringold, Borehole DH-7.

Core samples outside the RRL show alternating sand, silt, and clay horizons similar to those observed in the White Bluffs (Fig. 2-14). Only the lowermost part of the upper Ringold section found at the White Bluffs is present in the RRL. It represents a low-energy, fluvial environment with some lacustrine facies, probably a floodplain of a major fluvial system. Pebble gravels indicate small channels or perhaps extensive sheet-wash periodically inundated the area, and paleosols represent extended periods of subaerial exposure. Sediments interpreted to be loess overlie the fluvial sequence and are included in the upper Ringold unit.

Erosion removed an unknown amount of the upper Ringold in the RRL; that which remained was buried by the sediments of the Quaternary Hanford formation. The timing of loess deposition relative to the major erosion of the upper section of this unit is not known. If the major erosion of the upper Ringold occurred before the deposition of the loess, as suggested by the caliche horizon below the loess, the loess unit may be considerably younger than the underlying fluvial sediments. The extensive caliche horizon on most of the upper erosional surface of the upper Ringold unit, be it loess or fluvial sediments, suggests that the surface existed for some time prior to deposition of the glaciofluvial Hanford formation. It also suggests that very little erosion took place during Pleistocene flooding in this area of the Pasco Basin as it was generally protected in the lee of the Umtanum Ridge-Gable Mountain structure.

HANFORD FORMATION

The Hanford formation, chiefly the Pasco Gravels, overlies the Ringold Formation throughout the RRL (Fig. 2-9 and 2-10). The sediments are made up of gravel to sand and represent relatively high-energy, subfluvial deposition during Pleistocene flooding. A thin sequence of Touchet Beds is present at or near the surface mainly to the west of the RRL.

The surface of the subfluvial bars is commonly armored with a lag gravel, resulting from the winnowing of fine sediments during waning stages of flooding. This has been further accentuated by eolian deflation during the Holocene.

Clastic dikes occur within the RRL. The surface expression of these dikes is polygonal-patterned ground with polygons up to tens of meters across.

Bergmounds are very common up the Cold Creek Valley and on the flanks of Rattlesnake Mountain (Fecht and Tallman, 1978). These relatively unique landforms resulted from the grounding of large, glacial icebergs on the surface of the Hanford formation, thus protecting the underlying sediments from erosion during draining of the floodwaters.

Pasco Gravels

The Pasco Gravels range from boulders to fine-grained sand and display varied bedforms (Routson and others, 1979). The best exposures of the

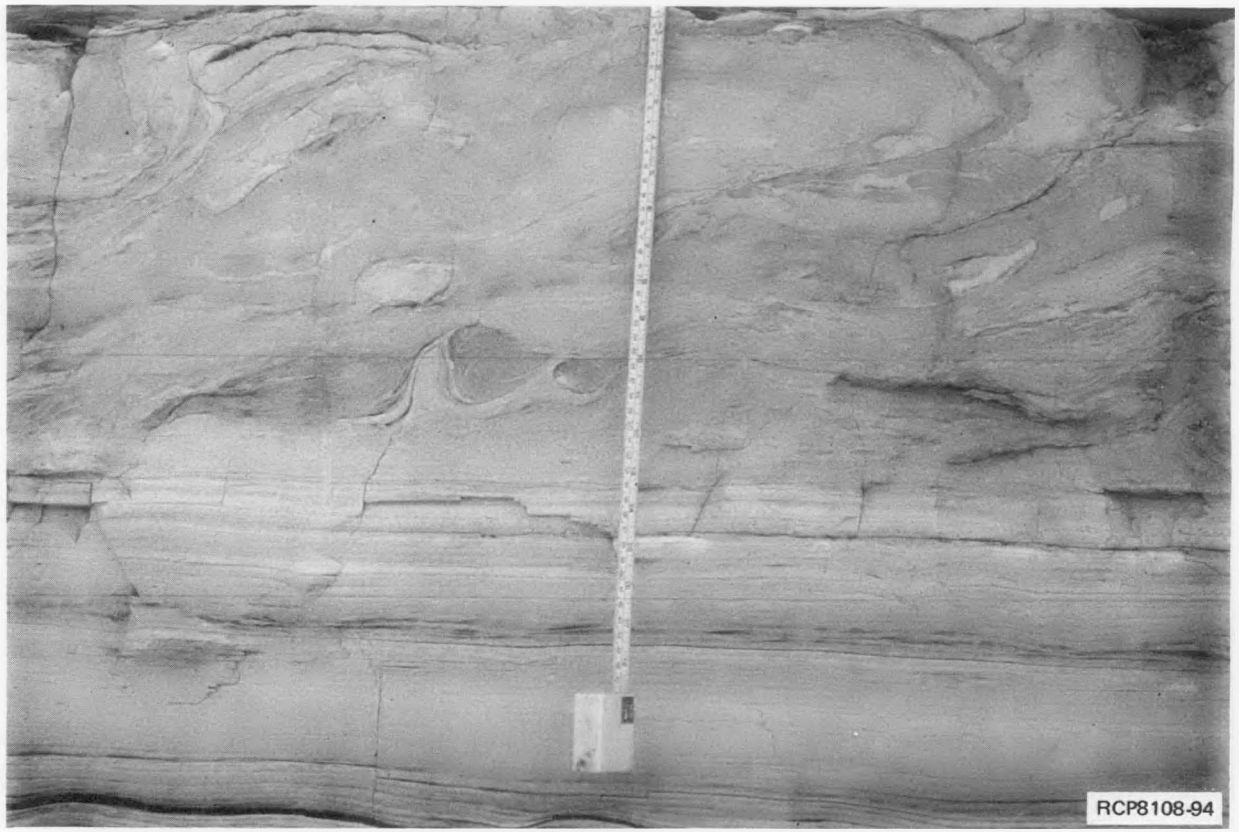

FIGURE 2-14. Laminated Upper Ringold Sediments, White Bluffs.

Pasco Gravels are in excavations for waste facilities east of the RRL. Massively bedded, horizontally bedded (often with fine laminations), cross-bedded, and graded-bed sequences have been observed in these excavations. Pasco Gravels are poorly exposed in the RRL, except for one, small, gravel pit in the northern part where the gravels are cross bedded (Fig. 2-4). Bedding present elsewhere in the Cold Creek syncline is assumed present in the RRL.

The gravel generally consists of <50% basalt, with some intrusive, igneous, metamorphic, and sedimentary rocks. Source areas for the non-basaltic rocks are the glaciated terrain to the north. Most of the sand is arkosic, with some horizons containing a relatively high basalt content. Mt. St. Helens Set S ash is locally present in the finer facies of the Pasco Gravels.

The Pasco Gravels are not generally indurated, but some horizons are moderately to well cemented with $CaCO_3$. These horizons are sometimes difficult to differentiate from the Ringold Formation in boreholes.

Two coarse- to fine-graded sequences are recognized in boreholes from the RRL. In areas where the Pasco Gravels form or fill channels in the Ringold Formation, as many as four, graded sequences are present. It is not known if these sequences represent separate floods or energy variations in the depositional environment during a single flood. Current interpretation honors two discrete floods and is based on borehole data, which include driller's logs (lithology, texture, and penetration rate), geophysical logs, and stratigraphic position relative to sediments known to represent multiple floods in the south-central Pasco Basin. Both graded sequences generally are composed of a relatively thin basal unit, consisting of poorly sorted silty-sandy-gravel with clasts ranging from pebbles to >30-cm boulders. This grades upward to a better sorted, silty-sandy, cobble-gravel unit overlain by sand and silt. The lower, graded sequence often has a calcic horizon on the upper surface, resulting in a slower drilling rate, and appears to be denser on geophysical logs.

Touchet Beds

The Touchet Beds are composed of rhythmically bedded silt to fine sand with stringers of coarse sand and gravel. A discrete horizon of Mt. St. Helens Set S ash is common.

Relatively minor, isolated exposures of Touchet Beds are present in the RRL. Touchet Beds in Cold and Dry Creek Valleys occur in generally protected areas distal to the main flood channel(s).

AGE RELATIONSHIPS

The age of the sediments overlying the Columbia River Basalt Group in the Pasco Basin is extremely important in the determination of deformation

rates. The Ringold and Hanford formations record deformation which may have taken place since the last basalt flow entered the Pasco Basin. To establish deformation rates, it is necessary to determine as precisely as possible the absolute age of the sediments. The methods used and results to date are discussed for both the Ringold and Hanford formations.

RINGOLD FORMATION

The Ringold Formation was assigned a Pliocene age by Gustafson (1973, 1978) based on vertebrate fossils. Caliche from the surface of the Ringold Formation at White Bluffs was dated using thorium/uranium methods at >500,000 yr before present, or beyond the limits of the method. Attempts to date Ringold ash horizons using fission-track methods have proved unsuccessful because of the lack of heavy minerals and large shards suitable for dating. The major emphasis in dating has been on the determination of the paleomagnetic stratigraphies and relating these to paleontologic data.

The upper Ringold at the White Bluffs contains microtine rodent fossils, 3.7 to 4.8 million years old (Repenning, in press). A Hemphillian (>4.8 million years old) rhinoceros was identified by Gustafson (1978) in the middle Ringold of the White Bluffs just above river level. This indicates that the predominantly reversed magnetic section of the White Bluffs (Packer and Johnston, 1979) represents the Gilbert Reversed Epoch, or 3.4 to 5.25 mybp.

The upper part of the Ringold Formation in the RRL is interpreted to be stratigraphically equivalent to the White Bluffs section. The erosional remnant of the upper Ringold in the RRL is, therefore, >3.7 million years and the middle Ringold is >4.8 million years. The underlying Elephant Mountain Member (10.5 million years) limits the maximum age of the Ringold Formation in the RRL. However, in the southern part of the Pasco Basin, the Ice Harbor Member (8.5 million years) and the Levey interbed are stratigraphically above the Elephant Mountain Member. Based on stratigraphic position, the basal Ringold in the Pasco Basin is interpreted to be post-Ice Harbor Member (8.5 million years) in age. Therefore, the Ringold Formation in the RRL is concluded to be >3.7 and <8.5 million years old.

HANFORD FORMATION

The number and age of Pleistocene floods that inundated the Pasco Basin is not known, but at least three events have been dated using ^{14}C and thorium/uranium methods and the Mt. St. Helens Set S ash horizon.

Pre-Wisconsinan Flood Deposits

Gravels cemented with $CaCO_3$ and assumed to be of Pleistocene flood origin are present in Badger Canyon. Three thorium/uranium age dates on the caliche from the petrocalcic horizons in these gravels yielded ages of

200,000 (+250,000 -70,000), 220,000 (+380,000 -70,000), and >210,000 yr (Tallman and others, 1978). These gravels may be correlative to flood gravels in the Cheney-Palouse channeled scabland tract north of the Pasco Basin (Patton and Baker, 1978; Baker and Nummedal, 1978). The Cheney-Palouse gravels are interpreted to be pre-Bull Lake in age (155,000 to 130,000 yr old) (Pierce and others, 1976). Gravels of this age range have not been identified in the RRL boreholes to date, but ∿8 km northwest of the RRL is an isolated outcrop of gravels which have similar field characteristics as the Badger Canyon gravels and may be correlative.

Wisconsinan Flood Deposits

The oldest ^{14}C date on the Hanford formation is in a normal-graded sequence containing clastic dikes located in the south-central part of the Pasco Basin. This sequence was eroded during a later flood that truncated the clastic dikes and deposited a later flood sequence. Wood fragments from the truncated clastic dike were dated at >32,000 radiocarbon years before present. The upper limit of the age is not known, but wood samples from flood gravels near Wanapum Dam were dated at 32,700 ± 900 radiocarbon years before present (Fryxell, 1965). These may represent the same flood.

The last major Pleistocene scabland flood occurred ∿13,000 yr ago, based on the occurrence of Mt. St. Helens Set S ash within the flood deposits and ^{14}C dates on organic sediments above and below Mt. St. Helens Set S ash near the source (Mullineaux and others, 1977). Mt. St. Helens Set S ash is present throughout the Pasco Basin, commonly occurring in the Touchet Beds, but also present in the Pasco Gravels. In Cold Creek and Dry Creek Valleys, Mt. St. Helens Set S ash is present in Touchet sediments under bergmounds (Fecht and Tallman, 1978).

Wood from a clastic dike in a flood bar southeast of Gable Mountain was dated at 18,705 (+1,515 -1,275) radiocarbon years. These sediments are stratigraphically related to the most recent, major, flood deposits and the current interpretation is that the wood was redeposited from older material. Another factor to support this conclusion is that evidence from radiocarbon dates in southern British Columbia indicate that the last major Wisconsinan advance in the northern United States began after 17,500 to 18,000 radiocarbon years before present (Clague and others, 1980). This makes an 18,705 (+1,515 -1,275) radiocarbon years flood in the Pasco Basin highly unlikely, if not impossible.

In summary, there are three, dated, flood sequences in the Pasco Basin: (1) a pre-Wisconsinan flood or floods with a well-developed calcic cement, (2) a Wisconsinan event >32,000 radiocarbon years before present, and (3) a late Wisconsinan flood(s) associated with Mt. St. Helens Set S ash ∿13,000 radiocarbon years before present (Fig. 2-1).

SUMMARY AND CONCLUSIONS

The post-Columbia River Basalt Group sediments of the Cold Creek syncline are composed of two major units: (1) Ringold Formation, a Miocene-Pliocene fluvial unit with some lacustrine facies; and (2) Pleistocene glaciofluvial sediments, informally termed the Hanford formation. Deposition of the Ringold Formation by ancestral streams flowing through the Pasco Basin started shortly after cessation of basalt flows. The Hanford formation was deposited by catastrophic floodwaters which inundated the Pasco Basin when glacial ice dams failed in Montana, Idaho, northern Washington, and southern British Columbia. Minor units include the Pleistocene and Holocene talus, colluvium, alluvium and loess, landslide debris, and Holocene dune sands.

The Ringold Formation overlies the Columbia River Basalt Group within most of the Pasco Basin. The division of the Ringold Formation into a basal, lower, middle, and upper facies, based primarily on texture, is appropriate for much of the central Pasco Basin. The predominant texture of each of these four facies is as follows: (1) basal--silty, sandy gravel to a gravelly sand; (2) lower--sand, silt, and clay; (3) middle--pebble-to-cobble gravel with a sand, silt, and clay matrix; and (4) upper--sand and silt.

In general, three representative stratigraphic sections can be used to describe the lateral variations of the Ringold Formation in the Pasco Basin. The central portion of the Cold Creek syncline and much of the central Pasco Basin are of representative section type I, the four vertical facies listed above. Section type II of the Ringold Formation north and east of Gable Mountain is composed predominantly of silt, sand, and clay. This section is interpreted to represent floodplain overbank sedimentation throughout Ringold time.

Section type III is the fanglomerate facies on the flanks of anticlinal ridges and includes the talus, slope wash, and side-stream facies which interfinger with the central basin deposits of section types I and II. This facies of the Ringold Formation is chiefly composed of basalt clasts with a matrix of quartz and feldspar or basalt sand. The unit is the result of mass wastage and runoff on the emerging ridges during the deposition of other Ringold section types in the lower elevations of the Pasco Basin. Section types I and II were deposited by a major river system which flowed through the Pasco Basin.

The sediments deposited in the Pasco Basin during catastrophic flood events are informally referred to as the Hanford formation. The Hanford formation is divided into two textural facies: (1) Pasco Gravels and (2) Touchet Beds. The Pasco Gravels range in texture from boulders to fine sand, representing varied energy environments during flooding. The Touchet Beds are made up of rhythmically bedded, fine-grained sediments deposited in low-energy, slackwater environments.

The number of Pleistocene floods in eastern Washington and the Pasco Basin is unknown. Within the Pasco Basin, multiple, graded sequences of Pasco Gravels and Touchet Beds have been observed in boreholes and outcrops. Whether each sequence represents an individual flood or merely changes in the energy environment during deposition is not known. Locally, three sedimentary sequences have been identified in the Pasco Basin boreholes and are interpreted to be three separate flood events.

The Ringold and Hanford formations record the deformation which has taken place since the last basalt flow entered the Pasco Basin. In order to establish deformation rates, it is necessary to determine, as precisely as possible, the absolute age of these sediments.

The major emphasis for age determination of the Ringold Formation has been on the determination of the paleomagnetic stratigraphy, and using paleontologic data, assigning age ranges to the formation. Fossils from the upper Ringold Formation indicate an age of 3.7 to 4.8 million years and that the predominantly reversed magnetic section represents the Gilbert Reversed Epoch. The basal Ringold is interpreted to be mainly post-Ice Harbor in age. Based on these assumptions, the Ringold Formation in the RRL is interpreted to be >3.4, but <8.5 million years old.

The number and age of Pleistocene floods to inundate the Pasco Basin are not known, but at least three events have been dated. These three flood sequences in the Pasco Basin are: (1) a pre-Wisconsinan flood or floods, (2) a Wisconsinan event >32,000 radiocarbon years before present, and (3) a late Wisconsinan flood(s) associated with Mt. St. Helens Set S ash ∿13,000 radiocarbon years before present.

CHAPTER 3 - WANAPUM AND SADDLE MOUNTAINS BASALTS OF THE COLD CREEK SYNCLINE AREA

S. P. Reidel
K. R. Fecht

INTRODUCTION

This chapter describes the stratigraphy of the Wanapum and Saddle Mountains Basalts (Fig. 3-1) in the Cold Creek syncline area of the Pasco Basin. More information is presently known about flows of these formations than the Grande Ronde Basalt because of the greater number of surface exposures and drill holes that penetrate them (Appendix A). Emphasis is placed upon primary physical and chemical characteristics that were used to map the area and to determine the distribution and emplacement history of the basalt flows. A discussion of the geologic history of the Cold Creek syncline area during Wanapum and Saddle Mountains time concludes this chapter.

Basic information on the stratigraphy of the Wanapum and Saddle Mountains Basalts is derived from the study of surface exposures (Fig. 3-2) and core and chip samples from drill holes. Surface exposures occur primarily along the edges of the Cold Creek syncline, where uplift along Yakima folds has exposed thick sections of the basalt. The spacing and depth of boreholes in the Cold Creek syncline area (Fig. 3-2) provide relatively good subsurface data coverage for the Saddle Mountains Basalt, but only fair coverage for the Wanapum and Grande Ronde Basalts (Appendix A); thus, less information is available. The stratigraphy of the basalt and correlations from borehole to borehole and from borehole to outcrop are determined by using chemical composition, paleomagnetism, and physical characteristics.

PREVIOUS WORK

The nomenclature and stratigraphic relationships of the Columbia River basalt in the Pasco Basin are based on that developed for the Columbia Plateau by Mackin (1961), Waters (1955, 1961), Schmincke (1967a and b), Wright and others (1973), Myers (1973), Bingham and Grolier (1966), Bingham and Walters (1965), Brown and Ledgerwood (1973), Myers and Brown (1973), Laval (1956), and ARHCO (1976). Swanson and others (1979b) summarized the important relationships discussed in these and other studies and related them to regional stratigraphic relationships. The nomenclature and stratigraphic framework for the Columbia River basalt that is currently used in the region and in the Pasco Basin and Cold Creek syncline area is shown in Figure 3-1. Myers, Price and others (1979) summarized the work

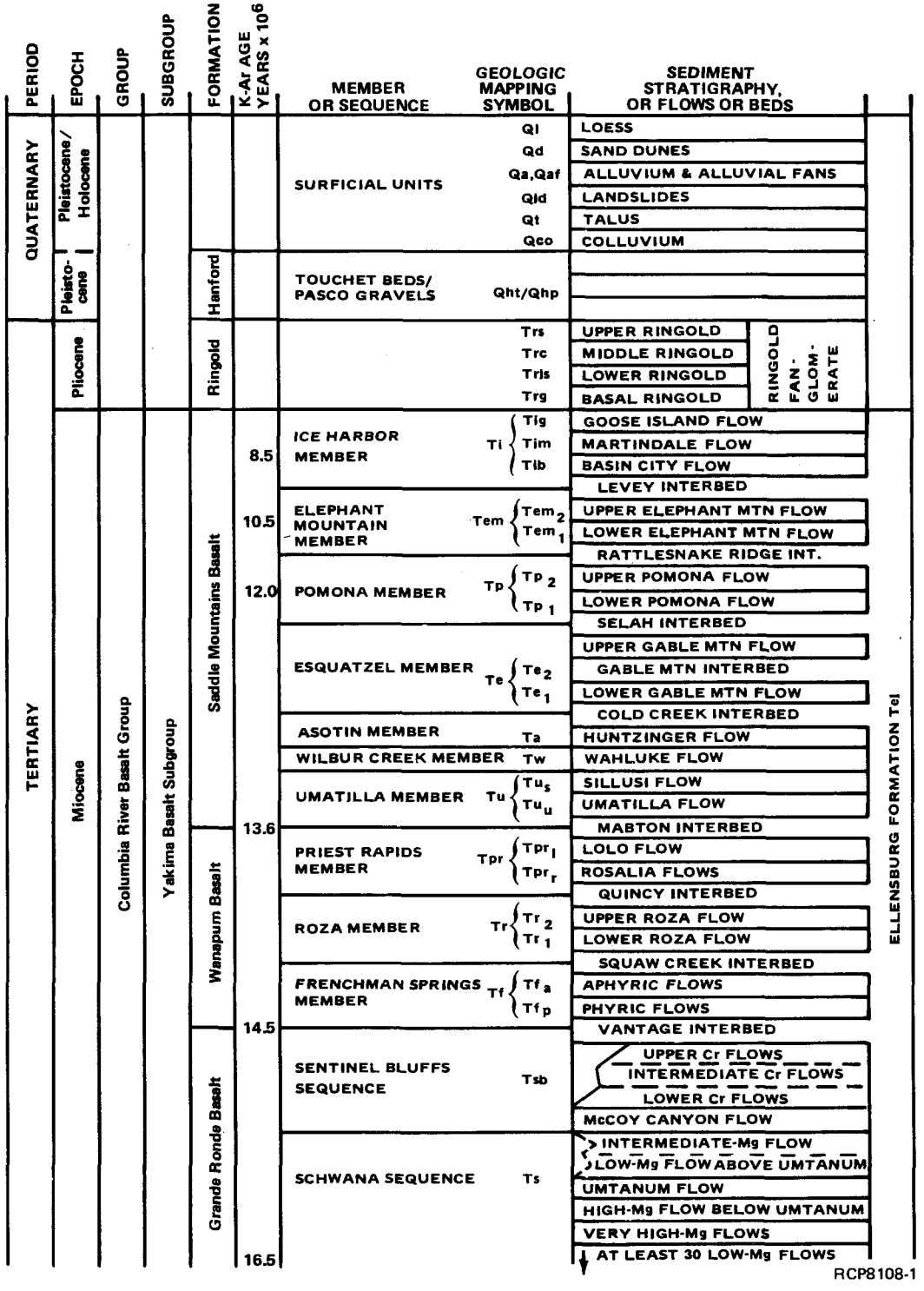

FIGURE 3-1. Stratigraphic Nomenclature, Columbia River Basalt Group, Pasco Basin.

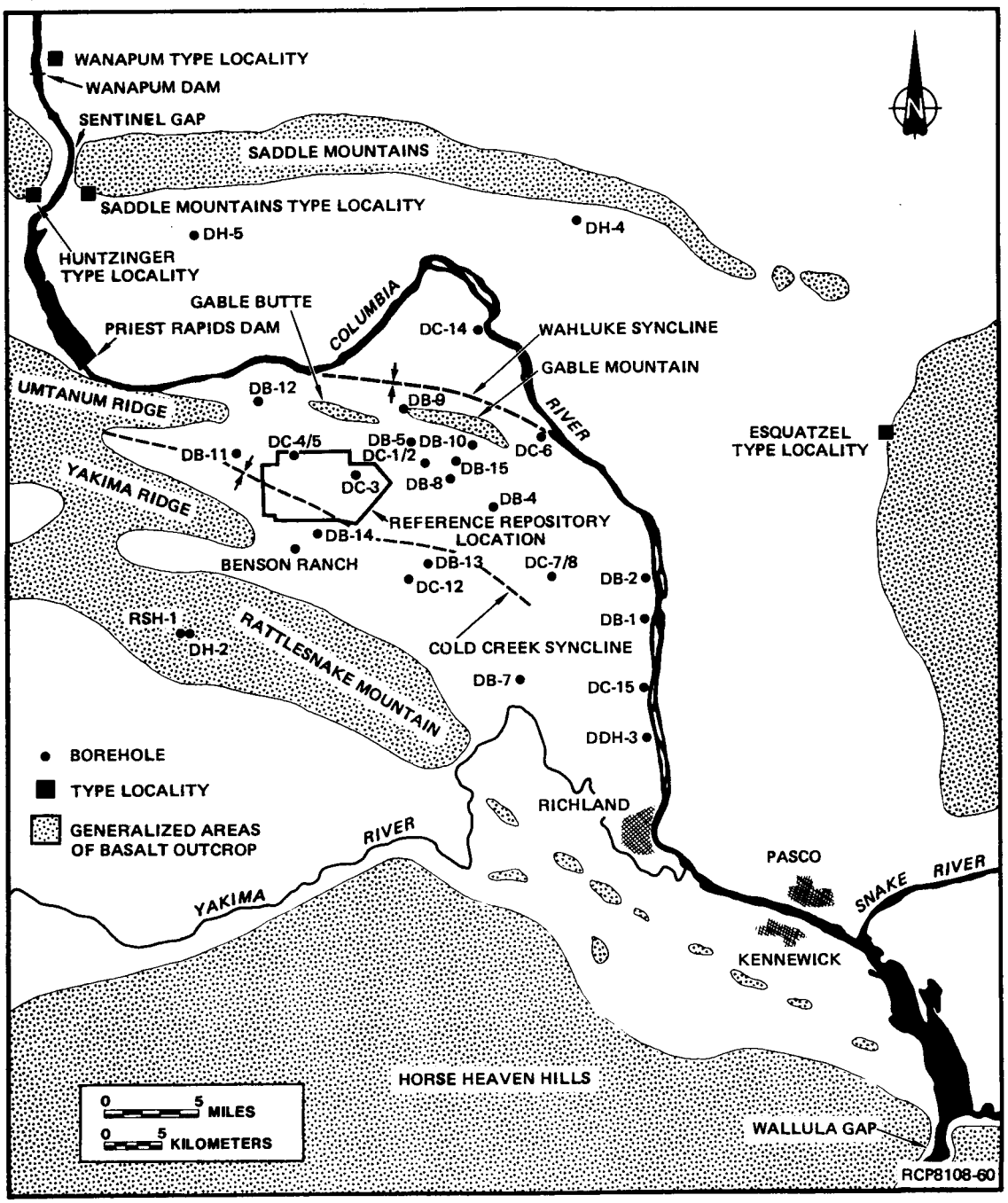

FIGURE 3-2. Location of Referenced Features, Pasco Basin and Nearby Area.

done by geologists for the BWIP. The results of a more detailed study on the Wanapum and Saddle Mountains Basalt flows were recently summarized by Reidel and others (1980). This study related the distribution of flows to the deformational history of the Pasco Basin.

WANAPUM BASALT

The Wanapum Basalt consists of three members in the Pasco Basin: (1) Frenchman Springs, (2) Roza, and (3) Priest Rapids. The Vantage interbed separates this formation from the underlying Grande Ronde Basalt; the Mabton interbed separates the Wanapum Basalt from the overlying Saddle Mountains Basalt (Fig. 3-1).

The Wanapum Basalt is typically fine to medium grained with some flows containing olivine and plagioclase phenocrysts. The petrographic characteristics combined with distinct chemical differences, termed the "TiO_2 discontinuity" (Siems and others, 1974), permit easy distinction of the Wanapum Basalt from the Grande Ronde Basalt.

The Wanapum Basalt is between 14.5 and 13.5 million years old (Watkins and Baksi, 1974) and was erupted from linear vents on the east side of the plateau (Swanson and others, 1979a). It is thickest in the central area of the Cold Creek syncline (Table 3-1; Fig. 3-3), but thins from west to east and over the Rattlesnake Mountain and Umtanum Ridge-Gable Mountain structures.

FRENCHMAN SPRINGS MEMBER

The Frenchman Springs Member is the oldest member of the Wanapum Basalt in the Pasco Basin and consists of seven to nine (possibly in borehole RSH-1) flows in the Cold Creek syncline (Fig. 3-4). It varies in thickness from ∿192 to ∿229 m (Fig. 3-4). The flows are all medium to fine grained and contain plagioclase pheocrysts. Within the Pasco Basin, the flows can be grouped into "phyric" and "aphyric" units based upon relative phenocryst abundance.

The average chemical composition of the Frenchman Springs Member is given in Table 3-2. It falls within the Frenchman Springs chemical type of Wright and others (1973), but there is no obvious difference in chemical composition between the phyric and aphyric flows from the Pasco Basin area.

The flows of the Frenchman Springs Member near Vantage were sampled for remanent magnetic polarity by Van Alstine and Gillett (in press) as part of BWIP stratigraphic studies. Their findings are comparable with those of Rietman (1966), Kienle and others (1978b), and Sheriff and Bentley (1980). Van Alstine and Gillett (in press) found that the magnetic polarity of the two lowest flows near Vantage, the Ginkgo and Sand Hollow flows (Table 3-3), are nearly identical with mean declinations of 146.1° and

TABLE 3-1. Map Explanation.

The following symbols are used throughout this report on maps and diagrams. In specific instances, additional special symbols are used and are defined for the specific diagram.

FOR ISOPACH MAPS

Isopach; line representing equal stratigraphic thickness; number is expressed in feet

Borehole location, identifying borehole (if applicable); thickness measured in feet

Field section location indicating thickness measured in feet

Contour interval in feet varies, but is indicated per each figure

FOR GEOLOGIC MAPS

Solid lines with stippling inside delineate areas of basalt outcrop

Contact; dashed where concealed

Fault; dashed where inferred; ball and bar appear on downthrown side

Map Units

Saddle Mountains Basalt

Ti	Ice Harbor Member
Tem	Elephant Mountain Member
Tp	Pomona Member
Te	Esquatzel Member
Ta	Asotin Member
Tw	Wilbur Creek Member
Tu	Umatilla Member

Wanapum Basalt

Tpr	Priest Rapids Member
Tr	Roza Member
Tf	Frenchman Springs Member

Grande Ronde Basalt

Tsb	Sentinel Bluffs Sequence
Ts	Schwana Sequence

FOR STRUCTURE-CONTOUR MAPS

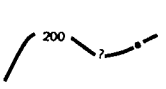

Structure contour; line representing equal elevation on a stratum; number is elevation in feet in relation to mean sea level; queried where trend or elevation is uncertain; shown with "e" where eroded, principal contours shown by bold line, intermediate contours by narrow line; contour interval varies, but is always in relation to the solid, continuous lines. Accuracy is ± one contour interval

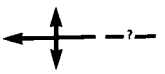

Anticline; showing trace of crest and plunge of crest; dashed where approximately located; queried where uncertain

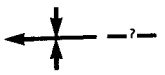

Syncline; showing trace of trough and plunge of trough; dashed where approximately located; queried where uncertain

Monocline; showing trace of axis; dashed where approximately located

Borehole location identifying borehole (if applicable); elevation measured in feet from mean sea level

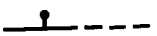

Fault; dashed where inferred; ball and bar appear on downthrown side

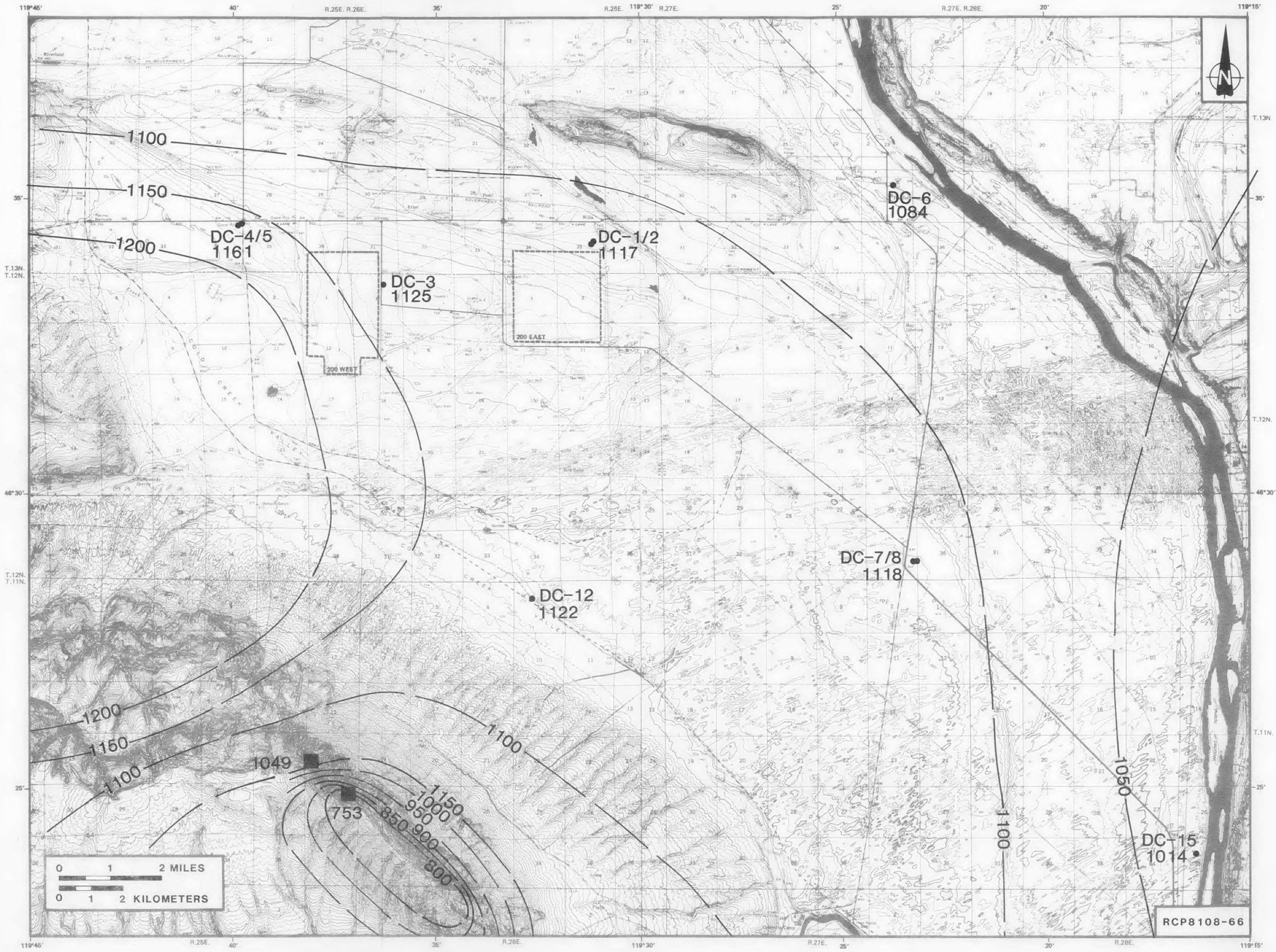

FIGURE 3-3. Isopach Map, Saddle Mountains Basalt, Cold Creek Syncline. Contour interval is 50 ft. See Figure 3-2 for location of structural features and Table 3-1 for explanation.

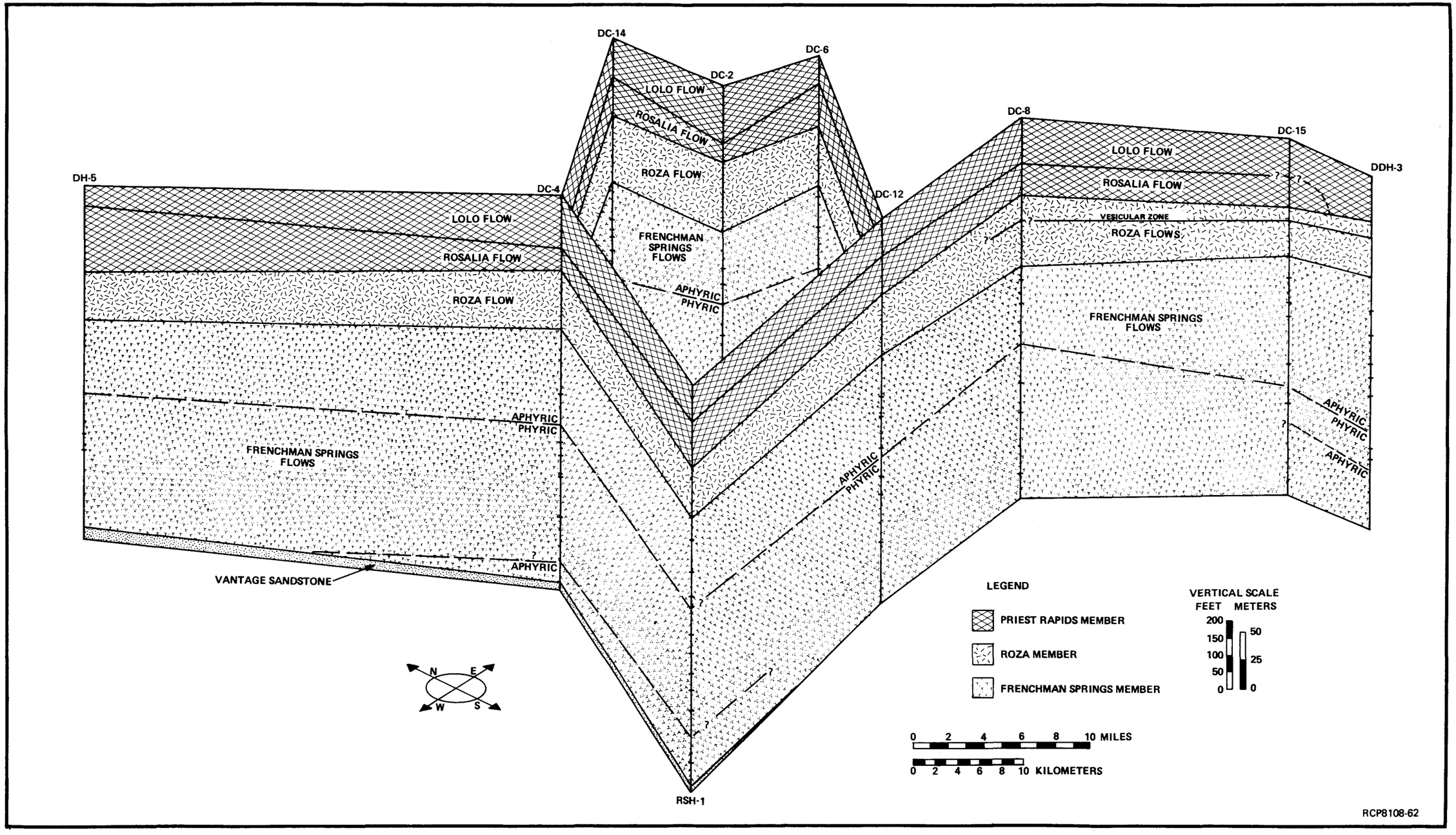

FIGURE 3-4. Fence Diagram, Wanapum Basalt, Cold Creek Syncline. See Figure 3-2 for location of boreholes. Individual flows or flow lobes are shown as horizontal lines on the boreholes and connections are shown only where there is confidence in the correlations.

TABLE 3-2. Average Chemical Composition of Flows from the Wanapum and Saddle Mountains Basalts, Pasco Basin. (Sheet 1 of 2)

Flow	Frenchman Springs Member plagioclase phyric flows		Frenchman Springs Member aphyric flows		Roza Member		Priest Rapids Member Rosalia flow	
	N = 43		N = 28		N = 13		N = 15	
Mean, One Std. Dev.	$\bar{X}$	1σ	$\bar{X}$	1σ	$\bar{X}$	1σ	$\bar{X}$	1σ
SiO_2	51.24	0.37	51.27	0.39	50.60	0.35	49.85	0.35
AL_2O_3	13.93	0.29	14.04	0.32	14.35	0.37	13.70	0.21
TiO_2	2.98	0.08	2.92	0.08	3.01	0.11	3.48	0.05
FeO*	12.83	0.44	12.69	0.37	12.44	0.54	13.47	0.31
MnO	0.24	0.01	0.23	0.01	0.23	0.01	0.24	0.01
CaO	8.34	0.17	8.34	0.15	8.65	0.20	8.55	0.19
MgO	4.22	0.25	4.21	0.23	4.59	0.31	4.49	0.22
K_2O	1.15	0.14	1.29	0.12	1.17	0.13	1.05	0.20
NA_2O	2.54	0.14	2.49	0.17	2.43	0.20	2.50	0.22
P_2O_5	0.53	0.05	0.52	0.04	0.54	0.03	0.66	0.02
Flow	Priest Rapids Member Lolo flow		Umatilla Member Sillusi flow		Umatilla Member Umatilla flow		Wilbur Creek Member Wahluke flow	
	N = 19		N = 26		N = 24		N = 4	
Mean, One Std. Dev.	$\bar{X}$	1σ	$\bar{X}$	1σ	$\bar{X}$	1σ	$\bar{X}$	1σ
SiO_2	49.87	0.53	54.31	0.73	53.65	0.59	53.43	0.35
AL_2O_3	14.28	0.30	14.70	0.60	14.51	0.27	15.01	0.28
TiO_2	3.15	0.09	2.83	0.30	2.99	0.11	1.87	0.02
FeO*	12.20	0.45	10.48	0.92	10.87	0.72	9.66	0.21
MnO	0.24	0.01	0.22	0.02	0.22	0.05	0.19	0.01
CaO	9.00	0.63	6.60	0.64	6.68	0.37	8.50	0.19
MgO	5.18	0.31	2.61	0.26	3.00	0.31	4.61	0.25
K_2O	0.98	0.11	2.62	0.36	2.52	0.14	1.90	0.16
NA_2O	2.45	0.17	2.82	0.25	2.84	0.24	2.37	0.15
P_2O_5	0.66	0.02	0.81	0.05	0.72	0.02	0.45	0.01

TABLE 3-2. Average Chemical Composition of Flows from the Wanapum and Saddle Mountains Basalt, Pasco Basin. (Sheet 2 of 2)

Flow	Esquatzel Member		Asotin Member Huntzinger flow		Pomona Member		Elephant Mountain Member Lower flow	
	N = 44		N = 45		N = 67		N = 23	
Mean, One Std. Dev.	$\bar{X}$	1σ	$\bar{X}$	1σ	$\bar{X}$	1σ	$\bar{X}$	1σ
SiO_2	52.78	0.47	51.43	0.82	51.81	0.38	50.76	0.33
AL_2O_3	14.24	0.27	16.06	0.56	15.41	0.28	13.76	0.30
TiO_2	3.02	0.10	1.58	0.12	1.63	0.06	3.49	0.06
FeO*	11.68	0.50	8.32	0.54	8.68	0.39	13.08	0.51
MnO	0.21	0.02	0.18	0.02	0.19	0.01	0.23	0.01
CaO	7.65	0.22	10.51	0.69	10.62	0.30	8.38	0.19
MgO	3.75	0.22	6.82	0.97	6.73	0.27	4.22	0.14
K_2O	1.78	0.13	0.67	0.42	0.53	0.10	1.30	0.10
NA_2O	2.50	0.14	2.16	0.20	2.16	0.12	2.29	0.21
P_2O_5	0.37	0.02	0.26	0.06	0.24	0.02	0.49	0.01
Flow	Elephant Mountain Member upper flow (Ward Gap)		Ice Harbor Member Basin City flow		Ice Harbor Member Martindale flow		Ice Harbor Member Goose Island flow	
	N = 10		N = 8		N = 14		N = 4	
Mean, One Std. Dev.	$\bar{X}$	1σ	$\bar{X}$	1σ	$\bar{X}$	1σ	$\bar{X}$	1σ
SiO_2	50.57	0.28	47.62	0.29	48.44	0.49	47.46	0.67
AL_2O_3	13.78	0.22	14.04	0.21	14.18	0.36	13.17	0.39
TiO_2	3.43	0.08	3.59	0.04	3.25	0.13	3.64	0.05
FeO*	13.26	0.39	13.54	0.28	12.38	0.87	15.32	0.44
MnO	0.22	0.01	0.23	0.01	0.23	0.01	0.28	0.01
CaO	8.54	0.13	9.71	0.28	10.20	0.59	8.85	0.11
MgO	4.26	0.24	5.57	0.20	5.65	0.36	4.31	0.15
K_2O	1.20	0.12	0.68	0.11	0.68	0.17	1.22	0.06
NA_2O	2.27	0.14	2.23	0.11	2.30	0.13	2.25	0.16
P_2O_5	0.47	0.02	0.78	0.04	0.68	0.04	1.49	0.04

NOTE: Analyses are in wt%. Samples are core that was collected from drill holes and specimens from type localities.
*Total Fe expressed as FeO.

TABLE 3-3. Paleomagnetic Polarity of Wanapum and Saddle Mountains Basalts.

Member	Flow or location	Mean declination	Mean inclination	α95	Source of information
Ice Harbor	Goose Island	51.3 33.5	+19.2 +31.9	11.7 13.3	1
	Martindale	185.1 168.2	-55.1 -65.0	3.0 3.3	1
	Basin City	317.0 319.3	+34.7 +49.5	4.2 6.3	1
Elephant Mountain	Site 1 Site 2	6.9 14.2	+59.6 +62.5	4.2 8.3	1
	Site 3 Site 4	111.5 127.9	-25.6 -39.5	9.3 9.8	1
		133.2	-39.2	8.6	2
Pomona	Site 1 Site 2	187.8 186.3	-519.1 -53.4	1.7 2.2	1
	Site 3 Site 4	203.4 195.4	-54.6 -50.6	2.0 2.9	1
		193.5	-52.7	9.5	2
Esquatzel	Site 1 Site 2	340.8 308.0	+63.0 +81.0	3.6 11.4	1
		348.4	+64.8	8.6	2
Asotin	Huntzinger	23.7	+80.6	4.5	2
Wilbur Creek	Wahluke	345.7	+72.1	3.4	2
Umatilla	Sillusi	321.7	+32.2	2.6	2
	Umatilla	324.3	+31.7	3.4	2
Priest Rapids	Lolo	190.5	-64.9	2.8	2
Roza	Site 1 Site 2	214.2 184.7	-14.7 -38.7	7.3 7.0	1
Frenchman Springs	Sentinel Gap	5.0	+62.8	2.2	2
	Sand Hollow	144.7	+39.8	3.6	2
	Ginkgo	146.1	+42.1	2.6	2

[1]Choinier and Swanson (1979)

[2]Van Alstine and Gillett (in press).

144.7° and mean inclinations of 42.1° and 39.8°, respectively. The youngest flow, the Sentinel Gap flow (Table 3-3), has a mean declination of 5.0° and a mean inclination of 62.8°. Packer and Petty (1979) found that the inclination of the lowest Frenchman Springs flow in core from borehole DC-2 (Fig. 3-2) had a mean inclination of 21° and all younger Frenchman Springs flows had higher inclinations. Van Alstine and Gillett (in press) suggested that the lowest flow in DC-2 could be either the Ginkgo or Sand Hollow flow and that the inclination of the younger flows in DC-2 were much closer to the Sentinel Gap flow. These results suggest that either the Ginkgo or Sand Hollow flow is not present in the Cold Creek syncline.

The total thickness of the Frenchman Springs Member thins from south to north and from east to west across the Pasco Basin (Reidel and others, 1980). The greatest number of flows is present near Wallula Gap (Fig. 3-2) in the southeastern part of the Pasco Basin and the least number in the northwestern part near Sentinel Gap (Fig. 3-2). In the central part of the Cold Creek syncline area, there are between seven and nine flows or flow lobes (Fig. 3-4). An abrupt thinning occurs onto the Rattlesnake Mountain structure at the southern edge of the Cold Creek syncline. The greatest thickness occurs on the east side of the Cold Creek syncline (Fig. 3-5). Due to the similarities between flows, the correlation of individual flows across the area is currently not possible.

ROZA MEMBER

Between one and two flows or flow lobes of similar physical and chemical composition comprise the Roza Member in the Pasco Basin. The Roza flows were erupted from a narrow, linear, vent system in eastern Washington and northeastern Oregon (Swanson and others, 1975). The member varies in thickness from 41 to 69 m. It is distinguished in hand specimen, typically by the presence of single plagioclase phenocrysts up to 1.5 cm in size set in a fine-grained groundmass.

The average chemical composition of the Roza Member from the Pasco Basin is given in Table 3-2. It generally falls within the Frenchman Springs chemical type of Wright and others (1973) and cannot be distinguished from the Frenchman Springs flows on chemical composition alone.

The magnetic polarity of the Roza Member was determined by Rietman (1966) to be transitional, but Choinier and Swanson (1979) found that in the southeastern part of the Columbia Plateau, the oldest Roza flow has reversed polarity. Van Alstine and Gillett (in press) found that the two Roza flows in core from DH-5 (Fig. 3-2) have low-mean inclinations (+3.3° and 7.5°), lower than that reported by Choinier and Swanson (1979) (Table 3-3). Packer and Petty (1979) sampled the Roza flow from core in DC-2 (Fig. 3-2) and found results similar to those of Van Alstine and Gillett (in press).

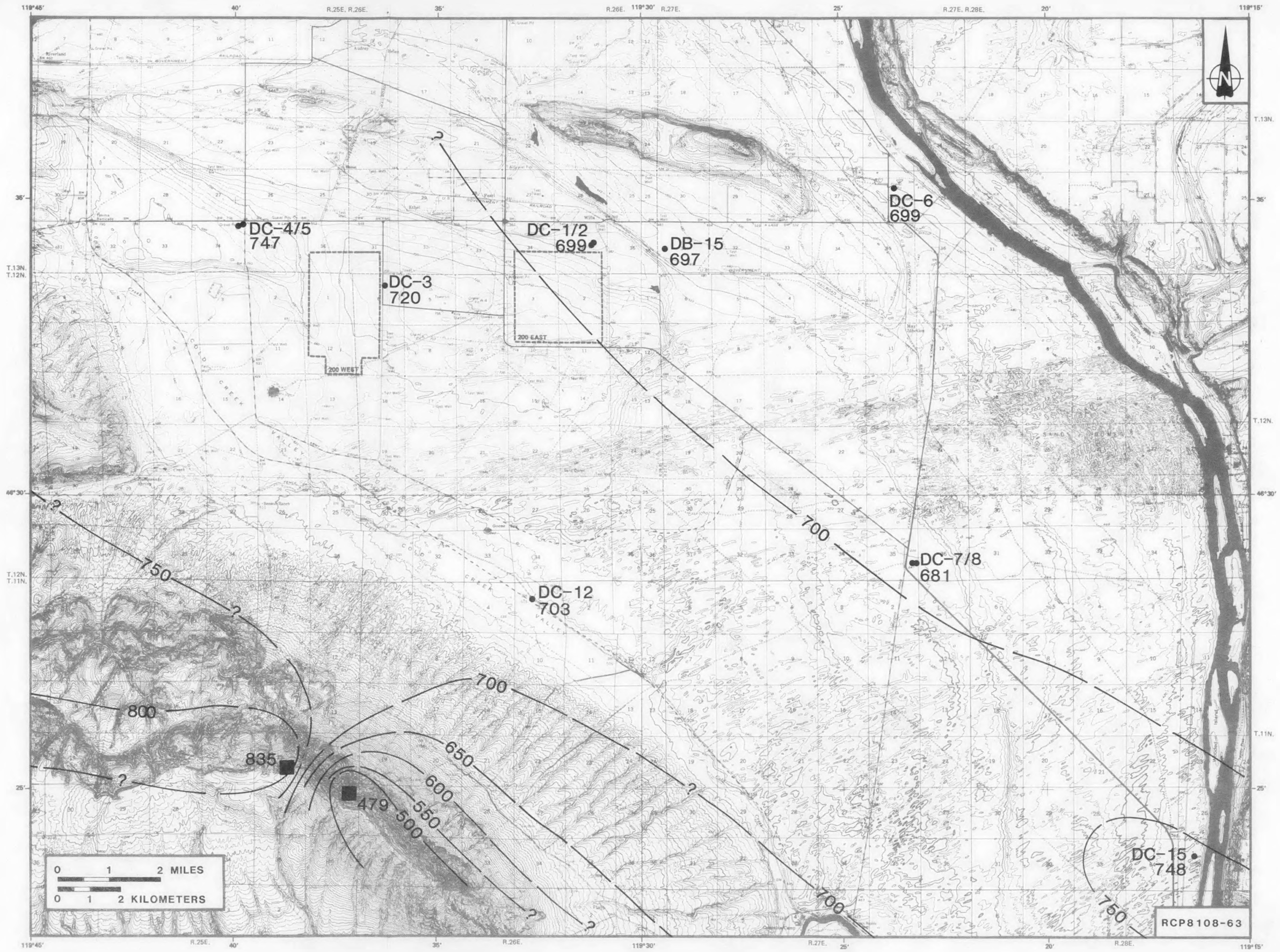

FIGURE 3-5. Isopach Map, Frenchman Springs Member, Cold Creek Syncline. Contour interval is 50 ft. See Figure 3-2 for location of structural features and Table 3-1 for explanation.

The Roza Member reaches its greatest thickness (Fig. 3-6) in the central part of the Cold Creek syncline and just north of Gable Mountain. It consists of one flow in the western part of the syncline, but is two flows or two flow lobes in the eastern part (Fig. 3-4). It thins across Rattlesnake Mountain and the Umtanum Ridge-Gable Mountain structure, but thickens along the northern flank of the Umtanum Ridge-Gable Mountain structure in the Wahluke syncline.

PRIEST RAPIDS MEMBER

The Priest Rapids Member is the youngest member of the Wanapum Basalt (Swanson and others, 1979b) and consists of two distinct flows in the Cold Creek syncline as elsewhere in the Pasco Basin. In core from the Priest Rapids Dam site (Fig. 3-2), four flows are present, but the three lowest are now considered to be flow lobes of the same flow (Reidel and others, 1980). The Priest Rapids flows were erupted from vents near the eastern margin of the plateau in Idaho (Camp, in Swanson and others, 1979a). The member varies in thickness from 40 to 75 m (Fig. 3-7) in the Cold Creek syncline. The older flow is typically coarser grained with rare olivine and plagioclase phenocrysts. The younger flow has small olivine phenocrysts (<5 mm) and rare glomerocrysts or phenocrysts of plagioclase. This texture varies from glassy to fine grained with distinct zones having a diabasic texture.

Both flows have distinct chemical compositions (Table 3-2). The older flow is chemically similar to the Rosalia chemical type of Swanson and others (1979b), while the younger flow is chemically similar to the Lolo chemical type of Wright and others (1973). The Lolo flow has lower TiO_2 and higher iron oxide (FeO) than the Rosalia flow.

Van Alstine and Gillett (in press) sampled a surface exposure of the Lolo flow in the Saddle Mountains for magnetic polarity. The flow was found to have a mean declination of 190.5° and a mean inclination of -64.9° (Table 3-3). These data are comparable to the inclination of the Lolo flow in core from DC-2 (Fig. 3-2) sampled by Packer and Petty (1979). Packer and Petty (1979) also found the Rosalia flow in DC-2 to have reversed magnetic polarity.

The Priest Rapids Member reaches its greatest thickness (Fig. 3-7) along the northern flank of Rattlesnake Mountain in the Cold Creek syncline, but thins abruptly across the structure. It also thins along the Umtanum Ridge-Gable Mountain structure and along a small, northwest-trending zone on the east side of the Cold Creek syncline.

Both the Rosalia and Lolo flows of the Priest Rapids Member are present throughout most of the Cold Creek syncline area (Fig. 3-4). The lower flow, the Rosalia, is thickest in the trough of the Wahluke syncline (Fig. 3-2) and Cold Creek syncline, and thins across the Umtanum Ridge-Gable Mountain structure and Rattlesnake Mountain (Reidel and others, 1980). It is thicker on the south side of the Cold Creek syncline and thins northward, abruptly pinching out on the southeast edge of the Cold Creek syncline between DC-15 and DDH-3 (Fig. 3-4).

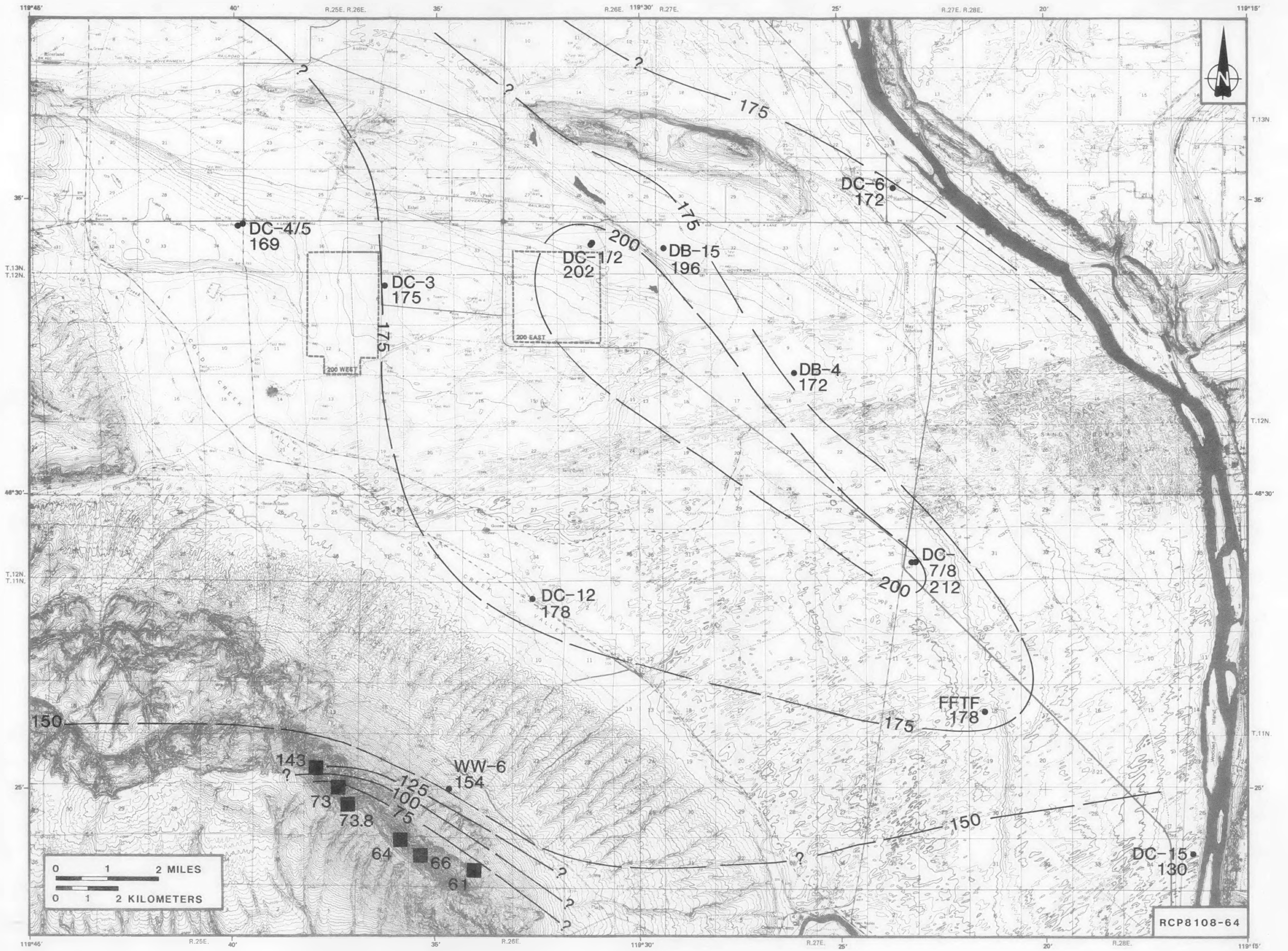

FIGURE 3-6. Isopach Map, Roza Member, Cold Creek Syncline. Contour interval is 25 ft. See Figure 3-2 for location of structural features and Table 3-1 for explanation.

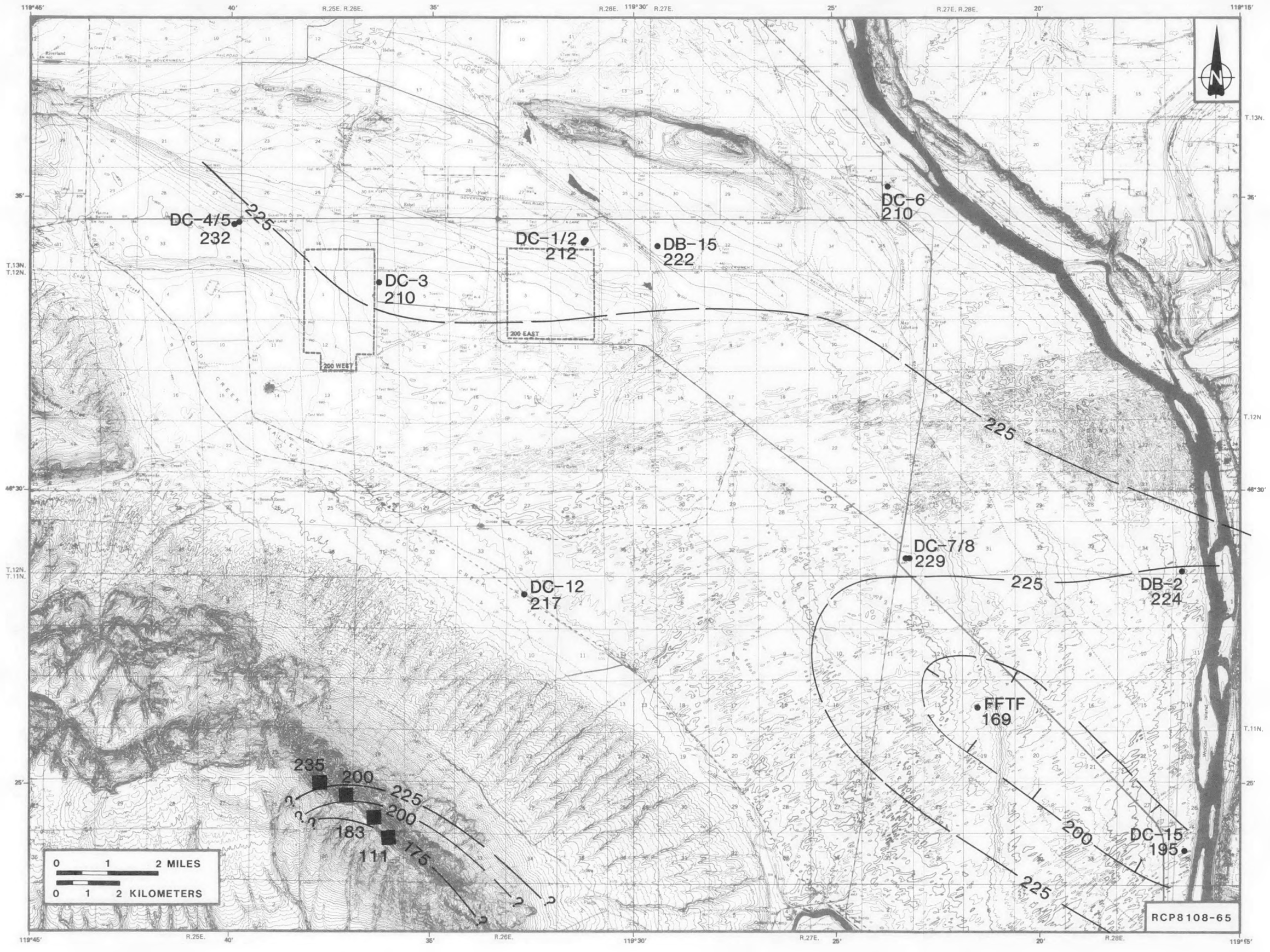

FIGURE 3-7. Isopach Map, Priest Rapids Member, Cold Creek Syncline. Contour interval is 25 ft. See Figure 3-2 for location of structural features and Table 3-1 for explanation.

The Lolo flow is also thicker on the southern margin of the Cold Creek syncline and thins across the Umtanum Ridge-Gable Mountain structure and Rattlesnake Mountain structure. The maximum thickness occurs in a northwest-southeast zone that parallels the present axis of the Cold Creek syncline. Evidence for ponding and slow cooling along the north side of Rattlesnake Mountain is apparent from areas where the basalt has a diabasic texture. The Lolo flow also pinches out on the east side of the Pasco Basin beyond the limits of the Cold Creek syncline (Reidel and others, 1980).

SADDLE MOUNTAINS BASALT

The Saddle Mountains Basalt consists of seven members (Fig. 3-1) in the Pasco Basin: (1) Umatilla, (2) Wilbur Creek, (3) Asotin, (4) Esquatzel, (5) Pomona, (6) Elephant Mountain, and (7) Ice Harbor. With the exception of the Wilbur Creek, all members are present in the Cold Creek syncline area. The Saddle Mountains Basalt in the Pasco Basin ranges in age from 13.5 to 8.5 mybp (Watkins and Baksi, 1974; McKee and others, 1977; ARHCO, 1976).

The Saddle Mountains Basalt flows were erupted over a much greater interval of time than the flows of any other formation of the Columbia River Basalt Group (Swanson and others, 1979b) and contain a wide diversity of petrographic characteristics, chemical types, and magnetic inclinations. Vents for the Saddle Mountains Basalt have been recognized in eastern Washington, northeastern Oregon, and western Idaho (Taubeneck, 1970; Price, 1977; Ross, 1978; Camp, in Swanson and others, 1979a).

Thickness variations in the Saddle Mountains Basalt (Fig. 3-8) are greater and more complex than in the Wanapum Basalt because of (1) thinning over structures, (2) a greater time between eruptions, and (3) the limited extent of many flows. Variations could also be attributable, in part, to the greater amount of information available for the Saddle Mountains Basalt than for other formations (Reidel and others, 1980).

UMATILLA MEMBER

The Umatilla Member consists of two flows in the Pasco Basin. Based upon chemical correlations with the type localities described by Laval (1956), the younger flow is the Sillusi flow and the older flow is the Umatilla flow (Fig. 3-1). The member varies in thickness from 35 to 85 m in the Cold Creek syncline (Fig. 3-9).

Both flows are fine grained to glassy with rare microphenocrysts of plagioclase and olivine and even rarer silicic xenoliths of basement rock. The flows are predominantly entablature with a small basal colonnade or pillowed base.

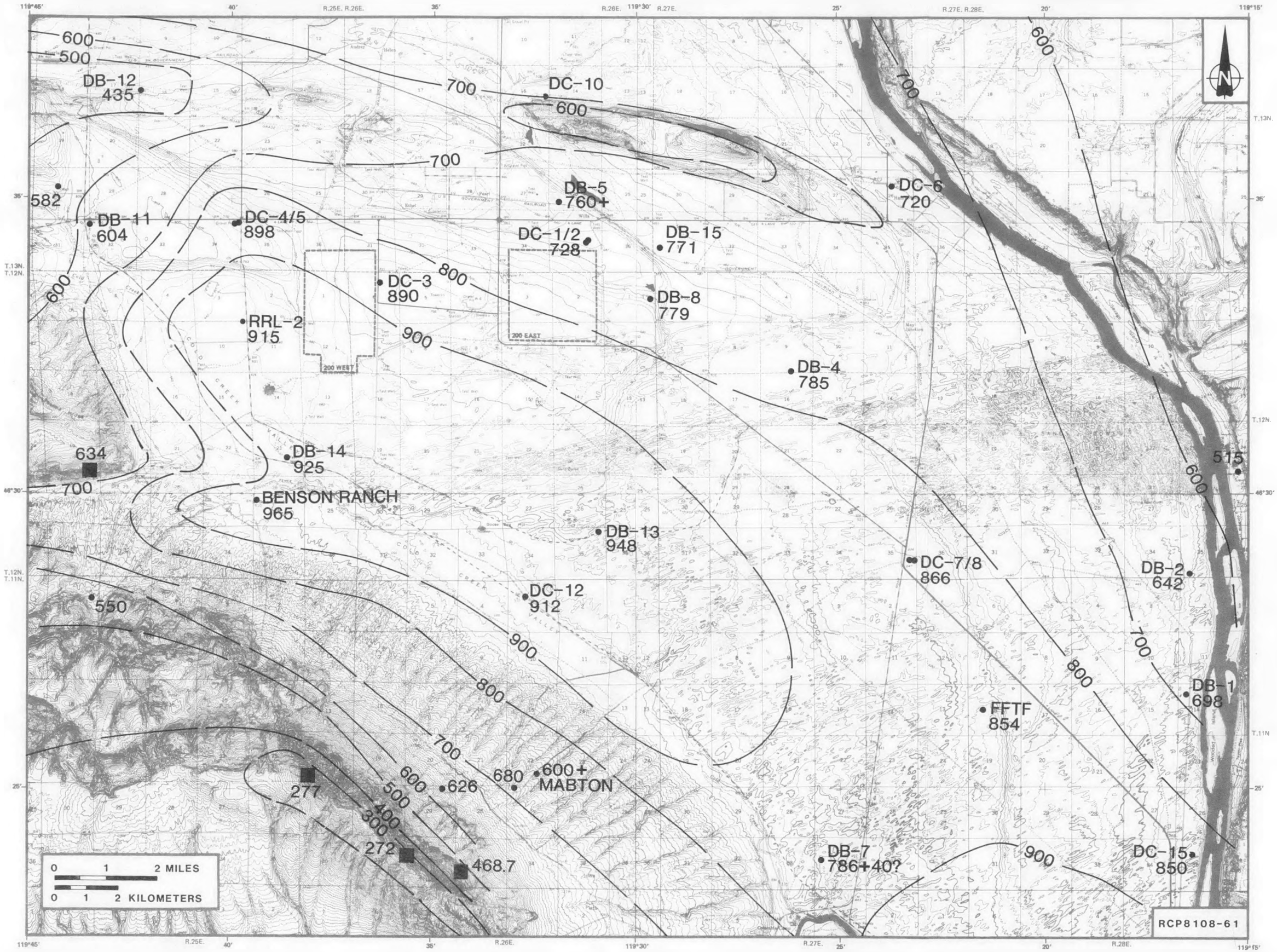

FIGURE 3-8. Isopach Map, Wanapum Basalt, Cold Creek Syncline. Data points shown on the map are thicknesses measured from boreholes and field sections. Contour interval is 100 ft. See Figure 3-2 for location of structural features and Table 3-1 for explanation.

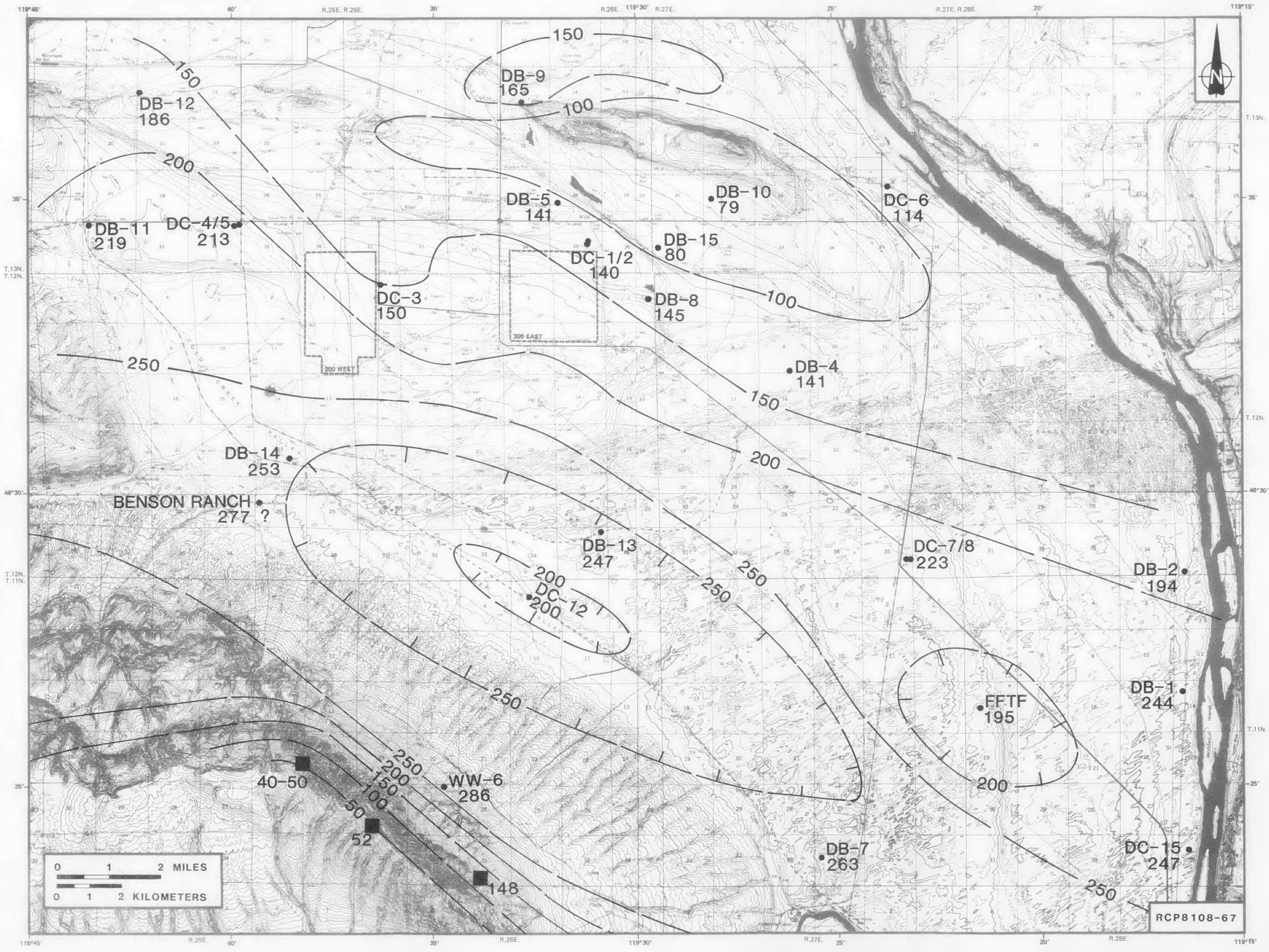

FIGURE 3-9. Isopach Map, Umatilla Member, Cold Creek Syncline. Contour interval is 50 ft. See Figure 3-2 for location of structural features and Table 3-1 for explanation.

Both the Umatilla and Sillusi flows have similar overall chemical compositions and fall into the Umatilla chemical type of Wright and others (1973). There are distinct differences in chemical composition, however, that allow the flows to be distinguished: The Umatilla has higher TiO_2, magnesium oxide (MgO), and lower phosphorus pentoxide (P_2O_5) than the Sillusi (Table 3-2).

Rietman (1966) found that the Umatilla Member has normal magnetic polarity. Van Alstine and Gillett (in press) found the Umatilla and Sillusi flows have nearly identical mean declinations of 324.3° and 321.7° and mean inclinations of +31.7° and +32.2°, respectively (Table 3-3). They suggested that this indicates the flows were erupted nearly contemporaneously.

Vent areas for the Umatilla Member have been located in eastern Washington and northeastern Oregon by Waters (1961), Price (1977), and Ross (1978). The flows of the Umatilla Member entered the Pasco Basin from the south and filled the Cold Creek syncline. The overall geometry of the Umatilla Member is that of a wedge that thins to the north (Fig. 3-10). The member pinches out just north of the Umtanum Ridge-Gable Mountain trend and just east of the Cold Creek syncline (Reidel and others, 1980). It is much thinner on the crest of Rattlesnake Mountain and on the extension of Yakima Ridge (Fig. 3-9). Thinning is also apparent across the subsurface extensions of Gable Mountain, Gable Butte, and an apparent southeast extension of a similar structure from Umtanum Ridge to DC-3. The subsurface extension of Yakima Ridge resembles the en echelon nature of the Gable Mountain and Gable Butte structures based upon thickness variations observed in the Umatilla Member.

Both the Umatilla and Sillusi flows are present throughout most of the Cold Creek syncline (Fig. 3-10). The Umatilla flow is the thicker flow in the western and southern parts of the syncline, but the Sillusi flow is the only flow present in the eastern part and is the thicker flow in the northern part of the syncline. In Figure 3-10, it is apparent that the western part of the Cold Creek syncline was covered first by the Umatilla flow. The Sillusi flow was later directed along the northern and eastern margins of the Umatilla flow, which it also onlapped. This distribution was probably a result of the Sillusi flow filling the low area formed between the gently westward-dipping, regional paleoslope and the northward-tapering margin of the Umatilla flow.

WILBUR CREEK MEMBER

The Wilbur Creek Member in the Pasco Basin consists of one flow, the Wahluke flow, and is generally <30 m thick. It is typically fine grained to glassy and aphyric with sparse microphenocrysts of plagioclase.

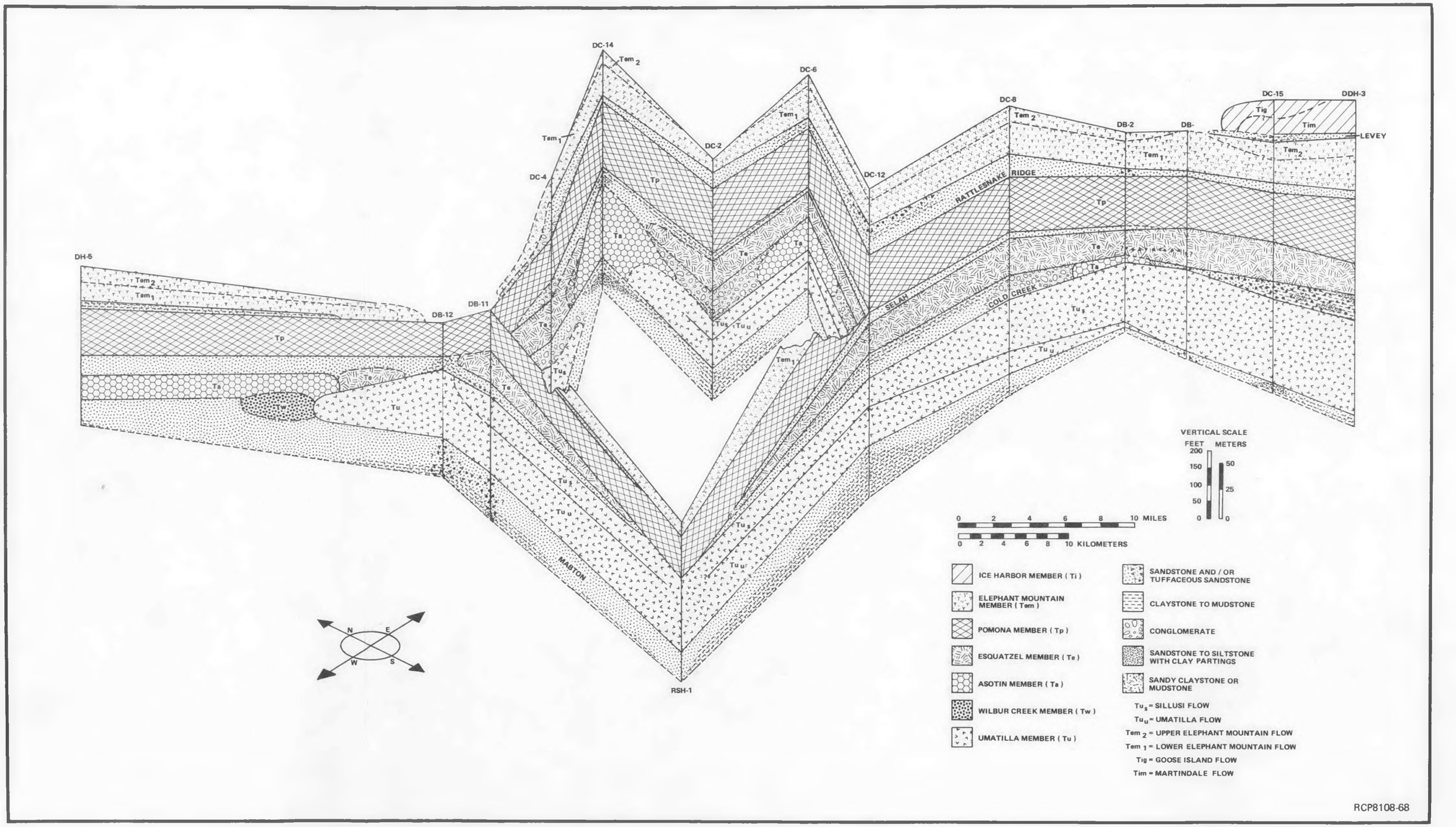

FIGURE 3-10. Fence Diagram, Saddle Mountains Basalt, Cold Creek Syncline. See Figure 3-2 for location of boreholes.

The chemical composition of the Wilbur Creek Member from the Pasco Basin falls within the Wilbur Creek chemical type of Swanson and others (1979b). The Wahluke flow has a mean magnetic declination of 345.7° and a mean inclination of +72.1° (Table 3-3; Van Alstine and Gillett, in press). The Wahluke flow was also sampled from core in DH-4 in the northeast part of the Pasco Basin by Packer and Petty (1979) who reported a 6° shallower inclination angle.

The Wahluke flow of the Wilbur Creek Member is not present in the Cold Creek syncline area of the Pasco Basin. This flow entered the Pasco Basin from the northeast and flowed southwest toward Umtanum Ridge. Just northwest of the Cold Creek syncline, the course of the Wahluke flow was partly controlled by the leading edge of the Umatilla Member (Reidel and others, 1980) (Fig. 3-10, DB-12 to DH-5).

ASOTIN MEMBER

The Asotin Member occurs as a single flow in the Pasco Basin. This was called the Huntzinger flow by Mackin (1961), Myers and Brown (1973), and ARHCO (1976). The flow varies from 23 to 66 m in thickness (Fig. 3-11) and is best exposed in the northern part of the basin along the Saddle Mountains (Reidel, 1978a).

The texture of the Huntzinger flow varies considerably throughout the Pasco Basin. The flow has abundant olivine, but sparse plagioclase, and its texture varies from fine grained and glassy to ophitic.

The chemical composition of the Asotin Member varies considerably throughout the Pasco Basin (Table 3-2). This extreme variation was first recognized by Myers (1973) and Ward (1976). The Asotin Member contains chemical compositions from two types defined by Swanson and others (1979b): (1) Asotin and (2) Lapwai. In Figure 3-12, the chemical composition of samples from a typical section of the Asotin Member (DH-4; Fig. 3-2) is shown and the approximate mean and range of the Lapwai and Asotin chemical types (from Wright and others, 1980) are plotted. It is apparent from this diagram that the Lapwai chemical type occurs at the top and bottom of the flow with Asotin chemical type in between and a complete gradation from one to the other. This indicates that the two chemical types are probably related by differentiation occurring in the flow at the surface. Myers (1973) related the chemical variation to olivine abundance and suggested that fractional crystallization of olivine is at least partly responsible. Based on sampling of surface exposures, Van Alstine and Gillett (in press) determined a mean declination of 23.7° and a mean inclination of +80.6° for the Asotin Member (Table 3-3).

The Asotin Member was erupted from an as yet undiscovered fissure, probably in eastern Washington or western Idaho (Camp, in Swanson and others, 1979a). The Asotin Member is confined to the northern part of the Cold Creek syncline and Pasco Basin (Reidel and others, 1980). As shown in Figure 3-10, the front of the Umatilla Member was a major factor controlling the edge of the Huntzinger flow. The Huntzinger flow is

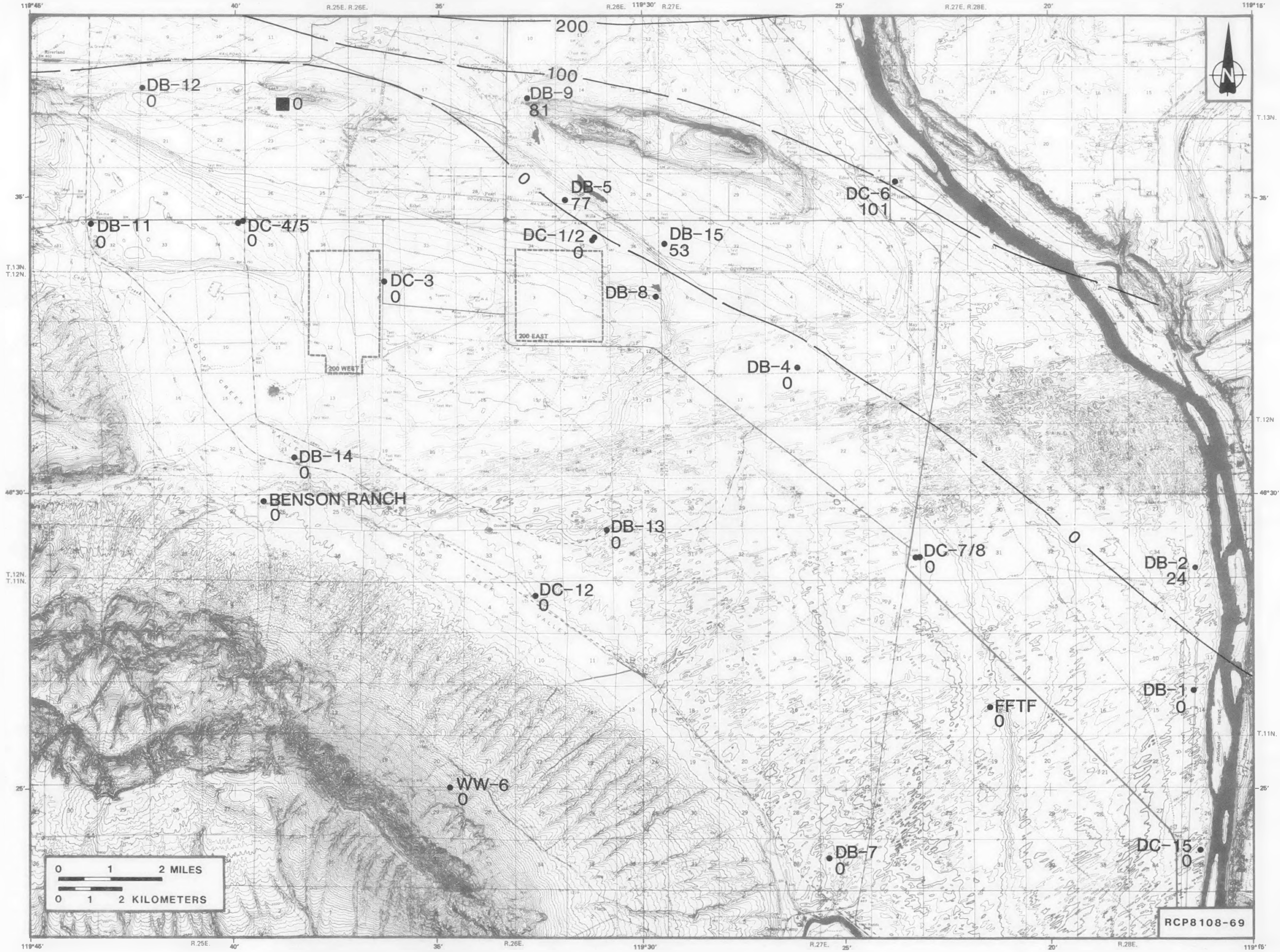

FIGURE 3-11. Isopach Map, Asotin Member, Cold Creek Syncline. Contour interval is 100 ft. See Figure 3-2 for location of structural features and Table 3-1 for explanation.

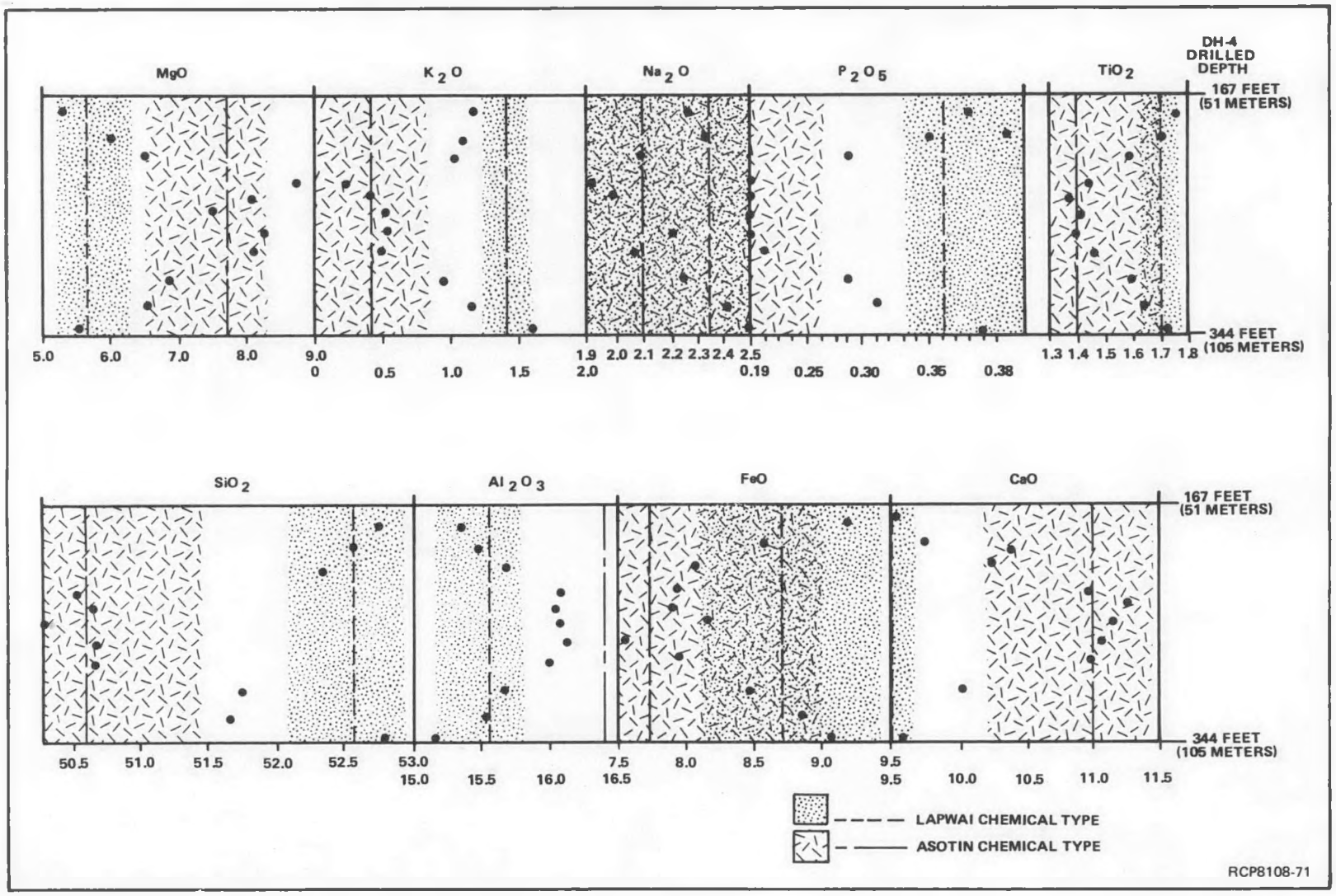

FIGURE 3-12. Chemical Variation of the Asotin Member, Borehole DH-4. Dots represent an analysis from a particular depth in the core. Dashed line represents the mean of the Lapwai chemical type and dotted pattern is the range (from Wright and others, 1980). Long dashed line is the mean of the Asotin chemical type and pattern is the range (from Swanson and others, 1979b).

interpreted (Reidel and others, 1980) to have entered from the east near Mesa and spread into the northern Pasco Basin. As it flowed south, a topographic low between the northward-tapering flow front of the Umatilla Member and the westward-dipping paleoslope channeled the Huntzinger flow. The Huntzinger flow lapped onto the Umatilla Member and pinched out on the slope formed by the flow front. The Umtanum Ridge-Gable Mountain structure also contributed to controlling the southern extent of the Huntzinger flow.

ESQUATZEL MEMBER

The Esquatzel Member in the Pasco Basin consists of one to two flows or flow lobes and varies in thickness from 21 to 38 m (Fig. 3-13) across the Cold Creek syncline. In the eastern Cold Creek syncline, there are two Esquatzel flows or flow lobes that occur locally with a vitric tuff between them (in core from DB-1 and DB-2).

The Esquatzel Member is plagioclase-phyric to glomerophyric and contains microphenocrysts of clinopyroxene. The abundance of phenocrysts is variable throughout the Cold Creek syncline area, with some localities completely void of phenocrysts.

The average chemical composition of the Esquatzel Member is given in Table 3-2 and falls within the Esquatzel chemical type of Swanson and others (1979b). Van Alstine and Gillett (in press) indicated that flows of the Esquatzel Member have normal polarity with a mean declination of 348.4^{o} and a mean inclination of $+64.8^{o}$ (Table 3-3). These results are similar to those determined by Choinier and Swanson (1979) for the Esquatzel Member.

Flows of the Esquatzel Member entered the Pasco Basin from the east near Mesa in a channel that was cut into the Priest Rapids Member (Swanson and others, 1979a; Reidel and others, 1980). It is confined to the south and east parts of the Pasco Basin and pinches out along and north of the Umtanum Ridge-Gable Mountain structure. It is thicker in the western Cold Creek syncline area north of the Yakima Ridge subsurface extension. It also thins across the subsurface extension of the Yakima Ridge and Rattlesnake Mountain structures and pinches out just south of the present crest of Rattlesnake Mountain. Flows of the Esquatzel, Asotin, and Wilbur Creek Members exited the Pasco Basin in channels to the west (Goff, 1981; Goff and Myers, 1978; Reidel and others, 1980).

Several factors probably controlled the distribution of the Esquatzel Member in the Cold Creek syncline. First, the margin of the Huntzinger flow of the Asotin Member formed a barrier that prevented the Esquatzel flow from spreading across the northern Pasco Basin. The channel that the Esquatzel flows occupies near Mesa is probably part of the same channel that is now filled by sediments along the southern margin of the Huntzinger flow in the Cold Creek syncline. The Umtanum Ridge-Gable Mountain structure was a structural high that influenced the spread of the Esquatzel flows to the west, as indicated by the absence of the Esquatzel Member west of Gable Butte and in DB-12 (Fig. 3-10). Rattlesnake Mountain was also important in controlling flows of the Esquatzel Member, as evidenced by its pinchout near the present crest.

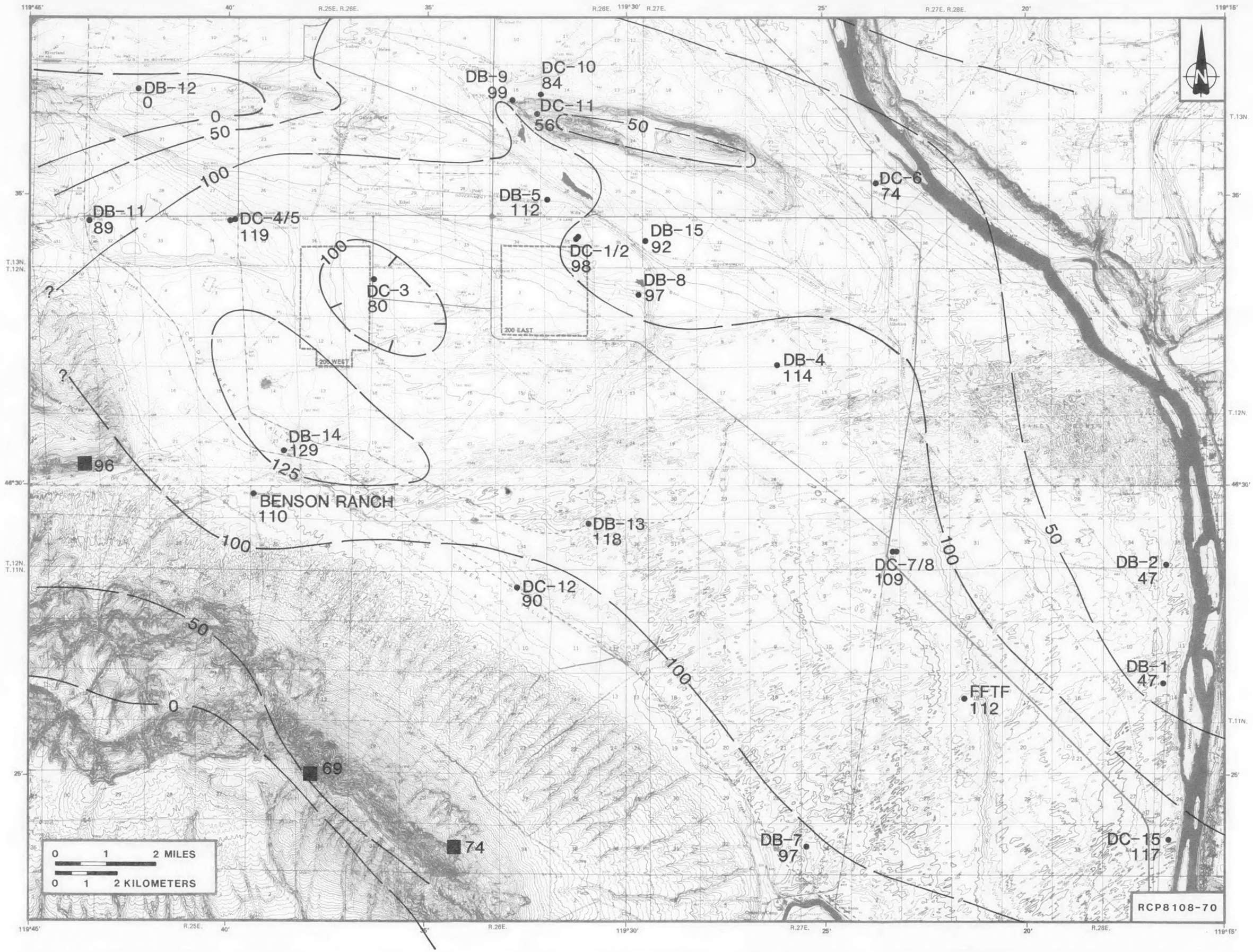

FIGURE 3-13. Isopach Map, Esquatzel Member, Cold Creek Syncline. Contour interval is 25 ft. See Figure 3-2 for location of structural features and Table 3-1 for explanation.

POMONA MEMBER

The Pomona Member was erupted from dikes near Orofino, Idaho (Camp, in Swanson and others, 1979a) and has been dated at 12 mybp (McKee and others, 1977). The member consists of one to two flows or flow lobes in the Pasco Basin and varies in thickness from 37 to 56 m (Fig. 3-14) in the Cold Creek syncline area.

The texture of the Pomona Member is relatively uniform across the Pasco Basin. It typically is fine grained to glassy with wedge-shaped plagioclase phenocrysts and rare olivine.

The Pomona Member has a distinct chemical composition (Pomona chemical type of Wright and others, 1973) with little overall variance (Table 3-2). The member has reversed magnetic polarity (Rietman, 1966; Choinier and Swanson, 1979). This polarity was corroborated by Van Alstine and Gillett (in press) who also found the Pomona has the tightest inclination and declination grouping of any flow analyzed from the Columbia River Basalt Group. The Pomona Member has a mean declination of 193.5^{o} and a mean inclination of -52.7^{o} (Table 3-3). It is proposed that the Pomona Member within the Pasco Basin may be comprised of two separate flows rather than two flow lobes. This premise is supported by the fact that the two distinct and separate flows of the Umatilla Member also have nearly the same chemical compositions and magnetic declinations and inclinations.

The Pomona Member is present throughout most of the Pasco Basin and reaches its greatest thickness in the southeast portion of the Cold Creek syncline and just north of Gable Mountain (DC-14; Fig. 3-2) in the Wahluke syncline. The Pomona Member thins over the Umtanum Ridge-Gable Mountain structure, Rattlesnake Mountain, and the subsurface extension of Yakima Ridge.

The volume of Pomona lava that was flowing into the Pasco Basin was considerably greater than that of the Umatilla, Wilbur Creek, Asotin, and Esquatzel Members. This volume overcame any effects of flow edges and topography, and the Pomona flow buried the topography of the Cold Creek syncline and much of the Pasco Basin.

ELEPHANT MOUNTAIN MEMBER

The Elephant Mountain Member consists of two separate flows: (1) Elephant Mountain flow of Waters (1955) and (2) Ward Gap flow of Schmincke (1967b). It varies in thickness from 0 to almost 46 m in the Cold Creek syncline area (Fig. 3-15).

The texture of the flows is medium to fine grained with abundant microphenocrysts of plagioclase. Where lava ponded, the flows exhibit a coarse-grained texture. Both flows (Table 3-2) fit the Elephant Mountain chemical type of Wright and others (1973).

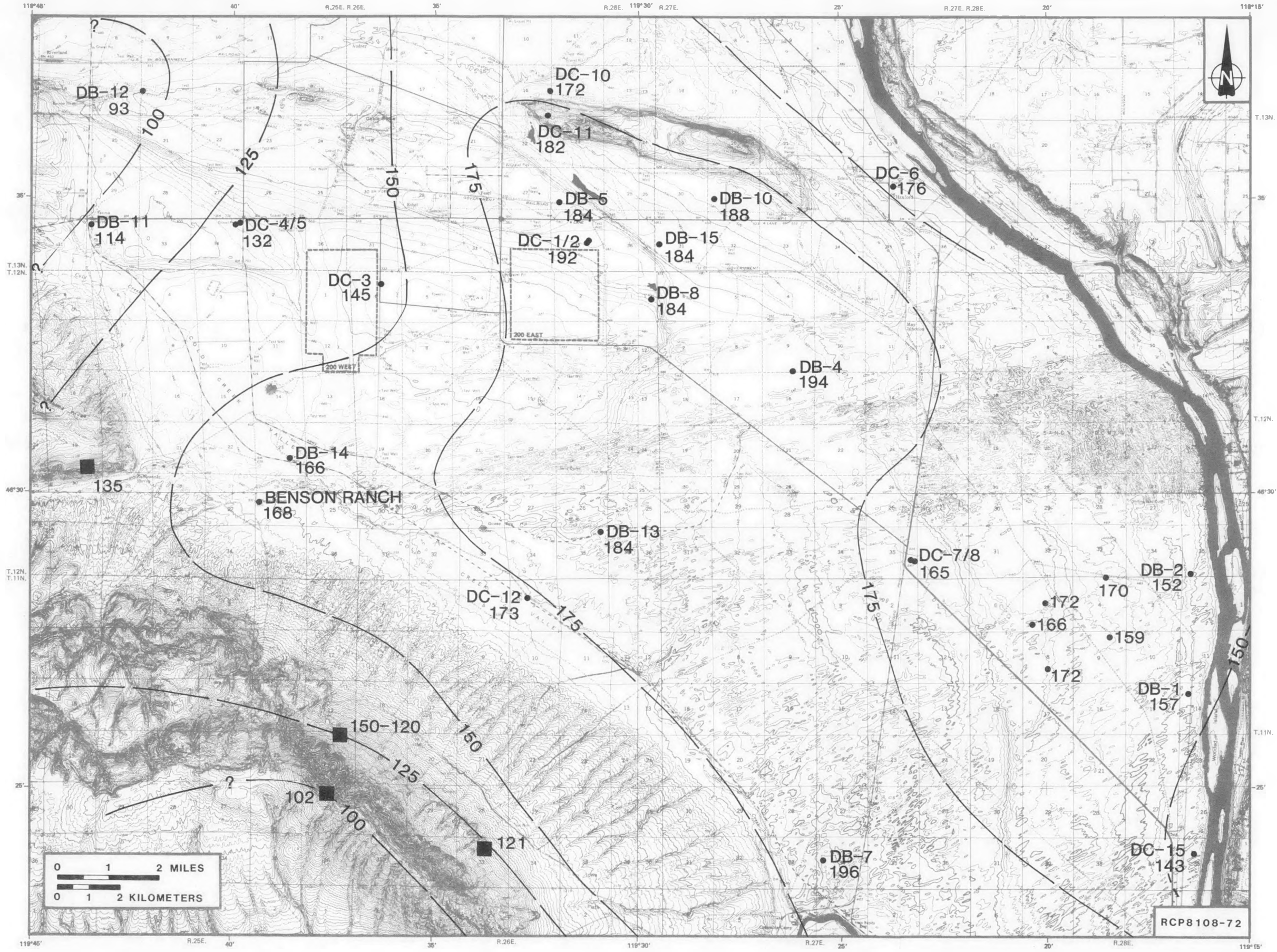

FIGURE 3-14. Isopach Map, Pomona Member, Cold Creek Syncline. Contour interval is 25 ft. See Figure 3-2 for location of structural features and Table 3-1 for explanation.

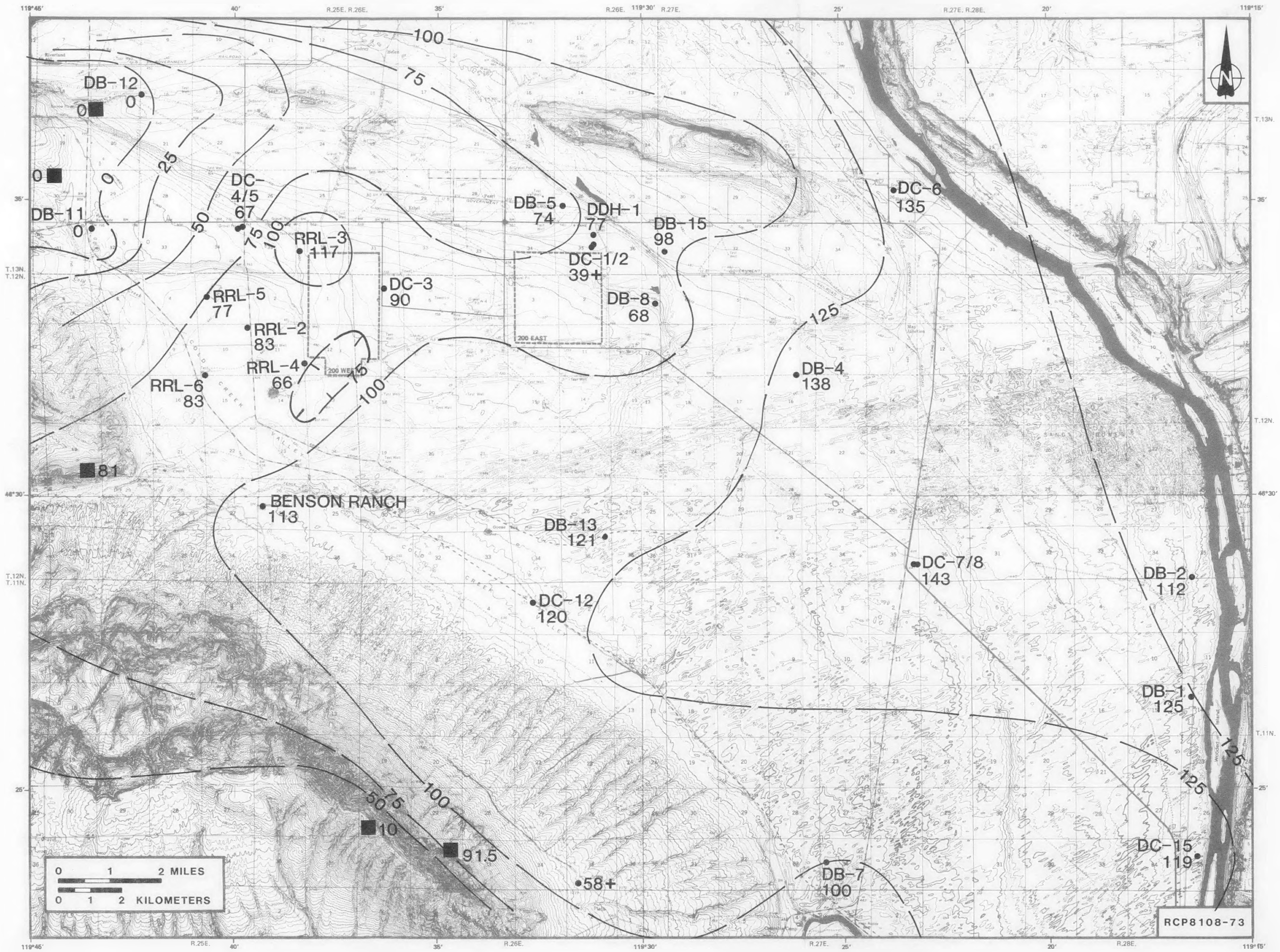

FIGURE 3-15. Isopach Map, Elephant Mountain Member, Cold Creek Syncline. Contour interval is 25 ft. See Figure 3-2 for location of structural features and Table 3-1 for explanation.

Choinier and Swanson (1979) and Rietman (1966) reported that the Elephant Mountain Member has transitional to normal magnetic polarity. Van Alstine and Gillett (in press) sampled surface exposures and found that both flows yielded a mean declination of 133.2° and a mean inclination of -39.2° (Table 3-3).

The Elephant Mountain Member is stratigraphically younger than the Rattlesnake Ridge interbed, but in many areas, an invasive relationship between basalt and sediment has been observed. Both Elephant Mountain Member flows pinch out in the northwest part of the Cold Creek syncline (Fig. 3-10). The member is thicker in the eastern part of the Cold Creek syncline area and thins toward Rattlesnake Mountain. The lower Elephant Mountain flow has a greater lateral extent than the upper flow (Ward Gap flow), but pinches out before reaching the DB-11/DB-12 area (Fig. 3-10). The Elephant Mountain Member defines the top of basalt (TOB) in the western Cold Creek syncline area.

ICE HARBOR MEMBER

The Ice Harbor Member is the youngest member of the Saddle Mountains Basalt present in the Pasco Basin and was erupted from vents on the east side of the basin 8.5 mybp (McKee and others, 1977). The member consists of three flows (Fig. 3-1): (1) Basin City, (2) Martindale, and (3) Goose Island. The flows of the Ice Harbor Member are generally no >30 m thick.

The flows are typically fine to medium grained with glomerocrysts and phenocrysts of olivine, plagioclase, and clinopyroxene. The overall petrography of the flows varies. Olivine occurs primarily in the Martindale and Basin City flows, while the Goose Island flow contains glomerocrysts of pyroxene and plagioclase. The average chemical compositions for flows of the Ice Harbor Member from the Pasco Basin are given in Table 3-2. These flows comprise three chemical types for the Ice Harbor Member (Swanson and others, 1979b).

Choinier and Swanson (1979) sampled flows of the Ice Harbor Member for remanent magnetic polarity. They found that the Goose Island and Basin City flows have normal magnetic polarity, while the Martindale flow has reversed polarity (Table 3-3).

Two flows of the Ice Harbor Member are present in the extreme southeast portion of the Cold Creek syncline: (1) Martindale and (2) Goose Island. The Martindale flow is present in DDH-3 and DC-15 (Fig. 3-10), but the Goose Island flow is present only in the most northern one, DC-15. The older, Martindale, flow front controlled the younger, Goose Island flow, forcing it along the lower topographic area between the Martindale flow front and the regional paleoslope.

ELLENSBURG FORMATION

Intercalated with and overlying the flows of the Columbia River Basalt Group in the western and central Columbia Plateau in Washington are sedimentary beds of the Ellensburg Formation (Smith, 1901; Schmincke, 1964, 1967a; Swanson and others, 1979b). As a unit, these sediments are relatively thick along the western margin of the plateau and thin eastward onto the central Columbia Plateau. Within the Pasco Basin, Ellensburg sediments are primarily interbedded in the Wanapum and Saddle Mountains Basalts. The lateral extent and thickness of the sediments generally increase upward in the section.

The Ellensburg Formation of the central plateau is composed of two, major, and distinct lithologies of different provenance (Schmincke, 1964, 1967a; Swanson and others, 1979b). One includes volcaniclastic sediments deposited as ashfall and by tributary rivers flowing onto the central plateau. The other includes clastic, plutonic, and metamorphic rock derived from Rocky Mountain terrain that was carried onto the plateau by westward-flowing, ancestral rivers. These two, major lithologies occur either as distinct or mixed deposits within the Ellensburg Formation of the Pasco Basin.

The nomenclature used for the individual interbeds within the Ellensburg Formation in the Cold Creek syncline is informal and is based on upper- and lower-bounding basalt flows (Fig. 3-1). Therefore, discussions of individual units are restricted to those units with consistent upper- and lower-bounding flows.

VANTAGE INTERBED

The Vantage interbed is comprised of sediments lying between the Frenchman Springs Member of the Wanapum Basalt and the Sentinel Bluffs sequence of the Grande Ronde Basalt in the Pasco Basin. This interbed is the lowest, relatively continuous, Ellensburg unit in the Pasco Basin. The Vantage interbed is ∿24 m thick in the northwestern Pasco Basin, but thins to the southeast and locally pinches out (Fig. 3-16). The northwestern area probably represents a low that formed between the regional paleoslope and the Hog Ranch structure, which was a topographic high during Grande Ronde time. Saprolite formed on the Grande Ronde Basalt beyond the area of sedimentation during this time.

The thicker sequences of Vantage consist of arkosic sandstone locally containing thin, clay stringers with a clay cap. The thinner sequences of Vantage consist of clays which are altered tuffs.

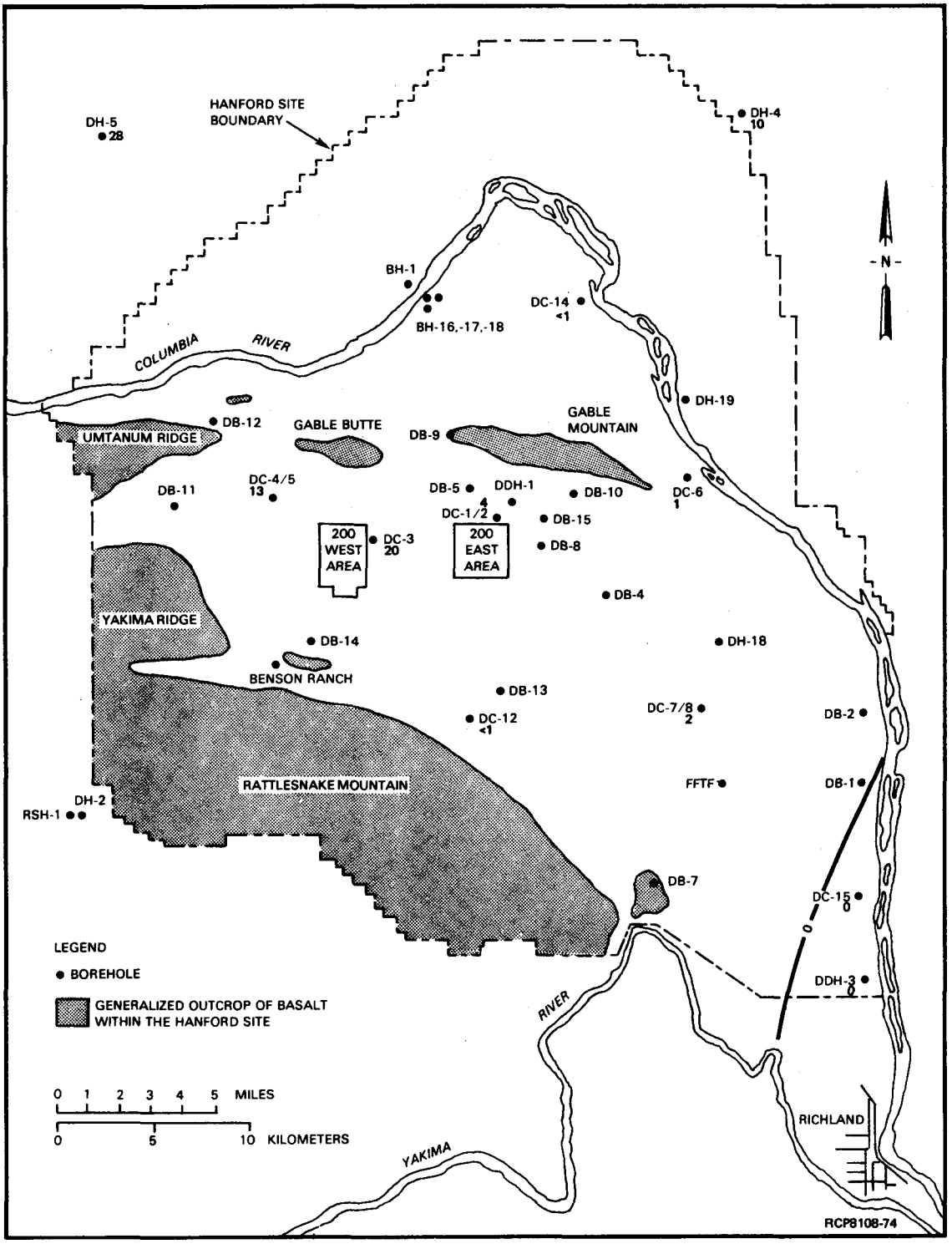

FIGURE 3-16. Isopach Map, Vantage Interbed. Contour interval is 50 ft. Thickness variations are less than contour interval. Thicknesses are shown for only those boreholes that penetrate the Vantage interbed.

MABTON INTERBED

The Mabton interbed is stratigraphically below the Umatilla Member and above the Priest Rapids Member in the Pasco Basin. The Mabton interbed is thickest in the central Pasco Basin area and thins in all directions (Fig. 3-17). Vertical lithologic and textural changes in the Mabton interbed are relatively uniform. From top to bottom, the interbed generally consists of (1) a well-indurated, lapilli tuffstone, locally baked; (2) a fine-grained, tuffaceous, clayey quartzitic sandstone; (3) a quartzitic to arkosic sandstone with interlayered, tuffaceous sandstones and siltstones; and (4) commonly a thin, basal, silty clay.

COLD CREEK INTERBED

The Cold Creek interbed refers to the sequence of Ellensburg sediments that occur stratigraphically between the Esquaztel and Umatilla Members of the Saddle Mountains Basalt. The Asotin Member partially controlled the distribution of part of the Cold Creek interbed. Three separate units of the interbed are identified on the basis of bounding flows. These intervals are the Umatilla-Esquaztel, Umatilla-Asotin, and Asotin-Esquatzel intervals.

Umatilla-Esquatzel Interval

The Umatilla-Esquatzel interval is the thickest interbed and has the largest areal extent (Fig. 3-18). This interval is divided into two textural facies: (1) a finer grained, tuffaceous sandstone facies and (2) a coarser sandstone and conglomerate facies with tuffaceous siltstone and clays. The coarser grained facies follows an arcuate trend that is subparallel to the flow front of the Asotin Member. The coarser grained facies represents the high-energy, main channel of a fluvial system which is interpreted to have flowed parallel to the flow front of the Asotin Member.

Umatilla-Asotin Interval

The Umatilla-Asotin interval which has a small, lateral extent (Fig. 3-19) is generally thin, <6 m, or not present. Where present, the unit is composed chiefly of tuffaceous siltstones and tuffaceous claystones.

Asotin-Esquatzel Interval

The Asotin-Esquatzel interval is generally thin (<3 m), but in the vicinity of DB-15 along the southern margin of the interval, it thickens to 29 m (Fig. 3-20). North and south of Gable Mountain the interval consists of tuffs and clay, arkosic to quartzose sandstones, and basaltic conglomerates. The interbed is not present along the Gable Mountain structure.

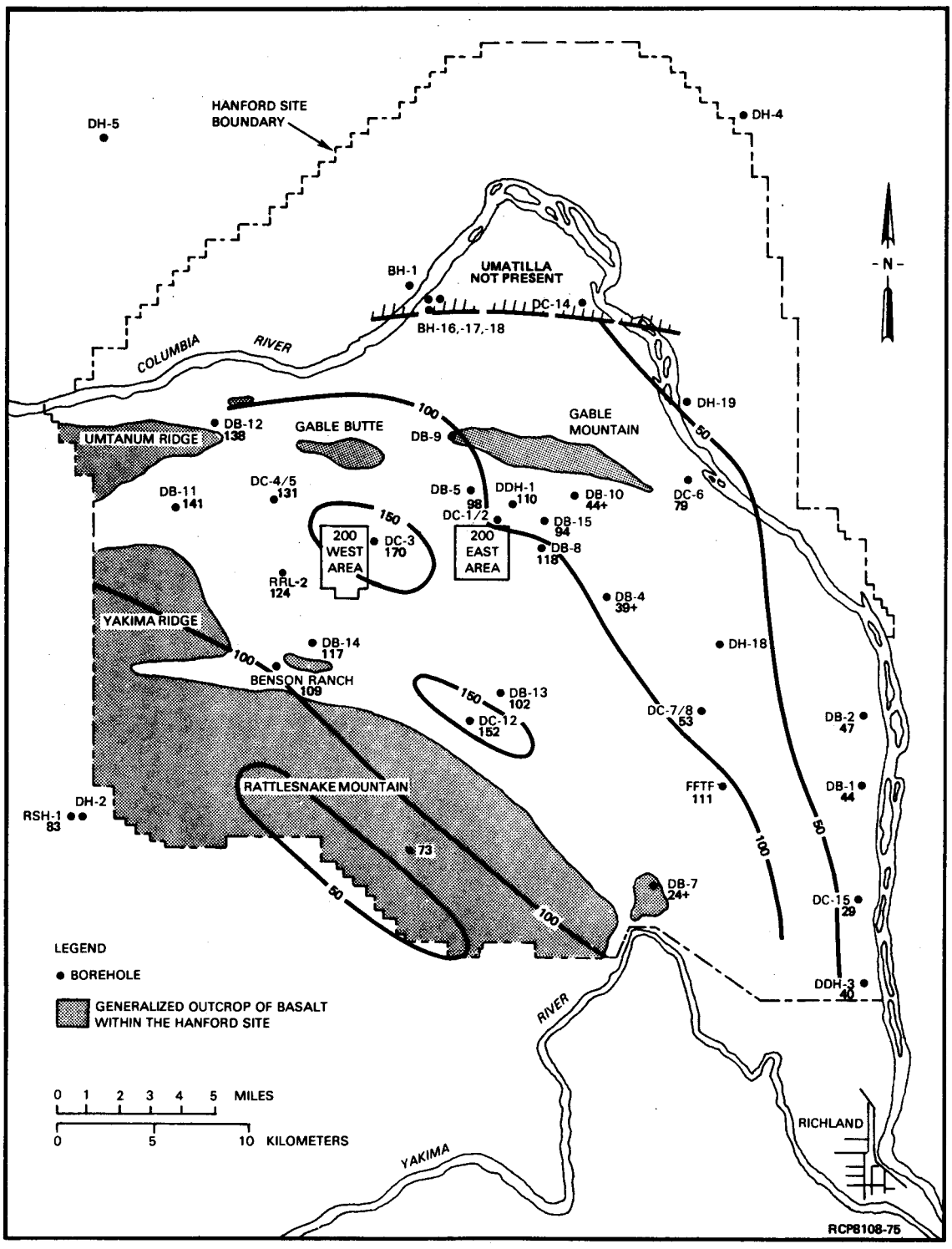

FIGURE 3-17. Isopach Map, Mabton Interbed. Contour interval is 50 ft. Thicknesses are shown for only those boreholes that penetrate the Mabton interbed. See Table 3-1 for explanation.

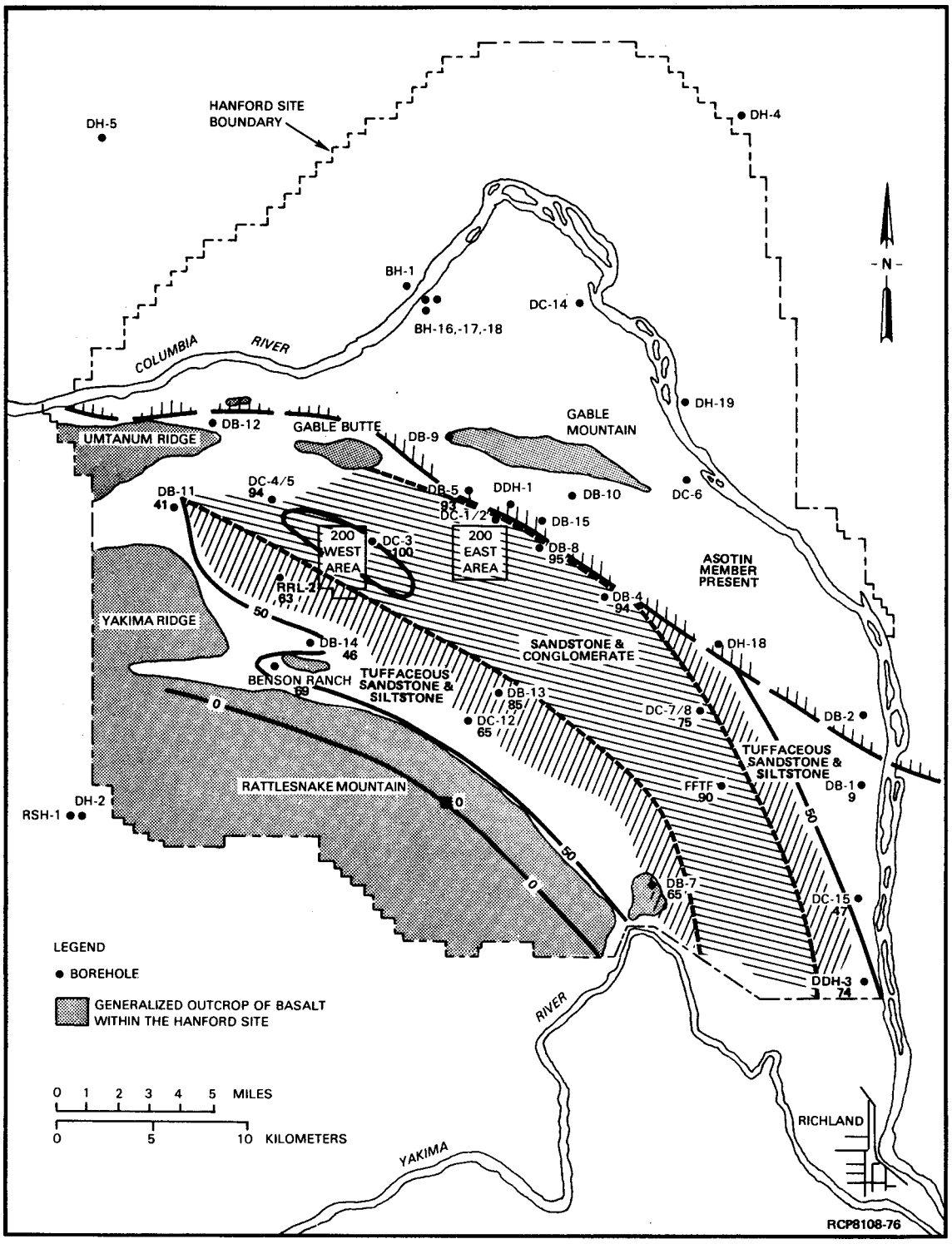

FIGURE 3-18. Isopach Map, Umatilla-Esquatzel Interval, Cold Creek Interbed, Cold Creek Syncline. Contour interval is 50 ft. Thicknesses are shown for only those boreholes that penetrate the sedimentary interval. See Table 3-1 for explanation.

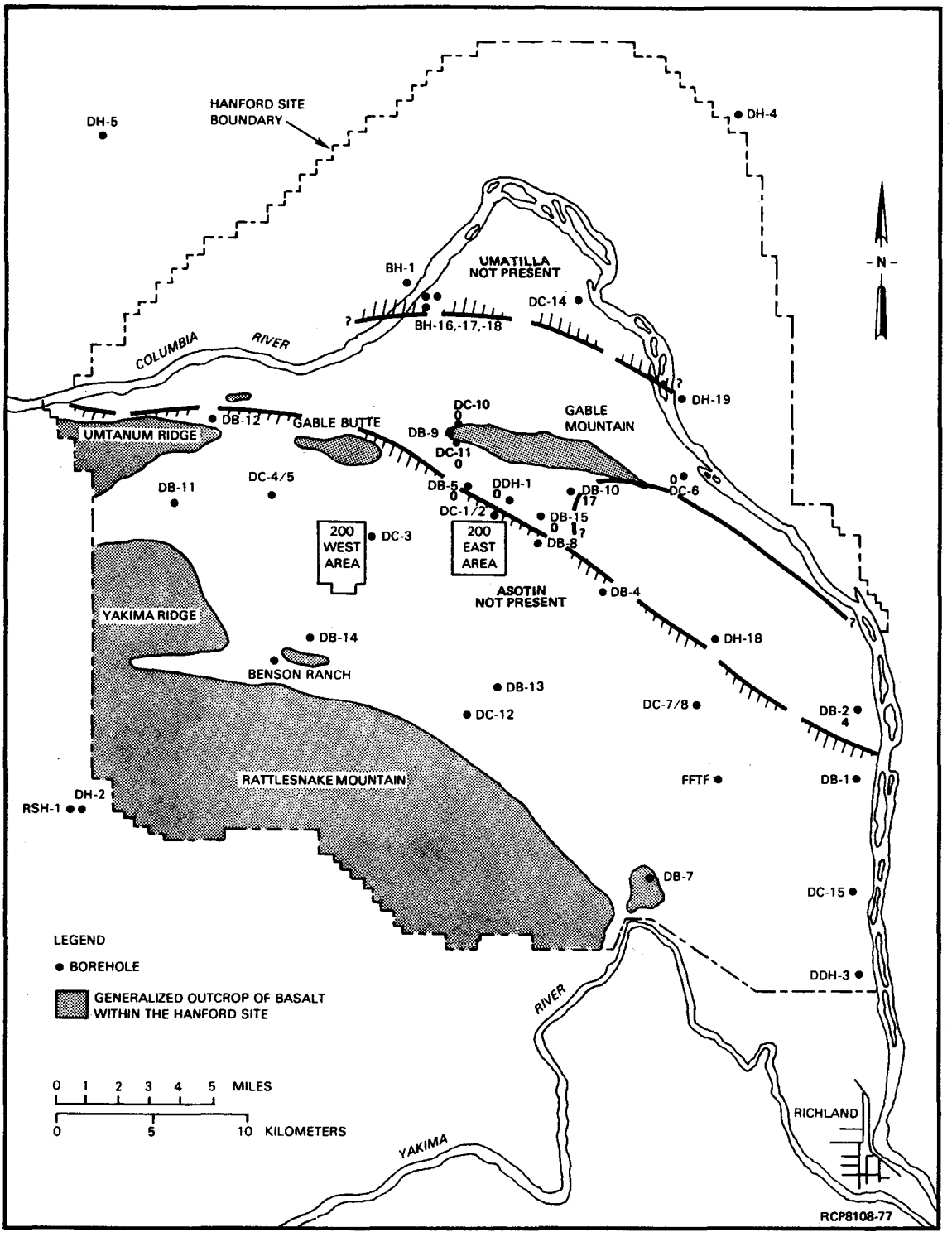

FIGURE 3-19. Isopach Map, Umatilla-Asotin Interval, Cold Creek Interbed, Cold Creek Syncline. Contour interval is 50 ft. Thicknesses are shown for only those boreholes that penetrate the sedimentary interval. See Table 3-1 for explanation.

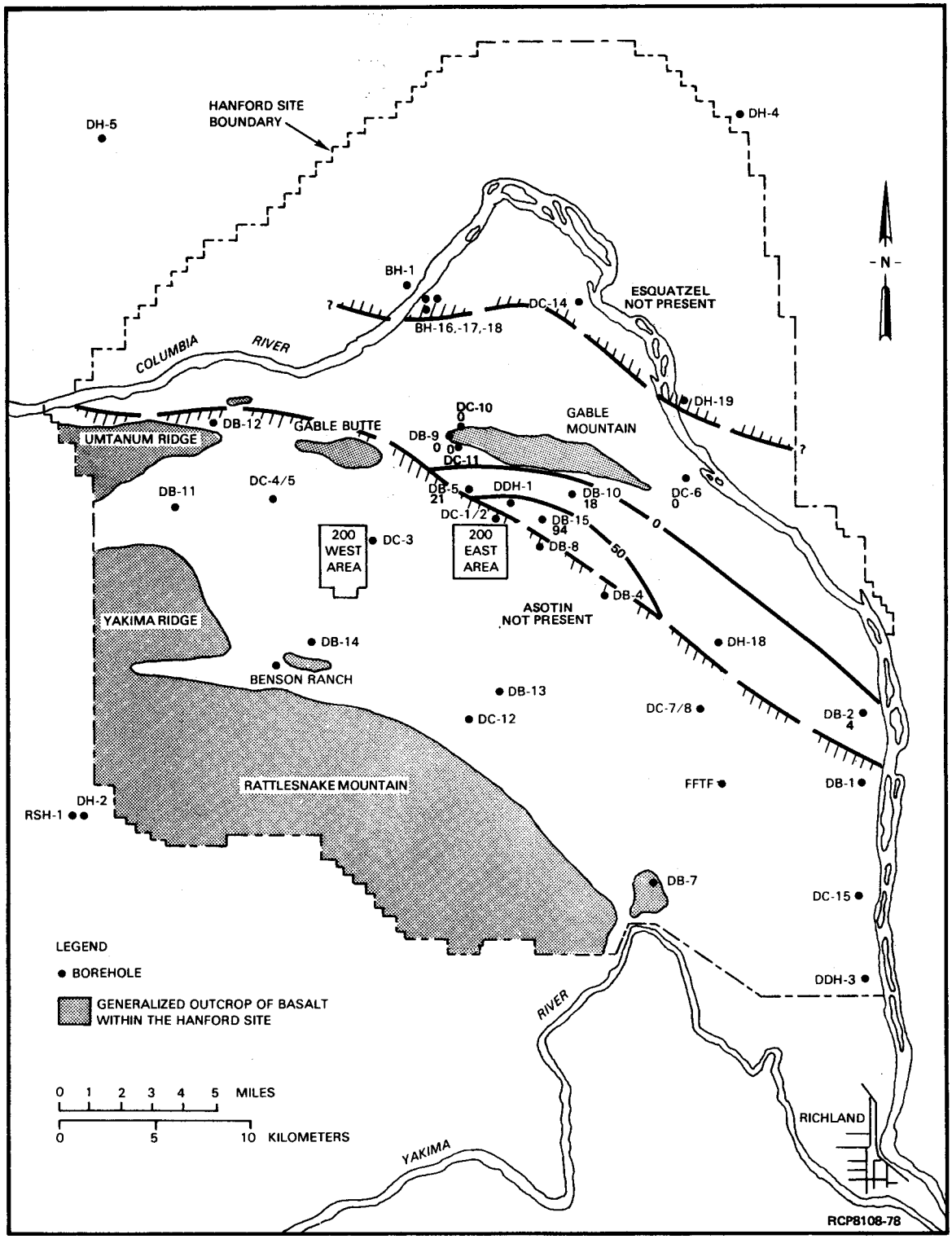

FIGURE 3-20. Isopach Map, Asotin-Esquatzel Interval, Cold Creek Interbed, Cold Creek Syncline. Contour interval is 50 ft. Thicknesses are shown for only those boreholes that penetrate the sedimentary interval. See Table 3-1 for explanation.

SELAH INTERBED

Interbedded between the Esquatzel and Pomona Members of the Saddle Mountains Basalt is the Selah interbed (Fig. 3-21). The lateral extent of the Selah interbed is restricted by the lateral extent of the Esquatzel Member. Lithologically and texturally, the interbed is a variable mixture of silty or sandy, vitric tuff, arkosic sands, tuffaceous clays, and locally thin stringers of predominantly basaltic gravels. The upper portion of the Selah interbed is a vitric tuff commonly fused to a perlitic vitric tuff by the overlying Pomona Member. Opaline silica and pepperite are common at the Pomona contact. In the northwestern Pasco Basin, sediments judged to be equivalent in age to the Selah of the central Pasco Basin consist of conglomerates containing plutonic and metamorphic clasts.

RATTLESNAKE RIDGE INTERBED

The Rattlesnake Ridge interbed (Fig. 3-22) is bounded by the overlying Elephant Mountain Member and the underlying Pomona Member. The interbed is present throughout the Pasco Basin, except locally on portions of structural ridges. In the Pasco Basin, the Rattlesnake Ridge interbed varies up to 33 m in thickness and can be divided into three facies based on lithology and texture. The first facies occurs in the central Cold Creek syncline area and generally consists of three units: (1) a lower clay or tuffaceous sandstone; (2) a middle, micaceous-arkosic and/or tuffaceous sandstone; and (3) an upper, tuffaceous siltstone or tuffaceous sandstone. The second facies is a single, tuffaceous, sandstone-to-siltstone unit and occurs where the interbed is relatively thin. The third facies occurs on the northwestern margin of the Pasco Basin. Here, the Rattlesnake Ridge interbed generally consists of three units. The upper two units are similar in texture and lithology to the first facies. The lower unit, however, is a conglomerate with plutonic and metamorphic clasts. On Yakima Ridge, the Rattlesnake Ridge interbed thins with only the upper tuffaceous unit and, locally, the conglomerate unit present.

LEVEY INTERBED

The Levey interbed is defined as the sediments between the Ice Harbor and Elephant Mountain Members of the Saddle Mountains Basalt. These sediments are the youngest Ellensburg sediments in the Pasco Basin and are found throughout the southeastern Pasco Basin from DC-15 to Wallula Gap and from Ice Harbor Dam to Red Mountain (Fig. 3-23). Along its northern extent, the Levey interbed is a tuffaceous sandstone which is known to be 5 to 9 m thick. Exposures of Levey interbed along the southern and western margins of the Pasco Basin are <6 m thick and consist of a fine-grained, typically tuffaceous silt or siltstone. The Levey interbed has been locally oxidized by the overriding Ice Harbor flow(s).

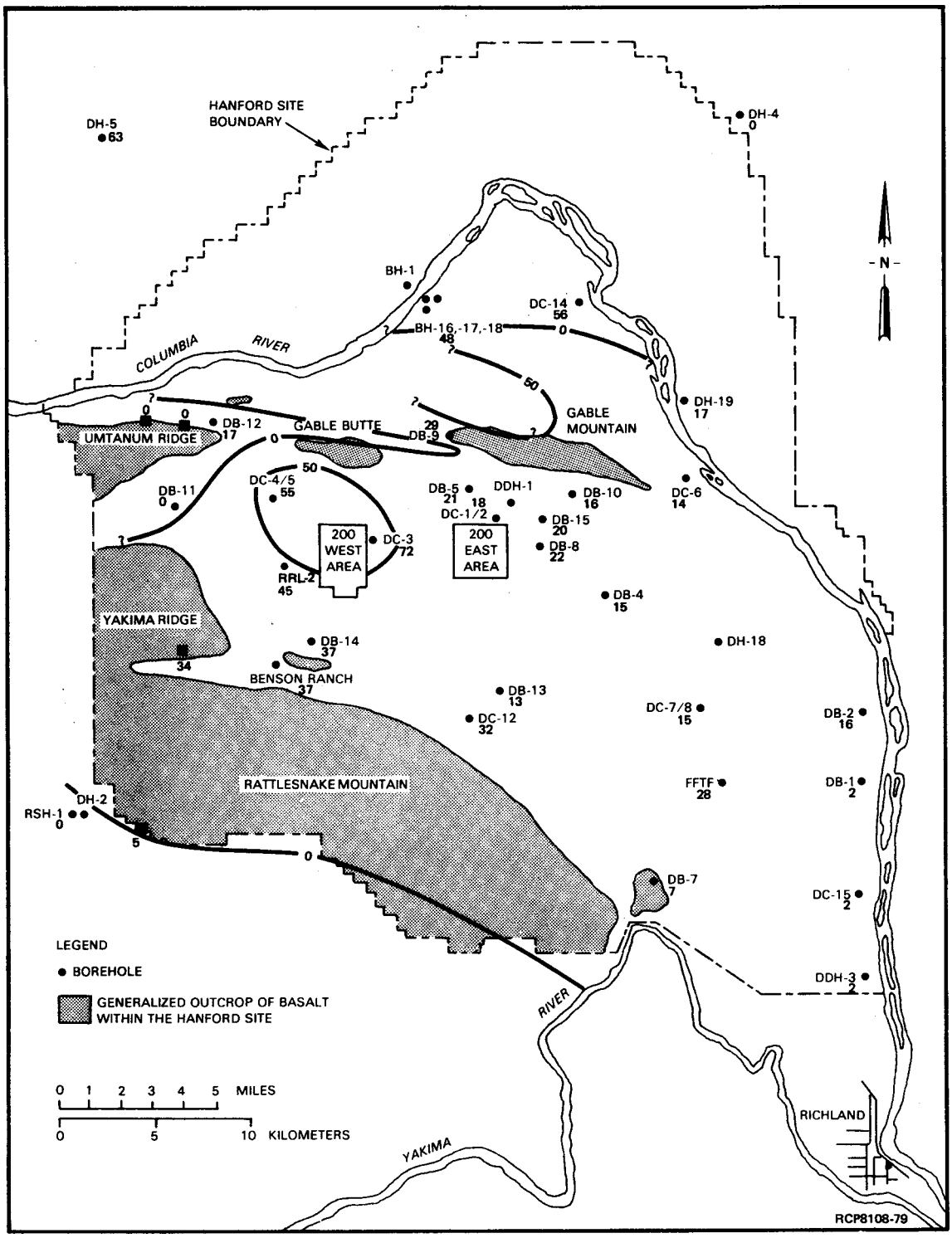

FIGURE 3-21. Isopach Map, Selah Interbed, Cold Creek Syncline. Contour interval is 50 ft. Thicknesses are shown for only those boreholes that penetrate the sedimentary interval. See Table 3-1 for explanation.

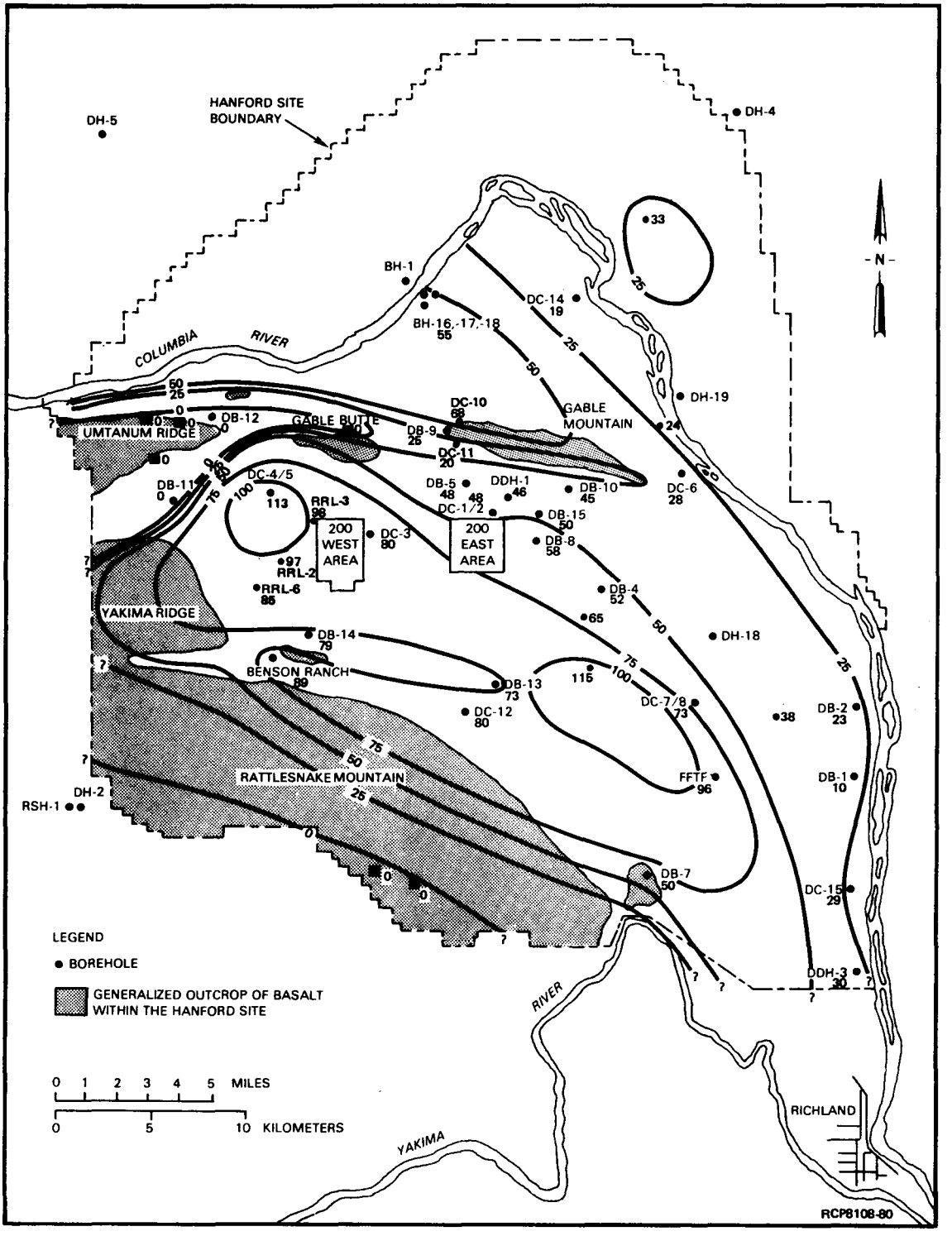

FIGURE 3-22. Isopach Map, Rattlesnake Ridge Interbed, Cold Creek Syncline. Contour interval is 50 ft. Thicknesses are shown for only those boreholes that penetrate the sedimentary interval. See Table 3-1 for explanation.

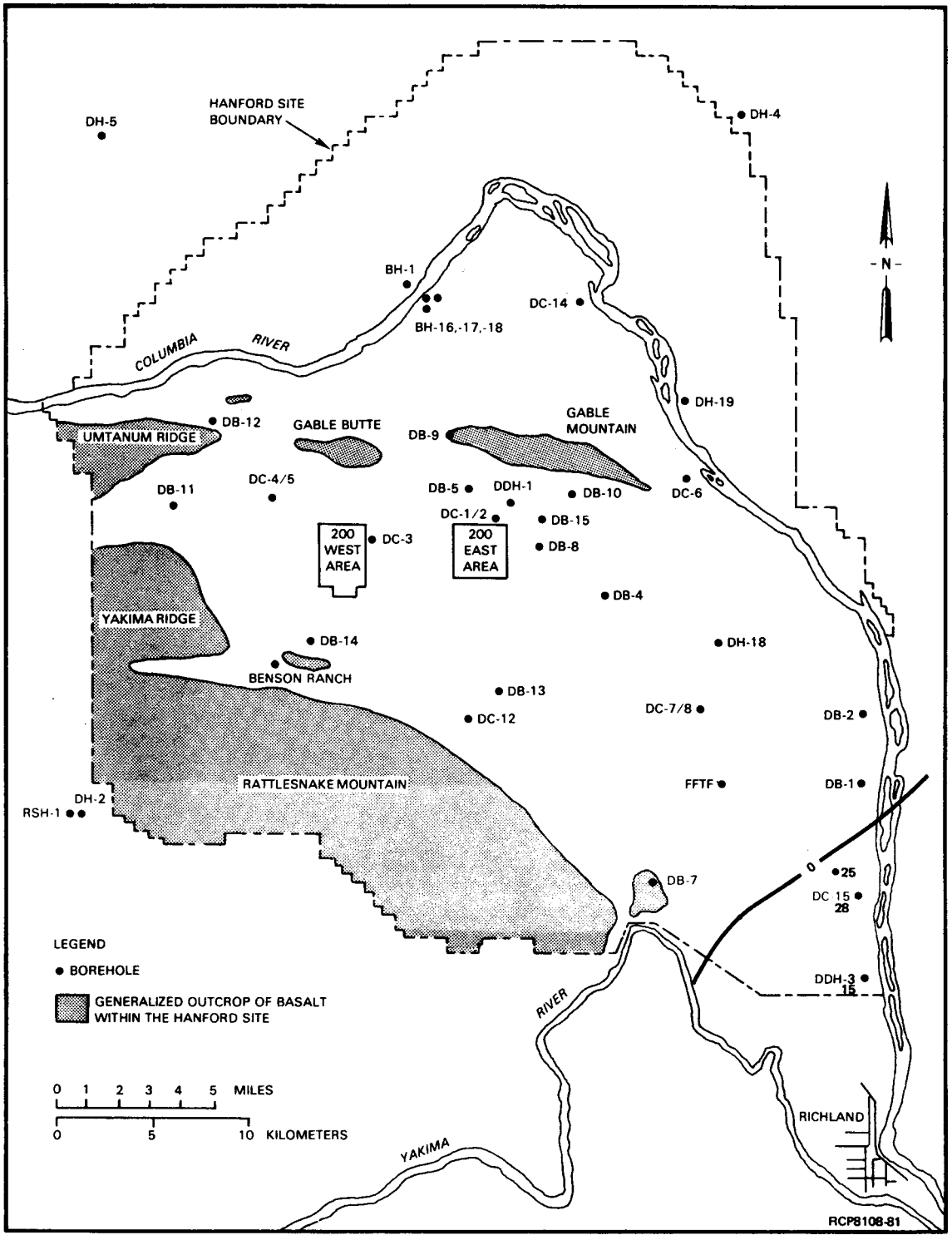

FIGURE 3-23. Isopach Map, Levey Interbed, Cold Creek Syncline. Thicknesses are shown for only those boreholes that penetrate the sedimentary interval. See Table 3-1 for explanation.

MEMBER THICKNESS VARIATIONS IN THE REFERENCE REPOSITORY LOCATION

The members of the Wanapum Basalt show very little thickness variation across the RRL (Fig. 3-2 and Table 3-4). Both the Roza and Priest Rapids Members have northwest-southeast thickness trends across the area, but the Frenchman Springs Member shows no apparent pattern. The total thickness variation for an individual member is <10 m, with the Frenchman Springs Member having the most (10 m) and the Roza Member having the least (3 m).

Considerably more variation in thicknesses of individual members occurs in the Saddle Mountains Basalt (Table 3-4) across the RRL. The Umatilla Member has 20 m of variation across the area, with an abrupt change along a northwest-southeast trend in the northeast part of the area. The thickness is relatively constant across the rest of the RRL. The Wilbur Creek, Asotin, and Ice Harbor Members are not present in this area. There is a 15-m-thickness variation in the Esquatzel Member along a northeast-southwest trend in the RRL. The Esquatzel Member is thicker in the northeast part of the RRL and thinner in the southwest. The Pomona Member has only 10 m of variation and this occurs along a northeast-southwest trend. There is an anomalous area of thinning near DC-3 (Fig. 3-2) which has an apparent northwest-southeast trend. The Elephant Mountain Member has a 21-m-thickness variation across the RRL, also with a northeast-southwest trend. The Elephant Mountain Member thickens across the zone of thinning in the Pomona Member near DC-3. This member is relatively consistent across the rest of the area.

TABLE 3-4. Variation of Member Thickness in the Reference Repository Location.

Member	Thickness trend	Maximum observed variation
Elephant Mountain	NE-SW	21 m (15 to 35 m)*
Pomona	NE-SW	10 m (36 to 46 m)*
Esquatzel	None	15 m (24 to 39 m)*
Asotin	None present	-
Wilbur Creek	None present	-
Umatilla	NW-SE	20 m (46 to 66 m)*
Priest Rapids	NW-SE	6 m (64 to 71 m)*
Roza	NS to NW-SE	1 to 3 m (51 to 53 m)*
Frenchman Springs	None apparent	10 m (219 to 229 m)*

*Thickness range

MODEL FOR THE EMPLACEMENT OF WANAPUM AND SADDLE MOUNTAINS BASALT FLOWS

The lateral extent and thickness variations among individual flows of the Wanapum and Saddle Mountains Basalts in the Pasco Basin are the product of the collective interplay of four factors: (1) volume of each flow that entered the basin, (2) location of flow margins of previously emplaced flows, (3) effect of uplift and subsidence, and (4) regional paleoslope. The flow eruption and emplacement rate and rate of uplift and subsidence are so closely related that a detailed evaluation of the flow history and structural development of the basin during the late Miocene is possible.

Based on the extent and thickness variations of the basalt flows, it is apparent that the Pasco Basin and Cold Creek syncline were active structural features by at least the beginning of Wanapum time. The combined rate of uplift and subsidence in the Pasco Basin was calculated for the period of time over which the Wanapum and Saddle Mountains Basalt flows were erupted (Reidel and others, 1980) and found to be <80 m/million years. An assessment of the contribution of uplift versus subsidence was made by extrapolating Swanson and others' (1975) regional paleoslope into the Pasco Basin, and using the extrapolated surface of this paleoslope as a datum. Based on this datum, both the rates of uplift and subsidence were found to be <40 m/million years. These low uplift and subsidence rates combined with a relatively rapid eruption rate for the Wanapum Basalt indicate that only a small amount of relief on the Yakima fold structures was present when flows of this formation were emplaced. These rates also indicate that any structural relief existing and developing in Grande Ronde time would have been obscured by the large volume of lava which was erupted over a short period of time. A much greater length of time occurred between the eruption of Saddle Mountains Basalt flows, allowing more relief to develop along the structures during periods of volcanic quiescence. Consequently, the topography exerted greater control on the thickness and distribution of Saddle Mountains Basalt flows (Fig. 3-10).

The westward-dipping, regional paleoslope also controlled the extent and thickness of the flows that entered the Pasco Basin. Typically, the thicknesses of flows with large volumes that entered the Pasco Basin and ponded against the Yakima fold structures were controlled more by the topographic relief on structures than by other flows. As a flow ponded against a structure, the eastern flow margin encroached on the paleoslope until the topography was buried and the lava could flow unhindered down the paleoslope.

The volume of the individual eruptions contributed significantly to their lateral extent. Flows of great volume were typically able to bury the topography, so their lateral extent was nearly unaffected. The extent of flows with volumes that could not fill the basin were significantly affected by the topography produced by growing structures and previous flows. The Wilbur Creek, Asotin, Esquatzel, and Ice Harbor Members were of such a sufficiently low volume that they were greatly affected by the topography. The margins of previous flows combined with the existing

structural relief to produce channels. These channels controlled stream drainage during the eruption of flows and after the flows were emplaced. As a result, each new flow ponded in low areas caused by the edges of previous flows, the structural relief, and the paleoslopes. The extent to which a flow spread beyond these low areas was controlled by the volume of lava available.

Unconformities between the basalt flows of the Cold Creek syncline are of two types: (1) angular unconformities and (2) paraconformities. The angular unconformities resulted from onlap of basalt flows onto structural ridges on the margins of the Cold Creek syncline. Gentle tilting of the basalt flows occurred as the ridges grew and, as younger flows were emplaced, they onlapped the ridges at relatively shallow angles. Angular unconformities ($<10^{0}$) were produced between successive flows. In the central part of the Cold Creek syncline, very little structural relief was produced, but other previously mentioned factors caused limitations on the extent of the flows. Here, paraconformities are the predominant unconformity; these occur predominantly between the Saddle Mountains Basalt flows.

The overall geometry of the voluminous flows fits the present geometry of the Cold Creek syncline. The present structural asymmetry of anticlines with steep north flanks and gentle south flanks is reflected in the thickness distribution of the large-volume flows that filled a similar shaped basin in Wanapum and Saddle Mountains time. The thickest parts of the flows are on the south side of the syncline, with thinning over Rattlesnake Mountain and the subsurface extension of Yakima Ridge, and with a gradual thinning toward the Umtanum Ridge-Gable Mountain trend. The westward-dipping paleoslope and the geometry of the flows suggest that the asymmetry of the present structural ridges is probably similar to the geometry of the ridges in Wanapum and Saddle Mountains time, except that the Miocene Cold Creek syncline had less relief.

SUMMARY AND CONCLUSIONS

Basic information on the stratigraphy of the Wanapum and Saddle Mountains Basalts has been derived from a study of surface exposures and core and chip samples from drill holes. The Wanapum Basalt consists of three members in the Pasco Basin: (1) Frenchman Springs, (2) Roza, and (3) Priest Rapids. The Vantage interbed separates this formation from the underlying Grande Ronde Basalt. The petrographic characteristics, combined with distinct chemical differences, permit easy distinction of the Wanapum Basalt from the Grande Ronde Basalt. The Wanapum Basalt (13.5 to 14.5 million years old) is thickest in the central area of the Cold Creek syncline, but thins from west to east and over both the Rattlesnake Mountain and Umtanum Ridge-Gable Mountain structures.

The Saddle Mountains Basalt consists of seven members in the Pasco Basin: (1) Umatilla, (2) Wilbur Creek, (3) Asotin, (4) Esquatzel, (5) Pomona, (6) Elephant Mountain, and (7) Ice Harbor. With the exception of the Wilbur Creek Member, all members are present in the Cold Creek syncline area. The Saddle Mountains Basalt in the Pasco Basin ranges in age from 13.5 to 8.5 mybp.

The Saddle Mountains Basalt flows were extruded over a much greater interval of time than the flows of any other formation of the Columbia River Basalt Group and contain a wide diversity of petrographic characteristics, chemical types, and magnetic inclinations. Thickness variations in the Saddle Mountains Basalt are greater and more complex than in the Wanapum Basalt because of: (1) thinning over structures, (2) greater time between eruptions, and (3) limited extent of many flows.

Intercalated with and overlying the flows of the Columbia River Basalt Group are sedimentary beds of the Ellensburg Formation. Within the Pasco Basin, Ellensburg sediments primarily occur interbedded in the Wanapum and Saddle Mountains Basalts. The lateral extent and thickness of the sediments generally increase upward in the section.

The Ellensburg Formation of the central plateau is composed of two major and distinct lithologies of different provenance. One includes volcaniclastic sediments deposited as ashfall and by tributary rivers flowing on the central plateau. The other includes clastic, plutonic, and metamorphic rock derived from Rocky Mountain terrain that was carried onto the plateau by westward-flowing ancestral rivers. These two major lithologies occur either as distinct or mixed deposits within the Ellensburg Formation of the Pasco Basin.

The lateral extent and thickness variations among individual flows of the Wanapum and Saddle Mountains Basalts in the Pasco Basin are the product of the collective interplay of four factors: (1) volume of each flow that entered the basin, (2) location of flow margins of previously emplaced flows, (3) effect of uplift and subsidence, and (4) regional paleoslope. The flow eruption and emplacement rate and rate of uplift and subsidence are so closely related that a detailed evaluation of the flow history and structural development of the basin during the late Miocene is possible.

Based on the extent and thickness variations of the basalt flows, it is apparent that the Pasco Basin and Cold Creek syncline were active structural features by at least the beginning of Wanapum time. The rates of uplift and subsidence in the Pasco Basin were calculated for the period of time over which the Wanapum and Saddle Mountains Basalt flows were erupted and the rates of uplift and subsidence were found to be <40 m/ million years. These low uplift and subsidence rates, combined with a relatively rapid eruption rate for the Wanapum Basalt, indicate that only a small amount of relief on the Yakima fold structures was present when flows of this formation were emplaced. These rates also indicate that any structural relief existing and developing in Grande Ronde time would have been obscured by the large volume of lava which was erupted over a short

period of time. A much greater length of time occurred between the eruption of Saddle Mountains Basalt flows, allowing more relief to develop along the structures during periods of volcanic quiescence. Consequently, the topography exerted greater control on the thickness and distribution of Saddle Mountains Basalt flows.

The present structural asymmetry of anticlines with steep north flanks and gentle south flanks is reflected in the thickness distribution of the large-volume flows that filled a similar-shaped basin in Wanapum and Saddle Mountains time. The thickest parts of the flows are on the south side of the syncline, with thinning over Rattlesnake Mountain and the subsurface extension of Yakima Ridge and a gradual thinning toward the Umtanum Ridge-Gable Mountain trend. The westward-dipping paleoslope and the geometry of the flows suggest that the asymmetry of the present structural ridges is probably similar to the geometry of the ridges in Wanapum and Saddle Mountains time, except that the Miocene Cold Creek syncline has less relief.

CHAPTER 4 - STRATIGRAPHY OF THE GRANDE RONDE BASALT

P. E. Long
R. D. Landon

INTRODUCTION

The Grande Ronde Basalt is a thick sequence of at least 50 basalt flows which underlie the Saddle Mountains and Wanapum Basalts. In the central Columbia Plateau, this thick sequence extends to a depth of at least 3.2 km. The thickness decreases toward the margins of the plateau, but nonetheless, significant thicknesses of Grande Ronde Basalt occur beneath much of the entire area. The occurrence of the Grande Ronde Basalt as a sequence of flows, many of which are relatively thick and laterally extensive, means that groundwater movement is in large part controlled by the sequence of flows. This is true principally because individual flows consist of a dense interior and a relatively porous and permeable, vesicular, flow top (see Chapter 5); hence, the layering of the sequence imparts a grossly planar anisotropy to groundwater movement. In spite of the folding and faulting that have distorted the original planar and nearly horizontal character of the layers (see Chapters 7 and 8), it is fundamentally important to understand the stratigraphy of the basalt layers as the first step to understanding the hydrology of the area. This chapter reports the current knowledge about Grande Ronde stratigraphy with particular emphasis on Grande Ronde flows adjacent to the reference repository horizon, the Umtanum flow.

PREVIOUS WORK

Work on the Grande Ronde Basalt prior to 1979 has been summarized by Swanson and others (1979b). This paper also established the Grande Ronde Basalt nomenclature now in widespread use for regional studies of the plateau. The Grande Ronde Basalt was subdivided into four paleomagnetic polarity units: R_1, N_1, R_2, and N_2. In addition, Swanson and others (1979b) noted the existence of at least three chemical types in the Grande Ronde Basalt: (1) low-Mg, (2) high-Mg, and (3) very-high-Mg chemical types. Publications specifically dealing with Grande Ronde Basalt of the Pasco Basin and vicinity (encompassing the Cold Creek syncline) include Myers (1973), ARHCO (1976), Long (1978), Myers, Price and others (1979), and Long and others (1980, 1981).

Atlantic Richfield Hanford Company (1976) and Myers, Price and others (1979) included available data on Grande Ronde Basalt stratigraphy up to their respective dates of publication. The principal stratigraphic feature of Grande Ronde Basalt recognized in ARHCO (1976) was the Mg horizon, a stratigraphic horizon which is underlain by relatively low-Mg basalts and overlain by relatively high-Mg basalts. Myers, Price and others (1979)

recognized that in addition to these two major subdivisions, it was possible to distinguish a very-high-Mg flow in the subsurface of the Pasco Basin and that it was possible to make stratigraphic correlations based on paleomagnetic inclination. Specifically, Coe and others (1978) discovered that the uppermost flow in the R_2 unit was exposed north of the Pasco Basin and that secular variation in the paleomagnetic inclination of N_2 flows could possibly be used to subdivide that thick sequence of flows. This and later paleomagnetic data (Beck and others, 1978; Packer and Petty, 1979) are reported in Myers, Price and others (1979). Additional paleomagnetic data have been collected and previous data reevaulated by Van Alstine and Gillett (in press). Stratigraphic interpretations from that data are included in this chapter.

Long and others (1980, 1981) reported on refinement of Grande Ronde stratigraphy based on major and trace element compositions of individual flows. This work, along with additional compositional data, is included in this chapter.

METHODOLOGY

The stratigraphy of Grande Ronde Basalt presented in this chapter is based first on the physical characterization of core samples and of outcrop exposures in stratigraphic sections (Fig. 4-1). For boreholes, geophysical logs are also utilized in picking contacts between flows, especially for boreholes for which no core is available (e.g., RSH-1, DC-3; see Fig. 4-1). The core is then sampled for major element analysis via X-ray fluorescence (XRF), trace element analysis via XRF and neutron activation analysis (NAA), and paleomagnetic analysis via alternating field and thermal demagnitization. The knowledge of the positions of contacts between individual flows coupled with the data obtained from these three analytical methods form the basis of the correlations reported here. In addition, over relatively short distances (approximately a few kilometers), the character of geophysical logs has been used as a correlation method for certain flows (Myers, Price and others, 1979). For one flow, the McCoy Canyon flow, photomosaics of cliff exposures have been used to physically trace it as a single unit for several kilometers. The results of this are discussed in more detail in Chapter 5.

The XRF analyses for major elements were performed at Washington State University under the direction of Dr. P. R. Hooper, according to procedures reported in Hooper and others (1976). The NAA and XRF analyses for trace elements were performed at the University of Oregon, Center for Volcanology, under the direction of Dr. G. G. Goles. The NAA data were obtained according to procedures reported in Goles (1977).

Paleomagnetic analyses have been performed by Coe and others (1978), Beck and others (1978), Packer and Petty (1979), and Van Alstine and Gillett (in press). Techniques used by each of these workers are reported in their respective reports. Van Alstine and Gillett (in press) include a summary and reanalysis of previous paleomagnetic data for Grande Ronde Basalt in the Pasco Basin.

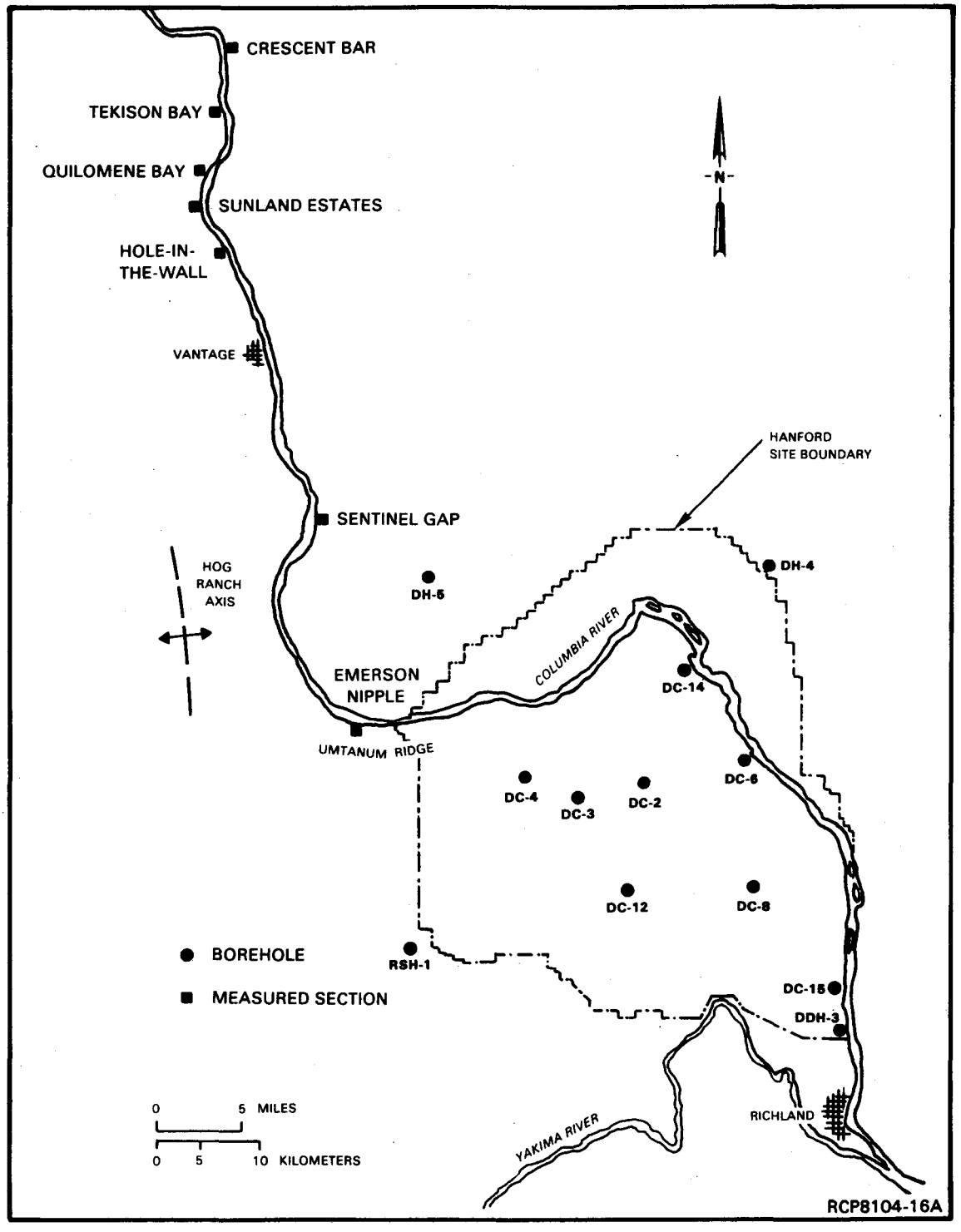

FIGURE 4-1. Location Map, Pasco Basin and Surrounding Areas (showing location of boreholes and surface sections).

RESULTS

CHARACTERIZATION OF SURFACE EXPOSURES AND CORE SAMPLES

Details of this work have been discussed in previous publications (ARHCO, 1976; Myers, Price and others, 1979). Those data are not repeated here; we simply note where additional data have been obtained and show examples of the types of results that have been obtained. Additional field sections were measured north of Vantage, including Crescent Bar, Tekison Bay, Quilomene Bay, Sunland Estates, and Hole-in-the-Wall sections (Fig. 4-1). Three new boreholes (DC-12, DC-14, and DC-15) were completed and a fourth deepened (DC-7). Examples of the information collected for the stratigraphic sections and for the core samples are provided in Figures 4-2 and 4-3, respectively. A typical geophysical log response to both flow top and dense flow interior is also shown in Figure 4-3.

In addition to stratigraphic sections at specific locations north of Vantage, the well-exposed cliffs in this area were photographed. A photomosaic was assembled and used to trace a single flow, the McCoy Canyon flow, from Crescent Bar to south of Sunland Estates. Results are shown in Chapter 5 and demonstrate that the flow is a laterally continuous, single sheet, although significant variations occur within the flow itself. Relatively thick flows, such as the McCoy Canyon flow, clearly may have great lateral extent. Furthermore, the uniform thinning of the McCoy Canyon flow to the north suggests that the distribution of individual flows was controlled in part by a relatively subdued, gentle topography.

MAJOR ELEMENT ANALYSES

More than 2,000 major element analyses have been performed on Grande Ronde Basalt samples. Typically two or three samples per flow are analyzed for any given section or borehole. The results are summarized in Table 4-1 and Figure 4-4. The three, major, Grande Ronde chemical types are evident in Figure 4-4, which shows high-Mg, low-Mg, and very-high-Mg chemical types. In addition, there are two subtypes of the low-Mg and high-Mg chemical types that are referred to as the Umtanum and McCoy Canyon chemical subtypes, respectively. The significance of these chemical features is that they are related to stratigraphy of Grande Ronde flows in the central part of the Columbia Plateau (Fig. 4-5). Major elements thus provide an important means of stratigraphic correlation which make it possible to distinguish groups of flows and, in some cases, individual flows (Reidel and Long, 1980).

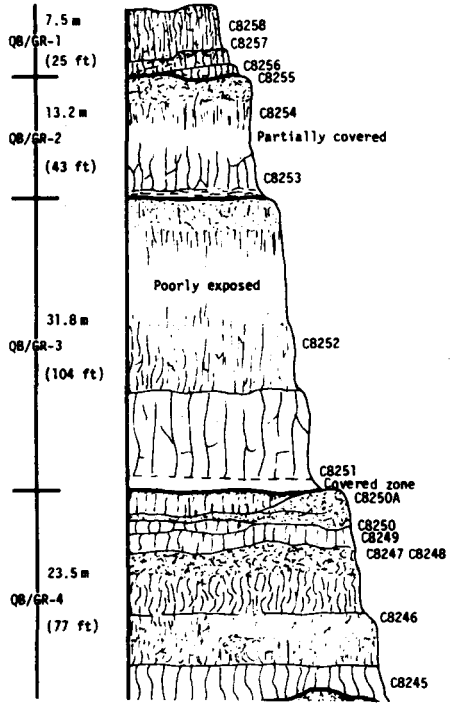

QB denotes Quilomene Bay section.

LITHOLOGY	SiO_2	TiO_2	Al_2O_3	Fe_2O_3	FeO	MnO	MgO	CaO	Na_2O	K_2O	P_2O_5	NUMBER OF ANALYSES	MAGNETIC POLARITY
Lower part of flow is a flow lobe of medium-grey, diktytaxitic, aphyric basalt with blocky internal structure, no well-defined columns. Sparse vesicle cylinders 1 to 2 cm in diameter. Upper, thickest part of flow is medium-to dark-grey, diktytaxitic basalt, aphyric to very sparsely phyric. Irregular columns ~0.4 m diameter grade upward to hackly columns ~0.2 m diameter.	54.29 *0.19	1.80 0.02	15.16 0.02	2.00	9.55 0.10	0.20 0.00	4.36 0.20	8.49 0.10	2.43 0.13	1.41 0.03	0.31 0.02	3	N
Dark-to medium-grey, diktytaxitic, medium-grained, aphyric basalt. Actual flow contact is not exposed. Lowest exposure is a platy zone overlain by poorly formed columns 0.5 to 0.7 m in diameter which grade upward into partly exposed hackly entablature. Gives way upward to blocky, vesicular flow top. Sparse, 1 cm-sized vesicles become abundant in upper 2 m of flow. Flow top is oxidized.	53.99 0.12	1.77 0.04	15.11 0.12	2.00	9.56 0.17	0.20 0.00	4.64 0.01	8.47 0.02	2.59 0.01	1.40 0.05	0.30 0.01	2	N
Dark-grey to black, aphyric basalt, poorly exposed. Colonnade consists of well-formed columns ~0.5 m diameter. Sharp contact with overlying entablature which is hackly, possibly some tiering, but poor exposure prohibits accurate description.	54.00 0.26	1.74 0.00	15.06 0.01	2.00	9.63 0.15	0.20 0.00	4.69 0.27	8.48 0.04	2.53 0.11	1.41 0.08	0.30 0.01	2	N
Dark-grey, aphyric basalt with plagioclase microphenocrysts readily visible. Colonnade exhibits well-formed columns 0.4 to 0.8 m in diameter with pinch-and-swell morphology and niche joints ~0.5 m apart plus irregular cross fractures. Thin, platy zones occur locally. Forms sharp contact with overlying hackly entablature which consists of fluted, 0.10 to 0.20 m-sized blocks. One mass of vesicular basalt occurs in the entablature. In places, an upper colonnade with moderately well-formed columns (0.2 to 0.4 m diameter) occur, but otherwise the upper third of the flow is hackly. Vesicles become abundant in the upper quarter of the flow. The flow top is very sparsely phyric. 1 to 2 flow lobes of black to dark-grey, medium-grained, diktytaxitic, aphyric basalt cap the flow. Radiating felted masses of plagioclase microlites are readily visible. Vesicle cylinders are abundant. Lower, thickest flow lobe has poorly formed, 0.4 to 0.6 m columns which degenerate upward to hackly basalt, fractured into 7 to 20-cm-sized blocks.	53.51 0.45	1.76 0.02	15.14 0.18	2.00	9.67 0.17	0.20 0.00	4.89 0.36	8.99 0.08	2.43 0.07	1.15 0.09	0.26 0.01	4	N

*One standard deviation values are given below the entry for each oxide. All analyses by X-ray fluorescence on a volatile free basis. Fe_2O_3 is arbitrarily set at 2.00 weight percent.

RCPB108-95

FIGURE 4-2. Example of Part of a Detailed Stratigraphic Section Taken at Quilomene Bay.

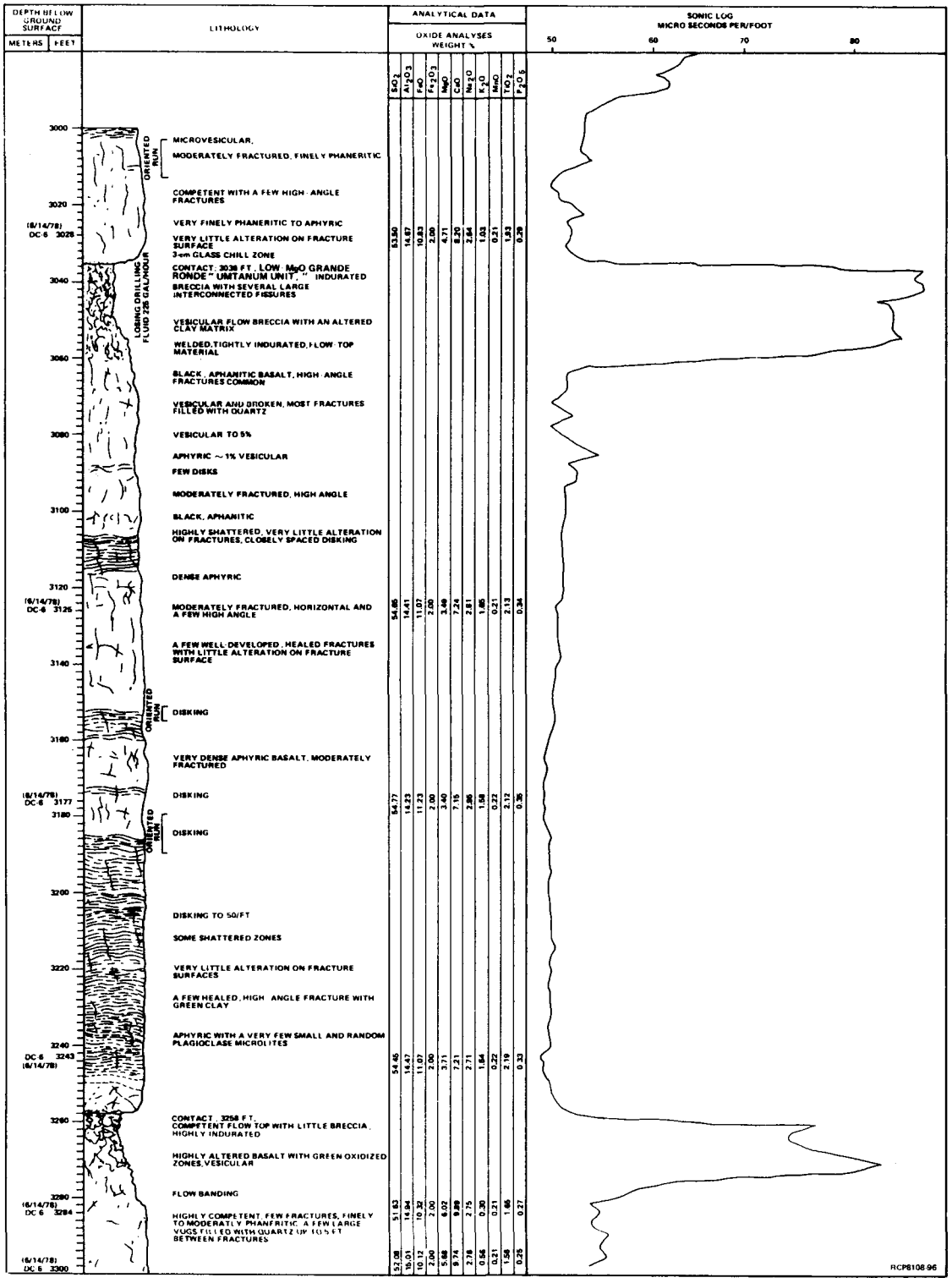

FIGURE 4-3. Example of Part of a Lithologic Log of Grande Ronde Basalt Core from Borehole DC-6. Geophysical log of same interval illustrating a typical response.

TABLE 4-1. Major Element Composition of Grande Ronde Flows (wt%).

	N	Mean	Standard deviation	Minimum** value	Maximum** value	Standard error of mean
High-Mg Flows						
SiO_2	50	53.61	0.43	52.61	54.45	0.06
Al_2O_3	50	14.88	0.27	14.26	15.51	0.04
FeO*	50	12.01	0.52	10.89	12.89	0.07
MgO	50	4.88	0.20	4.38	5.34	0.03
CaO	50	8.75	0.19	8.36	9.20	0.03
Na_2O	50	2.60	0.17	2.13	3.17	0.02
K_2O	50	0.97	0.15	0.51	1.31	0.02
TiO_2	50	1.81	0.10	1.62	1.96	0.01
P_2O_5	50	0.28	0.02	0.25	0.38	0.00
MnO	50	0.21	0.01	0.19	0.23	0.00
Low-Mg Flows						
SiO_2	13	55.45	0.63	53.82	56.01	0.18
Al_2O_3	13	14.88	0.19	14.44	15.19	0.05
FeO	13	11.95	0.30	11.25	12.40	0.08
MgO	13	3.55	0.12	3.41	3.84	0.03
CaO	13	7.35	0.13	7.11	7.55	0.04
Na_2O	13	2.82	0.18	2.45	3.11	0.05
K_2O	13	1.63	0.33	1.17	2.47	0.09
TiO_2	13	1.91	0.03	1.87	1.96	0.01
P_2O_5	13	0.30	0.01	0.28	0.32	0.00
MnO	13	0.20	0.01	0.19	0.21	0.00
Umtanum Flow						
SiO_2	13	54.90	0.25	54.45	55.45	0.07
Al_2O_3	13	14.34	0.15	14.08	14.59	0.04
FeO	13	13.10	0.21	12.70	13.39	0.06
MgO	13	3.48	0.09	3.38	3.71	0.03
CaO	13	7.30	0.14	7.14	7.64	0.04
Na_2O	13	2.66	0.26	1.86	2.95	0.07
K_2O	13	1.48	0.24	0.94	1.71	0.07
TiO_2	13	2.17	0.04	2.12	2.23	0.01
P_2O_5	13	0.35	0.01	0.33	0.36	0.00
MnO	13	0.22	0.00	0.21	0.23	0.00
Very-High-Mg Flow						
SiO_2	10	51.87	0.42	50.82	52.42	0.13
Al_2O_3	10	15.09	0.24	14.79	15.57	0.07
FeO	10	11.89	0.21	11.50	12.16	0.07
MgO	10	5.75	0.15	5.53	6.02	0.05
CaO	10	9.93	0.22	9.68	10.43	0.07
Na_2O	10	2.80	0.18	2.50	3.01	0.06
K_2O	10	0.53	0.17	0.29	0.76	0.05
TiO_2	10	1.64	0.07	1.57	1.79	0.02
P_2O_5	10	0.27	0.02	0.25	0.30	0.01
MnO	10	0.22	0.03	0.20	0.30	0.01

*Total Fe given as FeO.
**Maximum and minimum values are for individual oxides.

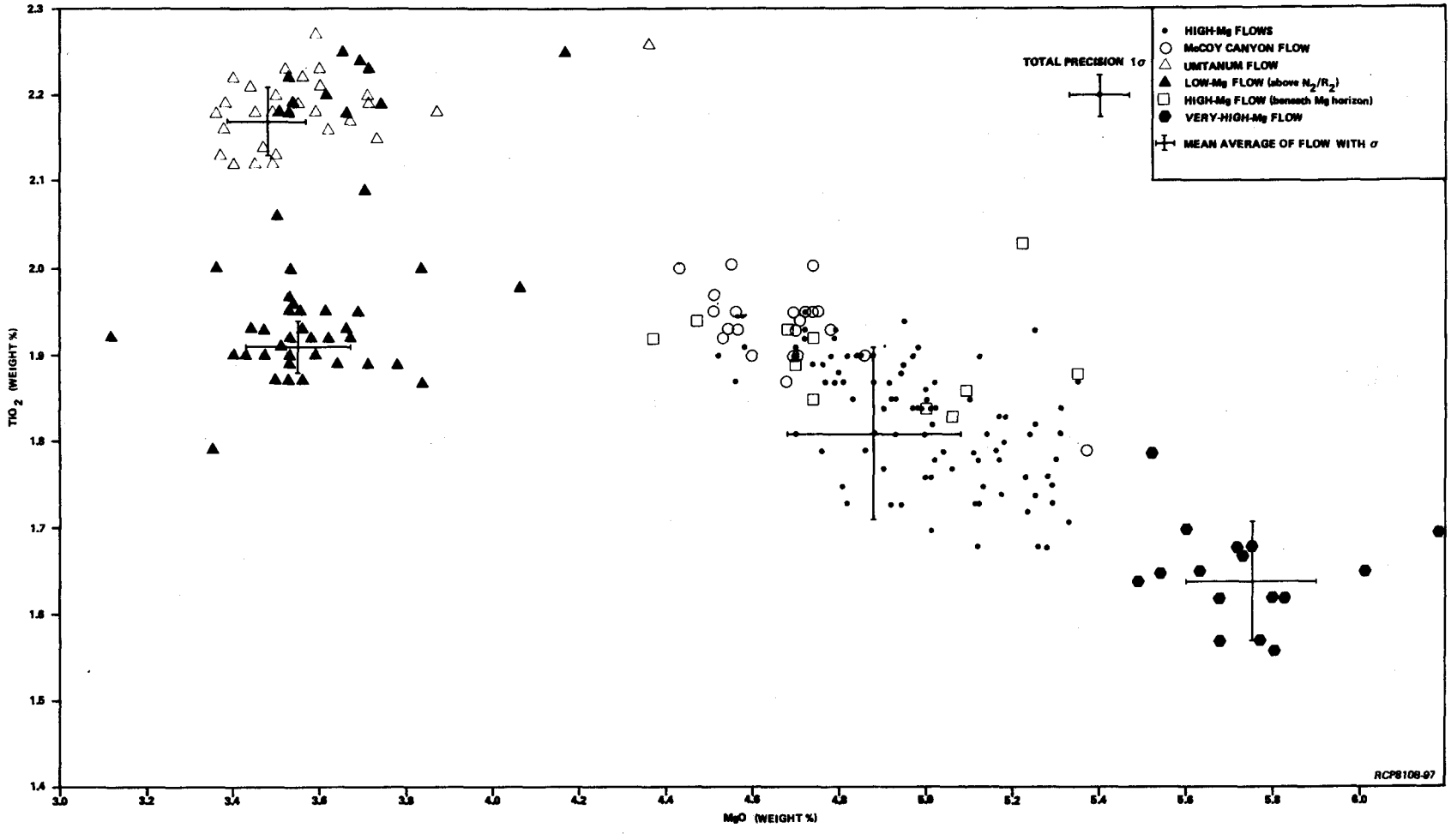

FIGURE 4-4. Magnesium Oxide Plotted Versus Titanium Dioxide for Grande Ronde Basalt Chemical Types and Subtypes.

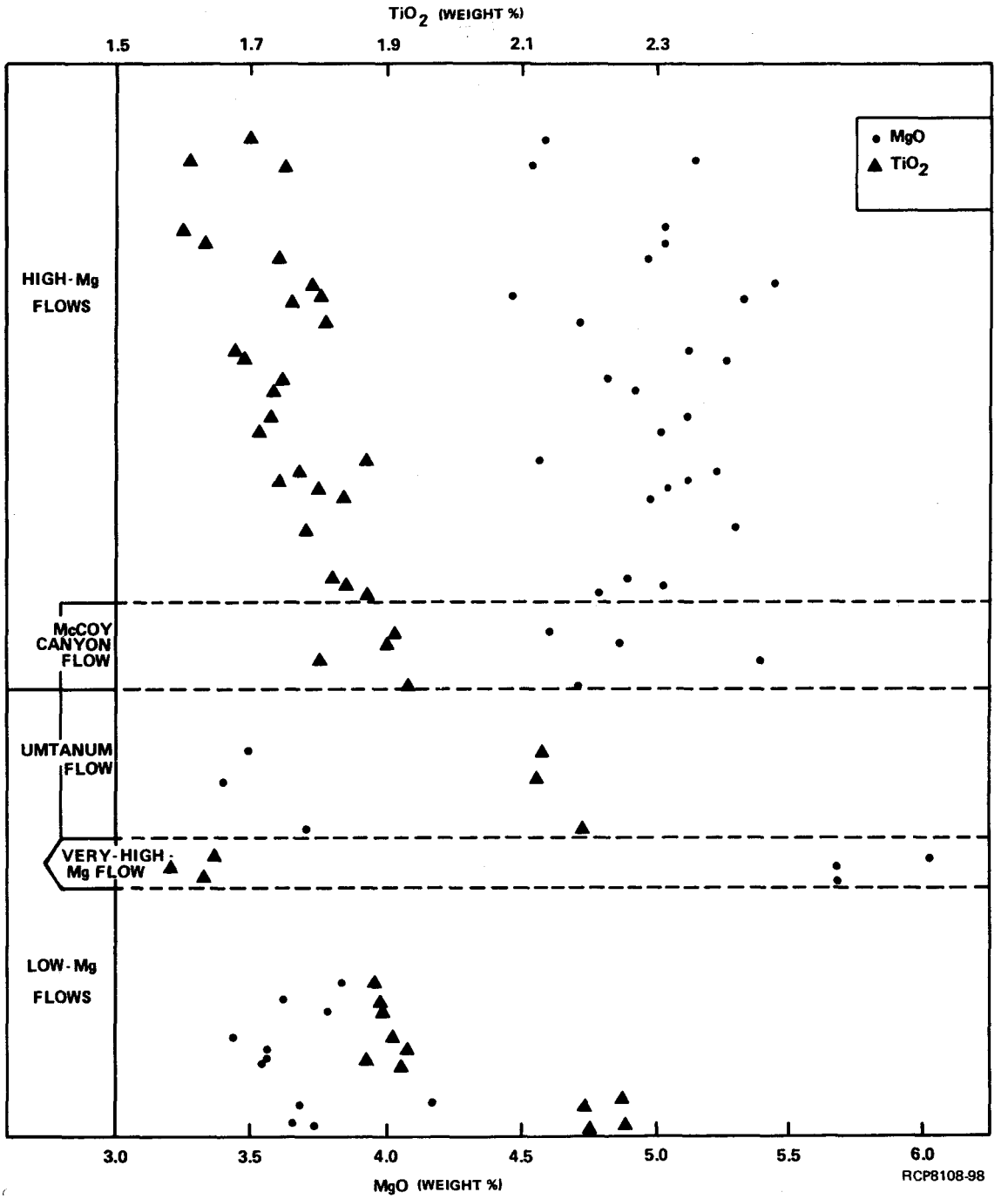

FIGURE 4-5. Magnesium Oxide and Titanium Dioxide Plotted Versus Stratigraphic Position in Borehole DC-6.

TRACE ELEMENT ANALYSES

Analyses for 21 selected trace elements have been made on more than 400 Grande Ronde Basalt samples. Selected analyses are summarized in Table 4-2, and the stratigraphic variation of zirconium (Zr) and chrome (Cr) illustrated in Figure 4-6. Trace element analyses have been used to strengthen the statistical significance of correlations based on major elements and to provide a basis for more detailed correlations within major element units. Chrome is particularly useful for subdivision of the high-Mg section, and forms the principal basis in conjunction with paleomagnetic data for correlating flows in this otherwise monotonous section.

PALEOMAGNETIC DATA

Paleomagnetic data on Grande Ronde Basalt have been obtained for two surface sections and all deep core holes, except DC-12, DC-14, and DC-15; these recently completed core holes are currently being sampled for analysis. Fully oriented, paleomagnetic-direction data have been obtained from the surface sections; whereas, from unoriented core, it is possible only to determine if a flow is normal or reversed and to determine its paleomagnetic inclination. An example of such data showing correlatable stratigraphic units is shown in Figure 4-7. Stratigraphic significance of these data is discussed in a later section of this chapter; the data on which paleomagnetic correlations are based are reported elsewhere (Van Alstine and Gillett, in press).

DISCUSSION

GENERAL STRATIGRAPHIC FRAMEWORK

Regional stratigraphy of Grande Ronde Basalt is based on four, paleomagnetic polarity units defined by reversals in the paleomagnetic polarity of the flows. These have been labeled in sequence from bottom to top: R_1, N_1, R_2, and N_2 (Swanson and others, 1979b). Core holes and surface exposures in the vicinity of the Pasco Basin include the N_2 and uppermost R_2 units. The N_2-R_2 horizon has, thus, been recognized and provides an important stratigraphic horizon. Presumably, N_1 and R_1 units underlie the central plateau, but this has yet to be demonstrated.

In addition to N_2 and R_2 Grande Ronde flows, two major sequences of flows have been recognized within the Grande Ronde Basalt in the Pasco Basin: (1) Schwana sequence, consisting almost entirely of flows with relatively low-Mg content (low-Mg chemical type) and (2) Sentinel Bluffs sequence, consisting entirely of flows with higher Mg content (high-Mg chemical type). The Schwana sequence lies stratigraphically below the Sentinel Bluffs flows. The contact between these two sequences is known as the Mg horizon. Generalized stratigraphic relationships among these sequences, the R_2-N_2 horizon, and the very-high-Mg flows are shown in Figures 4-8 and 4-9.

TABLE 4-2. Element Compositions of Grande Ronde Flows Determined by Instrumental Neutron Activation Analysis.

	N	Mean	Standard deviation	Minimum value	Maximum value	Standard error of mean
			High-Mg Flows (p/m)*			
Fe	70	8.83	0.34	8.05	9.54	0.04
Sc	70	36.31	1.45	31.50	39.10	0.17
Cr	70	35.66	9.04	19.60	51.20	1.08
Co	70	41.25	4.56	33.50	57.20	0.54
Zr	66	153.50	5.51	142.50	168.80	0.67
Hf	70	4.09	0.34	3.51	5.24	0.04
Nb	66	13.21	1.66	9.10	17.90	0.20
Ta	65	0.82	0.34	0.41	2.11	0.04
Th	70	3.74	0.46	2.49	4.79	0.05
U	7	1.12	0.32	0.80	1.80	0.12
Na	60	2.17	0.09	1.95	2.35	0.01
Sr	66	308.00	7.00	291.80	323.40	0.90
Ba	64	445.00	58.00	300.00	553.00	7.26
Rb	70	29.20	5.00	15.60	39.60	0.64
Cs	52	0.67	0.21	0.19	1.04	0.02
La	70	17.85	1.21	15.40	20.70	0.14
Ce	69	38.77	2.81	33.60	48.30	0.33
Nd	5	18.02	1.17	16.10	19.00	0.52
Sm	70	5.62	0.32	4.86	6.44	0.03
Eu	70	1.76	0.08	1.60	2.01	0.01
Tb	68	0.88	0.14	0.48	1.14	0.01
Yb	68	3.17	0.31	2.24	3.90	0.03
Lu	66	0.52	0.06	0.30	0.74	0.00
			Low-Mg Flows (p/m)*			
Fe	28	9.32	0.52	8.52	10.14	0.10
Sc	28	32.79	1.79	29.40	36.10	0.33
Cr	21	7.89	2.33	5.10	13.20	0.51
Co	28	38.01	3.00	35.10	50.00	0.66
Zr	24	185.00	5.00	177.00	201.20	1.12
Hf	28	4.82	0.30	4.22	5.65	0.05
Nb	24	15.55	1.58	11.60	18.10	0.32
Ta	24	0.91	0.27	0.50	1.72	0.05
Th	28	5.99	0.62	4.73	7.27	0.11
U	9	1.45	0.22	1.02	1.70	0.07
Na	28	2.35	0.10	2.02	2.53	0.01
Sr	24	320.00	13.00	304.40	365.00	2.74
Ba	25	636.00	75.00	450.00	850.00	15.15
Rb	28	46.36	9.37	17.60	68.30	1.77
Cs	24	1.33	0.54	0.56	2.43	0.11
La	28	23.30	2.02	15.20	26.70	0.38
Ce	28	49.85	2.53	45.50	57.70	0.47
Nd	4	30.50	6.55	25.00	40.00	3.27
Sm	28	6.69	0.28	6.16	7.26	0.05
Eu	28	1.98	0.11	1.81	2.29	0.02
Tb	25	1.02	0.12	0.75	1.21	0.024
Yb	28	3.53	0.46	2.90	4.59	0.088
Lu	27	0.57	0.07	0.38	0.69	0.014
			Very-High-Mg Flow (p/m)*			
Fe	8	8.69	0.29	8.00	8.91	0.10
Sc	8	40.16	1.30	38.70	41.80	0.46
Cr	8	109.10	11.08	90.00	123.30	3.91
Co	8	43.23	3.69	40.40	50.00	1.30
Zr	7	119.00	5.51	112.10	130.20	2.08
Hf	8	3.39	0.22	3.11	3.75	0.07
Nb	7	13.38	1.98	10.20	15.50	0.75
Ta	7	0.57	0.17	0.36	0.83	0.06
Th	8	2.21	0.14	2.01	2.44	0.05
U	0	-	-	-	-	-
Na	8	2.14	0.09	2.00	2.24	0.03
Sr	7	356.00	17.14	344.70	394.00	6.47
Ba	7	401.00	49.47	340.00	470.00	18.69
Rb	8	13.00	5.58	6.40	24.20	1.97
Cs	5	0.46	0.06	0.37	0.54	0.02
La	8	14.25	0.89	12.90	15.40	0.31
Ce	8	32.35	2.61	28.30	37.50	0.92
Nd	1	19.70	-	19.70	19.70	-
Sm	8	4.89	0.19	4.58	5.17	0.07
Eu	8	1.62	0.11	1.44	1.84	0.04
Tb	8	0.76	0.15	0.49	0.93	0.053
Yb	8	2.81	0.39	2.24	3.30	0.140
Lu	8	0.46	0.045	0.36	0.51	0.016

*Except values for Fe and Na which are percent.

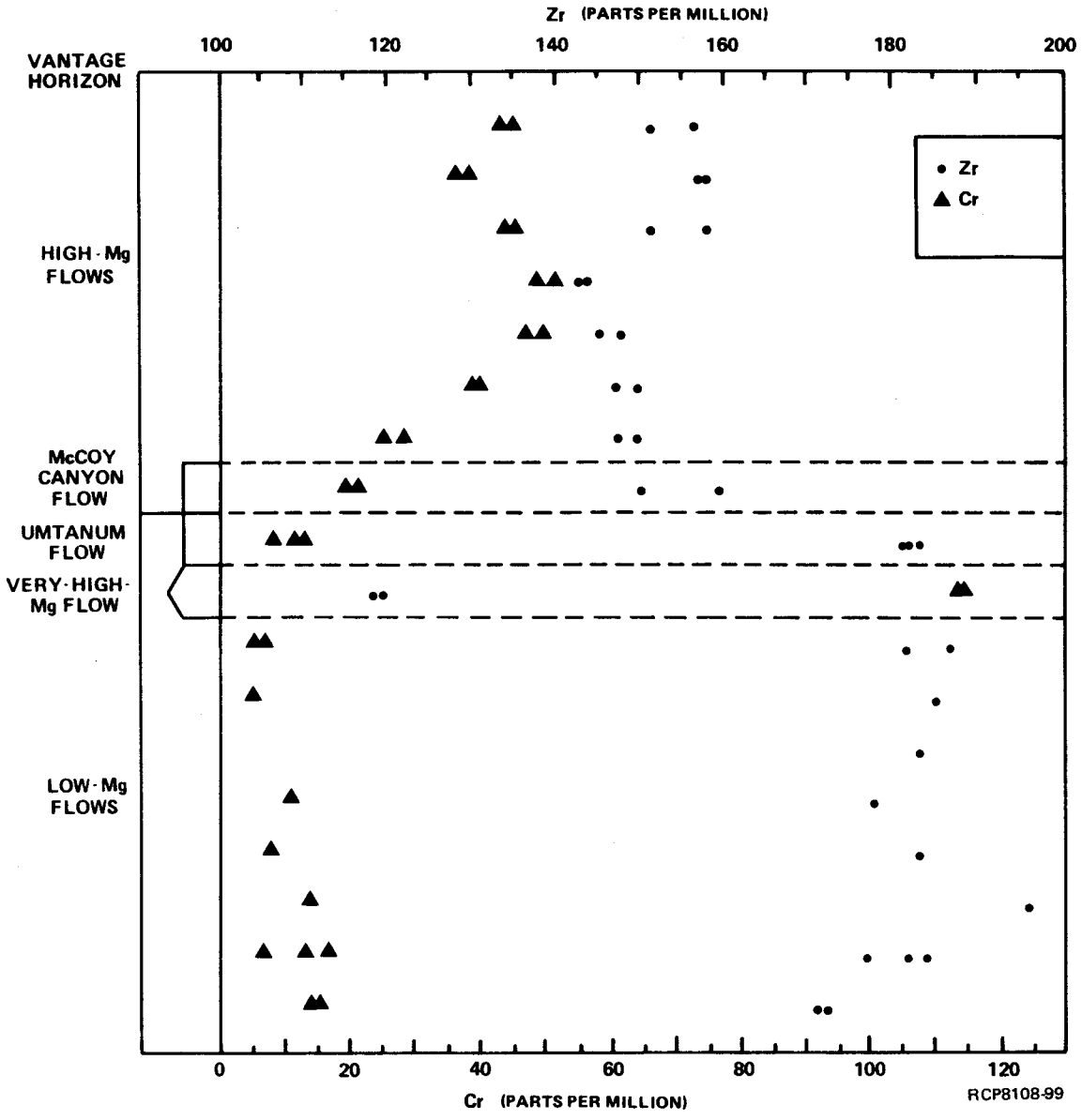

FIGURE 4-6. Zirconium and Chrome Plotted Versus Stratigraphic Position in Borehole DC-6.

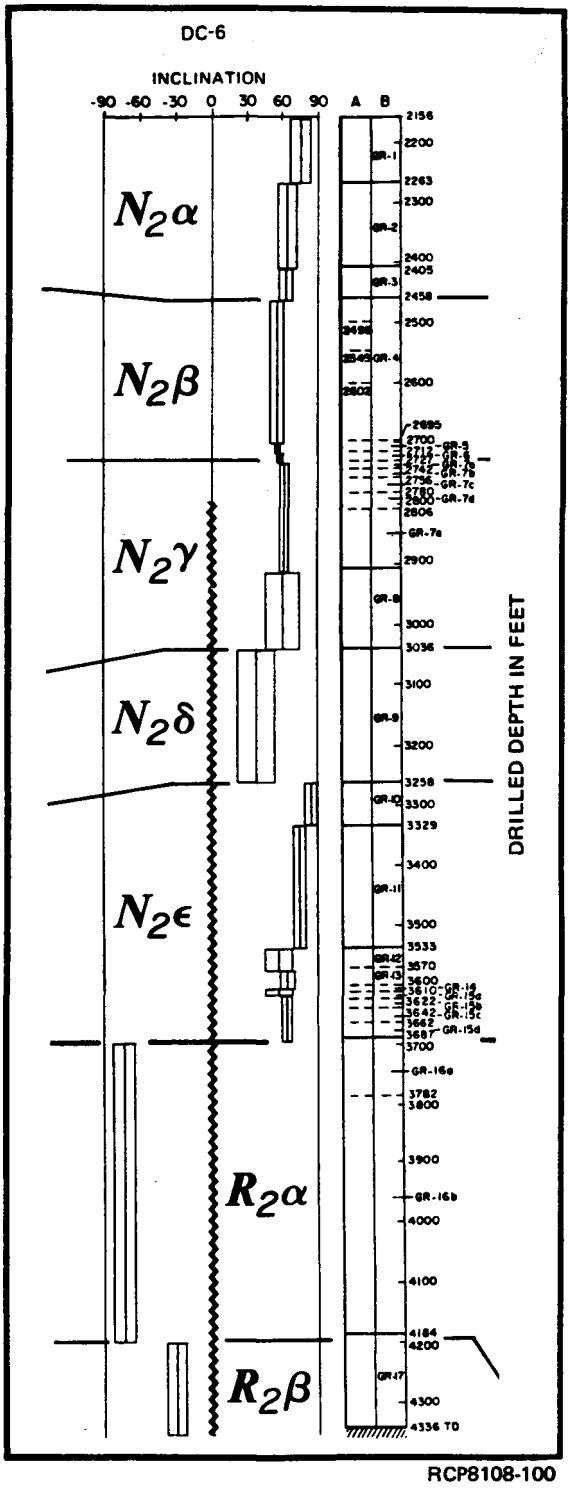

FIGURE 4-7. Paleomagnetic Inclination Data from Borehole DC-6.

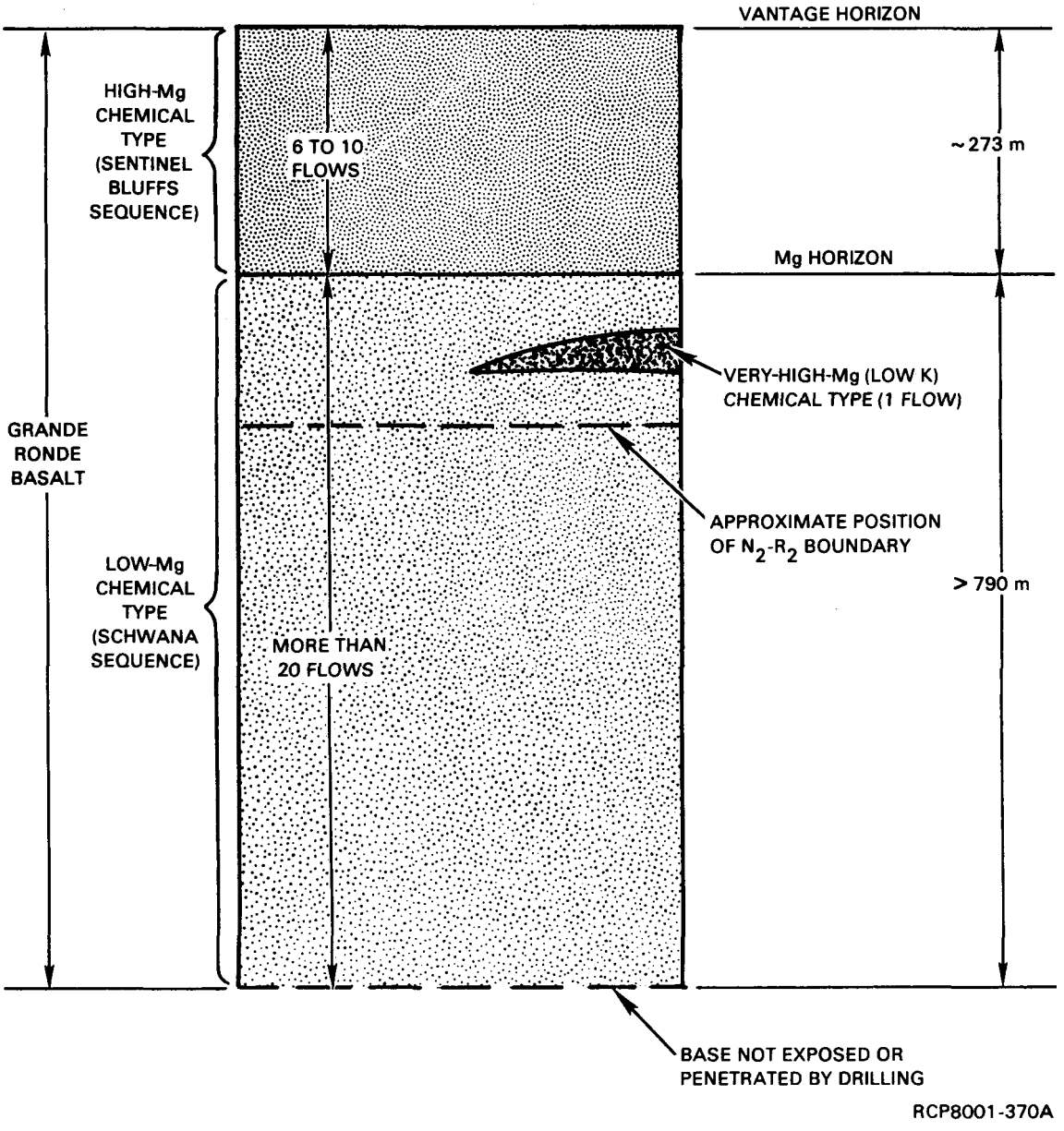

FIGURE 4-8. General Stratigraphic Relationships Among Grande Ronde Basalt Flow Sequences in the Pasco Basin. Thickness figures and numbers of flows based on core drilling and exposures in the Pasco Basin and vicinity. Analysis of chip samples from a deep, rotary-drilled well (RSH-1) indicate that Grande Ronde Basalt extends to a depth of at least 3.2 km.

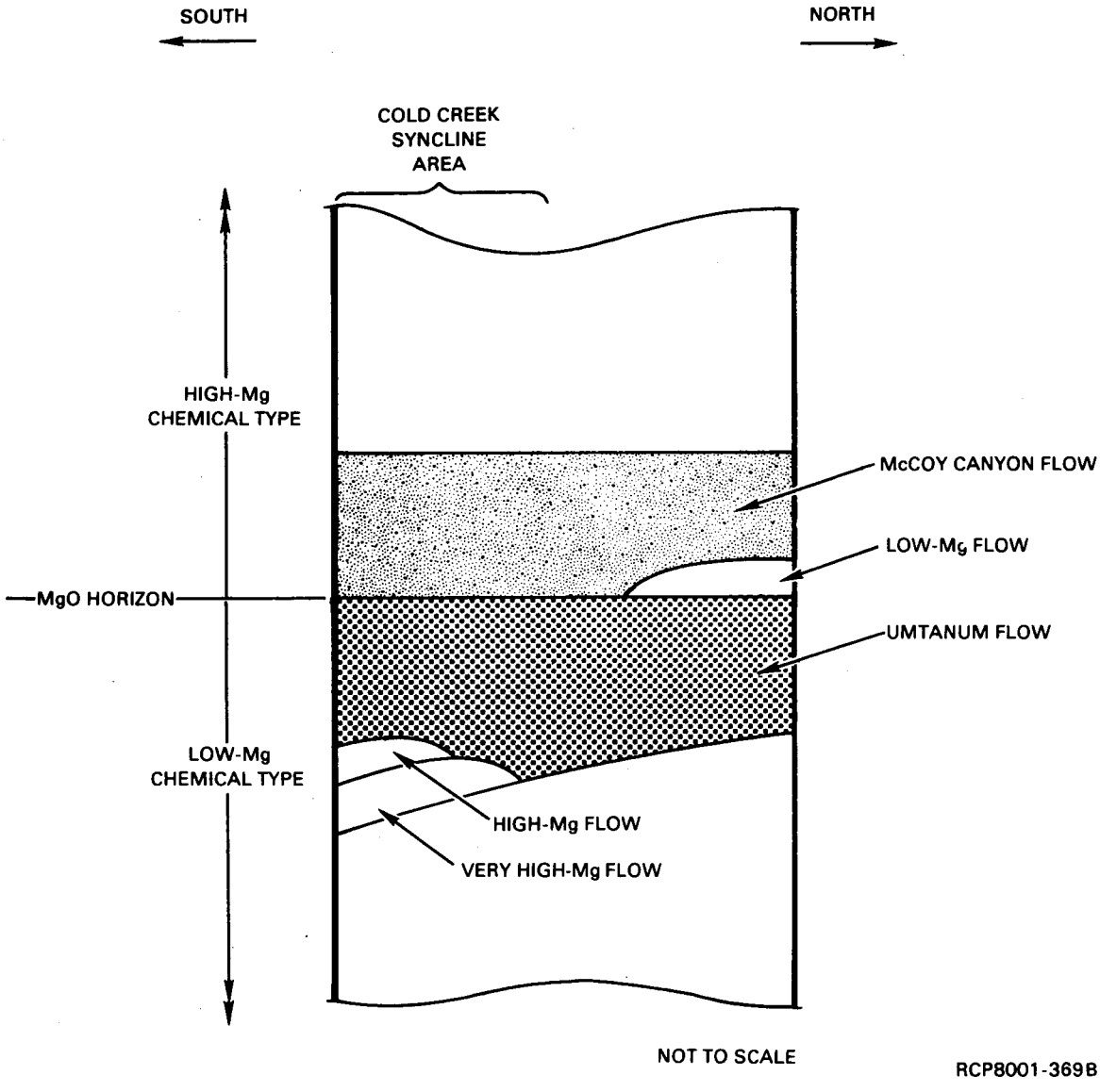

FIGURE 4-9. Stratigraphy of Grande Ronde Basalt Flows Proximal to the Magnesium Horizon. Stratigraphic relationships are based on major element chemical composition of flows.

SCHWANA SEQUENCE

The entire Schwana sequence consists of low-Mg flows, except for three flows occurring near the top of the sequence. The lowermost of these three flows is the very-high-Mg chemical type described in Long and others (1980); this flow occurs two to four flows below the Mg horizon (Fig. 4-9). It is recognized by MgO content (≥5.53%) and TiO_2 content (≤1.80%) (Fig. 4-4) and apparently occurs as a single flow which is limited to the central and southeast parts of the basin (Fig. 4-10). This is based solely on correlation between boreholes, because the very-high-Mg flow does not crop out in the Pasco Basin or surrounding area. It is possible, however, that it correlates or is related to a very-high-Mg flow cropping out to the east along the Snake River (Swanson and others, 1979b).

Two flows of high-Mg chemical type are intercalated with the low-Mg flows in the upper part of the Schwana sequence. The lower of these flows is found only in DC-12 and RSH-1 (Fig. 4-11), where it is stratigraphically equivalent to the very-high-Mg flow. The age relation between these two flows is indeterminant, but flow distributions suggest that the very-high-Mg flow is the older flow. The upper high-Mg flow in the Schwana sequence is found only in the extreme southern portion of the basin and has not been penetrated north of DC-7/8 or DC-12 (Fig. 4-11).

The Umtanum flow lies directly below the Mg horizon (except in DH-4). This flow is recognized on the basis of unusual thickness, major and trace element chemistry, and paleomagnetic inclination. It has distinctly higher TiO_2 content (Fig. 4-4) than other low-Mg flows in the upper portion of the Schwana sequence; hence, it is considered a chemical subtype of the low-Mg chemical type.

In DH-4, a single flow 26 m thick of low-Mg chemical type overlies the Umtanum flow; this is the only core well in which the Umtanum is not the youngest flow of the Schwana sequence. However, a similar situation occurs west of the Emerson Nipple section where a single thin flow of intermediate-Mg composition crops out between the Schwana and Sentinel Bluffs sequences. This flow directly overlies the Umtanum flow (Price, in press). It is noteworthy that, whereas the flow overlying the Umtanum in DH-4 is considered to have low-Mg chemical composition, it does lie more toward the high-Mg composition than most low-Mg flows. Thus, it may be closely related to the intermediate-Mg flow west of Emerson Nipple.

Within the low-Mg flows underlying the Umtanum flow, five chemical units have been suggested by Myers, Price and others (1979). These units occur in DH-4 and DH-5 and are based on Mg and Ti variations between flows in these two boreholes. Data from two additional boreholes (DC-7 and DC-12; Appendix A) which have been drilled to depths great enough to encounter extensions of these units in the southern part of the basin are currently being examined.

Three paleomagnetic, secular-variation units have been found in the R_2 polarity unit: $R_2\alpha$, $R_2\beta$, and $R_2\gamma$ (Van Alstine and Gillett, in press). Lack of paleomagnetic data from sufficiently deep boreholes prevents extensive correlation of these units. Data currently being acquired will help determine their lateral extent.

Within the normal polarity portion of the Schwana sequence, two secular-variation units occur: $N_2\delta$ and $N_2\varepsilon$ (Fig. 4-7). All flows above the R_2-N_2 polarity horizon are within the N_2 , except for the upper one to three flows of the Schwana sequence which are contained in the $N_2\delta$. The $N_2\delta$ secular-variation unit consists principally of one flow, the Umtanum flow, except in DH-4 and the Sentinel Gap field section where one or two additional flows are present. Also, in DDH-3 and possibly DC-4, the Umtanum flow exhibits flow lobes near its top which are part of the $N_2\delta$.

SENTINEL BLUFFS SEQUENCE

The Sentinel Bluffs sequence consists of 7 to 10 flows all of high-Mg chemical type and all within the N_2 polarity unit. The McCoy Canyon flow is the lowermost flow in the Sentinel Bluffs sequence. It is the type flow for the McCoy Canyon chemical subtype (Long and others, 1980) of the high-Mg chemical type flows. On an MgO versus TiO_2 variation diagram (Fig. 4-4), the McCoy Canyon flow plots at the low-Mg/high-TiO end of the high-Mg flows, and its mean and standard deviation are different from the mean and standard deviation of high-Mg flows in general (Fig. 4-4).

Within the Sentinel Bluffs sequence, two Cr horizons occur (Long and others, 1981). The lower horizon is marked by a lower Cr content in flows underlying the horizon and higher Cr content in flows overlying it. The upper horizon is marked by a single flow of low Cr overlying three to four flows of somewhat higher Cr content. These horizons are illustrated in Figure 4-6.

Three, magnetostratigraphic, secular-variation units occur in the Sentinel Bluffs sequence. The base of the $N_2\gamma$ coincides with the Mg horizon. The top of the $N_2\gamma$ lies one to four flows above the base and corresponds to the lower Cr horizon. The $N_2\beta$ unit is the next recognizable unit and its upper boundary lies two to four flows below the top of the Sentinel Bluffs sequence and is coincident with the upper Cr chemical horizon. The $N_2\alpha$ unit contains the upper two to four flows of the sequence.

Paleomagnetic secular variation and Cr content thus provide two independent bases of subdividing the Sentinel Bluffs sequence. These two techniques are consistent with each other, providing nearly identical correlation of flows. Only one correlation discrepancy occurred in one borehole and, in this case, the paleomagnetic data may be subject to reinterpretation. Moreover, these correlations reduce the numbers of flows (one to four) in each unit such that individual flows can be correlated from borehole to borehole on the basis of their thickness and/or position

in the unit. Trace element and paleomagnetic analyses are two extremely valuable techniques which allow the subdivision of an otherwise monotonous sequence.

One flow or group of flows may be correlated using borehole lithologic logs. This is the Sentinel Bluffs through-runner described in Myers, Price and others (1979). This unit consists of a single cooling unit with a well-defined vesicular zone two-thirds from the base into the flow. This vesicular zone has a characteristic signature on density and transit time geophysical logs and is traceable throughout the basin, except in DC-15 and DDH-3 where the unit thins abruptly. This is interpreted to mean that two separate flows or lobes from the same flow erupted nearly simultaneously with one covering the other before the lower unit could cool completely. They then cooled as a single cooling unit; apparently, there was sufficient time for the lower flow to vesiculate prior to burial by the later unit. The later unit apparently did not extend as far south as DC-15 and DDH-3.

THICKNESS AND LATERAL CONTINUITY

Several factors govern flow thickness and lateral extent of individual flows in the Grande Ronde Basalt. They include flow volume, rate of eruption, flow viscosity, and topographic features which may be the result of structural deformation, erosion, or constructional topography caused by previous flows.

Flow volume is a primary control on the lateral extent of a flow as well as its thickness. All other factors being equal, a flow with a small volume is unlikely to extend as far as one with a larger volume. Large differences in viscosity, on the other hand, could cause flows of equal volume to differ in lateral extent and thickness (assuming they were extruded onto planar surfaces of equal dip). The flow with high viscosity would tend to be thicker, but less extensive. The great lateral extent of many Columbia River basalt flows (e.g., the Roza [Swanson and others, 1979a]) suggests that these flows were necessarily of relatively low viscosity. Compositional ranges of Grande Ronde Basalt are not great and do not suggest large differences in viscosity among flows. For this reason, we assume that viscosity of flows does not play a large role in determining extent and thickness of flows. Apparently, Grande Ronde flows were highly fluid and thus tended to form an accurate mold of topography over which they were emplaced, <u>if</u> they were of sufficient volume.

Eruption rate may affect flow thickness and extent by determining, in part, the ability of a flow to build natural levees. Presumably, a relatively low or pulsating eruption rate will lead to higher natural levees and greater channelling of the flow. Thus, a flow erupted onto a planar surface might develop differences in thickness as a result of the channelling. There is considerable evidence, however, that Columbia River basalt flows were emplaced rapidly (Shaw and Swanson, 1969). This does not rule out the possibility that levees and channelling could occur, but rapid emplacement and low viscosity together suggest that such effects will be minimal, on an order of 10 m at most for a thick flow.

This suggests that for thick (>40-m), widespread flows, the principal control on flow thickness is topography (also see Chapter 5). Structural deformation is obviously an important cause of topography on the Columbia Plateau and this is reflected in Wanapum and Saddle Mountains Basalt flow distributions (Reidel and others, 1980) and to a lesser extent in Grande Ronde Basalt flows (Long and others, 1980). Flows typically may thin over a developing anticlinal structure or they may thin over a larger area in response to more regional tilting or subsidence. Topography can also result from erosion. The formation of incised canyons is particularly significant for the plateau, in that such features form natural channelways for lava and give rise to intracanyon flows with narrow, tongue-like distribution. Moreover, flows that are intracanyon in one area are known to spread laterally where the canyon they flowed down broadened into basins (e.g., the Pomona flow [Swanson and Wright, 1976]). During Grande Ronde time, the rate of extrusion was extremely high, such that there probably would not have been sufficient time between each flow to allow for significant incisive erosion. Rapid succession of flow emplacement is also suggested by magnetostratigraphy of Grande Ronde Basalt. Nevertheless, this possibility cannot be ruled out entirely; intracanyon flows may exist in the Grande Ronde Basalt of the Pasco Basin subsurface.

Topography results from constructional features associated with the flows themselves, such as flow edges occurring due to lack of volume, pressure ridges, or the previously mentioned lava levees. These almost certainly created topography during Grande Ronde time, but with the possible exception of flow edges, these features appear to be very limited in magnitude (i.e., on the order of a few to several meters). They also create thickness changes which occur on a spacing too fine to ascertain with borehole spacings at intervals similar to those shown in Figure 4-1. Consequently, the isopach maps which follow must be regarded as generalized, recognizing that local, minor variations in thickness must exist and that these variations likely exert a minor impact on placement of contours. The likely magnitude of fine-scale thickness differences which occur in a relatively thick flow are discussed in Chapter 5.

The principal controls, then, on the general thickness of a Grande Ronde flow are flow volume, topography created by structural deformation, and topography created by flow edges.

It is possible to distinguish among these factors if sufficient stratigraphic information is available. The effects of structural deformation, for example, should be consistently developed through time as a particular structure or basin develops. Flows should both decrease in thickness and in total number across an anticline or onto the flanks of a basin. If only a single flow thins, and the number of flows in a given area does not decrease relative to surrounding areas, then either inadequate volume or a flow edge is responsible. These two cases can be distinguished if the stratigraphy is sufficiently well known, such that an underlying or slightly earlier flow can be shown to have exerted control on the distribution and thickness of the flow in question. If no such control can be identified or if the thickness ignores distribution of surrounding flows

and the adjacent flows vary in thickness according to identified structural trends, then it can be concluded that lack of volume is controlling the thickness and distribution of the flow.

All three of the above effects occur in Grande Ronde flows and are illustrated in the isopach maps that follow. These maps are for several flows which lie stratigraphically close to the Umtanum flow, and also for the entire thickness of the Sentinel Bluffs sequence. Data from these isopachs (Fig. 4-10 through 4-16) and from a fence diagram (Fig. 4-17) show that the dominant factor controlling thickness of voluminous flows is tectonic deformation, principally regional subsidence. The distribution of one relatively thin flow is apparently controlled by lack of volume; whereas, another is controlled by constructional topography of a previous flow. It is also clear that, for some flows, limited volume and structural topography combine to limit the distribution of a flow.

The isopach maps discussed below have been drawn using two methods: (1) by using linear interpolation between points; and (2) by computer, in which a contouring program was used to fit a smooth surface to the data points. These two maps were then compared and a composite isopach was constructed. As noted above, contours represent generalized thickness trends; their placement is thought to be accurate within $\sim$2 or 3 km, but this is highly dependent on borehole spacings and upon thickness gradient. In a worst case, we expect contours could shift by no more than one contour interval as more boreholes are drilled. In the central part of the Cold Creek syncline, we expect changes to be much less; isopachs constructed prior to the drilling of DC-12 predicted the thickness of the Umtanum flow to within 0.3 m.

Very-High-Mg Flow

The very-high-Mg flow is a single flow with very limited extent (Fig. 4-10). Long and others (1980) suggested on the basis of limited data that the flow was emplaced from the east, southeast, or southwest, and showed a general thickening trend to the southwest. Two new boreholes (DC-12 and DC-15) and reanalysis of chips from a rotary borehole (RSH-1) have significantly changed this interpretation. The new data show that the flow is a single lobe apparently emplaced from the east or southeast. The flow thins and pinches out to the north, south, and west.

The observation that a later flow (Umtanum) thickens significantly to the west and northwest of the very-high-Mg flow strongly suggests that distribution of the very-high-Mg flow was principally limited on the west and southwest by lack of volume. Tectonic uplift may have played a role in determining its northern boundary.

EXPLANATION

The following isopach maps are provided in sets: (a) shows the flow thickness variation in the Pasco Basin; whereas, (b) shows the thickness variation in the Cold Creek syncline area.

See Table 3-1 for explanation.

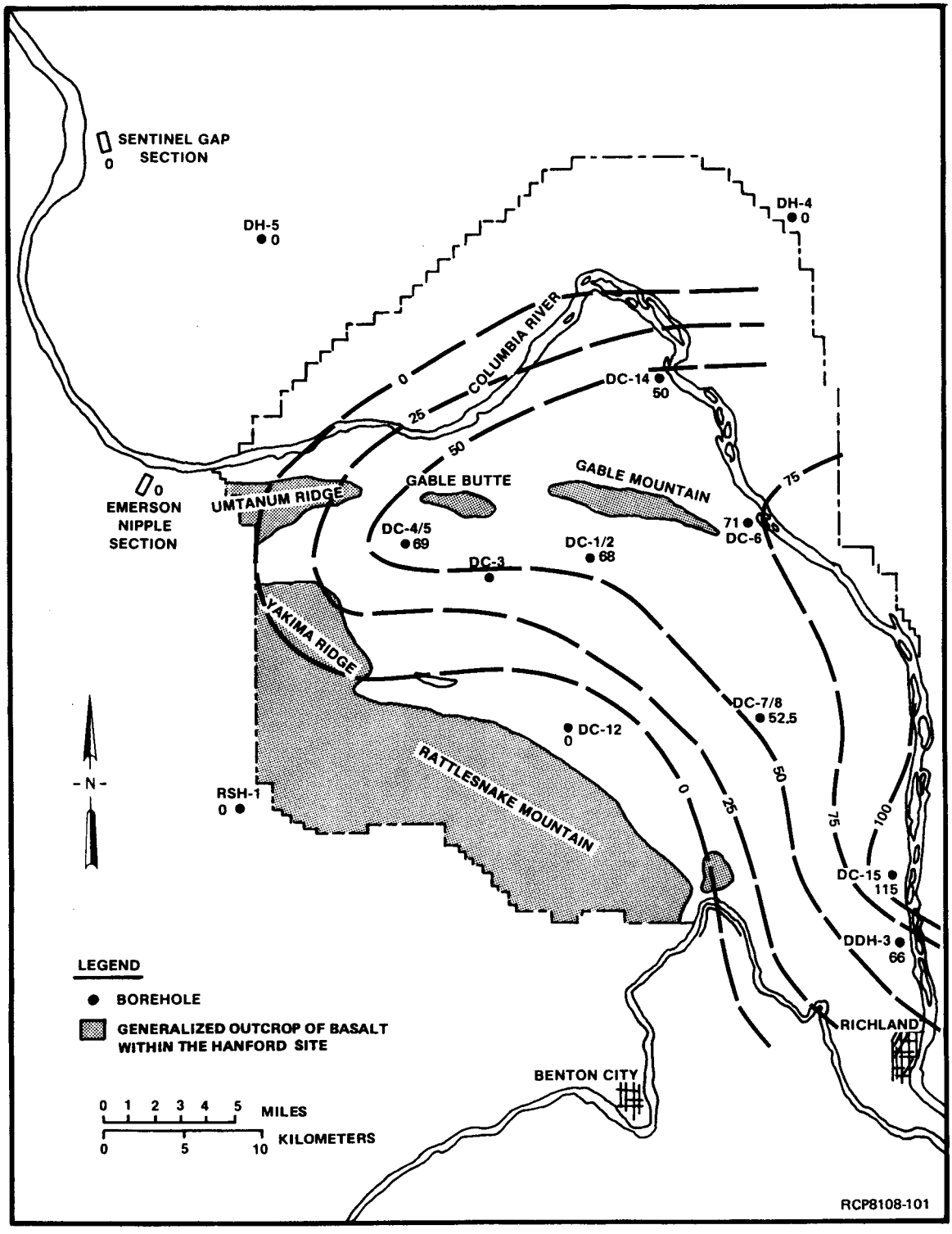

FIGURE 4-10a. Isopach Map, Very-High-Mg Flow, Pasco Basin and Vicinity.

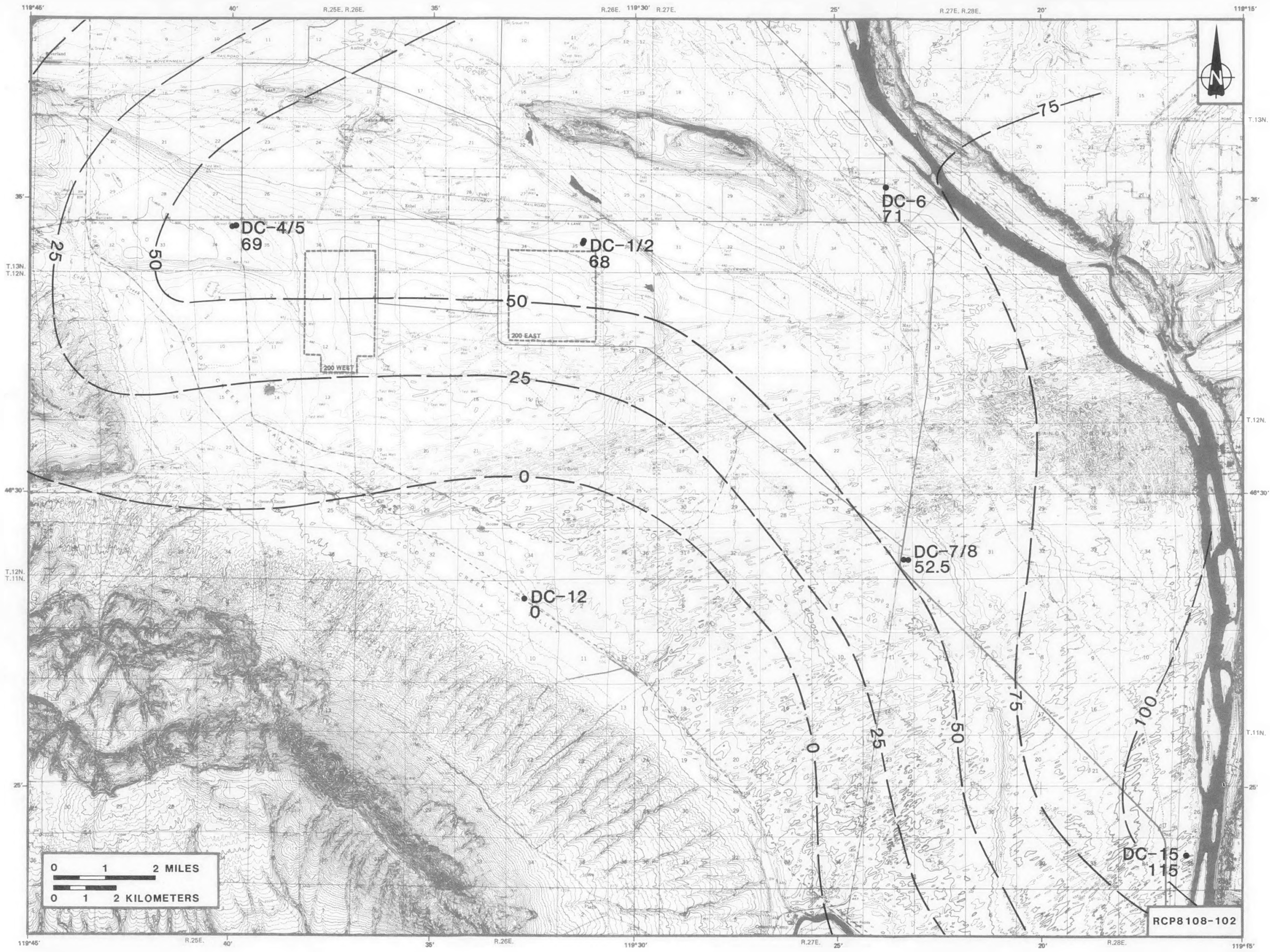

FIGURE 4-10b. Isopach Map, Very-High-Mg Flow, Cold Creek Syncline.

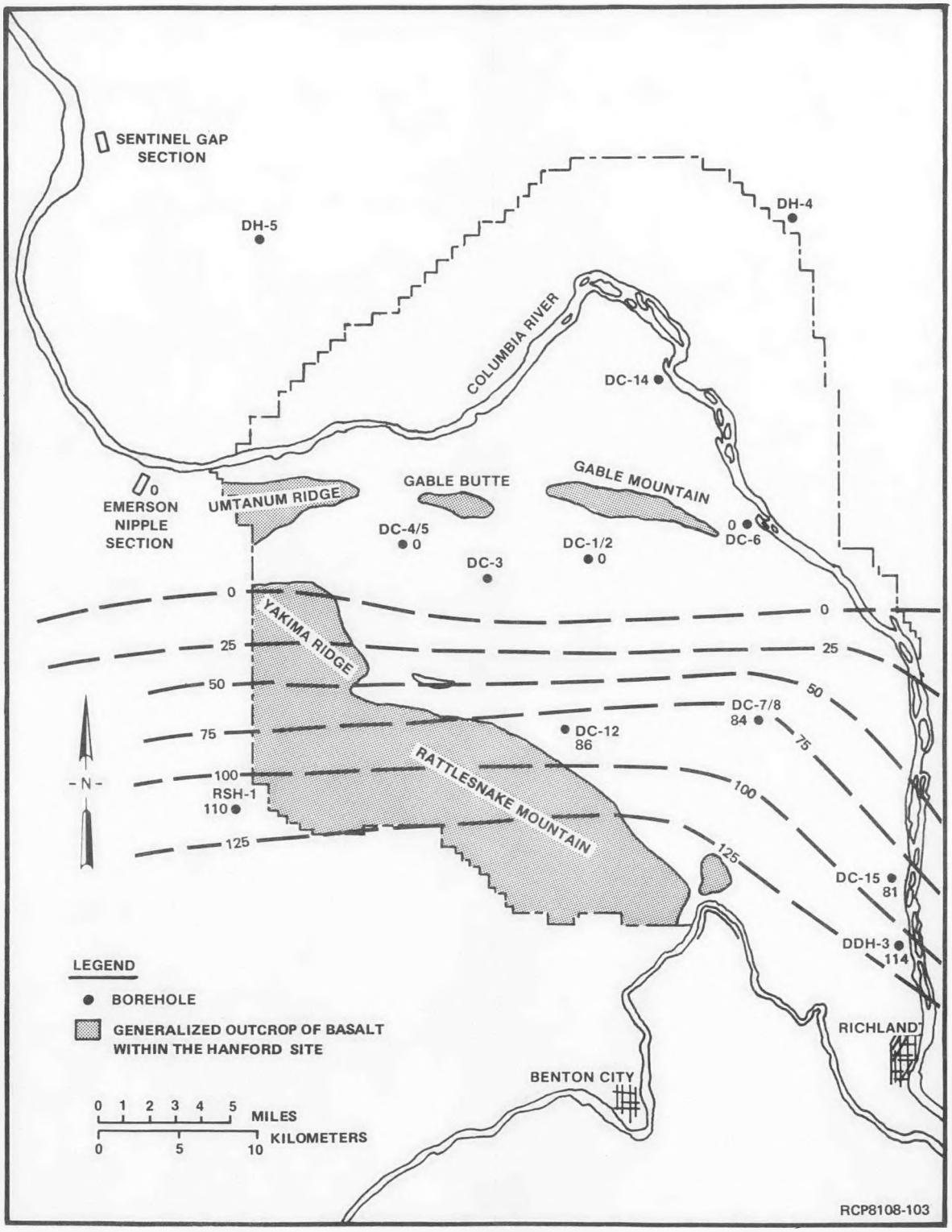

FIGURE 4-11a. Isopach Map, High-Mg Flow, Upper Schwana Sequence, Pasco Basin and Vicinity.

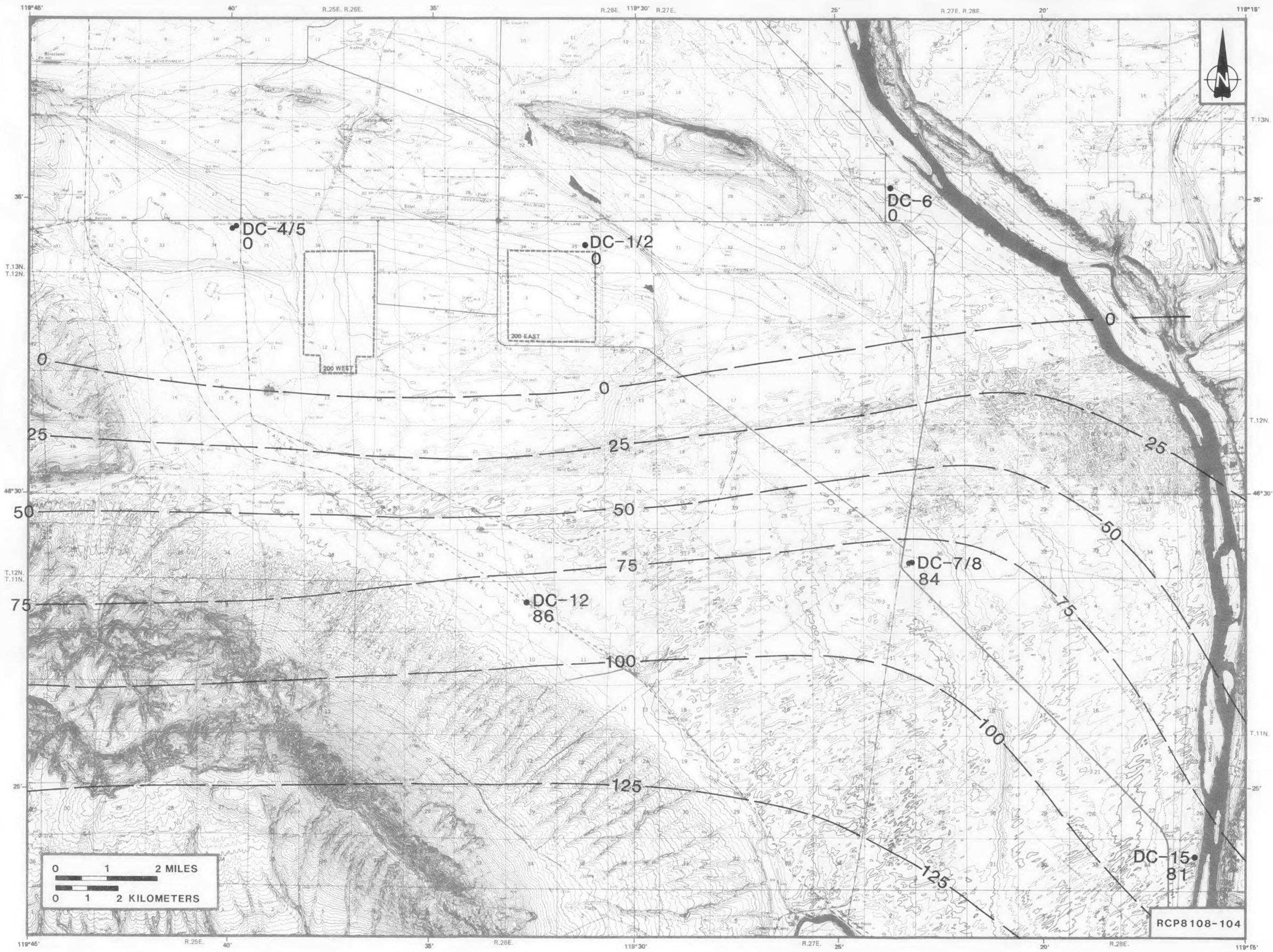

FIGURE 4-11b. Isopach Map, High-Mg Flow, Upper Schwana Sequence, Cold Creek Syncline.

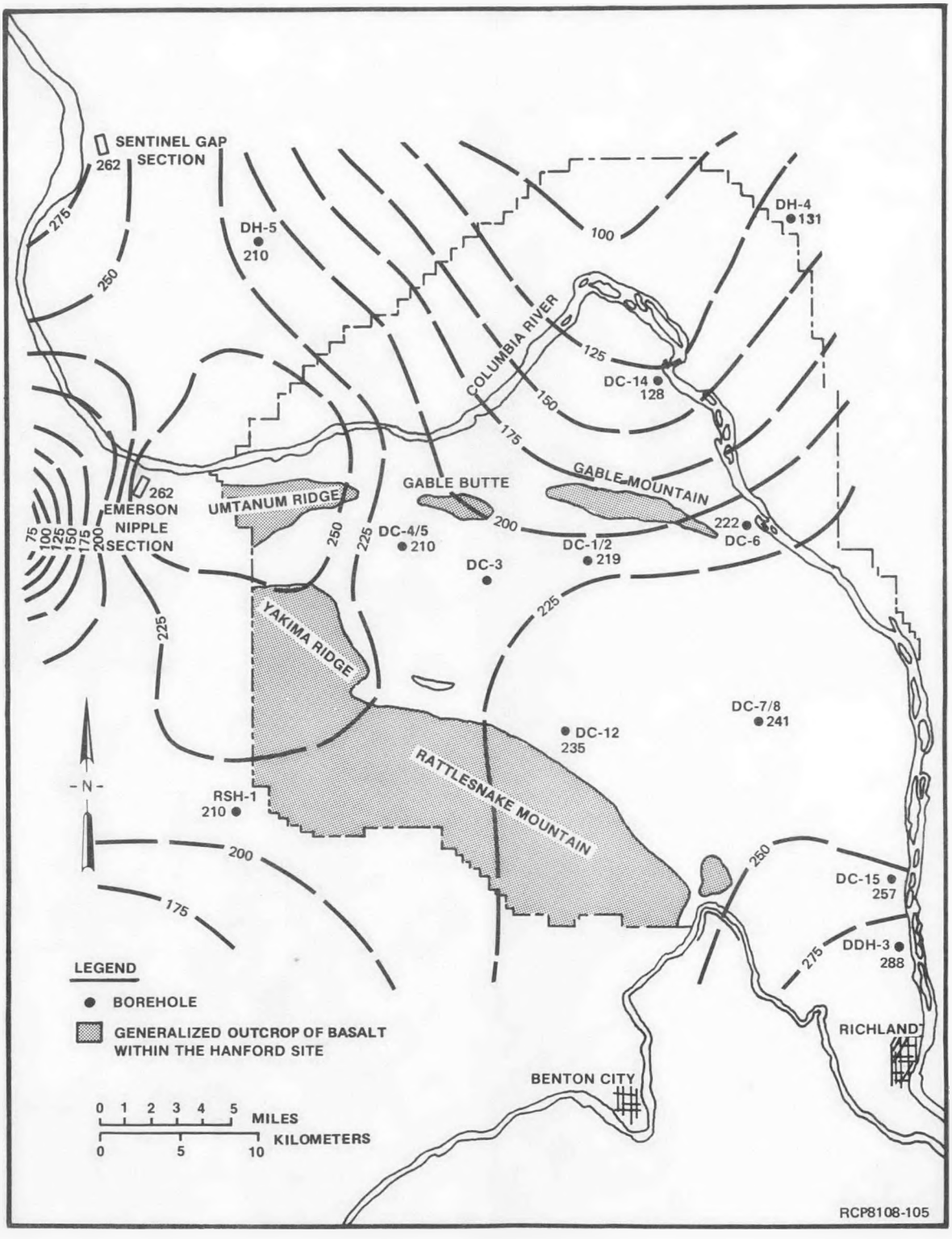

FIGURE 4-12a. Isopach Map, Umtanum Flow, Pasco Basin and Vicinity.

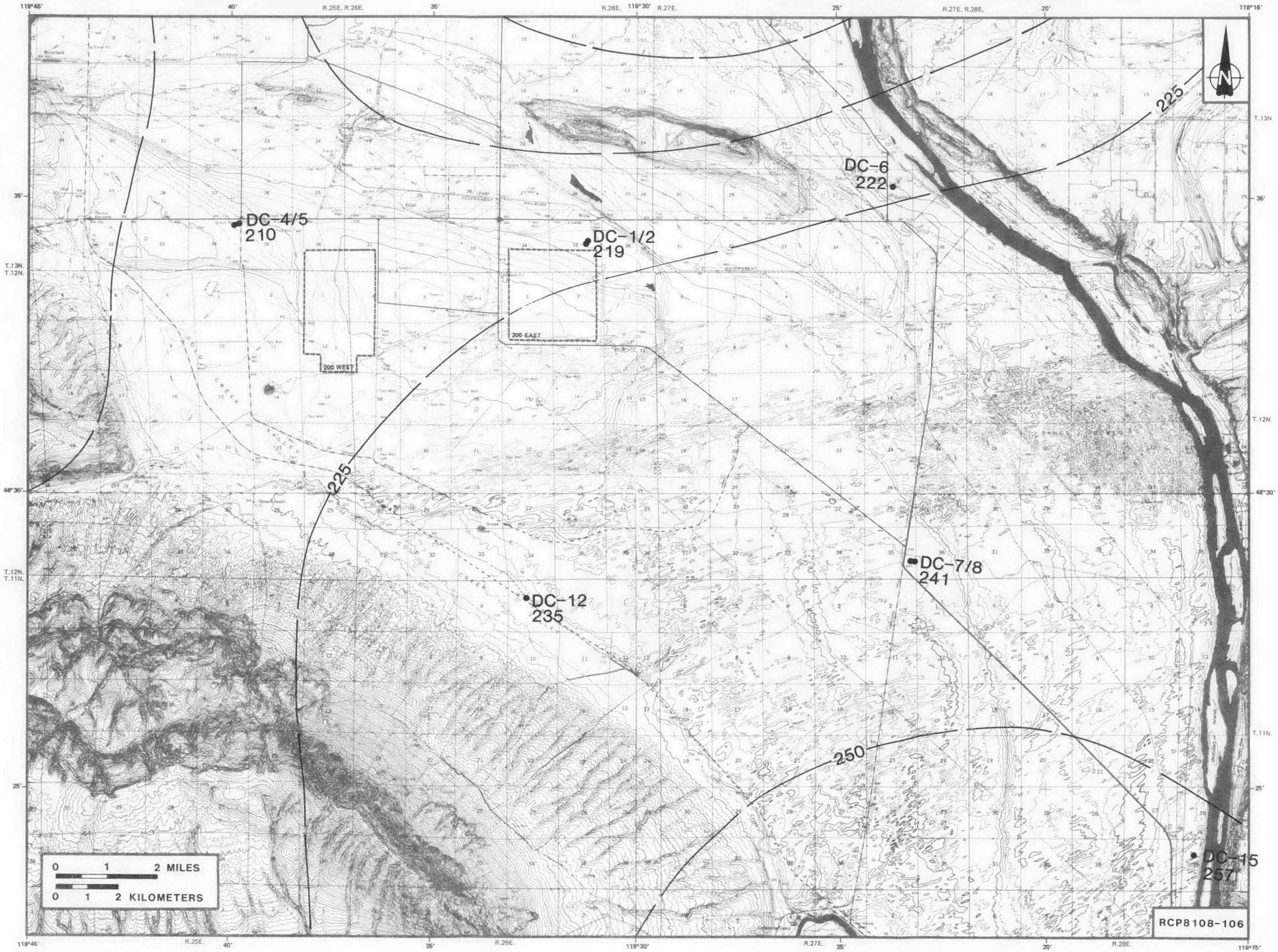

FIGURE 4-12b. Isopach Map, Umtanum Flow, Cold Creek Syncline.

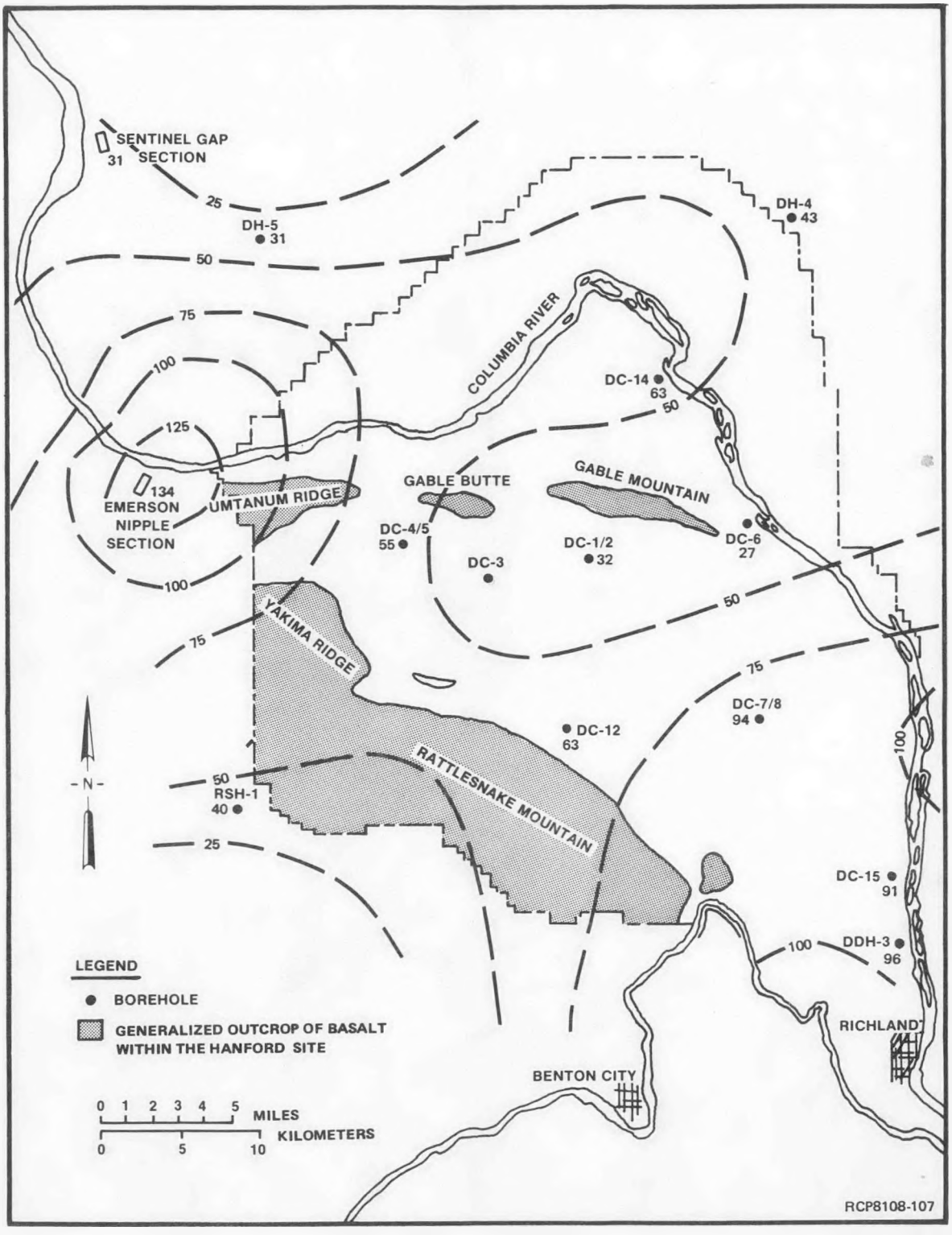

FIGURE 4-13a. Isopach Map, Flow Top of Umtanum Flow, Pasco Basin and Vicinity.

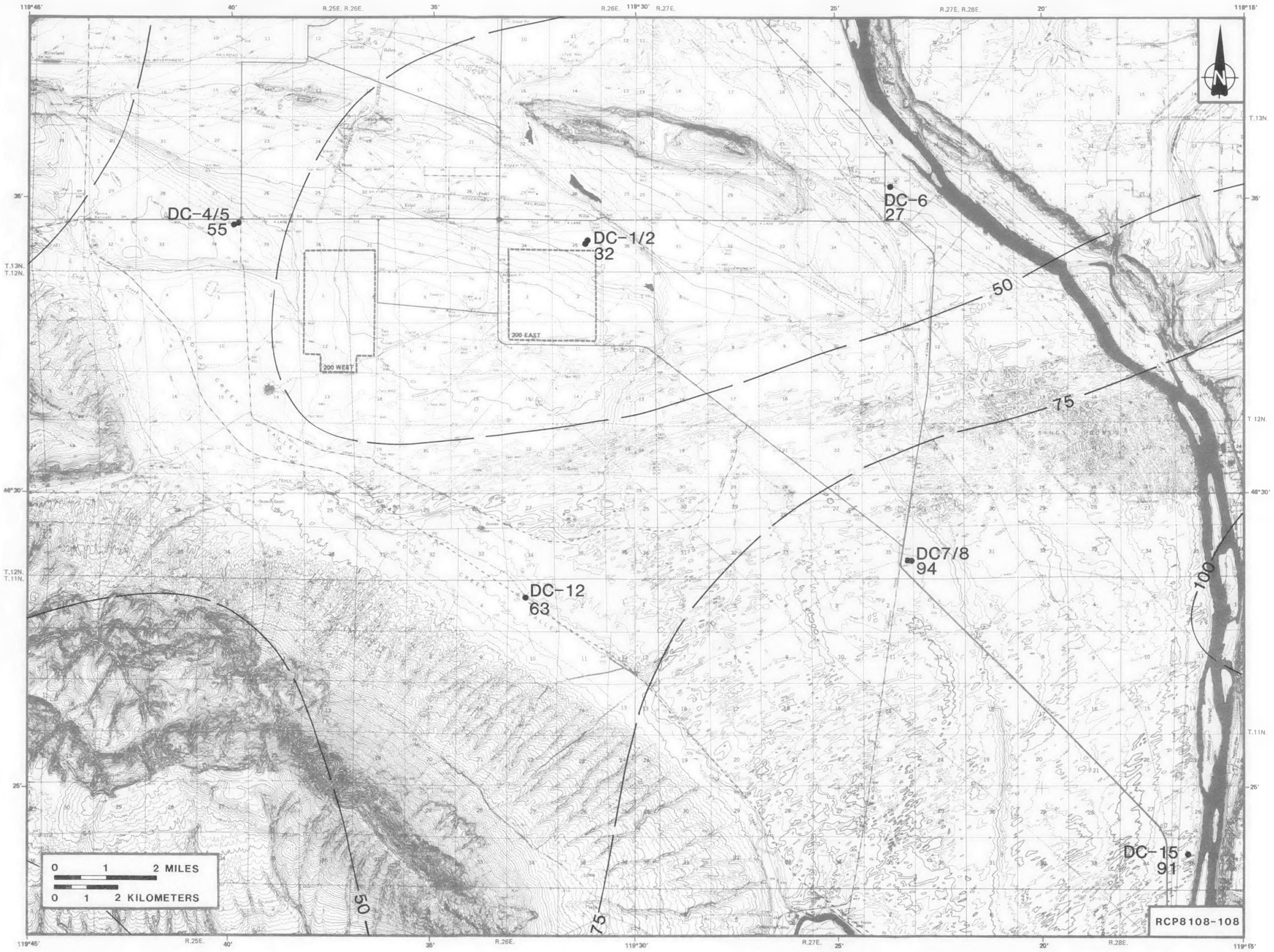

FIGURE 4-13b. Isopach Map, Flow Top of Umtanum Flow, Cold Creek Syncline.

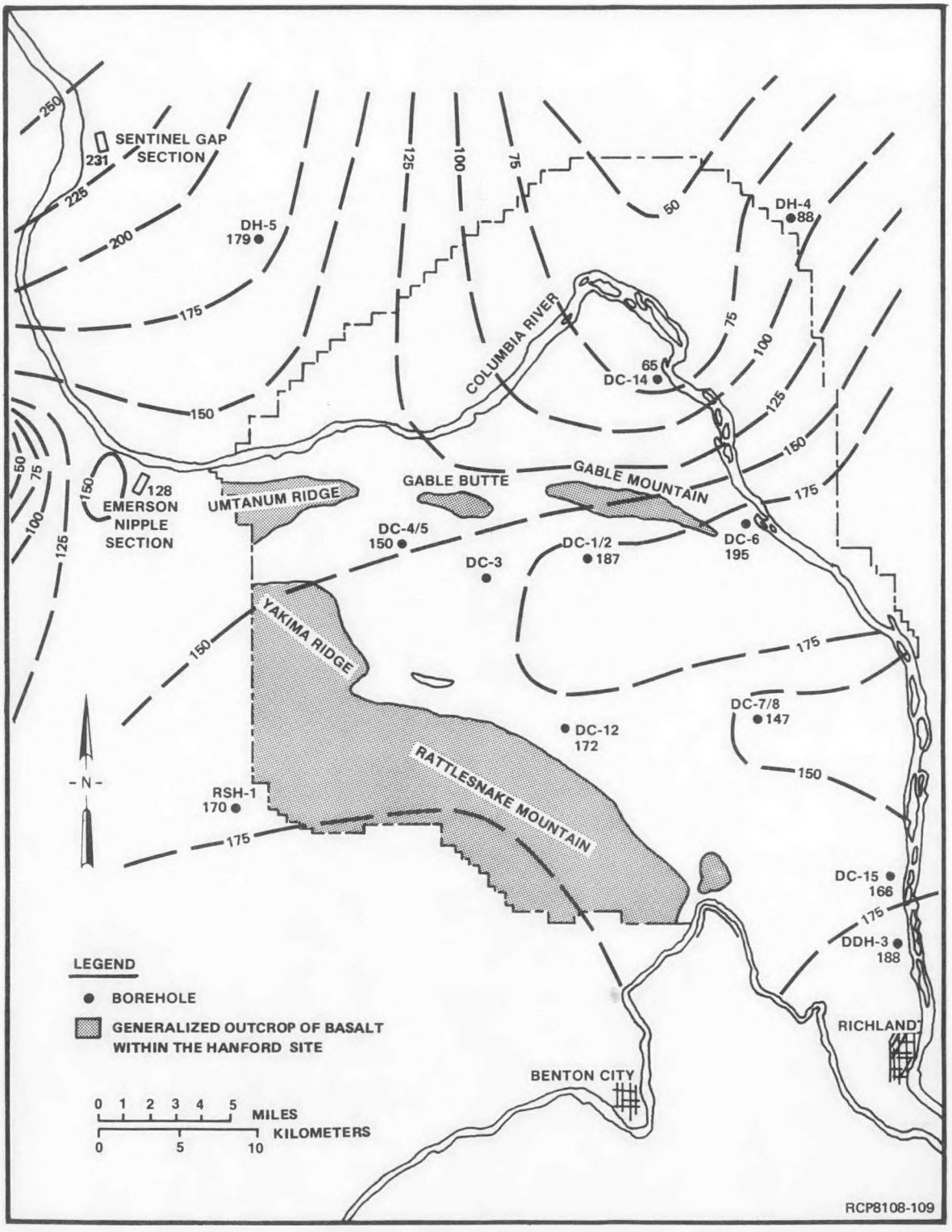

FIGURE 4-14a. Isopach Map, Interior of Umtanum Flow, Pasco Basin and Vicinity.

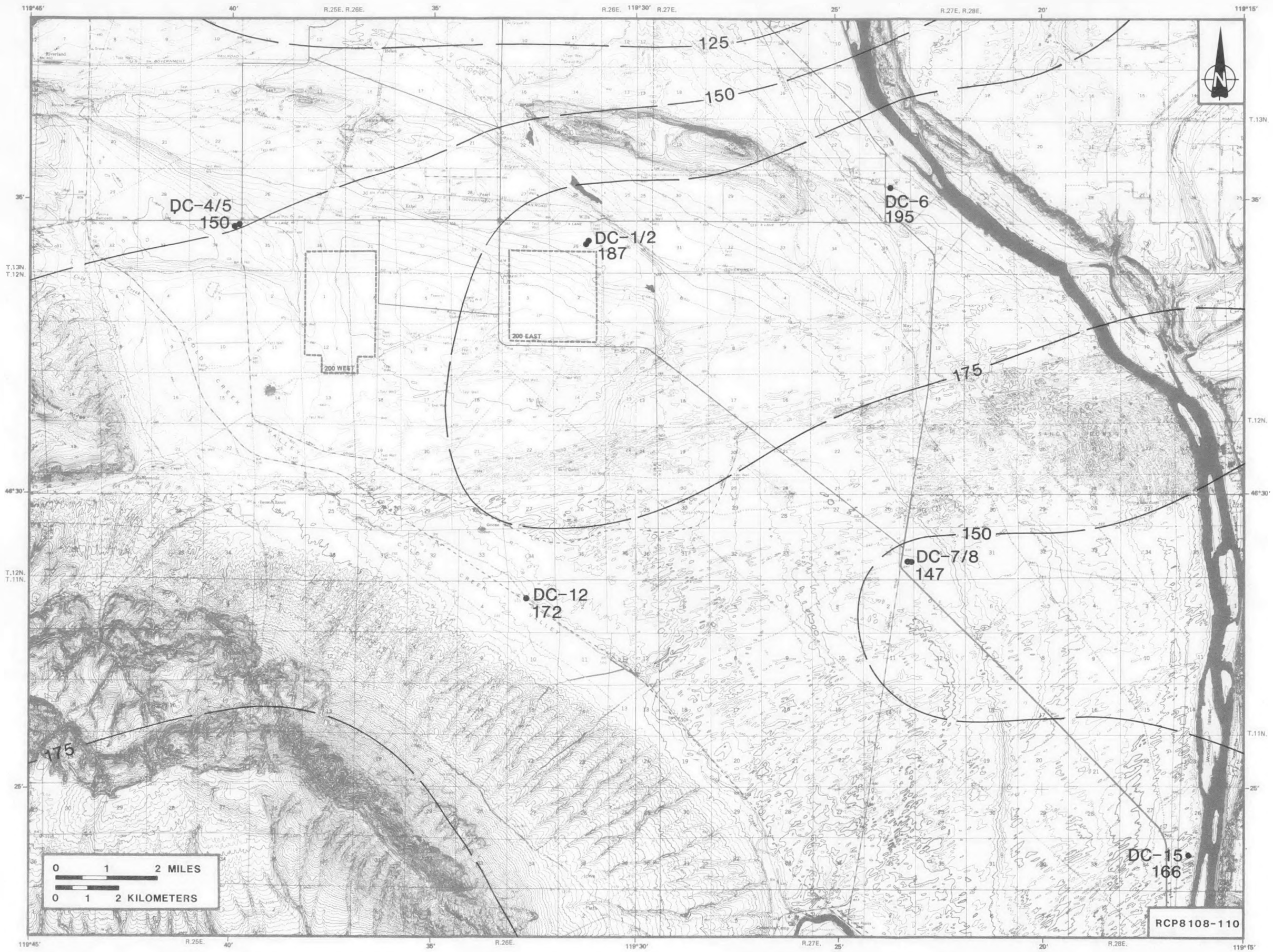

FIGURE 4-14b. Isopach Map, Interior of Umtanum Flow, Cold Creek Syncline.

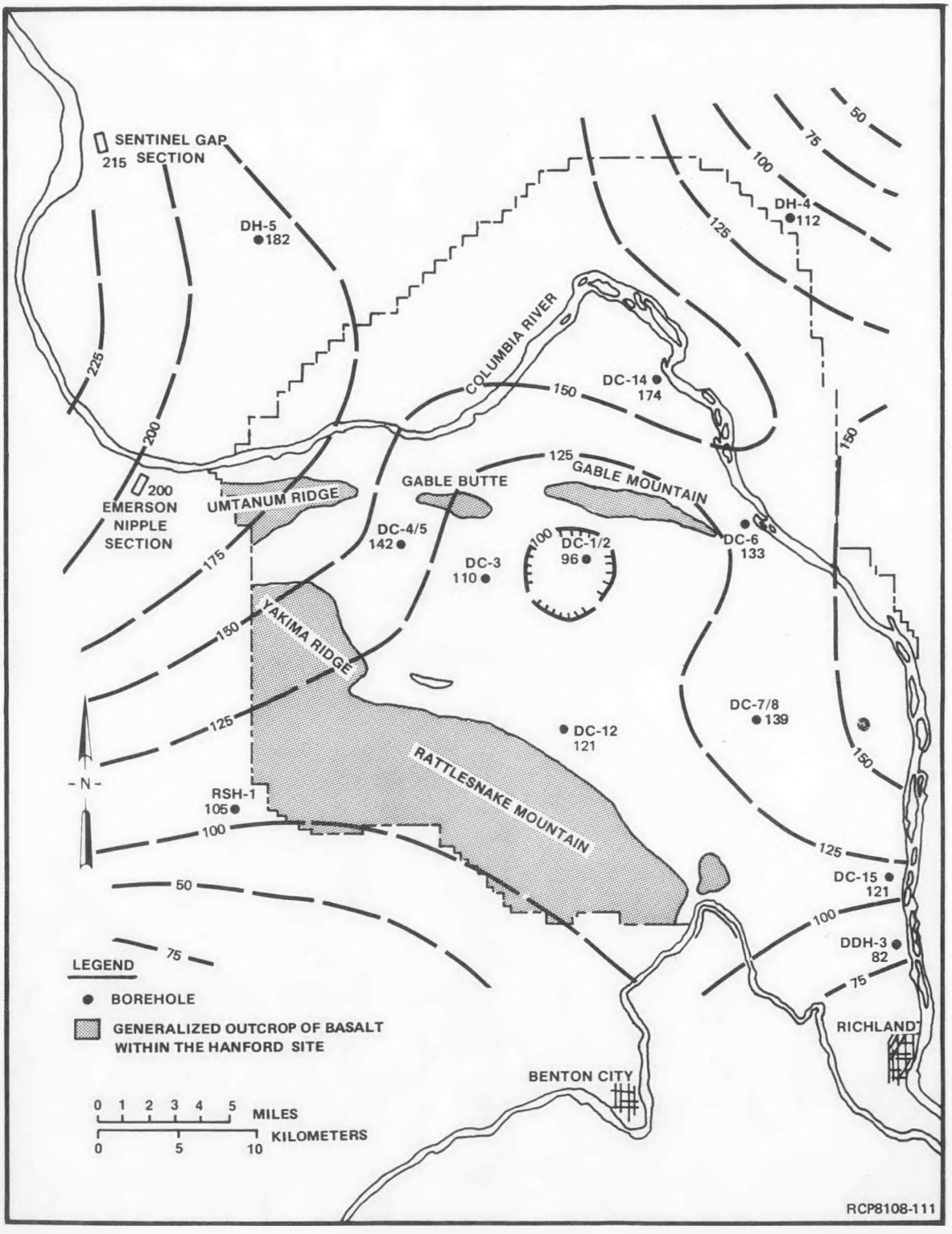

FIGURE 4-15a. Isopach Map, McCoy Canyon Flow, Pasco Basin and Vicinity.

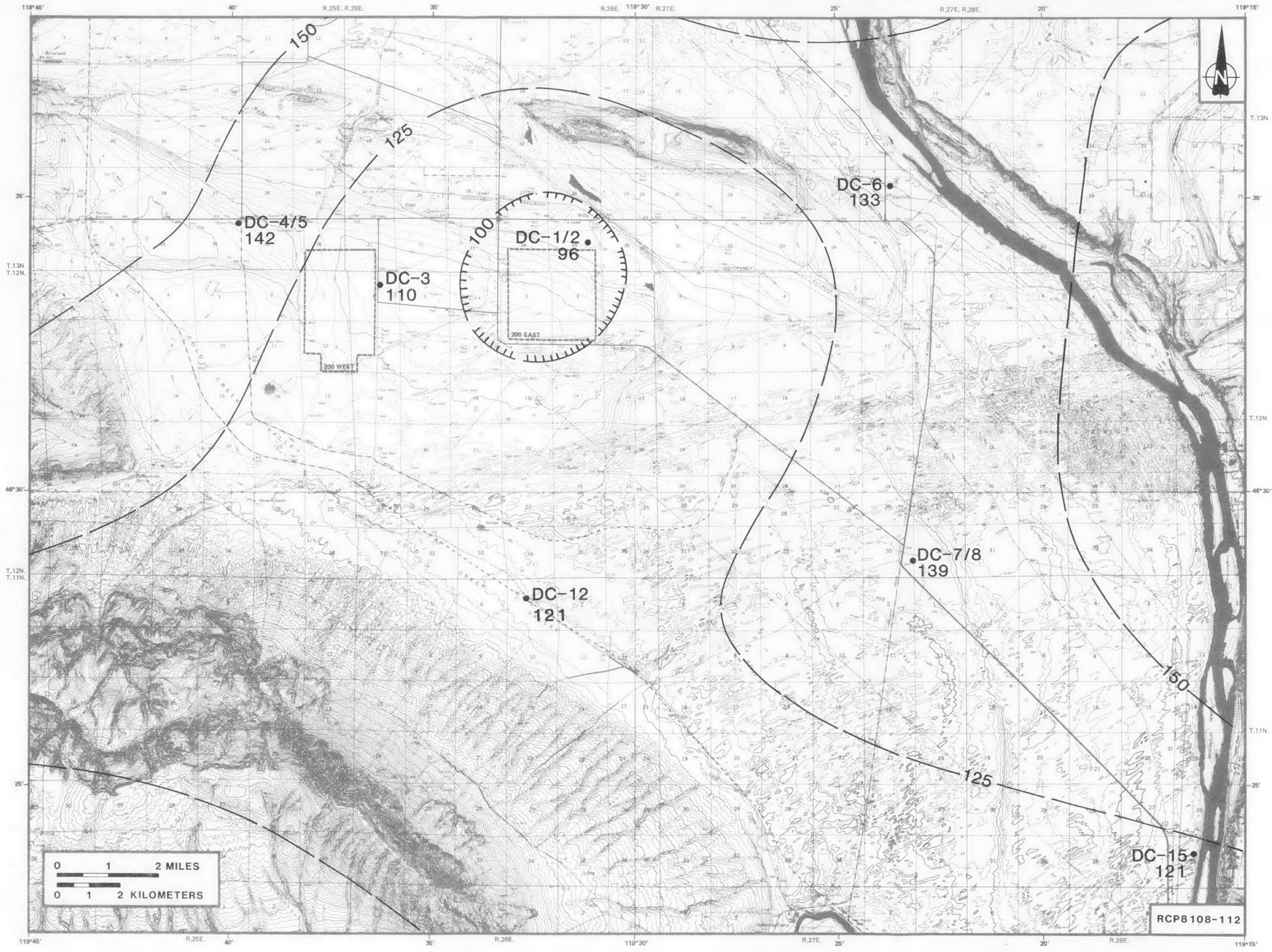

FIGURE 4-15b. Isopach Map, McCoy Canyon Flow, Cold Creek Syncline.

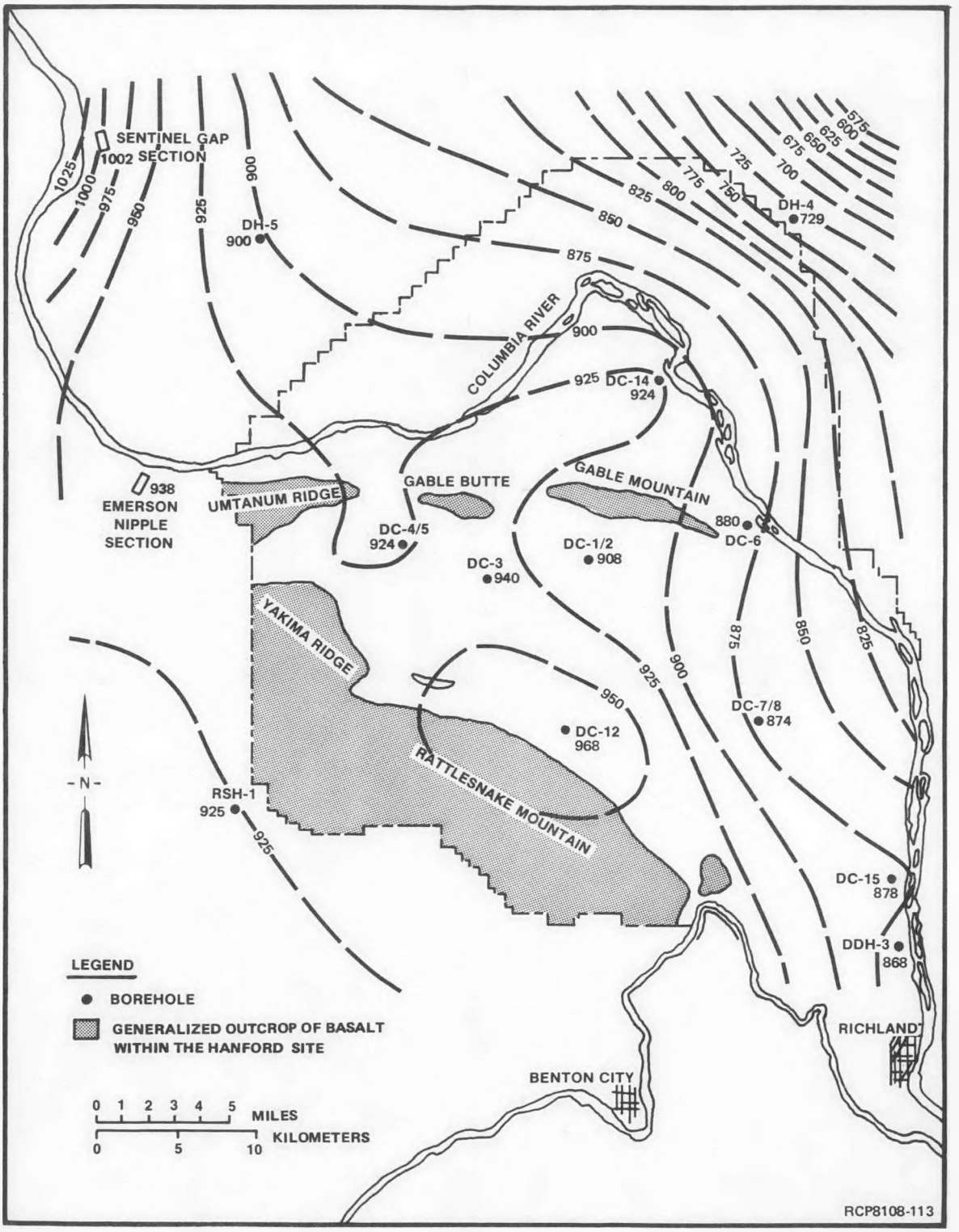

FIGURE 4-16a. Isopach Map, Sentinel Bluffs Sequence, Pasco Basin and Vicinity.

RHO-BWI-ST-14

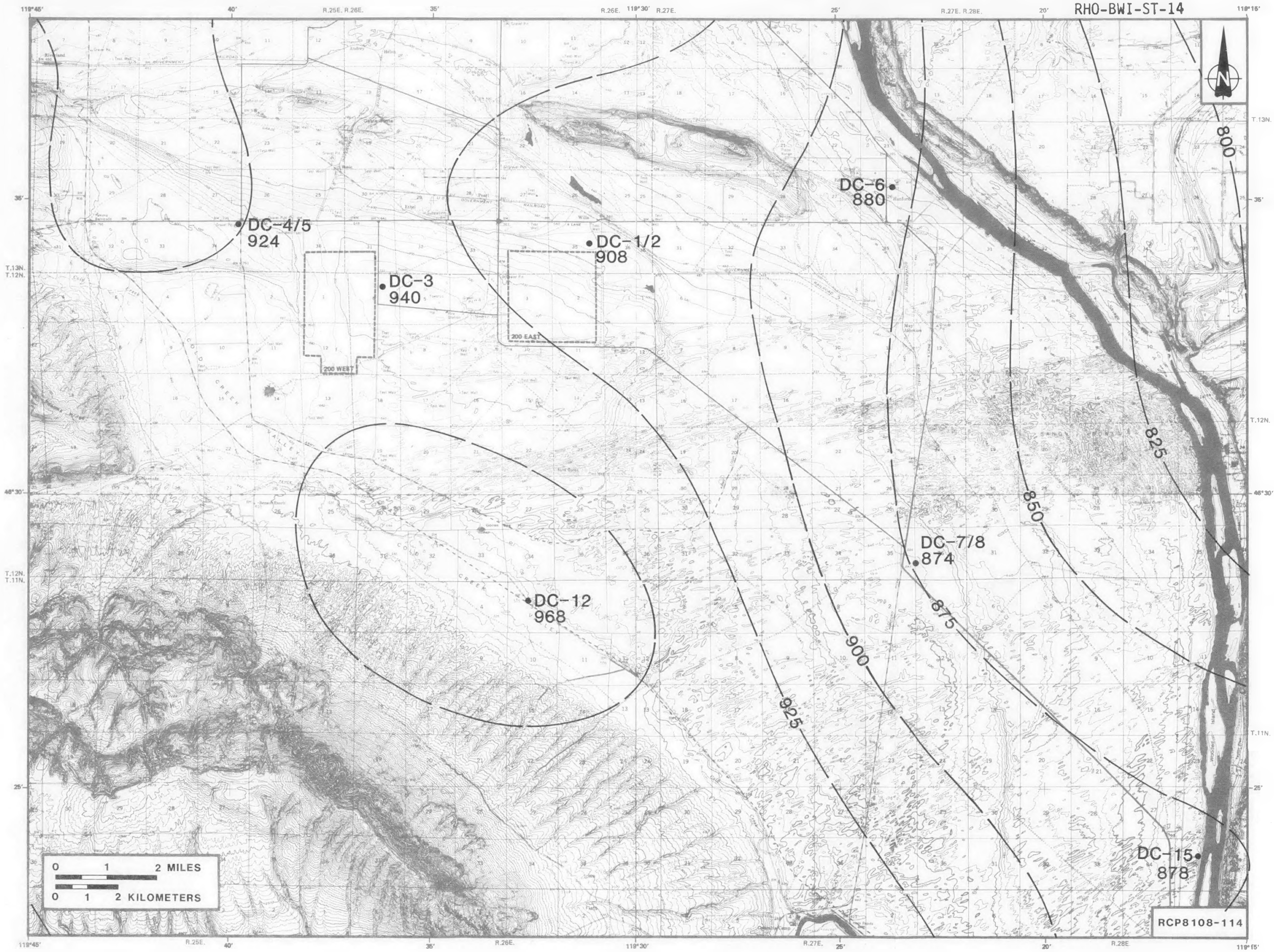

FIGURE 4-16b. Isopach Map, Sentinel Bluffs Sequence, Cold Creek Syncline.

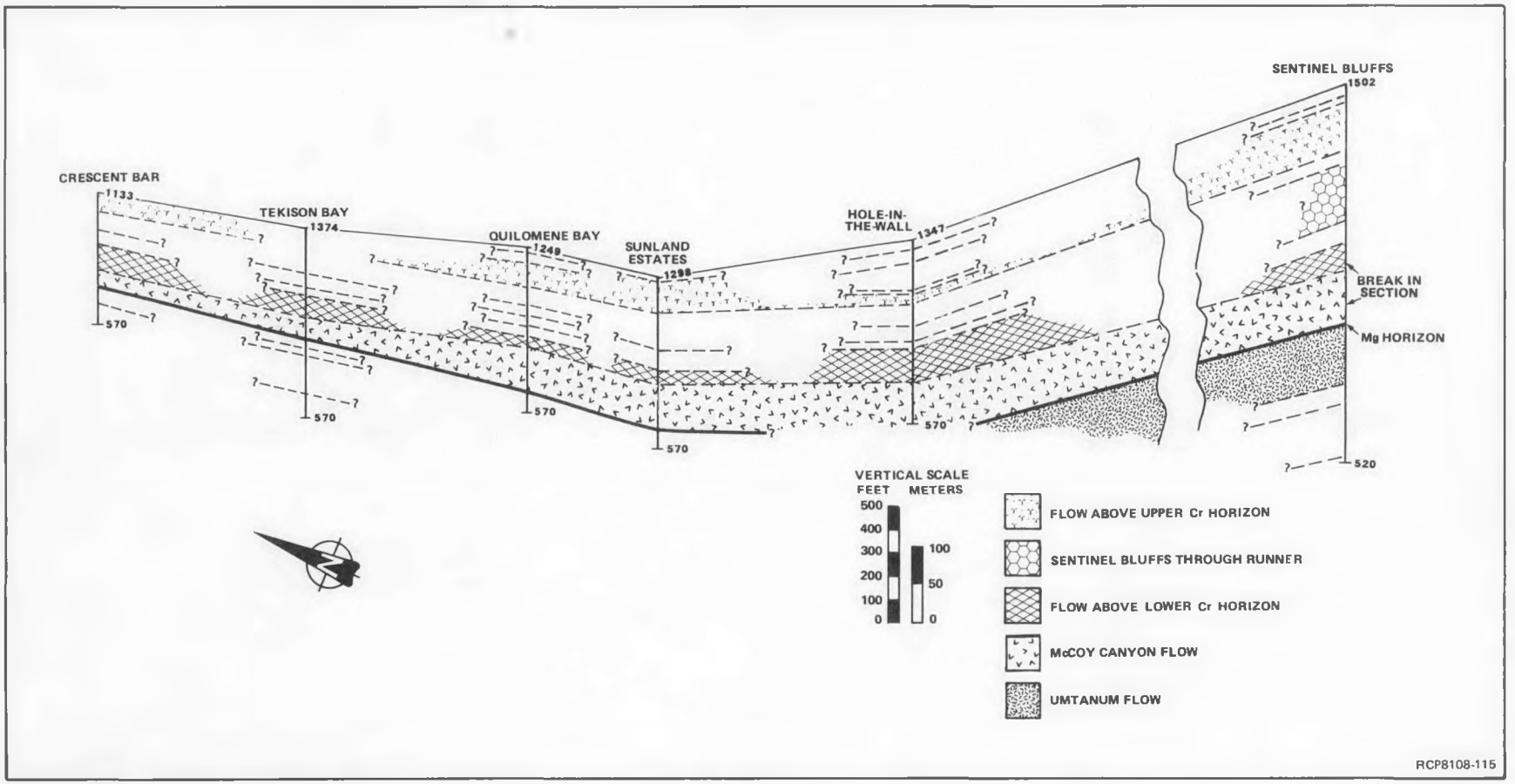

FIGURE 4-17a. Fence Diagram, Upper Grande Ronde Basalt, Crescent Bar to Sentinel Bluffs.

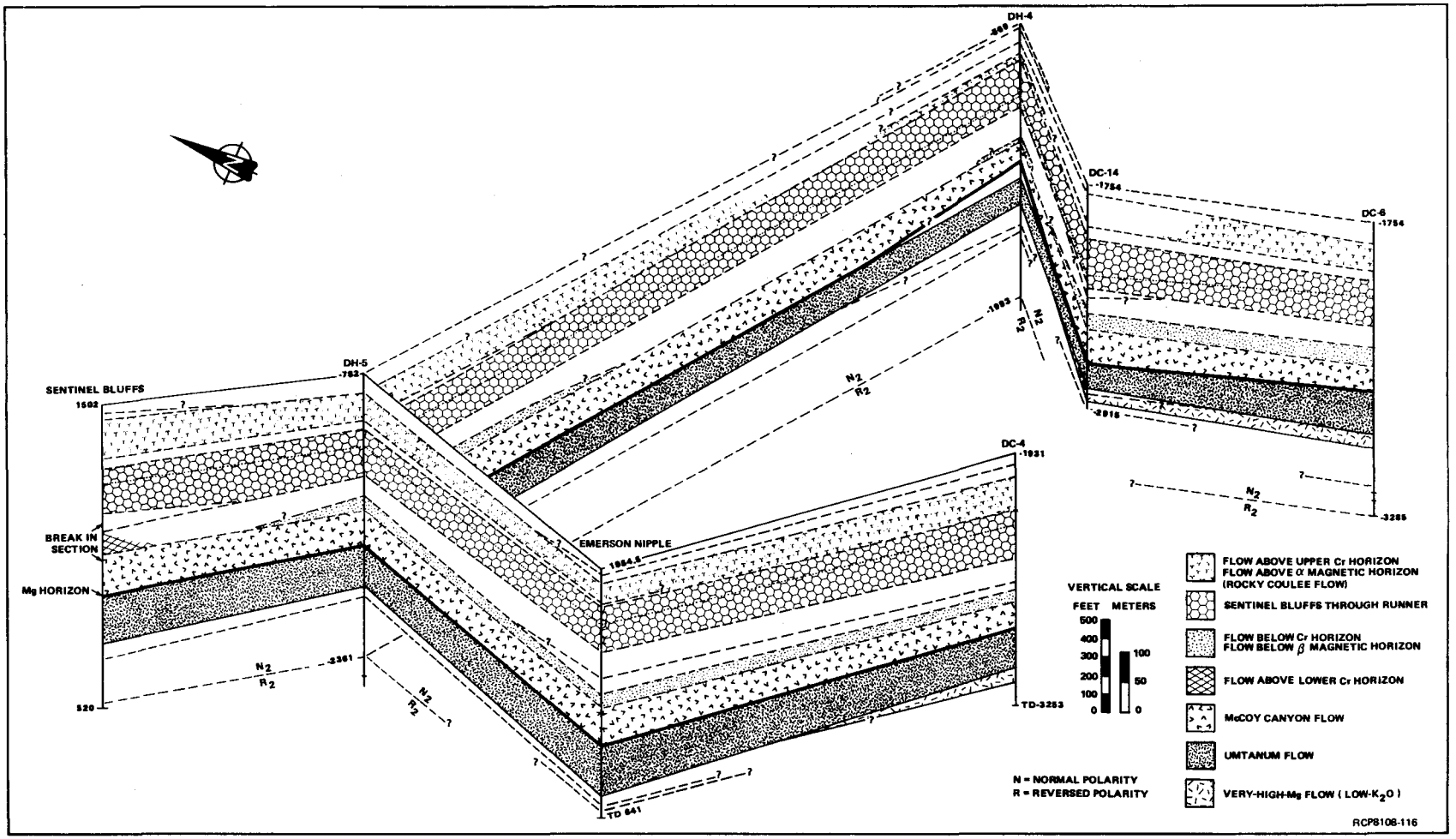

FIGURE 4-17b. Fence Diagram, Upper Grande Ronde Basalt, Sentinel Bluffs to Borehole DC-6.

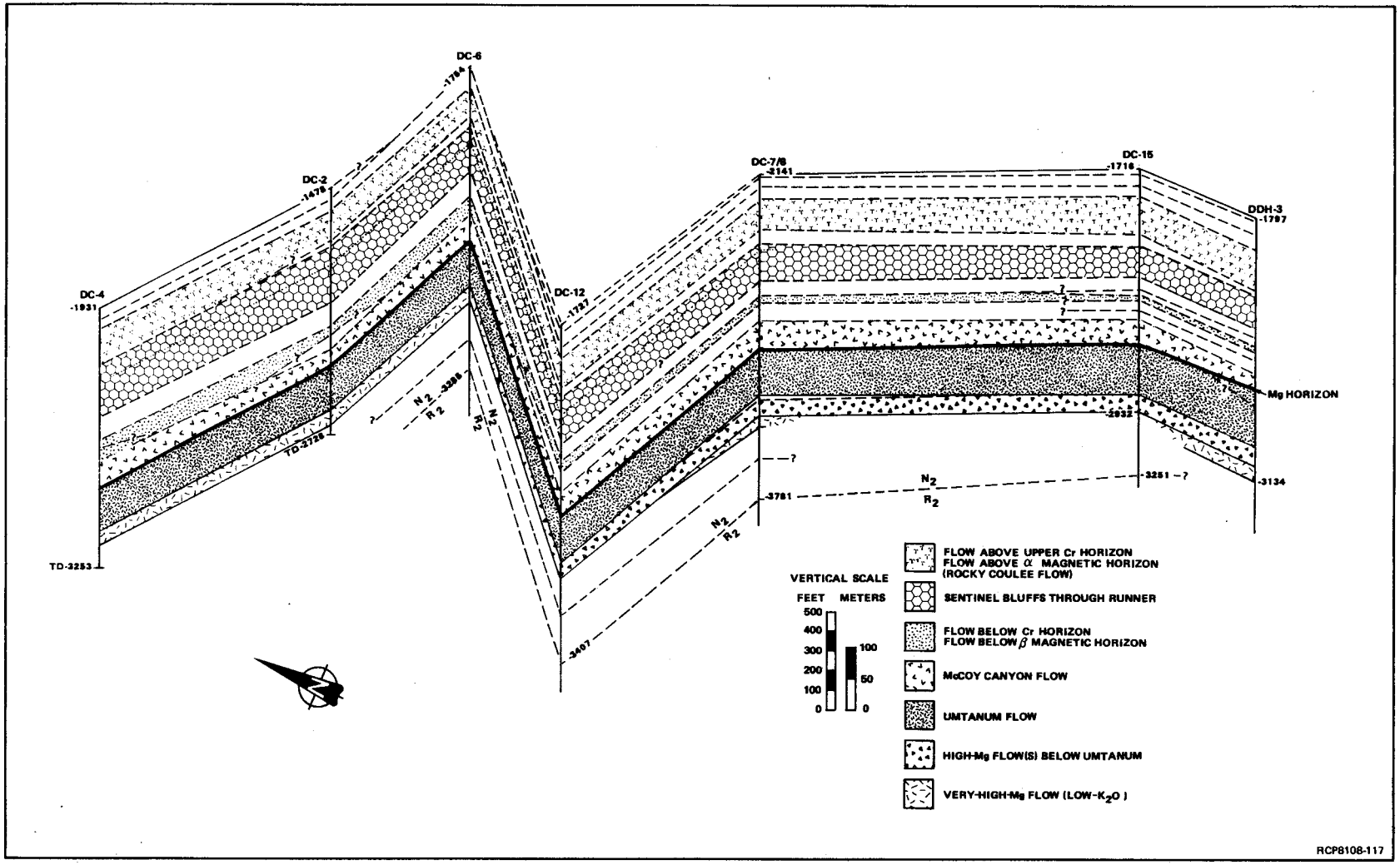

FIGURE 4-17c. Fence Diagram, Upper Grande Ronde Basalt, Boreholes DC-4 to DDH-3.

High-Mg Flows

The two high-Mg flows found within the Schwana sequence have only limited distribution and are not found north of RSH-1, DC-12, and DC-7/8 (Fig. 4-11). The lower flow is found only in RSH-1 and DC-12. The upper flow is found in RSH-1, DC-12, DC-7/8, and in wells farther south.

The distribution of very-high-Mg and high-Mg flows is an interesting problem. Was the southern extent of the very-high-Mg flow limited by the northern flow front of the lower high-Mg flow or was the very-high-Mg flow already in place and blocked the northward movement of the lower high-Mg flow? Although either model may be argued, the latter model is the simplest and seems to be the most internally consistent. The very-high-Mg flow would then be the oldest of the three flows; the two high-Mg flows were emplaced later, probably in rapid succession, from a southerly or southeasterly source. The lower high-Mg flow partially reduced the constructional topography created by the very-high-Mg flow and enabled the upper high-Mg flow to flood both the lower high-Mg flow and the southern part of the very-high-Mg lobe.

Umtanum Flow

The Umtanum flow is found throughout the Pasco Basin, but thins to the northeast (Fig. 4-12) and is not present in surface sections north of Sentinel Gap. It also thins dramatically west of the Emerson Nipple section and to a lesser degree to the southwest. It is thickest in the area of Emerson Nipple and Sentinel Gap and in the southeast near DC-15 and DDH-3. A broad zone of relatively constant thickness occurs in the central Pasco Basin.

The relatively narrow zone of thickening at the western edge of the basin may represent ponding of the flow in a structurally subsided area. A paleochannel may have been localized by the structural low and may help explain the unusually thick flow top at the Emerson Nipple section (Fig. 4-13 and 4-14).

It is suggested that the thickness variations in the north half of the Umtanum isopach are a reflection of structural topography in which broad paleoslopes converged from the northeast and east to culminate in a structural low formed against either the Hog Ranch anticline or the embryonic Umtanum Ridge structure. Thickening of the flow to the southeast probably also represents structurally developed topography, but part of it could be related to a greater volume of magma due to proximity to the source area. It is not possible to prove that the source of the flow lay to the southeast or east, but because the flow thins in all other directions, we infer that other source directions are unlikely. This assumes that these flows do indeed thicken somewhat toward their source areas; something that need not always be true. Hawaiian flows are known to deflate via degassing and downslope flow of magma and, thus, become thinner near their source. It is not known how Columbia River basalt flows behaved in this regard. Considering distances they typically traveled from their source areas and the very gentle slopes onto which they were erupted,

it seems unlikely that deflation would be significant. Flows adjacent to their source areas would obviously be an exception. In any case, the notion of an easterly or southeasterly source direction for the Umtanum flow is consistent with a known Grande Ronde dike swarm (Price, 1977; Swanson and others, 1979b).

A northeasterly trend of slight thinning which passes through the central basin may represent very mild development of a northeast-southwest structural trend.

Isopach maps of the Umtanum flow-top breccia and the Umtanum flow interior are included here for reference to the total flow thickness of the Umtanum. These isopachs are discussed in detail in Chapter 5.

McCoy Canyon Flow

The McCoy Canyon flow is present throughout the Pasco Basin and is interpreted to extend as far north as Crescent Bar, ∿80 km north of the Cold Creek syncline. The total thickness of the flow varies from 65 m at Sentinel Gap to 25 m at DDH-3 (Fig. 4-15). A thick zone in the northwest and west is similar to that found for the Umtanum flow; apparently, a similar structural low existed when the McCoy Canyon flow was emplaced. This may have resulted from continued deformation after emplacement of the Umtanum flow or perhaps the Umtanum flow incompletely filled the previous structural low.

To the southeast, where the McCoy Canyon flow thins, it may have covered constructional topography formed by the Umtanum flow. The flow also thins progressively to the northeast, indicating continued development of a gently dipping paleoslope in that area.

Figure 4-17a illustrates the progressive thinning of the McCoy Canyon flow north of Sunland Estates (also see Chapter 5). It may thicken slightly between Hole-in-the-Wall and Sunland Estates and this, perhaps, represents the position of the structural low at this latitude. This is confirmed by the presence of abundant pillows (see Chapter 5). Decreasing thickness of the flow to the north, however, is caused by the flow onlapping a broad, structural high as evidenced by the general thinning, decrease in thickness of the pillow zone, and loss of flows in the overlying section. Apparently, there was progressive tilting forming a paleoslope in this area during late Grande Ronde time. Moreover, foreset pillows in the pillow zone indicate a generally northward direction of emplacement in the vicinity of Quilomene Bay and Sunland Estates. If this is taken in light of the thickness variations in Figure 4-15, then the flow may have been emplaced from the east or southeast at about the latitude of DC-7/8 and was deflected to the north by the structural high which lies just to the west of the map area.

The McCoy Canyon flow, then, when taken in conjunction with the underlying and overlying flows, indicates that slight but progressive deformation was occurring, apparently at a rate sufficient to create noticeable topographic change between the emplacement of individual

flows. By knowing the approximate time period over which these flows were emplaced, it is possible to estimate the minimum rate of deformation involved. This is done in a later section.

Sentinel Bluffs Sequence

The isopach of the total Sentinel Bluffs sequence (Fig. 4-16) shows principally a pronounced thinning trend to the northeast. The sequence thickens in the vicinity of Sentinel Gap and to the southwest, but is relatively uniform in thickness in the central Pasco Basin. Figure 4-17a shows that the sequence thins markedly to the north. Thinning to the north and northeast apparently represents a southeast-dipping paleoslope of regional extent that developed progressively during deposition of the Schwana sequence. This is based on the observation that individual flows thin toward the north and northeast along with the thinning of the total sequence, and individual flows pinch out in the same direction. Examples of flows that pinch out are the Umtanum flow and several thin flows in the middle and upper parts of the sequence (Fig. 4-17). The upper flows are of particular interest from the standpoint of nomenclature, in that Waters (1961) and Taylor (1976) referred to the uppermost two flows as the Museum and Rocky Coulee flows. Figure 4-17 indicates that these two flows are overlain by two younger flows in the vicinity of DC-15 and DDH-3. This is consistent with a general thickening trend to the south and southwest, and demonstrates that it is inappropriate to arbitrarily refer to the upper two flows in the Grande Ronde Basalt as the Museum and Rocky Coulee flows.

The Sentinel Bluffs isopach (Fig. 4-16), as well as isopachs of individual flows, also reveals that the Pasco Basin did not exist during late Grande Ronde time. Instead, what is now part of the Pasco Basin was a slight decrease, or step, in the regional paleoslope. The tectonic significance of this slight step is not clear, but it is conceivable that it is a very weak expression of the earliest development of the Pasco Basin and associated Yakima folds (see Reidel and others, 1980, and Chapter 3 for a discussion of the effects of Yakima folds on the distribution of Wanapum and Saddle Mountains Basalts).

ESTIMATES OF RATES OF DIFFERENTIAL TECTONIC UPLIFT

If we assume that the surface of each flow was approximately horizontal after it was emplaced, and we are able to refer a sequence of flows to an identifiable level datum, it then becomes possible to calculate the rate of tilting if the time over which the flows were emplaced is known or can be estimated. The Mg horizon and the top of Grande Ronde Basalt both provide identifiable reference horizons. Long and others (1980) used the Mg horizon and adjacent flows in DH-4, DC-6, DC-8, and DDH-3 and estimated that the rate of tilting of the paleoslope was 37 m/million years over a distance of 10 km.

This was based on the conservative assumption that the very-high-Mg, high-Mg, and Umtanum flows were erupted over a period of not more than

500,000 yr; hence, the calculated rate is a minimum rate. A similar calculation for the interval between the Mg horizon and the top of Grande Ronde yields a minimum rate of uplift of 30 m/million years over a distance of 10 km. This calculation assumes that the interval was emplaced during a 1-million-year-period and compares the thickness of the sequence between Crescent Bar and DC-4 (Fig. 4-17). Again, this is a minimum value because the time span of 1 million years allowed for deposition of the Sentinel Bluffs sequence is the maximum credible length of time over which it might have been deposited.

This rate of creation of differential relief is approximately the same as rates calculated by Reidel and others (1980) for late Wanapum and Saddle Mountains time. The style of deformation during Wanapum and Saddle Mountains time had shifted from regional uplift or subsidence to development of Yakima folds, but nonetheless, the general suggestion that the rates of development of differential uplift were at least as high during Grande Ronde time as they were later appears valid and must be accounted for in any tectonic model of the Columbia Plateau.

SIGNIFICANCE OF STRATIGRAPHY OF GRANDE RONDE BASALT TO REPOSITORY PERFORMANCE

This chapter reports our ability to establish a flow-by-flow stratigraphy for much of the upper Grande Ronde. It is this stratigraphy that must form the basis of any detailed hydrologic modeling of the near- or far-field hydrology and subsequent risk analysis. It must be recognized, of course, that those models must take structural features as well as stratigraphy into account. It is worthwhile, however, to point out purely stratigraphic features which may have significant effects on groundwater flow and which may be important to the design of the hydrologic models.

First, the general character of the N_2 part of the stratigraphic sequence is significant. As pointed out by Myers, Price and others (1979), it consists of relatively thick, laterally continuous flows intercalated with relatively thin flows, some of which are discontinuous. The thick, laterally continuous flows are likely to be hydrologic barriers; whereas, the intervening thin flows, with possibly a higher total proportion of porous flow top, are likely to provide the most transmissive zones. In addition, the discontinuous character of some of the thin flows may result in a significant increase in vertical permeability relative to the parts of the section with thick flows. Examination of Figure 4-17 suggests that for far-field models, a minimal number of six layers is required to represent the hydraulic properties of the system. For near-field models, the system should be represented on a flow-by-flow basis.

Secondly, the occurrence of flow pinchouts stratigraphically adjacent to the Umtanum may create increased vertical permeability in the strata directly underlying the Umtanum flow. One such example has been discussed previously and is illustrated in Figure 4-17 in the vicinity of DC-4, DC-6,

and DC-7/8. Comparison of Figures 4-10 and 4-11 shows that the intersection of these two flows, in plan view, lies along an east-west line which passes through the central part of the Cold Creek syncline (i.e., the reference repository horizon). Because this intersection may be characterized by a rubble zone which could be expected to increase permeability from one stratigraphic horizon to another, this area should be a target of future boreholes and hydrologic testing. A borehole (DC-16) currently being drilled is sited directly above this zone and partially fulfills this need. It will provide a direct test of the accuracy with which flow edges can be predicted.

Another facet of the pinchout of the very-high-Mg flow beneath the Umtanum flow is that it may have created a flow edge or cusp which may have controlled stream drainage after the flow was emplaced. Later emplacement of the Umtanum flow could then have encountered this drainage and a pillow zone created as a result. This could have an effect similar to a flow edge in creating a zone of high permeability at the base of the Umtanum flow. This scenario is discussed in more detail in Chapter 5. There are a number of reasons why this scenario is unlikely, but it appears to be of sufficient importance to merit status, as noted above, as a drilling objective.

SUMMARY AND CONCLUSIONS

Grande Ronde Basalt occurs to a depth of at least 3,200 m beneath the Pasco Basin, has a total thickness of ∿2,500 m, and consists of at least 50 flows. Stratigraphic subdivisions of the Grande Ronde Basalt within the Cold Creek syncline are based primarily on paleomagnetic and chemical data. Regional Grande Ronde Basalt stratigraphy is based on four horizons, defined by reversals in paleomagnetic polarity of the flows. These have been labeled (oldest to youngest) R_1, N_1, R_2, and N_2. The upper 1,000 m of Grande Ronde Basalt of the Pasco Basin include the N_2 and part of the R_2 units. The boundary between the N_2-R_2 polarity units provides an important stratigraphic horizon. The N_2 and part of the R_2 are further subdivided into paleomagnetic secular-variation units based on inclination differences among flows and groups of flows.

In addition to N_2 and R_2 Grande Ronde Basalt polarity units, two major sequences of flows have been recognized within the Pasco Basin: (1) Schwana sequence, consisting almost entirely of flows with relatively low magnesium (Mg) content and (2) Sentinel Bluffs sequence, consisting entirely of flows with higher Mg content. The Schwana sequence lies stratigraphically below the Sentinel Bluffs flows. The boundary between these two sequences is known as the Mg horizon.

The Umtanum flow generally lies directly below the Mg horizon. This flow is recognizable on the basis of its unusual thickness, major and trace element chemistry, and paleomagnetic inclination. It has a

distinctly higher titanium dioxide (TiO_2) content than other low-Mg flows in the upper portion of the Schwana sequence. Hence, it is considered a chemical subtype of the low-Mg Schwana sequence.

The Sentinel Bluffs sequence consists of 7 to 10 flows, all of high-Mg chemical type and all within the N_2 polarity unit. The McCoy Canyon flow is the lowermost flow in the Sentinel Bluffs sequence.

Several factors govern flow thickness and lateral extent of individual flows in the Grande Ronde Basalt. They include flow volume, rate of eruption, flow viscosity, and topographic features which may be the result of structural deformation, erosion, or constructional topography caused by previous flows. Apparently, Grande Ronde flows were highly fluid and, thus, formed an accurate mold of topography over which they were emplaced, if they were of sufficient volume.

The Umtanum flow is found throughout the Pasco Basin, but it generally thins to the northeast and is not present in surface sections north of Sentinel Gap. A broad zone of relatively constant thickness occurs in the central Pasco Basin. The relatively narrow zone of thickening at the western edge of the basin may represent ponding of the flow in a structurally subsided area.

The thickness variations in the north half of the Umtanum flow are a reflection of structural topography in which broad paleoslopes converged from the northeast and east to culminate in a structural low formed against either the Hog Ranch anticline or the embryonic Umtanum Ridge structure. An easterly or southeasterly source direction for the Umtanum flow is consistent with a known Grande Ronde dike swarm in northeastern Oregon.

The McCoy Canyon flow is present throughout the Pasco Basin and is interpreted to extend as far north as Crescent Bar, $\sim$70 km north of the Cold Creek syncline. Apparently, there was progressive tilting of a paleoslope in this area during late Grande Ronde time. The McCoy Canyon flow then, when taken in conjunction with the underlying and overlying flows, indicates that slight, but progressive, deformation was occurring, apparently at a rate sufficiently great relative to magma extrusion to create noticeable topographic change between the emplacement of individual flows.

The total Sentinel Bluffs sequence shows principally a pronounced thinning trend to the northeast. The sequence thickens in the vicinity of Sentinel Gap to the northwest, but is relatively uniform in thickness in the central Pasco Basin. Thinning to the north and northeast apparently represents a southeast-dipping paleoslope of regional extent that developed progressively during deposition of the Schwana sequence. This is based on the observation that individual flows within the Schwana sequence thin toward the north and northeast along with the thinning of the total sequence and that individual flows pinch out in the same direction. Examples of flows that pinch out are the Umtanum flow itself and several thin flows in the middle and upper parts of the Schwana sequence.

The thickness distribution of the Sentinel Bluffs sequence, as well as other individual Grande Ronde Basalt flows, also reveals that the Pasco Basin did not exist during late Grande Ronde time. Instead, what is now part of the Pasco Basin was a slight decrease or step in the regional paleoslope. The structural significance of this slight step is not clear, but it is conceivable that it is a very weak expression of the earliest development of the Pasco Basin and associated Yakima folds.

Based on the assumption that the surface of each flow was approximately horizontal after it was emplaced, each sequence of Grande Ronde flows serves an identifiable level datum. The Mg horizon and the top of Grande Ronde Basalt provide identifiable datums. Based on these datums, the minimum rate of tilting of the paleoslope is estimated to be 30 to 40 m/million years over a distance of 10 km. This rate of development of differential relief is approximately the same as rates calculated for late Wanapum and Saddle Mountains time. However, the style of deformation during Wanapum and Saddle Mountains time had shifted from regional uplift or subsidence to development of Yakima folds. Nonetheless, the general suggestion appears valid that the rates of development of differential uplift were at least as high during Grande Ronde time as they were later.

The general character of the N_2 polarity unit, Sentinel Bluffs sequence, is significant. It consists of relatively thick, laterally continuous flows intercalated with relatively thin flows, some of which are discontinuous. The thick, laterally continuous flows are likely to be hydrologic barriers; whereas, the intervening thin flows with possibly a higher total proportion of porous flow top are likely to provide the most transmissive zones. In addition, the discontinuous character of some of the thin flows may result in a significant increase in vertical permeability relative to the parts of the section containing thick flows.

CHAPTER 5 - LITHOLOGY OF THE GRANDE RONDE BASALT WITH EMPHASIS ON THE UMTANUM AND McCOY CANYON FLOWS

P. E. Long
N. J. Davidson

INTRODUCTION

This chapter reports the results of examination of the internal structures, petrographic textures, and mineralogy of Grande Ronde Basalt flows in the vicinity of the Cold Creek syncline. These features have been studied in a general way for a number of Grande Ronde flows and in considerable detail for two flows: (1) Umtanum and (2) McCoy Canyon. The Umtanum flow is the principal candidate to host a nuclear waste repository in the subsurface beneath the Cold Creek syncline; consequently, it is important to know the geometry and abundance of fractures in this and surrounding flows to assess their influence on long-term migration of radionuclides. Additionally, the mineralogy and textures of the basalts, particularly along fractures, will also influence radionuclide migration by absorption or desorption of the radionuclides themselves and by hydration or dehydration of clay minerals and zeolites. Dehydration of these secondary minerals may influence permeability of the basalts in the immediate vicinity of the repository during and after the thermal phase. Thus, it is important to understand the distribution and abundance of these minerals.

This problem has been approached by studying the kinds of intraflow structures and textural features that occur generally in Grande Ronde flows, followed by a more intensive, detailed study of the Umtanum flow and the flow directly overlying it, the McCoy Canyon flow. This study was conducted by first examining and sampling Grande Ronde flows to the west and north of the Cold Creek syncline where they are exposed along the Columbia River (Fig. 5-1). Several, detailed, stratigraphic sections were measured and intraflow structures were described and illustrated for these sections. Where exposure permitted, photomosaics of cliff faces were constructed and the McCoy Canyon flow was traced directly on the photomosaics.

Some of the same flows examined and described in outcrop were then sampled and examined in core from several deep boreholes in the Pasco Basin and Cold Creek syncline (Fig. 5-1). Earlier work (Long, 1978) indicated that, whereas fractures, per se, in core were not an accurate guide to intraflow structures, petrographic textures correlated well with intraflow structures. Close examination revealed that the petrographic differences associated with intraflow structures could be commonly observed on core samples by examination with a hand lens. This made it possible to qualitatively identify intraflow structures by examining core samples and later check the identification by petrographic examination of polished thin sections.

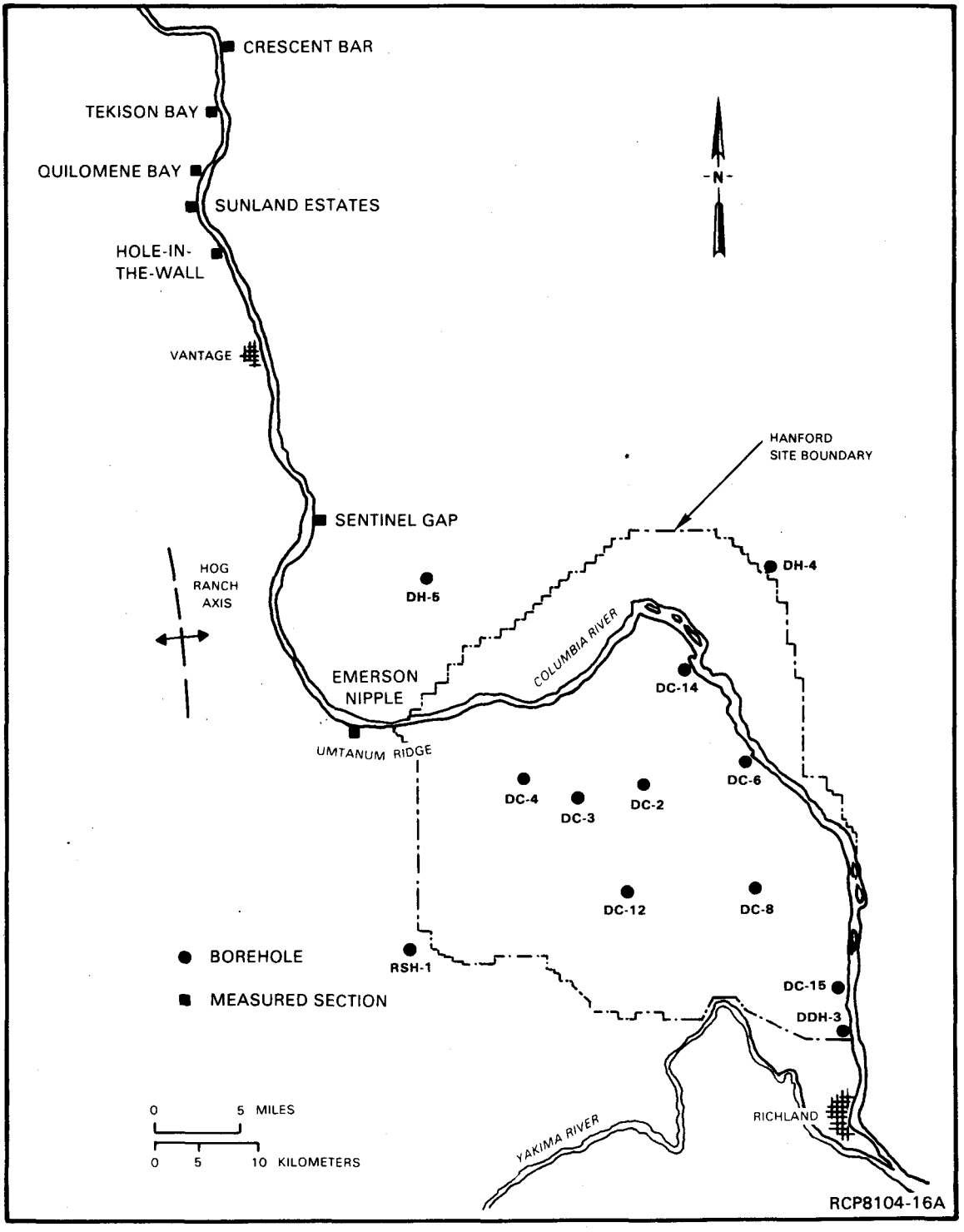

FIGURE 5-1. General Location Map, Pasco Basin Boreholes and Grande Ronde Surface Stratigraphic Sections Used in the Study of Intraflow Structures.

Results of preliminary petrographic examination are also reported in this chapter. This work was accomplished by routine qualitative examination with a petrographic microscope in reflected and transmitted light and by quantitative image analysis with a Cambridge IMANCO image analyzer. In addition, the results of several previous studies on the mineralogy and composition of both primary and secondary minerals are summarized here.

Previous work on intraflow structures and petrographic textures of Grande Ronde flows in the vicinity of the Cold Creek syncline includes work by Long (1978) and Myers, Price and others (1979).

General discussion of Grande Ronde petrography and intraflow structures are included in Waters (1961), Mackin (1961), Camp (1976), Holden and Hooper (1976), Ross (1978), Reidel (1978b), Price (1977), and Swanson and others (1979b).

Intraflow structures of basalt include columnar basalt which has attracted the attention of geologists since the latter part of the last century. No attempt is made here to review the voluminous literature on columnar jointing; several papers provide excellent bibliographies and provide a basis for comparing Grande Ronde jointing characteristics with other well-studied occurrences. Particularly noteworthy among these papers are Mallet (1875), Iddings (1886), Tomkeieff (1940), Spry (1962), Jaeger (1961), Peck and Minakami (1968) and Ryan and Sammis (1978).

GENERAL INTRAFLOW STRUCTURES OF GRANDE RONDE BASALT FLOWS

The term intraflow structure is used here to refer to internal units of basalt flows defined by regions within the flow of relatively uniform macroscopic features. These features are principally fractures (abundance and geometry), but also include size and abundance of vesicles, brecciation (flow top), and the occurrence of globular masses of chilled magma known as pillows. Intraflow structures of Grande Ronde flows are similar to those of basalt flows that have been described from other subaerial basalt terrains (e.g., Iddings, 1886; James, 1920; Tomkeieff, 1940; Spry, 1962).

Intraflow structures observed in this study from top to bottom of a flow may include:

- A ropy to brecciated vesicular flow top
- Upper colonnade with relatively large (0.7- to 2.2-m-diameter), irregular columns with or without vesicles
- Entablature consisting of relatively small, hackly to regular (0.2- to 0.9-m-diameter) columns
- Lower colonnade consisting of well-formed to irregular or massive, large (0.5- to 1.5-m-diameter) columns

- A glassy basal zone that varies greatly in thickness and may be highly fractured, vesicular, or pillowed.

Figure 5-2 illustrates these features in a hypothetical flow and compares the nomenclature used here with that of three previous studies.

The flow top typically occupies <15% of the flow thickness, although in one part of the Umtanum flow, the flow-top breccia constitutes ∿50% of the flow thickness. The flow top, per se, is vesicular, but vesiculation may also extend downward into the upper colonnade or upper part of the entablature. Abundance and size of vesicles ordinarily decrease downward in the flow. The flow top itself is marked by the presence of either brecciation or ropy structures or both (Fig. 5-3). Much of the flow top may be highly vesicular, up to 40% estimated porosity, but this property varies greatly. The vesicles are commonly arranged in undulating, slabby layers that constitute a kind of contorted crust at the top of the flow. Vesicles that extend downward into the upper colonnade or entablature commonly occur as vesicle sheets. Other flow tops are highly brecciated with an admixture of vesicular and non-vesicular clasts cemented by glassy or palagonitic basalt.

The lower parts of the flow top locally grade downward to the upper colonnade and are typified by the irregular occurrence of vugs with a wide range of sizes, some >40 cm in maximum dimension. In some flows, however, there is a relatively sharp break between flow-top breccia and underlying entablature with little or no vesiculation in the entablature.

Upper colonnade (Fig. 5-4), where present, consists of relatively large, irregular columns up to 2.2 m in diameter with or without vesicles. It is the least distinct of intraflow structures, with gradational top and bottom contacts; indeed, it is present in <50% of the exposures we have examined. Locally, however, it constitutes a prominent feature. The largest column diameters we have measured are upper colonnade columns (∿2.25 m in diameter). Column faces are typically well developed, but the column cross sections ordinarily are poor approximations to regular polygons and, hence, do not produce the impression of a consistent columnar structure typical of a lower colonnade.

Entablature consists of relatively small, hackly to regular columns (0.2 to 0.9 m in diameter) that most commonly occupy the middle portion of a flow (Fig. 5-5). Entablature "columns" weather to hackly pieces characterized by fluted surfaces. Contacts with adjacent intraflow structures range from sharp to gradational over several meters. Orientation of columns varies greatly within most entablatures. In some places, columns are horizontal, but in other cases they form fanning arrays.

Basal colonnade columns are larger than overlying entablature columns and are typically the closest approximation to regular polygons: four, five, or six sided (Fig. 5-6). Columns are upright in most places, but radiate locally and exhibit a variety of internal features such as niche joints and ball-and-socket fractures. Vesiculation in some places extends upward from the base of the flow into the lower colonnade as much as 1 to 2 m. In the majority of flows, however, vesicles are sparse and extend <0.5 m above the flow base.

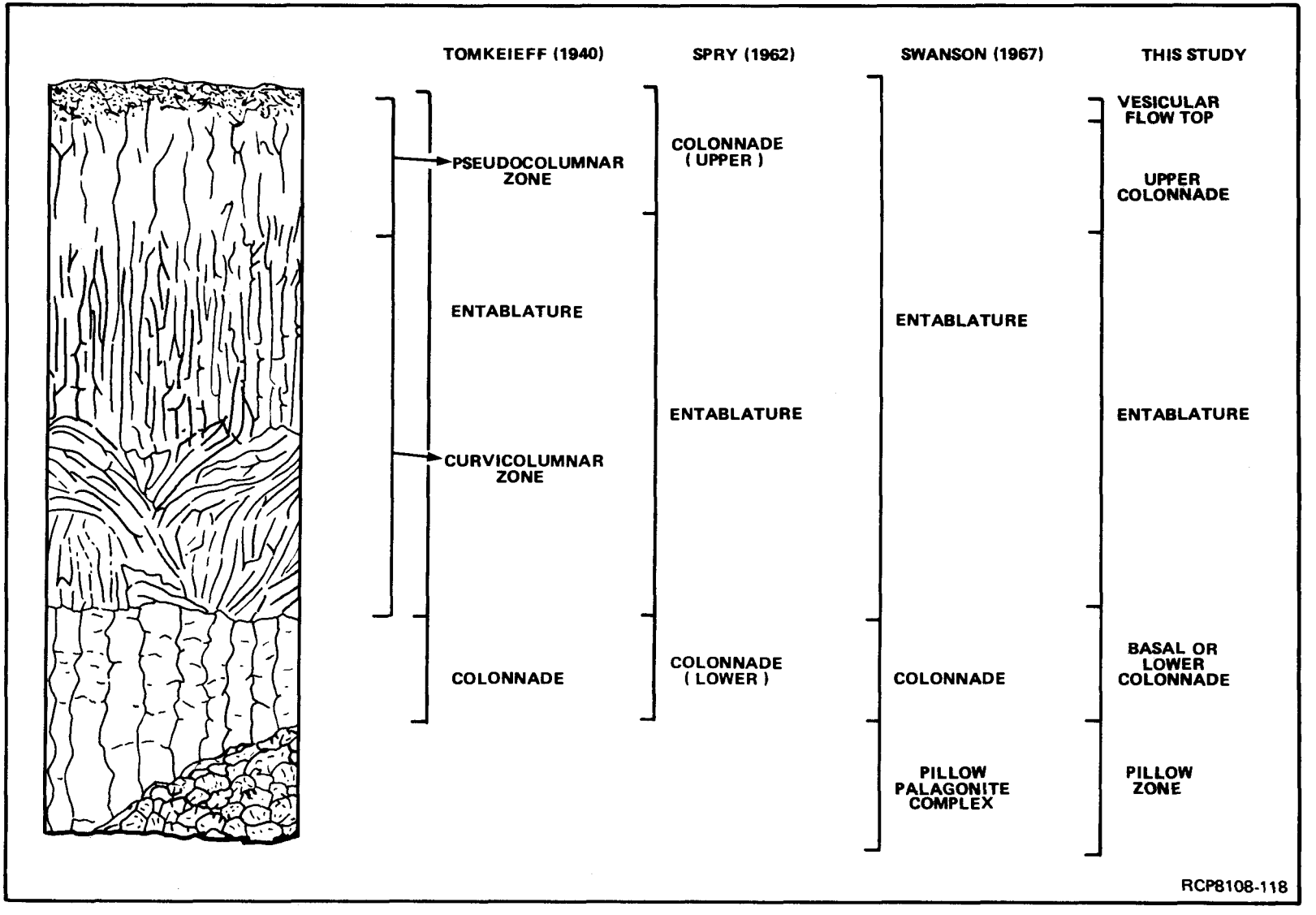

FIGURE 5-2. Typical Intraflow Structures Present in a Grande Ronde Basalt Flow. Nomenclature used in previous studies is compared with that used here.

FIGURE 5-3. Exposure of Flow-Top Breccia. Note scoriaceous and highly vesicular basalt fragments. Base of overlying flow shown in upper left. Width of photograph is ∿1.2 m.

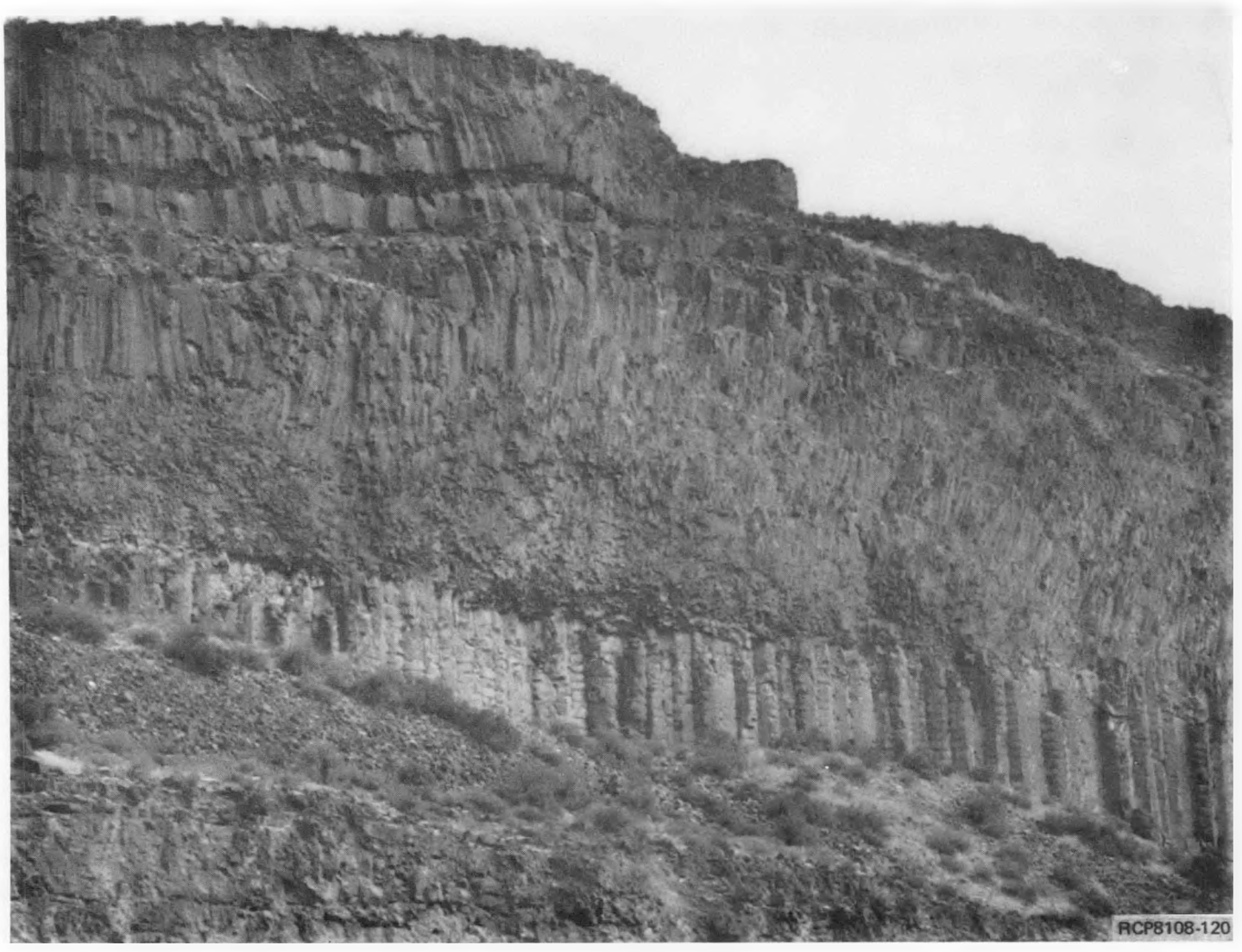

FIGURE 5-4. Well-Developed Upper Colonnade (upper third of exposure) along East Side of Columbia River North of Vantage, Washington. Entablature and lower colonnade underlie the upper colonnade. Height of colonnade is ∿5 m.

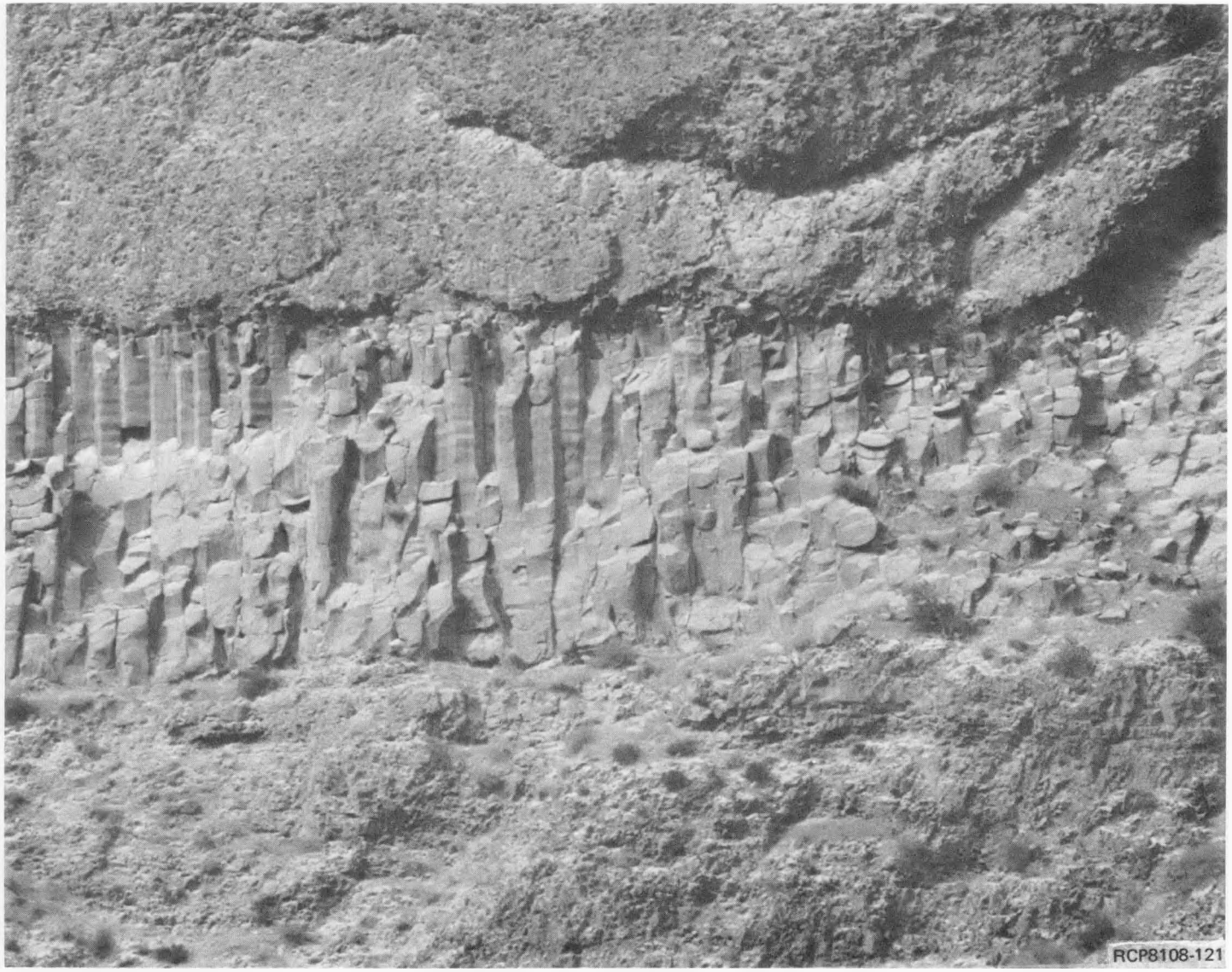

FIGURE 5-5. Well-Developed Entablature (upper part of photograph). Note well-formed colonnade. West side of Columbia River near Sunland Estates, Washington. Colonnade is ∿8 m in height.

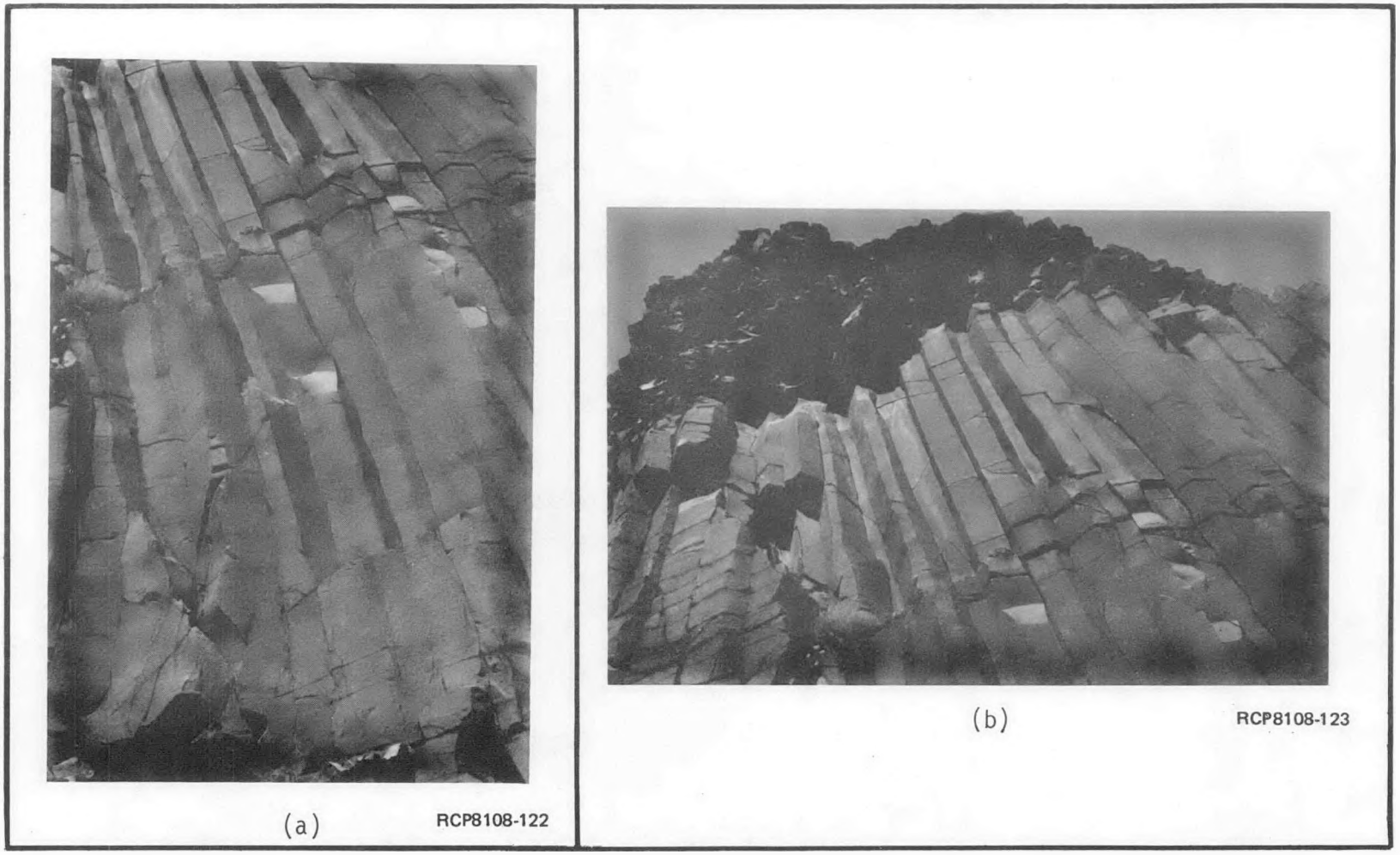

FIGURE 5-6. Basal Colonnade of a Grande Ronde Flow. Note well-formed columns and niche joints: (a) columns fan slightly at base of flow, (b) overlying entablature at top of colonnade. Columns are ∿0.5 m in diameter.

In the majority of flows in the Pasco Basin, the lowest intraflow structure consists of a glassy basal zone (0.5 to 1 m in thickness) that is both highly fractured and slightly vesicular (Fig. 5-7). The actual contact with the underlying flow is commonly a 1- to 3-cm-thick, glassy rind. Certain flows, however, developed pillows extensively at their bases when they entered a significant depth of water (Fuller, 1931). In some flows, the pillows occupy 50% or more of the flow thickness (Fig. 5-8). The pillows range in diameter from 0.3 to several meters and vary considerably in shape from elongate, cylindrical features to rounded, bulbous masses. The pillows are typically packed closely together and the void space between pillows is locally filled with palagonite. In places, however, a palagonite matrix is sufficiently abundant such that it supports the pillows.

INTRAFLOW STRUCTURE TYPES

The intraflow structures discussed above may vary greatly in thickness, be absent entirely from any given flow, or occur repeatedly within a single flow. Patterns in the way intraflow structures occur, however, allow classification of flows into general intraflow structure types (Long, 1978).

Type I flows are relatively thin (10 to 30 m thick), consisting primarily of irregular, tapering columns 1 to 2 m in diameter (Fig. 5-9 and 5-10). These flows lack a distinct entablature and have a poorly developed vesicular flow top. Such flows are invariably diktytaxitic and commonly contain vesicle cylinders. Type II flows are very thick (45 to 76 m thick), exhibiting columnar tiers of alternating entablature and colonnade-type columns in the lower half of the flow which grade upward into a hackly entablature (Fig. 5-9 and 5-11). Another kind of tiering occurs in the upper third of the flow, where tiers are defined by thin zones of abundant fractures or vesicles. An oxidized flow top with large, frothy blocks is common and vesicles are abundant in the upper third of the flow. Fanning of columns in the entablature occurs locally. Type III flows are moderately to relatively thick (30 to 80 m), in which a sharp break between entablature and colonnade defines a marked difference in fracture abundance and column size (Fig. 5-9 and 5-12). The colonnade in these flows commonly shows pinch-and-swell structure in the columns, and the entablature is a complex pattern of smaller, radiating columns. A crude upper colonnade caps the entablature along parts of many type III flows.

Examples of the three intraflow structure types are best exposed in the Sentinel Bluffs stratigraphic section. Other sections, such as the Emerson Nipple section on Umtanum Ridge and sections north of Vantage (Fig. 5-1), show similar features, but examination of a number of flows in many localities shows that intraflow structure types are best thought of as end members with nearly continuous gradations between all of the types.

FIGURE 5-7. Glassy Basal Zone Overlying Flow-Top Breccia. Hammer head marks contact. Glassy zone grades upward into basal colonnade.

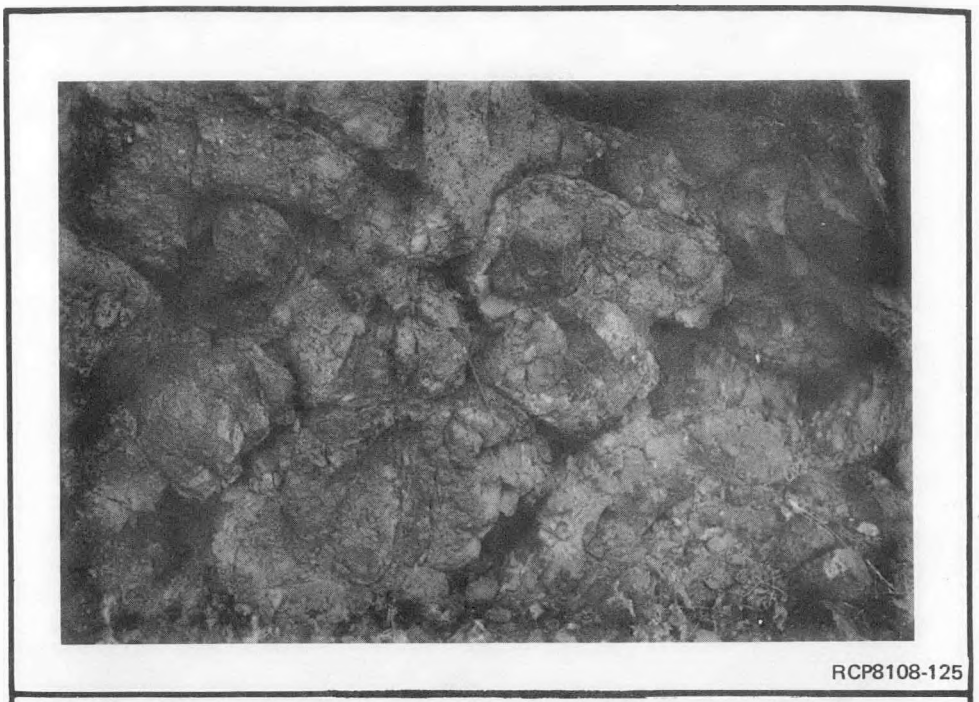

RCP8108-125

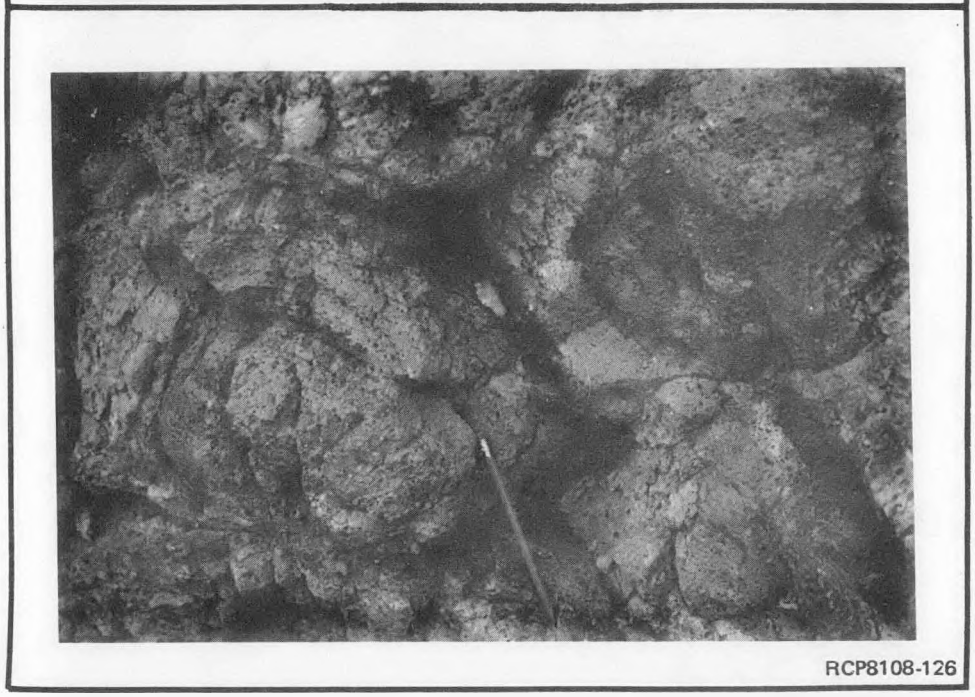

RCP8108-126

FIGURE 5-8. Detail from Pillow Zone. Note chill margins and highly vesicular interior of pillows. Pillows form the upper part of such a zone in a Grande Ronde flow north of Vantage, Washington. The upper photograph shows the general size (0.3 to 1.0 m) and shape (ellipsoidal) of the pillows. The lower photograph is a detail of the upper photograph and shows the chilled rind of the pillows. Notice also the highly vesicular interior of the pillow. This is common in pillows near the upper part of a pillowed zone.

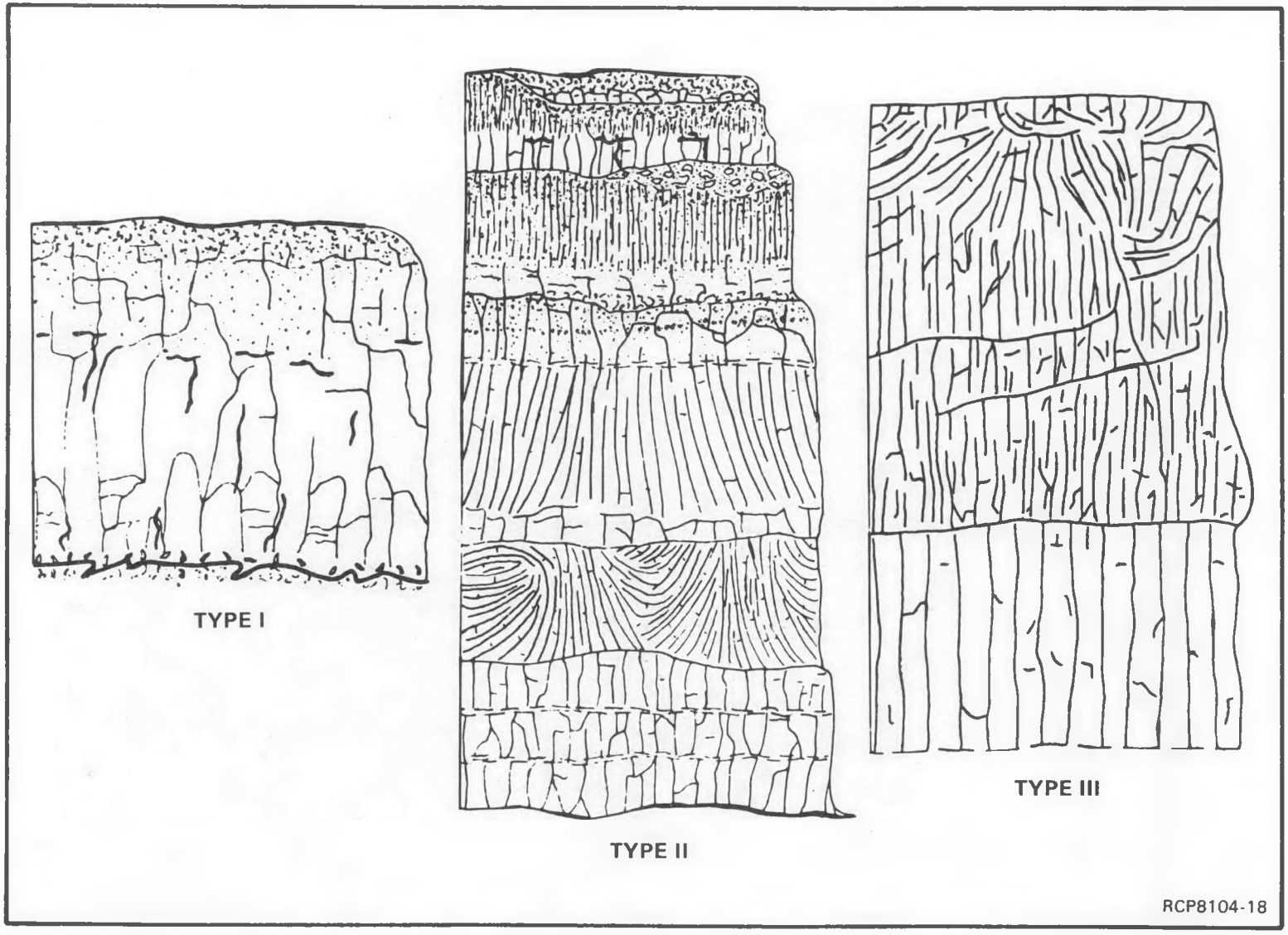

FIGURE 5-9. Comparison of General Intraflow Structure Types (after Long, 1978). See text for discussion.

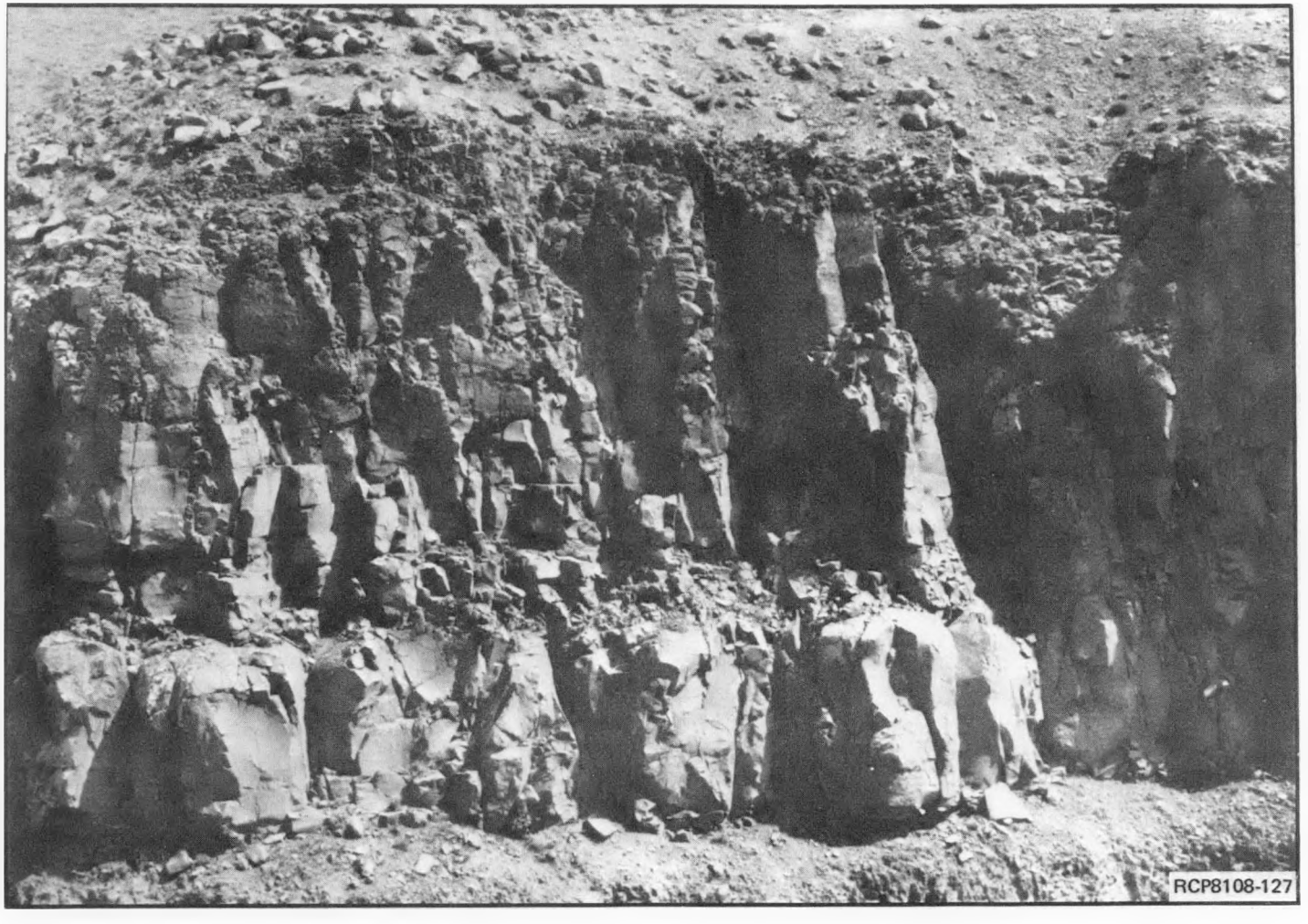

FIGURE 5-10. Type I Flow. A platy zone occurs in the central part of the flow. Above the platy zone, columns taper gradually toward top of flow. This flow is the uppermost flow of Grande Ronde Basalt in the Sentinel Gap field section. Total thickness of flow is ∿14 m.

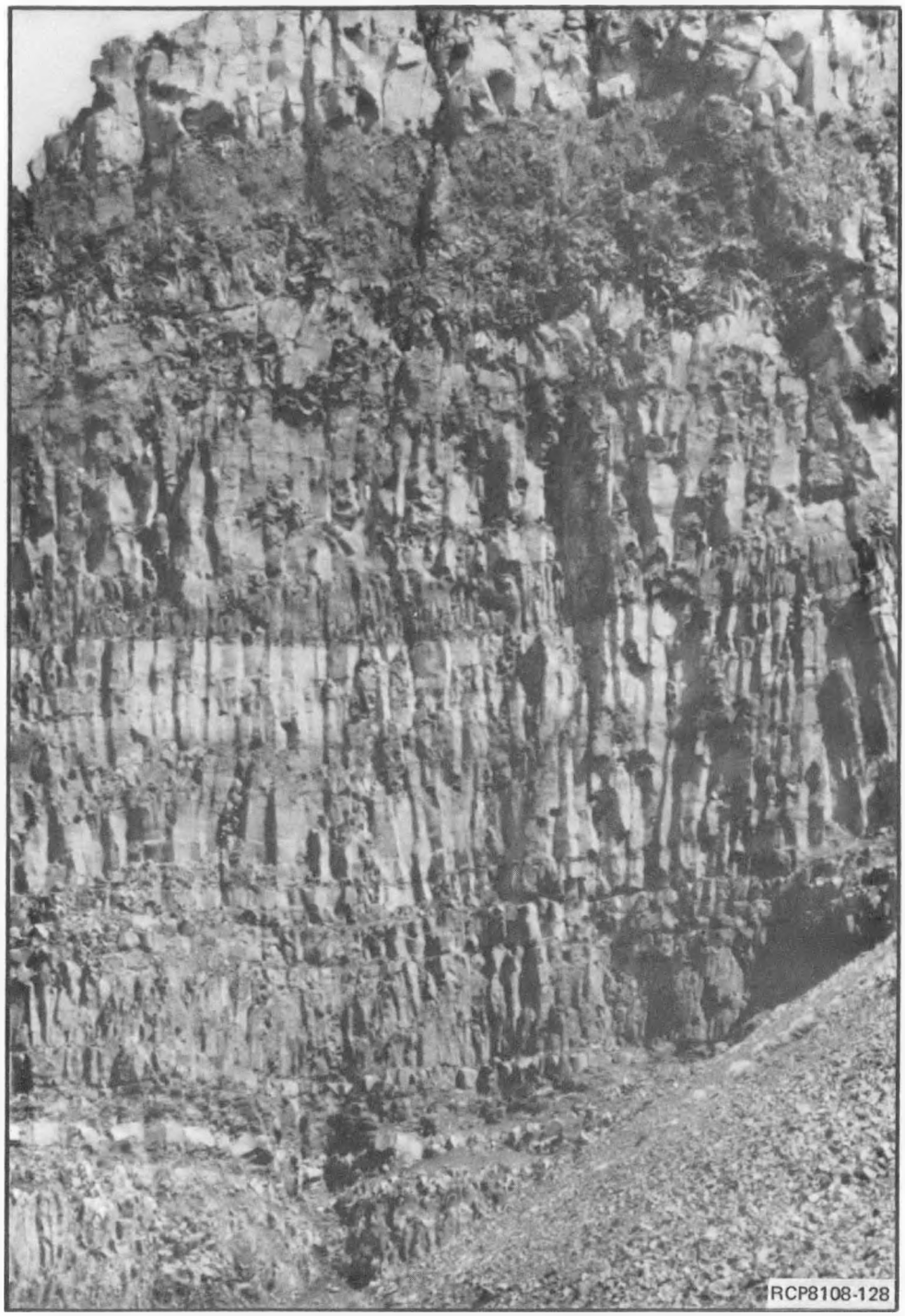

FIGURE 5-11. Type II Flow. Multiple tiers occur both in the thick entablature and as alternating colonnade and entablature in the lower part of the flow. A relatively thick, oxidized, clinker flow top marks the top of the flow. Located at Sentinel Gap field section. Height of the cliff exposure is ∿70 m.

FIGURE 5-12. Type III Flow. Sharp contact occurs between entablature and colonnade in the lower half of the flow. Colonnade columns are typically well formed; whereas, entablature exhibits a hackly fracture pattern. McCoy Canyon flow, Sentinel Gap field section. Colonnade is ∿20 m in height.

FRACTURE CHARACTERISTICS

Fractures that occur in Grande Ronde flows can be described qualitatively by examining the shape and orientation of fracture surfaces as exposed in surface outcrop and quantitatively by measuring fracture spacing and orientation both in surface exposures and core samples.

Qualitatively, the dominant fractures range from those that define well-formed, regular, polygonal solids to those that define irregular, elongate to equant blocks (compare Fig. 5-6 and 5-10). There is nearly an entire spectrum from regular, well-formed columns to irregular (hackly) blocks. Both columns and blocks range widely in size; 0.2 to 2.3 m for columns and 0.1 to 0.7 m for the more equant blocks. In plan view, the fractures are arranged as four-, five-, or six-sided polygons (Fig. 5-13 [a and b]). Commonly, well-formed columns (Fig. 5-13 [a and b]) possess five or six sides; whereas, less-regular columns (Fig. 5-13 [b and c]) either possess three or four sides or their sides are not well defined. The columnar character of the fractures is commonly lost in the entablature of type III flows. That is, most single, column-defining fractures on the colonnade cannot readily be traced as single fractures through the entablature. Entablature in these flows is, instead, commonly fractured into fluted, hackly blocks 0.15 to 0.3 m in maximum dimension. The blocks may be elongate, forming a crude columnar structure in some flows. In other flows, columnar structure is well developed, but column diameter is smaller in the entablature than it is in the colonnade. Also, hackly entablatures are commonly interspersed with well-formed columns occurring as fans.

Virtually all columns or blocks are subdivided into smaller blocks by cross fractures. These cross fractures occur in a wide range of orientations and formed mainly after the primary, column-defining fractures; cross fractures typically are terminated by the primary fractures. In outcrop, the secondary fractures rarely exhibit the rough surface that is common on column faces. They are also curviplanar and range from highly regular "ball-and-socket" joints (see below) to irregular fractures that constitute platy zones (Fig. 5-14).

Certain fracture morphologies occur extensively in basalt flows and have been described previously by a number of workers (e.g., Spry, 1962). These include pinch-and-swell along columns, ball-and-socket joints, chisel marks, and niche joints.

Pinch-and-swell columns are shown in Figure 5-15. Colonnade columns in these flows range from extremely well formed and regular to poorly formed and highly irregular. The well-formed columns typically exhibit well-formed pinch-and-swell structures; whereas, the irregular columns exhibit gently curving, irregular surfaces, but without pronounced sinusoidal undulation.

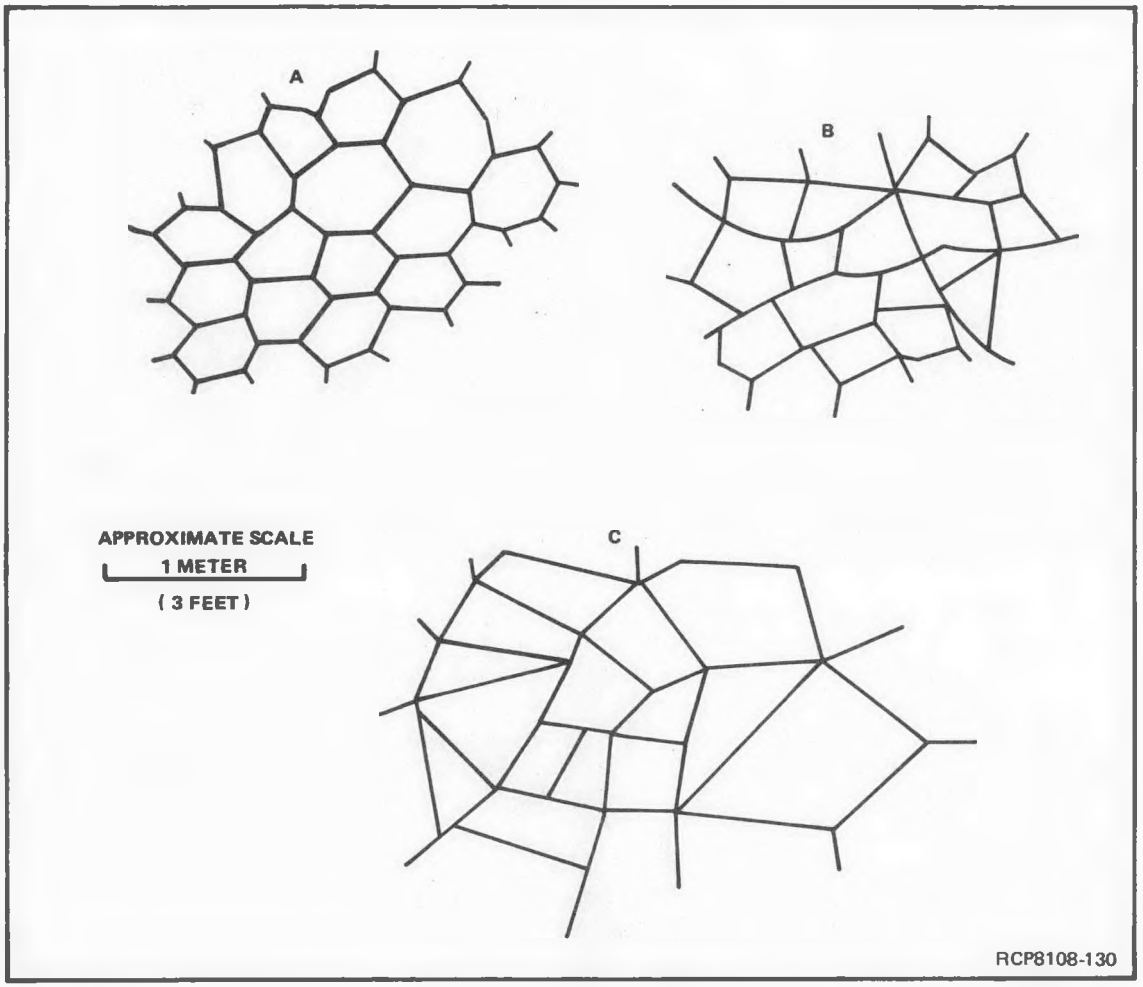

FIGURE 5-13. Line Drawings Illustrating Plan Views of Various Columnar Jointing Patterns. These range from regular polygons (a) to hackly, irregular, fracture patterns (c).

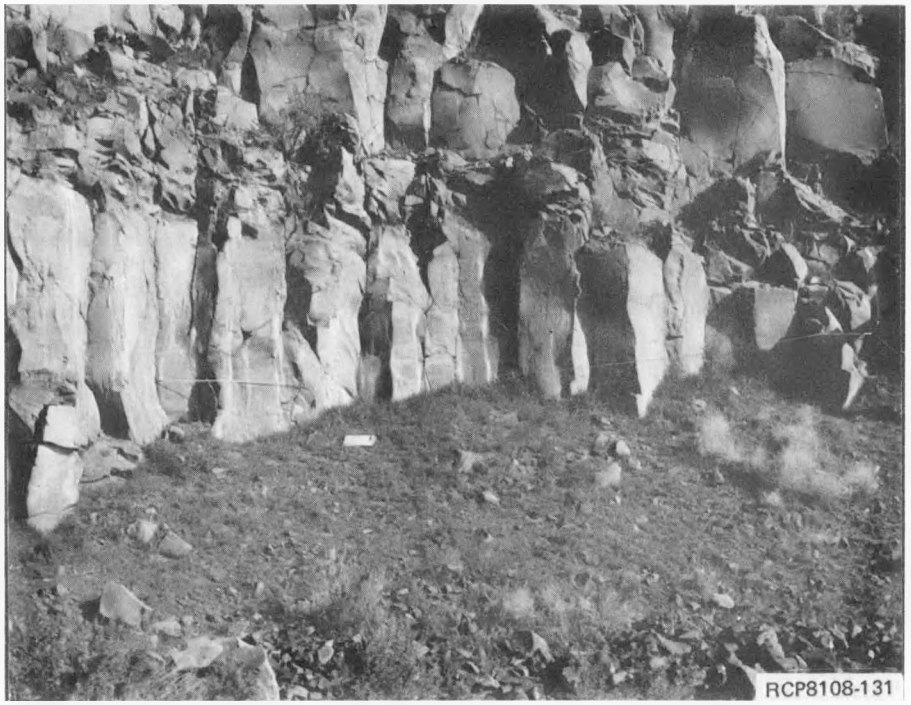

FIGURE 5-14. Platy Zone in Colonnade of a Type II Flow. Irregular fracture patterns such as this in colonnade typically lack lateral continuity. Subhorizontal, narrow, platy zones within the entablature, however, may be laterally continuous for distances of several hundred meters.

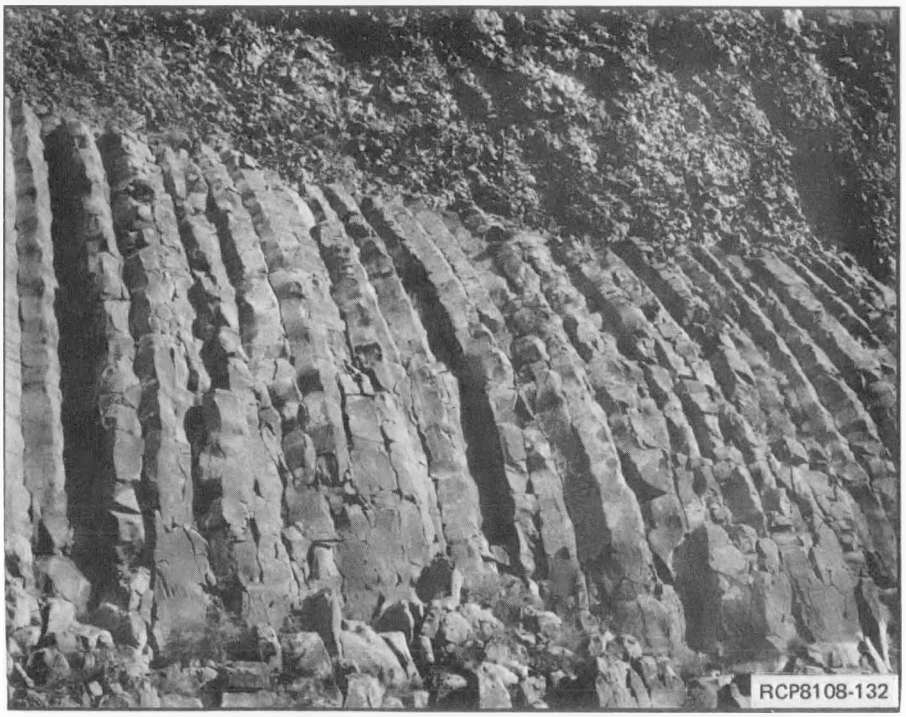

FIGURE 5-15. Pinch-and-Swell Features in the McCoy Canyon Flow. Note the sharp entablature colonnade contact and the "stack of Dutch cheeses" effect in some columns. Columns are ~0.7 m in diameter.

Ball-and-socket joints (Fig. 5-16) occur in the colonnade of some flows, particularly those with well-formed columns. Regularly spaced ball-and-socket and/or niche joints create a feature known as a "stack of Dutch cheeses" (Spry, 1962); they occur in the upper part of the flow in Figure 5-15.

Chisel marks are steps or grooves which occur on fracture surfaces at a scale of 0.5 to 1.0 cm. These steps are commonly associated with a change in surface roughness along a fracture (Fig. 5-17 and 5-18). Ryan and Sammis (1978) suggested that differences in surface roughness occurring in bands on colonnade column faces represent elastic ("smooth") and inelastic ("rough") modes of fracturing. Also, surface roughness differs in a general way from flow to flow and within flows. In Grande Ronde flows, colonnade columns are generally smoother than many entablature columns, but areas of smooth fracturing in the entablature also occur and both the roughest and the smoothest fracture surfaces occur in the entablature.

Platy fracture zones (Fig. 5-14) typically parallel the flow base and occur in almost all flows, but the degree and character of the development varies greatly from flow to flow. Some platy zones have distinct undulatory fractures; in others, platy zone fractures are curvilinear and subhorizontal. The origin of either type of platy fracture is not well understood, but is related to emplacement and primary cooling and, perhaps, enhanced by later deformation. Holmgren (1968) studied platy fractures in Columbia River basalt and concluded that they formed after the formation of the major vertical cooling joints. He ascribed them to alignment of elongated minerals and flattened vesicles in basalt. Locally, at Sentinel Gap, nearly horizontal, platy, fracture zones occur which are clearly tectonic in origin. These are shear features that transect column tiers, and in places show brecciation and sigmoidal tension fractures (Myers, Price and others, 1979).

Nearly vertical, closely spaced fracture zones have been observed in the Grande Ronde flows at Sentinel Gap and between Vantage and Crescent Bar. These vertical fractures are also tectonic in origin. They transect portions of the interior of individual flows and in some places cross flow boundaries.

FRACTURE ABUNDANCE MEASUREMENTS

Abundance of fractures has been measured both in surface outcrops and in drill core. These measurements were made to determine if fracture characteristics can be used to identify intraflow structures at depth from drill core and to provide basic information on fracture abundance for use in estimating mechanical strength, fracture porosity, and fracture permeability of large, basalt, rock masses.

Fractures logged in drill core were defined as any subplanar or planar crack, either filled or unfilled, which transects or partially transects the core. Most core fractures have narrow apertures (<0.5 mm) and contain secondary minerals (see section on secondary minerals below).

FIGURE 5-16. Ball-and-Socket Joint in the McCoy Canyon Flow. The lower surface in the example is concave upward. Pen is 13 cm long.

FIGURE 5-17. Chisel Marks in the Rocky Coulee Flow. These chisel marks and associated banding are related to propagation of fractures toward the center of the flow.

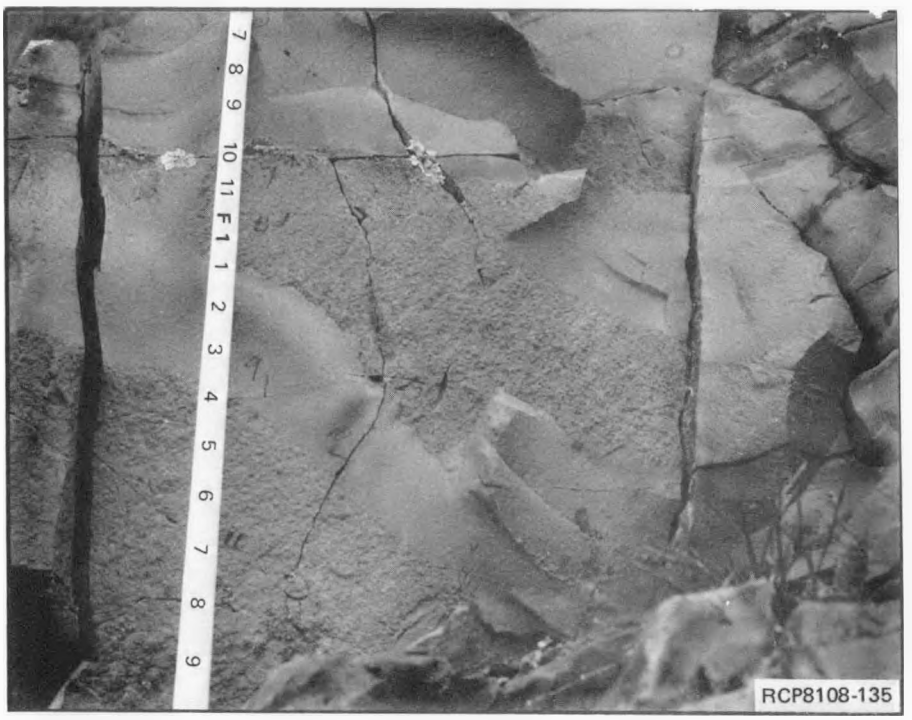

FIGURE 5-18. Differences in Surface Roughness on a Fracture Surface in the Entablature of the McCoy Canyon Flow. These features may represent different stages of fracture propagation or they may represent elastic (smooth) and inelastic (rough) stages of cyclical fracturing (Ryan and Sammis, 1978).

The majority of fractures are filled with multiple generations of secondary minerals, although relatively rare fractures or fissure openings that are 6 to 12 mm in width exhibit unfilled or partially filled apertures.

Fracture logging at surface outcrops was conducted in order to intersect fractures as they would occur in drill core. This was done by taking a series of vertical segments along well-exposed vertical cliff faces. Position of each segment was determined by outcrop accessibility; segments were arranged so that the base of one segment was at the same elevation as the top of the next lower, adjacent segment. In addition, horizontal segments were measured in order to estimate average column diameter. In outcrop, the majority of fractures lack secondary mineral infillings because they have been removed by dissolution and weathering.

Thus, little can be said about secondary minerals in fractures from observations of surface outcrops. In addition, slight slumping of surface blocks renders any measurements of fracture aperture invalid. Consequently, no attempt was made to measure fracture apertures in surface outcrops.

Fracture abundances for the same flow (McCoy Canyon flow) in drill core and in surface outcrop are compared in Figure 5-19. Average fracture abundance in drill core (DH-5; Fig. 5-1) for this flow is ∿10 fractures/m; no obvious changes occur within the flow, except for a subtle decrease in abundance near the base. Surface fracture abundance, on the other hand, shows an increase from ∿5 fractures/m to as high as ∿27 fractures/m across a narrow zone in the flow. This abrupt increase in fracture abundance delineates the entablature-colonnade contact and was anticipated from casual inspection of the outcrop. The lack of such a feature in the fractures from drill core, however, was not anticipated. The explanation for the difference between surface and subsurface fracture abundance probably has to do with fundamental differences between fracture measurement in drill core versus in outcrop, as well as the effect of weathering and unloading in revealing fractures that are not readily visible in core samples. Further study is required to determine if the entablatures of type III flows have consistently less fracture abundance in the subsurface than in surface outcrop.

In spite of directional bias and inadequate cross section of sampling, drill core fracture data do provide invaluable information on in situ fracture widths (apertures) and on the secondary minerals filling those fractures. Secondary minerals are discussed in a later section; fracture apertures are discussed here as a quantitative characteristic of fractures, which has important implications for both permeability and mine stability of a repository. Figures 5-20 and 5-21 are histograms of fracture apertures which show both filled and unfilled* fractures. They clearly demonstrate that fractures classified as unfilled tend toward relatively narrow apertures (Fig. 5-21) or have a frequency distribution similar to that of the filled fractures (Fig. 5-20). Mean fracture widths for all fractures, filled or unfilled, average between 0.1 and 0.3 mm. On Figures 5-20 and 5-21, notice that the unfilled fractures do not occur in widths ≥0.7 mm.

Information from fracture logging of drill core can also be used to calculate the volume percent of fracture openings (filled or unfilled) in the core. The results of such calculations for three different flows in DH-5 are presented in Figure 5-22. The total volume percent of all fractures is clearly very small, but the volume percent of unfilled fractures is even less, ranging from 0.025 to 0.059. The small volume of unfilled fractures, particularly in the dense interiors of Grande Ronde flows, limits the total fracture porosity of these rocks.

*The term unfilled is here defined as a fracture which is either devoid of secondary minerals or whose filling is obviously discontinuous along the plane of the fracture. Naturally occurring fractures in the former category are extremely rare. Most fractures are drilling or hammer breaks and these are not included in the fracture histograms.

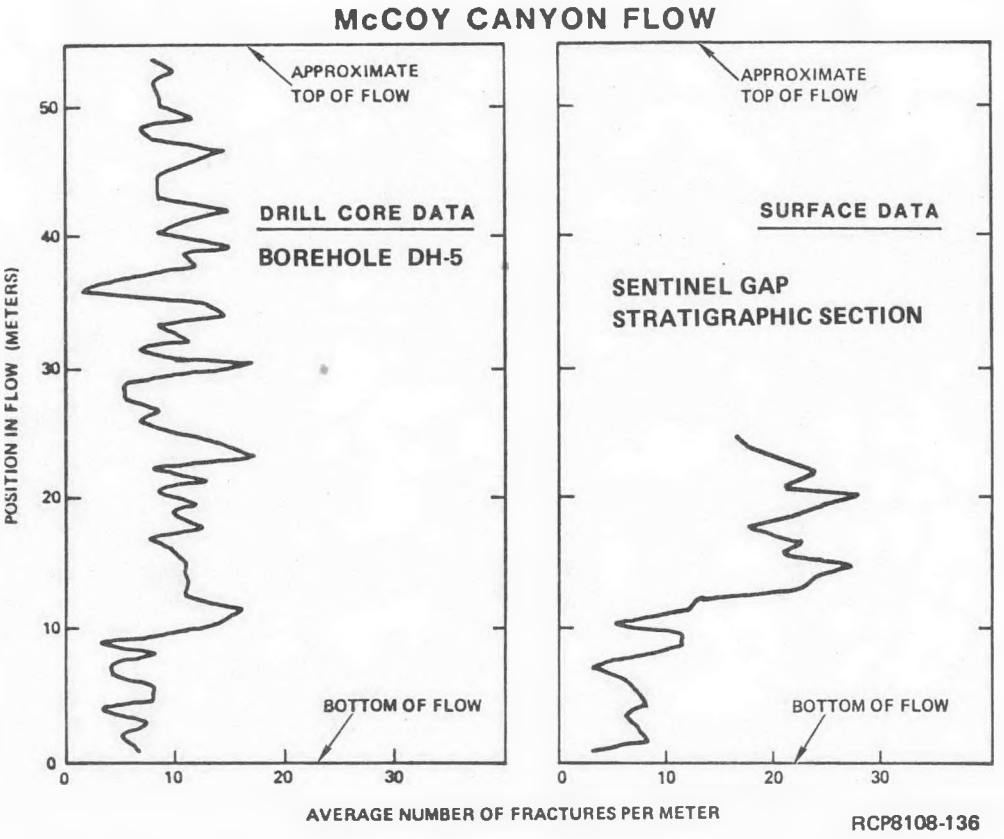

FIGURE 5-19. Results of Fracture Logging of Drill Core and Surface Exposures of Basalt. These plots compare fracture abundance versus position in a flow. Fracture data from drill core are not as sensitive to the entablature-colonnade contact as the fracture data from a surface outcrop of the same flow. These plots suggest a general level of fracture abundance in the flows and that the fractures in drill core cannot be readily related to internal structures observed in surface exposures. Examination of other ways of determining internal structures from subsurface samples resulted in the discovery that petrographic texture of the flows is a good indicator of their internal structures.

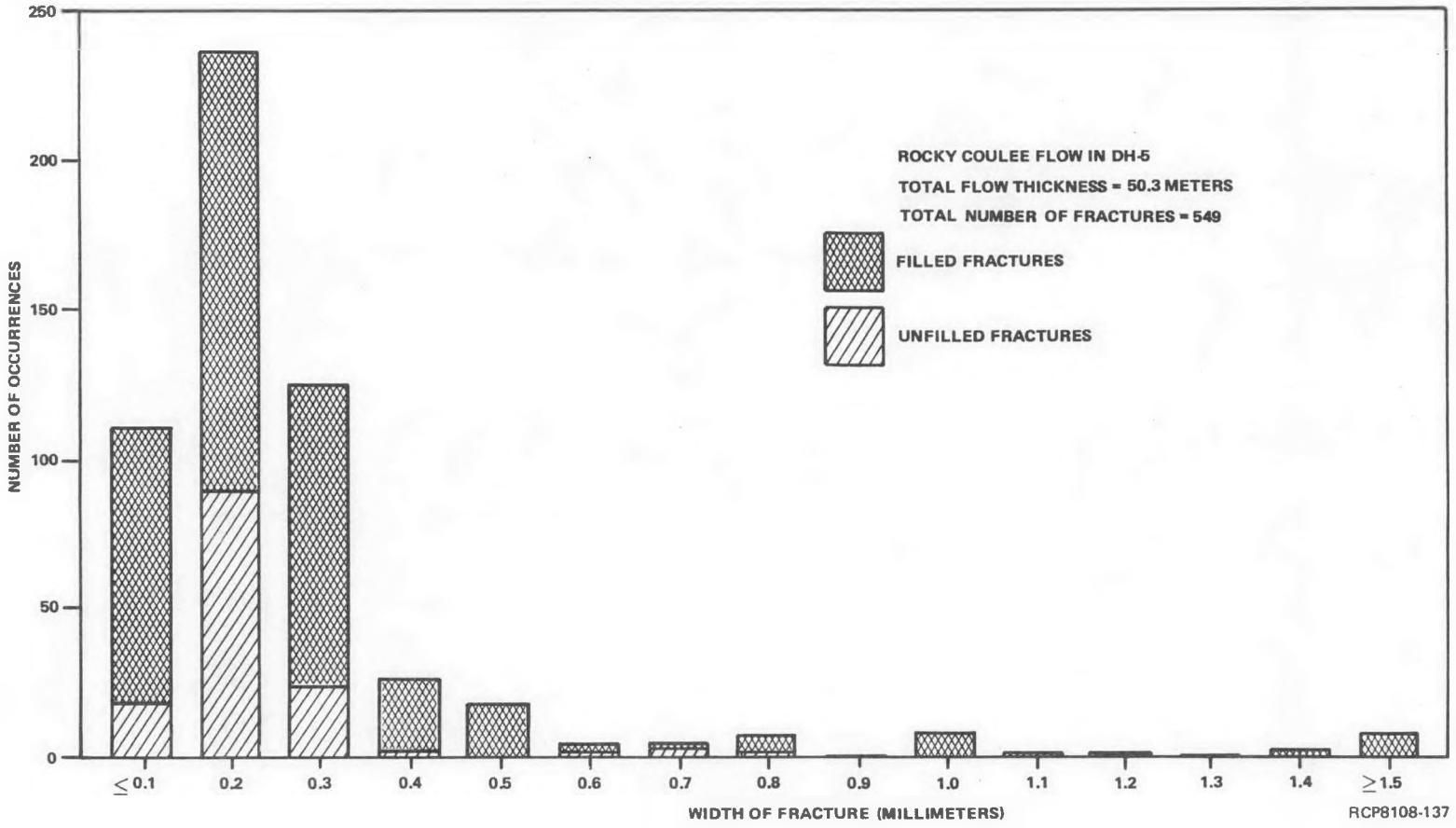

FIGURE 5-20. Histogram, Fracture Widths, Rocky Coulee Flow, Borehole DH-5. Mean fracture width is ∿0.2 to 0.3 mm. Filled and unfilled fractures have approximately the same distribution of widths, although unfilled fractures are much less abundant than filled ones.

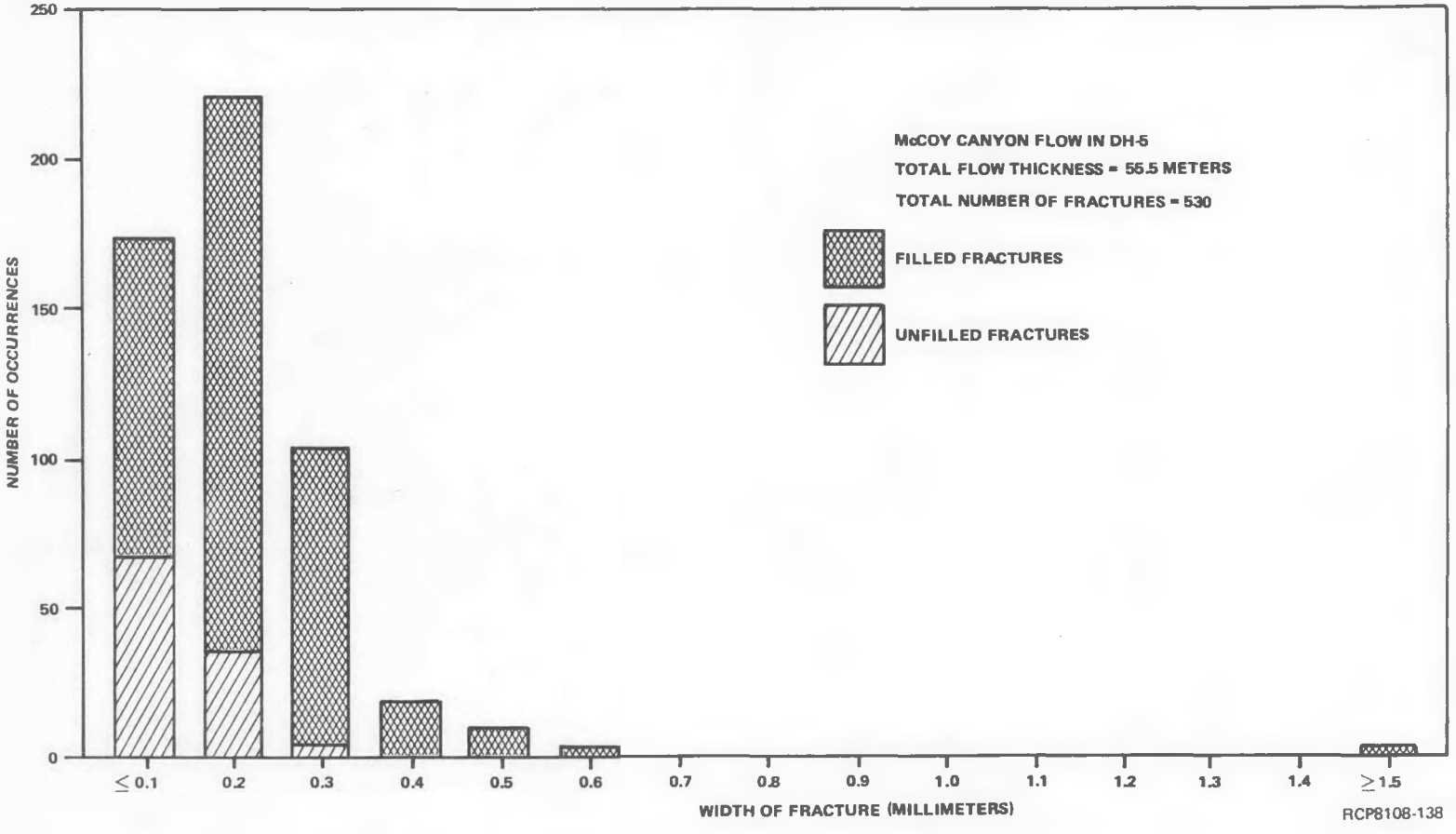

FIGURE 5-21. Histogram, Fracture Widths, McCoy Canyon Flow, Borehole DH-5. Mean fracture width is 0.1 to 0.2 mm. Unfilled fractures are definitely skewed toward smaller widths compared to the unfilled fractures.

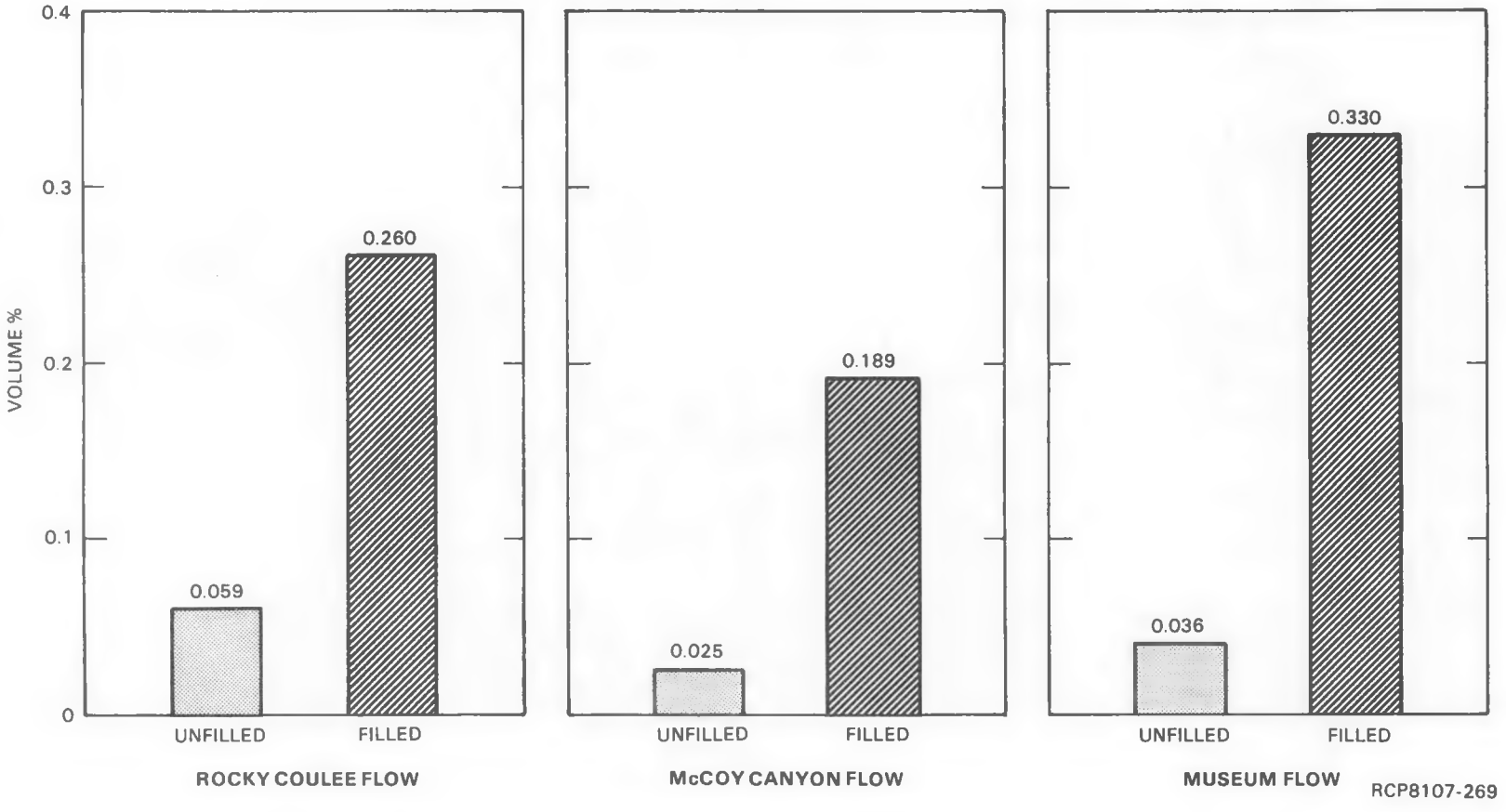

FIGURE 5-22. Volume Percent, Filled and Unfilled Fractures, Rocky Coulee, McCoy Canyon, and Museum Flows. Values presented are calculated by summing fracture widths and dividing by total length of core over which the fractures occur. From these examples, it appears that the maximum fracture volume (filled and unfilled) is <0.4 vol%.

LATERAL CHANGES IN INTRAFLOW STRUCTURES

Intraflow structures are commonly characteristic of a particular flow over the very limited distance of typical exposures (≤1 km). It is generally agreed that intraflow structures are not constant over relatively large distances of several or tens of kilometers (Swanson and others, 1979b), but little is known about what lateral changes might occur.

We have attempted to remedy this situation by studying Grande Ronde flows that are nearly continuously exposed along the Columbia River from Sunland Estates to Crescent Bar, a distance of nearly 20 km (Fig. 5-1). This is the area closest to the Pasco Basin where good exposures of Grande Ronde Basalt are laterally continuous for a significant distance.

McCoy Canyon Flow

Study has been concentrated on a single flow, the McCoy Canyon flow (Long and others, 1980; and Chapter 4), which is well exposed near the base of cliffs along this part of the Columbia River. This flow occurs near water level, so it is readily photographed from a boat. These photographs were pieced together to form a long photomosaic and the flow and its intraflow structures were traced on mylar overlays. Vertical control was established by five measured sections north of Vantage (Fig. 5-1).

The results demonstrate that the McCoy Canyon flow is a laterally continuous, single flow over the area of study. Its consistent variation in thickness and its consistent stratigraphic position relative to the Mg horizon lends confidence to the interpretation that it extends into the Pasco Basin subsurface at least as far south as Richland (DDH-3; Fig. 5-1). Intraflow structures in the exposed portion, then, provide valuable insight into the kinds of intraflow structural variations that occur in the subsurface of the Pasco Basin, both in this flow and in other thick flows.

The results of the intraflow structure study of the McCoy Canyon flow are illustrated in Figure 5-23. This figure depicts the flow from Crescent Bar, where it is thinnest, to just south of Sunland Estates, and it includes isolated exposures of the flow farther south at the Sentinel Gap and Emerson Nipple sections. The flow thickens continuously as far south as the Emerson Nipple section, ranging from 21 m in the north to 65 m in the south. At about the latitude of the Tekison Bay section, the flow develops a prominent pillowed zone which thickens southward to at least the Sunland Estates section. It probably occurs in the Hole-in-the-Wall section, but only the top part of the flow is actually exposed, so thickness of the pillowed zone, if present, cannot be determined. Significant pillowed zones do not occur to the south in either the Sentinel Gap or Emerson Nipple sections. Entablature and colonnade are present all along the flow, except for local areas where the entablature and the pillow zone are in direct contact. The entablature-colonnade contact is sharp in almost every exposure, but it becomes less distinct toward the north in the vicinity of the Crescent Bar section.

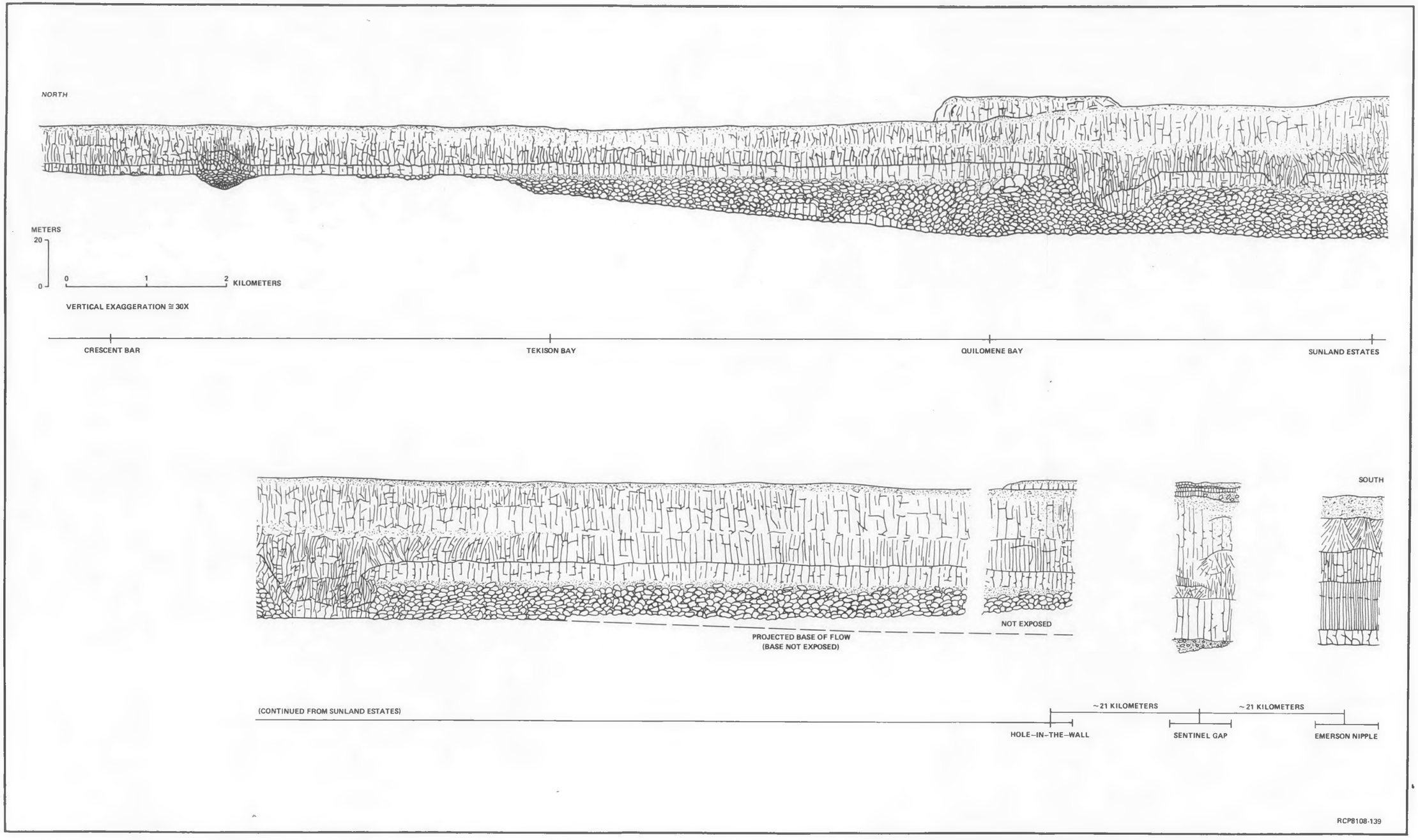

FIGURE 5-23. Depiction of Lateral Variation, McCoy Canyon Flow. This figure is based on "mapping" of the flow on a mosaic of photographs of cliffs from Crescent Bar to Hole-in-the-Wall (Fig. 5-1). Many of the internal structures of the flow are shown diagramatically due to the large vertical exaggeration (30 X).

Here, the contact remains fairly sharp, but the difference between entablature and colonnade in terms of average column diameter is less than in exposures to the south.

Upper colonnade is well developed along much of the exposure, but it is not a uniform, continuous feature. Thickness, column diameter, and vesicularity vary significantly. Such lateral differences are typically gradual. For example, well-developed upper colonnade grades laterally into what appears to be a distinct flow lobe, but which may actually be a sharp lower contact of the upper colonnade. These types of changes in the expression of upper colonnade come and go over distances of a few kilometers or less. Thicknesses and character of vesicular zones also vary significantly. Vesiculation occurs at the top of the pillowed zone in this flow and in the upper one-third to one-eighth of the flow. Between the Quilomene Bay and Sunland Estates sections, the lowest vesiculation (excluding the pillowed zone) occurs approximately two-thirds of the way up in the flow. Abundant, pin-head-sized vesicles are commonly overlain by basalt with less abundant, larger vesicles which then increase in abundance toward the flow top. In some areas, this feature is sufficiently developed to suggest that the flow may have been emplaced as two pulses.

The vesicular, rubbly flow top itself in the McCoy Canyon flow is relatively thin between Crescent Bar and Hole-in-the-Wall. For this part of the flow, the flow top makes up <10% of the flow thickness. The flow top thickens slightly to the south as the flow thickens. At Sentinel Gap, it is even thicker and consists of a vesicular flow top overlain by two to three vesicular flow lobes with slabby, vesicular flow tops. Farther south at the Emerson Nipple section, the flow top is still thicker (8 m or 13% of the flow thickness).

Umtanum Flow

Exposures of the Umtanum flow are limited to two localities: (1) Emerson Nipple area and vicinity and (2) Sentinel Gap area. The flow pinches out to the north, somewhere between Sentinel Gap and Sunland Estates (see Chapter 4); hence, laterally extensive exposures are not available for study. Exposures that are available, however, provide considerable information about intraflow structures. One exposure has been photographed and mapped in order to illustrate the types of internal differences that occur across this exposure (Fig. 5-24). At Emerson Nipple section, the Umtanum flow has an anomalously thick flow top that comprises ∿50% of the flow and has a thickness of 40 m. This flow top is principally a flow-top breccia with clasts of vesicular and nonvesicular basalt cemented by basalt or palagonite. These clasts range in size from ∿2 to ∿30 cm with a mean size of ∿10 cm. Across ∿400 m of exposure at the Emerson Nipple section, the flow top maintains a great thickness, although it is somewhat variable (Fig. 5-24). In contrast, the Umtanum flow at the Sentinel Gap section has a thin (∿5 m) flow top which is vesicular, but has little or no breccia.

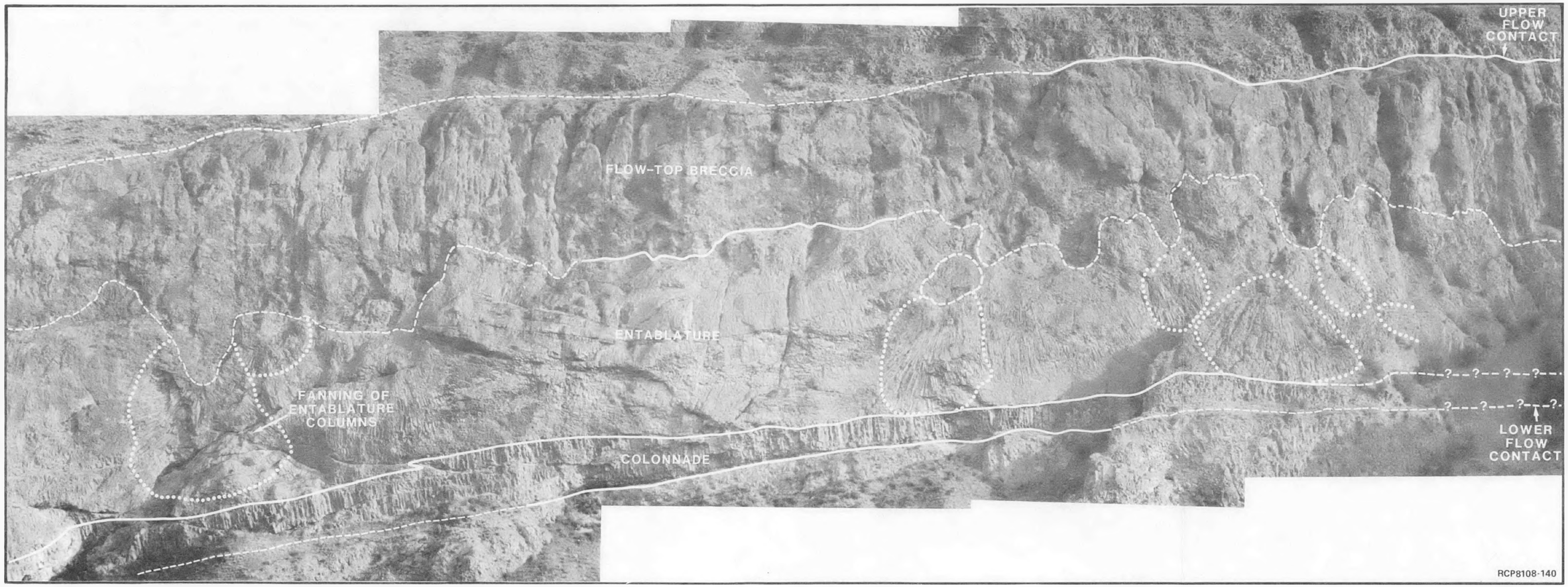

FIGURE 5-24. Cliff Exposure, Umtanum Flow and Emerson Nipple Section. Note the thick flow breccia and thin colonnade. Prominent fanning arrays occur in the entablatures and these features are spatially associated with areas of thickening of the overlying flow top. The radiating columns of the fan in conjunction with the flow top and lower colonnade may be of hydrologic significance.

The entablature at both localities is thick relative to the colonnade. At Emerson Nipple, the colonnade is 5 to 8 m thick; whereas, the entablature is 30 to 75 m thick. The entablature at Sentinel Gap is 40 m thick; whereas, the colonnade is at least 15 m thick. Poor exposure may conceal a second, lower entablature which would make the Umtanum flow here a type II flow.

Evidence from limited exposure of the Umtanum flow suggests, then, that a major intraflow structure, the flow-top breccia, thins markedly in the 20 km from Emerson Nipple to Sentinel Gap. It is also possible that the flow changes from a type III to a type II flow over that same distance.

The details of fracture patterns within the entablature also vary significantly between the two exposures of the Umtanum flow. At the river-level exposure at Sentinel Gap, the entablature exhibits a distinctive, hackly fracture pattern with only a suggestion of a columnar structure. At Emerson Nipple, columnar structure is well developed as well-formed, slender columns. Locally, these columns radiate as inverted fans (Fig. 5-24) with centers spaced at intervals ranging from a few to 160 m. From these observations, it is predicted that orientation of column-defining fractures, especially in the entablature, will vary considerably. On the other hand, parts of the Umtanum flow interior are expected to have a very hackly character with approximately random orientation of fractures.

Figure 5-24 also illustrates that the radiating fans in this particular exposure have flow-top breccia at their apices. This breccia is connected to the main body of flow-top breccia and, thus, it forms a dimple on the interface between the flow-top breccia and the underlying entablature. The origin of the dimple is uncertain, but it has apparently affected the formation of cooling joints locally, thus creating the inverted fans. The occurrence of the dimples is particularly significant, because the relatively porous nature of the flow top combined with the well-developed columnar fractures of the inverted fans may significantly reduce the amount of hydrologic isolation provided by the host flow itself. In order to check this possibility, it will be necessary to hydrologically test these features; this probably can only be accomplished in a test facility at repository depths.

Basal colonnade at the Emerson Nipple locality ranges from $\sim$7 to 13 m in thickness. As previously stated, there may be two colonnades at Sentinel Gap. The exact way in which the transition from one to two colonnades takes place is uncertain, but judging from exposures north of Vantage, the transition would be gradual rather than abrupt. The lower colonnade at Emerson Nipple may correlate with the lowest colonnade at Sentinel Gap. This means that major changes in fracture abundance or average column diameter are to be expected in a least some parts of the Umtanum flow interior; that is, colonnade may occur in what would otherwise be homogeneous entablature. Evidence for such occurrence has been obtained from subsurface cores and is presented in a later section of this chapter.

DISCUSSION

Studies of laterally extensive surface exposures of Grande Ronde Basalt indicate that intraflow structures of flows change laterally. They do so, however, within certain limits. Some of the changes, such as appearance or disappearance of pillowed zones, can be predicted if paleogeography is known or can be assumed. The locations of other features, such as thinning of colonnade, multiple tiers of entablature, or colonnade and fanning of entablature columns, probably cannot be predicted with any certainty. These features should, however, be anticipated in the Umtanum and other Grande Ronde flows and they can be objectives for hydrologic testing at depth in an exploratory test facility. With additional data from field observations and from deep boreholes, the number and spacing of these features that might occur in any given volume of the Umtanum flow could be predicted.

GENERAL MINERALOGY AND PETROGRAPHY OF GRANDE RONDE BASALT

Grande Ronde flows are aphyric to microphyric or very sparsely phyric basalt with higher hyalo-ophitic, intersertal, intergranular, or slightly ophitic textures. Subequant to lath-shaped pyroxene grains (0.05 to 0.2 mm) and lath-shaped plagioclase grains (0.07 to 0.3 mm) are set in a glassy mesostasis. Equant to cruciform or dendritic titaniferous magnetite grains are scattered throughout the rock, but tend to be most common in glassy areas. Accessory minerals, apatite, orthopyroxene, pigeonite, and olivine occur as primary phases. Alteration products include clay minerals, principally smectite clays; zeolites, mainly clinoptilolite and mordenite; and silica in a variety of forms ranging from opal to crystalline quartz and including cryptocrystalline calcedony, crystobalite, and tridymite. Sulfides, notably pyrite and chalcopyrite occur mainly as secondary minerals along cooling joints; some occurrences of sulfides as primary phases have been noted (Ames, 1980). Minor amounts of other phases have been identified in vesicles in Grande Ronde Basalt, such as erionite, chabazite, calcite, vermiculite, phillipsite, and gypsum (Benson and Teague, 1979).

Primary phases are summarized in Table 5-1 and secondary phases in Table 5-2. Each of the principal (primary and secondary) phases in Grande Ronde Basalt are discussed individually in the following sections.

PRIMARY PHASES

Plagioclase

Plagioclase is the most abundant mineral phase in Grande Ronde Basalt. It most commonly occurs as euhedral to subhedral laths that range in length from $\sim$0.2 to $\sim$1 mm and in width from $\sim$0.05 to $\sim$0.5 mm. Microphenocrysts are common, but typically not abundant; they impart a slightly bimodal

TABLE 5-1. Petrographic Characteristics of Primary Phases in Grande Ronde Basalt.

Characteristic phase	Abundance (vol%)	Compositional range	Compositional zoning	Grain size (mm)	Texture	Special features
Plagioclase	25 to 50	An_{45} to An_{65}	Generally moderate, normal. Locally reversed and/or oscillatory	0.1 to 1.0, Average ≃0.25	Lath-shaped	Microphenocrysts common; contains melt inclusions and symmetrically arranged pyroxene inclusion
Augite	20 to 45	Wo_{30} En_{38} Fs_{32} to Wo_{33} En_{45} Fs_{22}	Moderate, normal, intergrown with pigeonite, some iron-rich rims	0.05 to 0.8, Average ≃0.20	Euhedral to subhedral prismatic grains	
Pigeonite	0 to 10	Wo_{13} En_{50} Fs_{37} to Wo_{9} En_{64} Fs_{29}	Intergrown with augite, occurs as rims on some clinopyroxene or orthopyroxene grains	∿0.1	Anhedral, equant	Mode of occurrence and textures suggest limited stability range in certain flows
Orthopyroxene	0 to trace	Wo_{4} En_{61} Fs_{35} to Wo_{6} En_{75} Fs_{19}	Unzoned to slight normal zoning	∿0.2	Subhedral, prismatic, commonly embayed	Resorbtion textures and reaction rims indicate instability at 1 atm
Titaniferous magnetite	0 to 7	TiO_2 = 28 to 32 wt%	Unzoned (?)	∿0.05 to 0.4	Octahedral, cruciform or dendritic	Oxidation lamellea occur in colonnade samples
Mesostasis	15 to 70	SiO_2 = 60 to 74 wt%	Compositional variation apparent adjacent to magnetite and clinopyroxene grains	∿0.1 to 0.3	Intersertal interstitial, with or without abundant tachelytic inclusions	Immiscible liquid blebs common. Highly tachelytic in entablature, relatively inclusion-free in colonnade.
Apatite	0 to 2	N. D.*	N. D.*	∿0.01 to 0.1	Acicular	Occurs both as discrete grains and as minute crystal aggregates within immiscible liquid blebs
Olivine	0 to 3	Fo_{67} to Fo_{47}	Moderate, normal zoning	∿0.05	Anhedral to subhedral, equant	Commonly absent from Grande Ronde flows. Occurrence limited to glassy rind of some flows.

*Not determined.

TABLE 5-2. Secondary Minerals Identified in Grande Ronde Basalt, Pasco Basin.

Clay Minerals		
Smectite*		
Montmorillonite	$(Ca,Na)_{0.66}(Al^{+3},Mg^{+2})_{4-6}(Si,Al)_8O_{20}(OH)_4.nH_2O$	dioctahedral
Beidellite	$(Ca,Na)_{0.66}(Al^{+3})_{4-5}(Si,Al)_8O_{20}(OH)_4.nH_2O$	dioctahedral
Nontronite	$(Ca,Na)_{0.66}(Fe^{+3})_{4-6}(Si,Al)_8O_{20}(OH)_4.nH_2O$	dioctahedral
Saponite	$(Ca,Na)_{0.66}Mg_6(Si,Al)_8O_{20}(OH)_4.nH_2O$	trioctahedral

Zeolites	
Heulandite	$(Ca,Na_2)(Al_2Si_7O_{18})\cdot 6H_2O$
Clinoptilolite*	$(Ca,Na_2,K_2)(Al_{1.5}Si_{7.5}O_{18.1})\cdot 6H_2O$
Mordenite	$(Na_2,K_2,Ca)(Al_2Si_{10}O_{24})\cdot 7H_2O$
Phillipsite	$(Ca,Na,K)_3(Al_3Si_5O_{16})\cdot 6H_2O$
Harmatome	$Ba(Al_2Si_6O_{16})\cdot 6H_2O$
Chabazite	$Ca(Al_2Si_4O_{12})\cdot 6H_2O$
Erionite	$(Na_2,K_2,Ca,Mg)_{4.5}(Al_9Si_{27}O_{72})\cdot 27H_2O$

Silica Polymorphs*	
Quartz	SiO_2
Tridymite	SiO_2
Cristobalite	SiO_2
Opal	$SiO_2.nH_2O$

Miscellaneous Species	
Gypsum	$CaSO_4.2H_2O$
Calcite	$CaCO_3$
Pyrite	FeS_2

*Identifies the dominant secondary minerals.

size distribution to the plagioclase grains. Samples from the interior of Grande Ronde flows exhibit no obvious preferred orientation of plagioclase laths; whereas, samples from the glassy basal zones and from vesicular flow tops do exhibit strong preferred orientation.

Even though plagioclase grains are almost invariably tabular or lath shaped, the details of crystal outlines, size distribution, and general arrangement create notable differences in rock textures. Plagioclase grains occur in felted masses with relatively little size variation in some samples; whereas, in others a seriate texture is dominated by intervening pyroxene grains. Typical textural variations are shown in a later section on intraflow structures.

Some individual plagioclase grains, especially microphenocrysts, exhibit prominent optical zoning which reflects anorthite-content variation of ∿13 mol% from ∿An_{45} to An_{58} (Ames, 1980). Zoning is oscillatory, with an overall normal trend. Zoning in microphenocrysts commonly reveals rounded to embayed morphologies in the crystal interiors.

Microphenocrysts also exhibit glass or devitrified glass inclusions which presumably represent melt trapped by the growing crystal. These inclusions commonly occur along twin planes or in association with embayed or corroded crystal interiors. Other inclusions are principally minute pyroxene grains arranged necklace-fashion along major changes in anorthite content.

Clinopyroxene

Clinopyroxene is the secondmost abundant phase in Grande Ronde Basalt. It includes augite and pigeonite. Pigeonite is discussed below. Early-formed augites exhibit typical prismatic forms. These are best developed in glassy rinds of pillows or at the base of flows. In the flow interiors, the prismatic morphology is obscured by late growth on early-formed crystals and by the formation of separate, smaller grains. This yields an overall subhedral, slightly shratty shape to the majority of pyroxene grains and imparts a seriate to bimodal size distribution. Seriate textures are most common in the colonnade; whereas, a bimodal size distribution is apparent in the entablature samples. Grain sizes range from ∿0.05 to 0.5 mm and average ∿0.15 mm. Prismatic grains are commonly ∿4 times as long as they are wide.

Slight normal zoning is nearly ubiquitous in augite grains. Magnesium/magnesium + iron (Mg/Mg+Fe) commonly spans a range of 55 to 70, with calcium (Ca) contents ranging from Wo_{27} to Wo_{34}.

Inclusions are less common in clinopyroxenes than in plagioclases, but both glass and unidentified crystalline inclusions do occur in the larger grains.

Pigeonite

Pigeonite occurs in moderate to low abundance in almost all Grande Ronde flows. It typically occurs as small, groundmass grains. Detailed microprobe studies are in progress to determine its exact abundance or mode of occurrence. Price (1977), however, has reported a value of 9 vol% for pigeonite abundance in the Grande Ronde type locality area. These pigeonites contained 19.9 wt% FeO, 20.1 wt% MgO, and 4.9 wt% CaO.

The small grain size, low abundance, and apparent lack of pigeonite in some flows suggest that it has a limited stability range.

Orthopyroxene

Orthopyroxene occurs rarely in Grande Ronde flows. It has been reported from widely scattered localities across the Columbia Plateau (Reidel and others, 1978), however, and this suggests that in spite of its low abundance, it may be of petrogenetic significance. Orthopyroxene grains may be prismatic or rounded and are ∿1 to 2 mm in length. Reaction rims and resorbtion features are ubiquitous. Textural association or even intimate intergrowth with large plagioclase grains is also very common. Zoning is slight to absent, with most grains exhibiting a uniform, inclusion-free interior.

Alumina (Al_2O_3) contents are low, ranging from 0.7 to 1.2 wt%, suggesting a low- to intermediate-pressure stability range (Reidel and others, 1978).

Titaniferous Magnetite

Titaniferous magnetite occurs as octahedral, cruciform, or dendritic grains that range in size from ∿0.2 to 0.05 mm. Octahedral or cruciform grains are typically imperfect or incomplete. Compositional range of this material is not well known, but analyzed samples for one flow (Umtanum) show a nearly constant TiO_2 content, ranging from 28 to 32 wt% (Noonan and others, 1980). Little other compositional data are currently available from Grande Ronde samples.

Optical examination, however, indicates oxidation sometimes occurs along grain boundaries of the blocky, octahedral grains. These are most common in the basal and upper colonnades.

Titaniferous magnetite typically constitutes from 3 to 7 vol% of Grande Ronde samples. Some samples, notably from very hackly entablature and from glassy rinds of pillows, flow bases, or flow tops, exhibit lesser percentages of extremely small magnetite grains.

Olivine

Olivine is relatively rare in Grande Ronde Basalt. Abundances range from zero to as high as 3 vol% with the majority of samples containing <0.25 vol%. Compositions typically range from Fo_{67} to Fo_{47}, with moderate, normal zoning. Grains are anhedral, equant, and ~0.05 mm in diameter, and are most readily observed in glassy pillow rinds. In certain flows, olivine is essentially restricted to the pillow rinds, suggesting that it may have a reaction relationship with the residual liquid (Schiffman, 1979).

Glassy Mesostasis

An interstitial glassy mesostasis occupies from 15 to 65 vol% of Grande Ronde flows. Samples with abundant mesostasis come from the entablature or glassy flow bases; whereas, the samples with the least glass occur in the colonnade. Texture within the mesostasis itself varies considerably with position in the flow. Glass from the colonnade, for example, is relatively inclusion free; whereas, glass or mesostasis from the entablature is invariably charged with tiny crystalline inclusions which are dominantly pyroxene, but which also include apatite and opaque oxide grains. Some of the crystalline inclusions occur as rounded blebs, clearly indicating that they represent crystallized, immiscible liquid. Evidence for liquid immiscibility is also present in colonnade samples, but is absent from glassy pillow rinds or from flow tops. The mesostasis of the flow tops is characterized by felted masses of extremely fine-grained material; presumably, this material is mainly pyroxene.

Compositional data on the mesostasis are sparse. A single study (Noonan and others, 1980) on the Umtanum flow indicates that, at least for that flow, the mesostasis has a highly fractionated bulk composition that is essentially granitic (SiO_2 = 61 to 73 wt%). Variations in cation abundances exist between the mesostasis of entablature and colonnade. The colonnade mesostasis exhibits more K_2O and SiO_2, but less CaO, Na_2O, FeO, and P_2O_5 than does the entablature mesostasis.

Apatite

Apatite abundance ranges from 0 to 2 vol% of most Grande Ronde flows. Its most predominant occurrence is as 0.01- to 0.1-mm accicular crystals in the mesostasis, but it also occurs as extremely fine grains within immiscible, liquid blebs. Preliminary microprobe data suggest that fluorine is present in the apatites at the ~1% level.

SECONDARY PHASES

Diagenesis of the Grande Ronde Basalt has produced secondary minerals along fractures, in vugs, and in relatively porous, vesicular rock. These secondary minerals are predominantly smectite clays, zeolites (clinoptilolite), and SiO_2. The data on these minerals reported here are based on

the work of Ames (1980), Benson and Teague (1979), and Teague (1980) and, in addition, on petrographic observations made as part of this study.

Numerous, other, secondary minerals have been identified, but typically in much lower abundance. These minerals are listed in Table 5-2.

The relative abundances of the principal secondary minerals are given in Table 5-3; note that smectite clays are more abundant in fractures than in vugs. The volume abundance of secondary minerals in fractures relative to the total rock mass is indicated by Figure 5-22; it is <0.4% in the flow with the most fracture fillings and <0.3% in the flow with the least filling material. The volume percent of vesicle fillings is nil in the interior of the flow, but increases to as much as 20 vol% in the flow top and vesicular base.

TABLE 5-3. Relative Proportions of Secondary Minerals in Grande Ronde Basalt, Pasco Basin.

Mineral	Vesicles	Fractures
Smectite	∿32*	∿75
Clinoptilolite	∿43	∿20
Silica	∿25	∿5

*Values are in percent by volume of total amount present. For abundance of fracture fillings as a percentage of total rock mass, see Figure 5-22. Data from Benson and Teague, 1979.

The order of crystallization of secondary minerals is smectite clay followed by clinoptilolite followed by silica. Silica is followed in some fractures or vugs by additional generations of zeolite or clay. Multiple, early, clay generations are also present in some samples (Benson and Teague, 1979).

Among the many, minor, secondary phases that occur in the basalt (Table 5-2), mordenite (a zeolite) is of particular interest. It occurs only below a depth of >950 m. This horizon is nearly horizontal between wells investigated thus far, and apparently is not deflected by folds in the basalt (Smith and others, 1980). This suggests that either the mordenite was not formed until after folding had occurred or the dissolution and formation of mordenite were able to keep pace with the rate of folding.

Experimental data on the stability of mordenite (Smyth and Caporuscio, 1981) imply that temperature at the depth at which mordenite first appears should be higher than it actually is. The first appearance of mordenite with depth, then, represents a fossil geothermal gradient somewhat higher than the one that currently exists.

Chlorophaeite, iddingsite, and mineraloid are terms that are commonly used to refer to secondary minerals in basalt. Mineraloid is a general term that refers to inorganic materials that are amorphous. The only identified alteration phases in these basalts that could be classified as mineraloid are opal and hydrated basaltic glass. In spite of liberal use of the term mineraliod in reference to secondary minerals in Columbia River basalt, including fracture and vug fillings, the majority of secondary phases are well-defined mineral species.

Chlorophaeite is a "specific" mineraloid which is similar to chlorite in composition (Mg-, Fe-, Ca-silicate). As with the more general term mineraloid, chlorophaeite is used to refer to vug and fracture fillings, as well as altered interstitial glass and pseudomorphs after olivine. Chlorophaeite is a useful, general term for field descriptions, but as applied to Columbia River basalt, it includes much material that is here reported as specific mineral species, particularly zeolites and clay minerals. Iddingsite refers to alteration products of olivine, and is considered to be a mixture of Mg, Ca, and Fe silicates. This term may be applied to olivine-bearing flows, but again, actual mineral species constituting iddingsite are probably specific zeolites and clay minerals. Specific mineral names should be used where they have been definitely identified. The use of the more general terms discussed above should be avoided where possible.

RELATIONSHIPS BETWEEN INTERNAL STRUCTURES AND PETROGRAPHIC TEXTURES

Figures 5-25, 5-26, and 5-27 illustrate the relationships between intraflow structures and petrographic textures. Type I flows show consistent intersertal to intergranular textures throughout the flow thickness, except for somewhat glassy basalt in the upper 10 to 15% of the flow. This is apparently related to relatively rapid cooling of the flow top that is typical of virtually every flow. Note that opaque morphology, glass abundance, and glass texture are similar in all parts of the flow beneath the flow top. Consistency of petrographic textures throughout the main body of the flow is characteristic of all type I flows we have sampled.

Type II flows exhibit textural differences that are spatially associated with the repeated entablature and colonnade tiers. Samples from the lower colonnade have intersertal to intergranular textures that are finer grained, but otherwise similar to the samples from type I flows. Octahedral magnetite grains and a relatively inclusion-free

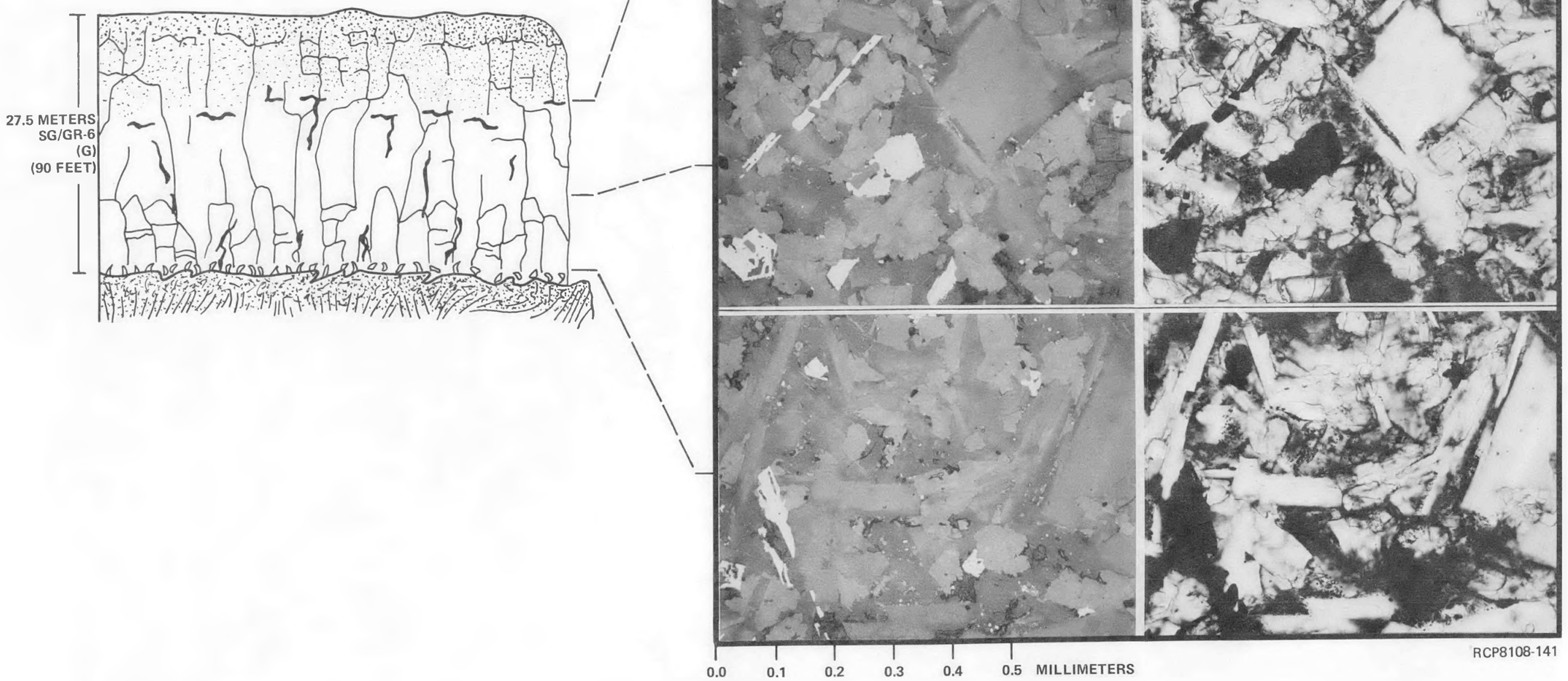

FIGURE 5-25. Petrographic Textures, Type I Flow, Sentinel Gap. Textures are similar throughout the interior of the flow.

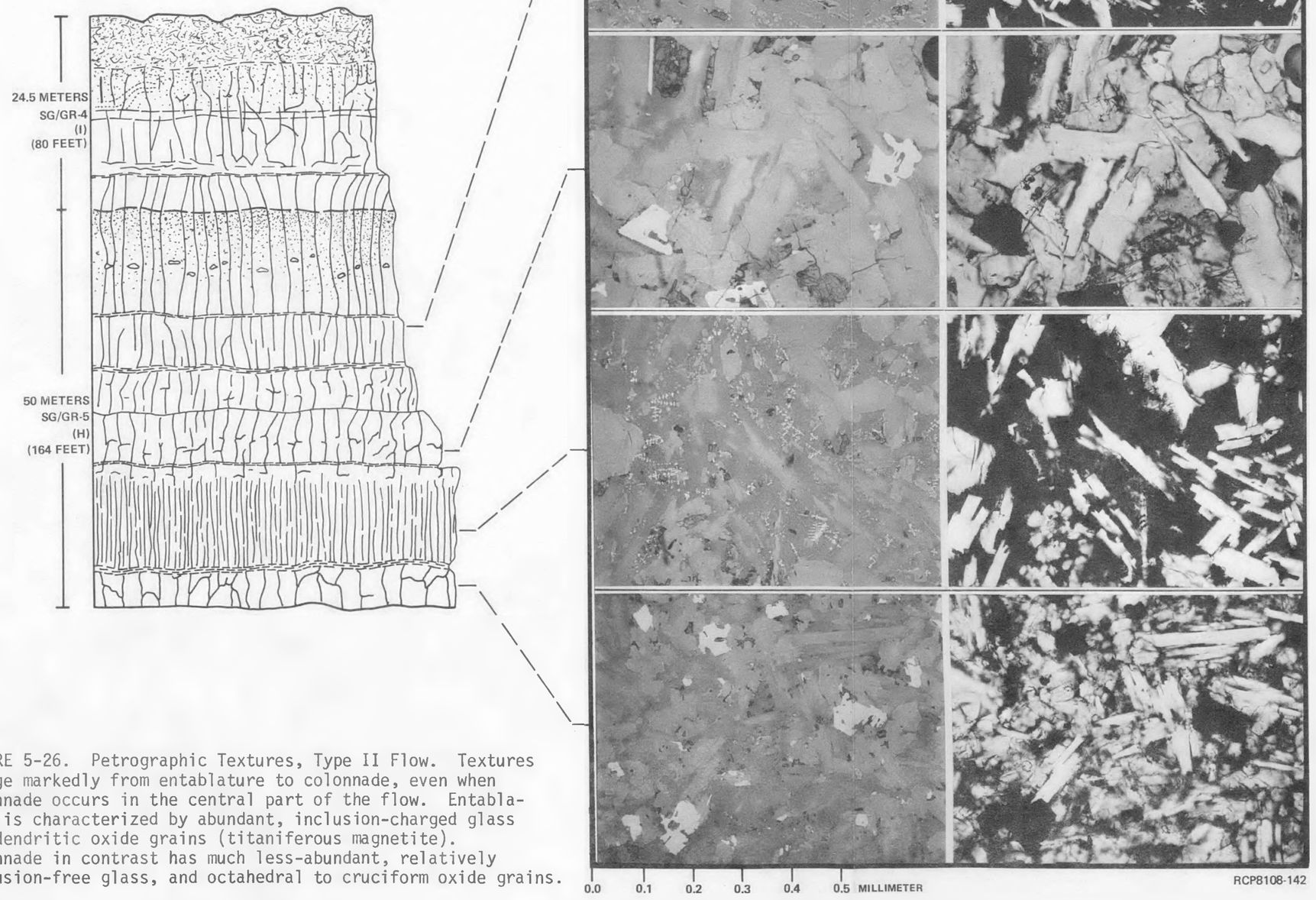

FIGURE 5-26. Petrographic Textures, Type II Flow. Textures change markedly from entablature to colonnade, even when colonnade occurs in the central part of the flow. Entablature is characterized by abundant, inclusion-charged glass and dendritic oxide grains (titaniferous magnetite). Colonnade in contrast has much less-abundant, relatively inclusion-free glass, and octahedral to cruciform oxide grains.

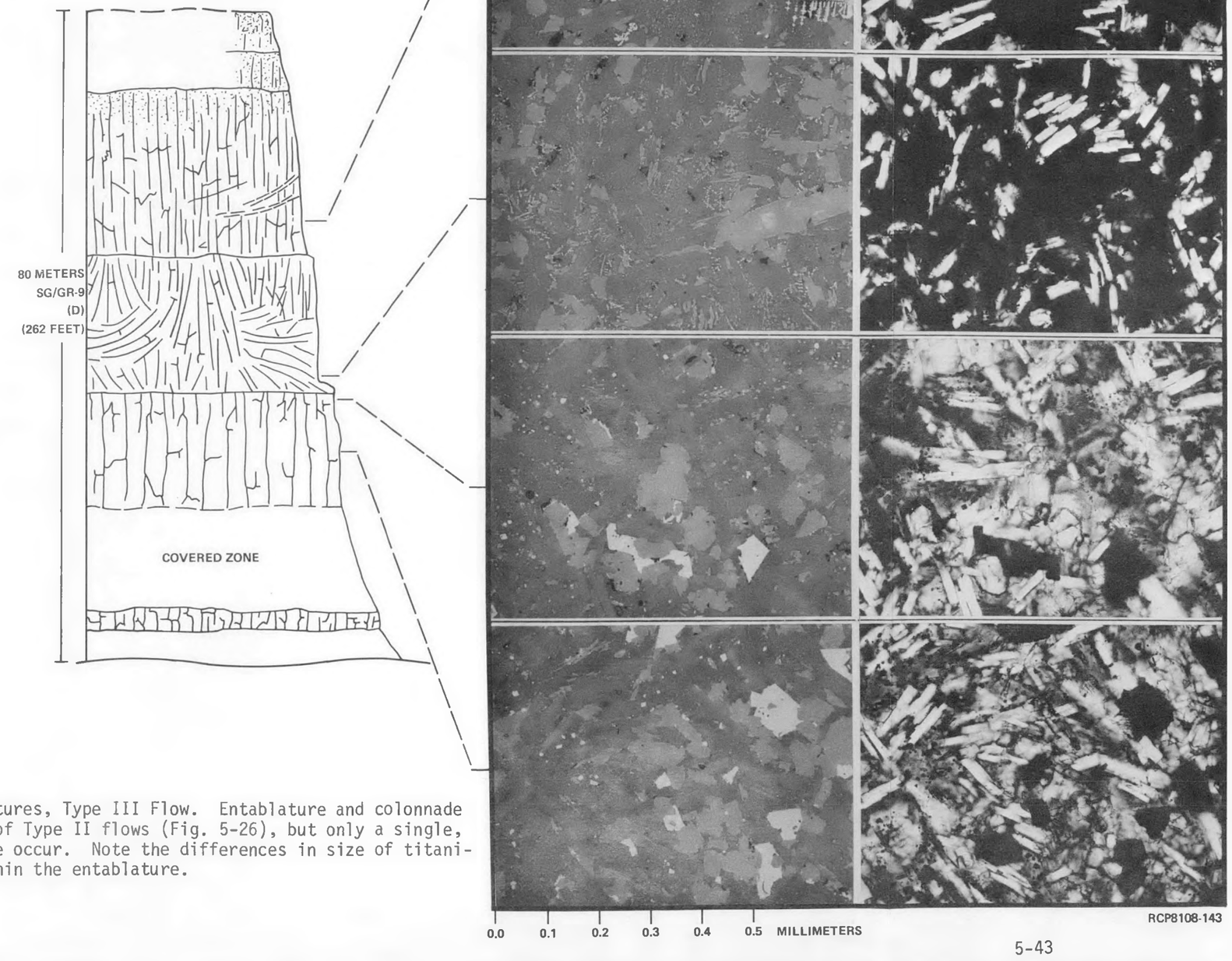

FIGURE 5-27. Petrographic Textures, Type III Flow. Entablature and colonnade textures are similar to those of Type II flows (Fig. 5-26), but only a single, lower colonnade and entablature occur. Note the differences in size of titaniferous magnetite dendrites within the entablature.

mesostasis are present in the colonnade. The entablature portions, however, are characterized by a subhyalo-ophitic texture, a dendritic morphology of titaniferous magnetite, and an inclusion-charged, glassy mesostasis. The abundance of mesostasis in the entablature zones is substantially greater than it is in the colonnade zones. Colonnade typically has ∿15 to 25 vol% mesostasis; whereas, the entablature mesostasis abundance ranges from ∿35 to as much as 70 vol%.

Type III flows exhibit similar textures associated with entablature and colonnade which are similar to those in type II flows. In type III flows, however, the entablature and colonnade sequence is not repeated. A single, sharp, entablature-colonnade contact occurs in the lower half of the flow. Samples ∿1 m apart on either side of this contact show the characteristic textures of entablature and colonnade. In the few flows where the entablature-colonnade contact is gradational, the associated textures are also gradational in accordance with sample position. Thus, the petrographic textures of these flows consistently reflect the internal characteristics of these flows, even where gradations occur.

The petrographic characteristics of entablature and colonnade are not identical in all flows. For example, the exact mesostasis abundance in the entablature may differ from flow to flow and the texture of the entablature mesostasis is rarely identical from one flow to another. Morphology of the opaque oxide grains is highly variable. In some flows, oxide phases are absent entirely in the entablature; whereas, the morphology of opaque grains may differ only slightly across the entablature-colonnade contact in others.

In spite of such variations, the sense of change in the abundance of mesostasis and in the abundance of inclusions in the mesostasis is consistent; mesostasis is markedly more abundant in the entablature than in the colonnade and the abundance of inclusions increases from colonnade to entablature in each case examined.

DISCUSSION OF THE PETROGRAPHIC TEXTURES

The consistency of the correlation of entablature and colonnade with their respective petrographic textures in these flows suggests that such textures universally characterize entablature and colonnade. The single entablature (curvicolumnar zone) sample for which Tomkeieff (1940) reported petrographic data supports this extrapolation. We suggest that future field work in basalt terrains include detailed sampling of entablature and colonnade for petrographic study.

The petrographic characteristics of entablature and colonnade clearly indicate that the entablature cooled at a more rapid rate than the colonnade. The abundance of mesostasis, texture of the mesostasis, and morphology and abundance of titaniferous magnetite relative to the colonnade all point to a more rapid cooling rate for the entablature. The high abundance of mesostasis in the entablature indicates that a cooling rate, which would have produced a colonnade texture, was interrupted by a more rapid cooling rate which quenched the residual glass. This resulted in the mesostasis

observed in entablature samples. The more rapid cooling rate, however, did not entirely stop crystallization; it gave rise, instead, to a higher nucleation rate which resulted in the high density of crystalline inclusions in the mesostasis (Lofgren, 1980). The dendritic morphology of the opaque oxide grains in the entablature is characteristic of a high degree of undercooling that results from a high-cooling rate. In some flows, titaniferous magnetites are absent, suggesting that the cooling rate was sufficiently rapid to suppress nucleation entirely (Lofgren, 1980). These same entablatures typically exhibit the finest grained mesostasis consistent with high-cooling rate compared to other entablature samples.

Lofgren (1980) has reviewed experimental evidence for relationships between crystal morphology, nucleation rate, growth rate, and cooling rate. No attempt will be made here to cite the extensive literature on the subject, but there seems to be little doubt that the morphological and textural features of the entablature are evidence for a cooling rate more rapid than that of the colonnade. For types II and III flows, this means that significant differences in cooling rate occur adjacent to one another across an entablature-colonnade contact. Thermal properties of silicate rocks suggest that this cannot occur if thermal conduction alone controls the cooling of the flow. Indeed, conductive cooling models (Jaeger, 1961) do not predict sharp differences in cooling rate anywhere in the flow. For this reason, the cooling history of flows has been investigated by a simple, one-dimensional, thermal model which mimics the effect of convective removal of heat by ingress of water along cooling joints.

The results of the model show that it is possible to quench the interior of a flow if the depth of water ingress is controlled by the position of the solidification front in the flow. Thus, if the flow were to be inundated by water from deranged drainage or perhaps heavy rainfall, the interior of the flow would cool at a much higher rate than the outer parts of the flow which would have crystallized prior to the flooding event. This process for creating entablatures and its implications for intraflow structures are discussed in a later section.

INTERPRETATION OF INTRAFLOW STRUCTURES OF THE McCOY CANYON AND UMTANUM FLOWS IN THE COLD CREEK SYNCLINE AND SURROUNDING AREAS

By utilizing the relationship between internal structures and petrographic textures, it is possible to determine the internal structures of a flow from drill core samples. We have done this for boreholes that penetrate the McCoy Canyon and Umtanum flows (see Chapter 4). By combining these data from subsurface samples with observed internal structures of surface exposures of these same flows, we have constructed fence diagrams which illustrate the lateral differences in internal structures of these flows.

McCOY CANYON FLOW

Figure 5-28 depicts the fence diagram for the McCoy Canyon flow. This flow is thickest in the area of the Sentinel Gap and Emerson Nipple sections. It thins to the northeast and southeast (see Chapter 4). This distribution reflects an easterly source area, with lava flowing westerly to southwesterly down a regional paleoslope (Long and others, 1980)--a topographic low in the Sentinel Gap area. The flow lapped onto a gentle topographic high to the north and probably terminated several kilometers north of Crescent Bar. Forset pillows indicate a northerly to westerly direction of emplacement in the area north of Vantage; apparently, the westerly direction of flow emplacement in more southerly areas was at least partly diverted to the north as it reached the base of the paleoslope.

The pillow zone is restricted to the northern portion of the flow, where it formed in a shallow lake that apparently formed behind an early lobe of the McCoy Canyon flow or behind a previous flow or flows. The pillow zone is thickest at the Quilomene Bay and Sunland Estates sections ($\sim$23 m). It thins to the north and to the south and is absent in both the Sentinel Gap and Crescent Bar sections. It is noteworthy that the pillow zone thins markedly as the flow thins to the north (Fig. 5-23). This is consistent with a shallow body of water occupying topographic lows and provides further basis for attributing northward thinning of the flow to a slight topographic high.

Entablature and colonnade thickness vary partly in relation to total flow thickness. In particular, the character of the entablature varies because several of the core holes exhibit repeated colonnade-entablature tiers or perhaps simply differences in column diameter related to fanning of columns. If these tiered portions of the flow are included in the entablature, then the entablature is thickest where the flow is thickest (DH-5, Emerson Nipple section; Fig. 5-1). The entablature also thins to the south and east, although there is not a one-to-one correspondence between entablature and total flow thicknesses. Basal colonnade thickness is apparently unrelated to total flow thickness. Upper colonnade occurs in two surface exposures and in DH-4, DC-4, and DC-2 (Fig. 5-1). It exhibits no consistent thickness or geographic occurrence pattern. This is consistent with observations of surface exposures where upper colonnade grades laterally into and out of entablature.

The thickness of flow-top breccia or vesicular flow top correlates well with total flow thickness. One slight exception to this occurs in DC-2 (Fig. 5-1), but no anomalous thicknesses of flow-top breccia have been discovered to date in the McCoy Canyon flow. The general correlation of flow-top breccia thickness with total flow thickness is consistent both with formation of the flow top from degassing of the underlying flow and with accumulation of flow-top breccias where the volume of the flow is greatest.

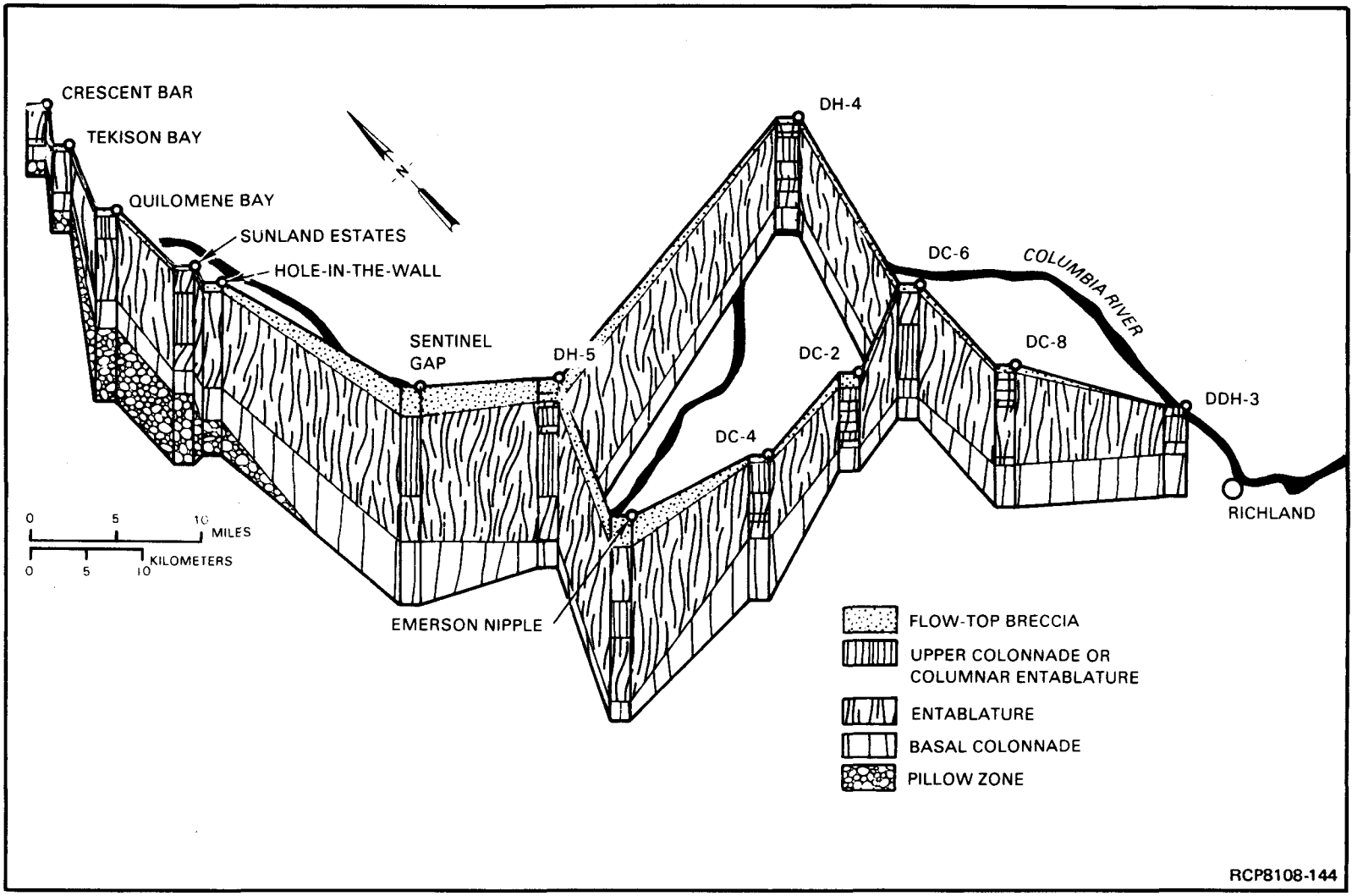

FIGURE 5-28. Fence Diagram, McCoy Canyon Flow. This figure is an illustration of the lateral variation of internal structures of the flow in subsurface borings and surface exposures.

UMTANUM FLOW

The Umtanum flow thins to the northeast and along a broad zone trending southwest-northeast to the central part of the Pasco Basin (Fig. 5-29). Like the McCoy Canyon flow, the Umtanum flow is thickest in the area of Sentinel Gap, Emerson Nipple, and DH-5 (Fig. 5-1), but thins farther west where the flow apparently lapped onto the north-south-trending Hog Ranch anticline or, alternatively, an early expression of the Umtanum Ridge structure (Price, in press). The northern edge of the flow lies several kilometers north of DH-4 and Emerson Nipple. Its exact location is not known; only that it pinches out between Sentinel Gap and Sunland Estates.

The thickness of the basal colonnade of the Umtanum flow is not consistently correlated with total flow thickness; in most core holes, however, it makes up <10% of the total flow thickness. The entablature is also variable in its thickness, but in general, it is relatively thick. It exhibits tiering in the southeastern portion of the Pasco Basin and in DH-5 (Fig. 5-1). In the area of the western Cold Creek syncline, however, DC-4 did not penetrate tiering. This core hole has a consistent, uniform, glass-rich texture, suggesting few differences in fracture abundance. Obviously, data are very limited in the area and additional boreholes are required to determine if the Umtanum flow in DC-4 is characteristic of a wider area. It must also be pointed out that if the tiering features encountered in the entablature are due to radiating columns, then drilling results obtained so far probably do not reflect the actual distribution of these features. Rather, we would anticipate the occurrence of fanning joints in any entablature on a fairly wide range of spacings, from a few to as much as several hundred meters.

Upper colonnade of the Umtanum flow has no consistent geographic occurrence. It occurs in five of the boreholes, but is highly irregular in its thickness. This is typical for a type III flow.

The flow-top breccia of the Umtanum flow is anomalously thick at the Emerson Nipple section, DC-8, and DDH-3. It apparently thins to the east from the Emerson Nipple section to DC-4, where it occupies a portion of the total flow thickness which is more characteristic of other flows in the area. Isopachs of the flow-top thickness suggest that it is ~18 m thick or 28% of the total estimated flow thickness in the RRL (Chapter 4). The possibility of a highly localized increase in the thickness of flow-top breccia related to fanning joints has been discussed previously.

The overall geographic distribution of the flow-top breccia suggests that it is thickest in a northwest-southeast-trending zone on the southwest margin of the Pasco Basin. It is also noteworthy that in DDH-3, outside the Cold Creek syncline study area, the flow top occurs as two units, suggesting the possibility of flow lobes occurring locally in the upper part of the Umtanum flow.

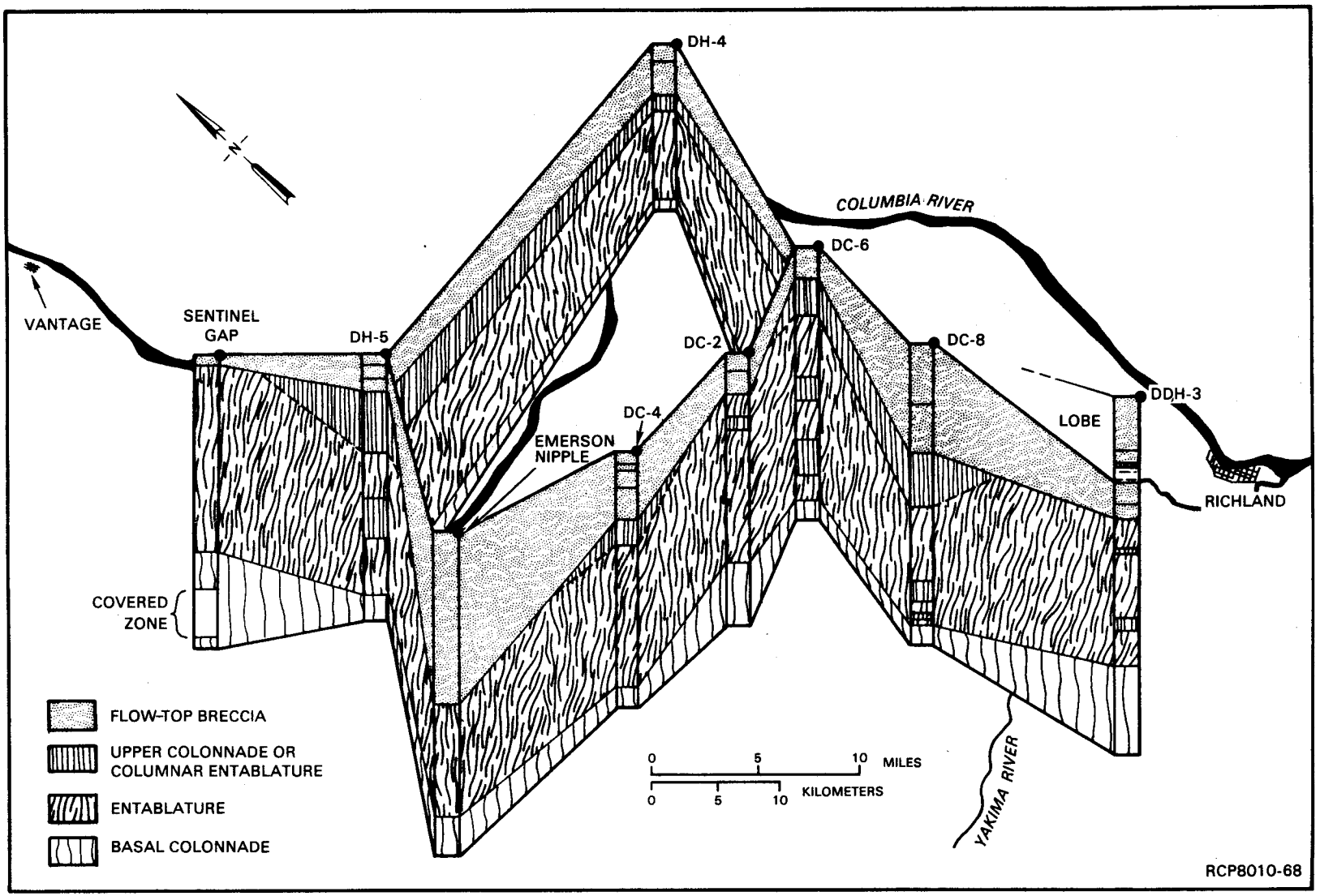

FIGURE 5-29. Fence Diagram, Umtanum Flow. This figure is an illustration of the lateral variation of internal structures of the flow in subsurface borings and surface exposures.

DISCUSSION OF INTRAFLOW STRUCTURES OF THE GRANDE RONDE BASALT AND THEIR IMPLICATIONS FOR REPOSITORY SITING AND PERFORMANCE

Primary intraflow structures of Grande Ronde Basalt result from processes which occur during the emplacement and subsequent cooling of each flow. The data presented in the previous sections of this chapter shed considerable light on these processes. The purpose of this section is to summarize interpretations of how intraflow structures form and the impact these interpretations have on repository siting and performance.

FLOW TOPS

Vesicular flow tops are ubiquitous in these flows. They stem from a combination of outgassing of volatile constituents and rapid chilling of the upper surface of the flow. This rapid chilling creates a thin crust which is repeatedly broken during movement of the flow and reincorporated into its lower, still molten portion. When combined with vesiculation due to outgassing, this process creates the typical flow top which occupies ∿10 to 15% of the flow thickness.

Anomalously thick flow-top breccias may have originated from a similar process which has, for some reason, affected a much greater thickness of lava or they may result from a different process entirely. One possibility is that deranged drainage could cause water to pour out over the top of molten material (prior to significant formation of chilled crust) and this could cause rapid turnover of the underlying magma with attendant chilling and brecciation. This would explain the admixture of vesicular and non-vesicular clasts in the Umtanum flow-top breccia.

An alternative is the possibility that the Umtanum flow top is a near-vent breccia. That is, it represents agglutinate and spatter which accumulated in greatest thickness in close proximity to the vent. This hypothesis has at least two difficulties: (1) there is no independent evidence that there is a nearby vent area for the Umtanum flow and (2) no flow-top sample has characteristics definitely identifiable as spatter. On the other hand, there is abundant evidence that significant bodies of water were present when the flows were erupted. Lack of modern analogs, however, make it unknown if inundation by water could actually create a flow-top breccia. There is circumstantial evidence that many flows were inundated (see later discussion on origin of entablature), but thick flow-top breccias are rare. This suggests that special circumstances had to exist in order for inundation to create a flow-top breccia.

In spite of our lack of knowledge as to the exact origin of the Umtanum flow-top breccia, its general thickness can be contoured (Chapter 4) and a consistent pattern of areal variations in thickness emerges. This is apparently true, even though thickness of the Umtanum flow-top breccia is known to vary significantly on a horizontal scale of meters (e.g., Fig. 5-24). Additional data will be required to test the consistency of the thickness of flow-top breccia in the RRL.

TYPE I FLOWS

The important distinction between type I and types II or III flows is that type I flows cooled without major perturbation of their cooling history by inundation with water. Type I flows were probably emplaced with a partially formed vesicular flow top, which continued to form for a brief period after the flow stopped moving. As the flow began to cool, the major columnar cooling joints formed at the top and bottom of the flow and propagated inward with further cooling. Cooling was principally by conduction, although some convection may have occurred in the upper part of the flow due to rainfall. The lack of chilling by inundation in these flows is consistent with the observation that type I flows are typically not as thick as types II or III. Because of this, they would be less effective in damming major drainages and, hence, would be less likely to be flooded by deranged drainage.

PILLOW ZONES

Pillow zones provide direct evidence that extensive, shallow lakes occurred in Grande Ronde time. As discussed previously, these features are known to form when lava flows enter bodies of water. The lateral distribution and thickness of these features indicate that these flows commonly entered lakes of ≥30 m depth, widths of a few to several kilometers, and lengths significantly greater. These lakes were probably displaced upstream by some flows, so the apparent size of the lake judged from extent of pillows may be somewhat exaggerated.

The significance of pillow zones to repository siting and performance is that they are almost certainly of higher permeability than flow interiors and probably higher than a typical Grande Ronde flow top. They have not been encountered in Grande Ronde Basalt by core drilling in the Pasco Basin, so no hydrologic tests have been run on these features at depth. However, springs issue from between pillows at one location between Vantage and Crescent Bar and the general mode of occurrence of pillows as bulbous masses with intervening void space or porous palagonite hyaloclastite suggests a highly permeable character for these zones. The lack of pillow zones associated with Grande Ronde flows within the Pasco Basin indicates the main paleodrainages lie to the west and northwest of the present-day Pasco Basin. Because this indication fits well with the observed locations of pillowed zones and with interpretation of a regional paleoslope extending westward to the base of the rising Cascade Range, we predict that major pillow zones will not be encountered by future drilling in the Pasco Basin. Thus, thick pillow zones are not believed to be a concern for repository performance considerations or for Pasco Basin hydrologic considerations. The possible occurrence of thin, highly localized pillow zones is of interest, however. Their occurrence seems unlikely due to the probable direction of emplacement of the Grande Ronde flows. They would have flowed parallel to the tributary drainage and, thus, not ponded water in front of them. Instead, these flows would have cut off drainages,

making the formation of pillows downslope unlikely (compare with Swanson and Wright, 1976). Nevertheless, a geophysical technique for detecting nearby, minor, pillow zones during repository construction is important not only for use during the construction process, but for the purposes of final hydrologic analysis.

ENTABLATURE-COLONNADE

Petrographic textures of entablature indicate that it forms when the typical conductive cooling rate has been markedly increased. A possible explanation for this increase in cooling rate is inundation by deranged fluvial drainage. The inundation causes downward percolation of water which rapidly cools the unsolidified interior of the flow. This rapid cooling creates the highly fractured character of the entablature and accounts for the high-mesostasis abundance and quench textures of the opaque oxides.

That abundant runoff was available to cause the inundation is evidenced by the occurrence of pillow zones. The paleogeography was clearly conducive to flooding, in that the paleoslope of the plateau extended westward to the rising Cascade Range. The line of intersection of these two physiographic provinces determined the course of the through-going drainage. Flows emplaced down the paleoslope would intersect this drainage, block it, and create a lava-dammed lake. This lake would eventually overflow its dam, thus chilling the interior of the partly solidified flow. Large areas could be inundated if a later flow entered the lake, displacing much of its water out across the earlier flow. This, in fact, must have happened repeatedly, judging from the abundant pillow zones in parts of the Grande Ronde Basalt north of the Pasco Basin.

The entablature-colonnade contact then represents the position of the solidification front at the time the quenching occurred. This means that there may be considerable variation in the position of this contact within a flow, depending on the length of time between emplacement of the flow and the quenching of the flow by inundation.

Quenching of the flow by flooding also creates fanning joints in the entablature because of preferential cooling along early-formed cooling joints or at dimples in the flow-top breccia-entablature contact. These fanning columns may be hydrologically significant, in that they may provide an interconnection between the flow-top breccia and the colonnade (e.g., Fig. 5-24). Outcrop exposures of the Umtanum flow suggest that the spacing of fanning columns ranges between ~160 to a few meters. Hence, underground workings more than a few hundred meters in length have a very high probability of intersecting such fans. Considerable effort should be made to hydrologically test these features; this probably can only be accomplished in a test facility at repository depths.

Repeated colonnade and entablature in the same flow apparently result from relatively short, multiple, flooding events in which periods between floods permitted the formation of colonnade. Again, the timing and duration of flooding events will control the final disposition and character of the entablature and colonnade layers. We anticipate considerable lateral variation in these features. It is probable, for example, that type II flows grade laterally into type III as the source of floodwaters is approached. The repeated layers of colonnade, however, are separated from each other by entablature, so it is not expected that these tiers will have significant impact on hydrologic properties compared to type III flows. Differences in joint spacing, however, may affect stability of a mined opening. Consequently, the mechanical impact of these features should be examined.

SUMMARY AND CONCLUSIONS

The mineralogy, internal structures, and petrographic textures of Grande Ronde Basalt flows in the vicinity of the Cold Creek syncline have been studied in a general way for a number of Grande Ronde flows and in considerable detail for two flows: (1) Umtanum and (2) McCoy Canyon.

Grande Ronde Basalt flows are aphyric to microphyric or very sparsely phyric basalt with hyalo-ophitic, intersertal, intergranular, or slightly ophitic textures. Subequant to lath-shaped pyroxene grains (0.05 to 0.2 mm) and lath-shaped plagioclase grains (0.07 to 0.3 mm) are set in a glassy mesostasis. Equant to cruciform or dendritic titaniferous magnetite grains are scattered throughout the rock, but tend to be most common in glassy areas. Accessory minerals, apatite, orthopyroxene, pigeonite, and olivine occur as primary phases. Alteration products include clay minerals, principally smectite clays; zeolites, mainly clinoptilolite and mordenite; and silica in a variety of forms, ranging from opal to crystalline quartz and including cryptocrystalline chalcedony, crystobalite, and tridymite. Sulfides, notably pyrite, occur mainly as secondary minerals along cooling joints; some occurrences of sulfides as primary phases have been noted. Minor amounts of other phases have been identified in vesicles in Grande Ronde Basalt, such as erionite, chabazite, calcite, vermiculite, phillipsite, and gypsum.

Intraflow structures are internal units of basalt flows defined by regions within the flow of relatively uniform macroscopic features. These features are principally fractures (abundance and geometry), but also include size and abundance of vesicles, brecciation (flow top), and the occurrence of globular masses of chilled magma, known as pillows.

Fractures that occur in Grande Ronde Basalt flows have been described qualitatively by examining the shape and orientation of fracture surfaces as exposed in surface outcrop and quantitatively by measuring fracture spacing and orientation in surface exposures and core samples. Most core fractures have narrow apertures (<0.5 mm) and contain secondary minerals.

Histograms of fracture apertures which show both filled and "unfilled" fractures show clearly that fractures classified as unfilled tend toward relatively narrow apertures or have a frequency distribution similar to that of the filled fractures. Mean fracture widths for all fractures, filled or unfilled, average between 0.1 and 0.3 mm. The unfilled fractures do not occur in widths ≥0.7 mm.

The total volume percent of all fractures is clearly very small, but the volume percent of unfilled fractures is even less (<0.1%). The small volume of unfilled fractures, particularly in the dense interiors of Grande Ronde Basalt flows, limits the total fracture porosity of these rocks.

Pillow zones provide direct evidence that extensive, shallow lakes occurred in Grande Ronde time. The lateral distribution and thickness of these features indicate that these flows commonly entered lakes of ≥30-m depth, widths of a few to several kilometers, and lengths significantly greater. These lakes were probably displaced upstream by some flows so the apparent size of the lake, judged from extent of pillows, may be somewhat exaggerated.

The significance of pillow zones to repository siting and performance is that they are almost certainly of higher permeability than flow interiors and probably higher than a typical Grande Ronde flow top. They have not been encountered in Grande Ronde Basalt by core drilling in the Pasco Basin. The lack of pillow zones associated with Grande Ronde flows within the Pasco Basin indicates the main paleodrainages were to the west and northwest of the present-day Pasco Basin. Because this indication fits well with the observed locations of pillowed zones and with interpretation of a regional paleoslope extending westward to the base of the rising Cascade Range, we predict that major pillow zones will not be encountered by future drilling in the Pasco Basin. The possibility of minor occurrences remains, however. The development of geophysical methods for detection of such features during repository construction is advised.

The intraflow structures of Grande Ronde Basalt flows exert a strong influence on the hydrologic characteristics of Grande Ronde Basalt. As a consequence, they clearly impact repository design, construction, and performance. The direct correlation of intraflow structures and petrographic textures provides a basis for determining intraflow structures which occur in core holes. The data so obtained have proved extremely useful in predicting general areal trends of the intraflow structures of the McCoy Canyon and Umtanum flows.

By utilizing the relationship between internal structures and petrographic textures, it is possible to determine the internal structures of a flow from drill core samples. In most core holes, the basal colonnade of the Umtanum flow makes up <10% of the total flow thickness. The entablature is also variable in its thickness, but in general, is relatively thick (>50 m). It exhibits tiering in the southeastern portion of the Pasco Basin. In the area of the western Cold Creek syncline, however, core holes have not penetrated tiering. The entablature drilled in this area to date has a consistent, uniform, glass-rich texture, suggesting few

differences in fracture abundance. Upper colonnade of the Umtanum flow does not occur consistently in the RRL. Isopachs of the flow-top thickness suggest that it is 18 m thick or 28% of the total flow thickness in the RRL.

Among the most significant petrographic features of the Grande Ronde Basalt are the occurrence of abundant mesostasis in the entablature and the occurrence of secondary minerals as fracture fillings. Both of these features enhance the isolation capability of basalt. The high mesostasis abundance in the entablature means that it will alter and, hence, react with and inhibit the migration of radionuclides more readily than will the colonnade. Alteration products, such as clay minerals and zeolites, will tend to sorb radionuclides and will tend to fill any void space in and around the repository, including newly formed fractures. The occurrence of fracture fillings of clay (smectite), zeolite (clinoptilolite), and silica acts to reduce the permeability of the basalts, as well as provide existing highly sorbtive minerals along pathways where most of the groundwater flow through these rocks would occur.

CHAPTER 6 - BOREHOLE GEOLOGIC STUDIES

D. J. Moak

INTRODUCTION

The purpose of this chapter is to describe results of fracture studies of basalt core and to compare the predicted versus observed stratigraphy in certain boreholes recently drilled by the BWIP. Information from these boreholes has been used extensively in studies described in preceding chapters. A detailed description of boreholes and geologic activities at borehole sites within the Pasco Basin is contained in Appendix A.

The locations of key boreholes discussed in this chapter are shown in Figure 6-1. Continuous core is available for most of these boreholes and has been the subject of detailed fracture and lithologic studies. The boreholes drilled into the Grande Ronde Basalt (Appendix A) have received particular attention and are the principal data points used in the discussion which follows.

STUDIES OF FRACTURES

Studies of the basalt fractures and breccias penetrated by BWIP boreholes are necessary for geologic characterization of the rock mass, evaluating hydrologic test results, and engineering design. All basalt core is fractured and/or brecciated to some degree. These features are of three main genetic types: (1) cooling fractures, (2) tectonic breccias, and (3) core disking fractures. Cooling fractures, by far the most common type of fracture penetrated by drilling, are discussed in detail in Chapter 5. Hence, this section contains only a summary of recently completed studies of cooling-fracture orientations in basalt core from the Near-Surface Test Facility (NSTF) located in Gable Mountain (Fig. 6-1). The principal fracture studies reported here are those concerned with tectonic breccia and core disking.

TECTONIC BRECCIA

Most deep boreholes in the Pasco Basin were intentionally located away from the hinge zones of Yakima folds to avoid complex structure that might produce unclear stratigraphic relationships and ambiguous hydrologic test results. Prior to 1978, the breccia zones that had been penetrated by coring were generally interpreted as flow-top breccias which originated as the result of flow emplacement or related processes and not as the

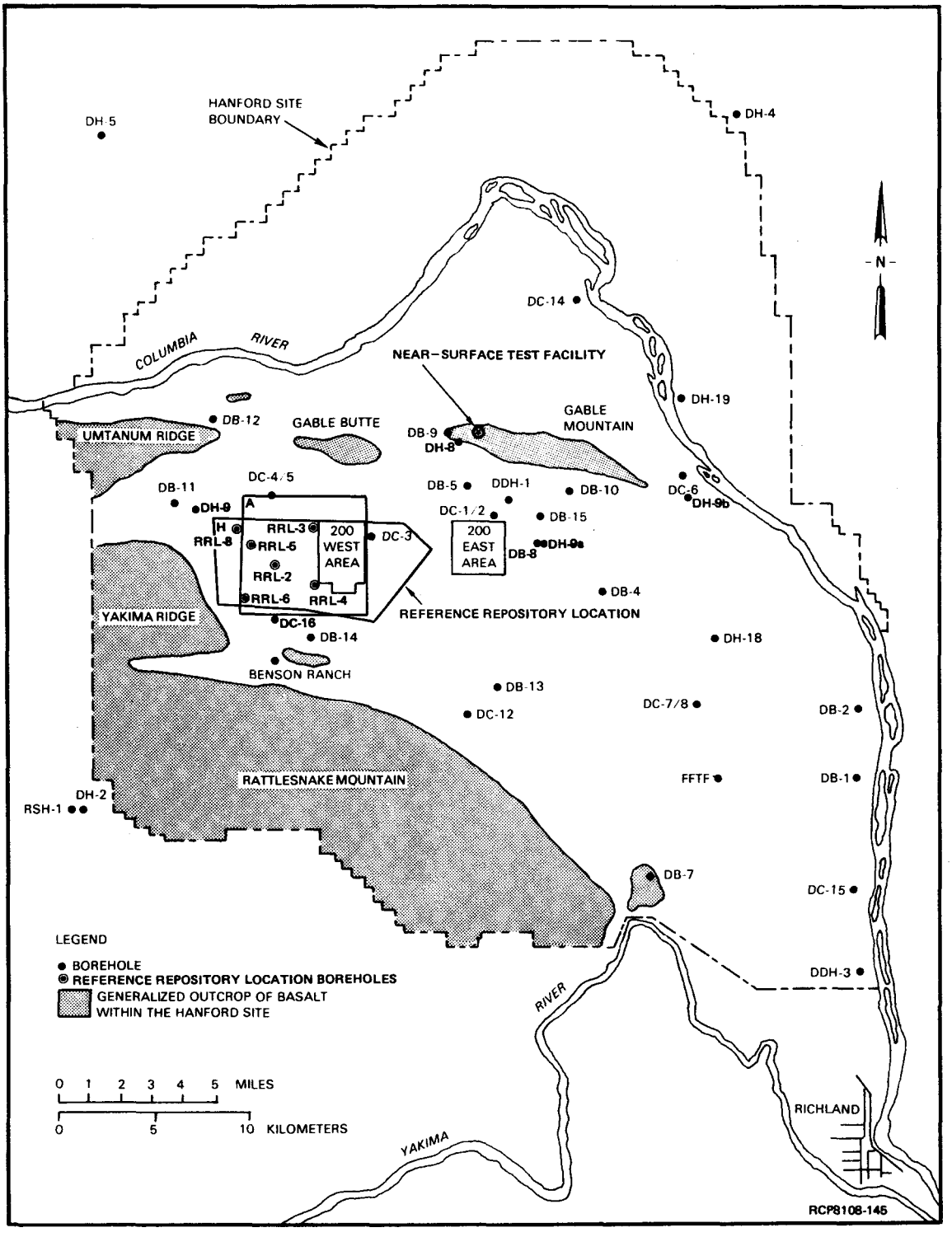

FIGURE 6-1. Location Map, Key Boreholes Used in Basalt Waste Isolation Project Studies. Boreholes DC-1/2, DC-4/5, and DC-7/8 are core hole/rotary hole pairs.

result of tectonic processes. Myers, Price and others (1979) reported tectonic fractures or breccias in only three boreholes: DB-10, DC-8, and DC-4. The repeated section in DB-10 is unequivocal evidence that it crossed a reverse fault. However, the fractures in DC-8 and DC-4 are much smaller. Although they were originally interpreted as tectonic in origin, an origin related to lava-flow-emplacement processes or to post-emplacement, non-tectonic processes, such as slumping, could not be entirely discounted.

In order to check for previously undetected tectonic breccia, zones logged as emplacement breccia or breccia in the deep and intermediate-depth boreholes cored on the Hanford Site were reexamined. Lithologic logs and core photographs from the DB- and DC-series boreholes were reviewed and breccia zones of possible tectonic origin were identified. The core from each of these zones was then examined, using features such as particle size, matrix content, and fabric to identify tectonic fractures and breccia (Goff, 1981; Long, 1978; Myers, Price and others, 1979; Price, 1980). Table 6-1 lists the boreholes, intervals examined, and general comments about the breccia zones. (The fault in borehole DB-10 was not reviewed because its character had been previously documented in Myers, Price and others, 1979.)

In general, tectonic breccias are infrequent in the thousands of feet (meters) of core drilled in the Cold Creek syncline area and elsewhere in the Pasco Basin. The breccia zones that were identified (Table 6-1) are generally intact and <4 in. (<10 cm) in thickness, although some are slightly thicker (Fig. 6-2). They appear in all deep boreholes within the Hanford Site and are principally in the Grande Ronde and Wanapum Basalts. As noted in the next chapter, such small tectonic breccia zones and their associated fractures are viewed as typical strain features of folded basalt and should be expected within the limbs of any of the Yakima folds, including the Cold Creek syncline. None of the tectonic breccias examined are judged as being associated with large displacements. This conclusion is based on comparisons with surface exposures of similar breccias and the lack of anomalously thick basalt flows that would be expected if the section were repeated.

Isolation and hydrologic testing of individual tectonic breccia zones has not been conducted. However, some hydrologic test intervals have included these tectonic breccia zones as part of a larger composite test (Table 6-1). These composite tests generally do not indicate the hydrologic properties of the discrete breccia zone.

Geophysical logs of selected boreholes were also examined. The geophysical logs from DC-1 (Fig. 6-1) indicate two anomalous zones: (1) at 3,970 to 4,010 ft (1,210 to 1,222 m) and (2) at 4,175 to 4,270 ft (1,273 to 1,301 m). The geophysical logs through these intervals have a slightly different character than is common for interbeds, flow tops, or flow interiors. These anomalous zones may reflect features of tectonic origin, such as open shears or breccia zones cemented with less-dense material.

TABLE 6-1. Tectonic Breccia in Core. (Sheet 1 of 3)

Borehole*	Drilled depth (ft)	Unit	Comments	Hydrologic test	Interval tested
DC-12	744 to 754	Umatilla	Primary vesicular breccia in middle of flow	no	
DC-2-A1	2,780	Sentinel Bluffs	Possibly a small tectonic feature; alteration to hard clay	no	
	3,051	Umtanum	Small (1-in.) tectonic breccia zone	no	
	3,319	Schwana	6-in. tectonic breccia and clay zone	no	
DC-2-A2	3,048 to 3,051	Umtanum	Tectonic fracture, very altered to hard clay along high-angle zone. Small breccia clasts	no	
DC-4	1,638	Priest Rapids (Lolo)	Well-healed, 3-in.-wide tectonic breccia zone	no	
	1,656	Priest Rapids (Lolo)	Small-scale tectonic breccia with slickensides	no	
DC-6	1,260	Priest Rapids (Rosalia)	Small (2-in.) tectonic shear zone with a cemented breccia	no	
	2,670	Sentinel Bluffs	Fractures with slickensides and breccia, possibly tectonic	yes	4,120 to 4,257
DC-7	4,147 to 4,148	Schwana	Probably not tectonic; associated with flow top	yes	4,140 to 4,257
	4,178	Schwana	Breccia associated with flow top primary feature	yes	4,120 to 4,257
	4,207 to 4,210	Schwana	Shattered and fractured, brecciated; appears tectonic, but could be primary and associated with flow contact at 4,205 ft	yes	4,684 to 4,827
	4,736	Schwana	Speculative, but probably primary feature; not typical tectonic clasts	no	

TABLE 6-1. Tectonic Breccia in Core. (Sheet 2 of 3)

Borehole*	Drilled depth (ft)	Unit	Comments	Hydrologic test	Interval tested
DC-8	1,741	Priest Rapids (Rosalia)	1/2-in. tectonic breccia zone with slickensides and minor fracturing	no	
	3,868	Schwana (Low K_2O)	8-in.-thick tectonic breccia zone at 45^o to core	no	
	3,892	Schwana	Small slickenside, little significance	no	
	3,930	Schwana	Brecciated, but probably primary and associated with the flow top		
DC-12	2,020	Frenchman Springs	Abundant fracturing with some slickensides; appears tectonic, but absence of gouge or breccia	no	
	2,227	Interbed	Clay with slickensides and few basalt inclusions; probably due to loading or settling	yes	2,218 to 2,260
	2,674	Sentinel Bluffs	Vesicular inclusions, but no breccia or slickensides; probably primary origin	no	
	2,831	Sentinel Bluffs	Glassy breccia associated with flow top; primary origin	yes	2,818 to 2,843
DC-14	1,389	Roza	1-in.-wide breccia zone with associated low-angle fractures for several feet; few slickensides; probably tectonic	no	
	3,030 to 3,031	Sentinel Bluffs (McCoy Canyon)	Well-healed, tectonic breccia zone with slickensides; irregular associated fractures for several feet	no	
	3,189	Umtanum	Low-angle tectonic fracture with small (1-in.) zone of clay and breccia; bounded by a few meters of low-angle, probably tectonic, fractures	no	

TABLE 6-1. Tectonic Breccia in Core. (Sheet 3 of 3)

Borehole*	Drilled depth (ft)	Unit	Comments	Hydrologic test	Interval tested
DC-15	1,970	Frenchman Springs	2-in.-wide tectonic fracture with breccia and slickensides in clay-filled matrix; slickensides are nearly horizontal	no	
	2,000	Frenchman Springs	3 in. of probably tectonic breccia, numerous slickensides in clay matrix	no	
	3,087 to 3,104	Umtanum	Silica-cemented breccia, probably primary, several discrete zones may be tectonized, but lack evidence of gouge or slickensides	yes	2,961 to 3,113, includes the Umtanum flow top
DDH-3	2,714	Sentinel Bluffs	4-in. brecciated zone, clay matrix; probably tectonic; abundant shattering on both sides of breccia	no	
	2,808 to 2,810	Sentinel Bluffs	Brecciation in flow contact, but several small zones appear tectonic	no	
DH-4	3,869 to 3,879	Schwana	Probably primary breccia, but not associated with a flow top	no	
DH-5	4,010	Schwana	Primary brecciation	no	
DB-11	730 to 737	Umatilla	Tectonic breccia; shattering back to 728 ft	no	
DB-15	1,165 to 1,170	Roza	Tectonic breccia; 1,165 to 1,166 and 1,169.8 to 1,170 ft with fracturing in between	no	

*See Figure 6-1 for borehole location.

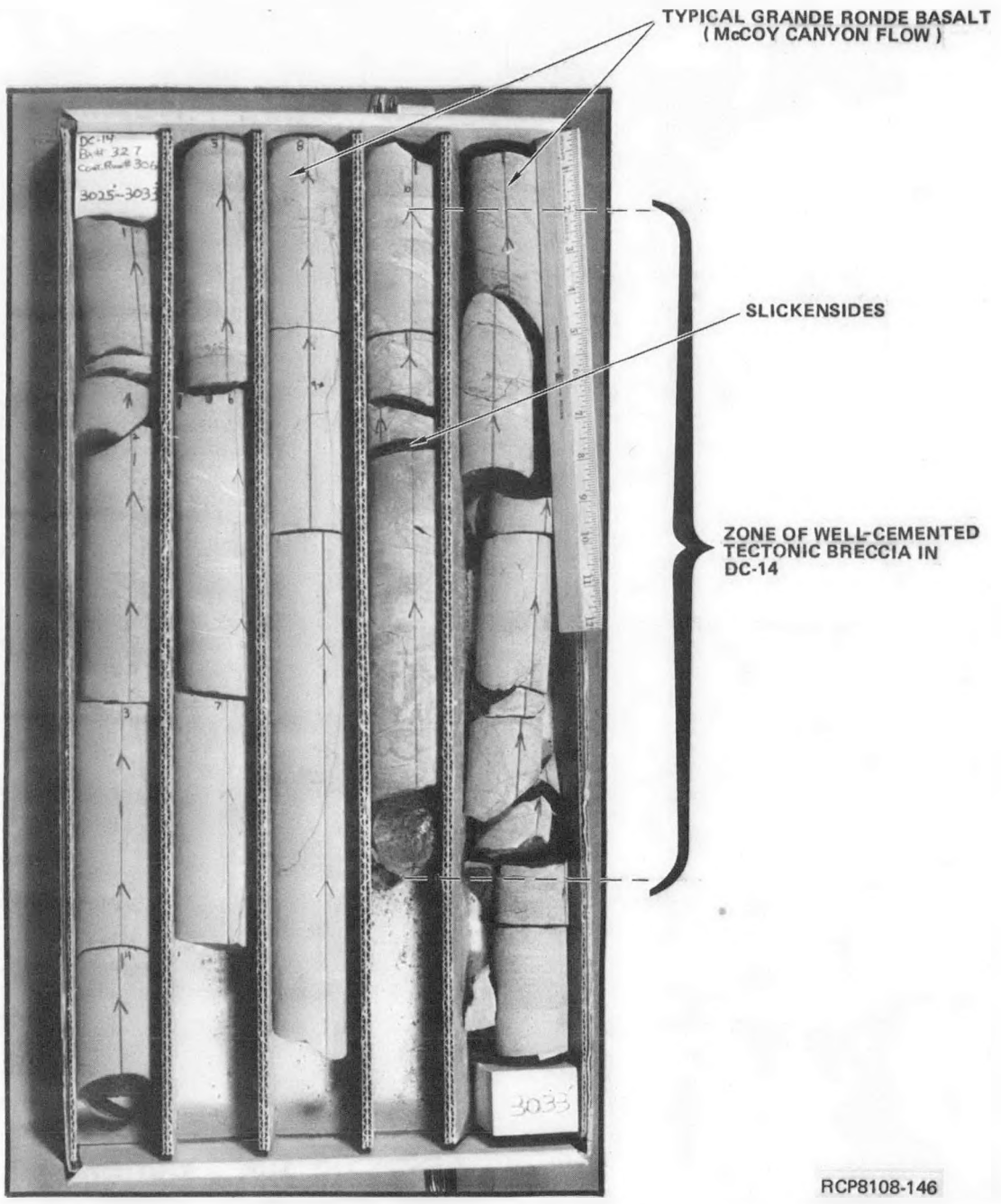

FIGURE 6-2. Tectonic Breccias, Grande Ronde Basalt, Borehole DC-14.

The zone from 3,970 to 4,010 ft (1,210 to 1,222 m) contains three areas with extremely low density and high porosity, possibly indicating open fractures or shear zones. In addition, the temperature log shifts and remains stable over the interval and the caliper log exceeds its measuring capability of 15 in. (38 cm) over much of the interval.

If the zone from 3,970 to 4,010 ft (1,210 to 1,222 m) in DC-1 is considered not to be a flow top, then the bounding flow contacts in DC-1 would be at 3,820 and 4,110 ft (1,164 to 1,253 m), giving a total flow thickness of 290 ft (88 m) and lower flow contact at 932 ft (284 m) below the Umtanum flow. The calculated thickness and flow contact locations are most consistent with the expected stratigraphic relationships in this area based on other boreholes in the vicinity.

Geophysical logs of the 4,175 to 4,270-ft (1,273 to 1,301-m) zone in DC-1 show a high-interval transit time, but an abnormally low density and spontaneous potential, possibly indicating a zone of gouge. Although porosity of this zone is only slightly less than the interiors of most basalt flows, the scale of the caliper log (15 in. [38 cm]) is exceeded throughout most of this zone. The caliper log returns to the drilled diameter on a "sharp ledge" at the bottom, indicative of a feature other than a flow top or interbed zone.

The significance of the 3,970 to 4,010 and 4,175 to 4,270-ft (1,210 to 1,222 and 1,273 to 1,301-m) zones in DC-1 is uncertain at this time. Further examination of their possible relationship to the regional stress field and to subsurface features detected by geophysical surveys is planned.

CORE DISKING

Core from deep boreholes in the Cold Creek syncline area often exhibits a type of fracturing known as disking (Myers, Price and others, 1979). The boreholes in which disking of core occurs include some of the DB-, DH- and DDH- series and most of the DC- series (Fig. 6-3). The degree of disking is variable, with individual disk thicknesses ranging from >0.5 to <0.2 in. (>1.3 to <0.6 cm). Generally, the core is only ruptured and not separated into discrete disks where the distance between the individual fractures is >3/8 in. (1 cm). However, where the distance between fractures is <0.4 in. (<1 cm), the disks are often completely separated (Fig. 6-4).

Location or frequency of disking relative to drilling activities at the BWIP has been examined. No definite relationship could be established between bit type, bit changes, drilling tools, or drill-string vibration. It is believed that a shearing mechanism caused by the drilling may contribute to the separation of discrete disks in the basalt, but a complete understanding of the phenomenon and possible contributing factors has not yet been developed.

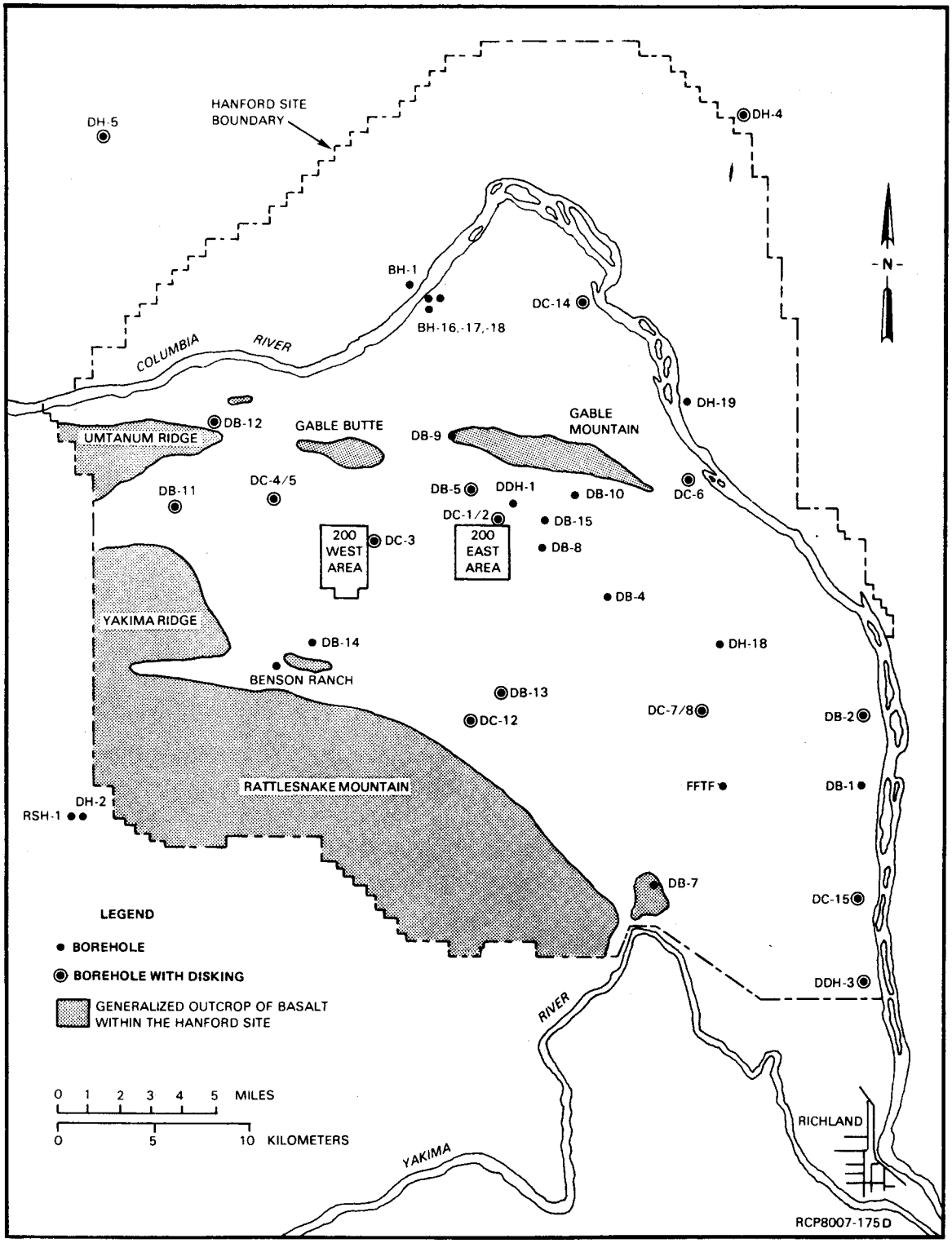

FIGURE 6-3. Location of Boreholes with Disked Core.

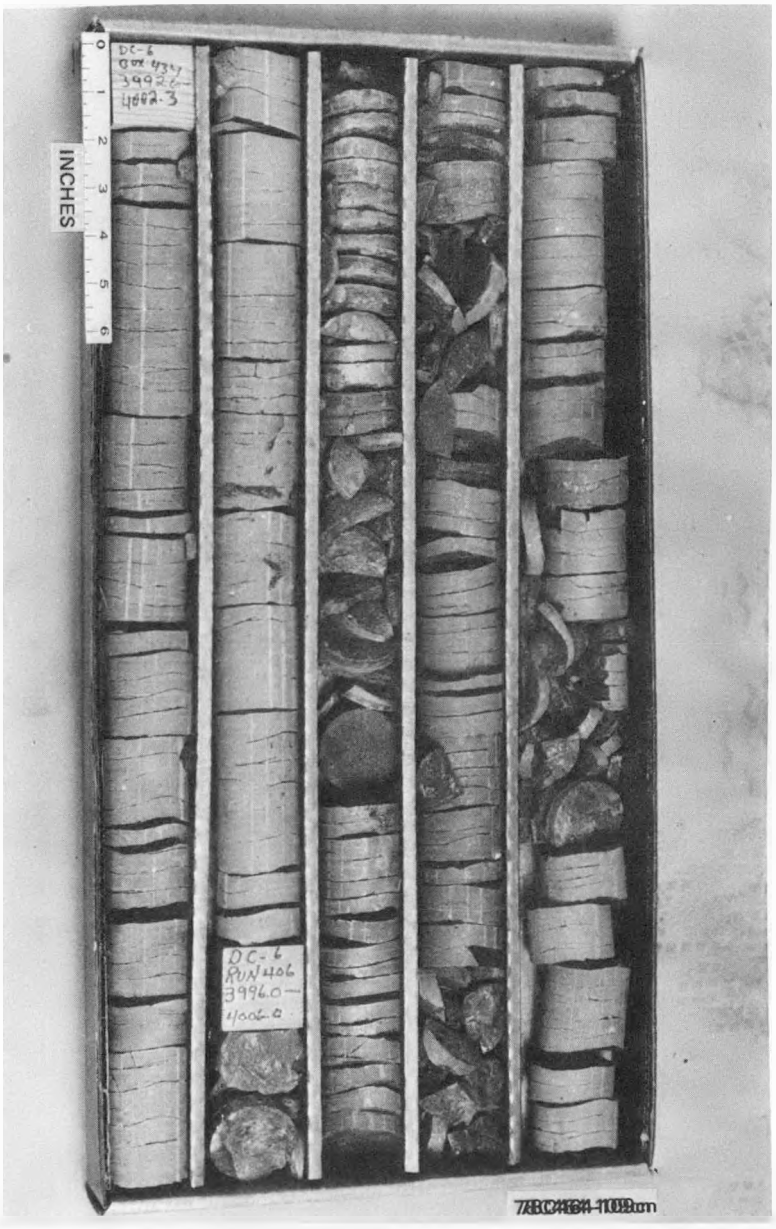

FIGURE 6-4. Core Disking.

The relation of geologic factors, such as stratigraphy, structure, intraflow structure, and mineralogy, to disking has also been examined. Two flows that are frequently disked are the Umatilla and Umtanum. The thickness, and possibly the lower unconfined compressive strength of the central parts of these flows, may account for this. The mineralogy and intraflow structures of the Umtanum core have been studied in detail and no correlation with disking is apparent, except that disking does not occur in the flow top.

Laboratory studies by Obert and Stephenson (1965) led them to conclude that for core disking to occur, the horizontal compressive stress must be numerically greater than the vertical compressive stress. They further concluded that the horizontal stress is probably numerically greater than one-half of the unconfined compressive strength of the rock.

To date, no in situ stress measurements have been made at depth in the Cold Creek syncline area. However, from the work of Obert and Stephenson (1965) and other laboratory testing, it is concluded that the disking phenomenon probably results from higher horizontal than vertical in situ stresses in the basalt. Further evaluation of core disking and its possible implications is under way.

CORE STUDIES OF THE POMONA FLOW AT THE NEAR-SURFACE TEST FACILITY

The NSTF is an underground facility constructed in Gable Mountain (Fig. 6-1) for thermomechanical testing relating to storage of high-level nuclear waste at depth. The facility is comprised of ∿2,953 ft (∿900 m) of tunnels and test rooms and provides the only unweathered and subsurface exposures of basalt in the Cold Creek syncline area. Geologic characterization studies around the area of the full-scale heater tests (Moak and Wintczak, 1980) were conducted to provide baseline data for identification of changes resulting from heating the basalt mass.

Geologic characterization studies involved detailed mapping of the joints of the tunnel walls and lithologic and geomechanical logging of 3,799 ft (1,158 m) of core from instrument boreholes drilled into the entablature of the Pomona flow. Data from both horizontal and vertical holes were evaluated in an attempt to reduce the sampling bias of the over 7,000 joints measured. The horizontal boreholes intersected mostly high-angle joints; whereas, vertical boreholes intersected mostly low-angle joints. By plotting equal numbers of joint-dips from horizontal and vertical boreholes, a dip-frequency histogram was obtained (Fig. 6-5). Three groups of joint-dip frequency are shown: (1) the 66° to 90° group that comprises 47% of the measured joints, (2) the 0° to 37° group that comprises 30%, and (3) the 38° to 65° group comprising the remaining 23%. The 66° to 90° group is the most conspicuous, in that these are the main cooling joints and have a continuous length of up to 7.9 ft (2.4 m) based on observations in the tunnels. The remaining two

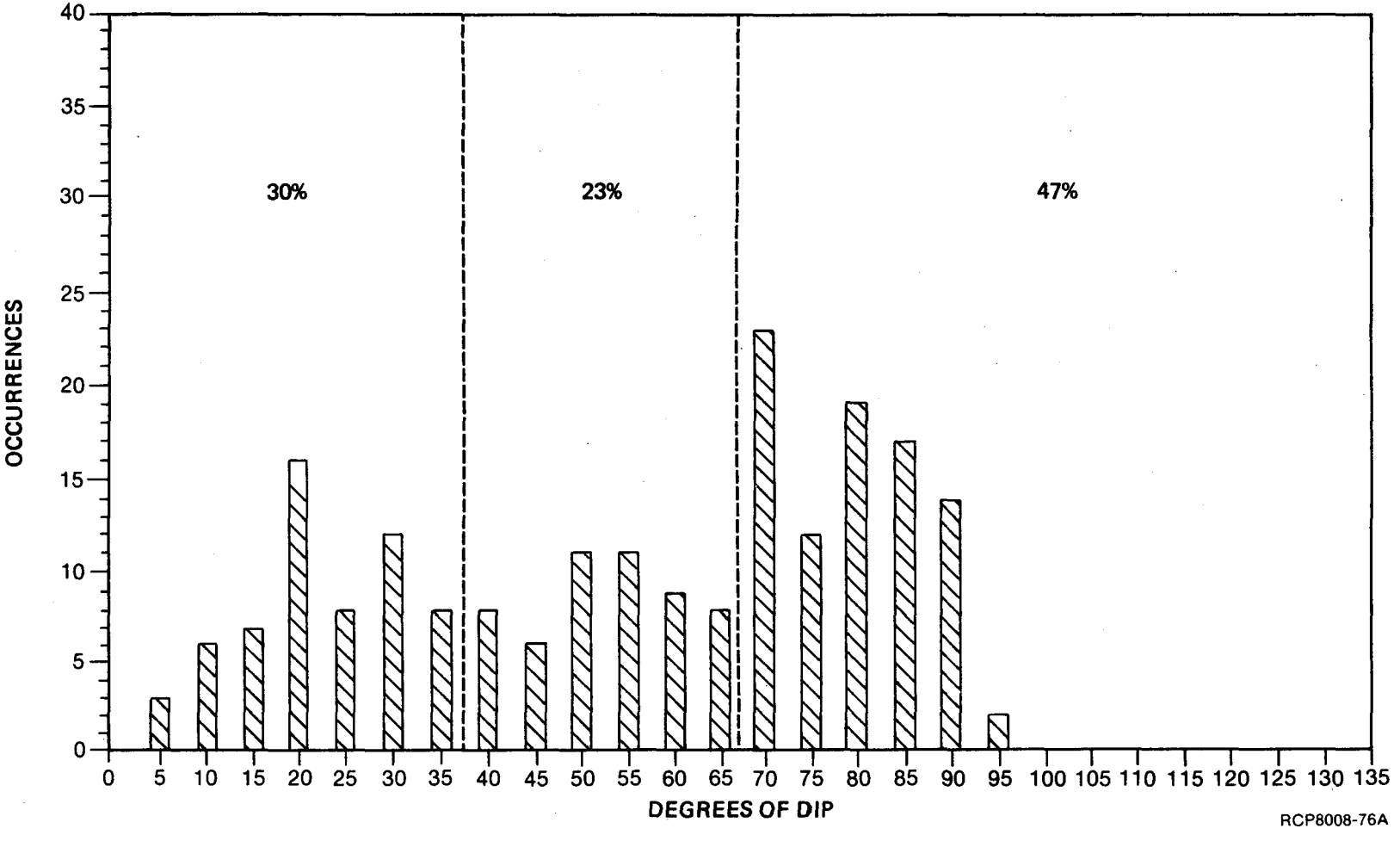

FIGURE 6-5. Histogram, Joint-Dip Frequency.

groups are discontinuous and seldom cross the joint boundaries of the 66° to 90° group. From the data available, there is no preferred orientations of these three joint groups. Stereonet plots with an equal population of joints from vertical and horizontal boreholes show a random orientation (Fig. 6-6).

PREDICTED VERSUS OBSERVED STRATIGRAPHY

The structure-contour and thickness-distribution maps in Myers, Price and others (1979) constitute a geometric model of the stratigraphy and structure of the upper basalt section. This model has been tested by later drilling, using the three new boreholes drilled in fiscal years 1980 and 1981: DC-12 and DC-15 within the Cold Creek syncline and DC-14 located 4 mi (6.5 km) north of the study area (Fig. 6-1).

Figure 6-7 shows the predicted and observed values for the thicknesses and drilled depths of rock units penetrated by DC-12, DC-14, and DC-15. Predictions of rock unit thicknesses were made using three different map sets in Myers, Price and others (1979): (1) isopach maps of individual flows and interbeds, (2) isopach maps of formations, and (3) thickness values derived by taking the difference between surfaces defined by structure contours.

The Saddle Mountains Basalt was not cored in DC-12 because the stratigraphy was thought to be correlatable with DB-13 located 1.5 mi (2.4 km) to the northeast. The observed stratigraphy and thicknesses were very close to those predicted, except that individual interbeds in the Wanapum and upper Saddle Mountains Basalts were, in general, consistently thicker than predicted. The total formation thickness is accurate because of the extensive knowledge gained from the drilling in the Saddle Mountains Basalt. The observed thickness of the Wanapum Basalt was 1,122 ft (343 m) and the prediction of 1,150 ft (350 m) is within 5% of the actual. Likewise, the thickness of the Sentinel Bluffs sequence of the Grande Ronde Basalt was within 5% of that predicted; individual flows were not differentiated in the Sentinel Bluffs sequence. The total thickness of the Umtanum was 235 ft (72 m), only 1 ft (<30 cm) less than that predicted based on the isopach map of the Umtanum flow (Long and others, 1980).

Borehole DC-14 is located in the northeastern part of the Hanford Site north of the Cold Creek syncline and was drilled principally for further definition of the Pasco Basin groundwater flow regime. Observed stratigraphy in the Saddle Mountains Basalt differs from previous interpretations. Lack of nearby boreholes and the structural characteristics of the area made the prediction less accurate than for the other boreholes. Although in DC-14 the total thickness of the Elephant Mountain Member was within 75% of that predicted, the presence of the upper flow of the member was not expected. In addition, the Pomona flow is almost double the thickness predicted, the Umatilla flow is unexpectedly absent, and the Asotin flow is over 200 ft (60 m) thick--more than twice that

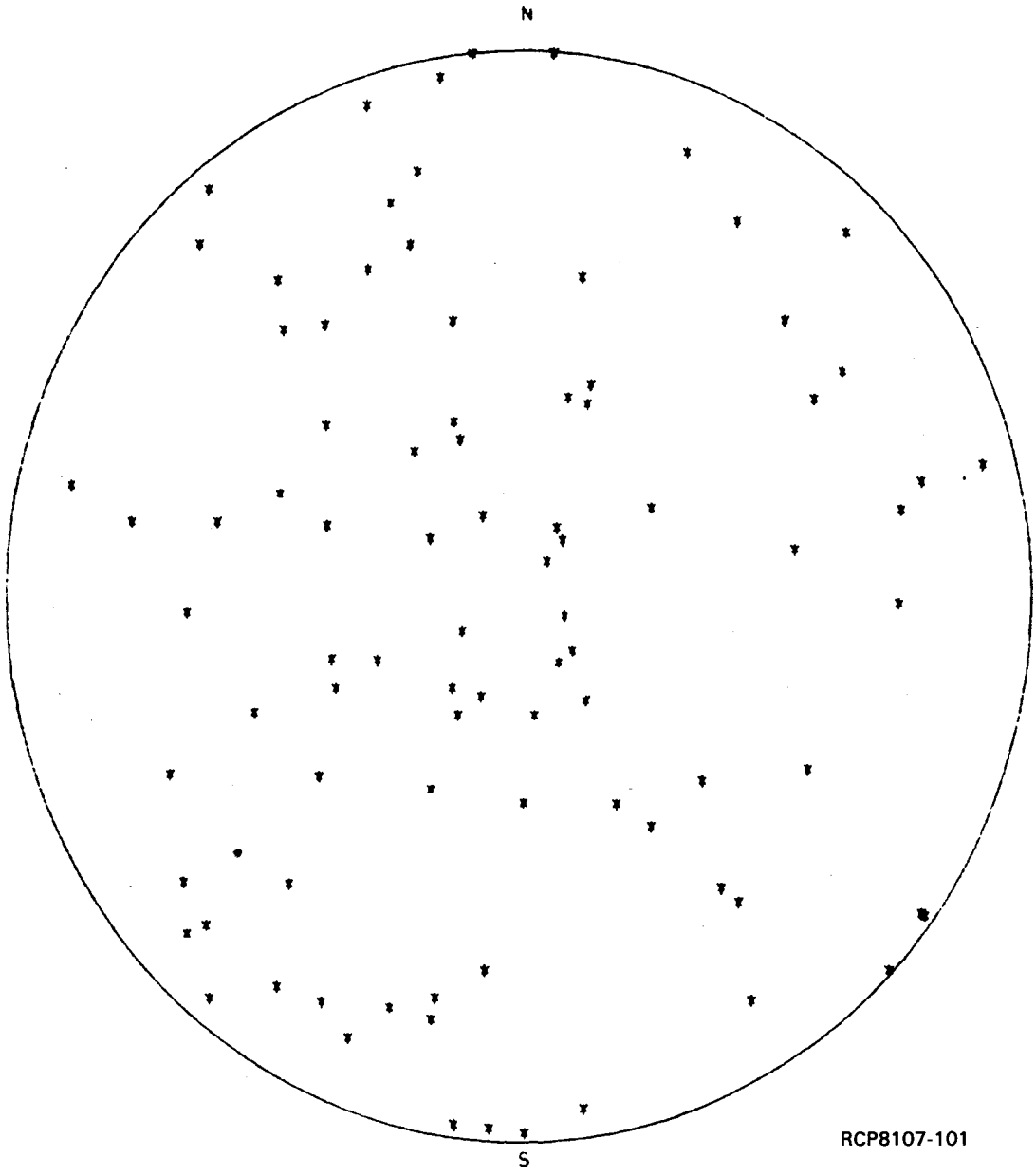

FIGURE 6-6. Stereonet Plot, Horizontal and Vertical Joints.

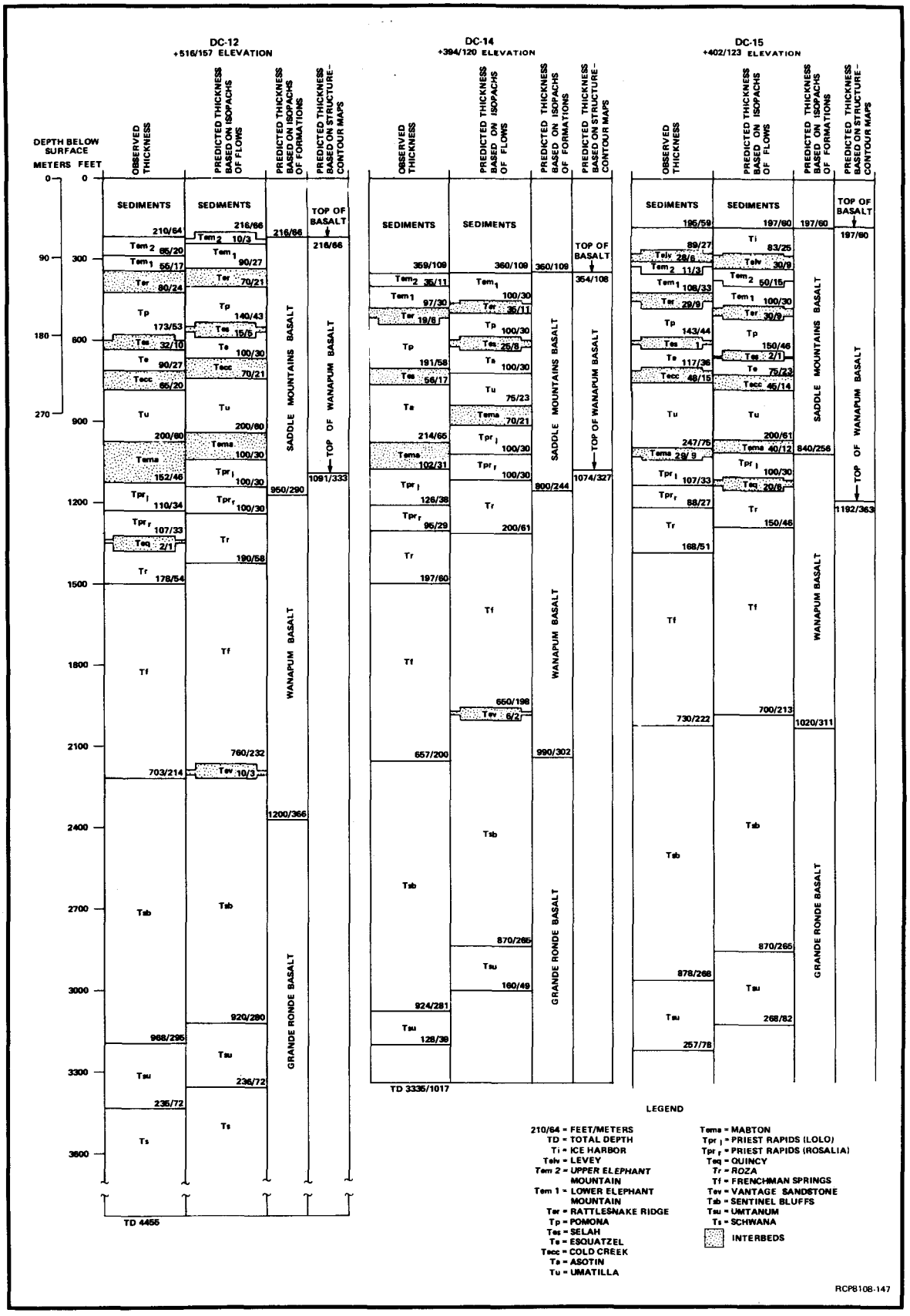

FIGURE 6-7. Predicted Versus Observed Stratigraphy in Boreholes DC-12, DC-14, and DC-15.

predicted. Revised interpretations of the structure and stratigraphy of the Saddle Mountains Basalt based on DC-14 are discussed in Chapter 3. The Wanapum Basalt stratigraphy and flow thicknesses were very close to that predicted, but the observed elevations are lower due to the greater thickness of the Saddle Mountains Basalt. Although the Umtanum flow was predicted to be 160 ft (48.8 m) thick (Long and others, 1980), preliminary interpretations suggest it is only 128 ft (39 m) thick. However, a small flow or lobe 31 ft (9.4 m) beneath the main flow may be related to the Umtanum; this possibility presently remains unconfirmed.

Borehole DC-15 is located ∿2 mi (∿3 km) north of DDH-3 and ∿3 mi (∿5 km) south of DB-1 (Fig. 6-1). The thickness and stratigraphy of the Saddle Mountains Basalt were predictable as evidenced by the close match of the observed and predicted data (Fig. 6-7). The upper section of the Wanapum was less predictable at DC-15; the occurrence of the Priest Rapids (Rosalia) and the absence of the Quincy interbed were unexpected. The remaining stratigraphy and flow thicknesses were similar to those predicted; however, their elevations were slightly lower due mostly to the presence of the Rosalia flow of the Priest Rapids Member. The Umtanum flow is 256 ft (78 m) thick and the drill core of the flow interior (149 ft [45.4 m]) was highly disked and broken, resulting in a 15% core loss through this zone. Testing of the predictive capability of structure-contour and thickness-distribution maps contained in this report will be made as additional boreholes are drilled.

SUMMARY AND CONCLUSIONS

Studies of the basalt fractures and breccias penetrated by BWIP core holes are necessary for geologic characterization of the rock mass, for evaluating hydrologic test results, and for engineering design. Zones logged as "emplacement breccia" or "breccia" in the deep and intermediate-depth holes cored in the Hanford Site were reexamined using features such as particle size, matrix content, and fabric to identify tectonic fractures. In general, tectonic fractures were found to be infrequent in the thousands of meters of core drilled in the Cold Creek syncline area and elsewhere in the Pasco Basin. The breccia zones that were identified are generally intact and <10 cm thick. They appear in all deep core holes within the Hanford Site and are principally in the Grande Ronde and Wanapum Basalts. Such small tectonic breccia zones and their associated fractures are viewed as typical strain features of folded basalt and should be expected within the limbs of any of the Yakima folds, including the Cold Creek syncline. None of the tectonic breccias examined were judged as being associated with large displacements.

Core from deep holes in the Cold Creek syncline area exhibit a type of fracturing known as disking. The degree of disking is variable, with individual disk thicknesses generally ≤1.5 cm. No definite relationship could be established between the location or frequency of disking relative to drilling activities. The relationship of geologic factors, such as

stratigraphy, structure, intraflow structure, and mineralogy, to disking has also been examined. Stratigraphically, two of the flows commonly disked are the Umatilla and Umtanum. Their thickness, and possibly the lower unconfined compressive strength of the central parts of these flows, may account for this. The mineralogy and intraflow structures of the Umtanum core have been studied in detail and no correlation with disking is apparent, except that disking does not occur in the flow top. It is concluded that the disking phenomenon probably results from higher horizontal than vertical in situ stresses in the basalt.

The existing geometric model of the stratigraphy and structure of the upper basalt section was tested using two new boreholes drilled within the Cold Creek syncline and one borehole drilled north of the study area. Predictions of rock unit thicknesses were made using three different map sets included in Myers, Price and others (1979): (1) isopach maps of individual flows and interbeds, (2) isopach maps of formations, and (3) thickness values derived by taking the differences between surfaces defined by structure contours. Within the Cold Creek syncline, the observed stratigraphy was, for the most part, close to that predicted. However, in the borehole to the north of the study area, the previous interpretations were less accurate. As additional boreholes are drilled, testing of the predictive capability of existing structure-contour and thickness-distribution maps will be carried out and the geologic models and maps updated.

CHAPTER 7 - DISTRIBUTION OF STRAIN FEATURES WITHIN SELECTED YAKIMA FOLD STRUCTURES AND EXTRAPOLATION OF THEIR NATURE INTO THE COLD CREEK SYNCLINE AREA

E. H. Price

INTRODUCTION

This chapter summarizes the results of a structural analysis of selected Yakima folds. These results are based on field mapping and geometric analysis of structural elements (i.e., folds, faults, and joints). Recent studies of the strain geometry within the Umtanum Ridge structure at Priest Rapids on the Columbia River, at the Baldy area in the Yakima River canyon, and within the Frenchman Hills structure at Hole-in-the-Wall canyon (Fig. 7-1) have shown a remarkable similarity of the strain geometry among these Yakima folds. Such consistency of strain geometry has allowed a mechanical fold model to be developed from which an accurate prediction of the location and character of strain features in the subsurface of the Cold Creek syncline can be made. The detailed analysis and interpretation of the strain geometry of these structures are given in Price (in press) from which the following information is abstracted.

STRUCTURAL ANALYSIS OF EASTERN UMTANUM RIDGE AT PRIEST RAPIDS

GEOLOGIC SETTING

Umtanum Ridge is the topographic expression of a linear anticlinal structure extending from the east end of Gable Mountain (T. 13 N., R. 27 E.) west-northwestward to south of Ellensburg (T. 16 N., R. 17 E.), a distance of 110 km (Fig. 7-1). In the Pasco Basin, the Umtanum Ridge structure is bounded to the north by the Wahluke syncline, Hanson Creek structure, and the Saddle Mountains, and to the south by the Cold Creek syncline and adjoining Yakima Ridge (Fig. 7-1). It is well exposed along the Yakima River canyon at Baldy south of Ellensburg and at Priest Rapids along the Columbia River.

The Umtanum Ridge structure at Priest Rapids is an asymmetric, box-shaped anticline in the hanging wall of the Umtanum fault. The distribution of strain elements (faults and other shear zones, shatter breccias, and tectonic joints) is systematically related to their position within the fold; therefore, the strain is interpreted to be related to the

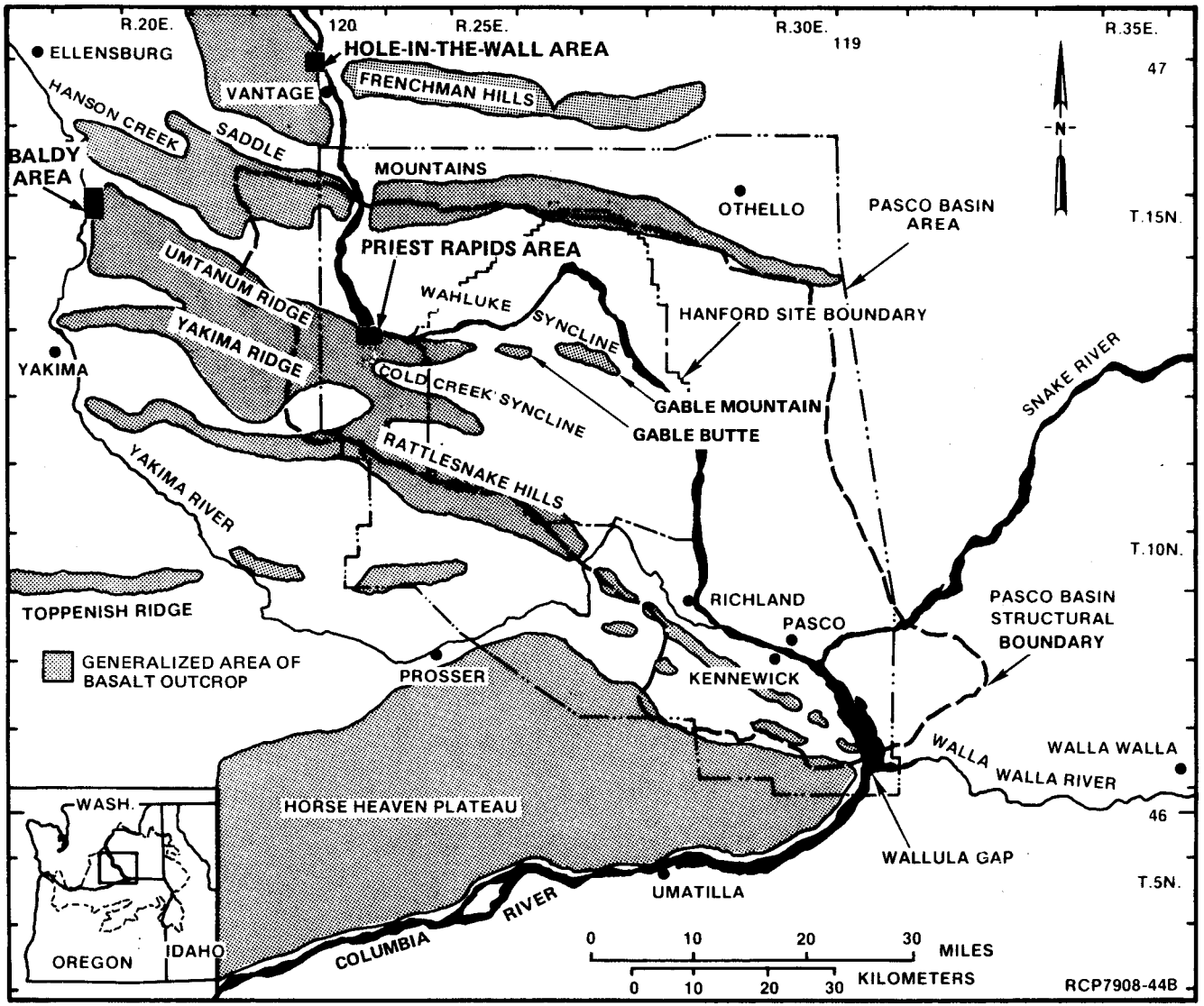

FIGURE 7-1. Index Map, Pasco Basin and Vicinity (showing Hanford Site and study areas described in this chapter).

folding process. All strain features observed within the Umtanum structure at Priest Rapids are in the Umtanum fault and in the hanging wall of the Umtanum fault. The basalt flows above the fault are continuous across the fold and remain intact even where the flows are vertical (Fig. 7-2). Flows of the Priest Rapids Member in the footwall show no definitive faulting or tectonic jointing.

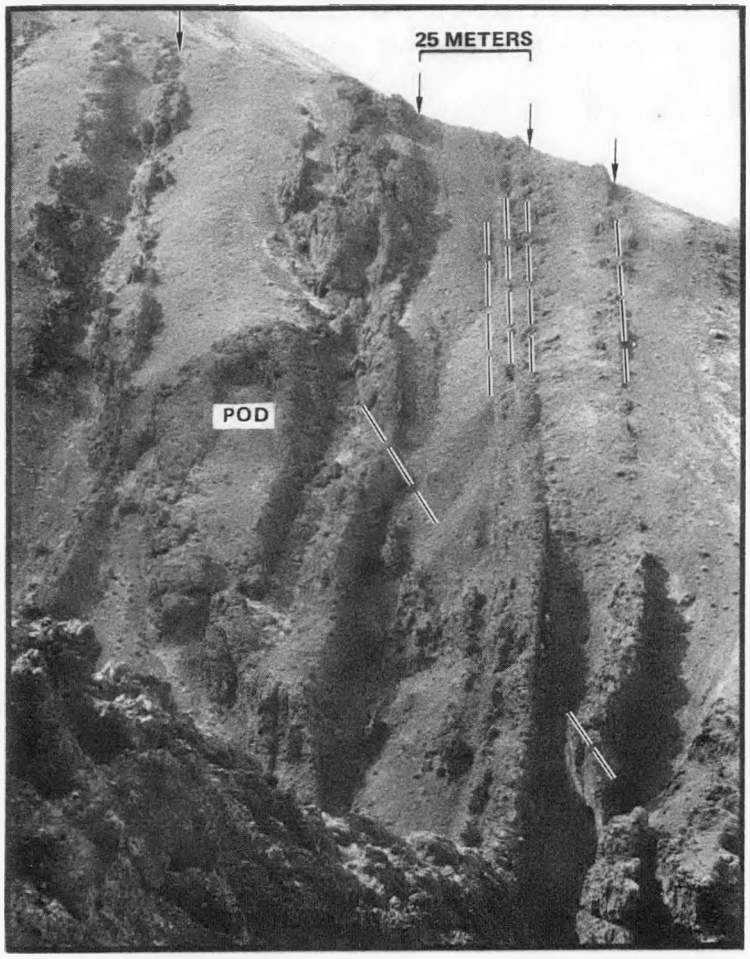

FIGURE 7-2. Vertically Standing Grande Ronde Basalt Flows in the Hanging Wall of Umtanum Fault at Priest Rapids (viewed toward the west). Small faults occur parallel and oblique to flow layering, but the continuity of primary cooling features is preserved because fault breccia is <5% of the total rock volume. "Entablature-like" material (POD) is surrounded by rubbly basalt of a complex flow top.

Most strain is concentrated in the northern part of the fold and consists of localized layer-internal faulting, extensive shattering, and limited layer-parallel faulting, both along flow contacts and along induced surfaces within steeply inclined layers. These features, their orientations, and distributions are generalized in a schematic cross section in Figure 7-3. Extension fractures associated with a limited number of faults indicate the northern sides of the faults have moved up relative to the southern sides. Faults that dip steeply southward in overturned flow layering are normal faults, and are reverse faults if they dip steeply northward in upright flow layering. Moderately northward- and southward-dipping faults (probably conjugate faults) also occur within flows and, in some cases, across flow layering (Fig. 7-3). Slickenside striae on most faults in the northern part of the fold are generally steeply inclined.

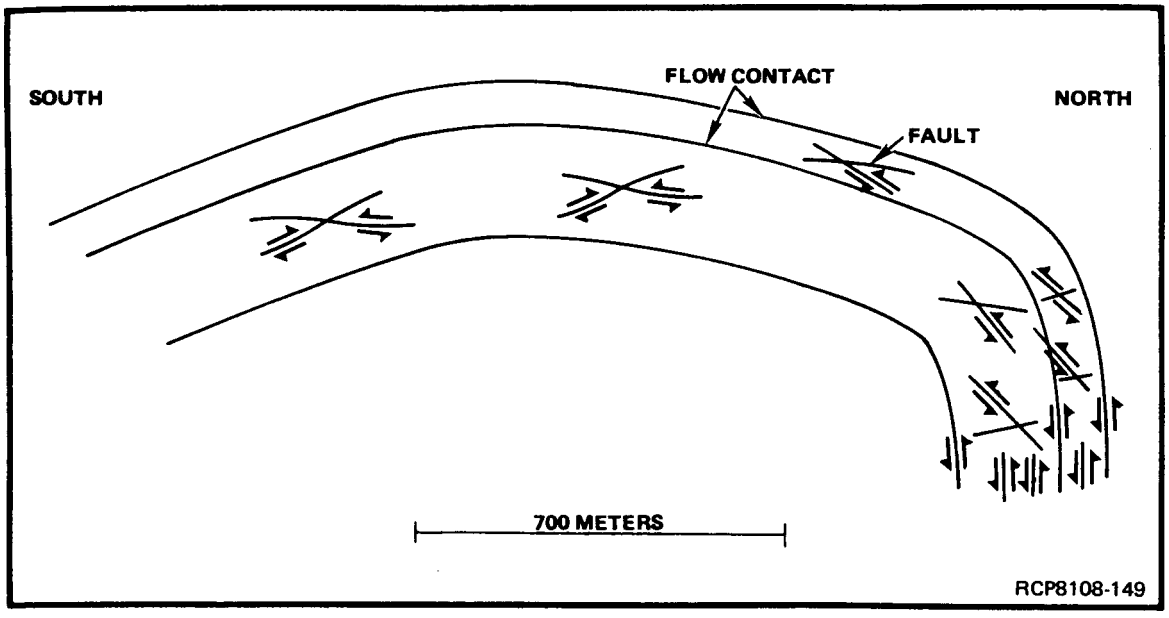

FIGURE 7-3. Schematic Cross Section, Two Representative Flows within Umtanum Anticline at Priest Rapids (illustrating the interpreted geometric relationship of faulting to position within the cross section from field observations). Faulting along flow contacts is limited to the northern part of the fold.

Fault orientations within the central part of the fold cross section have different geometries from those of the northernmost area. All faults that trend subparallel to the strike of flow layering dip toward the north as does layering. Faults oblique to flow layering commonly are found in conjugate sets (Fig. 7-3). Orientations of slickenside striae found within the central part of the fold cross section are of intermediate plunge and trend generally perpendicular to the fold axis.

The exposed southern limb of the fold is characterized by a few low-dipping faults that generally strike subparallel to flow layering, but whose dip is at an acute angle to that of flow layering. These faults are interpreted, in cross section, to be conjugate sets of undulatory slip surfaces whose acute-angle bisectors are at an acute angle to flow layering. Slickenside striae within this part of the fold are necessarily of low plunge because of the low fault dips and of generally high, but variable, rake.

In the northern and central parts of the fold, a few faults strike obliquely to the axial trend of the fold. These faults, therefore, cannot be portrayed accurately in the schematic cross section. Because trends of slickenside striae on these fault-slip surfaces are consistent with those of the faults described above, and because they occur in the same areas, these faults are also interpreted as part of the folding strain. Too few of these oblique-trending faults were mapped to allow a definitive geometric analysis of their relationship to the fold geometry.

MECHANICAL MODEL FOR THE FORMATION OF THE UMTANUM RIDGE STRUCTURE

The model for the Umtanum Ridge structure must be one of folded basalt that has subsequently been faulted. Folding is the primary deformation because the strain features observed within the Umtanum Ridge structure are spatially and geometrically related to the anticline geometry and not to the Umtanum fault. The conceptual mechanical model proposed here involves buckling of the basalt flow layering accompanied by reverse slip parallel to flow contacts and by internal shear and bending strains within individual basalt flows.

The strain distribution and geometry have been modeled in a reconstructed cross section of the Umtanum anticline (Fig. 7-4) after the mechanism of flexural flow buckling described by Ramsay (1967). Only one parameter was assigned to the strain model construction--that there was little or no strain in the southern hinge. This assumption is supported by field observations. Passive strain markers that would have been originally rectilinear and perpendicular to flow layering are shown on Figure 7-4. Generalized strain ellipses due to only simple shear show directions of local, principal, strain axes and relative amounts of strain. The total strain would also include bending strains. Bending strains should be small compared to the simple shear strains, except in the core of the anticline where the curvature of flow layering is greatest. The fold model shows a slight simple shear within layers on either side of the fold crest. Slip between the flow layers and more extreme simple shear within flow layers occurs in the northern fold hinge where the curvature of folding is greatest. The most extreme shearing and, therefore, the

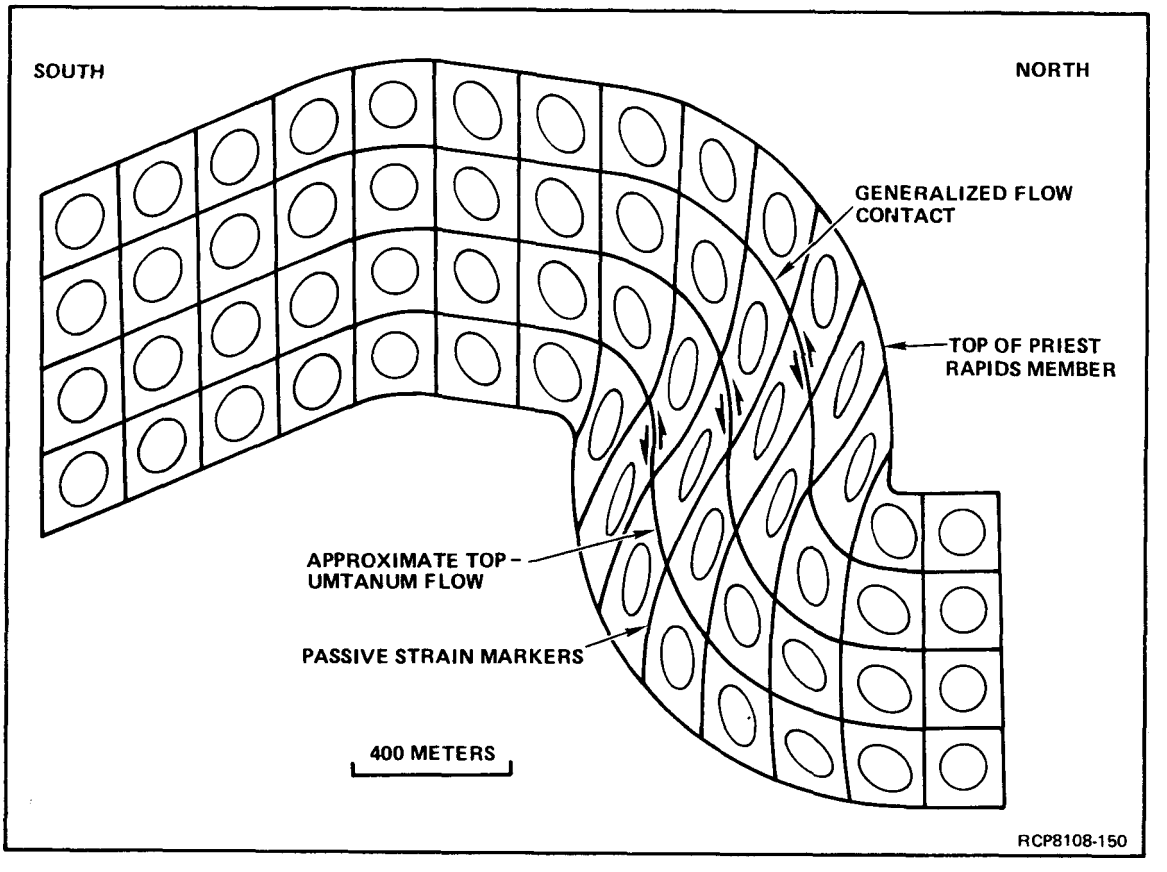

FIGURE 7-4. Cross-Sectional Strain Geometry Interpretation for the Umtanum Anticline at Priest Rapids. No vertical exaggeration. Generalized finite strain ellipses are shown as strain indicators.

most extensive flattening of the strain ellipses occur where flow layering is nearly vertical. The change from the area of minor shearing to extreme shearing occurs over a narrow region in the lowermost layers toward the fold core. Horizontal flow layering north of the fold core shows little or no strain.

A comparison of the model with a field exposure is shown in Figure 7-5. This figure shows an "eroded version" of the mechanical model with a photomosaic cross section along a canyon at the western boundary of the Priest Rapids area. Region a (Fig. 7-5) consists of basalt flows with minor shear zones and faults. Between regions a and b, flow-layering curvature and the degree of brecciation increase noticeably over a distance of a few meters. Intraflow structures in region a are essentially pristine, but in region b, shattering and anastomosing brecciation are so extensive that intraflow structures are difficult to recognize. In regions c and d, faults occur parallel to flow layering and minor faults occur in conjugate sets oblique to flow layering. The generally subhorizontal and undeformed Priest Rapids flows in the area north of Umtanum Ridge (Fig. 7-5, off the photograph to the north) correspond to the unstrained syncline in the mechanical model. Overall, the fold geometry and strain distribution accord remarkably with that predicted in the mechanical model.

PROJECTION OF THE UMTANUM STRUCTURE TO DEPTH

The structural geometry of the rocks below the exposed part of the Umtanum anticline could not be determined. The strain geometry of the Umtanum anticline suggests that the Umtanum reverse fault grew outward from the fold core because of mass imbalances inherent in concentric folding. Therefore, faulting along the Umtanum fault below the level of the fold core is not required to explain the observed displacement at the surface.

The fold profile of the Umtanum structure and other Yakima folds (see below) is intermediate between a sinusoidal buckle and a conjugate kink band. Conjugate kink bands (box folds) cannot be projected indefinitely to depth. In empirical models and field observations, such folds attain a single-hinged, chevron-fold profile at depth if the mechanical anisotropy of the layering is great enough (for example, see Ghosh, 1968; Cobbold and others, 1971).

The mechanical anisotropy of the basalt layering under the exposed part of the fold could have kinked and shortened while the underlying, more mechanically homogeneous basement either: (1) shortened in a ductile manner (thick skinned) or (2) remained rigid while the overlying basalt shortened by sliding over the basement along a decollement (thin skinned). A third possibility is that the mechanical anisotropy of layering could have decreased at depth because of increased lithostatic pressure. A decreased mechanical anisotropy of layers would lessen the kinking effect and favor more sinusoidal folding or homogeneous shortening (Cobbold and others, 1971). In such a model, kinking at the surface would grade into rocks thickened in a ductile manner at depth. The interpreted strain geometry of the Umtanum fold does not permit differentiation of the most applicable of the above models.

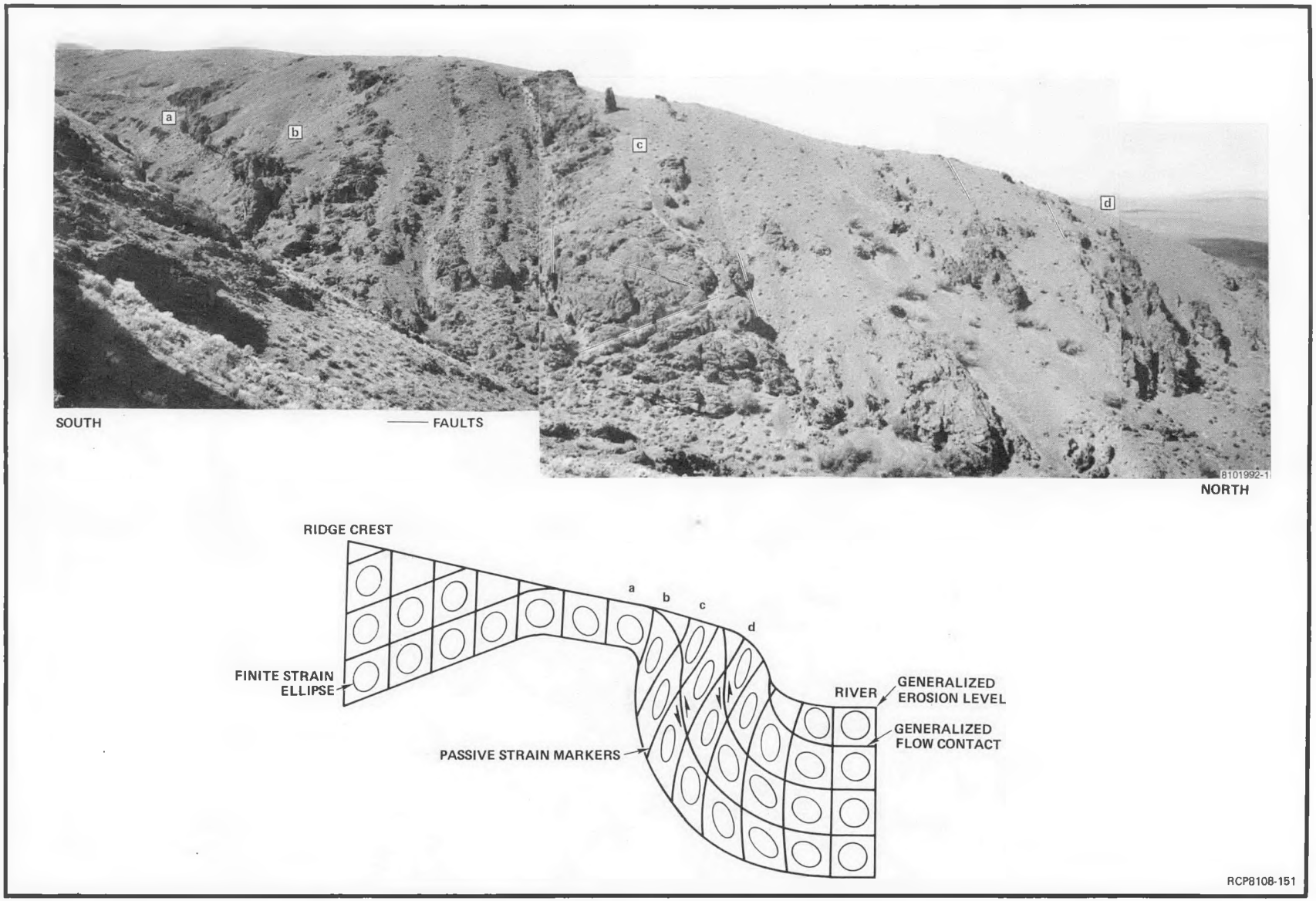

FIGURE 7-5. Comparison of Buckle Fold Model, Umtanum Anticline, with a Photomosaic of the Canyon Just West of the Priest Rapids Map Boundary. Regions designated a, b, c, and d on the model are interpreted to correspond with areas noted on the photomosaic by like symbols. No vertical exaggeration. Photomosaic shows folded basalt flows and typical fault orientations found within the northern hinge area. For scale, distance from b to c is ~200 m.

STRUCTURAL ANALYSIS OF THE UMTANUM RIDGE STRUCTURE AT THE BALDY AREA IN THE YAKIMA RIVER CANYON

GEOLOGIC SETTING

The Umtanum Ridge structure in the Yakima River water gap at Baldy (Fig. 7-1) is an asymmetric, overturned, box-shaped, concentric anticline in Columbia River basalt (Fig. 7-6). Erosion has exposed one of the deepest sections of Grande Ronde Basalt in the western Columbia Plateau and has removed most of the Wanapum Basalt. The anticline is bounded by two broad synclines: (1) Squaw Creek syncline to the north and (2) Burbank Creek syncline to the south (Fig. 7-7). The structure along the river has been examined by Smith (1903), Hammer (1934), Mackin (1961), Diery (1967), and Bentley (1977). The most recent geologic mapping of the area was by Bentley in Swanson and others (1979a).

The Burbank Creek syncline (Fig. 7-7) has one of the few exposed synclinal troughs within the Yakima Fold Belt. Basalt exposed along road cuts and outcrops exhibits no obvious tectonic jointing or faulting, except for three, small, strike-slip faults. These faults are defined by steeply inclined clay gouge zones up to 0.5 m wide, trending between N10°W and N44°E. Slickenside striae plunge between 3° and 54°. Because the gouge is not cemented, these faults are interpreted to be younger than the other faults associated with the anticline. These faults have no obvious geometric relationship to the fold; hence, these few younger faults are not considered to be directly related to folding.

Brecciated and overturned Grande Ronde Basalt within the anticline has been thrust northward over relatively undeformed and essentially horizontal flows of the Frenchman Springs and Roza Members of the Wanapum Basalt. The thrust fault, named the Wymer fault by Bentley (1977) (Fig. 7-7), is present in a gully along the north side of Baldy. Strain features observed at Baldy include shatter breccia and faults and other shear zones, the same as those observed at Priest Rapids. Locally, brecciation is so extensive that intraflow structures cannot be recognized. The angular southern hinge of the fold and its associated brecciation have been misinterpreted as a fault zone by previous workers (Diery, 1967; Kienle and others, 1978a; Bentley in Swanson and others, 1979a).

COMPARISON OF STRUCTURAL GEOMETRY OF UMTANUM RIDGE STRUCTURE AT BALDY WITH THAT OF PRIEST RAPIDS

The Umtanum Ridge structure at Baldy and at Priest Rapids has several structural features in common:

- The fold is doubly hinged and concentric.
- A narrowly defined, reverse fault superposes brecciated and overturned basalt over undeformed and essentially horizontal basalt of the synclinal trough to the north.

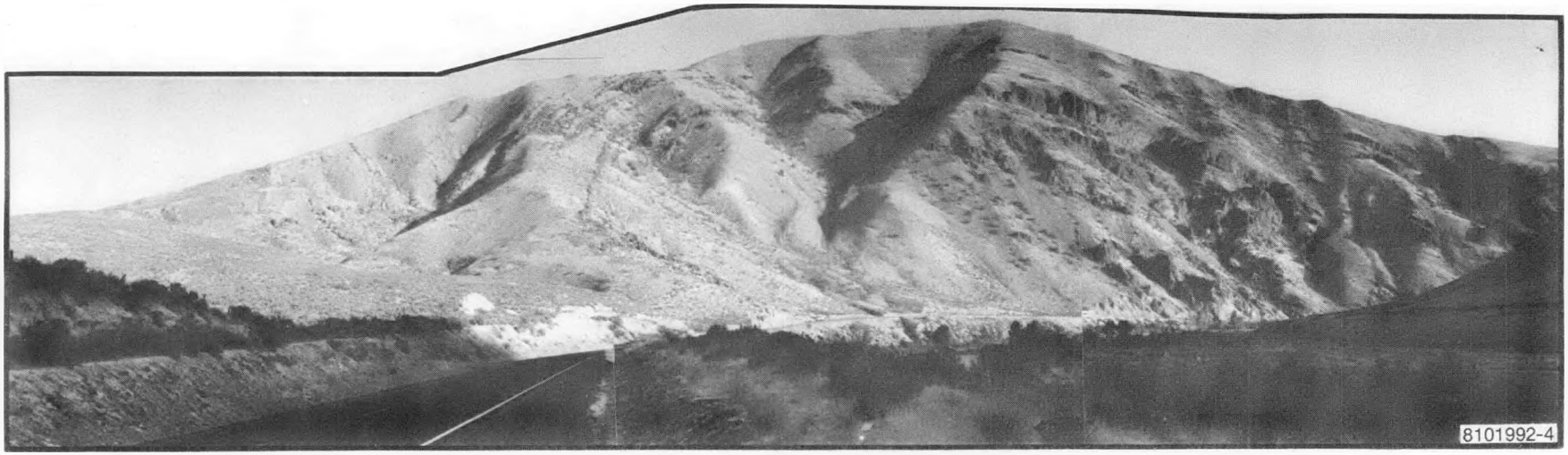

FIGURE 7-6. Cross-Sectional Photomosaic, Umtanum Ridge Structure at Baldy (viewed toward the southeast). Note highway in left foreground for scale.

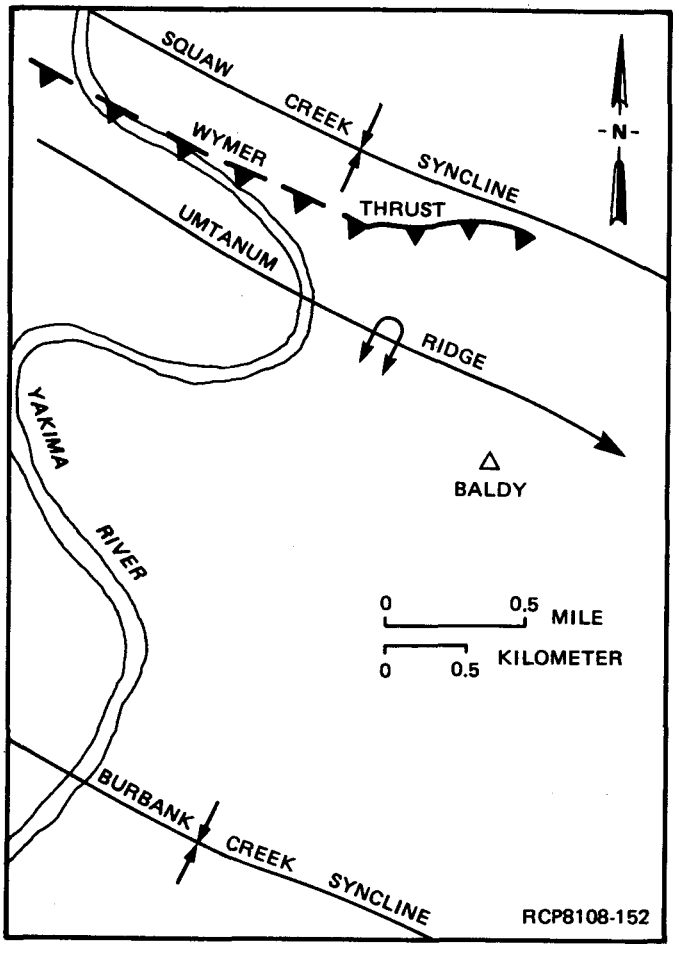

FIGURE 7-7. Structure Index Map, Baldy Area, Umtanum Ridge Structure. See Figure 7-1 for index map.

- Basalt flows can be traced across the fold.
- The degree of brecciation is spatially related to the dip, with more steeply dipping flows generally more brecciated.
- Layer-parallel faulting is present in hinge zones, but is not present in the fold crest or south limb.
- Slickenside striae on fault slip surfaces generally trend perpendicular to the fold axis.
- Movement on almost all faults has been dip-slip.
- Tectonic jointing strikes almost perpendicular to the fold axes.

The similarities of these structural elements indicate that both areas have essentially the same strain geometry and structural history. This suggests that the flexural flow buckle mechanical model is applicable to the Umtanum Ridge structure at both Baldy and Priest Rapids.

STRUCTURAL ANALYSIS OF HOLE-IN-THE-WALL AREA OF THE FRENCHMAN HILLS STRUCTURE

GEOLOGIC SETTING

The Frenchman Hills structure extends from north of Othello (T. 15 N., R. 29 E.) for ~85 km west (Fig. 7-1). The Frenchman Hills anticline has a noncylindrical character and appears to terminate eastward in low-amplitude folds. It is well exposed in a water gap along the Columbia River north of Vantage. Grande Ronde Basalt exposed in the gorge has been described by Mackin (1961) and Myers (1973). The structure east of the river has been mapped by Grolier and Bingham (1971) and by Swanson and others (1979a). The west side of the river has been mapped by Bentley (1977) and by Bentley, Swanson, and Byerly in Swanson and others (1979a).

The Frenchman Hills structure in the gorge is an asymmetric anticline with a thrust fault along the more steeply dipping north side. The thrust fault superposes gently dipping Frenchman Springs flows over a Roza flow and sandstone which Grolier and Bingham (1971) believed to be the Ringold Formation. On the west side of the river, a very open, anticlinal crest is exposed at Hole-in-the-Wall canyon (Fig. 7-8), but the hinge has been eroded. Numerous, low-dip, conjugate shear zones are exposed along the river cliffs (Fig. 7-9). Because of the good exposure, the Hole-in-the-Wall area was chosen for a geometric analysis of the shear zones. Of interest was whether the shear zones are associated with folding in the crest area (as at Priest Rapids) or whether they are associated with a different deformation geometry due to thrust faulting to the north.

ORIENTATIONS OF STRUCTURAL ELEMENTS

Flows in the Hole-in-the-Wall section dip 6^{o} to 10^{o} in both the north and south limbs. The regional reconnaissance geologic mapping of Swanson and others (1979a) shows the anticlinal trace trending east-northeast in this area.

Intraflow structures are well preserved and cross-cutting tectonic structures can be easily identified. Faults and shear zones are only locally developed and widely separated. Almost all observed faults and shear zones occur in conjugate sets. Orientations of shear zones in the Hole-in-the-Wall area are shown on equal-area projections (Fig. 7-10 [a]). All observed faults have a very low dip, and strike generally east-northeast. Field observations suggest that poles to the conjugate faults can be divided into two groups (Fig. 7-10 [b]): (1) a horizontal to gently north-dipping group and (2) a gently south-dipping group. Reverse or thrust movement is interpreted on each fault on which associated extension

FIGURE 7-8. Cross-Sectional View, Hole-in-the-Wall Area, Frenchman Hills Anticline. North is to the right. Cliff immediately above the water on left side of photograph is ~50 m high.

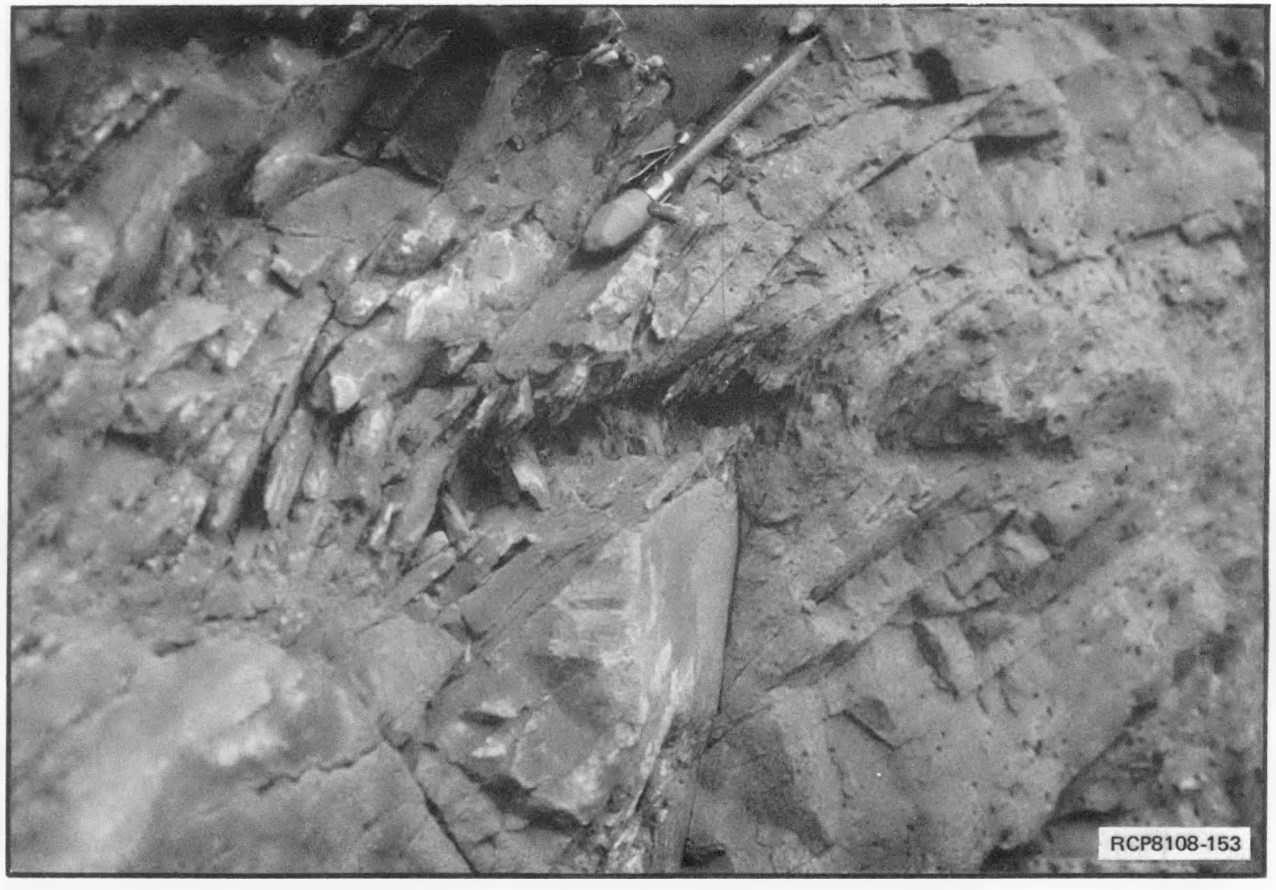

FIGURE 7-9. Incipient Brecciation with Rotation of Basalt Blocks within a Shear Zone at Hole-in-the-Wall. Apparent amount of shear (1 to 2 cm) decreases within 1 m laterally from the center of the photograph. Note pencil for scale.

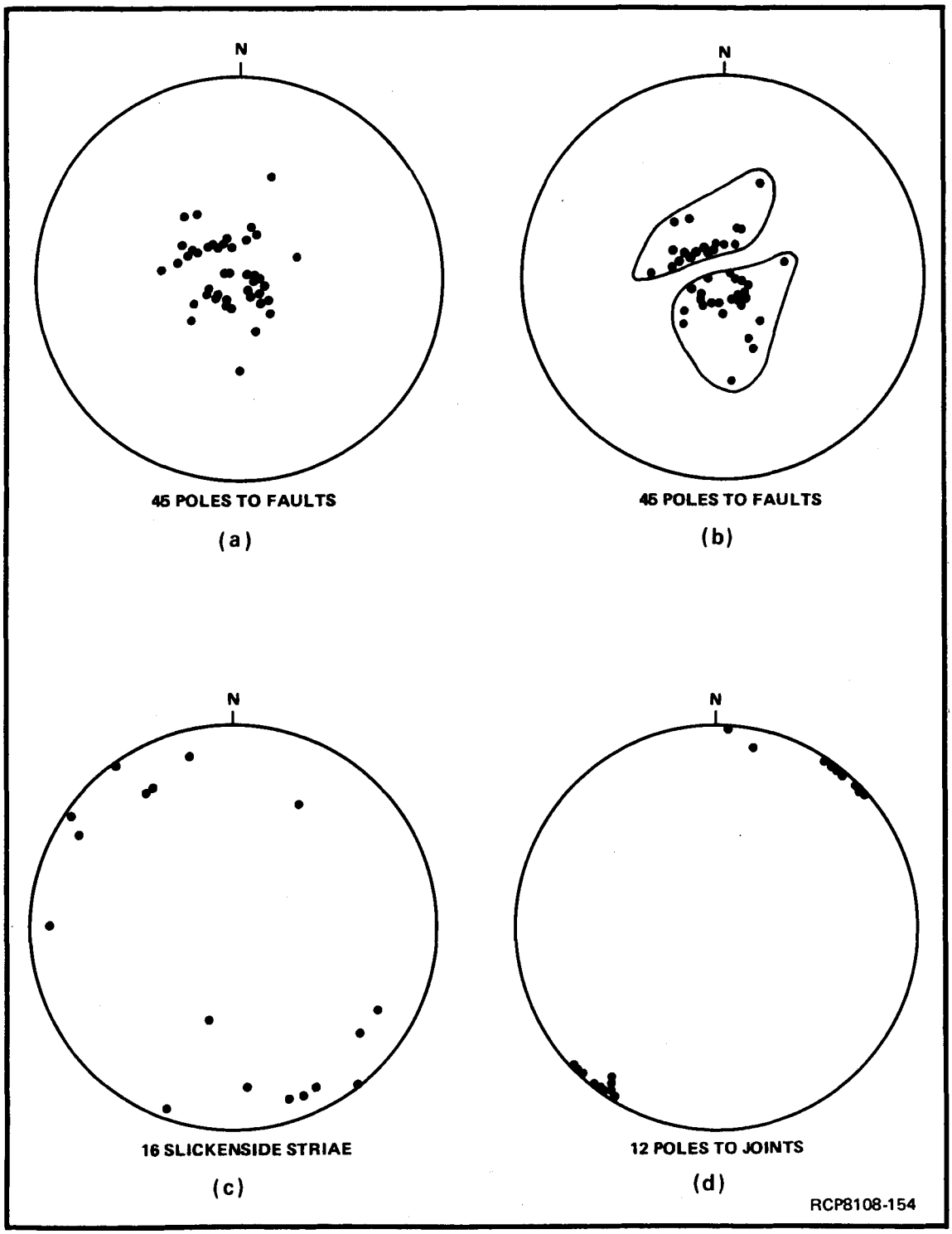

FIGURE 7-10. Equal-Area Projection of Structural Elements within the Hole-in-the-Wall Area, Frenchman Hills Anticline. (a) Poles to faults, (b) groupings of poles to faults based on field observations, (c) slickenside striae lineations, (d) poles to tectonic joints.

fracture angular relationships, as described in Price (in press), are recognized. Typical shear zones have an apparent maximum displacement of 1 to 2 cm, which diminishes to no recognizable displacement within 1 m laterally along dip (Fig. 7-9).

Orientations of slickenside striae are shown in equal-area projection in Figure 7-10 (c). Slickenside striae plunge moderately toward the northwest and southeast, generally perpendicular to or at a high-oblique angle to the fold trend. This plunge direction is essentially perpendicular to fault strikes. Thus, the faults are dip-slip.

Tectonic jointing is well developed, but widely spaced. Differential erosion has accentuated some joints that now appear as small, linear depressions traceable across the Hole-in-the-Wall area. Orientations of tectonic joints are shown in equal-area projection in Figure 7-10 (d). All joints are essentially vertical and strike northwest at a high-oblique angle to the fold trend.

COMPARISON OF THE FRENCHMAN HILLS STRUCTURE GEOMETRY AT HOLE-IN-THE-WALL WITH THAT OF THE UMTANUM RIDGE STRUCTURE GEOMETRY AT PRIEST RAPIDS

Orientations of faults in the Hole-in-the-Wall area (Fig. 7-10 [a] and [b]) are taken from the north and south limbs of the fold. In both limbs, orientations of the conjugate fault sets are the same, but the limbs dip in opposite directions. In both limbs, the acute bisector of the conjugate sets lies at an acute angle with flow layering (Fig. 7-11).

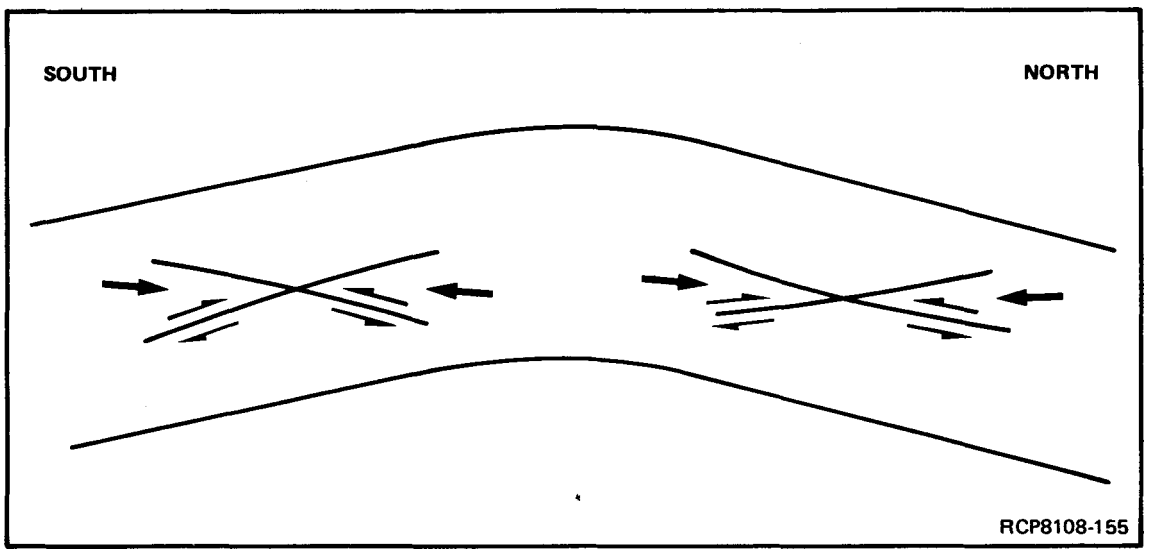

FIGURE 7-11. Schematic Cross Section, Flow Layer of Hole-in-the-Wall Area, Frenchman Hills Structure (showing the relationship between orientation of conjugate faults and shear zones relative to position within the fold). Whole arrows indicate interpreted local compression directions; half arrows indicate interpreted relative shear directions.

The conjugate fault geometry and reverse movements on the faults suggest that local compression was at an acute angle with flow layering and was symmetrically distributed about the fold crest. Strain geometry at Hole-in-the Wall is analogous to the strain geometry observed near the crest of the Umtanum Ridge structure at Priest Rapids (Fig. 7-3). This suggests that the flexural flow buckle mechanical model is also applicable to the Frenchman Hills structure; however, more detailed mapping across the entire structure is necessary to be more definitive.

EXTRAPOLATIONS OF THE NATURE OF STRAIN FEATURES INTO THE SUBSURFACE OF THE COLD CREEK SYNCLINE AREA

Structural analysis of two folds at three localities suggests that the flexural flow buckle model may be characteristic of deformation of the Yakima folds. Because the Cold Creek syncline is a Yakima fold, bedrock strain features within the basalt in that area are probably due predominantly to flexural flow buckling.

The structural analyses show that relatively little deformation, other than tectonic jointing, has taken place in the anticlinal crests and that little to no deformation occurred in the synclinal troughs. The gently dipping limbs of the anticlines contain widely disseminated shear along small, conjugate faults; whereas, the steeply inclined flows contain the most extensive faulting and brecciation.

The overall consistency of these strain features suggests that similar strain distributions are within the Cold Creek syncline subsurface, as shown in a schematic cross section in Figure 7-12. Anticlinal crests should show little deformation, other than steeply inclined tectonic jointing. Individual joints may cross flow contacts and represent possible, vertical, groundwater flowpaths. Because the folds are asymmetric, more extensive shearing and large, reverse faults may underlie the crestal areas at depth. Within the gently dipping limbs of the anticlines, discrete shear zones or faults a few centimeters to a meter wide may be present. A recent examination of small breccia zones in basalt core from core holes within the Cold Creek syncline basalts by D. J. Moak (Chapter 6 and Appendix A) and this writer indicates that these small breccia zones have been penetrated by drilling in the Pasco Basin and Cold Creek syncline. Such small faults can extend across flow contacts and, on Umtanum Ridge, have been observed with groundwater flowing from them. Therefore, based on surface observations, these faults should be considered possible upward groundwater flowpaths.

The synclinal trough areas exposed in the Burbank Creek syncline and at Priest Rapids exhibit the least strain of any part of the fold structures. The synclinal trough areas observed do not show pervasive tectonic jointing or small-scale faulting related to folding. However, in the Burbank Creek syncline, strike-slip faults relatively younger than other faults associated with the folding do occur. Younger strike-slip faults transverse to the Yakima fold trends have not been observed within the Cold Creek syncline area, but may be present.

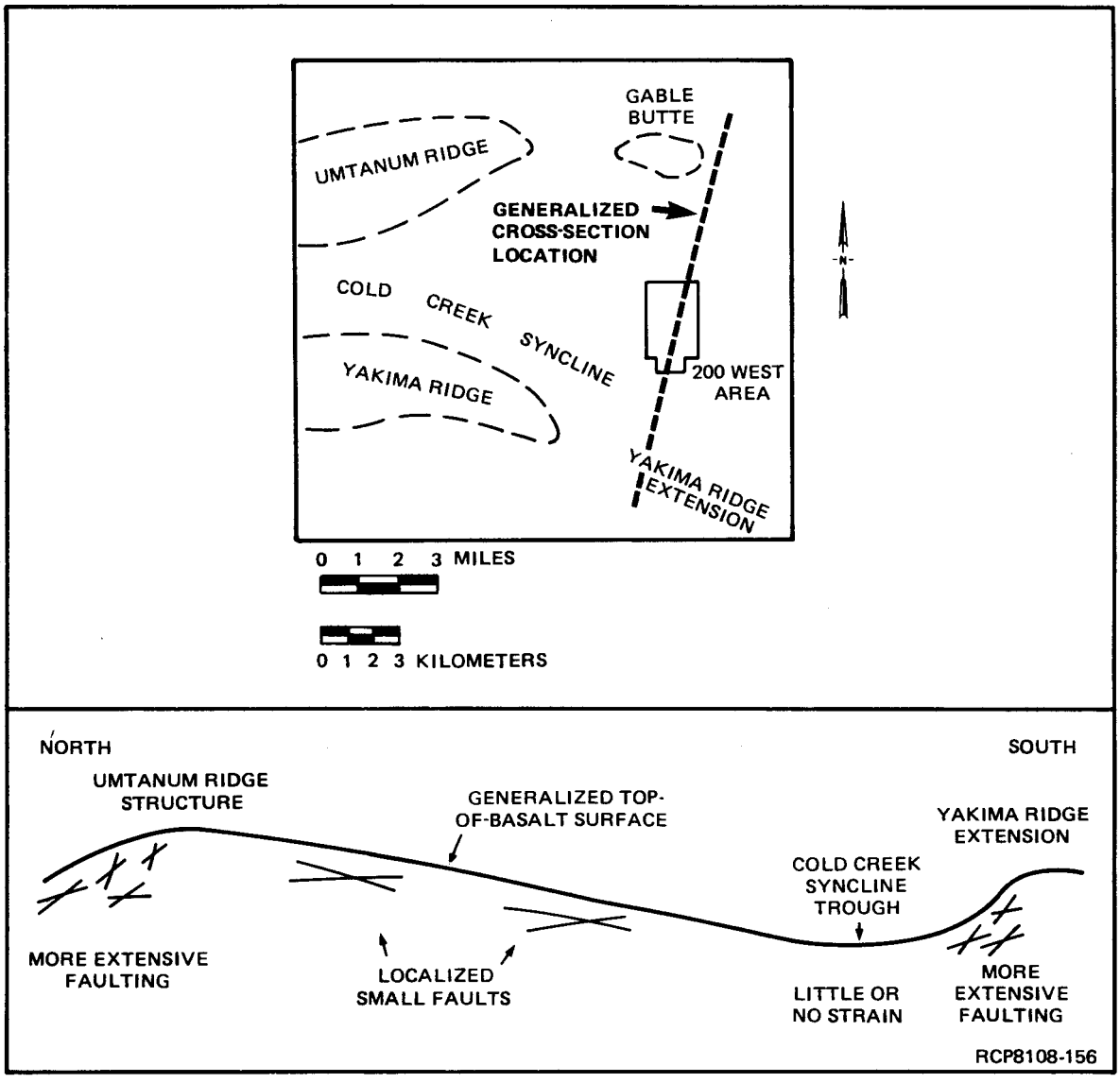

FIGURE 7-12. Schematic Cross Section, Cold Creek Syncline (illustrating predicted distribution of faults with respect to folds).

En echelon anticlines comprising Gable Butte and Gable Mountain are essentially buckles and should have their own geometrically related strain features. Faults such as those mapped on Gable Mountain (Myers, Price and others, 1979) and the DB-10 fault (Chapter 6) might be geometrically related to such second-order folding, but, due to the poor bedrock exposure and lack of strain features in the exposures of Gable Mountain and Gable Butte, their geometry is not yet adequately understood.

SUMMARY AND CONCLUSIONS

A structural analysis of selected Yakima folds was made based on field mapping and geometric analysis of structural elements (i.e., folds, faults, and joints). Recent studies within the Umtanum Ridge structure at Priest Rapids on the Columbia River, at the Baldy area in the Yakima River canyon, and within the Frenchman Hills structure have shown a remarkable similarity of the strain geometry among these Yakima folds. Such consistency of strain geometry allows a more accurate prediction of the location and character of strain features in the subsurface of the Cold Creek syncline. The structural analysis data suggest that the flexural flow buckle model is characteristic of deformation of the Yakima folds. Because the Pasco Basin and Cold Creek syncline lie mostly within the Yakima Fold Belt, bedrock strain features within that area would be due predominantly to flexural flow buckling.

The structural analyses show that relatively little deformation, other than tectonic jointing, has taken place in the anticlinal crests and that little to no deformation has occurred in the synclinal troughs. The gently dipping limbs of the anticlines contain widely disseminated shear along small, conjugate faults; whereas, the steeply inclined flows in hinge areas contain the most extensive faulting and brecciation.

CHAPTER 8 - BEDROCK STRUCTURE OF THE COLD CREEK SYNCLINE AREA

C. W. Myers

INTRODUCTION

The purpose of this chapter is to discuss the bedrock structure of the Cold Creek syncline area (Fig. 8-1) based on an integration of the results contained in the preceding chapters and following appendices. The interpretations presented are an update and expansion of those included in Myers, Price and others (1979). Locating and evaluating bedrock structures (i.e., folds, fractures, faults, and joints) is necessary because: (1) the spacing and orientation of such structures determine the geometry of the relatively intact volumes of basalt host rock within which a repository could be constructed and (2) bedrock structures might represent zones of vertically oriented fractures that could affect shallow and deep groundwater flow systems toward or away from a repository.

In the discussion that follows, emphasis is given to shallow bedrock structures within the upper 1,200 m of the bedrock section. These structures might modify the isolation potential of the Umtanum flow within the RRL (Fig. 8-1). Interpretations of the geometry of the Umtanum flow and the locations of bedrock structures relative to candidate repository sites are based largely on extrapolations to depth using the top of basalt (TOB) as datum. Hence, the structure of the TOB across the Cold Creek syncline area is described in greatest detail.

APPROACH

The description of the structural geologic setting of the Cold Creek syncline presented in this chapter has been produced through the analysis and integration of results from four separate, but related, field investigations: (1) surface geologic mapping of bedrock (see maps in Myers, Price and others, 1979), (2) borehole geologic studies (Chapter 6 and Appendix A), (3) structural analysis of Yakima folds (Chapter 7), and (4) geophysical surveys (Appendices B through E). Current interpretations of the bedrock geology of the Cold Creek syncline are shown on the following figures:

- Bedrock geologic maps (Fig. 8-2)
- Structure-contour maps
  - Top of basalt (Fig. 8-3)
  - Top of Wanapum Basalt (Fig. 8-4)
  - Top of Grande Ronde Basalt (Fig. 8-5)
  - Top of Umtanum flow (Fig. 8-6)
- Structure cross sections (Fig. 8-7)
- Interpretive bedrock-structure map (Fig. 8-8).

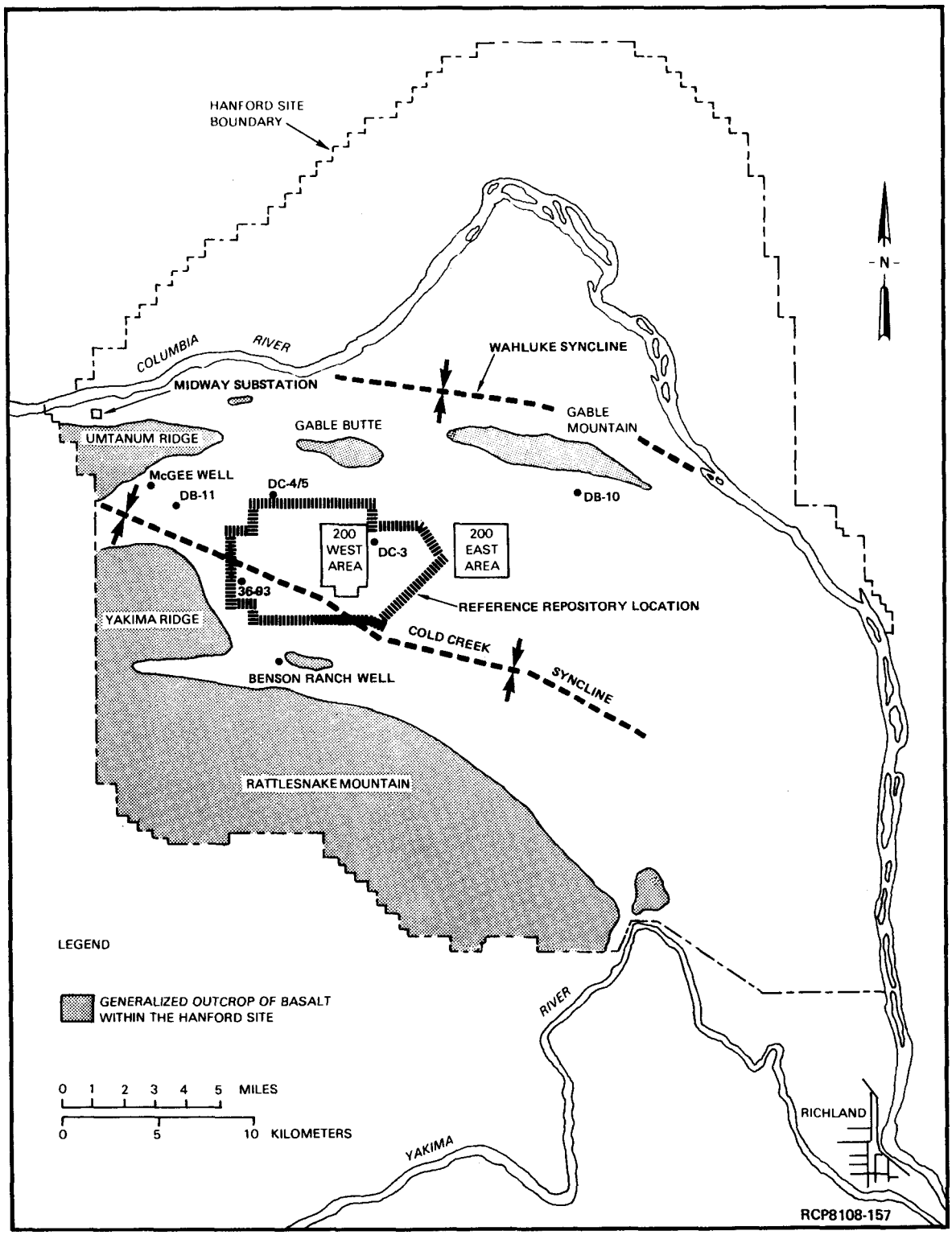

FIGURE 8-1. Location Index Map.

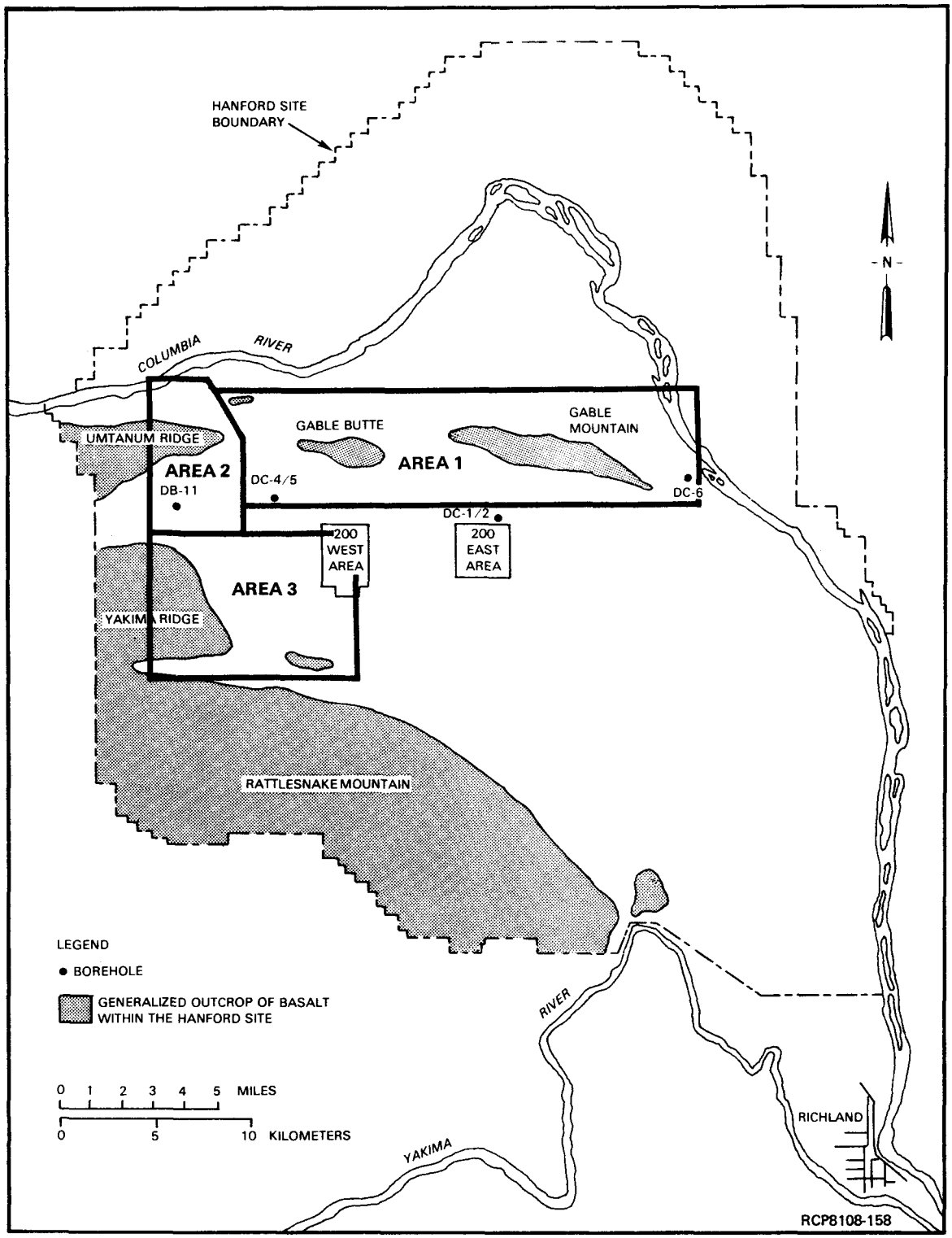

FIGURE 8-2a. Index Map Showing Locations of Bedrock Geologic Maps.

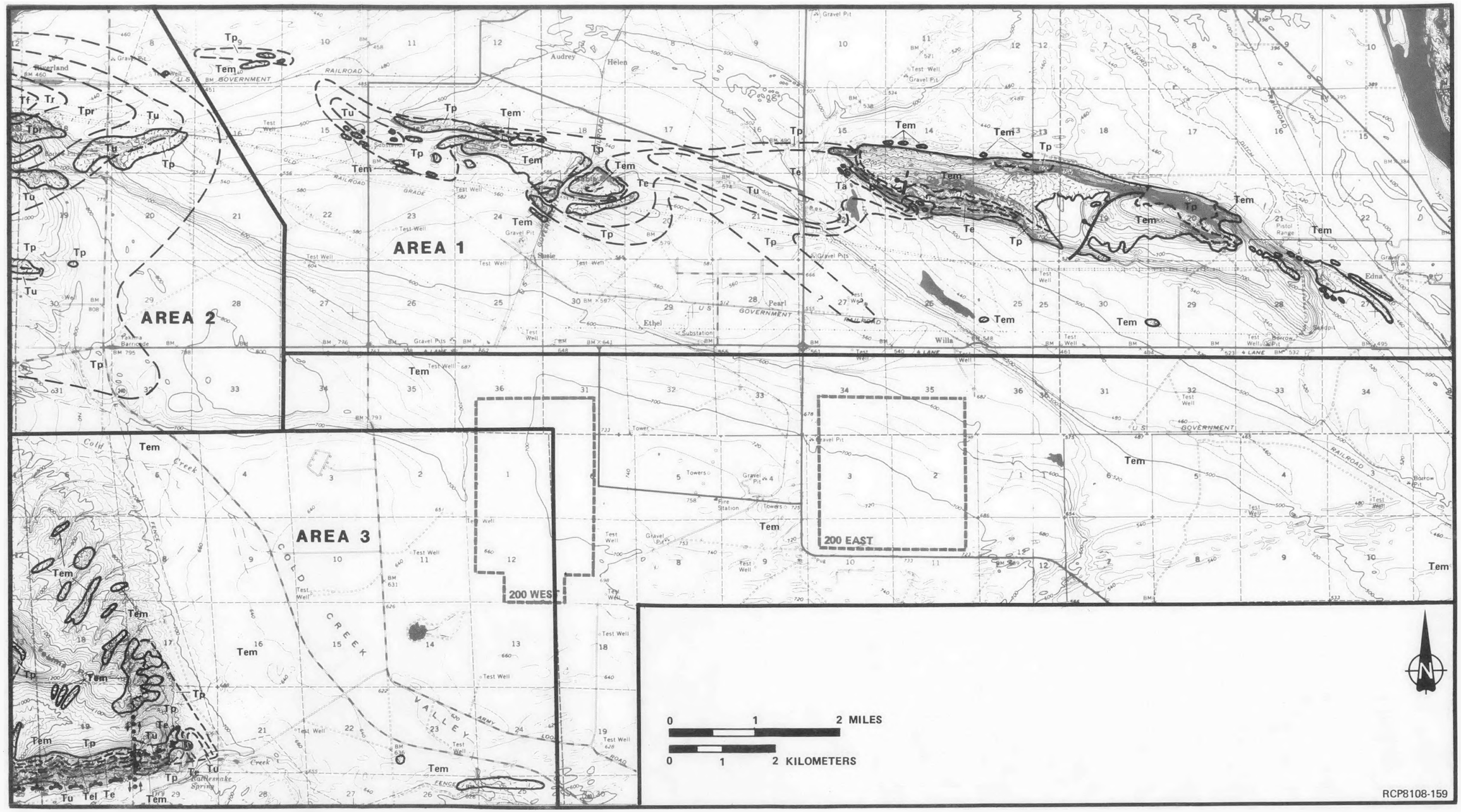

FIGURE 8-2b. Bedrock-Geologic Map, Areas 1, 2, and 3. See Table 3-1 for explanation.

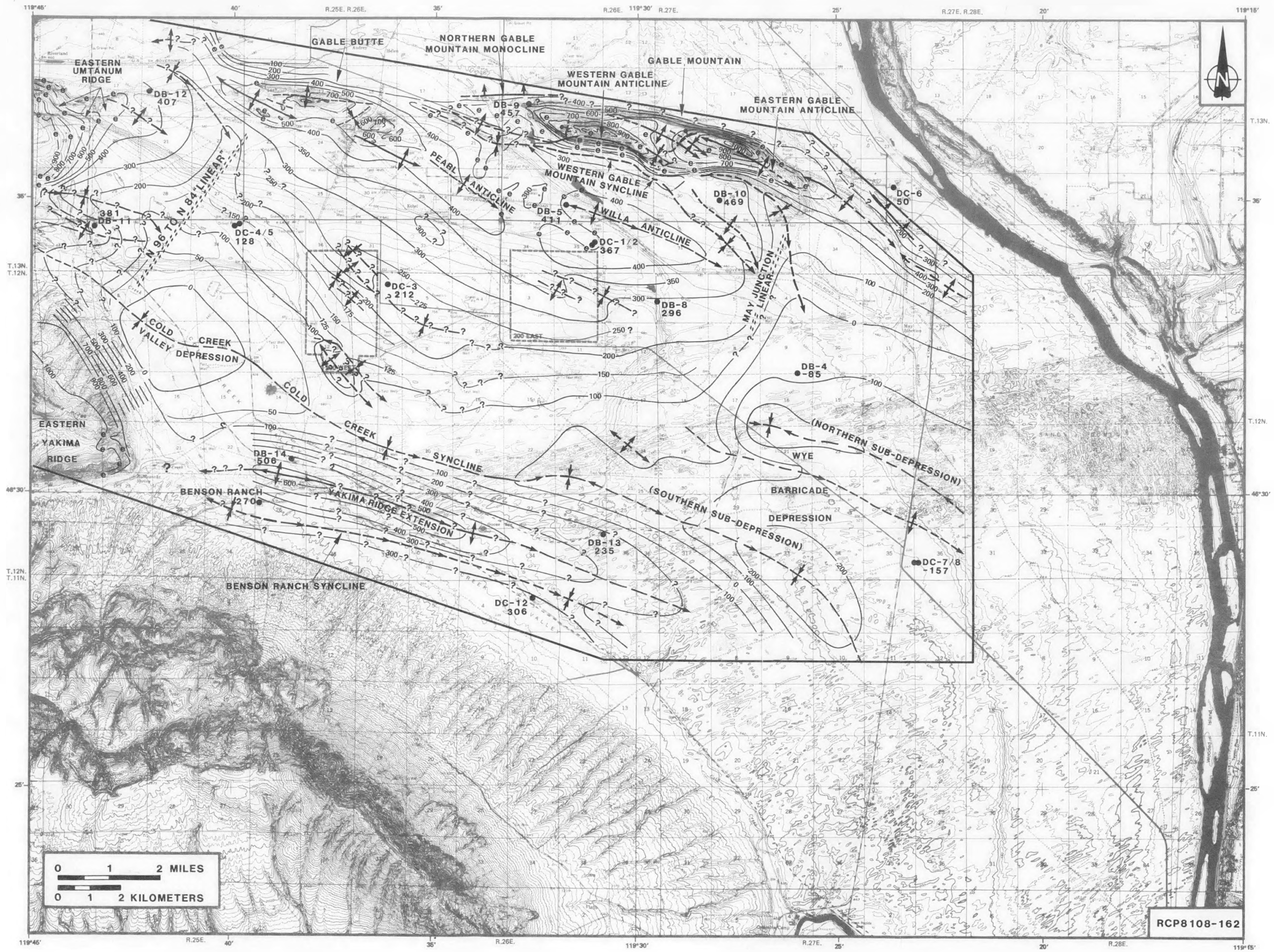

FIGURE 8-3. Top-of-Basalt Contour Map (see text for discussion and Table 3-1 for explanation).

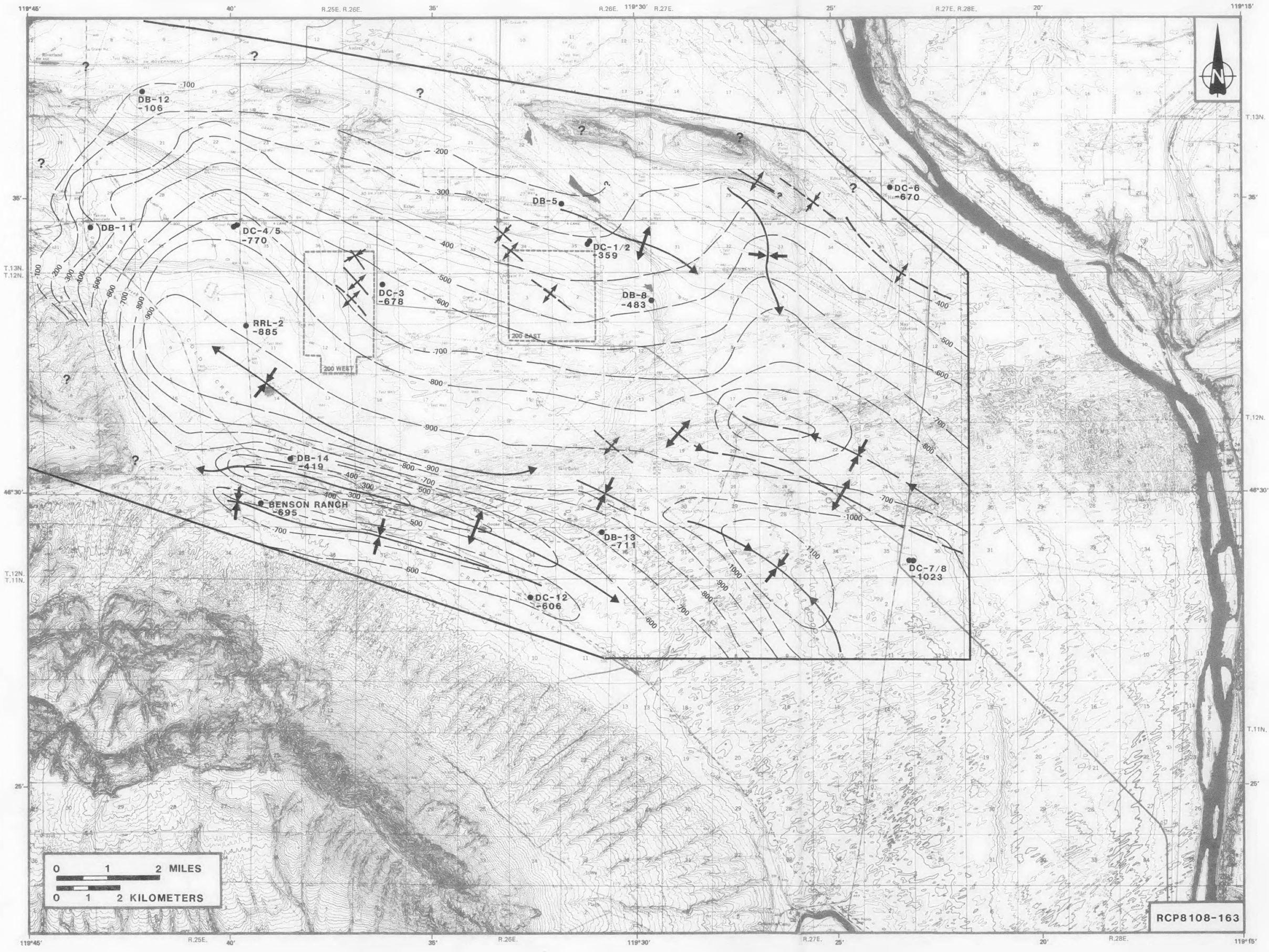

FIGURE 8-4. Top of Wanapum Basalt Structure-Contour Map (see Table 3-1 for explanation).

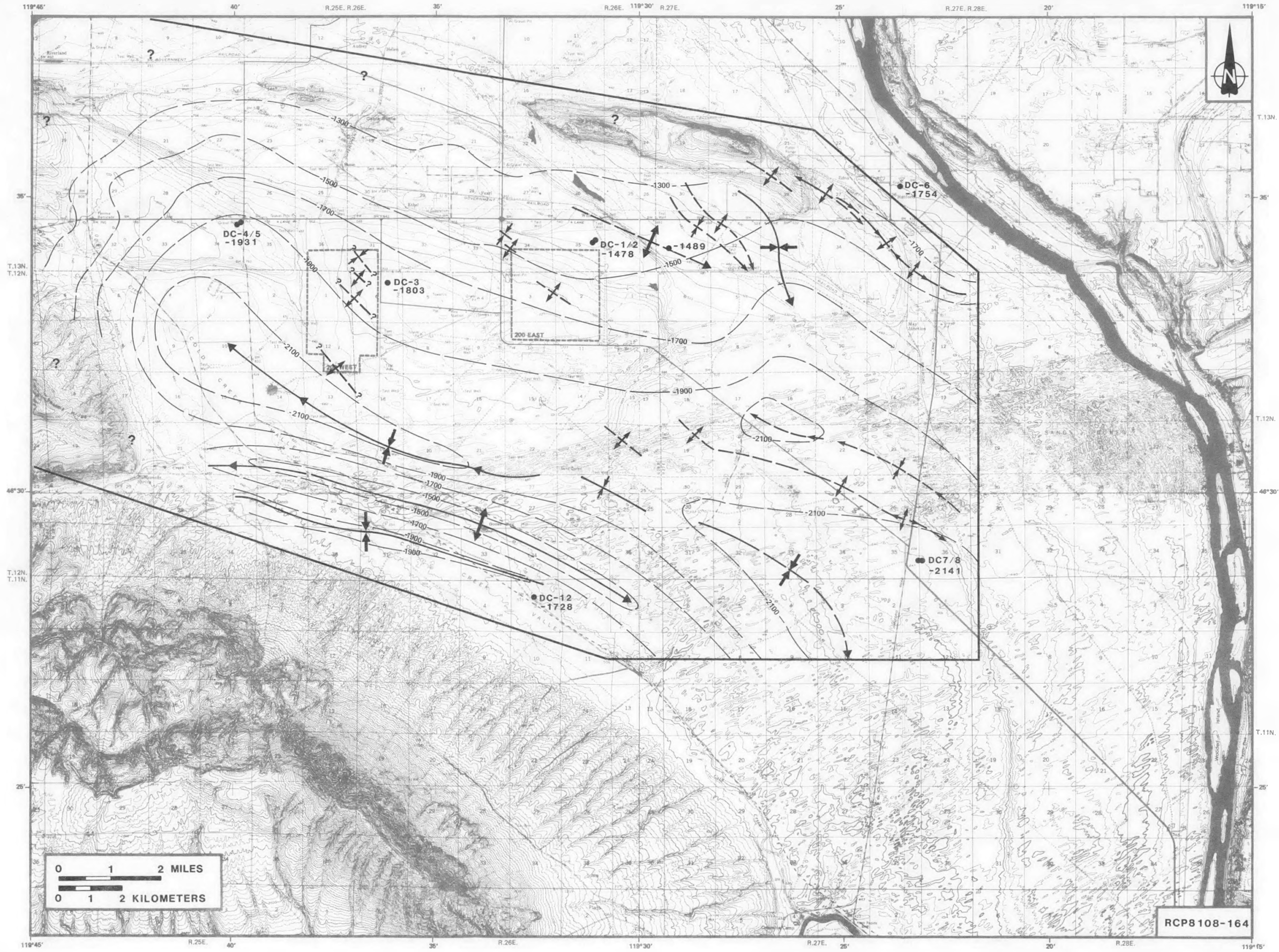

FIGURE 8-5. Top of Grande Ronde Basalt Structure-Contour Map (see Table 3-1 for explanation).

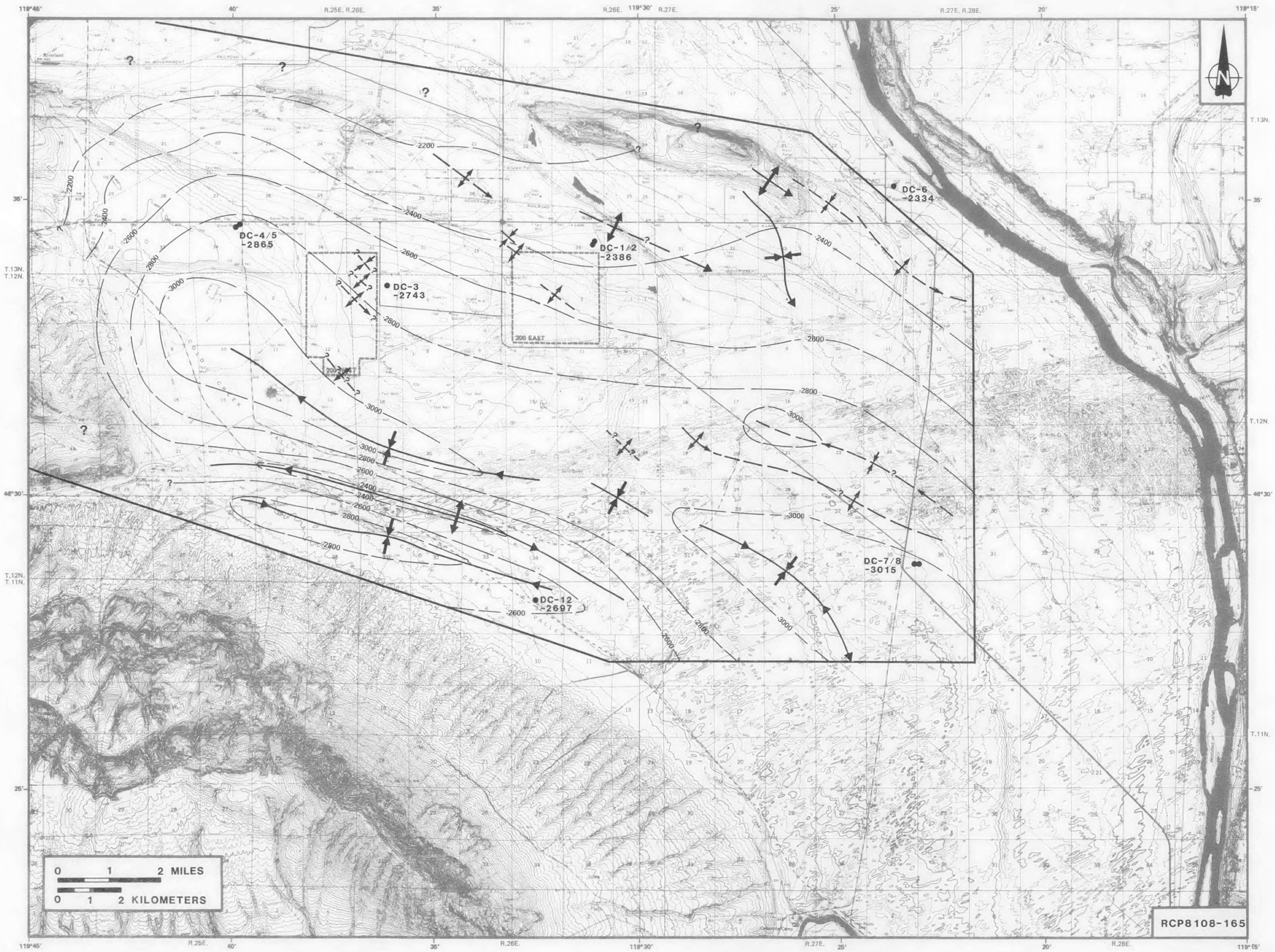

FIGURE 8-6. Top of Umtanum Flow Structure-Contour Map (see Table 3-1 for explanation).

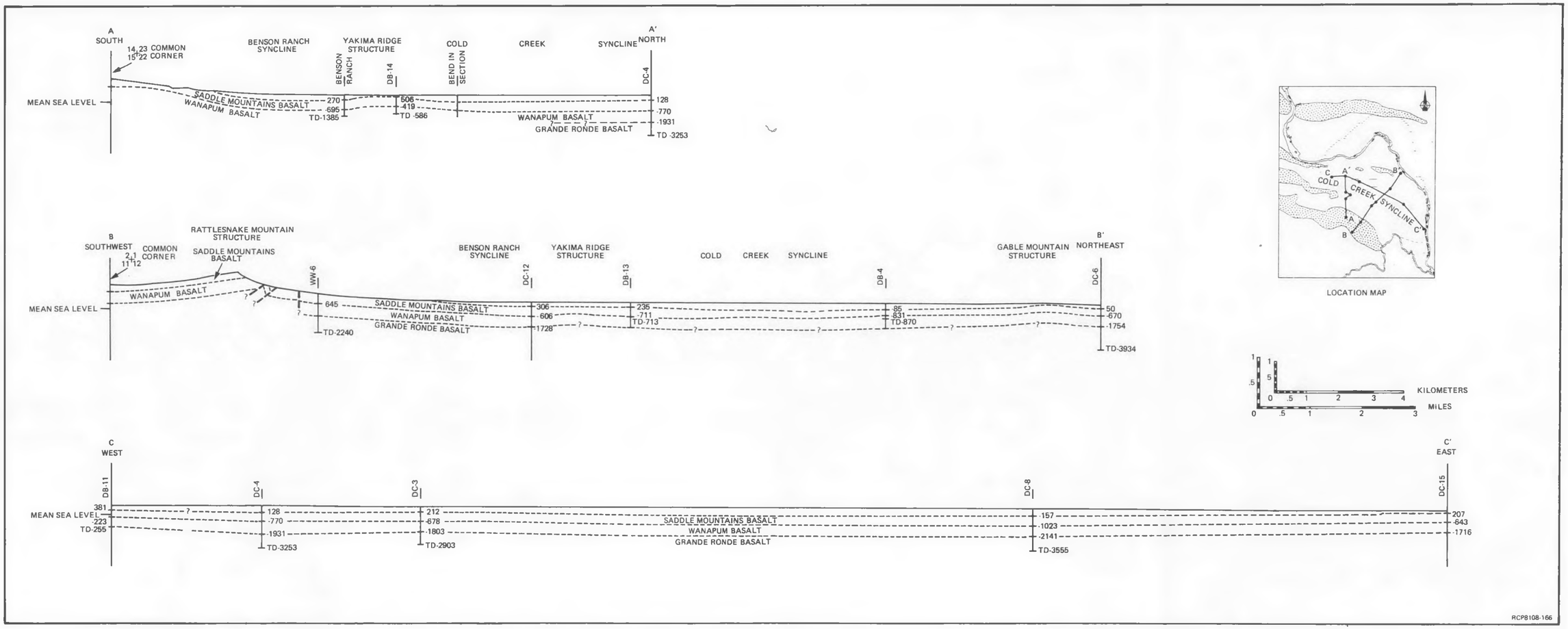

FIGURE 8-7. Structure Cross Sections.

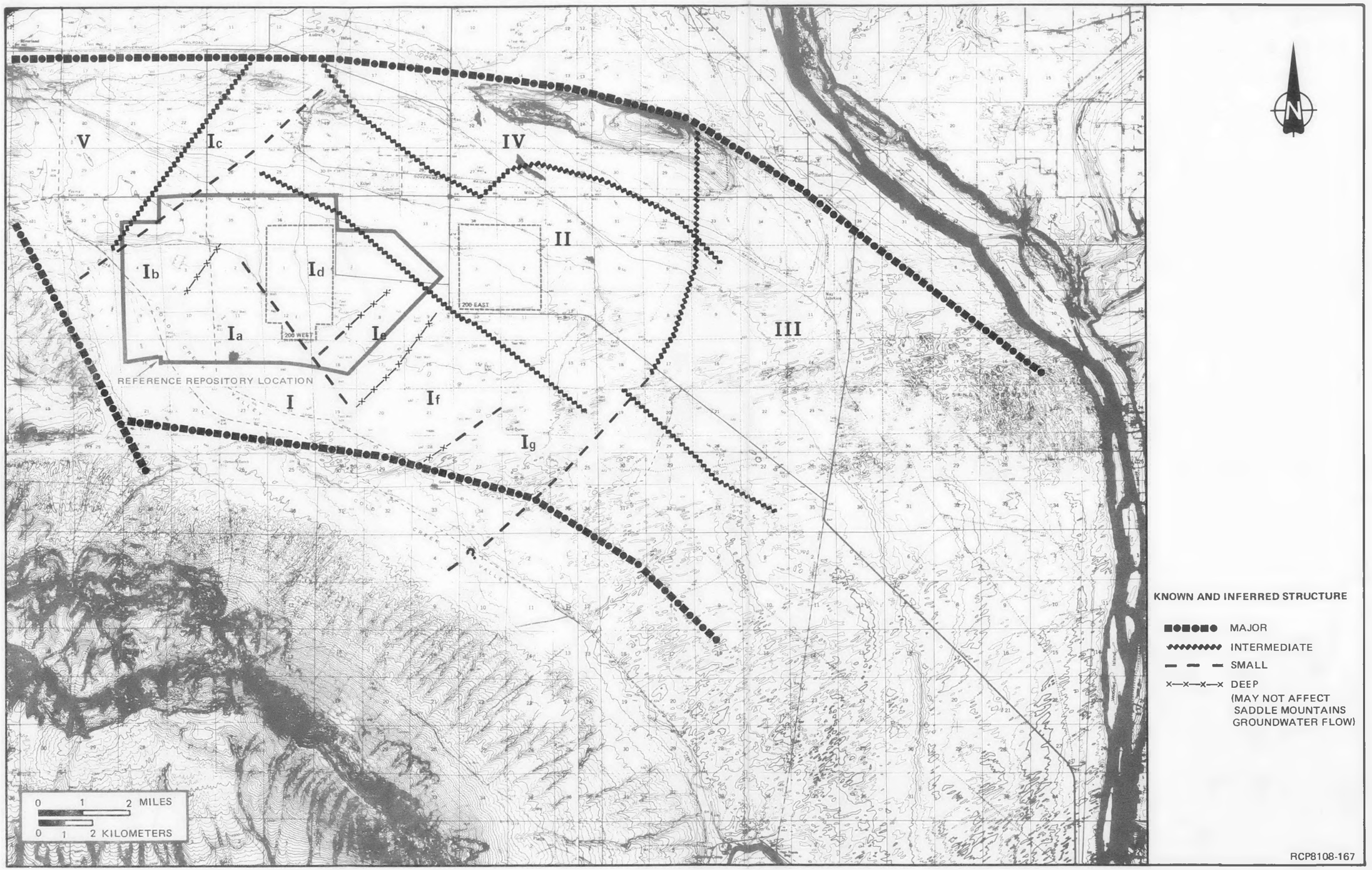

FIGURE 8-8. Interpretive Bedrock-Structure Map. Areas I through V are plan views of large, relatively intact volumes of bedrock with boundaries defined by known and inferred structures as shown. Areas Ia through Ig are subdivisions of Area I, also based on known and inferred structures.

Isopachs of the Saddle Mountains and Wanapum Basalts (which include the thickness of the Ellensburg Formation; Chapter 3) were combined with the TOB-contour map (Fig. 8-3) to generate structure-contour maps of the top of Wanapum Basalt (Fig. 8-4) and top of Grande Ronde Basalt (Fig. 8-5), respectively. The isopach map of the Sentinel Bluffs sequence (Chapter 5) was combined with the top of Grande Ronde Basalt structure-contour map to generate the top of Umtanum flow structure-contour map (Fig. 8-6). The manual method described by Low (1977) was used to combine the isopach maps and structure-contour maps. Structures shown at horizons below the TOB are based on downward projections from the TOB. Many structures shown on the TOB map are not honored by contour lines on the structure-contour maps of the deeper horizons because of the uncertainty of their presence or location at depth. Such structures are shown by the use of symbols to call attention to their possible presence (Fig. 8-4 through 8-6).

The TOB map (Fig. 8-3) was prepared in accordance with basic principles for constructing structure-contour maps (Low, 1977). Data utilized to construct the map included borehole information and indications of the configuration of the TOB surface from geophysical surveys. Interpretation of geophysical data was conducted on a line-by-line (two-dimensional) basis, then extrapolated into three dimensions. During this interpretive process, seismic reflection, multilevel aeromagnetic, ground magnetic, and gravity profiles were collated and compared to identify geophysical features in common between data sets. The degree of agreement among geophysical and borehole data was used as an indication of whether geophysical anomalies were indeed related to a geologic feature or were spurious. Ground magnetic, gravity, and seismic reflection (SR) sections were used to show TOB structural highs and lows, direction of apparent dip, and the uniformity and rate of apparent dip on the TOB. Aeromagnetic total field highs and lows were used as general indicators of broad highs and lows in the TOB.

Two types of borehole data were used to draw the TOB map: (1) interpreted elevation of the basalt-sediment contact and (2) identity of the uppermost basalt unit. The elevation of the basalt-sediment contact was determined in ∿300 boreholes within the Hanford Site. (By way of comparison, the elevations of the top of Wanapum Basalt and top of Grande Ronde Basalt are based on data from ∿25 and ∿15 boreholes, respectively.) The elevation of the basalt-sediment contact was identified using chip cuttings and, if available, core (Fecht and Lillie, in press) and geophysical logs. The identity of the uppermost basalt unit (based on chemical analysis of core or chip samples) was used to distinguish erosional from structural control of the TOB elevation. Where the contact has been cored, identification of the basalt-sediment contact and the uppermost basalt unit is relatively precise; however, cores are available for only ∿5% of the boreholes that penetrate the basalt-sediment contact (Appendix A).

A deliberate effort was made to have the pattern of contours on the TOB closely reflect the structural fabric and structural style revealed by surface mapping of bedrock exposures within and around the margins of the

Pasco Basin (Myers, Price and others, 1979; Fig. 8-2). Such mapping indicates that most deformation in the Yakima Fold Belt was by folding, and that folds can easily be misinterpreted as faults, especially where outcrops are sparse. However, any structure mapped as a fold in the TOB in the Cold Creek syncline might have associated faults, and some of the structures mapped as folds might actually be faults. The current lack of distinction between faults and folds is not judged as a serious problem at this stage of subsurface mapping for the BWIP geologic studies. The important point is that buried structures be located and recognized as such so that their potential influence on groundwater flow can be evaluated.

The Umtanum flow is ∿750 m stratigraphically below the TOB across most of the Cold Creek syncline, particularly in the trough area where the TOB is the virtually uneroded surface of the Elephant Mountain Member. A prime concern in using the TOB as a structural datum is that it adequately reflect the structure of the underlying bedrock, particularly at the level of the Umtanum flow. There are five possible reasons why the structure of the TOB might not exactly coincide with the structure of the Umtanum flow everywhere across the Cold Creek syncline area: (1) the TOB itself might represent a slightly unconformable surface; (2) the basalt section beneath the TOB and above the Umtanum flow might contain slight unconformities, buried folds or faults, or might have significant lateral variations in thicknesses of its major units; (3) fault planes or axial planes of asymmetric folds might be inclined from the vertical so much that structures could "migrate" significantly with depth; (4) concentric folding of the first-order and second-order folds might cause significant changes in structural attitudes with depth; and (5) shallow, third-order structures might not extend to depth.

The structural interpretations presented in this chapter are also based on the premise that all major bedrock structures that deform the Grande Ronde Basalt flows in the Pasco Basin have some expression in the uppermost flows of the Saddle Mountains Basalt. This premise appears justified based on our current understanding of the structural history of the Pasco Basin (Myers, Price and others, 1979; Caggiano and others, 1980; Chapters 3, 4, and 7). Use of this premise does not preclude the possibility that certain structures of post-upper Grande Ronde age may have developed with a different style and different trend during the early stages in the evolution of the Yakima Fold Belt. Such early-formed structures might have ceased their development before late Saddle Mountains time and, thereafter, become buried by later floods of Saddle Mountains Basalt lavas. Thus, the possibility exists that there may be buried structures in the Pasco Basin that have no expression in the TOB surface. Aeromagnetic data (Appendix B), although not conclusive, support this possibility. The location and trend of some aeromagnetic highs and lows suggest that some structures buried beneath the TOB have no expression in the bedrock surface.

STRUCTURE-CONTOUR MAP OF TOP OF BASALT

The structure of the Cold Creek syncline area (Fig. 8-1) is characterized by: (1) areas of nearly flat-lying basalt; (2) three, east-southeast-plunging, first-order anticlines (Umtanum Ridge, Yakima Ridge, and Rattlesnake Mountain structures); (3) two, southeast-plunging, second-order anticlines (Gable Butte and Gable Mountain); (4) third-order folds within the hinge zones of the second-order anticlines and on the limbs of the first-order anticlines; and (5) northwest- and possible northeast-trending cross structures whose exact nature is unknown. The dominant structural trend in the Cold Creek syncline area is east-west to northwest-southeast. Structural relief is ∿300 m in the western part of the Cold Creek syncline area and decreases to the east.

The Cold Creek syncline is an asymmetric, open, broad, and relatively flat-bottomed fold (Fig. 8-7) with a steep south limb. The syncline lies between the buried Yakima Ridge structure and the Umtanum Ridge-Gable Mountain structure; it plunges east and dies out in the vicinity of the Wye Barricade depression (Fig. 8-3).

For purposes of this discussion, the Cold Creek syncline study area (Fig. 8-3) is subdivided into the following sub-areas on the basis of bedrock structure:

1. Umtanum Ridge-Gable Mountain structure
   - Eastern Umtanum Ridge
   - Gable Butte
   - Gable Gap
   - Gable Mountain
   - South limb of the Umtanum Ridge structure

2. Cold Creek syncline
   - Cold Creek Valley depression
   - Wye Barricade depression

3. Yakima Ridge structure
   - Eastern Yakima Ridge
   - Buried extension of the Yakima Ridge structure.

UMTANUM RIDGE-GABLE MOUNTAIN STRUCTURE

Umtanum Ridge is a structure interpreted here to include at least three orders of folding (Fig. 8-3). The first-order fold is Umtanum Ridge itself, a Yakima fold of regional extent with a wavelength of 5 to 15 km. In the central Pasco Basin, the Umtanum Ridge structure is delineated by two, en echelon, second-order anticlines, with wavelengths of ∿5 km. The Gable Butte second-order anticline extends from sec. 10, T. 13 N., R. 25 E. to sec. 5, T. 12 N., R. 27 E.; the Gable Mountain second-order anticline extends from sec. 17, T. 13 N., R. 26 E. southeast out of the Cold Creek syncline study area (Fig. 8-3). Both anticlines are well marked by strong,

linear highs in the aeromagnetic total field (Appendix B) and by Werner deconvolution solutions (N-61, D-21, N-51, N-41, N-226, N-68, D-63, D-26, D-214, N-227, N-52, and D-216; Appendix B). Third-order folds with wavelengths of ≤1 km occur within the closure of the two second-order anticlines and, apparently, far down the south limb of the first-order Umtanum Ridge anticline.

Eastern Umtanum Ridge

Eastern Umtanum Ridge is a tight, asymmetric, box-shaped anticline that plunges eastward into the Pasco Basin. The north limb of the structure dips more steeply than the south limb. Chapter 7 contains a detailed description of the hinge zone of the Umtanum Ridge structure exposed at Priest Rapids, located ~16 km northwest of the Cold Creek syncline study area. Exposures of the Wanapum and Saddle Mountains Basalts are the easternmost outcrops on Umtanum Ridge (sec. 17 and 18, T. 13 N., R. 25 E.) (Fig. 8-2). These outcrops are near the crest of the first-order Umtanum Ridge structure.

The Umtanum fault, a reverse fault, is exposed on the north side of eastern Umtanum Ridge at Priest Rapids (Goff, 1981). The fault is covered toward the east, so its exact eastward extent is unknown. However, because strain in Yakima folds appears to be related to the folding process (Chapter 7), fault displacement should decrease as structural relief decreases. Current judgment is that the Umtanum fault probably dies out west of the Midway Substation (Fig. 8-1).

The TOB in sec. 17 and 21, T. 13 N., R. 25 E. (Fig. 8-3) shows a broad anticline nosing to the southeast, suggesting that the crestal zone (and the underlying hinge zone) does not trend east at this location. The anticline appears to be en echelon with the folds exposed on Gable Butte 3 km to the east. The location of this structure is probably indicated by a southeast-trending, elongated, aeromagnetic high in that same area (Appendix B).

Bedrock structures in sec. 29, 30, 31, and 32, T. 13 N., R. 25 E. (Fig. 8-3) are not well understood. The TOB contours were drawn to show an anticline and syncline plunging east-southeast, even though a Werner deconvolution solution (D-33; Appendix B) trends northeast. The aeromagnetic total-field-contour map shows both northeast and northwest trends (Appendix B). The overall structure here is one of southeasterly dip as far east as the N-96 to N-84 linear (Fig. 8-3), beyond which the dip is to the southwest (Fig. 8-3).

Gable Butte

Gable Butte (Fig. 8-1) is at the northern end of a second-order anticline, here named the Gable Butte fold. This fold extends southeasterly into sec. 5, T. 12 N., R. 27 E. near the May Junction linear (Fig. 8-3). Gable Butte itself includes three, approximately en echelon,

third-order anticlines (Fig. 8-3). The third-order anticlines are symmetrical and have rounded closures and open, interlimb angles, except for the northernmost which is asymmetrical and open to tight. Borehole and geophysical data around Gable Butte (Fecht, 1978; Appendix D) indicate that the southeasternmost, third-order anticline plunges southeastward into the subsurface, and is either en echelon with, or connects with, the Pearl anticline (Fig. 8-3). The northwestern plunge of the westernmost third-order anticline has been traced into the subsurface (Appendix E) using geophysical surveys. A southeast-plunging syncline is located ∿0.5 km southwest of the westernmost, third-order anticline on Gable Butte. This syncline is en echelon with the Gable Butte anticlines and with the previously discussed inferred anticline that plunges southeasterly off eastern Umtanum Ridge.

Gable Gap

Gable Gap is the informal name given to the sediment-covered, synclinal area between Gable Butte and Gable Mountain (Fig. 8-1). Floodwaters from the catastrophic Pleistocene floods (Bretz, 1923) swept southward across the northern Pasco Basin (Fecht, 1978) and were preferentially channeled through the Gable Gap area where they scoured and eroded the bedrock surface. The bedrock in Gable Gap is deformed by five folds (Fig. 8-3): (1) Pearl anticline, (2) Willa anticline, (3) western Gable Mountain anticline, (4) western Gable Mountain syncline, and (5) northern Gable Mountain monocline. The western Gable Mountain anticline is parallel to the western Gable Mountain syncline, a syncline whose trough is located ∿0.5 to 1 km south of the crest of the anticline. This anticline and syncline are third-order folds associated with the larger, second-order, Gable Mountain fold. The Pearl and Willa anticlines are en echelon, third-order folds associated with the larger, second-order, Gable Butte fold.

The following discussion of the Gable Gap area includes the results of work by Fecht (1978), Holmes and Mitchell (Appendix B), and Ault (Appendix D). The TOB on the north side of the western end of Gable Mountain does not dip uniformly into the Wahluke syncline (Fig. 8-1), but is sharply flexed (perhaps with some faulting). This flexure forms the northern Gable Mountain monocline, which extends from sec. 14, T. 13 N., R. 26 E. at the base of Gable Mountain through sec. 16, T. 13 N., R. 26 E. (Fig. 8-3). The monocline is indicated by SR data (line 4, shotpoint [SP] 1080 to 1100; line 2, SP 210 to 230; Appendix B) and coincides with a Werner deconvolution solution (N-61; Appendix B). The monocline either dips smoothly into the Wahluke syncline or, on the basis of the continuity of Werner deconvolution solutions (N-68, N-61, and N-51; Appendix B) and other geophysical data, the monocline might be much more extensive. The monocline is perhaps associated with the dip of the northern limb of the first-order Umtanum structure into the Wahluke syncline.

The western Gable Mountain syncline is asymmetric and is located 0.5 to 1 km south of the crest of the western Gable Mountain anticline. The steep limb common to these two asymmetric folds has been preferentially

eroded; portions of the north limb of the anticline have been stripped back, exposing flows as old as the Esquatzel Member (Fecht, 1978). Western Gable Mountain anticline plunges west and east from its culmination in the NE1/4 sec. 23, T. 13 N., R. 26 E. (Fig. 8-3). West of the NW1/4 sec. 23, T. 13 N., R. 26 E., the western Gable Mountain anticline is buried. Ault (Appendix D) used geophysical survey data, supplemented by borehole data, to interpret the location of the anticline through sec. 21 and 22 and into sec. 17, T. 13 N., R. 26 E.

Western Gable Mountain anticline plunges southeasterly from its culmination in sec. 23, T. 13 N., R. 26 E. and is buried to the east of the SE1/4 sec. 24, T. 13 N., R. 26 E. (Fig. 8-3). It continues to the east at least to the May Junction linear (Fig. 8-3). The reverse fault penetrated by DB-10 (Fig. 8-1; Myers, Price and others, 1979) is interpreted to be associated with this southeastern continuation of the western Gable Mountain structure.

Willa anticline is clearly shown by elevation data obtained from boreholes in sec. 25 and 26, T. 13 N., R. 26 E. and sec. 35 and 36, T. 13 N., R. 26 E. (Fig. 8-3). It is also indicated by SR data (line 3; Appendix B) and is associated with an east-west aeromagnetic high (Appendix B). The relatively steep dips of the TOB indicated by boreholes in sec. 25 and 26 and down-to-the-north Werner deconvolution solutions (N-227 and N-52; Appendix B) strongly imply that the Willa anticline is asymmetric, with a steep north limb.

Pearl anticline (Fig. 8-3) plunges south, but appears to die out before reaching the 200 East Area. The Pearl anticline might also plunge north and die out in sec. 29 and 20, T. 13 N., R. 26 E. Alternatively, it might connect with the previously discussed southeasternmost anticline exposed on Gable Butte. Existing SR data (line 4; Appendix B) do not resolve this question. Based on available aeromagnetic data (Appendix B), the Willa anticline, western Gable Mountain syncline, and western Gable Mountain anticline are tentatively interpreted as not continuing east beyond the May Junction linear.

Gable Mountain

Gable Mountain (Fig. 8-3) is the topographic expression of two, en echelon, northwest-trending anticlines: (1) western Gable Mountain anticline (sec. 21, 22, and 23, T. 13 N., R. 26 E.) and (2) eastern Gable Mountain anticline (sec. 19, 20, 21, and 28, T. 13 N., R. 27 E.). The western Gable Mountain anticline is a doubly plunging, tight fold with an angular hinge; the fold is asymmetric, with a steeper southeast limb. The eastern Gable Mountain anticline is similar to the western Gable Mountain anticline, except that it is asymmetric with a steeper northeast limb. The synclinal area between the two anticlines contains a very-low-amplitude anticline en echelon with the two larger folds. The extreme eastern end of Gable Mountain (sec. 27, T. 13 N., R. 27 E.; Fig. 8-3) is expressive of another northwest-trending, en echelon anticline with an open-to-tight interlimb angle and angular hinge.

Three faults have been identified on Gable Mountain (Bingham and others, 1970; Newcomb and others, 1972; Fecht, 1978). One fault near the west end of Gable Mountain (sec. 23, T. 13 N., R. 26 E.; Fig. 8-3) trends north and dips 30° to the east (Bingham and others, 1970). Stratigraphic relationships and dip of the fault plane indicate that it is a reverse fault with ∿25 m of offset. The two other faults are in the central portion of Gable Mountain along a northeast-trending escarpment (sec. 19, T. 13 N., R. 27 E.; Fig. 8-3). These faults were exposed after extensive trenching programs and have been examined most recently by Golder Associates, Inc., for Northwest Energy Services Company. Data acquired by Golder suggest that the faults are reverse faults with a maximum displacement of ∿50 m on the northernmost fault.

South Limb of the Umtanum Ridge Structure

The TOB along the southern limb of the Umtanum Ridge-Gable Mountain structure between the N-96 to N-84 linear and the May Junction linear (Fig. 8-3) is a broad, arcuate surface with an average slope of 10 to 20 m/km to the southwest. The crest of this arcuate surface projects toward the southwest between the 200 East and 200 West Areas and forms a broad culmination in the trough of the Cold Creek syncline. This culmination separates the Cold Creek Valley depression from the Wye Barricade depression (Fig. 8-3). The southern limb of the Umtanum Ridge-Gable Mountain structure is locally deformed by what are interpreted to be small, southeasterly trending, third order, parasitic folds (Fig. 8-3). Otherwise, the TOB on the south limb of the Umtanum Ridge structure appears to be relatively undeformed. Possible exceptions are indicated by Werner deconvolution solutions which have depth-to-magnetic sources near the TOB (N-235, D-214, N-232, N-231, the southeast end of D-217, and D-27; Appendix B). Several other Werner deconvolution solutions have depth-to-magnetic sources well below the TOB. These solutions possibly represent structures that are deeply buried in the basalt section, perhaps at the level of the Wanapum and Grande Ronde Basalts; these possible structures apparently have no expression in the TOB.

COLD CREEK SYNCLINE

Cold Creek Valley Depression

Two depressions lie along the trough line of the Cold Creek syncline: (1) Cold Creek Valley depression and (2) Wye Barricade depression (Fig. 8-3). The Cold Creek Valley depression is the nearly 25 km^2, triangular-shaped area that coincides approximately with the area enclosed by the 15-m elevation contour line (Fig. 8-3). Structural closure of the depression is estimated at ∿30 m.

The southwest side of the Cold Creek Valley depression is bounded by a northwest-trending structure that cuts across the generally west-to-east-trending Yakima Ridge structure. Relatively high structural

relief and a high gradient in the aeromagnetic total field (Appendix B) suggest the existence of this northwest-trending structure although it is covered by sediment. The structure was interpreted as a fault in Myers, Price and others (1979), but it may be a monocline. The strike of bedrock outcrops on the southwestern edge of the structure (sec. 7, 8, and 17, T. 12 N., R. 25 E.; Fig. 8-3) and the trend of the aeromagnetic total field contours over the structure are N25°W to N30°W. Two Werner deconvolution solutions (N-97 and N-98; Appendix B) are also associated with the structure. The location of the structure is constrained to a 1.5-km-wide zone located east of the basalt outcrops on northeastern Yakima Ridge (Fig. 8-2) (and west of SP 360 on line 8; Appendix B). The difference of ∿270 m in elevation between the TOB outcrops on northeastern Yakima Ridge and the TOB in borehole 36-96 (Fig. 8-1), located within the Cold Creek Valley depression (Fig. 8-1 and 8-3), defines the minimum slope of the TOB within the structure to nearly 200 m/km. The southern end of the northwest-trending structure intersects the axis of the Yakima Ridge structure near Rattlesnake Springs (sec. 20 and 21, T. 12 N., R. 25 E.; Fig. 8-2 and 8-3) and is assumed to be related to the steep eastward plunge of the Yakima Ridge structure into the subsurface. Although outcrops and subsurface data are sparse, it is clear that the plunge of the Yakima Ridge structure into the Pasco Basin in this area is not uniform. The elevation of the TOB in the Benson Ranch well (Fig. 8-1), in a borehole 2.5 km northeast of Rattlesnake Springs (Fig. 8-2), and at the bedrock outcrop in the SW1/4 sec. 23, T. 12 N., R. 25 E. (Fig. 8-2 and 8-3) indicate a westward plunge of the Yakima Ridge structure. The Rattlesnake Springs area appears, therefore, to be one of relatively complex bedrock structure. The structure of this area is currently under investigation.

The northwest boundary of the Cold Creek Valley depression extends northeastward from the center of sec. 5, T. 12 N., R. 25 E. into sec. 23, T. 13 N., R. 25 E. (Fig. 8-3). This boundary, which corresponds with a relatively high gradient in the aeromagnetic total field (Appendix B) and two Werner deconvolution solutions (N-96 and N-84; Appendix B), is informally referred to as the N-96 to N-84 linear (Fig. 8-3). The position of this linear coincides approximately with that of the Nancy linear (WPPSS, 1977). Borehole and geophysical data indicate that the TOB surface southeast of the N-96 to N-84 linear is relatively smooth, dips uniformly to the southwest, and gradually flattens to form the Cold Creek Valley depression. The TOB surface northwest of the N-96 to N-84 linear, however, has tentatively been interpreted to be folded into an east-southeast-plunging syncline and anticline, each ∿3 km long. Nonetheless, the following two observations indicate that the TOB structure northwest of the N-96 to N-84 linear is almost certainly more complex than that to the southeast.

1. Boreholes between eastern Umtanum Ridge and the N-96 to N-84 linear show that the TOB has an overall dip to the southeast. However, the presence of two elliptical highs in the aeromagnetic field (Appendix B) and two Werner deconvolution solutions (D-33 and D-32; Appendix B), suggest that this dip is not uniform.

2. Borehole DB-11 and the McGee well (Fig. 8-1) have anomalous hydraulic heads in the Saddle Mountains and Wanapum Basalts (Gephart and others, 1979a). These anomalous hydraulic heads, although perhaps related to stratigraphic changes known to occur in this area, might be associated with bedrock structure.

The northeastern side of the Cold Creek Valley depression has no well-defined structural boundaries similar to those on the southwestern and northwestern sides. Seismic reflection lines 3 and 5 (Appendix B) are positioned across the southern limb of the Umtanum Ridge-Gable Mountain structure in east-west and north-south directions, respectively (Appendix B). The two lines intersect at DC-4/5 (Fig. 8-1). Records from these lines and from gravity and ground magnetic surveys run south of DC-4/5 (Appendix C) have been interpreted (Appendix B) to indicate the presence of a smooth, southwest-dipping, TOB surface for the area to the east of the N-96 to N-84 linear and to the west and northwest of the 200 West Area. Two exceptions are: (1) the slight flexure intersected along line 5 (Appendix B) ∿1 km south of DC-4/5 (this flexure is judged as very small and is not shown on the TOB map) and (2) a broad, open, anticlinal flexure located along line 5 ∿1.5 km north of DC-4/5 (Werner deconvolution solution N-262 [Appendix B] is interpreted to be associated with this flexure). This latter flexure apparently continues to the southwest where it was intersected along line 3 ∿2.5 km west of DC-4/5. Other seismic anomalies and undulations in the TOB surface were interpreted to be caused by facies changes in the sediments overlying the TOB or induced by the processing of the seismic data (Appendix B). Two Werner deconvolution solutions (N-512, on the 1,680-m level, and N-85; Appendix B) have a calculated magnetic source depth of ∿600 m below sea level (Appendix B). They might correspond to a feature at the Wanapum or Grande Ronde Basalt level, but are interpreted to have no expression in the TOB.

Although the eastern and northeastern sides of the Cold Creek Valley depression have no well-defined structural boundary, TOB elevations from boreholes in the 200 West Area are inconsistent with an interpretation of a smooth, uniform dip to the southwest. Locally, steep dips and even dip reversals to the northeast are indicated (Fig. 8-3; also see borehole TOB elevations in the NE1/4 sec. 1 and SE1/2 sec. 12, T. 12 N., R. 25 E). Previous interpretations of this TOB elevation data (Tallman and others, 1979) showed a northeast-trending syncline passing through the eastern part of the 200 West Area with maximum relief in the vicinity of DC-3 (Fig. 8-1). Borehole elevation data in the 200 West Area have been reinterpreted here to show small, third-order, parasitic folds with northwest-southeast structural trends (Fig. 8-3). This interpretation is judged as being more consistent with the regional structural trend. A Werner deconvolution solution (D-218; Appendix B) coincides with a TOB dip reversal shown by boreholes in the southern part of the 200 West Area. This dip reversal is interpreted as a small anticline that projects southeasterly toward the culmination in the trough of the Cold Creek syncline. This small anticline and culmination, both of which are above the 15-m elevation contour, are used as the eastern boundary of the Cold Creek Valley depression.

Small folds similar to those interpreted to be present in the 200 West Area are also interpreted to be present in the northern part of the 200 East Area. Such folds apparently do not occur in the southern part of the 200 East Area. It is important to note that not all of these small folds in the 200 West and 200 East Areas produce a strong response on the geophysical surveys. Such small folds might likewise be undetected by drilling unless boreholes are spaced sufficiently close enough (such as in the 200 East and 200 West Areas), or unless high-resolution, gridded geophysical surveys are made. Small folds similar to those in the 200 East and 200 West Areas probably exist elsewhere on the south limb of the Umtanum Ridge-Gable Mountain structure, but have not been detected because of the wide borehole spacing. However, because the closely spaced boreholes in the southern half of the 200 East Area failed to reveal any small folds, it appears that these folds, if present elsewhere, are not evenly distributed.

The TOB in the center of the Cold Creek Valley depression is nearly flat, except perhaps for small monoclinal flexures such as those detected along line 8 (which extends east-west through the depression; Appendix B). Six boreholes are now being drilled in the RRL in the Cold Creek Valley depression (Appendix A) to evaluate the uniformity of the low dip currently interpreted for that area. The TOB elevations to date from these new boreholes are consistent with the interpretation presented in the preceding paragraphs.

Wye Barricade Depression

The Wye Barricade depression is a large, irregular-shaped area in the eastern Cold Creek syncline area. The geometry of the depression is interpreted here differently than in Myers, Price and others (1979). The depression appears to be divisible into a northern sub-depression and a southern sub-depression (Fig. 8-3). These sub-depressions are separated by a buried, asymmetric anticline that plunges eastward through sec. 20, 21, 27, 26, and 25, T. 12 N., R. 27 E. (Fig. 8-3). This buried anticlinal ridge is indicated by seismic data (line 11; Appendix B) and by recent drilling and gravity surveys by Northwest Energy Services Company. The lowest point of the northern sub-depression appears to be centered near SW1/4 sec. 16, T. 12 N., R. 27 E. (Fig. 8-3). This depression is bounded on the west by the May Junction linear. In the vicinity of this linear, TOB dip is a minimum of 40 to 60 m/km. The eastern side of the depression opens out into the westward-plunging trough of a subtle syncline. The southern sub-depression extends as far west as sec. 23, T. 12 N., R. 26 E. (Fig. 8-3), and consists of two smaller depressions: one centered near the SW1/4 sec. 23, T. 12 N., R. 26 E. and the other centered near the SE1/4 sec. 33, T. 12 N., R. 27 E. (Fig. 8-3). The western, smaller depression is bounded on the west by a feature interpreted as a short, monoclinal flexure that corresponds to two Werner deconvolution solutions (N-72 and N-243; Appendix B). A slight culmination in the trough of the Cold Creek syncline (sec. 25, T. 12 N., R. 26 E.; Fig. 8-3) separates the western, smaller depression from the eastern depression. The eastern depression is elliptical and trends northwest-southeast.

YAKIMA RIDGE STRUCTURE

Eastern Yakima Ridge

Eastern Yakima Ridge extends east-southeast from the area of the city of Yakima to the western edge of the Pasco Basin where it plunges beneath sediments (Fig. 8-2). It has been traced eastward through the Cold Creek syncline. At the eastern edge of Yakima Ridge, a northwest-trending structure (Fig. 8-3) is interpreted to separate the surface exposure of the ridge from its subsurface extension. The inferred geometry of the subsurface extension suggests that the ridge is en echelon to the main fold structure of Yakima Ridge.

Buried Extension of the Yakima Ridge Structure

The eastern portion of the Yakima Ridge structure (Fig. 8-2 and 8-3) is almost entirely buried by sediments; its surface expression is limited to a 2-km-long train of Elephant Mountain basalt. The structure extends through the subsurface from near Rattlesnake Springs (Fig. 8-3) east-southeasterly. The geometry of the anticline is not well known, but aeromagnetic, SR, and limited borehole data (Appendices A and B) suggest that the northern limb of the anticline dips more steeply than the southern limb. The SR data (lines 4, 5, and 12; Appendix B) reveal the steep edge of the northern limb. The SR data (lines 1, 9, and 14; Appendix B) also show undulations in the TOB similar to trends in the aeromagnetic total field (Appendix B). These undulations suggest that the subsurface extension of the Yakima Ridge structure might consist of en echelon folds or contain second-order folds similar to those of Gable Mountain and Gable Butte.

STRUCTURE-CONTOUR MAPS OF DEEP HORIZONS: TOP OF WANAPUM BASALT, TOP OF GRANDE RONDE BASALT, AND TOP OF UMTANUM FLOW

As previously stated, structure-contour maps on the top of the Wanapum and Grande Ronde Basalts and Umtanum flow (Fig. 8-4, 8-5, and 8-6) were generated using isopachs of the Saddle Mountains and Wanapum Basalts and the Sentinel Bluffs sequence, and using the TOB map (Fig. 8-3) as a structural datum. Hence, these structure-contour maps show a pattern very similar to the contour map of the TOB. The strike directions in the northwestern part of the Cold Creek syncline area (T. 13 N., R. 25 E.; Fig. 8-3 through 8-6) are to the northeast and the dips are southeastward toward the Cold Creek Valley depression. Although the eastward-plunging anticline and syncline near DB-11 (Fig. 8-1) are shown, the abrupt change in strike at the intersection of the N-96 to N-84 linear (Fig. 8-3) with the structure that defines the southwest boundary of the Cold Creek Valley

depression has been smoothed. The isopach of the Saddle Mountains Basalt (Chapter 3) indicates thinning to the west in the area between and south of DC-4/5 and DB-11 (Fig. 8-1). Due to this westward thinning, the deepest part of the Cold Creek Valley depression is ∿1.5 km farther to the east on Figures 8-4 through 8-6 than on Figure 8-3. The Wye Barricade depression and the east-west-trending anticline separating the Wye Barricade northern sub-depression from the Wye Barricade southern sub-depression are also shown on Figures 8-4 through 8-6, as are the locations and trends of the Gable Butte and Gable Mountain second-order folds. The trough of the Cold Creek syncline is maintained in the same position on all maps; the position of the crest of the buried extension of Yakima Ridge and the trough of the Benson Ranch syncline is also maintained.

IDENTIFICATION OF INTACT BEDROCK VOLUMES IN THE COLD CREEK SYNCLINE AREA

A key aspect of site-identification work has been the delineation of relatively intact volumes of Saddle Mountains, Wanapum, and upper Grande Ronde Basalts in the Cold Creek syncline. These relatively intact volumes of bedrock are bounded by known or inferred geologic structures, excluding intraflow structures. Locating and evaluating structures that define the boundaries of intact bedrock volumes are considered important for site identification because: (1) the spacing and orientation of structures determine the available size and effective geometry of the relatively intact layers of basalt host rock that could be used for repository construction and (2) the structures represent zones of potentially significant fracture anisotropy. These zones could connect shallow hydrologic flow systems to deeper hydrologic flow systems which include the stratigraphically controlled flowpaths above and below repository host rock layers. They might also affect repository design and construction.

Based on the results of geophysical surveys (Appendices B through E) and surface and subsurface mapping, the western Cold Creek syncline area is tentatively interpreted as consisting of five (I through V) large, relatively intact volumes of bedrock (Fig. 8-8) whose boundaries are defined by the following major or intermediate structures:

1. The hinge zone and steep limb of the Umtanum Ridge structure
2. The hinge zone and steep limb of the Yakima Ridge structure
3. The northwest-trending structure that intersects and appears to crosscut the Yakima Ridge structure
4. The hinge zone and steep limb of the Gable Butte second-order fold
5. The axial zone of the possible bedrock structure represented by the N-96 to N-84 linear

6. The axial zone of the possible bedrock structure represented by the May Junction linear

7. The axial zone represented by the possible bedrock structure which corresponds to the alignment of four Werner deconvolution solutions (D-27, D-217, D-28, and D-22; Appendix B).

The interior of the RRL lies within intact bedrock volume I (Fig. 8-8). The interior of intact bedrock volume I contains six Werner deconvolution solutions: N-85, N-512 (shown on the 1,680-m level), D-218, N-70, N-86, and N-243 (Appendix B). Because these solutions might correspond to bedrock structures, they have been used to further subdivide intact bedrock volume I into smaller volumes designated Ia through Ig (Fig. 8-8). The RRL is almost entirely within Ia, Ib, and Id. The Cold Creek Valley depression is almost entirely within Ia and Ib. Werner deconvolution solution N-85 is of questionable significance; nonetheless, it has been honored and has been used to form the boundary between Ia and Ib. The boundary between Ia and Id is formed by Werner deconvolution solution D-218. Overall, the central and eastern parts of the Cold Creek Valley depression appear to be free of potentially adverse bedrock structures relative to other parts of the Cold Creek syncline area and the Hanford Site. The structure of the TOB and deeper horizons within this area is interpreted as being nearly flat lying with very gentle dips toward the trough of the Cold Creek syncline, and with a slight westward component of dip toward the deepest point of the Cold Creek Valley depression. Additional drilling and geophysical work will be designed to detect and characterize subtle structures within this depression.

SUMMARY AND CONCLUSIONS

Locating and evaluating bedrock structure within the Cold Creek syncline is necessary because: (1) spacing and orientation of such structures determine the size and geometry of the relatively intact volumes of basalt host rock within which a repository could be constructed and (2) bedrock structures represent zones of vertically oriented fractures that might affect shallow and deep groundwater flow systems. Emphasis is given to the bedrock structures within the upper 1,200 m of the bedrock section. These structures might modify the isolation potential of the Umtanum flow within the RRL.

The description of the structural geologic setting of the Cold Creek syncline has been produced through the integration of results from four, separate, but related field investigations: (1) surface geologic mapping of bedrock, (2) borehole geologic studies, (3) structural analysis of Yakima folds, and (4) geophysical surveys. The current interpretations of bedrock geology of the syncline are represented by: (1) bedrock geologic maps; (2) structure-contour maps for the TOB, top of Wanapum

Basalt, top of Grande Ronde Basalt, and top of Umtanum flow; (3) cross sections; and (4) an interpretive map which delineates relatively intact bedrock volumes bounded by known or inferred structures.

Interpretations of the geometry of the Umtanum flow and the locations of bedrock structures relative to candidate repository sites are based largely on extrapolations to depth using the TOB as a datum. The interpretations presented are based on the premise that the major bedrock structures that deform the Grande Ronde Basalt flows in the Pasco Basin do have some expression in the uppermost flows of the Saddle Mountains Basalt. This premise appears justifiable based on the current understanding of the structural history of the Pasco Basin. A deliberate effort was made to have the patterns of contours on the TOB closely reflect the structural fabric and structural style that have been revealed by surface mapping of bedrock exposures within and around the margins of the Pasco Basin.

Because the TOB map was used as a structural datum, structure-contour maps of the top of Wanapum Basalt, top of Grande Ronde Basalt, and top of Umtanum flow show a pattern very similar to the TOB map. However, a number of structures included on the TOB map are not honored on the structure-contour maps of the deeper horizons because of the uncertainty of their presence or location at depth. Instead, such structures are shown using symbols to call attention to their possible presence.

The structure of the Cold Creek syncline area is characterized by: (1) areas of nearly flat-lying basalt; (2) two east-southeast-plunging, first-order anticlines (Umtanum Ridge and Yakima Ridge); (3) two southeast-plunging, second-order anticlines (Gable Butte and Gable Mountain); (4) third-order folds in the hinge zones of the second-order folds and on the limbs of the first-order folds; and (5) northwest- and possibly northeast-trending cross structures whose exact nature is unknown. The dominant structural trend in the Cold Creek syncline is east-west to northwest-southeast. Structural relief is $\sim$300 m in the western part of the Cold Creek syncline area, but decreases to the east.

The Cold Creek syncline is an asymmetric, open, broad, and relatively flat-bottomed fold. The steeper limb is the south limb. The syncline lies between the buried Yakima Ridge structure and the Umtanum Ridge-Gable Mountain structure. Two depressions lie along the trough line of the Cold Creek syncline: (1) Cold Creek Valley depression and (2) Wye Barricade depression. The TOB in the center of the Cold Creek Valley depression is nearly flat, except, perhaps, for small, monoclinal flexures. The Wye Barricade depression is a large, irregular-shaped area. The depression appears to be divided into northern and southern sub-depressions separated by a buried, asymmetric anticline. The Cold Creek syncline plunges and dies out to the east in the vicinity of the Wye Barricade depression.

A key aspect of site-identification work has been the delineation of relatively intact volumes of Saddle Mountains, Wanapum, and upper Grande Ronde Basalts in the Cold Creek syncline area. These relatively intact volumes of bedrock are bounded by known or inferred geologic structures, excluding intraflow structures. Based on the results of geophysical

surveys and surface and subsurface mapping, the western Cold Creek syncline area is tentatively interpreted to consist of five, large, relatively intact volumes of bedrock whose boundaries are defined by major or intermediate structures. The interior of the RRL lies within one of these large, intact bedrock volumes.

Overall, the central and eastern parts of the Cold Creek Valley depression, which includes the RRL, appear to be free of potentially adverse bedrock structures relative to other parts of the Cold Creek syncline area and Hanford Site. The structure of the TOB and the structure at deeper horizons within this area are interpreted as being nearly flat lying with very gentle dips toward the trough of the Cold Creek syncline, and with a slight westward component of dip toward the deepest point of the Cold Creek Valley depression. Additional drilling and geophysical work will be designed to delineate subtle structures within this depression.

APPENDIX A - SUMMARY OF BOREHOLE LOCATIONS AND GEOLOGIC ACTIVITIES AT BOREHOLE SITES

D. J. Moak

INTRODUCTION

This appendix describes the borehole coverage across the Hanford Site and Pasco Basin area, and the types of geologic data-gathering activities performed at Basalt Waste Isolation Project (BWIP) borehole sites. The BWIP borehole-drilling program supports various studies in geology, geophysics, hydrology, and rock mechanics, and is an essential data-gathering task. The BWIP borehole studies through 1978 are also described in Myers, Price and others (1979).

DESCRIPTION OF BOREHOLES

Locations of key boreholes used in BWIP studies are shown in Figure A-1. Stratigraphic levels penetrated by all boreholes on the Hanford Site are shown in Figure A-2.

Cable tool and rotary boreholes have been drilled into the shallow sediments at ~2,000 locations. About 300 of these boreholes reach or penetrate the top of basalt. Most of these boreholes were drilled for detailed groundwater monitoring and characterization of small areas within the Hanford Site and Cold Creek syncline area, primarily in the 200 East and 200 West Areas.

Cable tool and rotary water-supply wells have been drilled at nearly 100 locations outside of the Cold Creek syncline area for domestic, agricultural, and industrial water supply. About 20 of these wells penetrate the top of basalt.

The deep rotary boreholes drilled in the Pasco Basin can be subdivided into three groups: (1) 27 boreholes drilled in the 1920s and 1930s to develop the Rattlesnake Hills gas field (Hammer, 1934); (2) Rattlesnake Hills Well Number 1 (RSH-1), a petroleum exploration borehole (Raymond and Tillson, 1968); and (3) four rotary holes drilled by the BWIP and its predecessors for hydrologic testing within the basalt beneath the Hanford Site. Thus, six, deep, rotary boreholes have been drilled in and near the Cold Creek syncline: WW-6, RSH-1, DC-1, DC-3, DC-5, and DC-7 (Fig. A-2). The first borehole, WW-6, was drilled to 803 ft (245 m) in 1926 and deepened to 3,660 ft (1,115 m) in 1933. The only information currently available from WW-6 is a driller's log. This log plus geologic cross sections and interpretations indicate that this

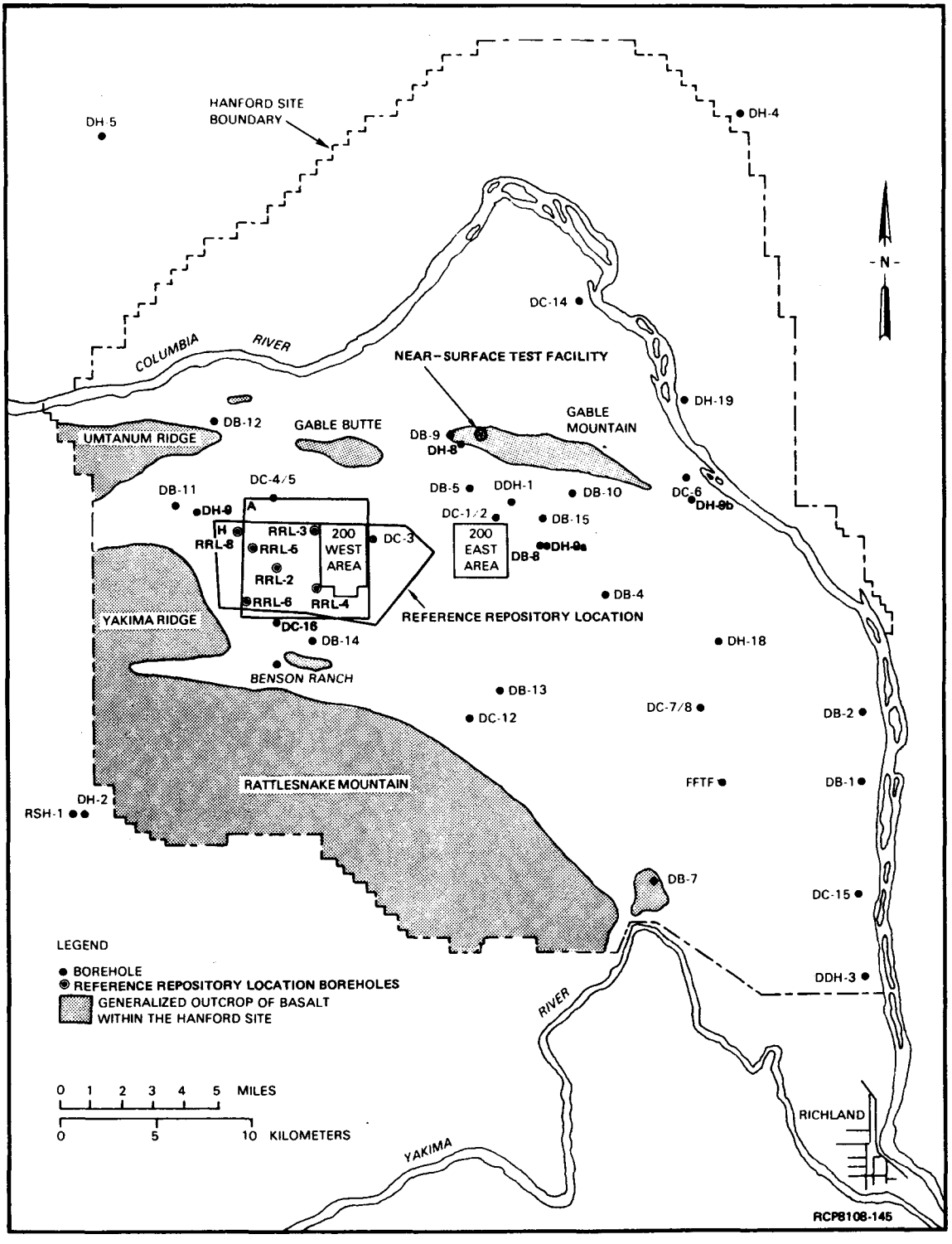

FIGURE A-1. Location Map, Key Boreholes Used in Basalt Waste Isolation Project Studies. Boreholes DC-1/2, DC-2/4, and DC-7/8 are core hole/rotary hole pairs.

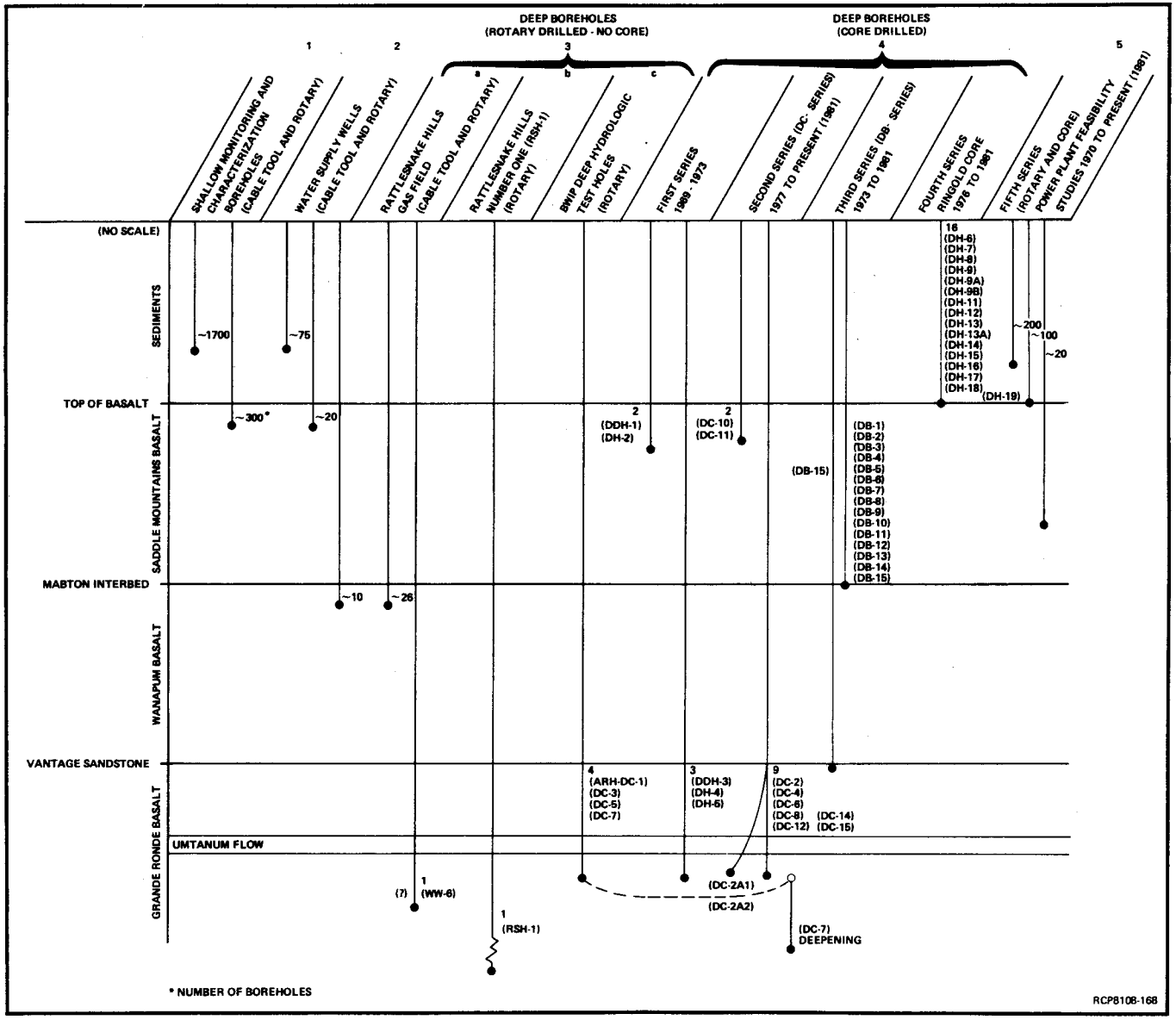

FIGURE A-2. Stratigraphic Levels Penetrated by Boreholes on the Hanford Site and Vicinity. Location of boreholes in parentheses are shown on Figure A-1, except DH-11 through DH-17. DC-2A1 and DC-2A2 are slant holes from DC-2.

borehole probably penetrated the Grande Ronde Basalt and probably the Umtanum flow. Borehole RSH-1 was drilled to 10,665 ft (3,250 m) from 1956 to 1957 and was reentered in 1977 for geophysical logging and testing (Gephart and others, 1979b). Borehole DC-1 was the first deep borehole drilled on the Hanford Site to obtain geologic and hydrologic data which could be used in evaluating the suitability of the basalt for underground storage of radioactive waste. Borehole DC-3 was drilled in 1977 into the Umtanum as part of the hydrologic testing program. Boreholes DC-5 and DC-7 were then drilled as companion holes to DC-4 and DC-8, respectively, for cross-hole hydrologic testing.

Five series of core holes have been drilled by the BWIP and its predecessors. The first series was five holes drilled by the Atlantic Richfield Hanford Company (ARHCO) during the initial basalt feasibility studies from 1969 to 1973. Two were relatively shallow boreholes, DDH-1 (1,165 ft [355 m]) and DH-2 (600 ft [185 m]), and were drilled to define the upper stratigraphy of nearby, deep, rotary holes (ARH-DC-1 and RSH-1, respectively). The other three (DDH-3, DH-4, and DH-5) are >3,000 ft (915 m) deep and were drilled to examine the stratigraphy of the upper Grande Ronde Basalt. Many fundamental stratigraphic relationships were recognized from the initial petrographic and geochemical analyses on samples from these three core holes (ARHCO, 1976; Myers, 1973, Myers and Brown, 1973).

The second series of core holes began in 1977. The first core hole (DC-2) was drilled to 3,300 ft (1,005 m). It was sited near an existing, deep, rotary hole (ARH-DC-1) to allow cross-hole testing and to verify the interpretation of the stratigraphic section penetrated by ARH-DC-1. During 1978, two slant holes (DC-2A1 and DC-2A2) were drilled from DC-2 and cored through the Umtanum unit at an angle of $\sim 25^{\circ}$ from vertical. Next were several deep core holes (DC-4, DC-6, DC-8, DC-12, DC-14, and DC-15) drilled for stratigraphic information and hydrologic testing, and two shallow exploratory holes (DC-10 and DC-11) drilled on Gable Mountain for siting the Near-Surface Test Facility (NSTF). In addition, rotary hole DC-7 was reentered and cored to a depth of 5,008 ft (1,526 m).

Figure A-3 is a stratigraphic summary sheet of the core and rotary holes (including paired holes) that penetrate into the Grande Ronde Basalt within the Pasco Basin area. Locations and information available from the most recent of these core holes (DC-7, DC-12, DC-14 and DC-15) are given in Table A-1.

The third series of core holes is the DB- series (Fig. A-4). These holes average about 1,000 ft (305 m) deep and were drilled through the Saddle Mountains Basalt and into or through the Mabton interbed principally for stratigraphic and groundwater-monitoring studies not part of the BWIP studies. However, DB-15 (Fig. A-3) was cored into the Grande Ronde Basalt as part of the BWIP studies.

The fourth series consists of the 16 core holes drilled to sample and correlate the Ringold Formation. These core holes are in the DH- series. The DH- holes in the 200 West and 200 East Areas are not located on Figure A-1.

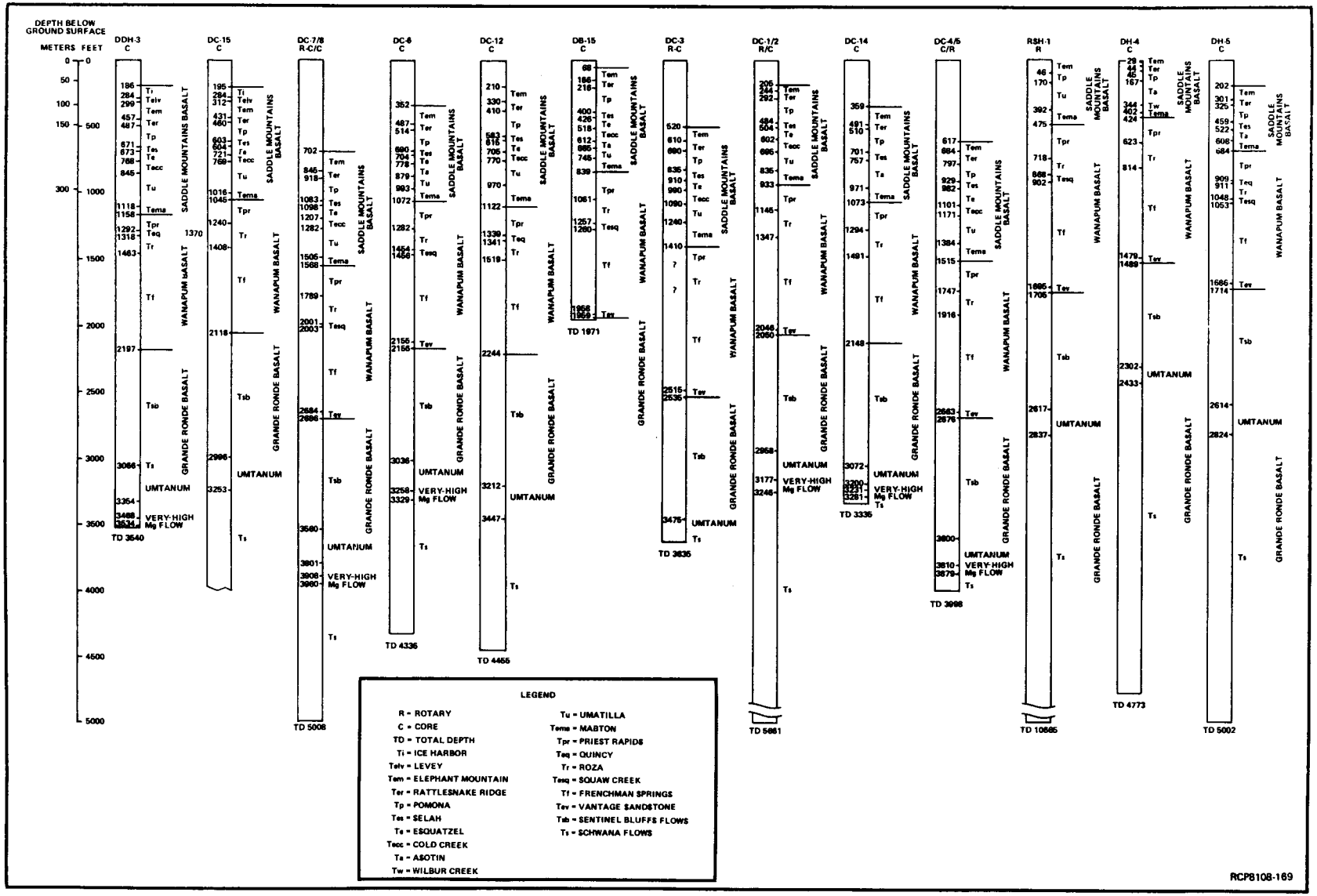

FIGURE A-3. Stratigraphic Summary Sheet for Core and Rotary Holes that Penetrate into Grande Ronde Basalt.

TABLE A-1. Geologic Data Summary of Core Holes DC-7, DC-12, DC-14, and DC-15.

Borehole designation	Type	Drilled depth	Location	Available information
DC-7	Rotary and core	5,008 ft (1,526 m)	PN 14910, W 14839 LN 420174, E 2280448 Lat 46°28'49" Long 119°23'12"	Hole history (Fenix & Scisson, 1977) Core and cutting samples (BWIP sample repository) Geophysical and lithological logs (BWIP library) Hydrological test results (Gephart and others, 1979b) Geomechanical and paleomagnetic results (BWIP library)
DC-12	Core	4,455 ft (1,358 m)	PN 10125, W 53687 LN 415290, E 2241612 Lat 46°27'40" Long 119°32'35"	Hole history (information not complete) Core and core pictures (BWIP sample repository) Hydrologic tests (information not complete) Geophysical, lithological, and geomechanical logs (BWIP library)
DC-14	Core	3,335 ft (1,017 m)	PN 84489, W 33860 LN 489704, E 2361248 Lat 46°40'20" Long 119°27'28"	Hole history (information not complete) Core and core pictures (BWIP sample repository) Hydrologic test (information not complete) Geophysical, lithological, and geomechanical logs (BWIP library)
DC-15	Core	Not completed; projected completion is 4,200 ft (1,280 m)	PS 15134, E 14990 LN 389809, E 2309775 Lat 46°21'30" Long 119°16'28"	Hole history (information not complete) Core and core pictures (BWIP sample repository) Hydrologic tests (information not complete) Geophysical, lithological, and geomechanical logs (BWIP library)

LN and E are Lambert North and East Coordinates.
PN, S, E, and W are Hanford Coordinates Plant North, South, East, and West.
This table represents a continuation of Table A-5 in Myers, Price and others (1979).

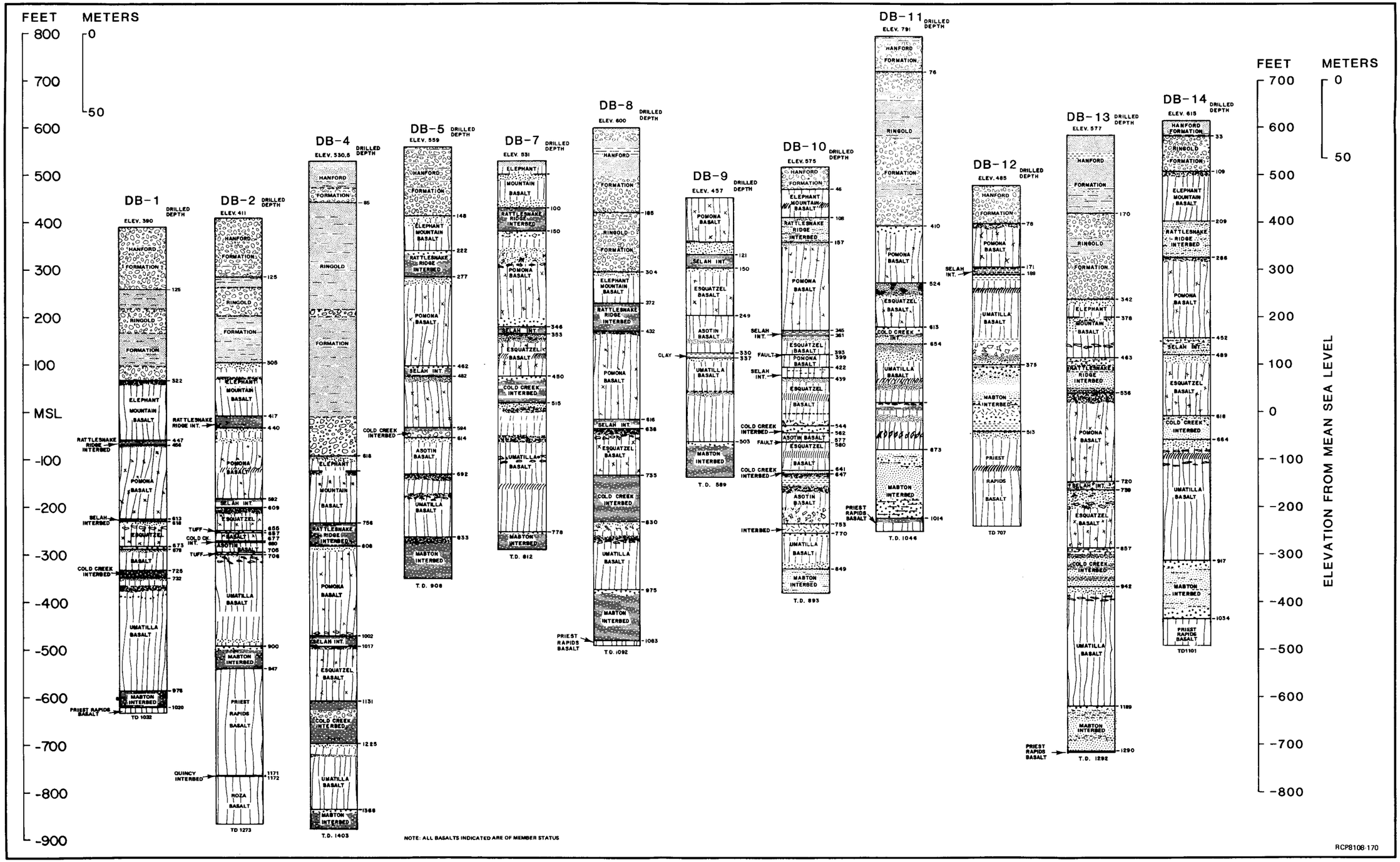

FIGURE A-4. Stratigraphic Summary Sheet for DB-Series Core Holes.

The fifth series of boreholes are non-BWIP boreholes (Fig. A-2). They consist of core and rotary holes used in feasibility studies for siting of nuclear power plants on the Hanford Site and associated foundation studies. This includes boreholes drilled in the early 1970s for the Washington Public Power Supply System, Inc. and over 175 boreholes recently drilled by Northwest Energy Services Company for siting two additional nuclear plants.

Table A-2 is a summary chart of the drilled depth, elevation, and drilled thicknesses for the principal stratigraphic units penetrated by the DB- and DC-series boreholes, and several other deep boreholes related to the BWIP.

Currently, the BWIP is drilling six boreholes in the reference repository location (RRL) to determine details of the shallow bedrock structure and stratigraphy of the Saddle Mountains Basalt. Additional, planned drilling in the RRL includes several core holes to be drilled through the Ringold Formation for stratigraphic correlation to evaluate the tectonic stability of the RRL. Coring has also begun on a deep core hole, DC-16 (Fig. A-1). This hole is to penetrate the Umtanum flow and will provide stratigraphic, structural, and rock-property data on the south side of the RRL. Existing boreholes near the Cold Creek syncline area that might provide key stratigraphic and structural detail, such as WW-6 and Benson Ranch, are to be reentered, cleaned out, and geophysically logged.

GEOLOGIC ACTIVITIES AT BOREHOLE SITES

Figure A-5 is a flow diagram for geotechnical activities performed at borehole sites. These activities provide the initial characterization of the core or drill cuttings.

ROTARY AND CABLE TOOL BOREHOLE SITES

Cable tool boreholes are generally used as entrance holes for the deep core holes and large-diameter, rotary boreholes used for hydrologic testing. Geologic activities during cable tool and rotary drilling are limited to preparing lithologic logs from the drill cuttings sampled at 5-ft (1.5-m) intervals and at changes in lithology, and correlating the lithologic log with drilling breaks and geophysical logs (when run). Cuttings are sampled for chemical and textural analysis as needed.

BASALT CORE HOLE SITES

Core drilling is the primary means used by the BWIP for collecting subsurface geologic data. Core holes have been drilled up to 5,008 ft (1,526 m) by standard methods, with an overall core recovery in excess

TABLE A-2. Stratigraphic Summary Table, Key Boreholes in the Hanford Site and Vicinity. (Sheet 1 of 4)

Well Number	DDH-3	DC-15	DB-1	DB-2	DB-7	FFTF[b]	DC-7	DC-8	DB-4
Ground Surface Elevation	400	402	390	411	531	547		545	533
SADDLE MOUNTAINS FORMATION	186/214[a] 972	195/207 850	322/68 698	305/106 642	0/531	612/-65 854		702/-157 866	618/-85
Ice Harbor Member	186/214 98	195/207 89	NP	NP	NP	NP		NP	NP
Levey Interbed	284/116 15	284/118 28	NP	NP	NP	NP		NP	NP
Elephant Mountain Member	299/101 158	312/90 119	322/68 125	305/106 112	0/531 100	612/-65 110		702/-157 143	618/-85 138
Rattlesnake Ridge Interbed	457/-57 30	431/-29 29	447/-57 9	417/-6 23	100/431 50	722/-175 96		845/-300 73	756/-223 52
Pomona Member	487/-87 184	460/-58 143	456/-66 157	440/-29 152	150/381 196	818/-271 112		918/-373 165	808/-275 194
Selah Interbed	671/-271 2	603/-201 1	613/-223 5	592/-181 16	346/185 7	930/-383 28		1083/-538 15	1002/-469 15
Esquatzel Member	673/-273 95	604/-202 117	618/-228 47	608/-197 47	353/178 97	958/-411 112	SAME AS DC-8	1098/-553 109	1017/-484 114
Interbed (Unnamed)	NP	NP	673/-283 55	655/-244 2	NP	NP		NP	NP
Esquatzel 2 Member	NP	NP	678/-288 47	657/-246 20	NP	NP		NP	NP
Cold Creek Interbed	768/-368 77	721/-319 48	725/-355 7	677/-266 3	450/81 65	1070/-523 90		1207/-662 75	1131/-598 94
Asotin Member (Huntzinger Flow)	NP	NP	NP	680/-269 24	NP	NP		NP	NP
Interbed (Unnamed)	NP	NP	NP	705/-294 1	NP	NP		NP	NP
Wilbur Creek Member (Wahluke Flow)	NP	NP	NP	NP	NP	NP		NP	NP
Umatilla Member	845/-445 273	769/-367 247	732/-342 244	706/-295 194	515/16 263	1160/-613 195		1282/-737 223	1225/-692 141
Mabton Interbed	1118/-718 40	1016/-614 29	976/-586 44	900/-489 47	778/-247	1355/-808 111		1505/-960 63	1366/-831
WANAPUM FORMATION	1158/-758 1040	1045/-643 1014	1020/-630	947/-536		1466/-919		1568/-1023 1118	
Priest Rapids Member	1158/-758 134	1045/-643 195	1020/-630	947/-536 224		1466/-919 169		1568/-1023 221	
Quincy Interbed	1292/-892 26	NP		1171/-760 1		1635/-1088 18		NP	
Roza Member	1318/-918 145	1240/-848 168		1172/-761		1653/-1106 178		1789/-1244 212	
Squaw Creek Interbed	NP	NP				NP		2001/-1456 2	
Frenchman Springs Member	1463/-1063 735	1408/-1006 710				1831/-1284		2003/-1458 681	
Vantage Interbed	NP	NP						2684/-2139 2	
GRANDE RONDE FORMATION	2197/-1797	2118/-1716						2686/-2141	
Sentinel Bluffs Sequence	2197/-1797 868	2118/-1716 878						2686/-2141 874	
Through Runner	2596/-2196 164	2505/-2103 154						2966/-2421 259	
McCoy Canyon Flow	2984/-2584 82	2878/-2476 118						3421/-2876 139	
Schwana Sequence	3066/-2666	2996/-2594						3560/-3015	
Low-Mg Flows Above Umtanum	NP	NP						NP	
Umtanum Flow	3066/-2666 288	2996/-2594 257						3560/-3015 241	
Very-High-Mg Flow	3468/-3068 66	3334/-2932 115						3908/-3363 52	
Low-MgO Flow		3449/-3047					3329/-2927	3960/-3415	
Total Depth	3540	4343	1032	1273	812	1964	5008	4100	1403
Bottom of Hole Elevation	-3140	-3941	-642	-862	-281	-1417	-4606	-3555	-870

TABLE A-2. Stratigraphic Summary Table, Key Boreholes in the Hanford Site and Vicinity. (Sheet 2 of 4)

Well Number	DC-6	DC-12	DB-13	DB-8	DB-15	DB-10	BENSON RANCH[b]	DB-14	DC-3
Ground Surface Elevation	402	516	577	600	470	515	615	615	732
SADDLE MOUNTAINS FORMATION	352/50 720	210/306 912	342/235 948	304/296 779	68/402 771	46/469	345/270 965	109/506 925	520/212 890
Ice Harbor Member	NP	NP	NP	NP	NP	NP	NP	NP	NP
Levey Interbed	NP	NP	NP	NP	NP	NP	NP	NP	NP
Elephant Mountain Member	352/50 135	210/306 120	342/235 121	304/296 68	68/402 98	46/469 62	345/270 113	109/506 100	520/212 90
Rattlesnake Ridge Interbed	487/-85 27	330/186 80	463/114 73	372/228 60	166/304 50	108/407 49	458/157 89	209/406 77	610/122 80
Pomona Member	514/-112 176	410/106 173	536/41 184	432/168 184	216/254 184	157/358 188	547/68 168	286/329 166	690/42 145
Selah Interbed	690/-288 14	583/-67 32	720/-143 19	616/-16 22	400/70 26	345/170 16	715/-100 30	452/163 37	835/-103 75
Esquatzel Member	704/-302 74	615/-99 90	739/-162 118	638/-38 97	426/44 92	361/154 35	745/-130 110	489/126 129	910/-178 80
Interbed (Unnamed)	NP	NP	NP	NP	NP	FAULT	NP	NP	NP
Esquatzel 2 Member	NP	NP	NP	NP	NP	NP	NP	NP	NP
Cold Creek Interbed	NP	705/-189 65	857/-280 85	735/-135 95	518/-46 94	544/-29 18	855/-240 69	618/-3 46	990/-258 100
Asotin Member (Huntzinger Flow)	778/-376 101	NP	NP	NP	612/-142 53	562/-47 15	NP	NP	NP
Interbed (Unnamed)	NP	NP	NP	NP	NP	FAULT	NP	NP	NP
Wilbur Creek Member (Wahluke Flow)	NP	NP	NP	NP	NP	NP	NP	NP	NP
Umatilla Member	879/-477 114	770/-254 200	942/-365 247	830/-230 145	665/-195 80	770/-225 79	924/-309 277	664/-49 253	1090/-358 150
Mabton Interbed	993/-591 79	970/-454 152	1189/-612 99	975/-375 108	745/-275 94	849/-334	1201/-586 109	917/-302 117	1240/-508 170
WANAPUM FORMATION	1072/-670 1084	1122/-606 1122	1290/-711	1083/-483	839/-359		1310/-695	1034/-419	1410/-678 1125
Priest Rapids Member	1072/-670 210	1122/-606 217	1290/-711	1083/-483	839/-369 222			1034/-419	
Quincy Interbed	NP	1339/-823 2			NP				
Roza Member	1282/-880 172	1341/-825 178			1061/-591 196				
Squaw Creek Interbed	1454/-1052 2	NP			1257/-787 3				
Frenchman Springs Member	1456/-1054 699	1519/-1003 703			1260/-790 697				
Vantage Interbed	2155/-1753 1	2244/-1728 <1			1958/-1488 1				2515/-1783 20
GRANDE RONDE FORMATION	2156/-1754	2244/-1728			1959/-1489				2535/-1803
Sentinel Bluffs Sequence	2156/-1754 880	2244/-1728 968							2535/-1803 940
Through Runner	2458/-2056 237	2605/-2089 223							2850/-2118 265
McCoy Canyon Flow	2903/-2501 133	3091/-2575 121							3365/-2633 110
Schwana Sequence	3036/-2634	3212/-2696							3475/-2743
Low-Mg Flows Above Umtanum	NP	NP							NP
Umtanum Flow	3036/-2634 222	3212/-2696 235							3475/-2743
Very-High-Mg Flow	3258/-2856 71	NP							
Low-MgO Flow	3329/-2927	3475/-2959							
Total Depth	4336	4455	1292	1092	1971	893	2000	1101	3635
Bottom of Hole Elevation	-3934	-3939	-713	-492	-1501	-378	-1385	-586	-2903

TABLE A-2. Stratigraphic Summary Table, Key Boreholes in the Hanford Site and Vicinity. (Sheet 3 of 4)

Well Number	DC-1	DC-2	DB-5	DB-9	DC-10	DC-11	DC-14	DC-4	DC-5
Ground Surface Elevation	572	572	559	457	-63° 438	764	394	745	745
SADDLE MOUNTAINS FORMATION		205/367 728	148/411	0/457	24/410	0/764	359/35 714	617/128 898	
Ice Harbor Member		NP	NP	NP	NP	NP	NP	NP	
Levey Interbed		NP	NP	NP	NP	NP	NP	NP	
Elephant Mountain Member		205/367 39	148/411 74	NP	24/410 32	0/764 76	359/35 132	617/128 67	
Rattlesnake Ridge Interbed		244/328 48	222/337 56	NP	56/387 69	76/688 20	491/-97 19	684/61 113	
Pomona Member		292/280 192	278/281 184	0/457 122	125/330 172	96/668 182	510/-116 191	797/-52 132	
Selah Interbed	SAME AS DC-2	484/88 20	462/97 20	122/335 28	297/168 49	278/486 28	701/-307 56	929/-184 53	
Esquatzel Member		504/68 98	482/77 112	150/307 99	346/130 84	306/458 56	NP	982/-237 119	
Interbed (Unnamed)		NP	NP	NP	NP	NP	NP	NP	
Esquatzel 2 Member		NP	NP	NP	NP	NP	NP	NP	
Cold Creek Interbed		602/-30 93	594/-35 20	NP	NP	NP	NP	1101/-356 70	
Asotin Member (Huntzinger Flow)		NP	614/-55 77	249/208 81	430/48	362/402	757/-363 214	NP	SAME AS DC-4
Interbed (Unnamed)		NP	NP	330/131 8			NP	NP	
Wilbur Creek Member (Wahluke Flow)		NP	NP	NP			NP	NP	
Umatilla Member		695/-123 140	691/-132 141	338/119 165			NP	1171/-426 213	
Mabton Interbed		835/-263 98	832/-273	503/-46			971/-577 102	1384/-639 131	
WANAPUM FORMATION		933/-361 1117					1073/-679 1075	1515/-770 1161	
Priest Rapids Member		933/-361 212					1073/-679 221	1515/-770 232	
Quincy Interbed		NP					NP	NP	
Roza Member		1145/-573 202					1294/-900 197	1747/-1002 169	
Squaw Creek Interbed		NP					NP	NP	
Frenchman Springs Member		1347/-775 699					1491/-1097 657	1916/-1171 747	
Vantage Interbed		2046/-1474 4					2148/-1754 <1'	2663/-1918 13	
GRANDE RONDE FORMATION		2050/-1478					2148/-1754	2676/-1931	
Sentinel Bluffs Sequence		2050/-1478 908					2148/-1754 924	2676/-1931 924	
Through Runner		2349/-1777 277					2427/-2033 259	2968/-2223 256	
McCoy Canyon Flow		2862/-2290 96					2898/-2504 174	3458/-2713 142	
Schwana Sequence		2958/-2386					3072/-2678	3600/-2865	
Low-Mg Flows Above Umtanum		NP					NP	NP	
Umtanum Flow		2958/-2386 219					3072/-2678 128	3600/-2865 210	
Very-High-Mg Flow		3177/-2605 69					3231/-2837 50	3810/-3055 69	
Low-MgO Flow	3246/-2674	3246/-2674					3281/-2887 28	3879/-3134	3879/-3134
Total Depth	5661	3300	908	589	456	385	3335	3998	3990
Bottom of Hole Elevation	-5089	-2728	-349	-132	35	379	-2941	-3253	-3245

TABLE A-2. Stratigraphic Summary Table, Key Boreholes in the Hanford Site and Vicinity. (Sheet 4 of 4)

Well Number	DB-11	DB-12	BH-16	WW-6[b]	RSH-1	DH-4	DH-5
Ground Surface Elevation	791	485	460	1420	2880	920	932
SADDLE MOUNTAINS FORMATION	410/381 604	78/407 435	525/-65		0/2880 475	29/891 395	202/730 482
Ice Harbor Member	NP	NP	NP		NP	NP	NP
Levey Interbed	NP	NP	NP		NP	NP	NP
Elephant Mountain Member	NP	NP	525/-65 116		0/2880 46	29/891 15	202/730 99
Rattlesnake Ridge Interbed	NP	NP	641/-181 55		NP	44/876 1	301/631 24
Pomona Member	410/381 114	78/407 93	696/-236 174		46/2834 124	45/875 122	325/607 134
Selah Interbed	NP	171/314 18	870/-410 51		NP	NP	459/473 63
Esquatzel Member	524/267 89	NP	921/-461 46	404/1016 30	NP	NP	NP
Interbed (Unnamed)	NP	NP	NP	NP	NP	NP	NP
Esquatzel 2 Member	NP	NP	NP	NP	NP	NP	NP
Cold Creek Interbed	613/178 41	NP	967/-507 1	434/986 3	NP	NP	NP
Asotin Member (Huntzinger Flow)	NP	NP	968/-508 33	NP	NP	167/753 177	522/410 86
Interbed (Unnamed)	NP	NP		NP	NP	NP	NP
Wilbur Creek Member (Wahluke Flow)	NP	NP		NP	NP	344/576 58	NP
Umatilla Member	654/137 219	189/296 186		437/983 268	170/2710 220	NP	NP
Mabton Interbed	873/-82 141	375/110 138		702/718 73	392/2488 83	402/518 22	608/324 76
WANAPUM FORMATION	1014/-223	513/-28		775/645	475/2405 1230	424/496 1065	684/248 1030
Priest Rapids Member	1014/-223	513/-28		775/645 254	475/2405 243	424/496 199	684/248 225
Quincy Interbed				NP	NP	NP	909/23 2
Roza Member				1029/391 154	718/2162 150	623/297 191	911/21 137
Squaw Creek Interbed					868/2012 34	NP	1048/-116 5
Frenchman Springs Member				1183/	902/1978 793	814/106 665	1053/-121 633
Vantage Interbed					1695/1185 10	1479/-559 10	1686/-754 28
GRANDE RONDE FORMATION					1705/1175	1489/-569	1714/-782
Sentinel Bluffs Sequence					1705/1175 912	1489/-569 729	1714/-782 900
Through Runner						1670/-750 258	2012/-1080 234
McCoy Canyon Flow						2106/-1186 112	2432/-1499 182
Schwana Sequence					2617/263	2218/-1298	2614/-1682
Low-Mg Flows Above Umtanum					NP	2218/-1298 84	NP
Umtanum Flow					2617/263 220	2302/-1382 131	2614/-1682 210
Very-High-Mg Flow					NP	NP	NP
Low-MgO Flow					2925/-45	2433/-1513	2824/-1892
Total Depth	1046	707	1001	3660	10665	4773	5002
Bottom of Hole Elevation	-255	-222	-543	-2240	-7785	-3853	-4070

NOTE: All measurements in feet; NP = Not Present

[a]Example: $\frac{205/367}{728}$ = $\frac{\text{Drilled Depth/Elevation}}{\text{Flow Thickness}}$

[b]Unconfirmed values.

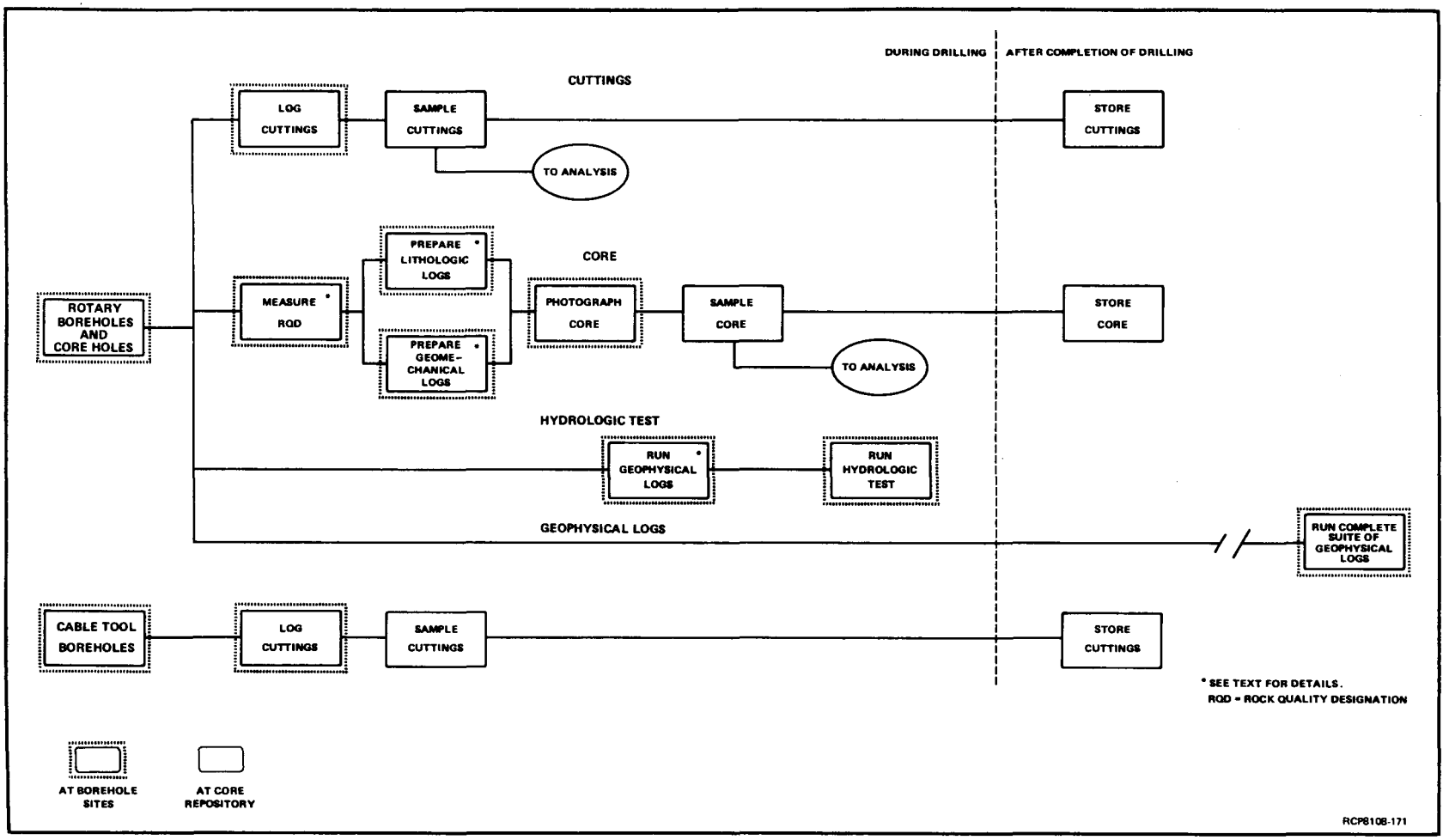

FIGURE A-5. Flow Diagram for Geotechnical Activities at Borehole Sites.

of 95%. Recovery of core in a nearly undisturbed condition was accomplished in 1981 by introduction of triple-tube core barrels in BWIP coring operations. Use of the conventional core barrel often caused disturbance of the core and prevented accurate interpretations of in situ fractures and rock mass quality.

The rock-quality designation (Deere, 1963) of the recovered core is measured immediately upon retrieval of each core run. This provides a fundamental measure of the competency of the rock mass and is a basic parameter used in other rock-mass classifications. The core lithology is then logged. The lithologic log includes a description of the structure, texture, mineralogy, and alteration of the core. This information is entered on standard forms to facilitate documentation and comparison. Other information recorded on the log includes zones of lost fluid circulation, location of artesian aquifers, percentage of core recovered, and drilling penetration rate.

Geomechanical logs are made through selected stratigraphic intervals. Discrete fractures and joints are measured and described following a standard procedure and the information is entered on a computer code sheet. Over 16,000 ft (4,877 m) of core fractures have been described and logged. The bulk of the geomechanical data collected to date is from the Grande Ronde Basalt. Fracture strike, dip, width, filling, appearance, and mineralogy were recorded. Fracture strike is measured relative to an arbitrary "north" line marked on the core using the natural remanent magnetic direction measured with a field fluxgate magnetometer. This method gives an internally consistent "north" direction for some flows; however, for other flows, it does not (Packer and Petty, 1979). The method is under evaluation. Analysis of data from the geomechanical logs has not been completed; complete analysis should provide a basis for computation of fracture frequencies, average fracture apertures, and possibly joint sets similar to that done for the NSTF (Moak and Wintczak, 1980).

Most of the core is photographed at the borehole site immediately after recovery from the hole. All core is boxed and photographed in color to record the original properties of the core before sampling or storage.

The BWIP boreholes are geophysically logged on an as-needed basis with a small, logging unit operated by Pacific Northwest Laboratory. These logs are used to assist in the selection of intervals for hydrologic testing. Only after casing and completion of several deep boreholes is it deemed economically feasible to run a complete log suite using an oil-field-type service firm. Variations in equipment, methods, and recording format used by the several logging firms that have worked at the Hanford Site have decreased the usefulness of the logs. The most useful logs for geological and geophysical purposes are the density, natural gamma, porosity, acoustic, and borehole gravimeter (obtained using a special-purpose tool). Dipmeter surveys have not proven useful due to the noise created by readings from the abundant cooling fractures in basalt flows and because most boreholes have been drilled in areas where structural dip is $<5^{0}$. A great susceptibility for error in dipmeter measurements occurs at such shallow dips (Fitzgerald and others, 1980).

Hydrologic testing includes hydraulic head measurements, groundwater chemical analyses, and other hydrologic property determinations. Hydrologic testing and groundwater sampling from interflow zones and interbeds are performed immediately after they are drilled to minimize the possibility of groundwater cross-flow contamination within the borehole. Testing of flow interiors occurs both during drilling and following completion of the borehole. Further information on the hydrologic testing program is detailed in Gephart and others (1979a) and in recent quarterly and annual reports from the BWIP.

APPENDIX B - SEISMIC-REFLECTION AND MULTILEVEL AEROMAGNETIC SURVEYS IN THE COLD CREEK SYNCLINE AREA

G. E. Holmes
T. H. Mitchell

INTRODUCTION

The purpose of this appendix is to discuss seismic-reflection and multilevel aeromagnetic surveys which were conducted to investigate bedrock structures within the Cold Creek syncline study area. Presented is a summary of methodologies and results which support subsurface geologic interpretations discussed in Chapter 8, particularly data which were used to prepare the top-of-basalt (TOB) map (Chapter 8). Discussions of additional geophysical surveys which were also used to prepare the TOB map are included in Appendices C, D, and E.

SEISMIC REFLECTION

INTRODUCTION

The Basalt Waste Isolation Project (BWIP) began a multichannel seismic-reflection survey in 1978. To date, a network of 14 profiles has been established across the Hanford Site and nearby areas (Fig. B-1) by Seismograph Service Corporation (SSC) under contract to BWIP. This section describes testing that led to the decision to use the seismic-reflection method. Results of the preliminary interpretations of those portions of the 14 profiles that pass through the Cold Creek syncline study area (Fig. B-2) are discussed in the concluding interpretation section.

PREVIOUS WORK: SEISMIC SURVEYS ON THE HANFORD SITE

Exploration seismic surveys on the Hanford Site were first conducted in 1959. Additional surveys followed in 1963, 1971, and 1974. The early surveys consisted mainly of short (<2 km) seismic-reflection profiles for engineering and foundation studies at specific sites, and for general exploration and testing of various methods. These early surveys were conducted primarily to measure the thickness of the sediments overlying the basalt and seismic velocities in different layers. The results of these surveys will be briefly reviewed.

In 1959, a series of short, seismic-refraction profiles was run as a test of the technique (Raymond and Ratcliffe, 1959). The research laboratories on the Hanford Site fabricated a single-channel chronometer which

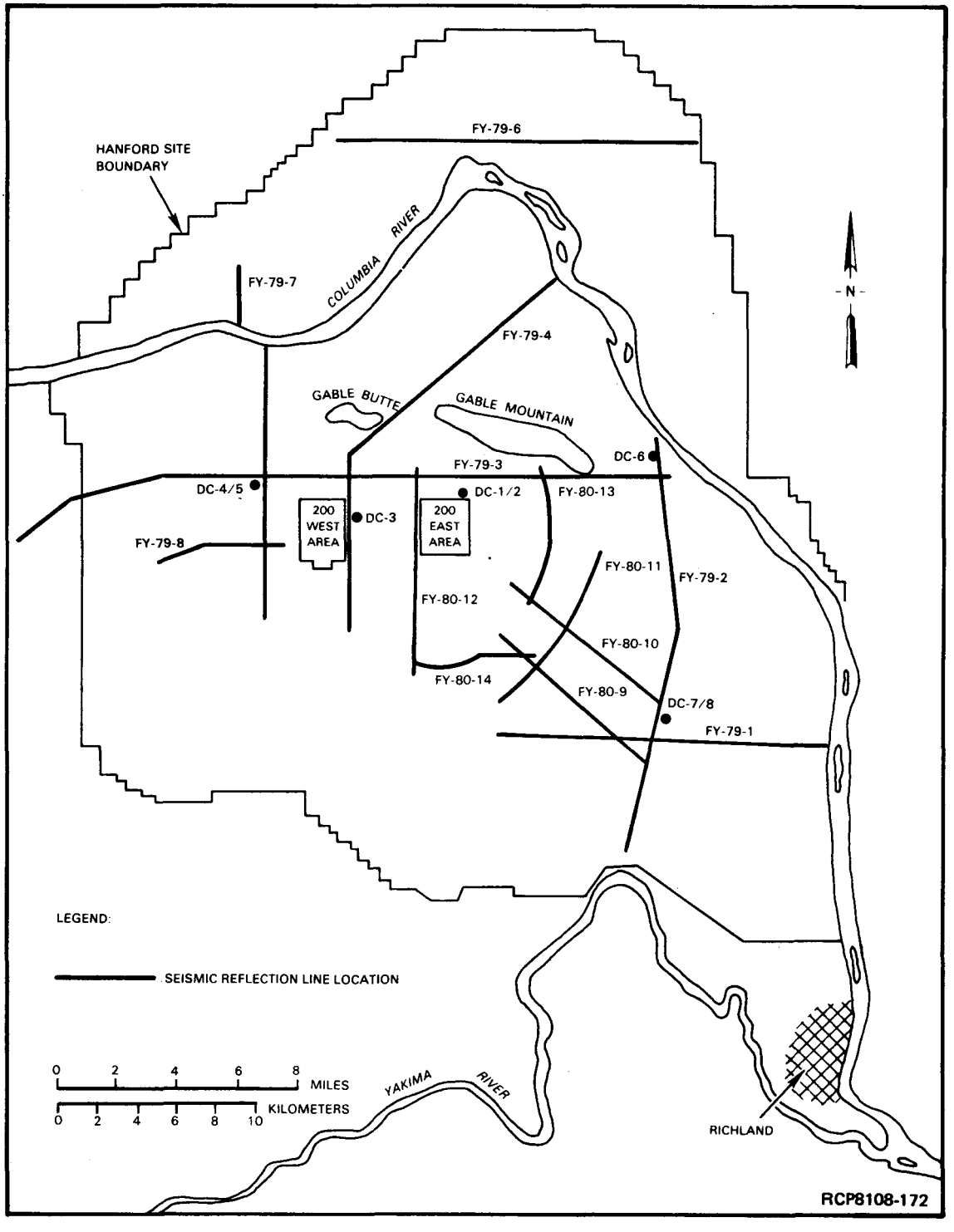

FIGURE B-1. Seismic-Reflection Line Locations.

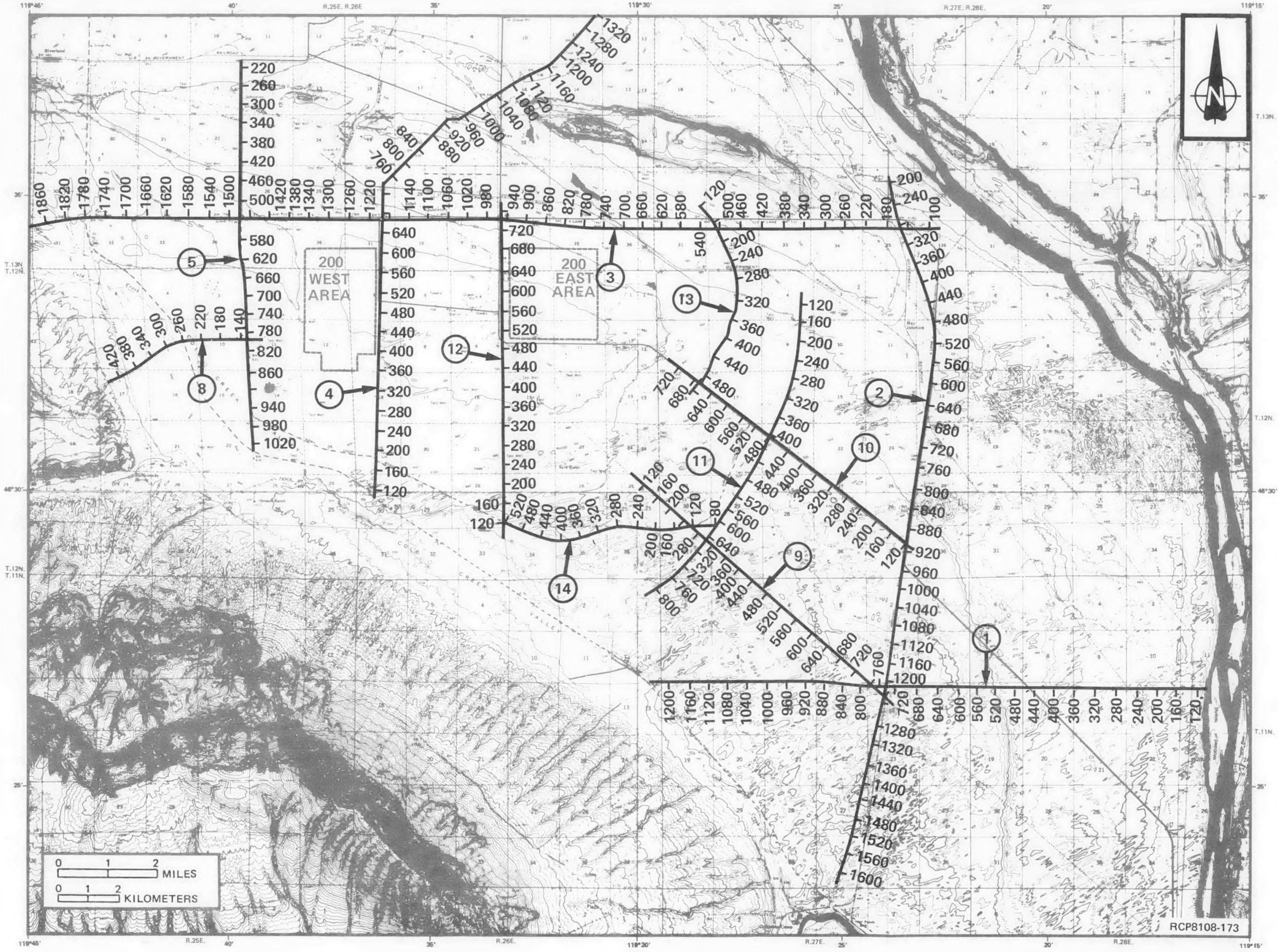

FIGURE B-2. Seismic-Reflection Line and Shotpoint Locations.

was coupled to a commercial blasting unit and a single geophone. Energy sources tested were single to partial sticks of dynamite and sledge hammer. Based on the test results, the refraction method was found useful for exploration at Hanford. Raymond and Ratcliffe (1959) recommended that geophysical surveys be made of the Hanford Site to support the waste-disposal activities.

In 1963, seismic-refraction and -reflection methods were tested as a means to determine "the depth of the top of the basalt section beneath the Hanford Site" (Brown and Raymond, 1964; Donaldson, 1963). The test consisted of refraction and reflection profiling using drilled shotholes. The basic recommendation from this test was that a combination of drilling and refraction profiling would be a cost-effective and definitive method to obtain data on the depth to basalt and on layering in the sediments overlying the basalt. Additional recommendations included running a grid of refraction lines, drilling shallow boreholes to the TOB at periodic intervals along the grid lines, running geophysical logs in the boreholes, and shooting velocity surveys in all boreholes. The test also showed that the continuous-profiling-reflection method could provide accurate information on the depth to basalt when coupled with advanced computer processing techniques. However, due to the necessary short spread length, it was noted that drilling costs of shotholes could be high (Donaldson, 1963). At the time this test was conducted (1963), digital recording and computer processing had just been developed and many seismic-recording systems still recorded in analog rather than in the present digital form.

In 1971 and 1974, refraction surveys were run for site investigation work at the Fast Flux Test Facility (Blume and Associates, 1971) and the Washington Public Power Supply System, Inc. nuclear plants 1, 2, and 4, respectively (WPPSS, 1974). These surveys were designed to determine depth to basalt bedrock and to provide data for shallow foundation studies. Survey design was based on the approach recommended by Donaldson (1963), relying on boreholes for depth and velocity control and shallow-drilled shotholes with large-charge sizes for better energy penetration. Although most of the work was shallow (30- to 60-m depth), some profiles reached the uppermost basalt (180- to 210-m depth).

These early tests and surveys demonstrated that the seismic-refraction method might be a good exploration technique for shallow investigations on the Hanford Site if proper borehole control were available. However, many of the refraction surveys which used borehole control discerned that the velocities within the sedimentary sequence were not laterally uniform, nor did they increase with depth, as was often assumed. Velocity inversions are difficult to locate in refraction interpretation and can cause erroneous depth estimates without borehole data. Additionally, seismic refraction was unable to resolve the thin basalt flows and interbeds below the TOB.

During the last decade, seismic-reflection techniques advanced rapidly with the development of modern digital computers. Research by oil companies, relying on seismic-reflection data for geophysical exploration, have improved the method far beyond the techniques tested at Hanford in 1963.

Improvements have been made in digital signal processing and in the speed of field data acquisition. Thus, an analysis of BWIP geologic data needs in 1977 showed that the costs of drilling seismic-refraction shotholes and the lack of resolution of the refraction method warranted a consideration of the use of seismic-reflection techniques.

METHODOLOGY

Fiscal Year 1978 Testing of Seismic Reflection

In 1978, a contract was let for the testing of seismic-reflection techniques to try to obtain penetration of the seismic signal down to and reflection from the level of the Umtanum flow within the Grande Ronde Basalt. This sequence of tests was reported in Heineck and Beggs (1978). The test consisted of a seismic-reflection survey of three short lines within the central Hanford Site at boreholes DC-1/2, DC-6, and DC-7/8 (Fig. B-1).

Three different energy sources were tested to determine which would give the best-quality data, as well as time and cost effectiveness. Primacord (a buried, rope-like, impulse source), dynamite (an impulse source), and VIBROSEIS (a vibrating source) were tested. The VIBROSEIS source was determined to be the best overall energy source. Field geometries, noise tests, and digital computer processing were also analyzed to determine an optimal data collection and processing sequence for this area.

The results of this test showed that the reflection method could give a rapid determination of the attitudes of basalt layers, especially the TOB. While the objective was to try to obtain reflections from the Umtanum flow itself, the ability of the technique to do so was only partially successful. Only limited areas of the Hanford Site were found to yield reflections from the flows in the Grande Ronde Basalt and possibly the Umtanum flow.

Fiscal Year 1979 Survey

In 1979, a contract was let for 113 km (70 line miles) of reflection profiling, all within the confines of the Pasco Basin. An additional 27 km (17 line miles) were subsequently added, for a total of 140 km (87 line miles). The 1979 seismic-line locations are shown in Figure B-1 with an FY-79- prefix. The seismic lines were located where the inferred trends of the Yakima folds (Fig. B-3) within the Pasco Basin were projected from geologic field mapping (i.e., where additional subsurface structural detail was required) (Fig. B-3).

Seismic lines 1 and 2 were positioned to cover the broad, open region of the eastern Hanford Site, south of Gable Mountain, to the Horn Rapids area of the Yakima River (the southern boundary of the Hanford Site).

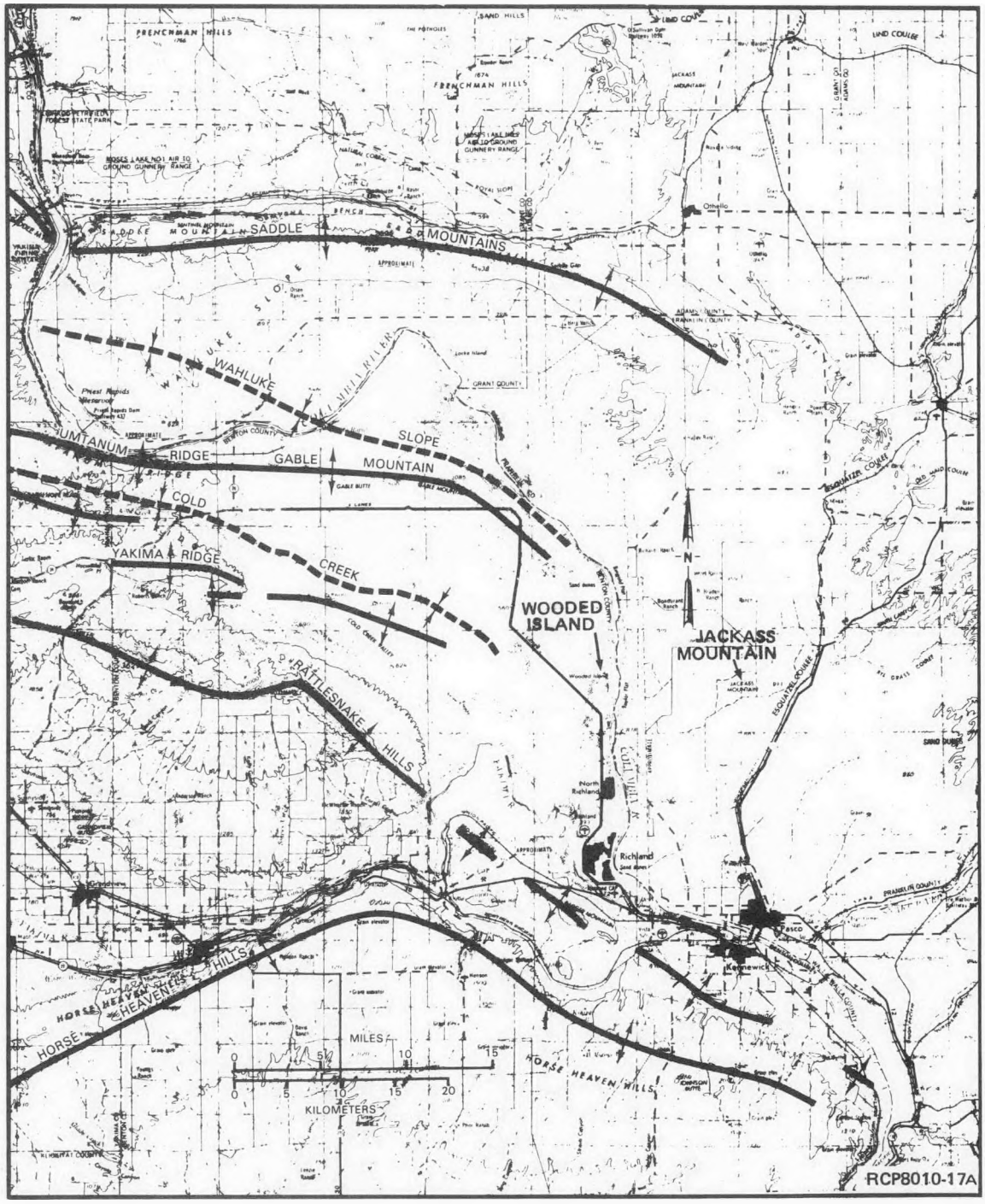

FIGURE B-3. Yakima Fold Structures.

Seismic line 3 runs east-west from just south of Gable Mountain to the western edge of the Hanford Site. This line essentially parallels the mapped axis of the Umtanum Ridge-Gable Mountain structure (Fig. B-3). The axis of the anticline has been interpreted to cross line 3 near the intersection with line 2. The structural trends of small, second-order folds along Gable Butte and Gable Mountain were interpreted by Fecht (1978) to be several degrees more northerly than the main axis, which was west-northwest to southeasterly. Seismic line 3 was designed to locate possible continuations of these small folds which could crosscut the Umtanum Ridge-Gable Mountain anticline and trend into the central part of the Cold Creek syncline.

Seismic line 4 begins at the southern edge of the Cold Creek syncline, runs north for several kilometers, then turns northeasterly to cross the mapped-projected axis of the Gable Mountain anticline, and then northeast to the Columbia River. The placement of this line was used to investigate the specific locations of the Cold Creek syncline axis, Gable Mountain axis, and Wahluke Slope syncline axis. Seismic line 5 runs north-south along the western edge of the site within the Cold Creek syncline and, again, was used to locate the main axis of the Umtanum Ridge-Gable Mountain structure.

Seismic line 6 was part of an extension of the original 113 km (70 line miles) and was placed to investigate any features trending southeast of the Saddle Mountains on the northern boundary of the Hanford Site. Seismic lines 7 and 8 were short lines placed to locate possible features indicated by aeromagnetic data and projected structures from geologic mapping (Reidel, 1978a).

Fiscal Year 1980 Survey

An additional 55 km (34 line miles) of data were collected in fiscal year 1980. This work was planned to complement the 1979 data and complete the regional Hanford Site coverage. Line placement was determined by the need to acquire data in the Cold Creek syncline area where there was previously little borehole control and limited geophysical data coverage. Figure B-1 shows the location of the 1980 seismic lines with an FY-80- prefix. The lines were generally based on structure projections represented on the geologic map of the Pasco Basin and TOB map contained in Myers, Price and others (1979).

Seismic lines 9 and 10 were placed on strike with the Cold Creek syncline and were intended to locate small, crosscutting features that might occur. Seismic line 11 was placed on the old Arc-5 test road to connect the other lines and crosscut the syncline in the dip direction. Seismic line 12 was placed in a similar location as lines 5 and 11, but in an intermediate position to locate the trough of the Cold Creek syncline. Seismic line 13 connects lines 10 and 3; trends from well data had suggested an anticline-syncline pair projected down from Gable Butte. Seismic line 14 closes the loop of data in the central area and provides data on both the southern limb of the Cold Creek syncline and the buried Yakima Ridge structure.

FIELD-COLLECTION PARAMETERS

The seismic-reflection surveys of 1978, 1979, and 1980 all used the VIBROSEIS as an energy source. Some modifications were made each year in the field techniques and data processing in an attempt to improve the quality of the data. Recording and processing parameters for the 1978 testing are discussed in Heineck and Beggs (1978). Similarly, the 1979 survey was discussed in Myers, Price and others (1979).

A modification in the 1980 seismic survey in field data acquisition and processing procedures attempted to optimize shallow TOB and Saddle Mountains Basalt reflections. The field-collection parameters are listed in Table B-1. The computerized data processing is summarized in Figure B-4.

SEISMIC-REFLECTION ANOMALY LOCATIONS

Figure B-5 shows the location of seismic-reflection anomalies. These anomalies were derived from the preliminary interpretations made by SSC. Several criteria for anomaly detection were established by SSC, such as severe and radical character changes, reflection time offsets, rapid changes in reflector dip, reflection discontinuities, and apparent diffraction patterns. Several specific anomalies interpreted by SSC are under question by BWIP. These BWIP interpretations are based on data from several geophysical surveys and geologic information. Using this additional geophysical and geological information, the anomalies have been interpreted and classified into the general categories listed in Figure B-5; the codes refer to the type of interpreted features. The categories presented in this figure represent a range of possibilities from a "real" bedrock or geologic structure to a data-processing phenomenon. Nevertheless, all SSC seismic anomalies were avoided in delineating potential repository sites. A more detailed discussion of seismic-reflection results for the Cold Creek syncline area is contained in the concluding interpretation section.

AEROMAGNETIC SURVEYS

INTRODUCTION

A multilevel, high-sensitivity, aeromagnetic survey was conducted for the BWIP by the Aero Service Division of Western Geophysical Company of America (Aero Service). The survey was flown between December 13, 1979 and March 10, 1980, and covered a 48- by 64-km area within the central Pasco Basin (Fig. B-6). The purpose of this survey was to provide high-resolution aeromagnetic data which could be used to support siting studies conducted by BWIP.

TABLE B-1. Seismic Field-Collection Parameters.

Recording Unit	
Instrumentation	Texas Instruments DFS IV digital recording system with 800 BPI 9-track tape drive and instantaneous floating point amplifiers
Number of channels	48
Gain mode	Instantaneous floating point
Low-cut filter	27 Hz 36 db per octave slope
Hi-cut filter	124 Hz 72 db per octave slope
Notch filter	60 Hz
Sample rate	2 ms
Format	SEG-B
Record length	11.25 s
VIBROSEIS Source	
Type vibrators	Y-600 with SSC VIBK electronics, center-mounted on trucks
Number of vibrators	3
Sweep generator	Pelton, radio-transmitted signals
Sweep frequency	30 to 120 Hz
Duration	10 s
Listening time	1.25 s
Vibrator pattern	3 in tandem 11.43 m (37.5 ft) apart
Number of sweeps	6 pr vibrator pattern
Pattern length	30.48 m (100 ft) total with 1.77-m (5.8-ft) move-up per sweep
Vibrator pattern interval	15.24 m (50 ft) (resulting in a 24-fold stack)
Spread Geometry	
Configuration	Split-straddle, 3-station gap between traces 24 and 25
Station interval	15.24 m (50 ft)
Near-trace offset	30.48 m (100 ft)
Far-trace offset	381 m (1,250 ft)
Detectors	
Geophone type	Mark Products L25E
Frequency	40 Hz
Number per trace	18 phones--3 strings of 6 connected in series--parallel
Phone pattern	Straddling station in-line, 30.48 m (100-ft) coverage (1.83-m [6-ft] uniform spacing)

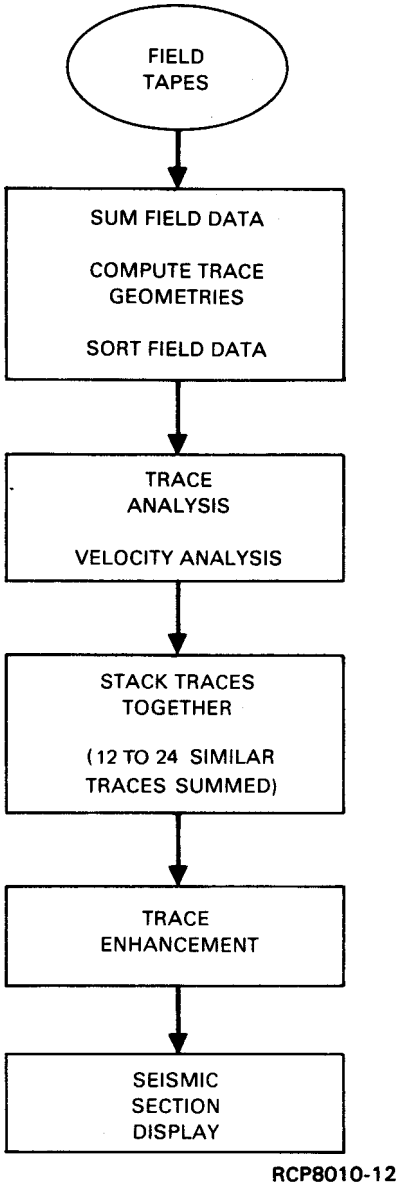

FIGURE B-4. Seismic-Reflection Data-Processing Flow Diagram (after Heineck and Beggs, 1978).

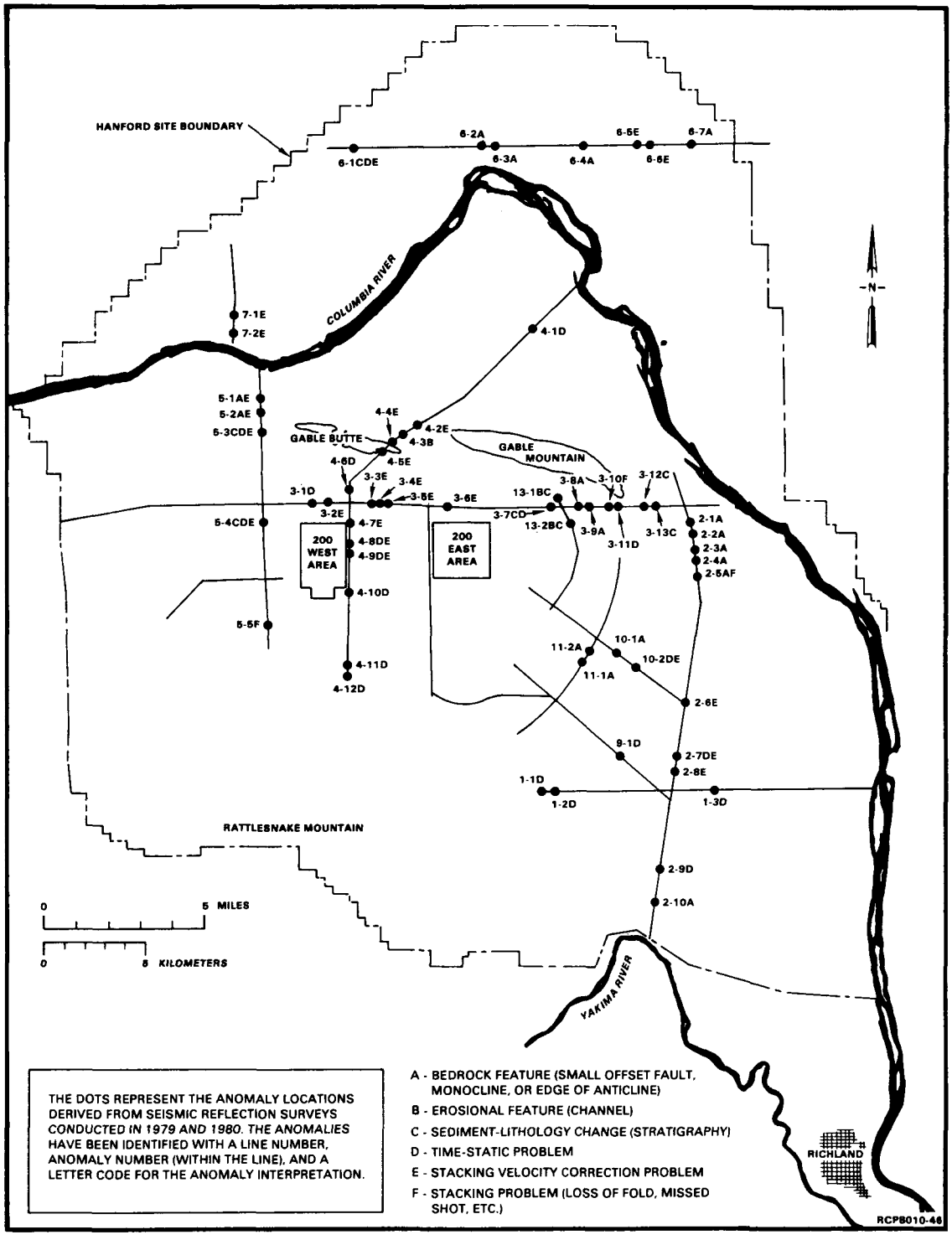

FIGURE B-5. Seismic-Reflection Anomaly Location Map.

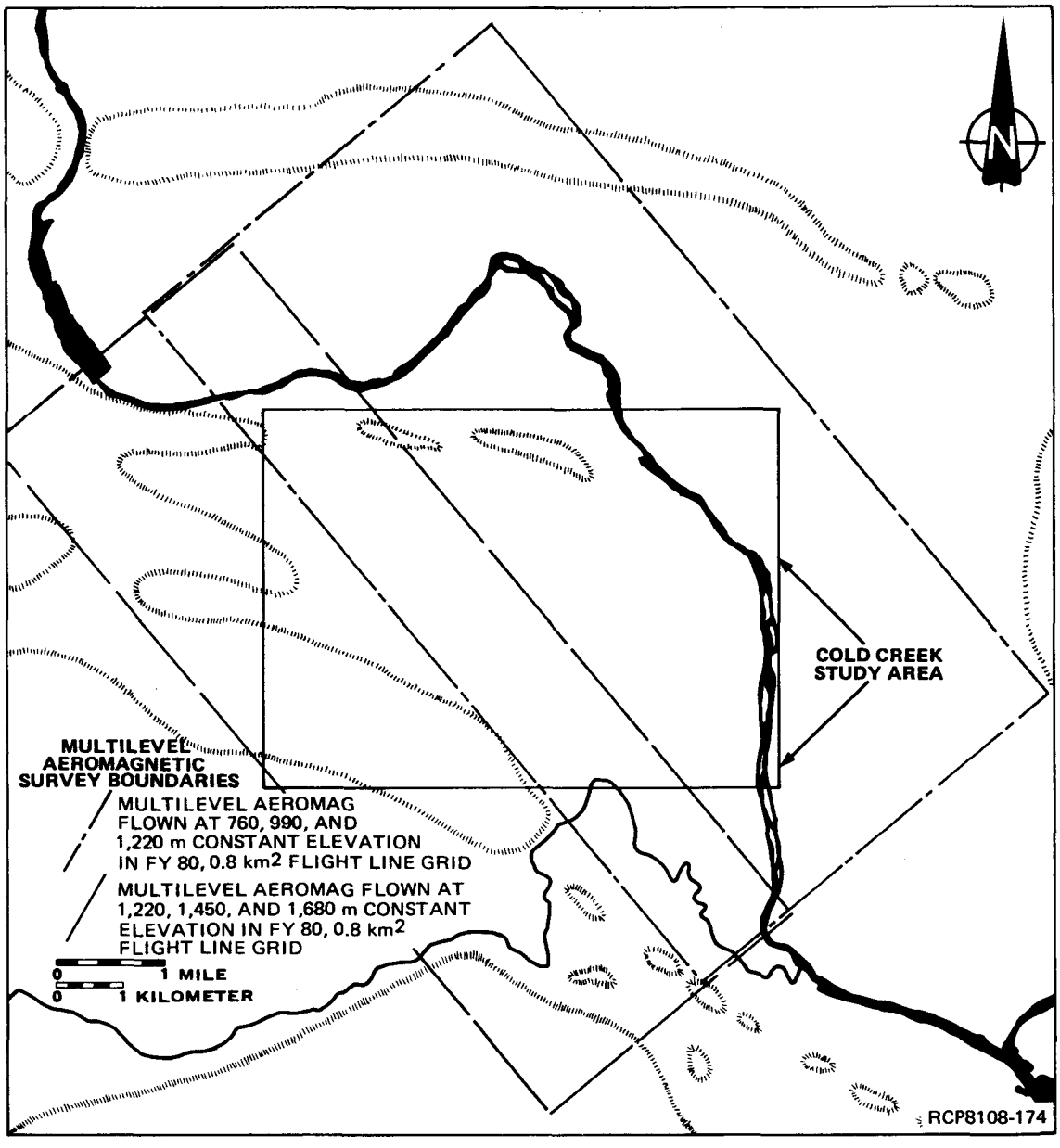

FIGURE B-6. Multilevel Aeromagnetic Survey Locations.

The multilevel survey was flown at five different altitudes: 760, 990, 1,220, 1,450, and 1,680 m constant elevation above mean sea level (MSL). Due to topographic constraints, only the 1,220-m-survey altitude covered the entire Cold Creek syncline study area (Fig. B-6). Therefore, this section will concentrate on a discussion of anomalies revealed by the 1,220-m level, with emphasis on the Werner deconvolution solutions derived from this level. Significant features unique to other survey levels are discussed briefly in the concluding interpretation section and in Chapter 8.

PREVIOUS WORK

A general chronology and description of the aeromagnetic surveys conducted over the Hanford Site prior to the multilevel survey are shown in Table B-2. Most of these surveys were regional and flown to obtain reconnaissance-type information.

The first reference to an aeromagnetic survey in the Hanford area was made by Raymond and McGhan (1963). They interpreted results of a reconnaissance aeromagnetic survey flown by U.S. Geological Survey personnel across the Hanford Site (Table B-2). Although a general configuration of the TOB was derived from the observed magnetic field, a quantitative analysis of magnetic data in this environment was reported to be difficult.

Zietz and others (1971) (Table B-2) presented results from a high-altitude, regional, aeromagnetic survey across the northwestern United States. The portion of the survey covering the Columbia Plateau was flown by Aero Service at a constant (barometric) flight elevation of 4,575 m above MSL. The area west of the Idaho Batholith, which includes the Hanford Site, is discussed as a subsection within the Zietz report. Also, Zietz and others (1971) noted that the overall magnetic amplitude was very low, considering the thick sequence of underlying basalt flows. They suggested that the low-magnetic intensity may be caused by an averaging effect due to interbedded basalt flows of normal and reversed polarities. The averaging effect was interpreted to mean that the basalt on the plateau acts magnetically as an imperfect window to the basement. If this were the case, Zietz and others (1971) concluded that primarily basement structures, not those of the basalt, should be shown by the magnetic data.

Blume and Associates (1971) provided subsurface geologic investigations for the Fast Flux Test Facility on the Hanford Site (Table B-2). An aeromagnetic survey was flown over the east-central Cold Creek syncline, utilizing a 3.2-km grid spacing. From Gable Mountain itself continuing to the southeast, there is a break in the magnetic highs which indicates that the anticlinal structures are in an en echelon arrangement similar to that of Gable Mountain and Gable Butte.

An aeromagnetic survey was flown over south-central Washington and north-central Oregon in 1957, compiled in 1970, and interpreted by Swanson and others (1979c) (Table B-2). This survey was flown with a 1.6-km north-south flight line spacing 150 m above the ground. Although the survey has much more detail than the one discussed by Zietz and others (1971), the results of both surveys are generally consistent.

TABLE B-2. Chronology of Aeromagnetic Surveys of the Hanford Site.

Survey reference	Survey elevation	Survey line spacing and orientation	Magnetometer
Raymond and McGhan (1963)	150-m terrain clearance	1.6-km north-south	Fluxgate
Zietz and others (1971)	4,575-m constant elevation above sea level (barometric)	8-km east-west	Alkali vapor and fluxgate
Blume and Assoc. (1971)	275- and 455-m barometric	3.2 x 3.2 km northeast-southwest northwest-southeast	Proton precession
Weston Geophysical (1978b)	300-m terrain clearance	0.8 x 8 km northeast-southwest traverse lines northwest-southeast tie lines	Optically pumped cesium vapor
Swanson and others (1979c)	150-m terrain clearance	1.6 km north-south	Fluxgate
Rockwell Records Retention Center	1,220-m barometric	0.8 x 0.8 km northeast-southwest northwest-southeast	Proton precession
Rockwell Records Retention Center	760, 990, 1,220, 1,450, and 1,680-m barometric	0.8 x 0.8 km northeast-southwest northwest-southeast	Optically pumped cesium vapor

In the qualitative interpretation presented by Swanson and others (1979c), anomalies are identified and categorized as relating to structurally controlled topography, dikes, faults, valley-filling basalt flows, or are of unknown origin. The Rattlesnake Hills, Yakima Ridge, and parts of Gable Mountain and Gable Butte anomalies were interpreted to be related to structurally controlled topography, particularly asymmetrical anticlinal ridges. The dipping flows and eroded ridge crests combine to expose flow sequences that are hidden in the "sandwich" of normal and reversed flows characterizing the areas between ridges. Another anomaly noted by Swanson and others (1979c) lies over Wooded Island (west of Jackass Mountain [Fig. B-3]). They interpreted this broad, negative anomaly as a possible reflection of a thick deposit of weakly magnetized, lacustrine clay, silt, and fine sand of Quaternary age (Grolier and Bingham, 1971).

Other aeromagnetic surveys over the Hanford Site include a 300-m terrain clearance survey flown for Weston Geophysical (1978b), and the first survey flown for Rockwell Hanford Operations (Rockwell) (Myers, Price and others, 1979) (Table B-2). Aeromagnetic highs, lows, and linears were generally correlative with known structures in the basalt, but some aeromagnetic linears were identified which did not correlate with any previously recognized bedrock structures.

DATA ACQUISITION

All of the Rockwell survey levels were flown in a square grid with flight lines spaced 800 by 800 m and oriented N45^{o}W and N45^{o}E. Table B-3 is a summary of the survey parameters used by Aero Service for compilation of the gridded data. The total field magnetic intensity was recorded digitally on magnetic tapes and monitored on an analog strip-chart recorder. Radar altimeter (height above the ground), barometric altimeter (altitude relative to MSL), fiducial interval, and photographic flightpath on 35-mm film were also recorded. The entire airborne system was controlled and triggered by a Doppler navigation system. Data points were collected at constant spatial intervals (46 m for this study).

A stationary, land-based magnetometer digitally recorded the total field magnetic intensity concurrently with the airborne data acquisition. An analog strip-chart recorder was used at the ground base station to identify when nonlinear variations in the geomagnetic field exceeded 5 gammas/5 min. Data recorded during these times were not used in map compilation, but, rather, were reflown.

DATA PROCESSING

Figure B-7 is a generalized flow diagram of the data compilation and processing utilized for the multilevel survey. The methodology involved two parallel procedures: (1) preliminary flightpath recovery using 35-mm flightpath film and (2) editing and processing of the digital data.

Initial flightpath recovery began in the field, where 35-mm photographic film was used to identify intersection points between tie lines,

TABLE B-3. Multilevel Survey Statistics.

Sensor	Optically pumped, 6-cell, cesium vapor magentometer
Installation	Tailstinger
Data acquisition system	CODAS*
Digital recording increment	0.01 gamma (nanoteslas)
Analog recorder	Hewlett Packard 25.4-cm rectilinear
Analog chart scale	4 gammas (nanoteslas)/cm
Analog chart speed	Doppler driven for a horizontal scale of 1:48,000
Altimeters	Minneapolis-Honeywell AN/APN 171 radar altimeter and Rosemount 124 A5 barometric altimeter
Analog recording scale	Radar 12 m/cm
Analog chart speed	Doppler driven for horizontal scale of 1:48,000
Digital recording increment	Radar 1.5 m, barometric 0.61 m
Flightpath camera	Automax, 35-mm, single frame
Fiducial interval	46 m
Ground monitor	Optically pumped, cesium vapor magnetometer
Digital recording increment	0.01 gamma (nanotesla)
Digital recording interval	1.00 s
Analog chart scale	0.4 gamma/cm: 4 gamma/cm
Analog chart speed	2.54 cm/min
Flight line spacing	800 m
Flight line direction	N45°E, N45°W
Base of operations	Pasco, Washington
Navigation	Singer SSK-1000 Doppler
Linear area	26,227 km
1,680-m	3,691 km
1,450-m	3,691 km
1,220-m	7,836 km
900-m	5,504 km
760-m	5,504 km
Map presentation scale	1:62,500
Total magnetic field intensity	
Maximum	56,570 nanoteslas (gamma)
Minimum	56,225 nanoteslas (gamma)
Average	56,390 nanoteslas (gamma)
Magnetic inclination	
Maximum	70°00'
Minimum	69°25'
Mean	69°40'
Magnetic declination	
Maximum	20°45'
Minimum	20°25'
Mean	20°30'

*CODAS: A computer-based, digital acquisition system designed and developed by Aero Service and based on the Hewlett-Packard 2100 series minicomputer.

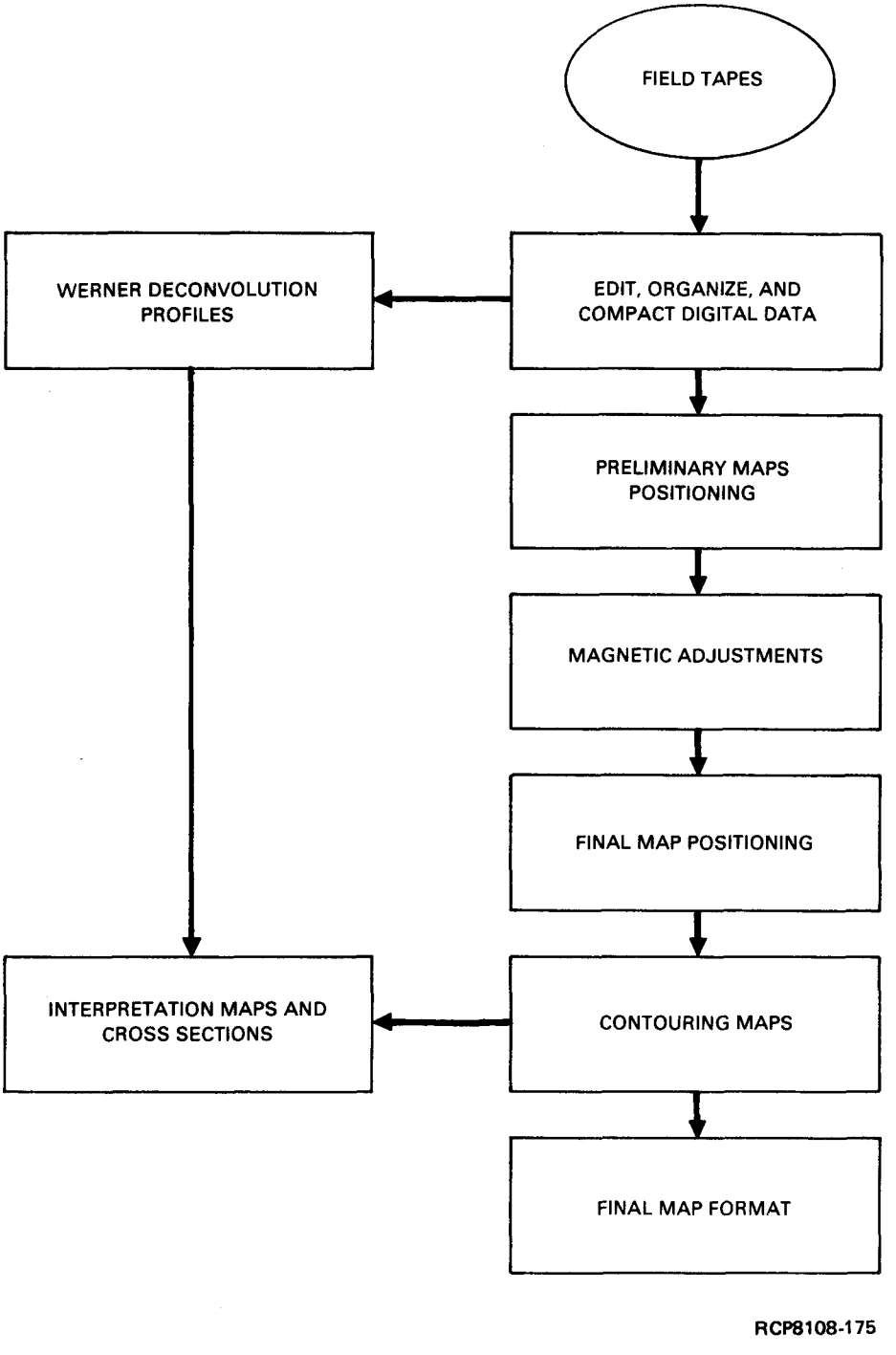

FIGURE B-7. Aeromagnetic Data Compilation and Processing.

traverse lines, and ground points on topographic maps of the area. This technique was used to identify significant flightpath errors, which were subsequently reflown.

The digital, total field, magnetic intensity data were edited, checked for noise spikes, organized, and compacted into a standard computer format. Magnetic adjustments were then made to eliminate differences at traverse line/tie line intersections. The major sources of differences at these intersections included diurnal variations, transients in the Earth's magnetic field, and deviations in altitudes of crossing lines. Lines were linearly shifted and tilted to minimize intersection differences. Most remaining intersection differences were then eliminated through an iterative process using higher orders of least-squares fit. Small, residual differences were distributed to the traverse lines.

Final map positioning was accomplished by positioning the flightpaths to an absolute coordinate system. This procedure allowed for removal of the Earth's regional magnetic field. A worldwide model of the International Geomagnetic Reference Field (Cain and others, 1968), described in terms of spherical harmonics and time deviations, was calculated and subtracted from the data. A constant (56,390 gammas), representing an average value of the Earth's field at the center of the survey area, was then added to the data.

Prior to contouring, data values from the combined flight lines were reduced to a square grid, 200 by 200 m, oriented N45^{o}W by N45^{o}E. The resultant grid was then contoured at a 10-gamma contour interval to produce the total-field-intensity maps. In areas of high-horizontal gradients, some contour lines were dropped, creating local-variable-contour intervals for display purposes. Various derivative maps were generated using the gridded total magnetic intensity data from the different flight levels. Included were horizontal gradient, residual, and vertical-gradient maps. Total-field-contour maps for the 760- and 1,220-m levels are included as Figures B-8 and B-9, respectively.

In addition to the contoured data, Werner deconvolution profiles were created for each flight line from all five survey levels. The Werner method is a digital computer technique which automatically calculates the depths, susceptibilities, and dips of tabular bodies, or interfaces between bodies, of contrasting susceptibility (Friedberg, 1975). Werner deconvolution profiles are printed on 76-cm Calcomp Plots, at the same horizontal scale as the magnetic contour maps. Figure B-10 represents a hypothetical example of a Werner deconvolution profile with some idealized solutions. The Werner profiles provided by Aero Service included the following data representation: (1) measured-total-field magnetic profiles, (2) calculated horizontal-gradient-magnetic profile, (3) sea-level line, (4) topographic profile from radar altimeter data, (5) calculated depth points from total-field and horizontal-gradient data, (6) calculated dip and susceptibility values, and (7) barometric elevation of aircraft.

The geometric solutions determined by Werner deconvolution are expressed graphically in three forms: (1) fault-like solutions, (2) dike-like solutions, and (3) structural disturbances. Structural

TOTAL FIELD CONTOURS
760-m AREA

CONTOUR INTERVAL	10 GAMMAS
FLIGHT INTERVAL	TIE 0,8 km
	TRAVERSE 0,8 km
SURVEYED AND COMPILED	1979 & 1980

RCP8108-176

FIGURE B-8. Aeromagnetic Total-Field-Contour Map (760 m).

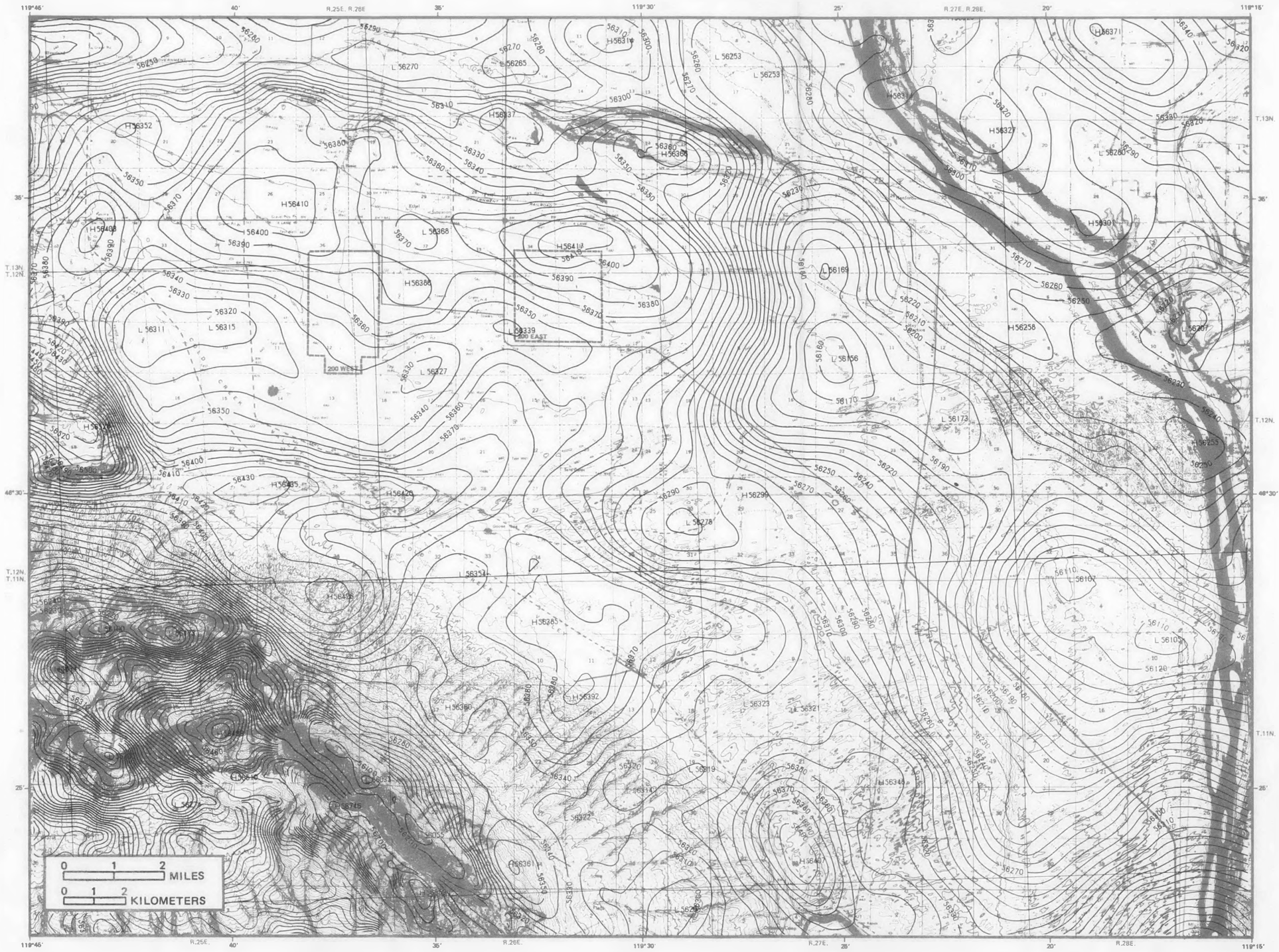

TOTAL FIELD CONTOURS

1,220-m AREA

CONTOUR INTERVAL	10 GAMMAS
FLIGHT INTERVAL	TIE 0,8 km
	TRAVERSE 0,8 km
SURVEYED AND COMPILED	1979 & 1980

RCP8108-177

FIGURE B-9. Aeromagnetic Total-Field-Contour Map (1,220 m).

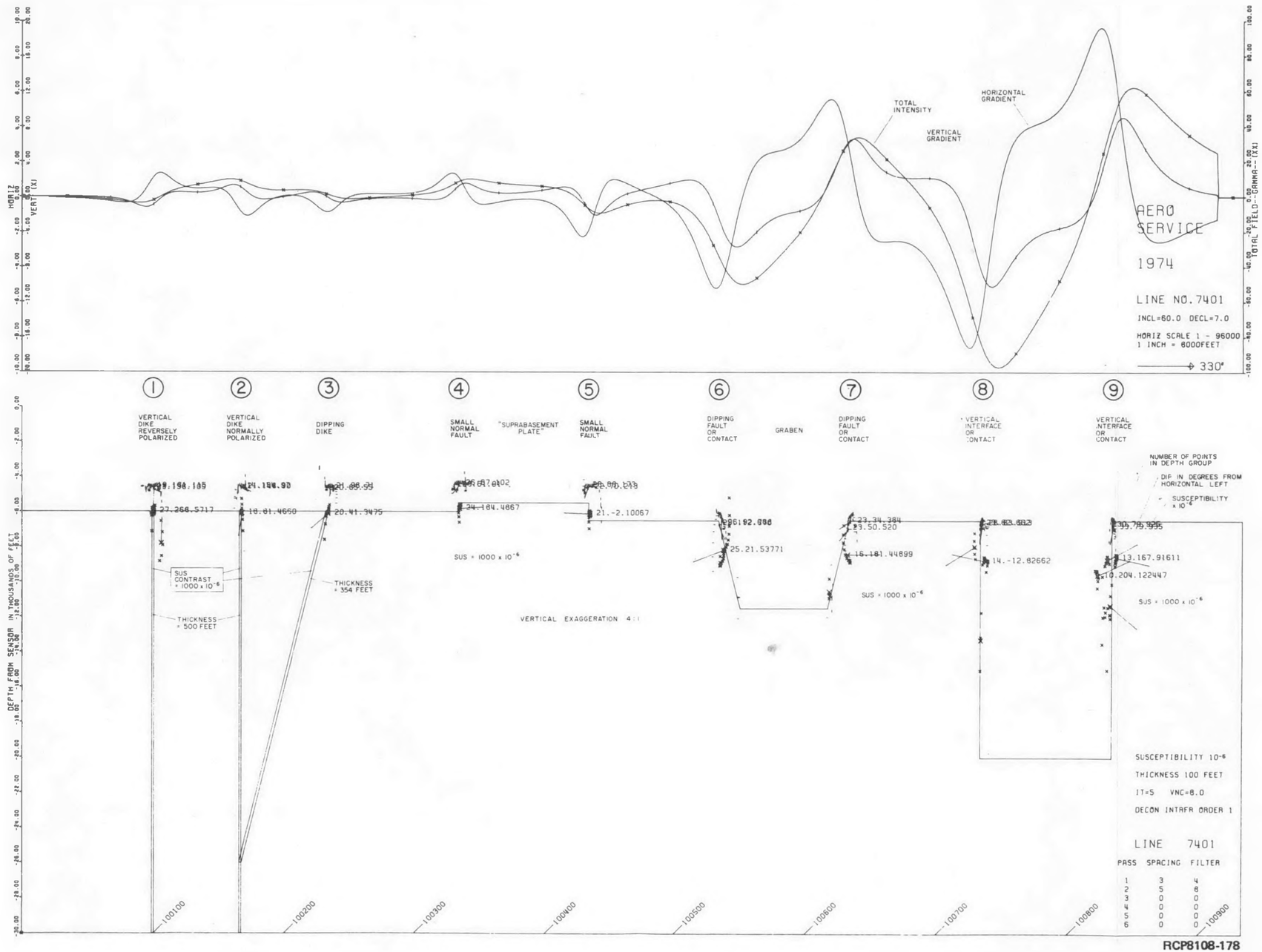

FIGURE B-10. Hypothetical Werner Deconvolution Profile with Idealized Solutions.

disturbances are generally combinations of both fault-like and dike-like geometric solutions. Aeromagnetic interpretive maps for the 760- and 1,220-m levels are included as Figures B-11 and B-12, respectively.

It should be emphasized that a fault-like solution does not necessarily mean that an actual fault is present. Rather, the fault-like solution indicates that a horizontal magnetic source terminates at a particular location. In the Cold Creek syncline, horizontal termination of magnetic sources (lava flows) can be caused by flow pinchout, possible abrupt changes in the magnetic properties of a flow, steep anticlinal/synclinal flanks, as well as fault displacement.

Generally, solutions of thin magnetic layers with a horizontal orientation ($\pm 45^{o}$) were considered fault bounded and were mapped as faults (Fig. B-11 and B-12). Many of the sheet solutions show an upward dip, indicative of thrust faulting. No thrust faults are indicated on the interpretative maps because of the known presence of strong, reversed, remanent magnetic polarization, which has been shown to affect the calculated dip of the sources.

Solutions of thin magnetic layers dipping vertically ($\pm 45^{o}$) are mapped as "dikes" on the interpretive maps (Fig. B-11 and B-12), although they may not represent true geologic dikes. A similar Werner deconvolution solution is obtained over anomalies caused by recognized anticlinal or synclinal structures. Structural disturbances, as noted on the interpretive maps, are generally solutions that do not meet the criteria for either dike-like or fault-like features. For example, structural disturbances may be mathematically resolved as a dike-like structure on one survey level, and possibly as two fault-like solutions from another flight level which represent the two edges of a dike-like body.

Aeromagnetic results to be discussed in the concluding interpretation section are primarily based on Werner deconvolution solutions from the 760- and 1,220-m flight levels (Fig. B-11 and B-12). Most anomalies seen on the 1,220-m level are also recognized from the other flight levels. Whenever possible, Werner deconvolution solutions have been correlated with known or inferred geologic structures. Anomalies that yielded dike-like solutions are designated D, while fault-like solutions carry either an N or F designation. Several general features evident on total-field-intensity maps for the 760- and 1,220-m levels (Fig. B-8 and B-9) are also discussed.

INTERPRETATION OF SEISMIC AND AEROMAGNETIC SURVEYS IN THE COLD CREEK SYNCLINE AREA

The geophysical interpretive process entailed an evaluation of results from a combination of the seismic-reflection and aeromagnetic surveys discussed in this appendix, and ground magnetic and gravity surveys discussed in the remaining appendices. This approach was deemed necessary, in that each geophysical technique "measures" a different base

GEOPHYSICAL INTERPRETATION

760-m AREA

⊥ ? ⊥ N – 1	NORMAL FAULT, HACHURES ON MAGNETICALLY DOWN-THROWN SIDE, DASHED WHERE INTERPOLATED, QUERIED WHERE DOUBTFUL
▲ ? ▲ T – 1	THRUST FAULT, DRAGON TEETH ON UPTHROWN BLOCK
⇄ ? ⇄ S – 1	STRIKE – SLIP FAULT
∿ ? ∿ F – 1	FAULT, SENSE OF MOVEMENT UNKNOWN
70° D – 1	DIKE, ARROW AND ANGLE INDICATE DIP OF FEATURE RELATIVE TO SURFACE
+27, 27, 27?	GRADED DEPTH OF MAGNETIC SOURCE, IN 100s OF ft RELATIVE TO SEA LEVEL
SD – 1	STRUCTURAL DISTURBANCE
2000	MAGNETIC SUSCEPTIBILITY IN MICRO – emu

RCP8108-179

FIGURE B-11. Aeromagnetic Interpretive Map (760 m).

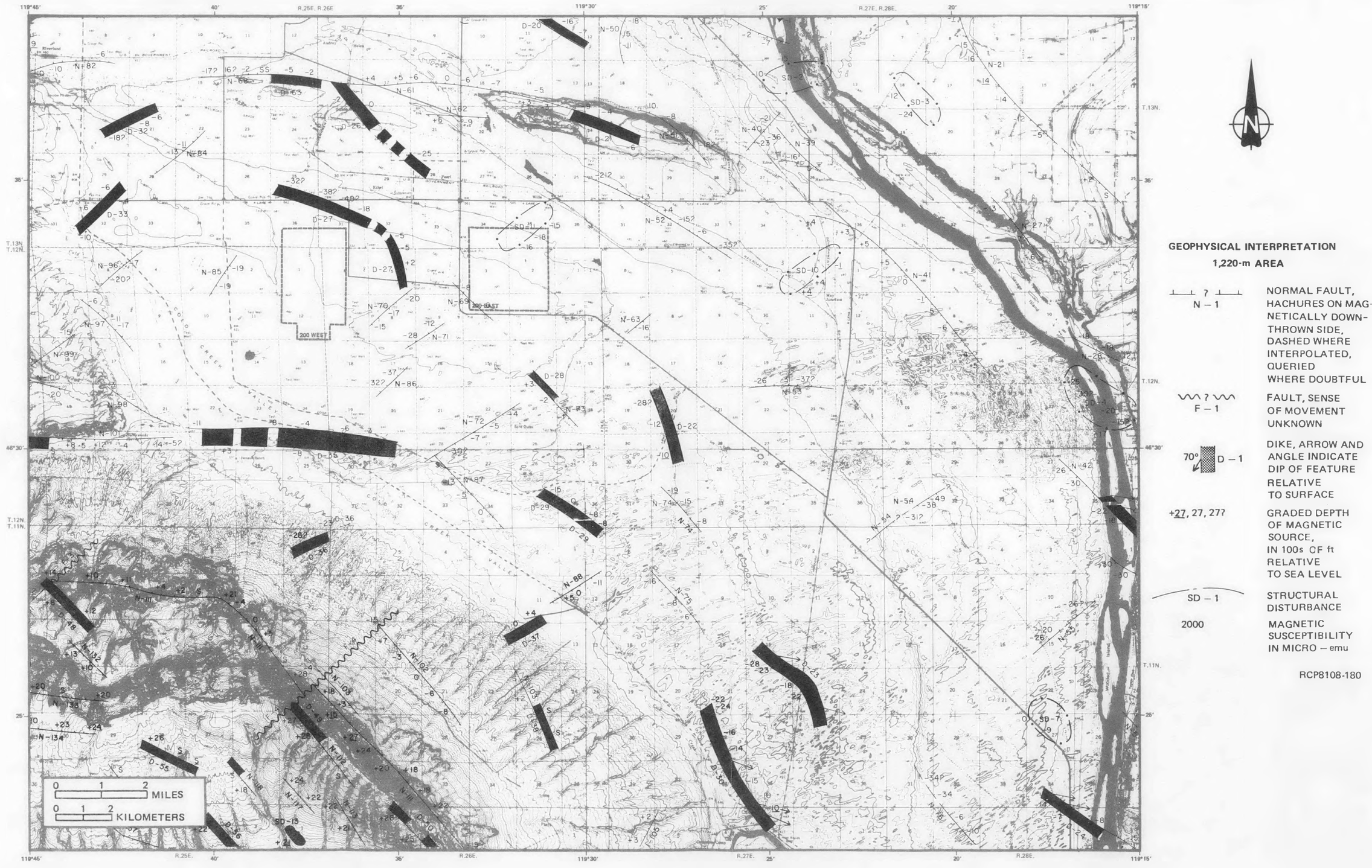

FIGURE B-12. Aeromagnetic Interpretive Map (1,220 m).

property of the rock. The reliability of interpretations was considered greatest when more than one technique indicated a similar subsurface geologic condition.

A demonstration of the need for multiple survey coverage can be shown by examining the results of a two-dimensional computer-modeling exercise. Figure B-13 is a summary plot of four, hypothetical, subsurface, geologic conditions that are interpreted to exist within the Hanford Site, including the Cold Creek syncline. These conditions have been generalized from borehole data or extrapolated from the surface-mapping work reported in Myers, Price and others (1979). These four conditions were computer modeled to determine and compare their geophysical responses. The models produced are shown in Figures B-14 through B-17. Table B-4 shows the stratigraphy, velocities, and densities for the models. The geologic parameters and geologic information were generalized from borehole stratigraphy, seismic-velocity logs, and borehole gravity surveys (Myers, Price and others, 1979; Robbins and others, 1979).

The models included as Figures B-14 through B-17 typify the type of geophysical responses that were observed in the Cold Creek syncline area. Modeling of gravity data, at the scale used for these models, was able to effectively portray a basalt bedrock structure such as a monocline (Fig. B-16) or a fault (Fig. B-17). However, for the same basalt-structure model, there is a much more subtle expression in the seismic-reflection response than in the gravity response. A small disruption in the reflection section could easily be confused with the response from a shallower feature such as a channel (Fig. B-14) or sediment lens (Fig. B-15); whereas, the gravity responses display a rather large, 1-mgal offset across the monocline (Fig. B-16) and fault (Fig. B-17). Conversely, a channel (Fig. B-14) or sediment lens (Fig. B-15) in the gravity response is minimal while causing a more noticeable data "dropout" on the seismic-reflection response. In the cases modeled, the seismic-reflection technique is seen to be more sensitive to vertical variations in geology, while the gravity technique tends to be more responsive to lateral variations in geology. Consequently, a combination of both techniques would be required to detect and evaluate a small bedrock structure of importance to a detailed analysis of the Cold Creek syncline subsurface. Modeling of responses to the various surveys has been used as a guide to the interpretation of actual field measurements.

The remainder of this section contains a summary of geophysical survey results that constrain the structural geology of the subsurface in the Cold Creek syncline area. Seismic survey and aeromagnetic survey results are emphasized in this discussion. Pertinent borehole data and high-resolution geophysical survey results (Appendices C, D, and E) which were used to complement these data are also included. This section focuses on the configuration of the TOB within that part of the Cold Creek syncline area which lies south of the Umtanum Ridge-Gable Mountain structure and north of the buried portion of the Yakima Ridge structure (Fig. B-3). This area includes the reference repository location (see Chapter 1). The overall utility of the TOB surface for interpreting bedrock structure in the Cold Creek syncline area is given in Chapter 8. For purposes of the

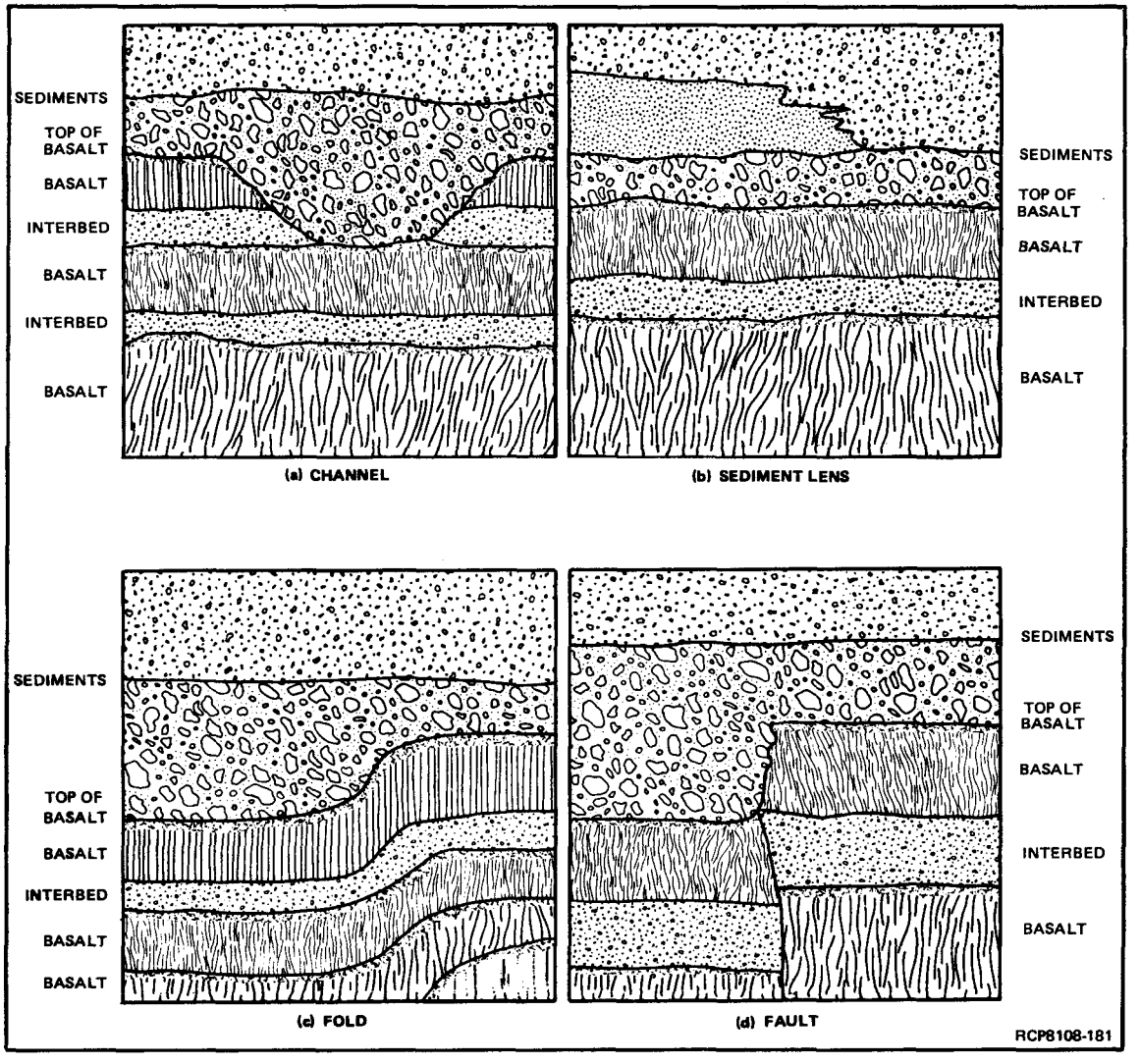

FIGURE B-13. Hypothetical Geologic Features That Can Produce a Geophysical Survey Response.

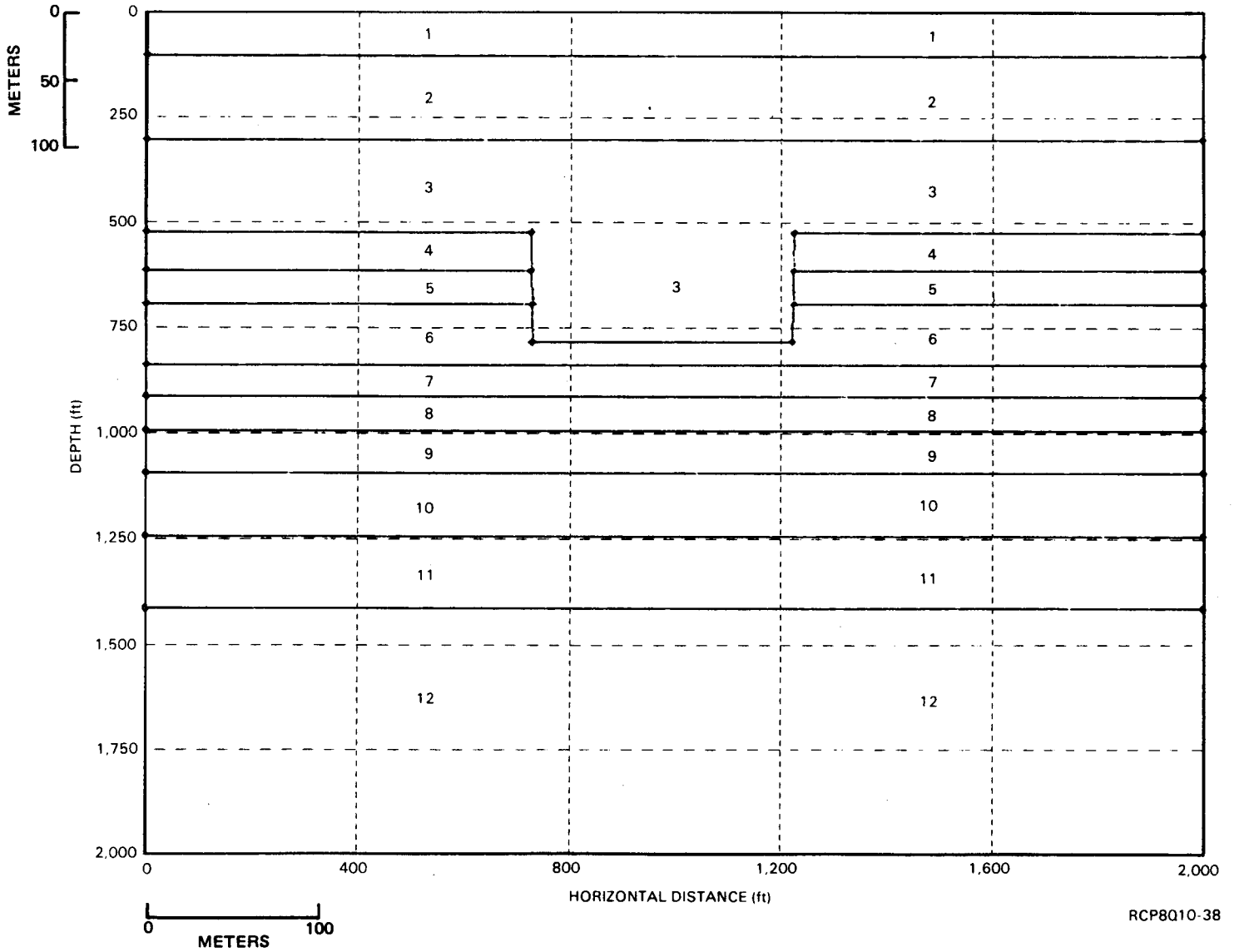

FIGURE B-14a. Geologic Model, Channel.

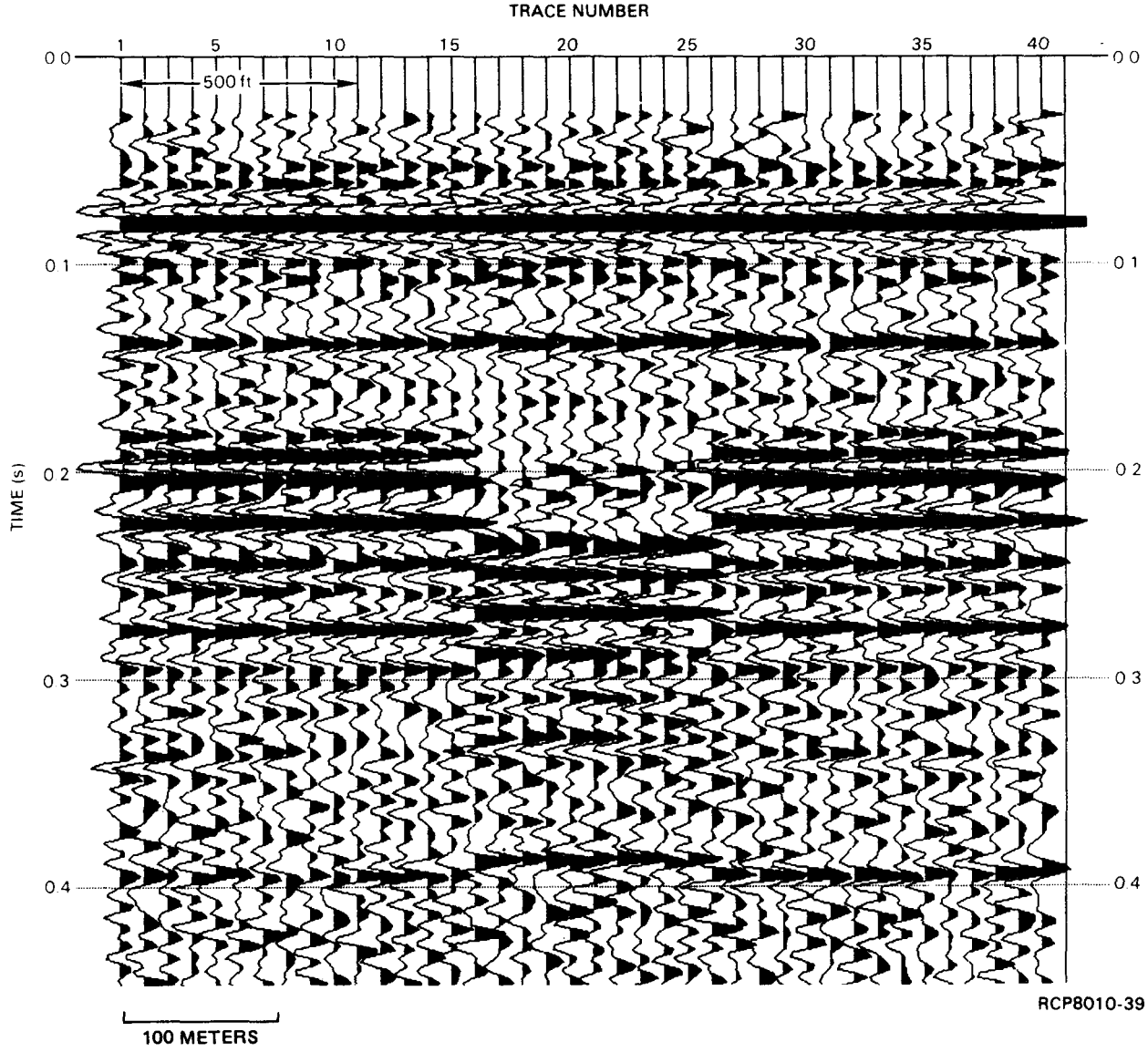

FIGURE B-14b. Seismic Response, Channel.

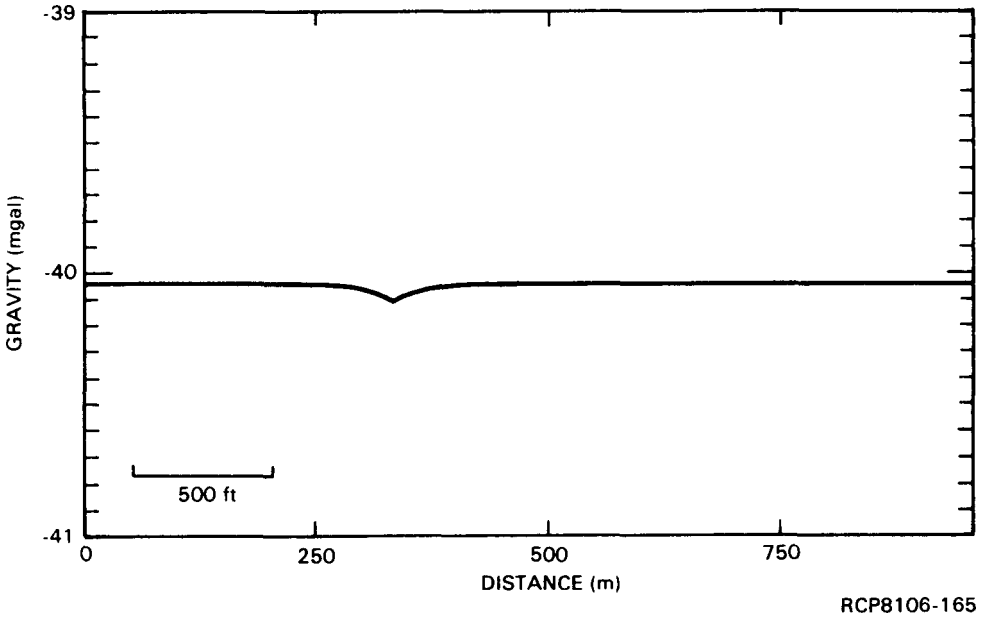

FIGURE B-14c. Gravity Response, Channel.

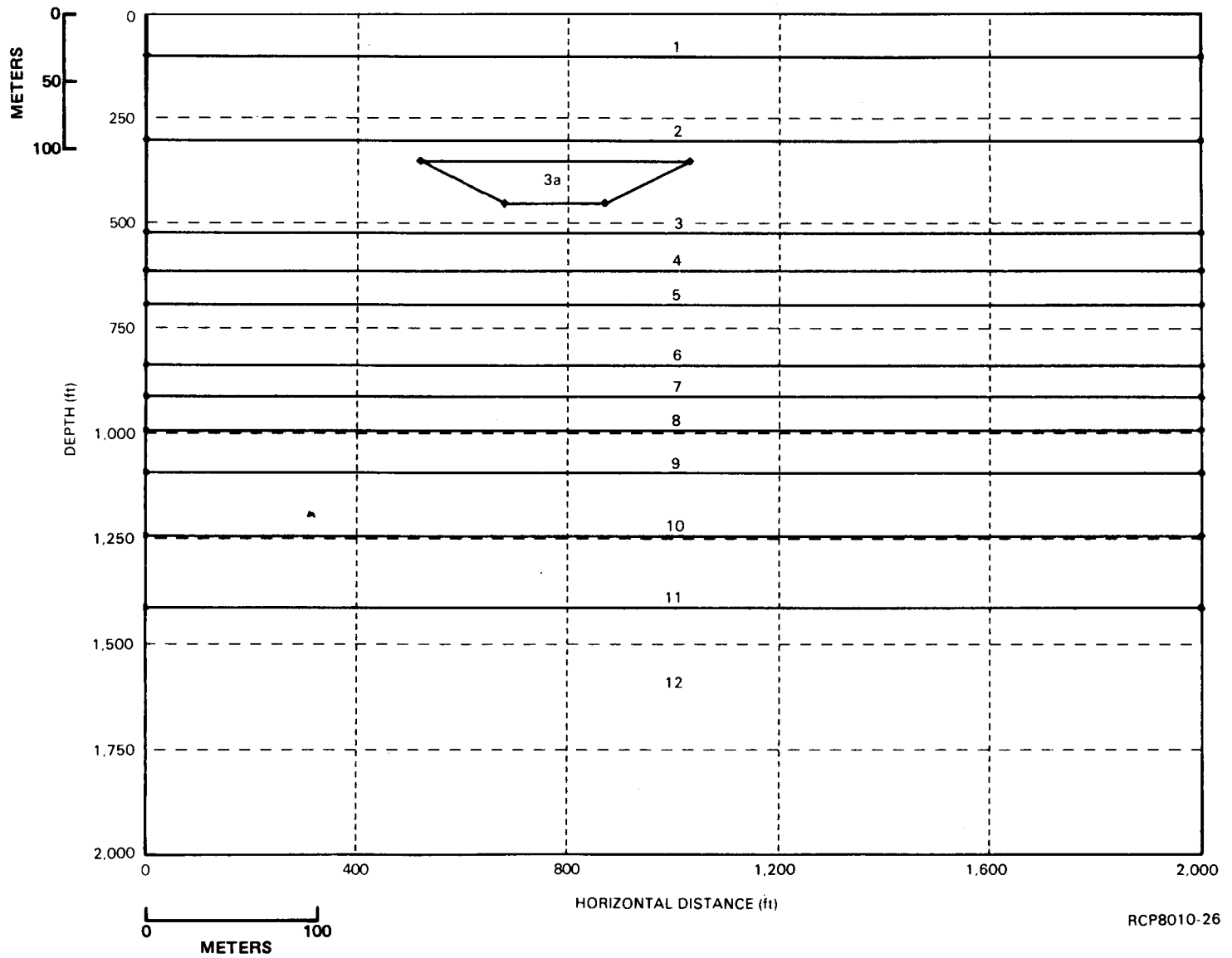

FIGURE B-15a. Geologic Model, Sediment Lens.

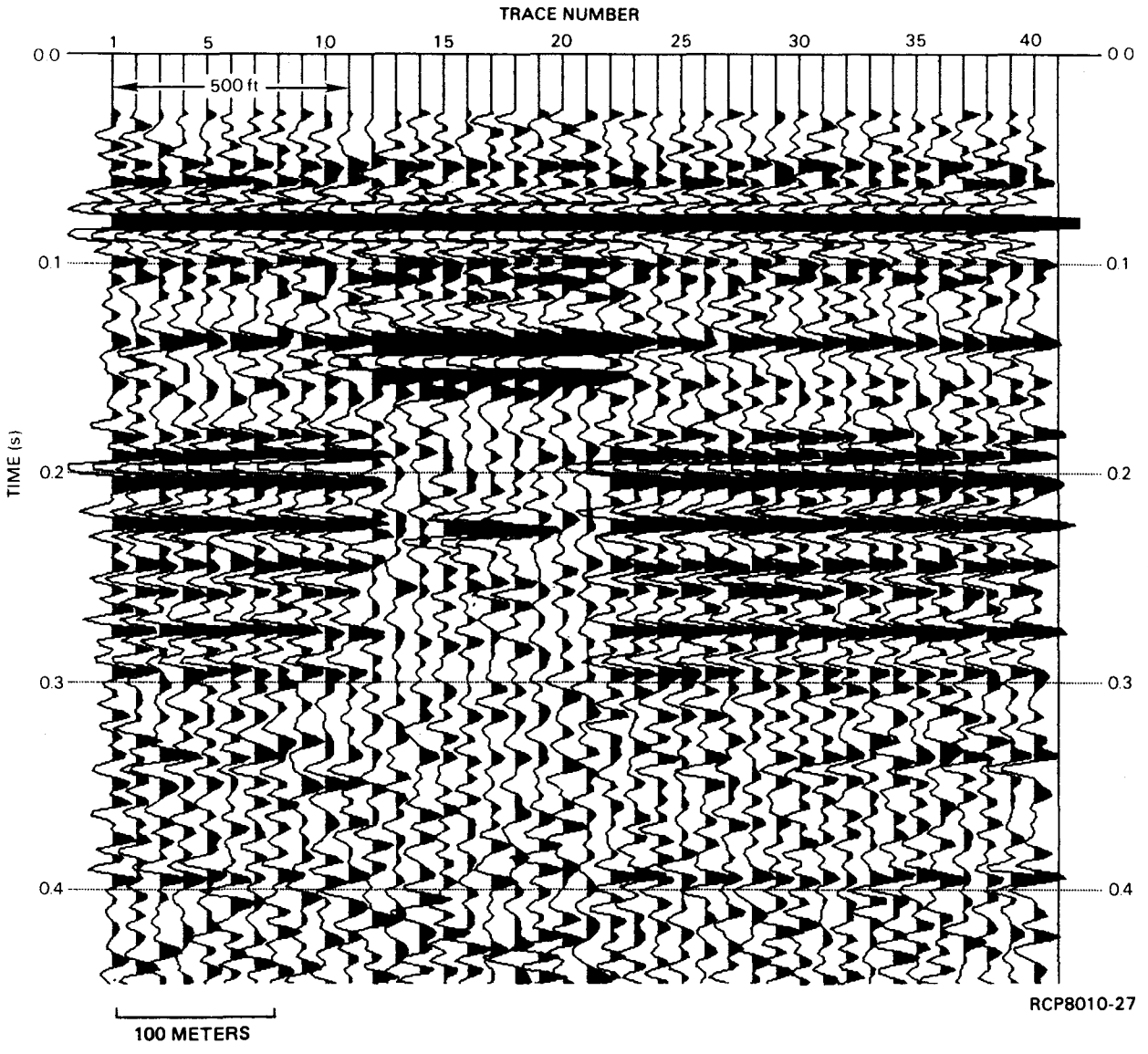

FIGURE B-15b. Seismic Response, Sediment Lens.

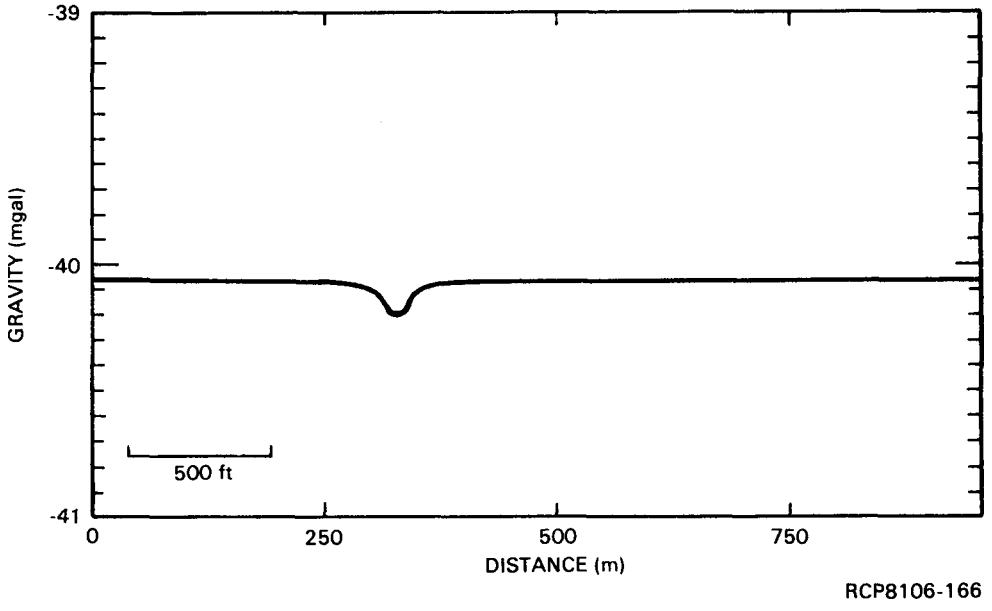

FIGURE B-15c. Gravity Response, Sediment Lens.

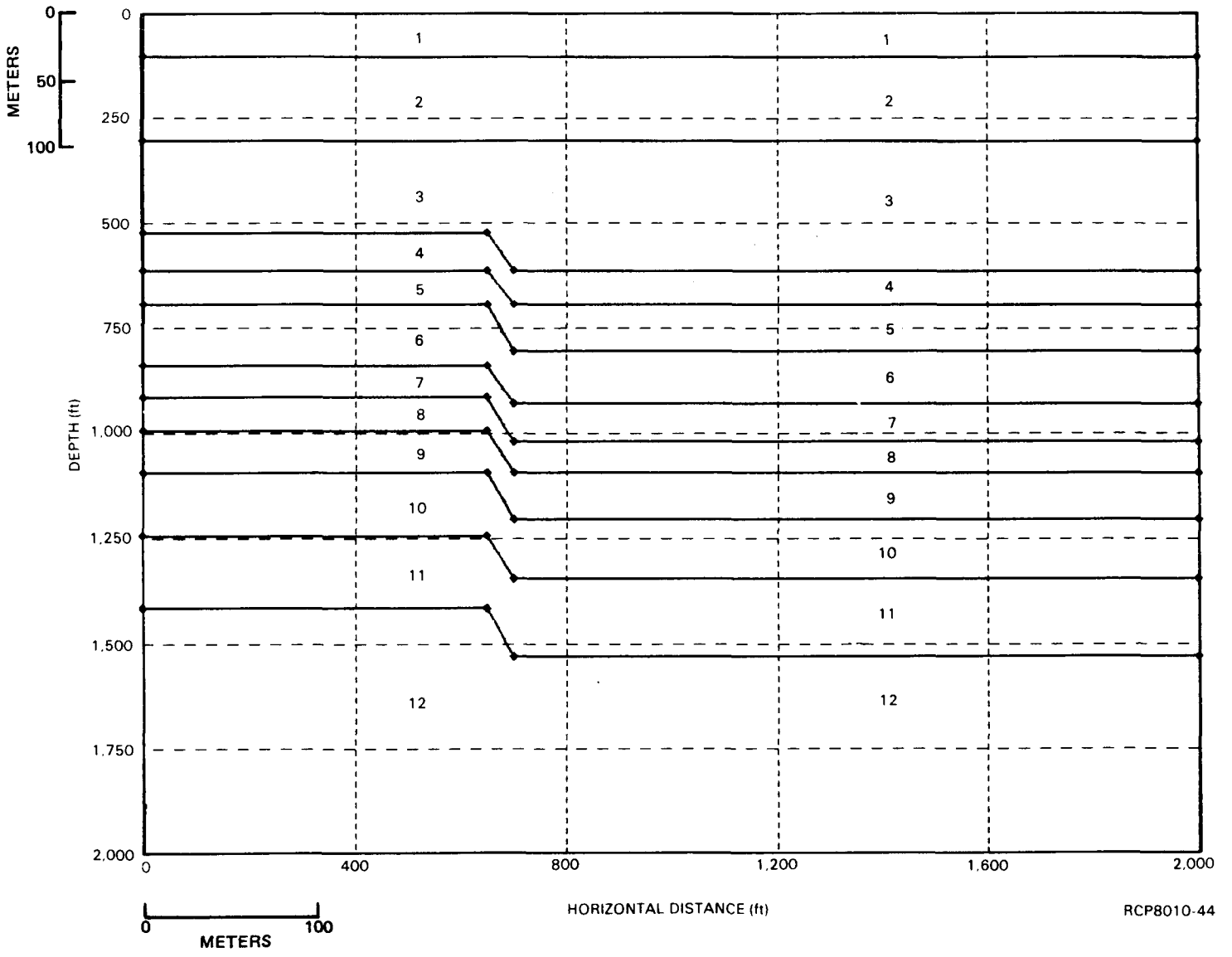

FIGURE B-16a. Geologic Model, Monocline.

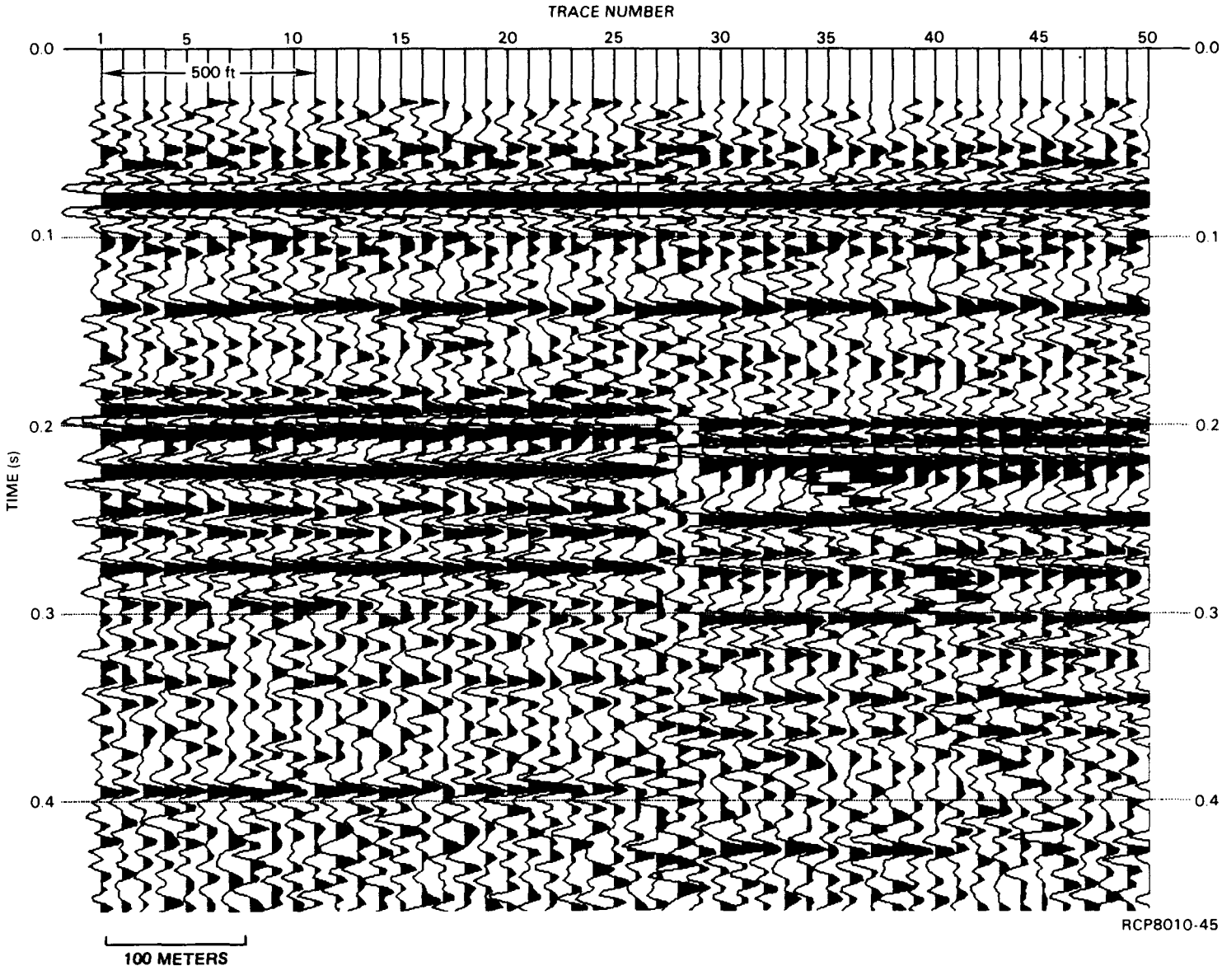

FIGURE B-16b. Seismic Response, Monocline.

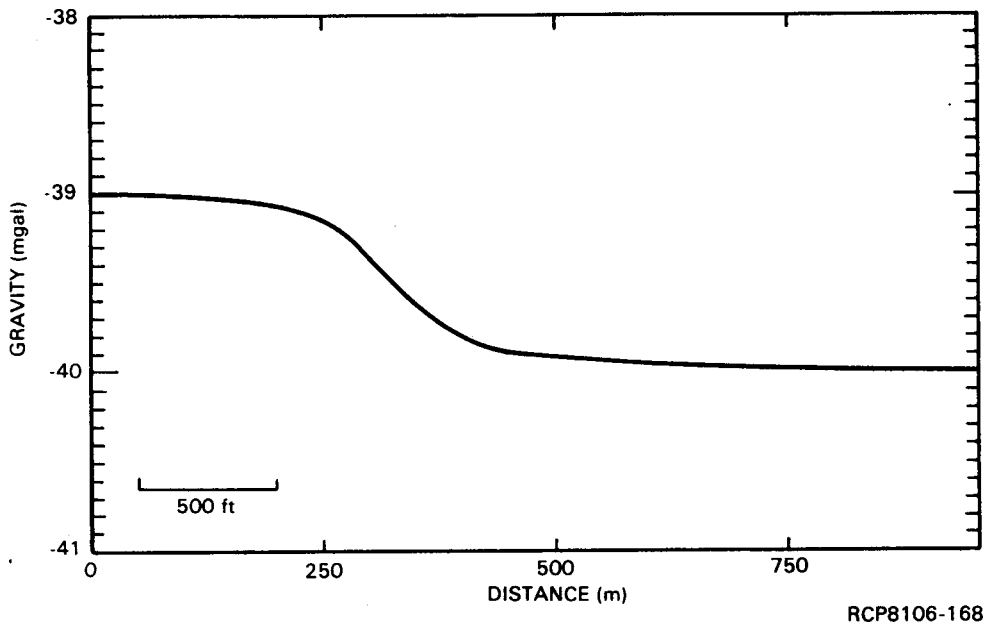

FIGURE B-16c. Gravity Response, Monocline.

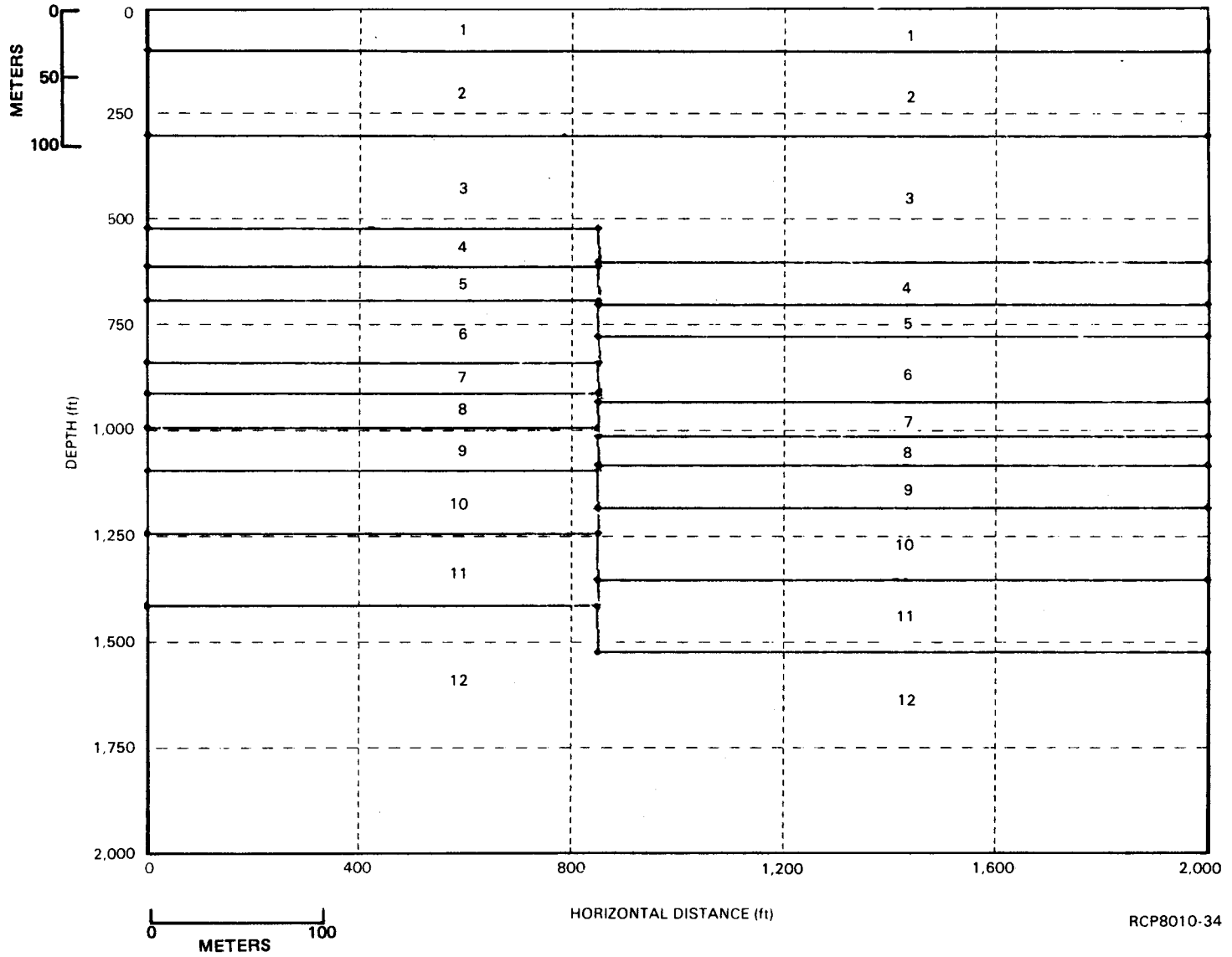

FIGURE B-17a. Geologic Model, Fault.

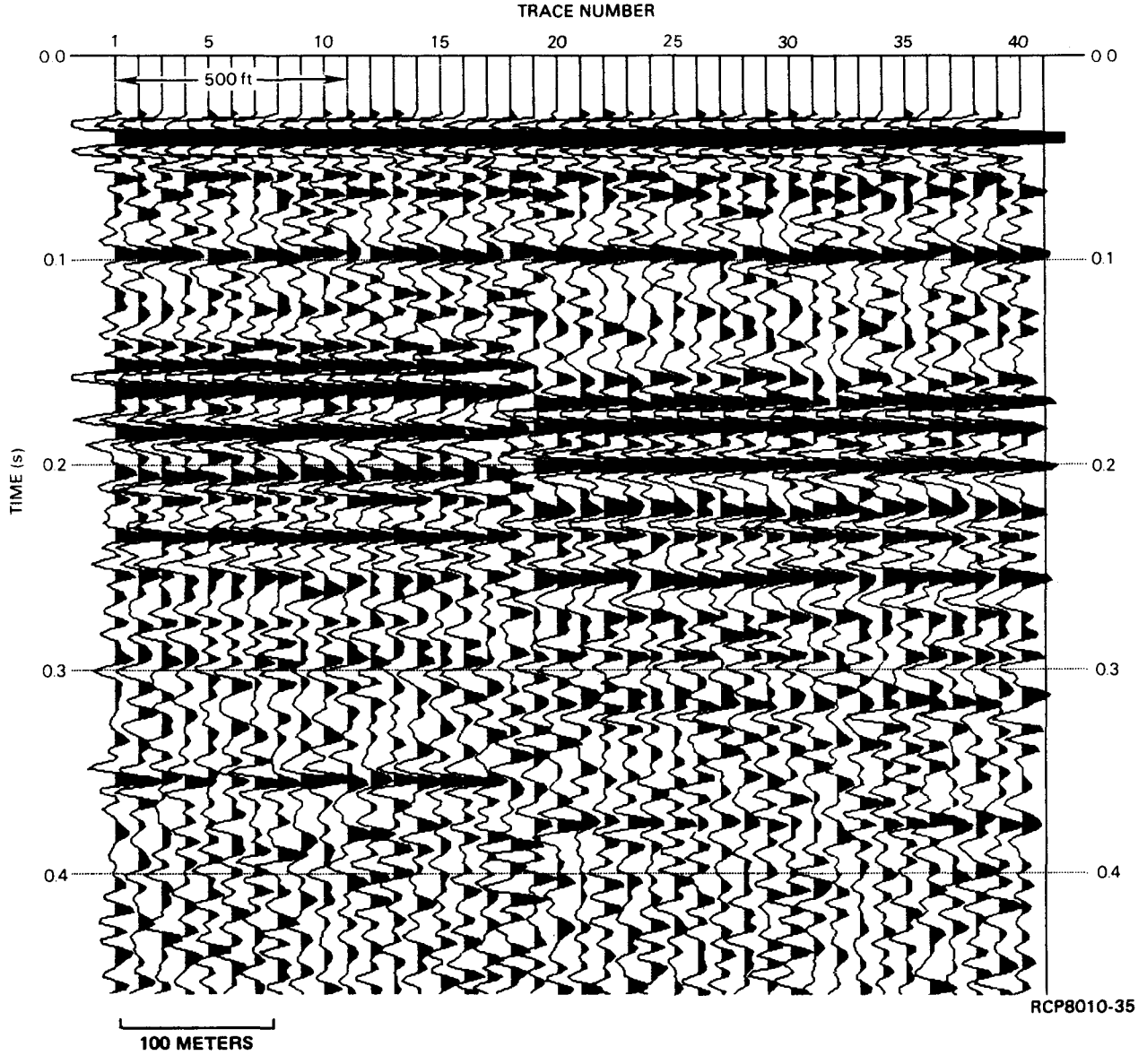

FIGURE B-17b. Seismic Response, Fault.

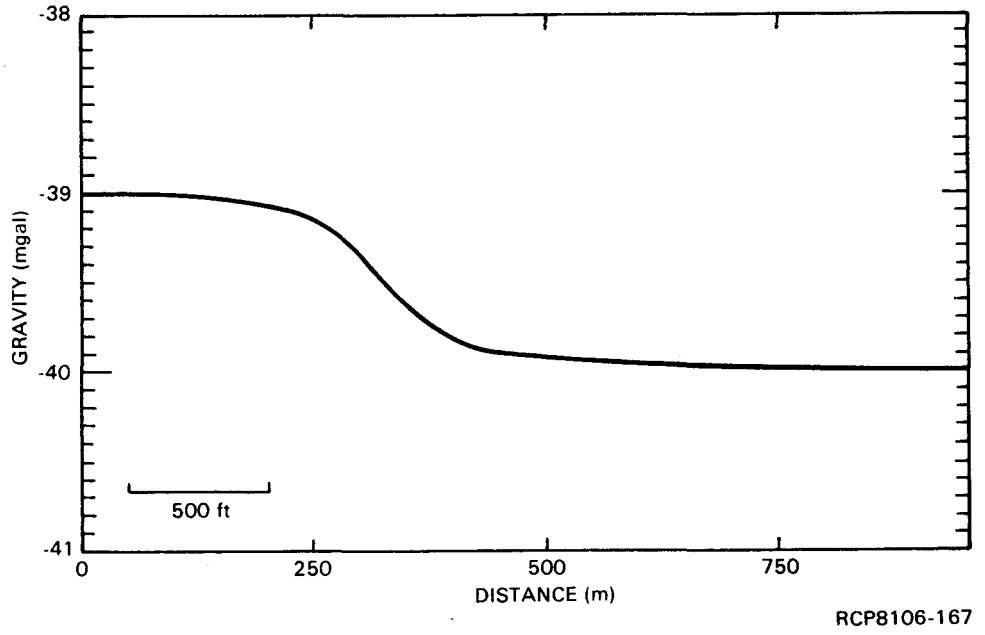

FIGURE B-17c. Gravity Response, Fault.

TABLE B-4. Stratigraphy and Geophysical Parameters Used for Modeling.

FORMATION	GEOLOGIC LAYER	VELOCITY (ft sec)	DENSITY (g cm^{-3})	LAYER NUMBER	DEPTH (ft BGS)
HANFORD	ALLUVIUM	2,500	1.9	1	
	PASCO GRAVELS	7,000	2.34	2	250
RINGOLD	UPPER, MIDDLE, AND LOWER RINGOLD	10,000	2.45	3	500
SADDLE MOUNTAINS	ELEPHANT MOUNTAIN MEMBER	11,000	2.85	4	
	RATTLESNAKE RIDGE INTERBED	6,000	1.94	5	
	POMONA MEMBER	11,000	2.85	6	750
	SELAH INTERBED	6,000	2.23	7	
	ESQUATZEL MEMBER	12,000	2.83	8	
	COLD CREEK INTERBED	7,500	2.11	9	1,000
	UMATILLA MEMBER	11,500	2.71	10	
	MABTON INTERBED	6,500	2.2	11	1,250
WANAPUM	(UNDIFFERENTIATED)	12,000	2.8	12	1,500
					1,750

(1 ft = 0.3048 m)

RCP8010-22

following discussion, the Cold Creek syncline area is arbitrarily subdivided into four areas: (1) western, (2) central, (3) eastern, and (4) northern (Fig. B-18).

WESTERN COLD CREEK SYNCLINE AREA

Geophysical surveys that are located in the western Cold Creek syncline area include:

1. Seismic-reflection line 3 (Fig. B-2 and B-19)
2. Seismic-reflection line 4 (Fig. B-2 and B-20)
3. Southern part of seismic-reflection line 5 (Fig. B-2 and B-21)
4. Seismic-reflection line 8 (Fig. B-2 and B-22)
5. Gravity lines 104, 440000, and 445000 (Appendix C)
6. Ground magnetics line 104 (Appendix C)
7. Multilevel aeromagnetics (Fig. B-8, B-9, B-11, and B-12).

Shotpoints (SP) referred to in the text are shown in Figure B-2.

Seismic-reflection line 5 and gravity and ground magnetics line 104 (Appendix C) were collected along the Army Loop Road, south of borehole DC-4/5 for a distance of 7.6 km (Fig. B-2). Seismic reflections from the TOB are discontinuous along line 5 (Fig. B-21), but generally indicate a gentle south dip.

Gravity and ground magnetics line 104 (Appendix C) was originally designed to investigate a seismic anomaly at SP 605 on line 5 (Fig. B-2). It was concluded that no response could be seen on the gravity or ground magnetics over the seismic anomaly.

An aeromagnetic anomaly (N-232) is plotted on Figure B-12 as having a fault-like source in the same general area as the seismic anomaly. Careful examination of the seismic-reflection sections, both line 5 (Fig. B-21) and line 3 (Fig. B-19), indicate that the nearest location of a shallow source for the aeromagnetic anomaly is 0.8 km to the northwest. Here, a fold is seen on both the seismic sections (lines 5 and 3). This aeromagnetic anomaly is discussed further in the section covering the northern Cold Creek syncline.

Continuous reflections on line 5 were recorded from the TOB south of SP 620 and the trough of the Cold Creek syncline at SP 820. The TOB here appears to be a smooth surface with a very low, apparent dip to the south. The original seismic section from the line segment shows three, broad, open undulations (centered at SP 720, 760, and 800) from reflections that appear to be from the TOB. The undulations have wavelengths of $\sim$600+ m and amplitudes (estimated using travel times) of $\sim$7 m. Reprocessing of this seismic

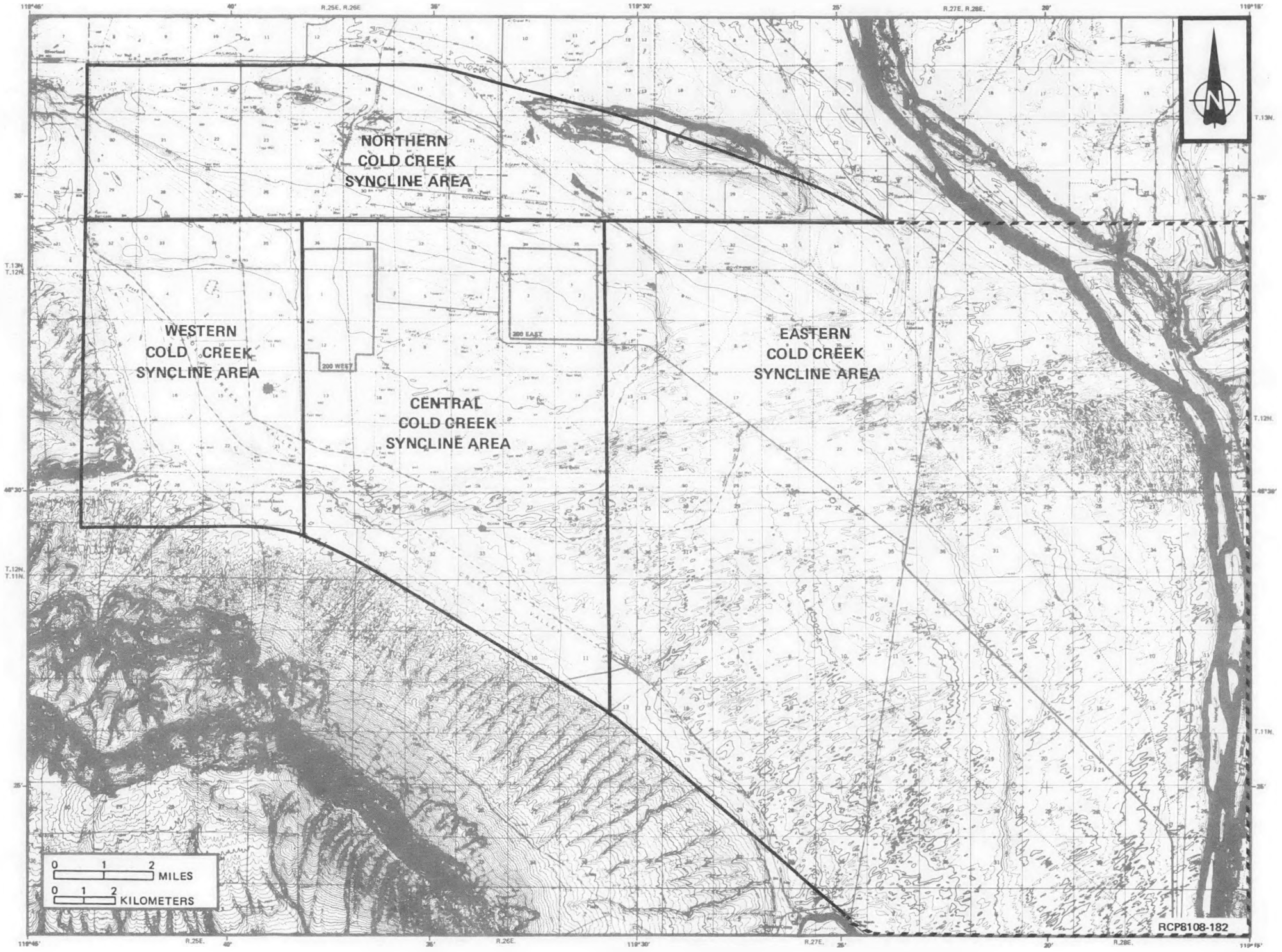

FIGURE B-18. Cold Creek Syncline Discussion Areas.

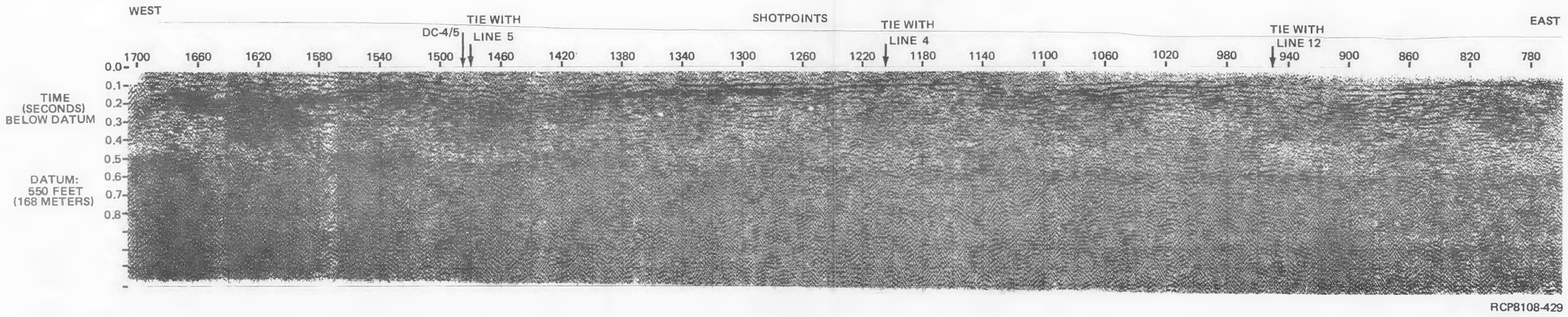

FIGURE B-19. Seismic Line 3.

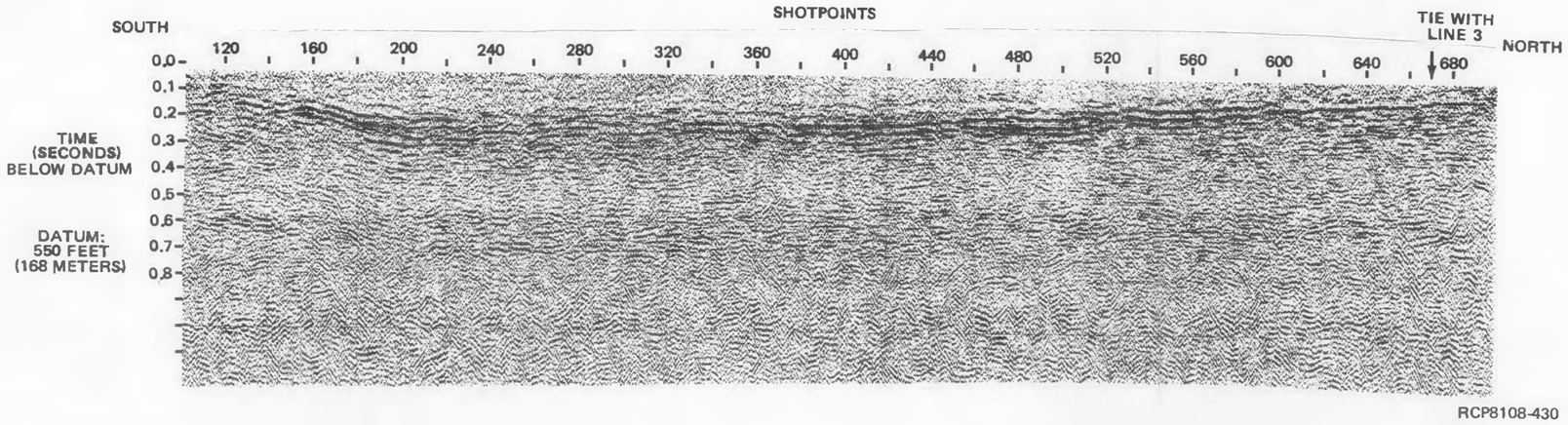

FIGURE B-20. Seismic Line 4.

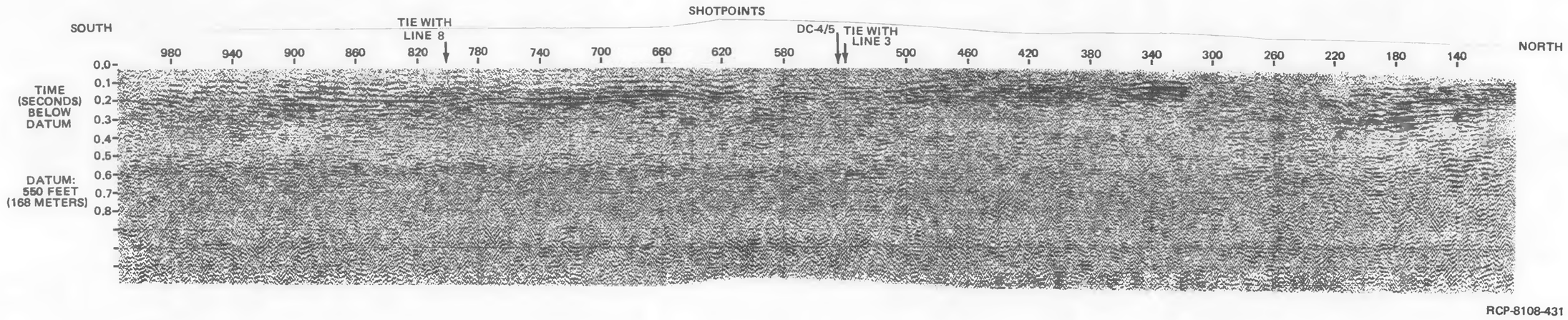

FIGURE B-21. Seismic Line 5.

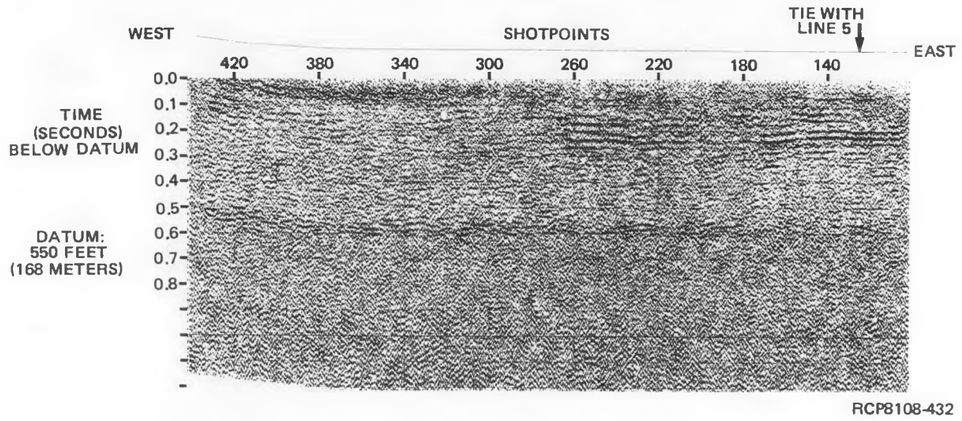

FIGURE B-22. Seismic Line 8.

section using different stacking velocities tended to smooth these undulations. This "smoothing" indicates that the undulations are probably caused by lateral variations in the velocities and densities of the sediments above the TOB.

Similar results are seen in the gravity data of line 104 which is located on top of line 5 (Fig. B-21). Between 1,500 and 7,500 m (see Appendix C), a general south dip is interpreted from decreasing gravity values toward the south. Undulations of ±0.5 mgal are seen on the profile and are similar to those seen on the seismic data. Gravity modeling has indicated that these undulations are probably due to shallow lenses of low-density material. The responses shown on both the seismic and gravity lines are indicative of the sediment variations at Hanford (see Chapter 2). A uniform, apparent dip to the south for the TOB is interpreted along the segment of line 5 between SP 650 and 820.

Aeromagnetic anomaly N-85 (Fig. B-12) has not been related to any anomalous features on line 5. The computer-calculated magnetic source depth of -579 m (-1,900 ft) MSL is well below the TOB and probably located in the Wanapum or upper Grande Ronde Basalts. No geologic interpretation is suggested for this anomaly at this time.

Segments of continuous and discontinuous reflections were recorded from the TOB along line 5 between SP 830 and 920. The TOB has been interpreted as a smooth surface with a uniform, low, apparent dip to the north.

All three data sets (seismic reflection, gravity, and aeromagnetics) indicate a broad, smooth, TOB surface centered about SP 820. The trough of the Cold Creek syncline was interpreted to be intersected by line 5 at SP 820. Gravity data (Appendix C) show broad undulations (discussed previously) which have a lowest value at ∿0.8 km to the south of SP 820. The gravity and seismic data have similar broad undulations superimposed on top of the low-dip rates into the syncline area.

Line 8 (Fig. B-22) was placed along an east-west traverse from borehole 37-82 to the eastern edge of Yakima Ridge, a distance of ∿4.8 km. The eastern end of line 8 intersects line 5 (Fig. B-21). Except for a small data dropout at SP 190 on line 8, continuous reflections from the TOB were recorded along the eastern segment of the line as far west as SP 260. West of SP 260, no reflections are identifiable from the TOB. A deeper horizon (of unknown depth) at a time of 600 ms on the seismic section indicates essentially flat-lying layers as far west as SP 360. At SP 320, the "deep" reflector appears to rise to the west. This rise is interpreted as the first indication of steeper dip associated with the Yakima Ridge structure (Fig. B-3).

Gravity survey grid lines 440000 and 445000 (Appendix C) were run along east-west traverses ∿1 km south and 1 km north, respectively, of line 8. These profiles suggest that the lowest point of the syncline (in this area) is west of line 5.

Additional indications of the configuration of the TOB are seen on the aeromagnetic data (Fig. B-8 and B-9). The Yakima Ridge structure is expressed as a large "high" which trends east.

Indications and constraints on the configuration of TOB indicated by geophysical survey results in the western Cold Creek syncline area are as follows:

1. Uniform apparent dip to the south between SP 620 and 820 on line 5

2. Uniform apparent dip to the north between SP 830 and 920 on line 5

3. Trough of the Cold Creek syncline at SP 820 on line 5

4. Zero apparent dip along line 8 between SP 140 and 260, except for two possible, small monoclinal flexures: one at SP 160 and the other at SP 240

5. Steeper northeast dip along line 8 constrained as being west of SP 360

6. Trough of the Cold Creek syncline on line 8 interpreted as near SP 210, but is not readily apparent

7. Crest of the buried Yakima Ridge structure roughly corresponds to the linear aeromagnetic high extending east from the eastern end of Yakima Ridge

9. The center of the Cold Creek Valley depression interpreted as corresponding to the low in the aeromagnetic total field located ∿3.2 km northeast of Yakima Ridge and centered near the common corner of sec. 4, 5, 8, and 9.

CENTRAL COLD CREEK SYNCLINE AREA

Geophysical surveys in the central Cold Creek syncline area include the following:

1. The southern part of line 4 (Fig. B-2 and B-20)

2. Lines 12 and 14 (Fig. B-2, B-23, and B-24)

3. Gravity and ground magnetic lines 102 and 103 (Appendix C)

4. Total coverage by a multilevel aeromagnetic survey (Fig. B-8, B-9, B-11, and B-12).

The southern part of line 4 (Fig. B-20) lies along an 8.5-km, north-south traverse which runs south of Route 11A (Yakima highway) and just east of the 200 West Area (Fig. B-2). Nearly continuous reflections were

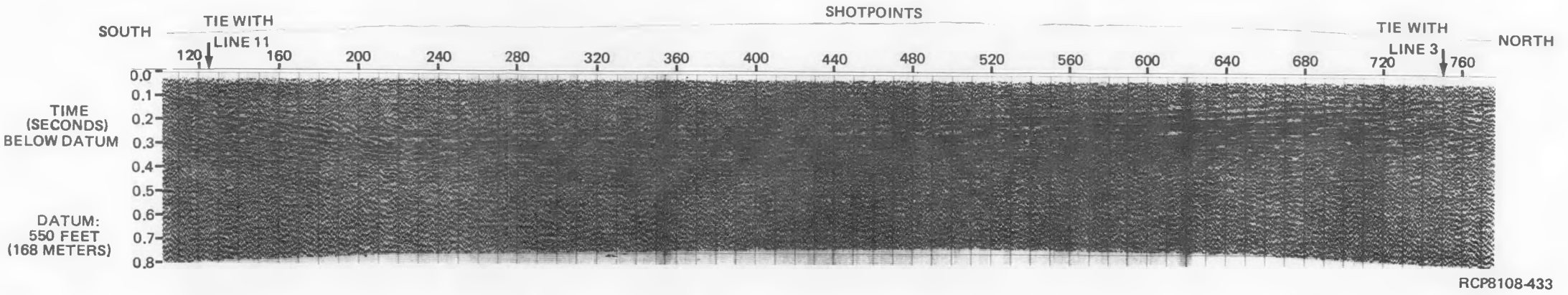

FIGURE B-23. Seismic Line 12.

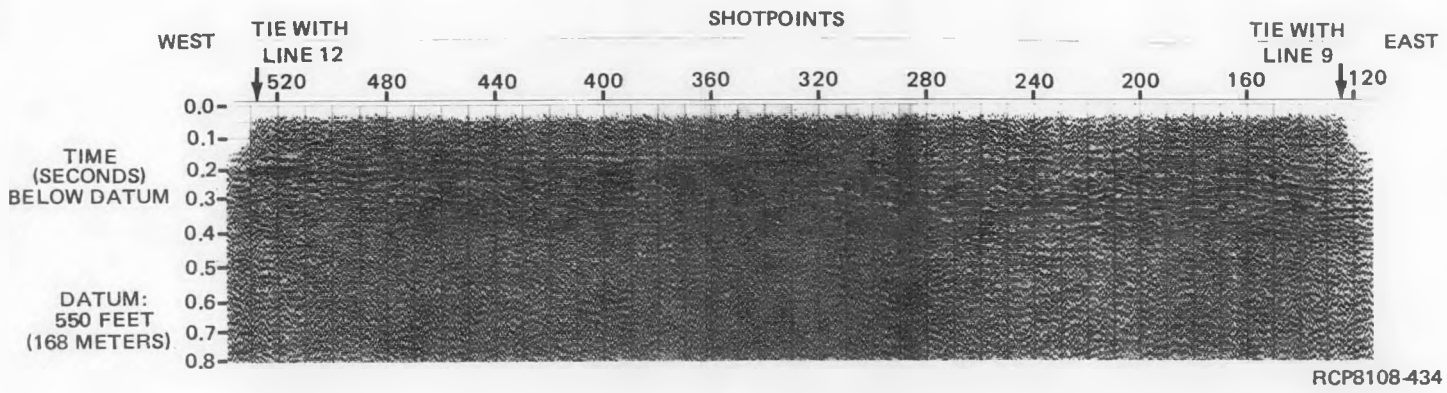

FIGURE B-24. Seismic Line 14.

recorded from the TOB along this entire traverse. The seismic section along line 4 (Fig. B-20) indicates a moderately smooth, south-dipping TOB between SP 670 and 540.

The aeromagnetic survey results (Fig. B-11 and B-12) indicate an anomaly (D-27) trending northwest and intersecting line 4 at SP 640 (see Fig. B-2). The estimate of the depth of the magnetic source for this anomaly is more than -305 m MSL elevation, well below the TOB. This anomaly appears to have no corresponding feature in the TOB on the record from line 4 (Fig. B-20).

Three seismic anomalies on line 4 are located at SP 590, 530, and 510 (Fig. B-2). These anomalies were evaluated (Appendix C) using ground magnetics and gravity in conjunction with available information on the sediment geology of that area (Chapter 2). The anomaly at SP 590 showed no determinable response to either the gravity or the ground magnetics methods (see Appendix C for more details). Based on gravity and ground magnetics data (Appendix C), the anomalies at SP 530 and 510 again revealed that little or no bedrock offset could be seen.

A uniform, apparent south dip on the TOB between SP 500 and 400 is shown on line 4 (Fig. B-20). The dip on the TOB reflectors appears to be slightly less at SP 400.

As in aeromagnetic anomaly D-27 above, no evidence of a source for aeromagnetic anomaly N-70 (Fig. B-11 and B-12) is seen on line 4. Although a seismic anomaly is located at SP 370, the reflection section indicates no change in dip across this anomaly.

No additional geophysical evidence (seismic or gravity) is available to dispute or support aeromagnetic anomaly N-235.

The trough of the Cold Creek syncline is interpreted between SP 400 and 200 and as being near SP 230. Sediments overlying the TOB are ~180 m thick along this section of line 4; this thickness probably causes the slight loss in reflector continuity that can be seen on the record. Seismic reprocessing has not appreciably improved the data quality.

Aeromagnetic anomaly D-218 (Fig. B-11) has a shallow source (estimated to be near the surface) and has been interpreted as a "high" in the TOB. The southeastward continuation of anomaly D-218 would intersect line 4 near SP 280, and the record from line 4 (Fig. B-20) does indeed show a slight high in the TOB near SP 280. The TOB has been contoured to honor this interpretation. The high at SP 280 is, thus, the only structure on line 4 that interrupts the overall uniform south dip between the anomaly at SP 510 and the trough of the Cold Creek syncline at SP 230.

South of SP 200, the TOB rises steeply along the north limb of the buried Yakima Ridge structure. A high gradient in the aeromagnetic total field (Fig. B-8 and B-9) corresponds with the steep "rise" in the seismic data.

Line 12 extends a distance of 9.6 km south of its intersection with Route 11A (Yakima Highway) to the southeast corner of sec. 28, T. 12 N., R. 26 E. just west of the 200 East Area (Fig. B-2). Reflections from the TOB between SP 750 and 240 on Figure B-23 show a remarkably uniform, apparent dip to the south with no undulations or other structures. However, a very slight monocline with less dip to the south is suggested near SP 350. No seismic anomalies were interpreted along the entire length of line 12.

The trough of the Cold Creek syncline was interpreted to be crossed on line 12 (Fig. B-23) at SP 240. South of SP 240, the TOB rises abruptly, but uniformly onto the buried north flank of the Yakima Ridge structure.

The apparent uniformity of the TOB dip along line 12 would seem to constrain the interpretation on the configuration of the TOB along this line.

Aeromagnetic anomalies N-86, N-71, and D-217 (Fig. B-11) are not seen to cross line 12. The computer-estimated depths of the anomalies are well below the estimated elevation for the TOB in this area (-300 to -700 m below MSL).

Aeromagnetic anomalies N-86, N-71, and N-243 (Fig. B-11) together bound a high in the aeromagnetic total field (Fig. B-8 and B-9) which strikes to the northeast from the buried Yakima Ridge structure. Again, no evidence is seen on the seismic lines for either of these features. This high might represent a basalt high buried beneath the younger flows and, therefore, have little or no expression in the TOB. Aeromagnetic features (anomalies and total-field contours) in this part of the Cold Creek syncline are still under investigation and the interpretation of some is questioned. Present interpretations of the TOB in this region of the central Cold Creek syncline have relied mainly on seismic reflection and borehole data to indicate the TOB surface configuration. Only in this area of the Cold Creek syncline are there found to be discrepancies between the interpretations of the seismic and aeromagnetic data. In the other areas of the Cold Creek syncline, especially the eastern section, much better agreement is found to indicate that the aeromagnetic method is very sensitive to bedrock structure.

Line 14 runs east-west, oblique across the northeastern limb of the buried Yakima Ridge structure which plunges southeast at this location. Line 14 (Fig. B-24) shows undulations in the TOB which are interpreted as second-order structures similar to the parasitic folds associated with the Umtanum Ridge-Gable Mountain structure in the Gable Mountain-Gable Butte area (Fecht, 1978). On Figures B-8 and B-9, the north side of the buried Yakima Ridge structure has a steep gradient in the western Cold Creek syncline, but a moderate gradient in the eastern Cold Creek syncline. The Yakima Ridge structure can be traced using the aeromagnetic and seismic data as far east as line 9 (Fig. B-25). Aeromagnetic anomalies D-29 and N-246 (Fig. B-11) are interpreted to represent the northern edge of the plunging structure as it dies out to the east.

Direct indication of the configuration of the TOB and constraints on the configuration of the TOB in the central Cold Creek syncline area are as follows:

1. South dip and uniform apparent dip rate between SP 660 and 600 and between SP 480 and 380 on line 4

2. Trough of Cold Creek syncline is probably at SP 230 on line 4

3. North dip from SP 100 to 200 on line 4, except for slight south dip at SP 150

4. South dip and very uniform apparent dip on line 12 between SP 750 and 240, except for a very slight monocline at SP 350

5. Uniform north dip from SP 120 to 240.

EASTERN COLD CREEK SYNCLINE AREA

Geophysical surveys in the eastern Cold Creek syncline area are:

1. Lines 9, 10, 11, and 13 (Fig. B-25, B-26, B-27, and B-28, respectively)

2. Lines 1 and 2 (Fig. B-29 and B-30, respectively)

3. A multilevel aeromagnetic survey (Fig. B-8, B-9, B-11, and B-12).

East of the 200 East Area (Fig. B-2), the aeromagnetic total field contour maps (Fig. B-8 and B-9) show a steep gradient of tightly spaced contours trending north-northeast to southwest. Seismic-reflection data on line 3 (Fig. B-19, east-west) and line 13 (Fig. B-28, mainly north-south) provide constraints of the steep gradient area of aeromagnetic maps.

Line 13 (Fig. B-28) indicates an apparent dip to the south, but is seen to be almost on-strike with the north-south trend of the aeromagnetic data. The reflectors are discontinuous for much of line 13, but are interpreted to indicate a uniform dip rate.

Line 3 (Fig. B-19) shows discontinuous reflectors which dip steeply to the east at SP 460 to 400. A zone of steep dip is constrained by the seismic-reflection and aeromagnetic data to be $\sim$1.6 km wide. This zone is located just east of line 13 in sec. 32 and 33, T. 13 N., R. 27 E., and sec. 4, 5, 8, and 9, T. 12 N., R. 27 E. (Fig. B-2). The trend of the zone is north-south in sec. 32 and 33 and northeast-southwest in sec. 8 and 9. Line 13 and the aeromagnetic contours (Fig. B-8) indicate that the zone of steep dip at the north becomes gentler toward the south. Near line 10 (Fig. B-26), the reflectors show gentle east dip from SP 747 to 530 as this steep gradient in the aeromagnetic total field swings around to the east.

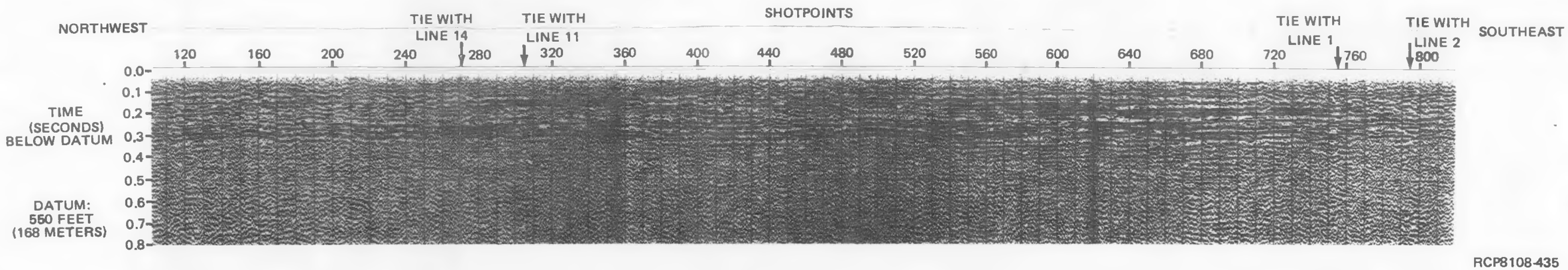

FIGURE B-25. Seismic Line 9.

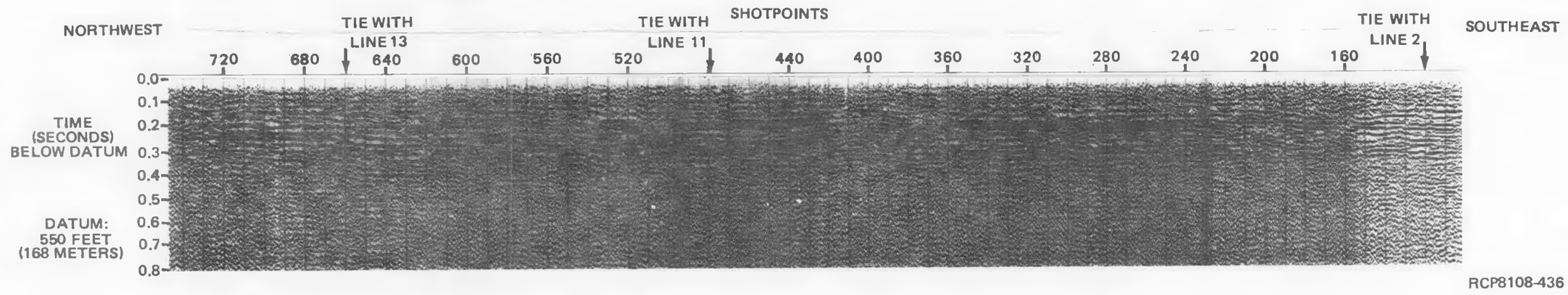

FIGURE B-26. Seismic Line 10.

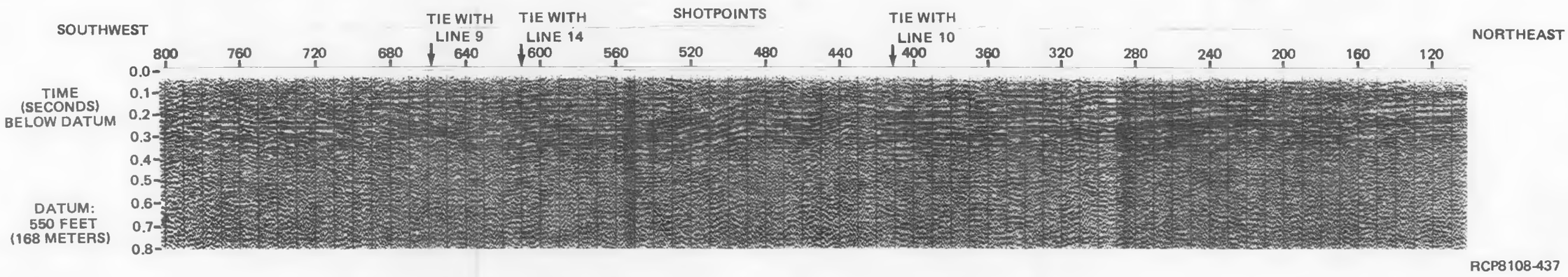

FIGURE B-27. Seismic Line 11.

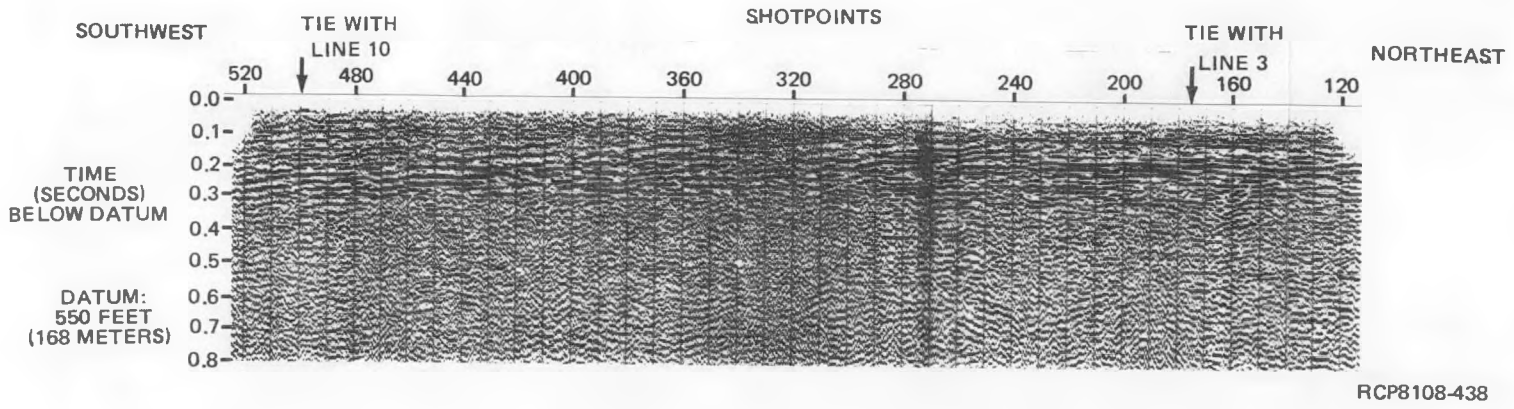

FIGURE B-28. Seismic Line 13.

FIGURE B-29. Seismic Line 1.

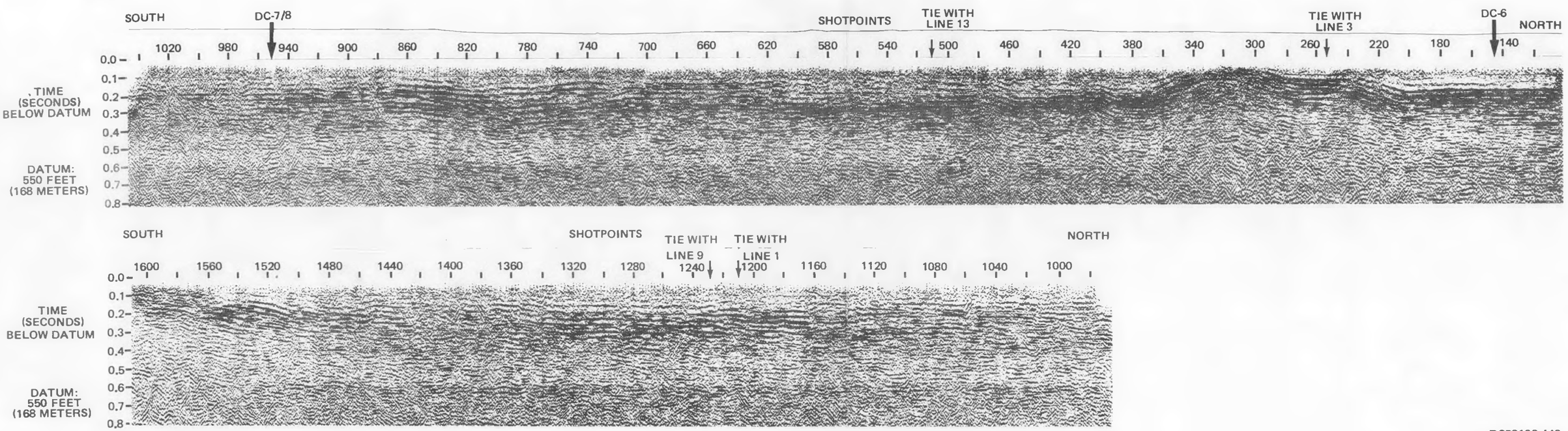

RCP8108-440

FIGURE B-30. Seismic Line 2.

South dip is seen on the seismic-reflection section of line 11 (Fig. B-27) between SP 101 and 420. The TOB reflections are fairly smooth, with some undulations.

South of borehole DB-4 (SP 259) on line 11 (Fig. B-27), there are several sets of reflectors, both shallow (sediment) and deeper (basalt). At SP 420, south of the intersection of line 11 with line 10, the lower reflectors are disrupted. Between SP 440 and 450 on line 11, the reflections dip abruptly south. An abrupt anomaly is indicated, yet the shallow reflectors continue smoothly across this zone between SP 420 and 460. Aeromagnetics on Figure B-8 and gravity data recently acquired by Weston Geophysical Research over this zone both show a north-dipping gradient. Both gravity and aeromagnetics indicate higher values to the south. This anomaly is interpreted as a deep (TOB at -45 m), buried anticline which has a steeply dipping north face. This same feature is expressed on line 10 (Fig. B-26) centered at SP 400. The aeromagnetic anomaly (D-22; Fig. B-11) is interpreted to represent this anticlinal feature.

Between SP 500 and 530 on line 11 (Fig. B-27), the reflections dip to the south into a depression. The low in the time of the reflections extends to SP 657 at the intersection of line 11 with line 9 (Fig. B-2). At this point, the reflections rise steadily to the southwest toward the end of the line. This depression between SP 530 and 657 corresponds to a relative low on the aeromagnetic contour maps. These lower magnetic total-field values south of the anticlinal feature at D-22 also trend northwest-southeast. This depression is interpreted to be the location of the trough of the Cold Creek syncline. The lowest point of the seismic data is between the intersection of lines 9, 11, and 14 (Fig. B-2).

Additional aeromagnetic anomalies are interpreted to define the TOB in this area. D-28 on Figures B-11 and B-12 is of shallow-source depth from ∿90 to -180 m MSL and strikes northwest-southeast similar to D-22. No additional geophysical data are currently available to compare with the aeromagnetic data, but a small fold could be present in this area. N-242 (Fig. B-11) is projected to cross line 9 where a small, anticlinal feature at SP 150 is seen. Southeast from N-242, line 9 shows smooth, flat, fairly continuous reflections down the length of the line. It is interpreted that line 9 is located over the strike line of the Cold Creek syncline.

Lines 9, 1, and 2 (Fig. B-2) intersect at a low point (on lines 1 and 2) which is interpreted as the trough of the syncline. The seismic-reflection data are discontinuous in this immediate vicinity. The lack of coherent reflection is probably due to loss of signal through the overlying, unconsolidated sediments. Line 1 (Fig. B-29) shows general trends of low dip to the east from the west end of the line to SP 950. A domal structure has been interpreted between SP 920 and 780. Between SP 750 and the eastern terminus of the line, a general west dip exists with minor undulations.

In the eastern Cold Creek syncline, the TOB configuration is seen to be:

1. Steep dip trends north-northeast to southwest, located just east of line 13

2. An anticlinal feature (a high in the TOB) trends west-northwest to east-southeast and is located near the intersection of lines 10 and 11

3. The Cold Creek syncline axis is located in a narrowed, northwest-southeast-trending trough centered at the intersection of lines 9, 11, and 14.

The syncline trough is also located beneath the intersection of lines 9, 1, and 2.

NORTHERN COLD CREEK SYNCLINE AREA

Geophysical data pertinent to this discussion of the northern Cold Creek syncline are:

1. Line 3 (Fig. B-2 and B-19)

2. The northern parts of lines 4 and 5 (Fig. B-2, B-20, and B-21)

3. Various gravity and ground magnetics profiles (see Appendices C, D, and E).

Discussion of geophysical surveys associated with the Umtanum Ridge-Gable Mountain structure are in Appendices D and E.

Line 3 (Fig. B-19) is an east-west profile crossing the center of the Hanford Site. The discussion of this line will center on that piece located between the Yakima Barricade and a point just west of borehole DC-1/2 (Appendix A; Fig. B-19).

Near SP 1680 on line 3, some segments of continuous reflectors are seen. A small anticline with a steep eastern face is shown by the basalt reflections at SP 1560 at 1500 just west of borehole DC-4/5 and line 5. A similar feature is also seen on line 5 at SP 440 to 480. It appears from the seismic-reflection data that DC-4/5 sits in a minor depression (on the seismic data), which is estimated to be 30 m lower than the high to the west.

Aeromagnetic data from the 1,220-m-level total field map (Fig. B-9) indicates a high at the same location as the seismic sections. This feature trends mostly east-west with a northeasterly elongation. Anomaly N-232 (Fig. B-11) would appear to be improperly placed by the Werner deconvolution computer analysis. A shift of only 750 m to the northwest would place it over the eastern edge of the small anticline seen on the seismic data. Recent gravity data collected by BWIP confirm the location of this small fold at the seismically derived location.

East of borehole DC-4/5 on line 3 between lines 5 and 4, the basalt reflectors rise at a low dip rate. This southwest dip is smooth and very gentle, except for several anomalies on the seismic data at SP 1340 and 1300. These anomalies have not been honored in constructing the TOB map.

Anomalies at SP 1340 and 1300 have most likely been caused by errors in the velocity correction and time-static computer programs used in the seismic data processing.

Velocity analyses are located at SP 1363, 1333, and 1263. The velocities listed on the seismic section, which have been used to make normal-moveout corrections, vary laterally by 760 m/s on the same reflecting horizon. Reflections from the TOB should generally possess similar velocities within an estimated range of ±180 m/s. This error in the data processing causes the reflections from the TOB within the common depth point gather to destructively stack when the gathers are combined to form the seismic section. Time-static corrections are calculated from the data after velocity corrections are applied. If the velocities are in error, then the time statics will generally also be in error. These data processing problems have occurred at SP 1340 and 1300. Even in the presence of these anomalies, the reflections from the TOB indicate a smooth, uniform dip to the southwest.

An aeromagnetic anomaly (D-27/N-231) (Fig. B-11 and B-12) is located near the intersection of lines 3 and 4. An additional anomaly (N-233) has been proposed ∿1.6 km to the east. Both of these anomalies trend northwest-southeast. The aeromagnetic anomalies are located near three seismic anomalies which bound a small depression at SP 1110 on line 3. The seismic anomalies are, again, poorly supported. Drastic lateral changes in the normal-moveout velocities were used to stack the common-depth point data. These velocities were judged to vary by too great a margin to be reasonable. Faulting at these seismic anomalies cannot be supported without further processing or another detailed geophysical/geological investigation. The seismic and aeromagnetic anomalies probably indicate the fold edges of a synclinal depression in the TOB.

The area near borehole DB-10 (Appendix A) is discussed in Appendix D and previously in Myers, Price and others (1979). In general, geophysical data support the presence of small, sympathetic folds generally paralleling those on Gable Mountain.

A steep gradient on the aeromagnetic, seismic, and recently collected gravity data (Weston Geophysical, 1978b) is indicative of steeply dipping basalt just east of borehole DB-10. As discussed in the earlier section on the eastern Cold Creek syncline, this feature is an abrupt structure to the north near Gable Mountain and broadens to the south.

Indications or constraints on the TOB from geophysical surveys in the northern Cold Creek syncline are:

1. Location of a small anticlinal fold just west of borehole DC-4/5 and trending northeast toward Gable Butte

2. Low, uniform dip to the southwest between lines 5 and 4

3. A depression in the TOB located at SP 1110 on line 3, which trends northwest-southeast based on aeromagnetic data

4. Fairly smooth southwest dip from SP 1080 to 960 on line 3

5. Steep east dip on the eastern edge of a northwest-southeast-trending high. The high is located at borehole DB-10 and the steep dip is centered 1,200 m to the southeast of borehole DC-10 on line 3 at SP 460 to 400.

CONCLUSIONS

In general, both the seismic and aeromagnetic survey data show the Yakima folds to be plunging and dying out (i.e., becoming smaller in size as they progress through the Hanford Site). Although the seismic data reveal a much smoother, flater surface than the aeromagnetic data seem to indicate, many small trends are correspondent.

Discrepancies between seismic and aeromagnetic interpretations have not yet been resolved. For this reason, modeling of both the seismic and aeromagnetic data is needed to investigate anomaly-causing structures which could be located near or in hydrologic flowpaths at the edges of the reference repository location. Additionally, a number of anomalies shown on Figures B-11 and B-12 seem to indicate structures which have a northeasterly trend within the Cold Creek syncline area. Detailed seismic velocity and magnetic parameter information is being gathered in and around the reference repository location to investigate these anomalies.

APPENDIX C - GEOPHYSICAL INVESTIGATIONS IN THE SOUTHWESTERN COLD CREEK SYNCLINE

J. R. Kunk

INTRODUCTION

Seismic-reflection surveys in the southwestern Cold Creek syncline area (Fig. C-1) located five anomalies, interpreted by Seismograph Service Corporation to be bedrock faulting (Appendix B). The anomalies were located at shotpoints (SP) 370, 510, 530, and 590 on seismic line 79-4 and at SP 605 on line 79-5 (Fig. C-2). Ground magnetic and gravity surveys were located over these five anomalies to further assess their structural significance.

Additional ground magnetic and gravity surveys were located in the extreme southwestern portion of the Cold Creek syncline to determine the configuration of the surface of the basalt in this area. Previous work reported in Myers, Price and others (1979) had relied on structural trends shown in nearby outcrops and sparse well data to construct a top-of-basalt contour map for this area. The question arose as to whether there might be unrecognized, buried basalt structures in the area described above.

PREVIOUS WORK

Previous gravity surveys in the southwestern Cold Creek syncline area (Fig. C-1) include the work of Peterson (1965, 1966), Weston Geophysical (1978a), Richard and Deju (1977), Konicek (1975), Robbins and others (1975), Deju and Richard (1975), Richard and others (1977), and WPPSS (1977). However, these surveys were regional in scope, with the station interval too large to supply the detail needed to evaluate the seismic anomalies or to determine the detailed configuration of the basalt surface. The gravity surveys by Lillie and Richard (1977) and Richard (1976) did prove useful, but weathering and erosion had disturbed their survey markers preventing the relocation of their stations. Recollection of data along these surveys was, thus, required.

Aeromagnetic surveys covering the southwestern Cold Creek syncline area consisted of a 150-m terrain clearance survey by Raymond and McGhan (1963), a 4,570-m constant elevation survey by Zeitz and others (1971), a 150-m terrain clearance survey by Swanson and others (1979c), and a 300-m terrain clearance survey by Weston Geophysical (1978b).

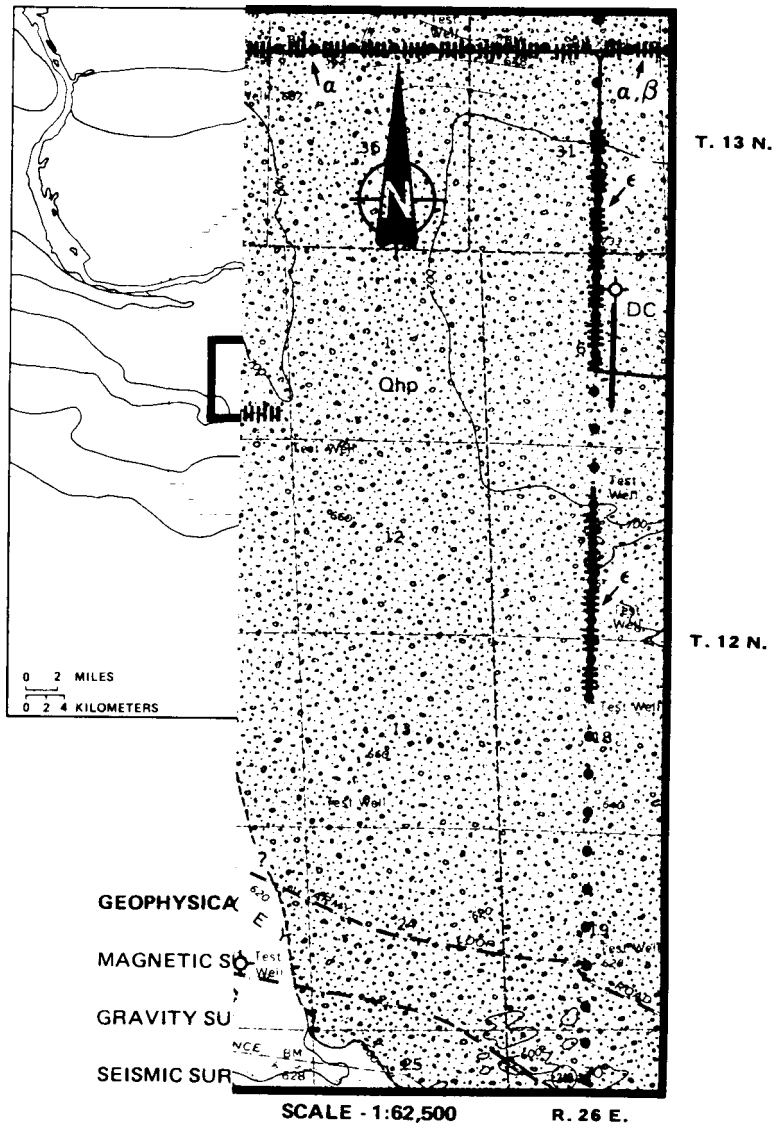
T. 13 N.
T. 12 N.
R. 26 E.
Qhp
DC
0 2 MILES
0 2 4 KILOMETERS
SCALE - 1:62,500
GEOPHYSICA
MAGNETIC SU
GRAVITY SU
SEISMIC SUR
OVERL
GRAVITY AND SEISM
GRAVITY, MAGNETI
'8a
RCP8108-193

FIGURE C-1. L

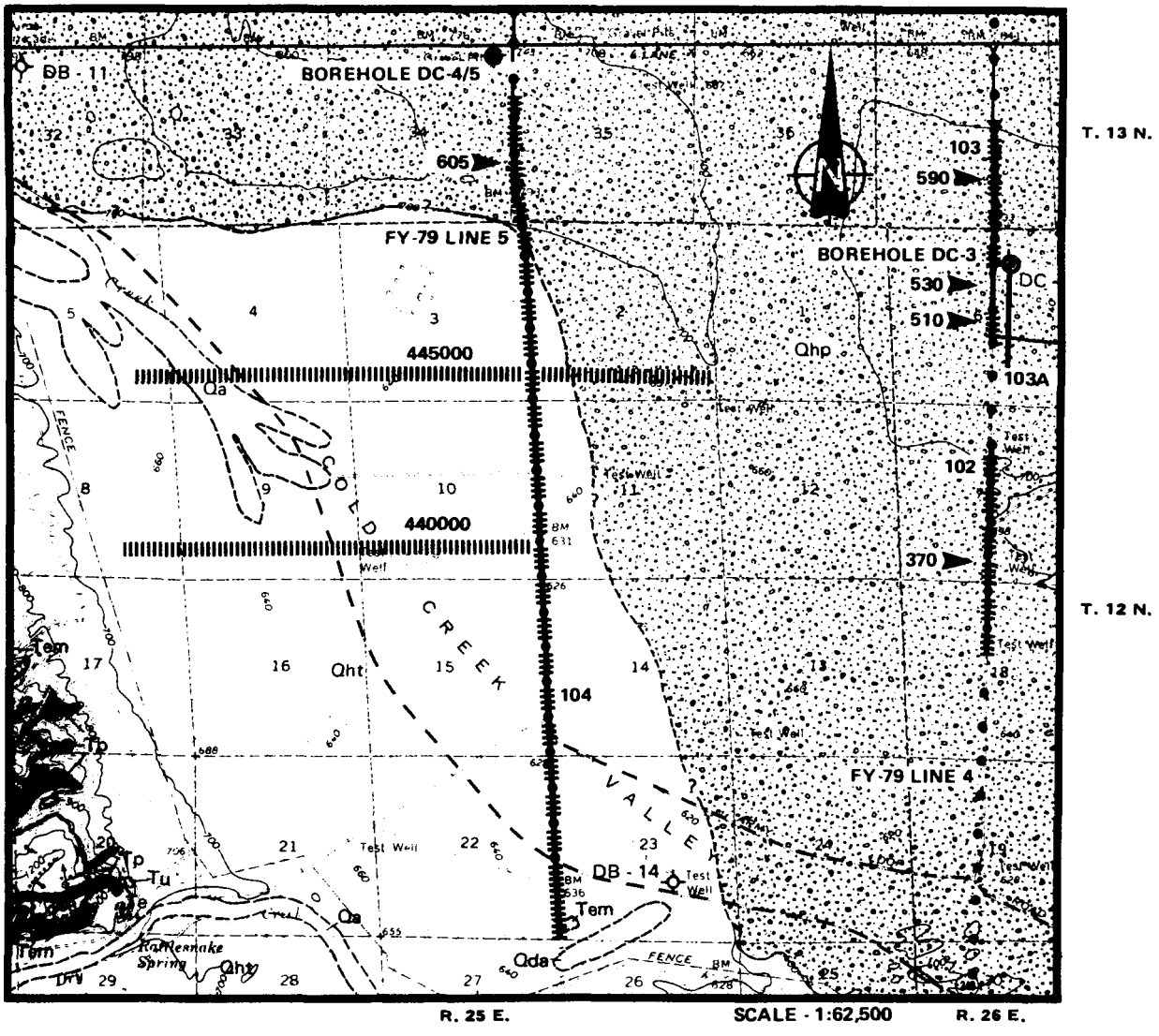

GEOPHYSICAL TRAVERSE SYMBOLS

MAGNETIC SURVEY	———
GRAVITY SURVEY	▮▮▮▮▮▮▮▮▮▮▮▮
SEISMIC SURVEY	• • •
TRAVERSE NUMBER	103
LOCATION OF SEISMIC REFLECTION ANOMALY	370 ▶

OVERLAPPING SURVEYS

GRAVITY, MAGNETICS, AND SEISMICS

REFER TO FIGURE C-1 FOR INDEX LOCATION

RCP8108-194

FIGURE C-2. Location Map of Basalt Waste Isolation Project Surveys.

Constant-elevation surveys at 750, 990, 1,200, 1,450, and 1,675 m, respectively, were flown for Rockwell Hanford Operations (Rockwell) (Appendix B). (Werner deconvolution solutions of the Rockwell multi-level aeromagnetic surveys identified anomalies near three of the five seismic anomalies [SP 370 and 570 on line 79-4 and SP 605 on line 79-5]).

Geologic information for this study was taken from that previously reported by Myers, Price and others (1979) and Tallman and others (1979). Density information was derived from borehole gravity meter (BHGM) data of Robbins and others (1979).

SURVEY STATIONS AND LINE LOCATIONS

Three of the five seismic-reflection anomalies (SP 510, 530, and 590) are located in or near sec. 6, T. 12 N., R. 26 E. (Fig. C-2). Line 103, consisting of ground magnetics and gravity (Fig. C-2), and line 103A, consisting of ground magnetics only, were constructed to evaluate these anomalies. Station intervals were 20 m along line 103 and 15 m along line 103A.

The fourth seismic-reflection anomaly (SP 370), located in sec. 7, T. 12 N., R. 26 E., was evaluated using data from line 102 (Fig. C-2). Station intervals along line 102 were 40 m from 0 to 400 m and from 1,200 to 1,880 m, with 20-m intervals from 400 to 1,200 m.

Line 104 was used to evaluate the fifth seismic anomaly (SP 605, line 79-5) located in sec. 34, T. 13 N., R. 26 E. (Fig. C-2). Station intervals along line 104 were 100 m from 0 to 5,700 m and decreased to 20 m from 5,700 to 7,640 m to supply detailed coverage over the seismic anomaly.

Line 104 completely crosses the trough of the Cold Creek syncline and was utilized along with gridlines 440000 and 445000 to assess the possibility of buried basalt structures not detected with well data. Station intervals on gridlines 440000 and 445000 are 150 m. Gravity data only have been acquired for these gridlines to date. Gridlines 440000 and 445000 are the first results from a 150 by 150-m, gridded, gravity survey for the reference repository location (RRL). The gridded survey is an ongoing project for characterization of the RRL.

SURVEY METHODS

Elevation control for lines 102, 103, and 104 was established by Rockwell personnel using a Zeiss Th 43 theodolite to acquire accuracies of ±0.03 m. The gridlines were surveyed by Vitro Engineering Corporation, retaining the same accuracies.

Horizontal distance between stations on lines 102, 103, and 104 was determined by tape measure. Locations along line 103A were established by pacing, using notes taken at cultural features to check actual distances. Gridline distances were established with an infrared, distance-measuring instrument and were checked using triangulation techniques.

Diurnal and meter drift for all gravity measurements were determined and removed for each line by looping back to a local base station at least once every 2 hr. All local bases were tied to the regional base established by Peterson (1965) at the Richland Airport.

Diurnal magnetic variations were recorded using a GeoMetrics Model G 826A base station. These variations were removed only when they were found to significantly affect the magnetic profile.

DATA AND DATA PROCESSING

The Bouguer gravity profile along line 103 (Fig. C-3) was calculated using a density of 2.15 g/cm^3 and a datum of 65 m above mean sea level. This density and datum were selected on the basis of BHGM work by Robbins and others (1979) in borehole DC-3 (Fig. C-2). Terrain corrections were not performed for this line, since the surrounding topography is relatively flat. Figure C-3 also shows the total field magnetic intensity profiles for lines 103 and 103A.

The Bouguer gravity profile for line 102 (Fig. C-4) was calculated using a density of 2.15 g/cm^3 and a datum at 60 m above mean sea level. These values were selected using the BHGM data of DC-3 and assuming that no major, lateral variations occurred within the sediment between DC-3 and the extent of this line. Terrain corrections were not performed due to the flat topography within the surrounding area. The total field magnetic intensity profile for line 102 is also shown in Figure C-4.

Gravity data for line 104 (Fig. C-5) were reduced, using a density of 2.17 g/cm^3 and a datum at 40 m above mean sea level. These values are based on BHGM results from DC-5 (Fig. C-2). Terrain corrections were performed using Hammer's (1939) template method from rings D through H, inclusive. Topographic variations for rings B and C were estimated in the field over the abrupt topographic rise (shown in the elevation profile of Fig. C-5). The total field magnetic intensity profile for line 104 is also shown on Figure C-5.

Gravity data from gridlines 440000 and 445000 (Fig. C-6) were reduced, using a density of 2.17 g/cm^3 and a datum at 40 m, assuming lateral continuity with respect to the BHGM data of DC-5 and line 104. Terrain effects were checked for several stations on these lines, but were not included as the maximum terrain-induced error found was to be <0.2 mgal. Normal or theoretical gravity values were calculated using the formula adopted in 1930 by the General Assembly of the International Association of Geodesy for all gravity lines.

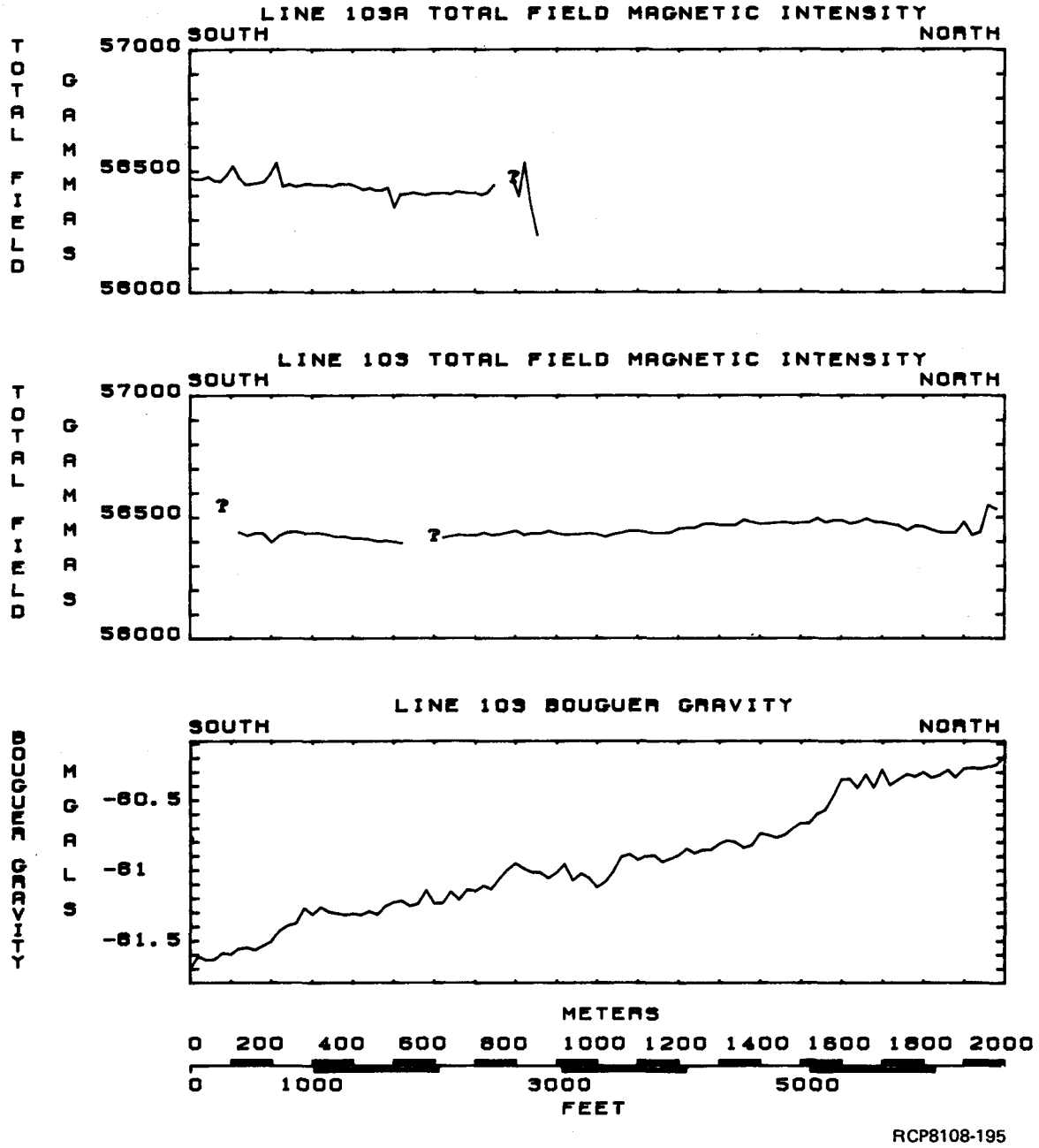

FIGURE C-3. Lines 103 and 103A.

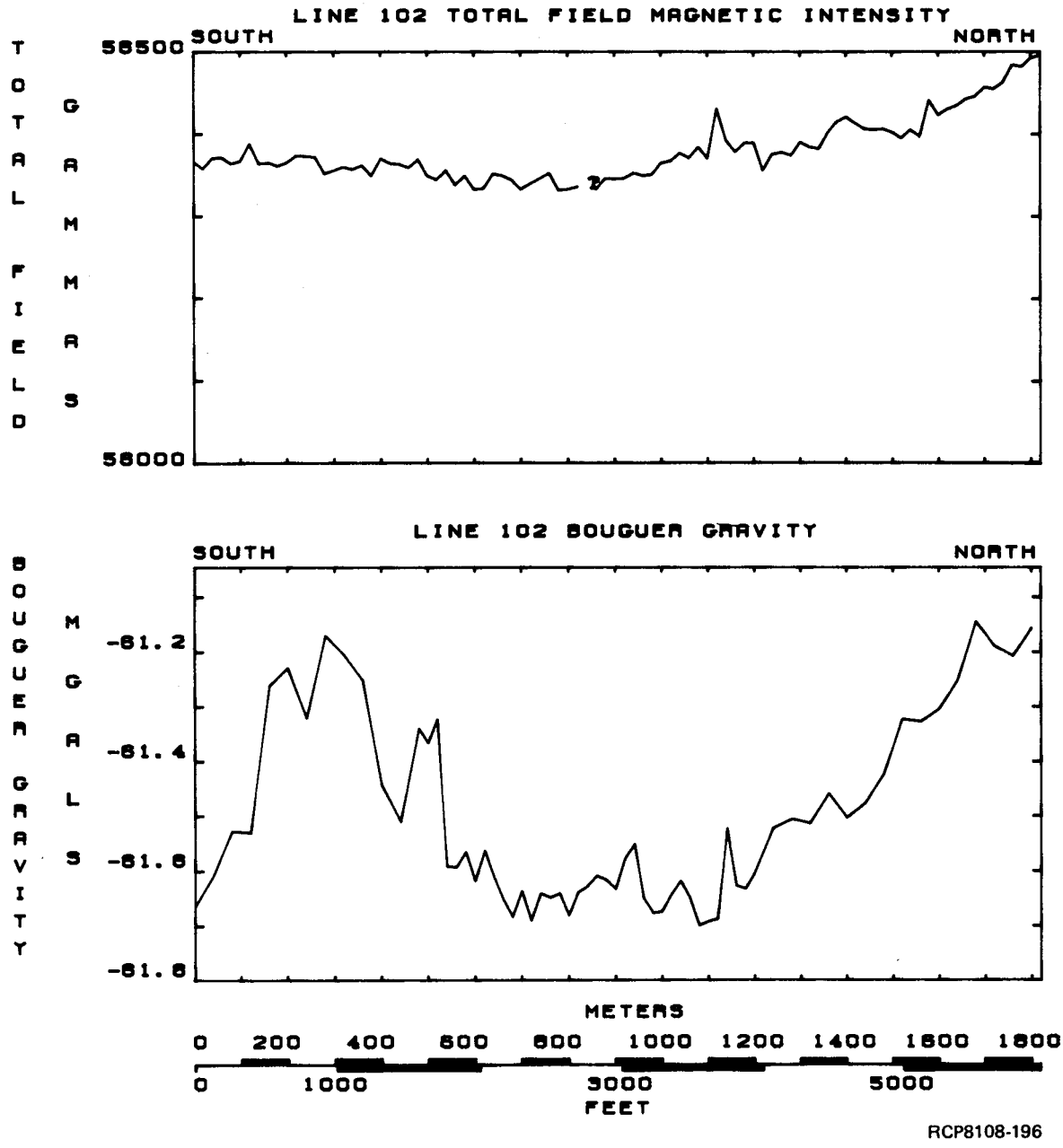

FIGURE C-4. Line 102.

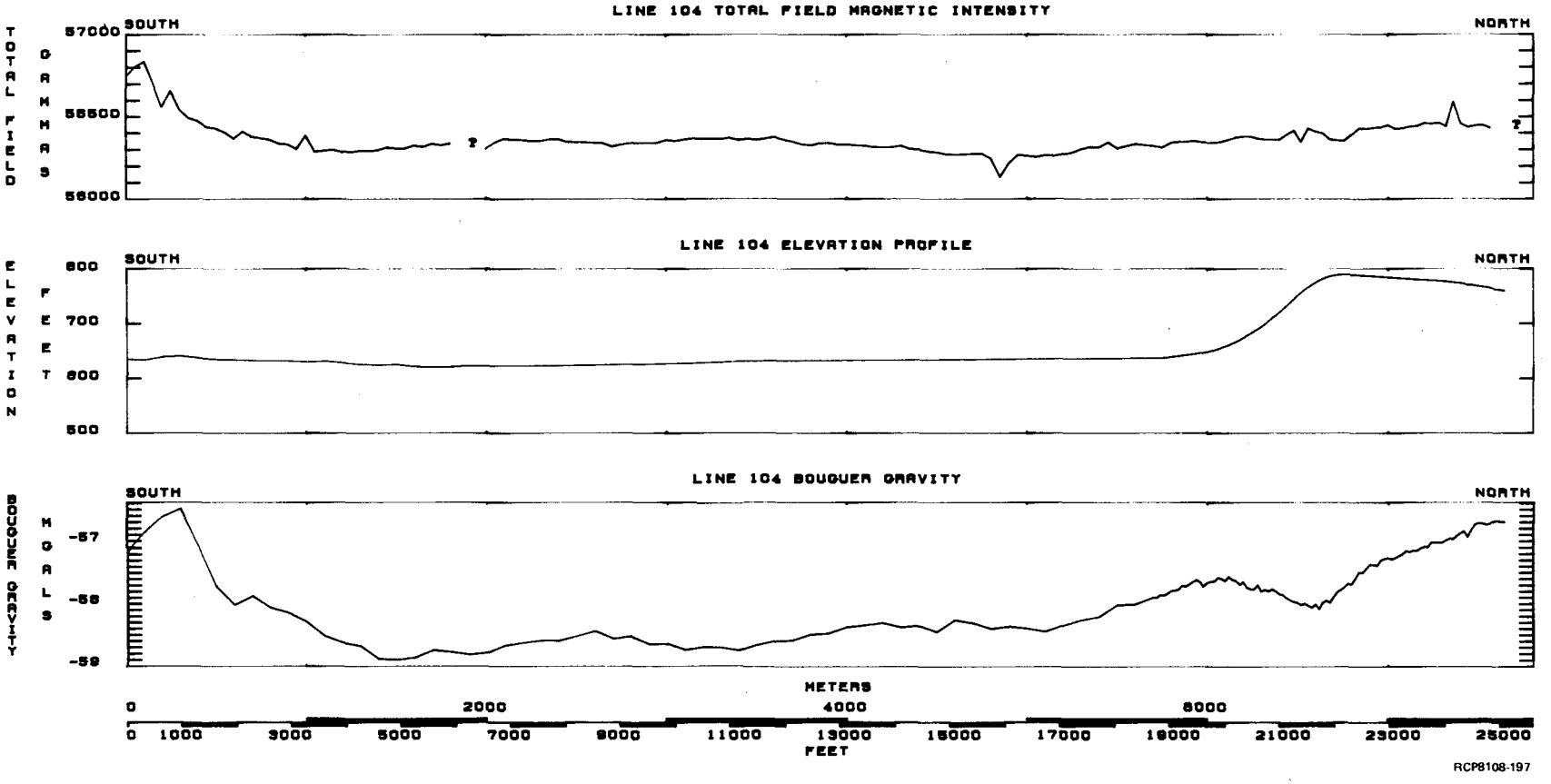

FIGURE C-5. Line 104.

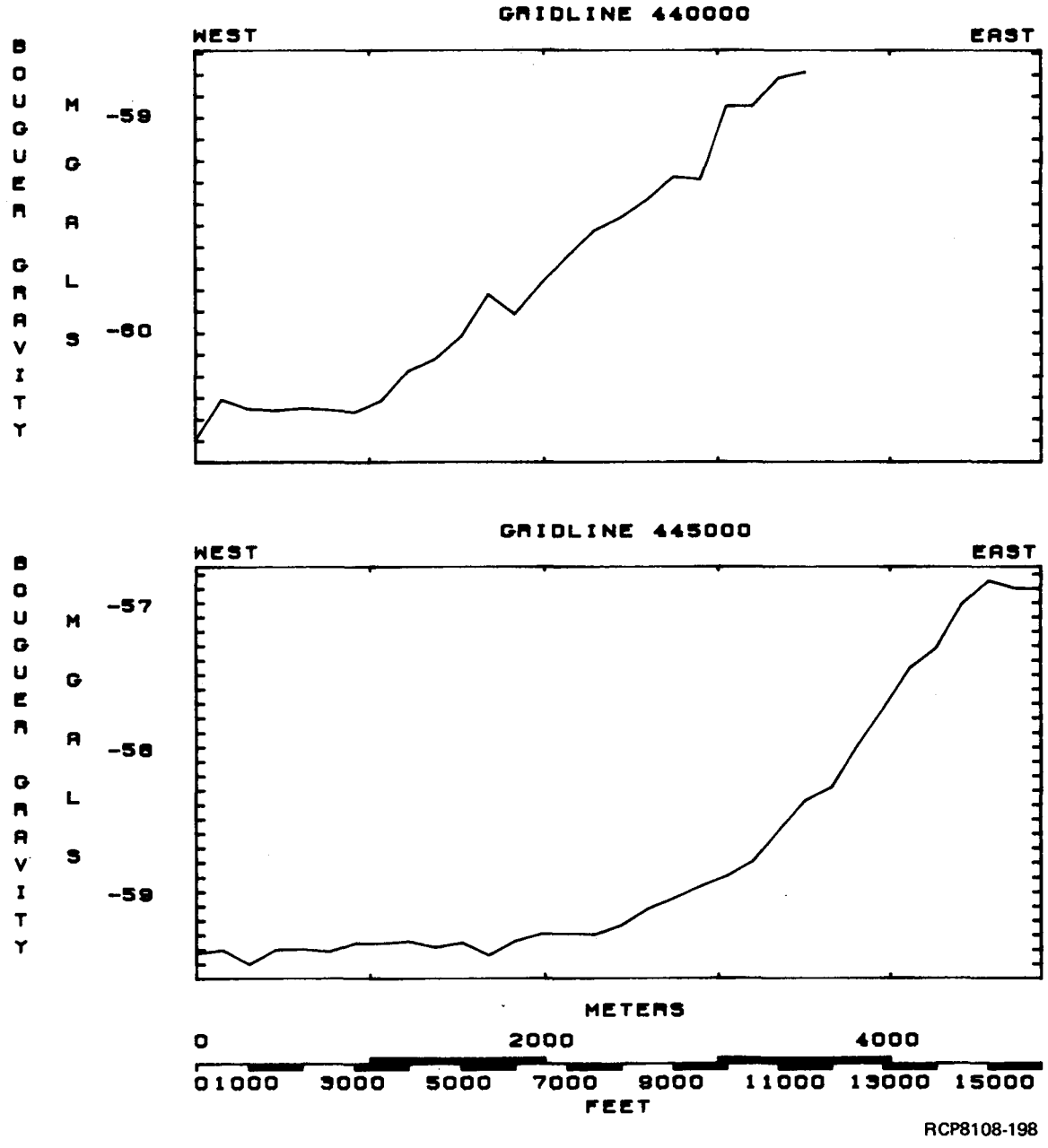

FIGURE C-6. Gridlines 440000 and 445000.

RESULTS AND INTERPRETATIONS

The seismic anomalies located at 150 m (SP 510), 430 m (SP 530), and 1,400 m (SP 590) along lines 103 and 103A (Fig. C-3) are not expressed on the Bouguer gravity profile nor the total-field magnetic profiles as structural displacement in the top-of-basalt surface. Moreover, the slight variations of the magnetic profiles show no significant anomalies attributable to the surface of the basalt. Minor anomalies, or spikes, are attributable to local cultural features (e.g., metal fence posts, well casings, etc).

Subsurface maps included in Tallman and others (1979) and Myers, Price and others (1979) indicate that the surface of basalt is >125 m below the land surface along lines 103 and 103A. A density contrast of 0.3 g/cm^3 exists at this sediment/basalt interface, according to Robbins and others (1979). This contrast should produce gravity anomalies of 0.2 mgal or greater, spanning at least 250 m as the seismic anomalies are crossed, assuming a vertical offset in the top of basalt of 15 to 23 m. The Bouguer gravity profile does not exhibit such features; therefore, either the offset across the structure is slight or the seismic anomaly is attributable to some other source.

The gravity profile does reveal a shallow anomaly between 200 and 400 m. The 0.3-mgal rise here is interpreted to be a lens of higher density material not >50 m below the surface, based on the half width of the anomaly. This lens is interpreted to have caused the two seismic anomalies (SP 510 and 530) in this area.

The rapid rise in the Bouguer gravity, beginning at 1,500 m along line 103, does not appear to be related to the seismic anomaly located at 1,400 m because of their respective distances. This gravity anomaly is interpreted as the replacement of a lower density sediment by a higher density layer in the sediment section overlying the basalt in this area. This probably corresponds to the termination of the Palouse soil or upper Ringold horizon, which is replaced by glaciofluvial material, as shown in Tallman and others (1979).

The seismic anomaly (SP 370) on line 79-4, located in sec. 7, T. 12 N., R. 26 E. (Appendix B), was investigated using line 102 (Fig. C-4). Neither the gravity traverse nor the magnetic traverse indicated any anomalies related to the basalt surface. A 0.5-mgal anomaly centered at 300 m (Fig. C-4) was located; however, it is not related to the seismic anomaly located at 820 m (Fig. C-4). The rapid change in slope on the gravity anomaly indicates a shallow source. The probable source is a near-surface channel filled with glaciofluvial flood gravels.

The magnetic field along line 102 is relatively uniform, but with a gradual change of 200 gammas between 1,000 and 1,880 m (Fig. C-4). This rise is too broad to reflect a significant structural disturbance at the basalt surface. The minor anomalies, or spikes, at 150, 1,140, and 1,600 m are related to cultural features (i.e., metal fence posts, well casings, etc).

Line 104 (Fig. C-5) was used to evaluate seismic anomaly SP 605 on line 79-5 (Appendix B), located in sec. 34, T. 13 N., R. 26 E. (Fig. C-2), and to provide a baseline for the gravity surveys across gridlines 440000 and 445000. A major portion of line 104 was previously collected by Lillie and Richard (1977), but due to the lapse of time, the survey markers had been so disturbed by weathering and erosion that infill of data was impossible, necessitating a resurvey.

Seismic anomaly SP 605 is located at 6,800 m along line 104 (Fig. C-5). The total magnetic field shows little variation in this area. The spikes at 1,000, 4,875, 6,500, and 7,300 m are cultural effects. The Bouguer gravity profile shows a 0.7-mgal drop south of the seismic anomaly between 6,600 and 7,000 m and a subsequent rise of 0.5 mgal from 6,000 to 6,600 m. The actual source of this anomaly is still under investigation, although it is not believed to be an offset in the basalt surface. If the anomaly was the result of faulting, the location of the gravity anomaly would be centered around the seismic anomaly. Furthermore, the seismic interpretation indicates that the northern side is upthrown, which is contrary to the overall character of the gravity traverse. The anomaly is believed to be due in part to terrain effects of the gravel bar which constitutes at least part of the topographic rise seen at this location (Fig. C-5). Gridded data are being acquired in this area to further evaluate this anomaly.

The remaining portion of line 104 (Fig. C-5) located three other anomalies. The first is located between 0 and 1,000 m and is displayed in both the gravity and magnetic data. This anomaly corresponds to the buried basalt high, defined by well and outcrop data as the eastern extension of Yakima Ridge. This extension crops out between 200 and 300 m on line 104.

Two other slight undulations occur in the gravity profile of line 104 (Fig. C-5). The first lies between 2,000 and 3,250 m and the second between 3,500 and 5,000 m. Both of these features are interpreted to be lateral variations in the sediment. For these to reflect the basalt surface, variations of the basalt would have to be extremely abrupt. Neither the seismic nor magnetic data support an abrupt change in the basalt surface.

Gravity data on gridlines 440000 and 445000 (Fig. C-6) were used to determine whether any unidentified subsurface structures exist at the basalt surface in this part of the Cold Creek syncline. Both traverses show similar characteristics: a smooth, flat, Bouguer profile toward the west, increasing toward the east. This increase is consistent with other well and geophysical evidence. The gravity rise is interpreted to be a gradual change in the near-surface sediments overlying the basalt, superimposed on a westward-dipping regional trend. Higher density, glaciofluvial gravels are abundant to the east, while fine, lower density loess is abundant to the west (Myers, Price and others, 1979). No evidence of buried basalt structures expressed in the top of basalt were observed in the Bouguer profiles along either gridline.

CONCLUSIONS

Fault interpretations proposed for the five seismic anomalies were not confirmed with ground magnetics or gravity. This may be attributable to three possibilities: (1) the seismic anomalies were caused by variations in the sediment above the surface of basalt, (2) the density and magnetic parameters were not sufficiently affected by the structural offset to cause detectable response in the gravity and magnetic fields, and (3) the offsets on the structures may be too small to be detectable with the gravity and magnetic surveys run to date.

The seismic anomalies located at 150 and 430 m along lines 103 and 103A (Fig. C-3) were interpreted, based on the Bouguer profile, to be sediment variations. The seismic-reflection anomalies located at 1,400 m along line 103 (Fig. C-3) and at 820 m along line 102 (Fig. C-4) were not detected with ground magnetics or gravity.

The seismic-reflection anomaly (SP 605) located at 6,800 m along line 104 (Fig. C-2 and C-5) is still under investigation. The seismic anomaly lies on the northern edge of a 1,000-m-wide gravity anomaly centered at 6,600 m (Fig. C-5). Gridded gravity data are presently being acquired in this area for further evaluation of this anomaly.

Both the ground magnetics and gravity along line 104 (Fig. C-5) display excellent responses where the line traverses the eastern extension of Yakima Ridge. Gridlines 440000 and 445000 (Fig. C-2 and C-6) did not reveal any unexpected anomalies identifiable as buried anticlines or synclines in the basalt surface.

APPENDIX D - GEOPHYSICAL INVESTIGATIONS OF THE GABLE MOUNTAIN-GABLE BUTTE AREA

T. D. Ault

INTRODUCTION

The purpose of this appendix is to summarize geophysical studies conducted in the Gable Mountain-Gable Butte area (Fig. D-1). The objective of these studies was to establish a better understanding of the structural relationship between Gable Butte, Gable Mountain, and the Cold Creek syncline to the south. The suite of geophysical surveys shown in Figure D-1 was specifically designed to examine the geometry of the subsurface basalt in the sediment-covered area near Gable Butte, Gable Mountain, and areas north of Route 11A (Yakima Highway).

PREVIOUS WORK

The Gable Mountain-Gable Butte area has been the object of a number of geologic, hydrologic, and geophysical studies. Previous geologic studies included mapping by Schmincke (1964), Bingham and others (1970), Newcomb and others (1972), Brooks (1974), Swanson and Wright (1976), WPPSS (1974), and Fecht (1978). Converse, Davis and Associates (1969, 1971) examined trenches on Gable Mountain to evaluate possible faulting. Hydrologic studies were performed on both the confined and unconfined aquifers on the flanks of Gable Mountain and Gable Butte by Hart and Frank (1954) and Mudd and others (1970).

Geophysical studies include local and regional gravity and magnetic studies reported by Raymond (1958), Raymond and McGhan (1963), Peterson and Brown (1966), Deju and Richard (1975), Lillie and Richard (1977), Richard and Lillie (1977), WPPSS (1977), Weston Geophysical (1978a), and Myers, Price and others (1979). An evaluation of data provided by previous hydrogeologic and geophysical work was conducted as part of this study. The preliminary results of ongoing work in the Gable Mountain area by Weston Geophysical Research, Inc. (for the Northwest Energy Services Company) were also considered.

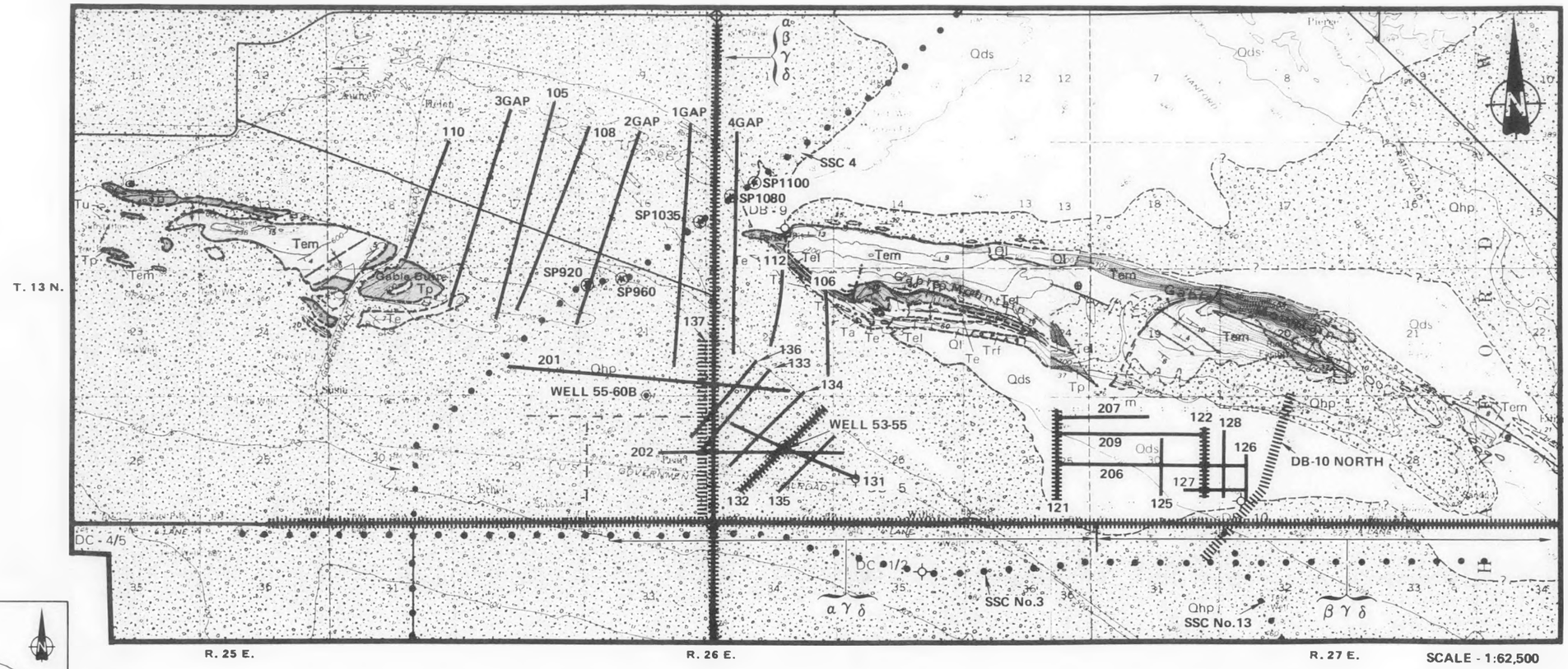

INDEX

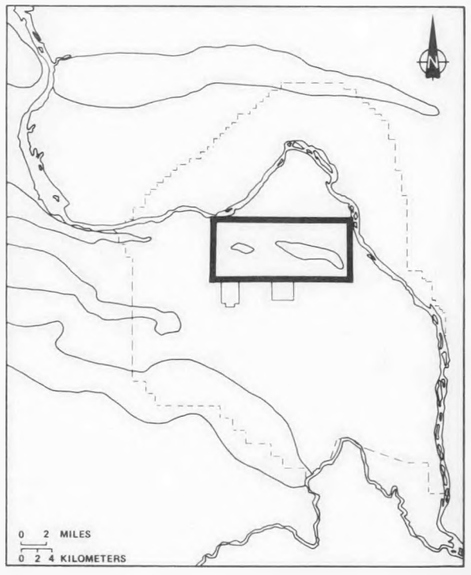

GEOPHYSICAL TRAVERSE SYMBOLS

MAGNETIC SURVEY

GRAVITY SURVEY

SEISMIC SURVEY

SHOTPOINT

OVERLAPPING SURVEYS

MAGNETICS AND GRAVITY

α	RICHARD,1976
β	LILLIE AND RICHARD, 1977
γ	RAYMOND, 1958
δ	WESTON GEOPHYSICAL, 1978a
GAP	GABLE GAP AREA SURVEY
SSC	SEISMOGRAPH SERVICE CORPORATION

RCP8108-199

FIGURE D-1. Gable Mountain-Gable Butte Survey Areas (see Table 3-1 for explanation).

SURVEY LOCATIONS AND METHODS

Surveys run by Basalt Waste Isolation Project personnel in the Gable Mountain-Gable Butte area include 28 gravity, ground magnetics, and resistivity profiles (Fig. D-2 through D-12). The lines having a GAP suffix relate to surveys performed in the Gable Gap area; the DB prefix indicates surveys in the area of borehole DB-10 (sec. 25, T. 13 N., R. 27 E.; Fig. D-1). The remainder of the survey lines are labeled in the order in which they were performed without reference to their areal locations.

As discussed in Appendix B, both seismic and aeromagnetic surveys have been conducted in the study area. Locations of pertinent seismic profiles are shown in Figure D-1. The area is covered by three elevations of the aeromagnetic survey: 760, 990, and 1,220 m.

The five gravity profiles were conducted at a station frequency ranging from 30 to 150 m. A Worden Master (#1088) gravity meter was used to collect all gravity data. Station elevations were surveyed to an accuracy of ±0.03 m with a Zeiss Th 43 theodolite. Gravity data reduction included drift, latitude, free-air, and Bouguer corrections on all profiles. Gravity data are presented as a graph of Bouguer values versus distance. A density of 2.67 g/cm^3 and datum of mean sea level were used to derive the Bouguer values.

Ground magnetic surveys were conducted using a GeoMetrics G 816 proton precession magnetometer with a sensitivity of 1 gamma. Twenty-six ground magnetic surveys were conducted at an elevation of 2.5 m above ground surface with a station frequency of 15 m. Stations were generally at pace intervals with tie points noted at prominent cultural and topographic features. Where magnetic profiles were coincident with gravity lines, gravity stations were used for location control. A recording base station magnetometer (GeoMetrics Model G 826A) was utilized to monitor the magnetic diurnal variations. Drift corrections were not applied to these magnetic profiles due to the minor amount of diurnal variation compared to the amplitude of the anomalies observed. Data are presented here as observed total magnetic field versus distance along profile (Fig. D-2 through D-12). Some magnetic profiles presented have had a 56,000-gamma constant removed before plotting.

Resistivity and induced polarization (IP) techniques were performed along line 122 primarily as a test of this method in this basalt type environment. The survey was conducted using a Scintrex Model IPC-7/1.5 kW IP control transmitter, an IPC-7/1.5 kW generator, and an IPR-8 receiver. The resistivity survey was conducted using both the pole-dipole and dipole-dipole arrays. Resistivity data are plotted in pseudosection of apparent resistivities. The IP technique yielded results of uncertain value and are not discussed further in this appendix.

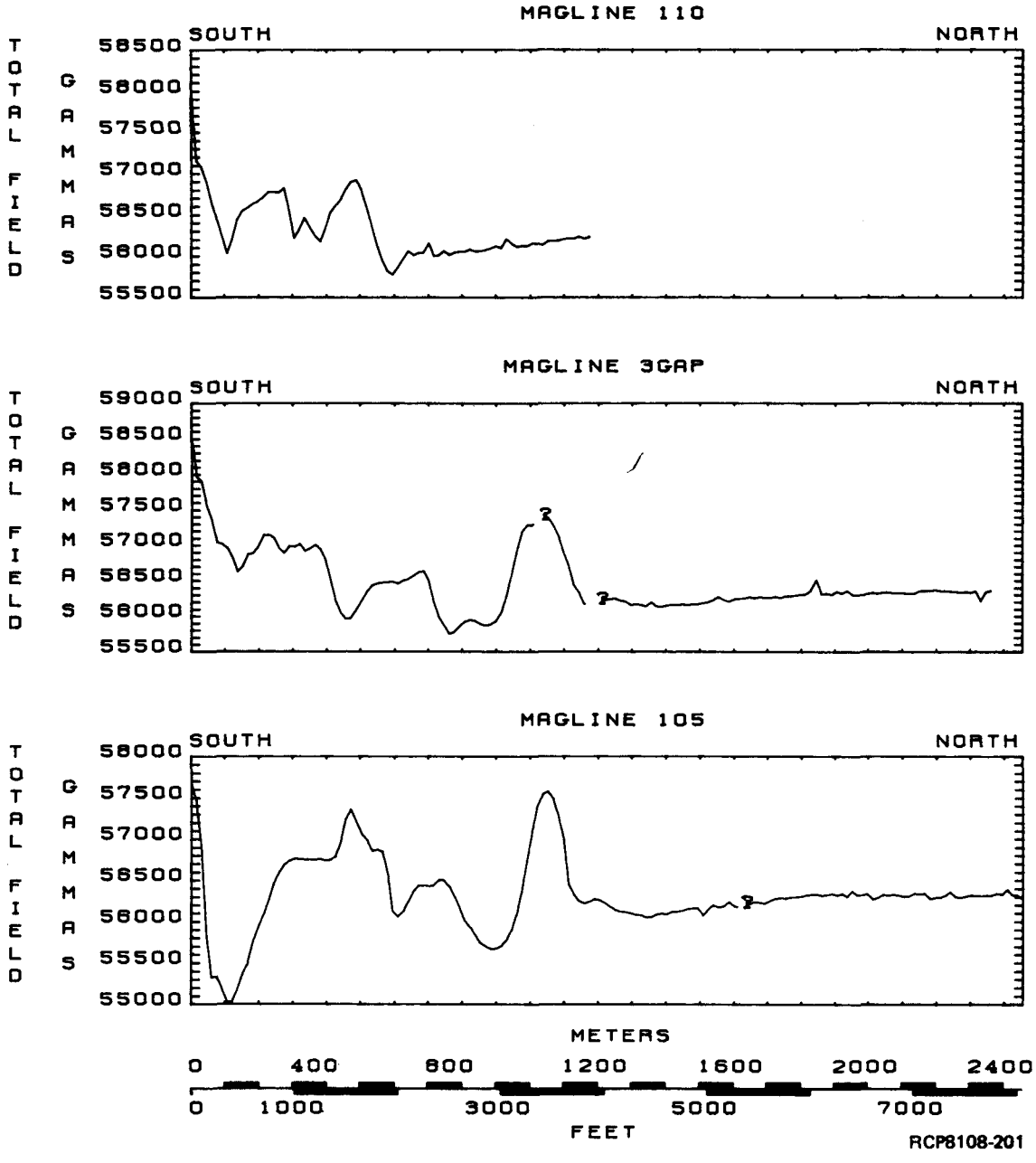

FIGURE D-2. Gable Gap Area Surveys, Lines 110, 3GAP, and 105.

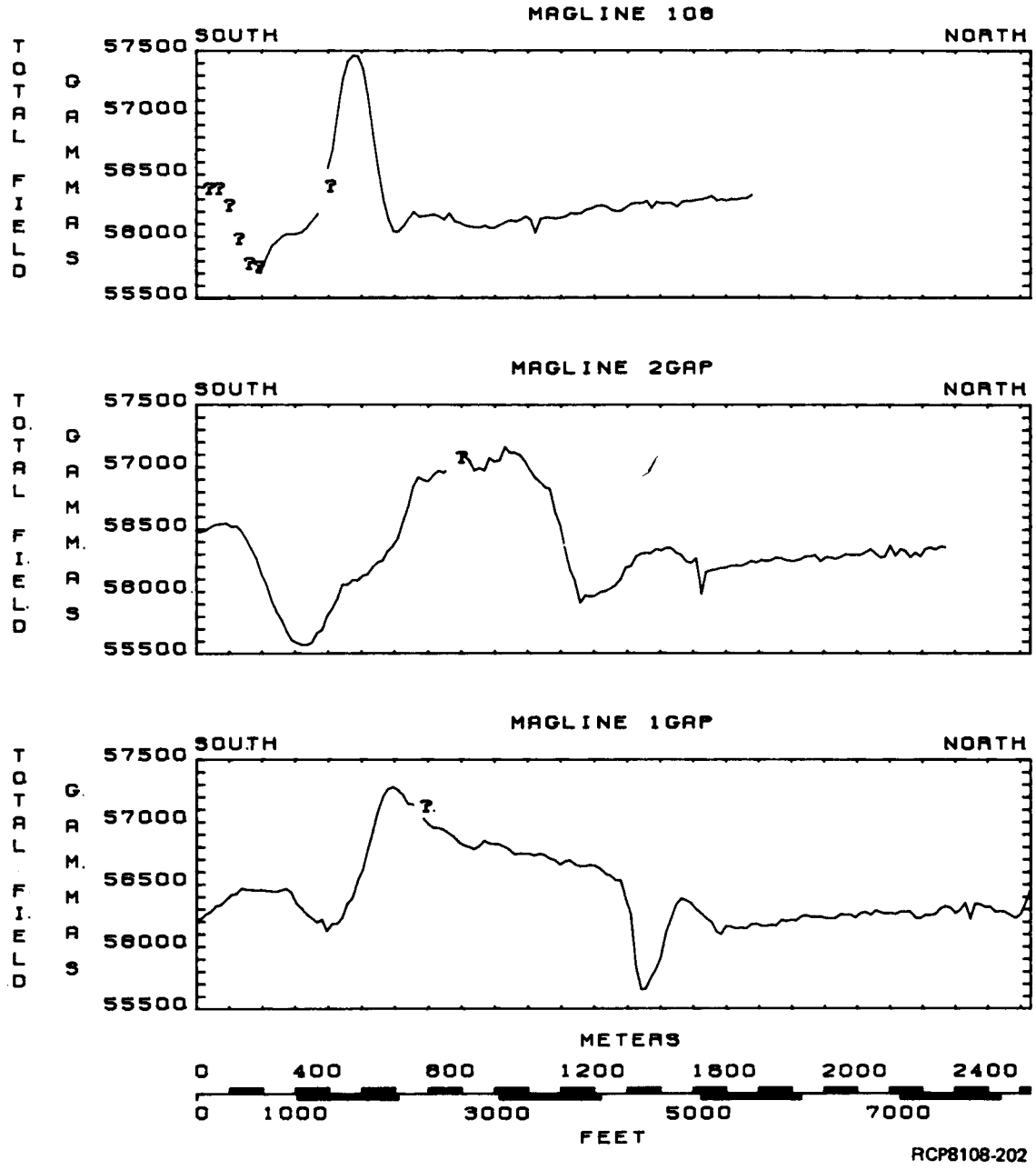

FIGURE D-3. Gable Gap Area Surveys, Lines 108, 2GAP, and 1GAP.

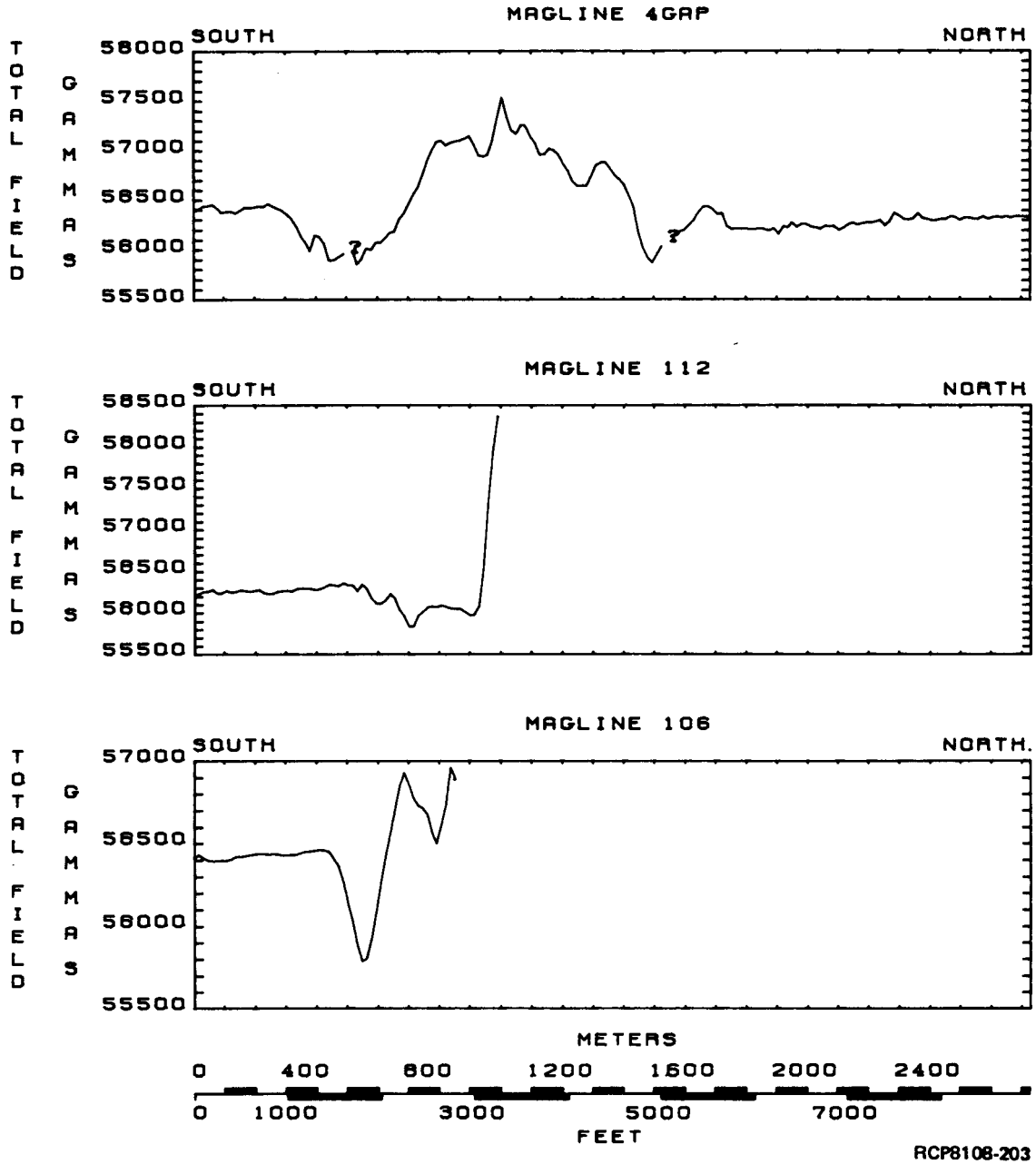

FIGURE D-4. Gable Gap Area Surveys, Lines 4GAP, 112, and 106.

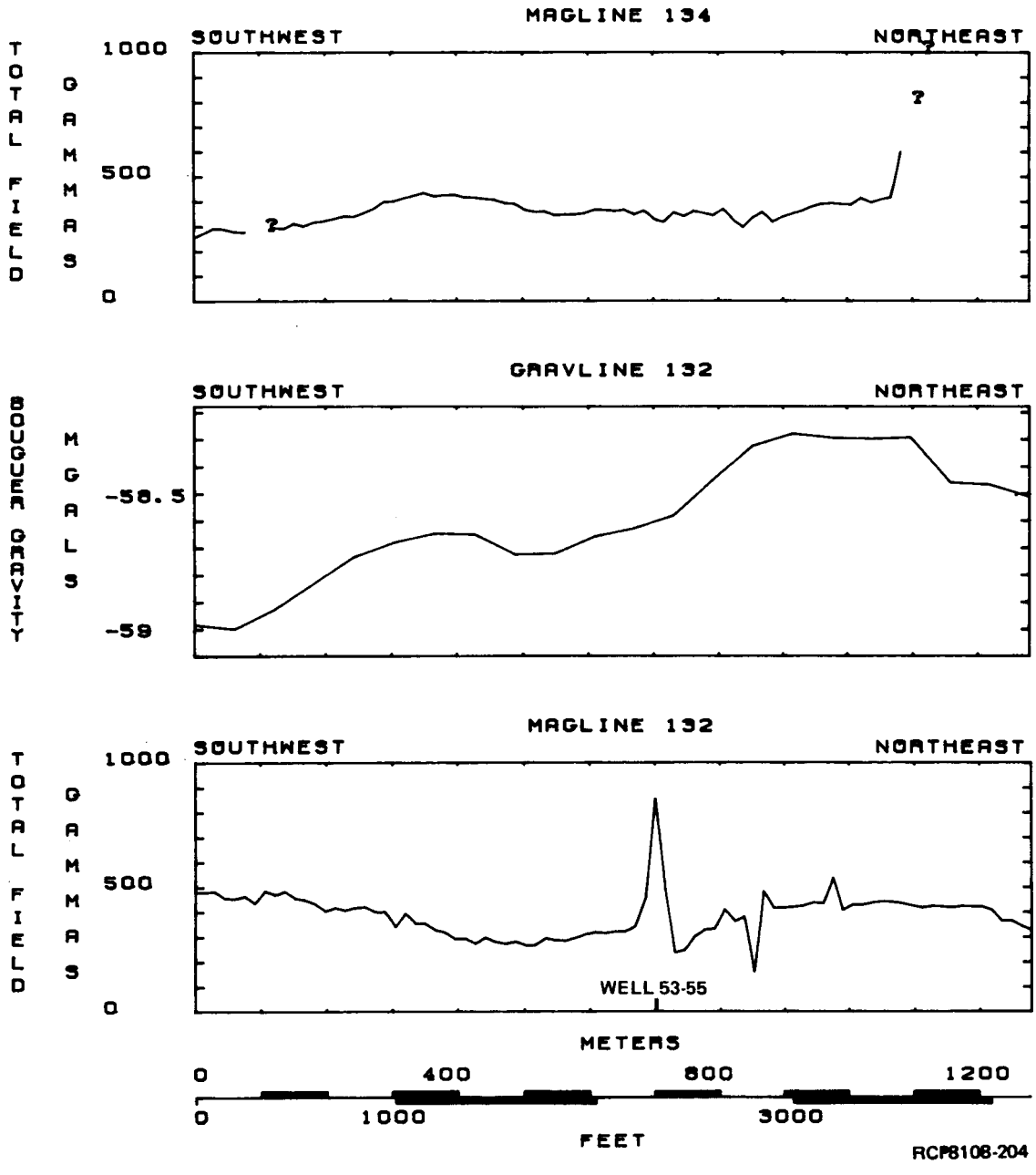

FIGURE D-5. Gable Gap Area Surveys, Lines 134 and 132.

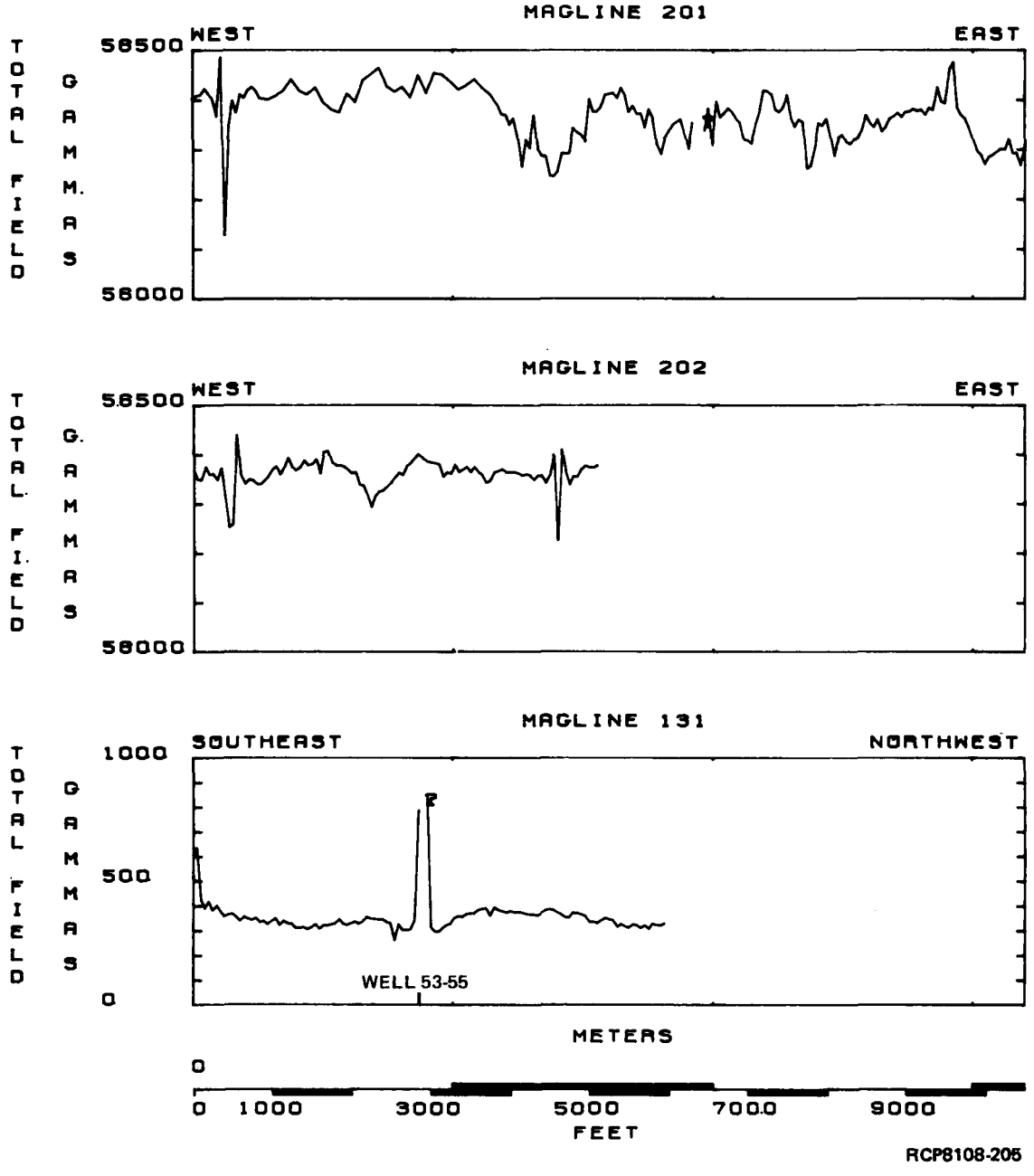

FIGURE D-6. Gable Gap Area Surveys, Lines 201, 202, and 131.

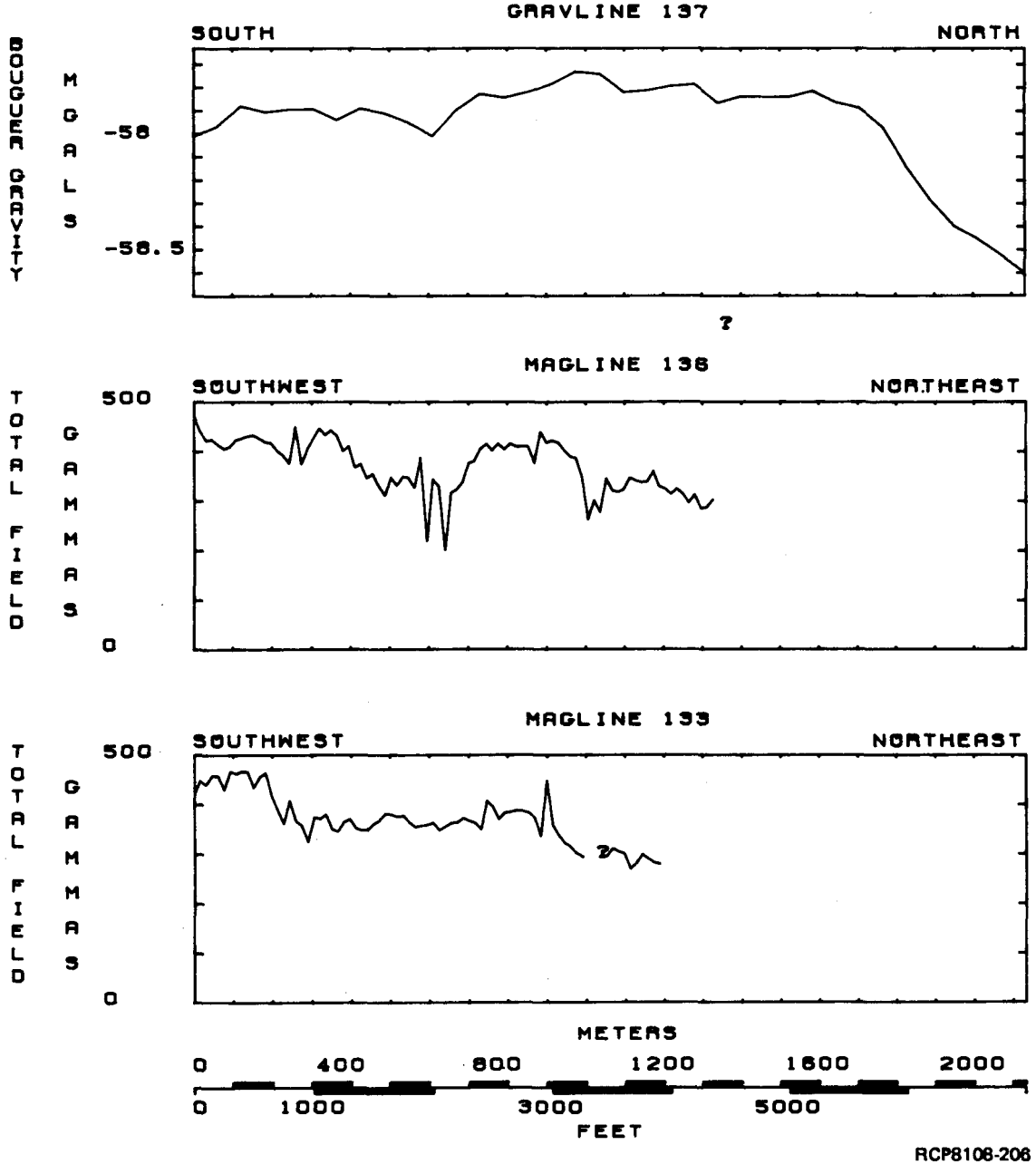

FIGURE D-7. Gable Gap Area Surveys, Lines 137, 136, and 133.

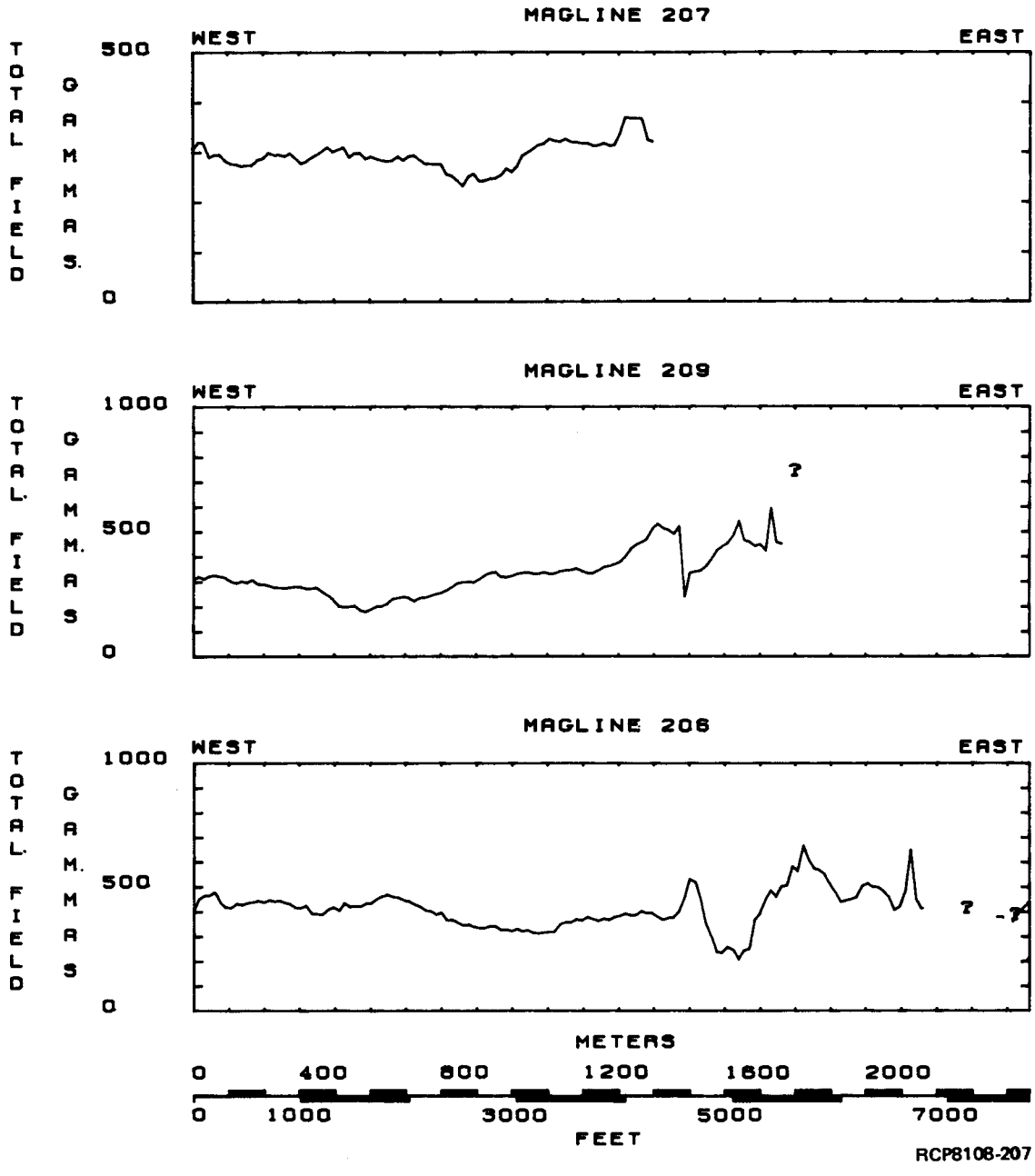

FIGURE D-8. DB-10 Area Surveys, Lines 207, 209, and 206.

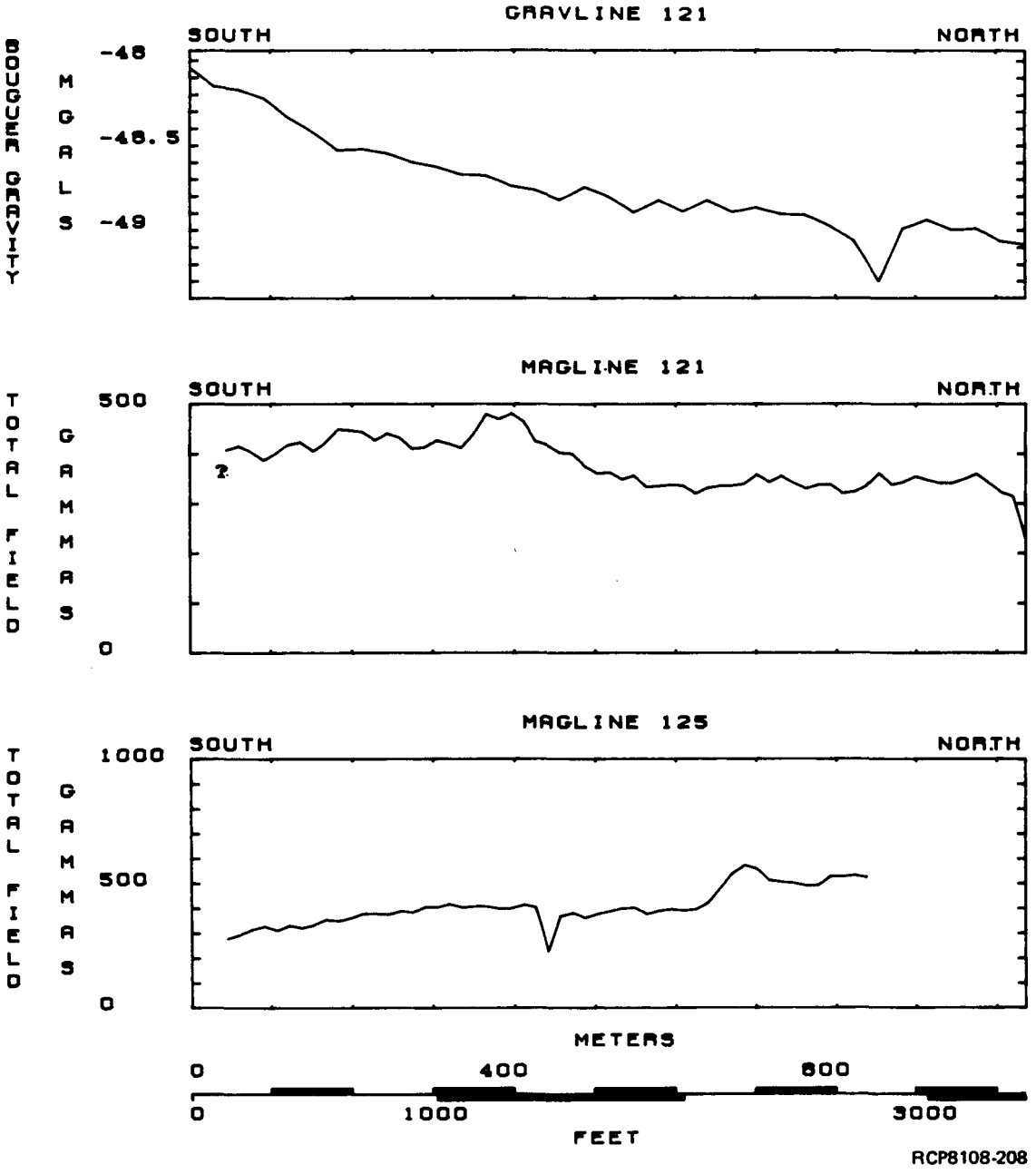

FIGURE D-9. DB-10 Area Surveys, Lines 121 and 125.

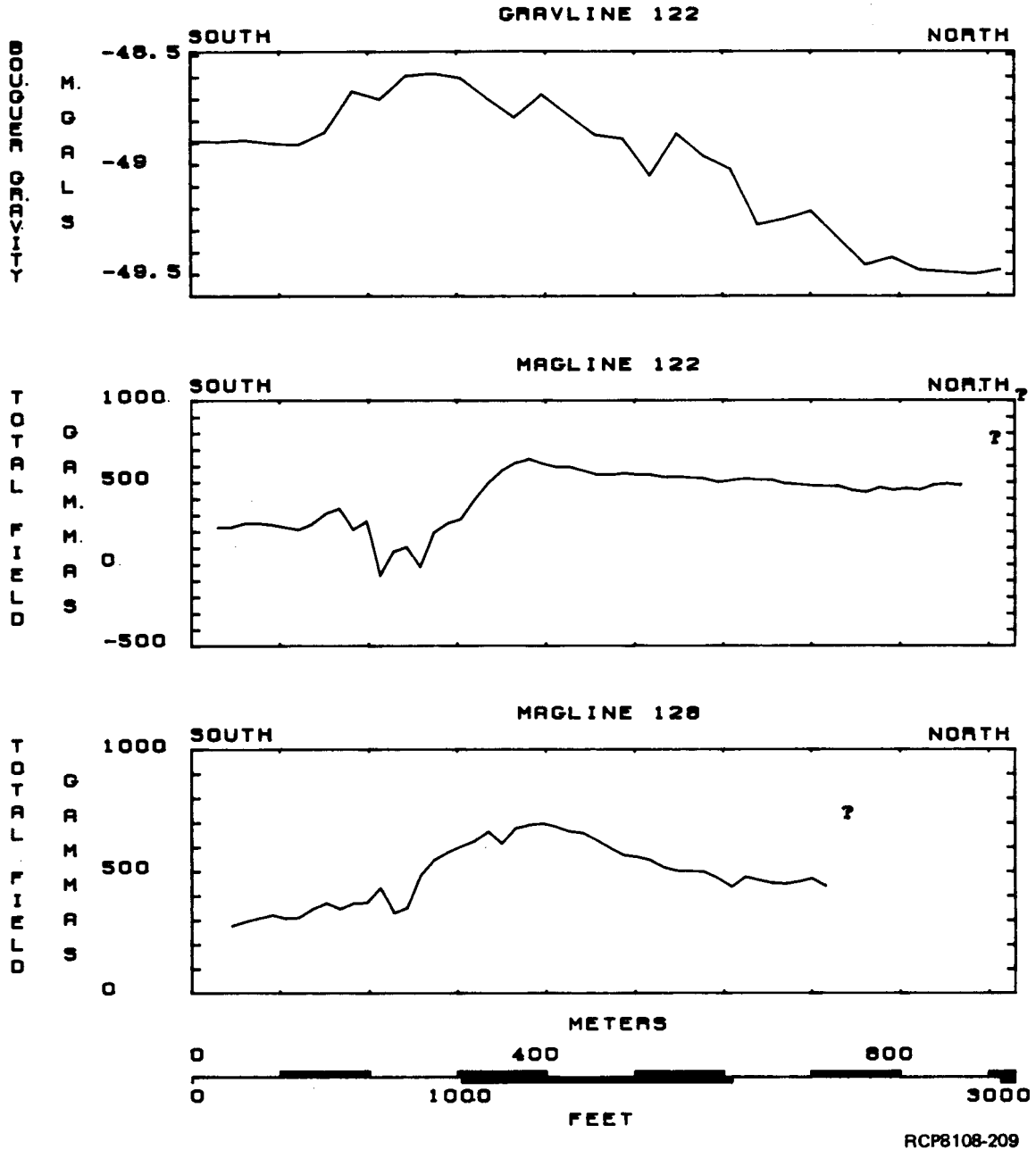

FIGURE D-10. DB-10 Area Surveys, Lines 122 and 128.

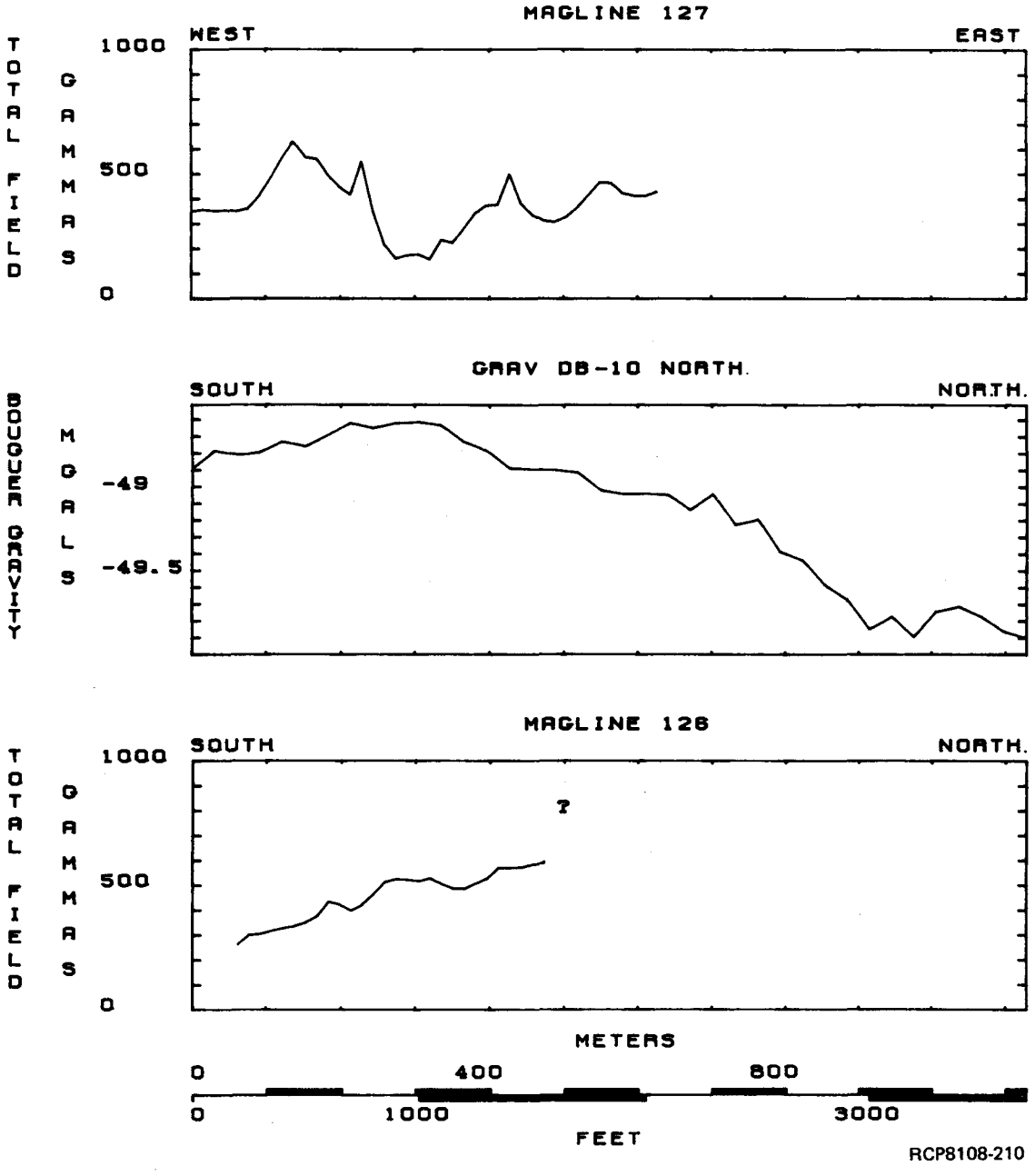

FIGURE D-11. DB-10 Area Surveys, Lines 127, DB-10 North, and 126.

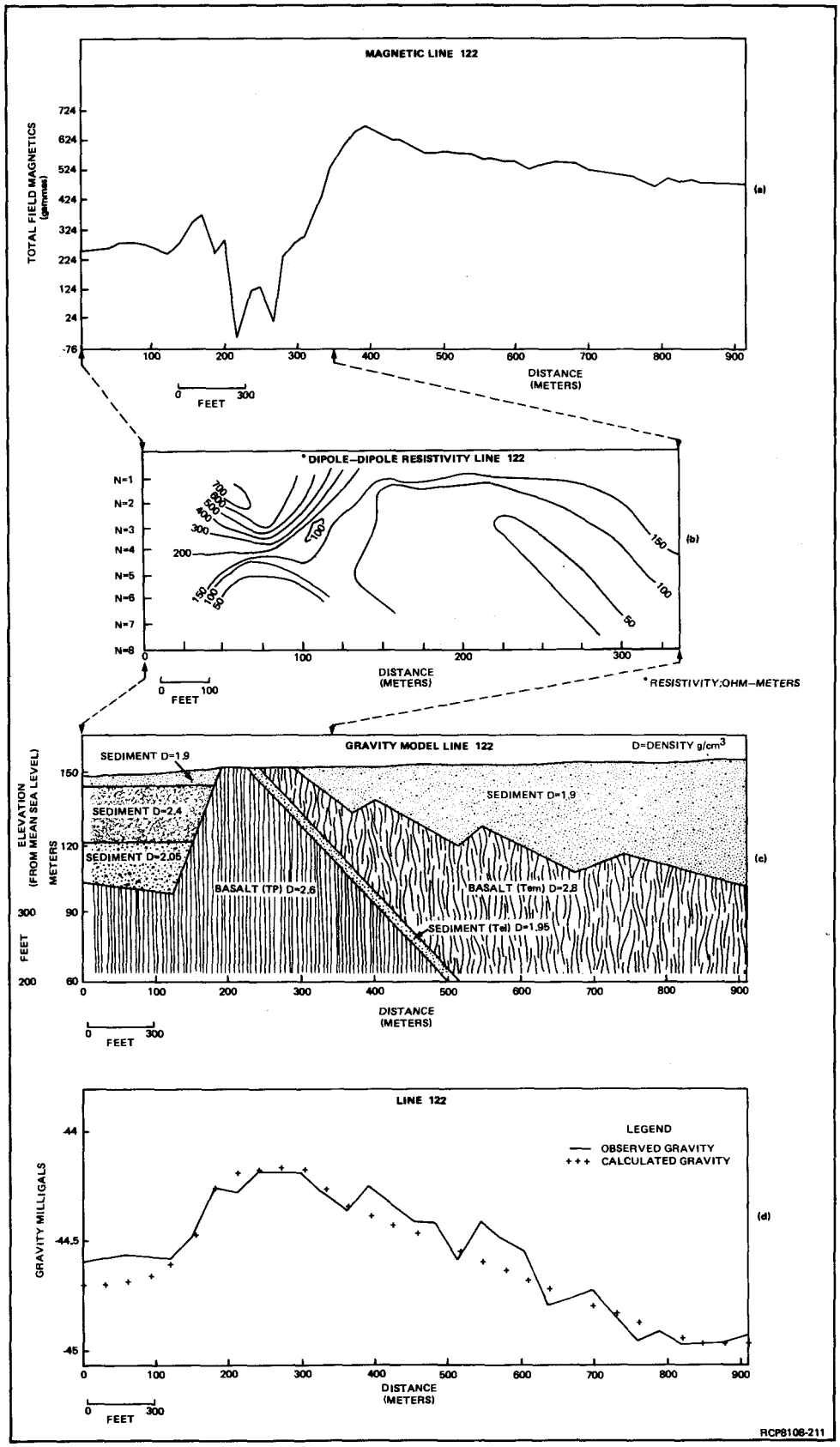

FIGURE D-12. DB-10 Area Surveys, Line 122.

DATA PROCESSING

Gravity data processing included examination of profiles plotted with various densities and datums, terrain corrections on selected profiles using Hammer's (1939) template method, and some preliminary two-dimensional modeling. Magnetic data processing included preliminary two-dimensional modeling to predict theoretical values for hypothetical bedrock geometries. No modeling was conducted on either the resistivity or IP surveys.

GABLE GAP AREA

The area between Gable Butte and Gable Mountain is referred to in this appendix as the Gable Gap area. Seventeen magnetic lines, two gravity lines, one seismic-reflection (SR) line, and the aeromagnetic survey (Appendix B) form the data base from which interpretations were made. Geophysical surveys in the area were designed to address: (1) the general structural relationship between Gable Butte, Gable Mountain, and the Cold Creek syncline; (2) features interpreted from the SR survey (Myers, Price and others, 1979); and (3) the existence of a paleochannel interpreted across the Gable Gap area by Fecht (1978).

Five major bedrock features are interpreted in the Gable Gap area and south of western Gable Mountain. The five major features include: (1) the abrupt decline in the top of basalt (TOB) corresponding with the northern flank of the major, first-order, Umtanum Ridge-Gable Mountain anticline; (2) the Pearl anticline, which forms a southeast-trending extension of Gable Butte; (3) the western Gable Mountain anticline, a northwest-trending, second-order, anticlinal feature below sediment cover west of Gable Mountain; (4) the western Gable Mountain syncline, a northwest-trending bedrock depression through the Gable Gap area thought to be modified by considerable secondary erosion; and (5) a previously mapped, northwest-trending, anticlinal feature south of Gable Mountain (Fecht, 1978), referred to here as the Willa anticline.

NORTH FLANK, FIRST-ORDER, UMTANUM RIDGE-GABLE MOUNTAIN ANTICLINE

Seismic-reflection profile 4 (Fig. D-1 and D-13) is interpreted to represent a general picture of the bedrock structure on a northeast-southwest profile across Gable Gap. The reflecting horizons are assumed to represent interfaces between sediments and basalt bedrock. The rapid increase of travel times of the uppermost reflectors in Figure D-13 north of shotpoint (SP) 1080 are interpreted to correspond to the northern flank of the major, first-order, Umtanum Ridge-Gable Mountain anticline. This feature was discussed by Myers, Price and others (1979) and was interpreted in that document as a dip slope modified extensively by secondary erosion.

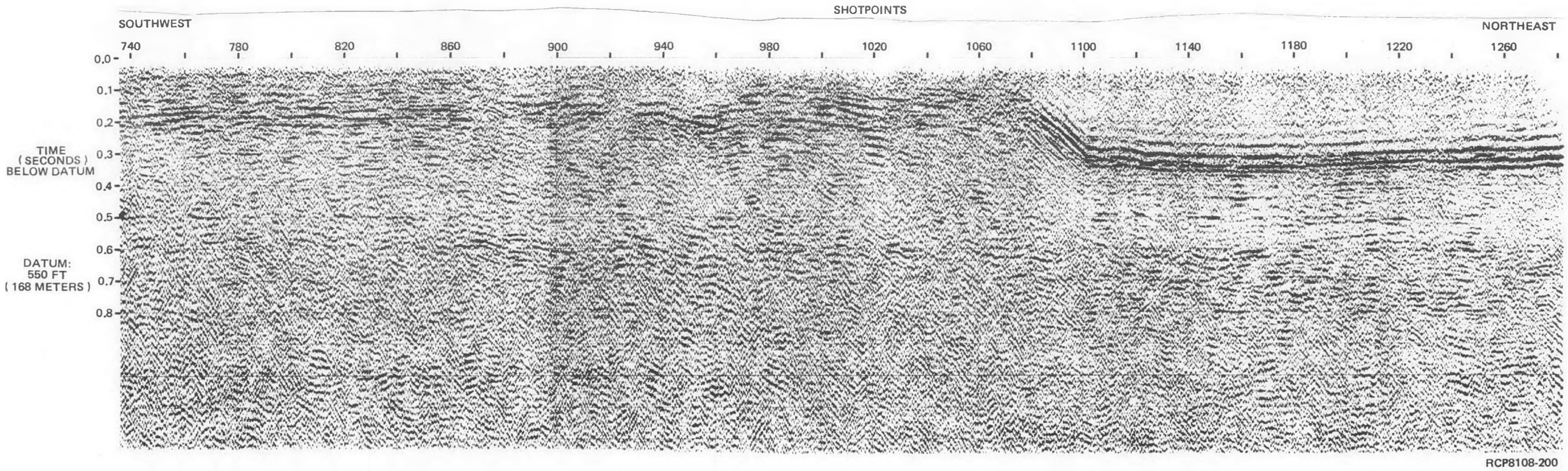

FIGURE D-13. Seismic-Reflection Profile 4.

WESTERN GABLE MOUNTAIN ANTICLINE

The western Gable Mountain anticline is interpreted on the basis of geophysical surveys to extend west from Gable Mountain beneath the sediment cover of the Gable Gap area. Seismic-reflection profile 4 (Fig. D-13) is interpreted to show an irregular bedrock high in the central Gable Gap area between SP 980 and 1080. This line is interpreted to represent a cross section of the western Gable Mountain anticline with its axis located between SP 980 and 1000. Magnetic line 4GAP (Fig. D-1 and D-4) is interpreted to represent a magnetic cross section of this anticlinal feature. The reduced magnetic intensities between the 300- and 800-m points correspond to a general low in the elevation of the basalt surface below the sediment cover.

It appears that the central portion of western Gable Mountain has been heavily eroded by Pleistocene catastrophic flooding, removing the upper basalt flows and exposing normal polarity Esquatzel and Umatilla flows. These normal polarity flows are probably bounded to the north by a more complete stratigraphic section containing the Pomona and magnetically transitional Elephant Mountain basalts, as indicated by the low in the total magnetic field near the 1,500-m point on line 4GAP (Fig. D-4). The higher frequency magnetic highs and lows to the south correspond to areas of differential erosion where remnants of reverse polarity basalt (Pomona) are left intact.

Continuation of the western Gable Mountain anticline to the west is interpreted on the basis of magnetic data. Magnetic profiles indicate a gradual narrowing to the west with fair continuity up to line 108 (Fig. D-3) where the central magnetic high narrows considerably from its configuration on line 2GAP. Possible explanations for this sudden change of character include the existence of a structural discontinuity (folding or faulting) between these two lines, differential erosion of the material during catastrophic flooding, or a rapid plunge of the anticlinal structure. The magnetic profiles to the west of this transition zone demonstrate an overall predominance of high-frequency anomalies. It is difficult to determine on the basis of current data whether these anomalies are due to variations in the basalt surface elevation or distribution of magnetically normal and reverse flow remnants.

The western Gable Mountain anticline appears to generally plunge to the west, as indicated by the narrowing of the magnetic anomalies across the gap. Strong, positive anomalies are present between 800 and 1,500 m on line 4GAP (Fig. D-4). These anomalies are correlatable with anomalies on magnetic lines to the west with similar wavelengths and amplitudes. The presence of strong, positive anomalies on lines west of 108 (lines 110, 3GAP, and 105; Fig. D-2) lead to the continuation of the anticline to the northern segment of Gable Butte, as shown in Figure D-14.

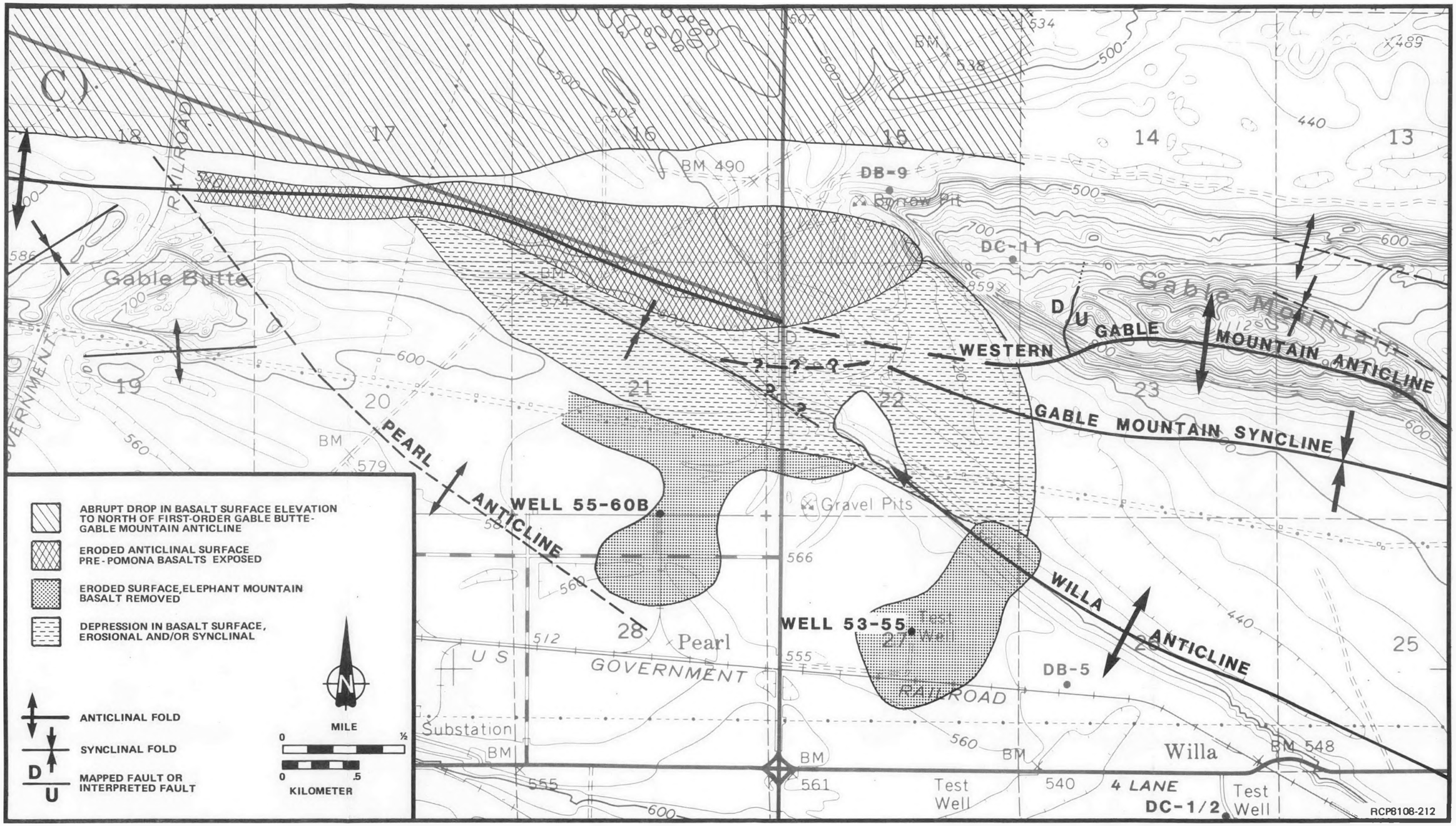

FIGURE D-14. Gable Gap Area Interpretation Map.

WESTERN GABLE MOUNTAIN SYNCLINE

A synclinal feature with considerable secondary erosional modification is interpreted to exist south of the anticline (discussed in the previous section). This is labeled the western Gable Mountain syncline and appears to coincide with the paleochannel interpreted by Fecht (1978) in the same general area. Seismic-reflection profile 4 (Fig. D-13) shows a termination of upper reflective horizons and a downward flexure of the lower horizons between SP 900 and 980. These reflective horizons are assumed to be basalt bedrock interfaces and the downward flexure is thought to be a syncline. Terminated reflectors probably represent the erosion of this syncline by either an ancestral Columbia River or by catastrophic flooding.

The westward continuation of the syncline away from line 4 could not be resolved by existing ground surveys. The presence of the Pearl anticline (Fig. D-14) to the southwest of the seismic feature, as interpreted from a Werner deconvolution solution (Appendix B) makes continuation in this direction unlikely. The total field aeromagnetic map for the 760-m survey elevation (Appendix B) shows a continuation of a magnetic low to the northwest from the syncline location on the seismic line. These data indicate a possible continuation of the syncline to the northwest across the axis of the western Gable Mountain anticline.

The eastward continuation of the syncline away from line 4 is suggested by the presence of magnetic lows on the southern ends of lines 1GAP, 4GAP, 112, and 106 (Fig. D-3 and D-4). A gravity low present in the same general location on a profile performed by Weston Geophysical (1978a) near line 4GAP supports the presence of this bedrock depression. The widening of the magnetic lows is interpreted to indicate a widening of the bedrock depression. This widening may be the result of increased erosion of the bedrock in this location. The bedrock depressions associated with this syncline are probably the result of both structural and erosional processes.

PALEOCHANNEL

Fecht (1978), on the basis of well data (Appendix A), interpreted a paleochannel to be located in the southern Gable Gap area and continuing to the southeast to a point near boreholes DC-1/2 (sec. 20, T. 13 N., R. 26 E.; Fig. D-1). The existence of this paleochannel is supported by interpretations of geophysical surveys as the western Gable Mountain syncline; however, the placement is changed somewhat and a structural as well as erosional origin is postulated. Gravity data from line 137 (Fig. D-7) failed to detect gravity lows interpretable as the paleochannel previously mapped by Fecht (1978) in sec. 27 and 28, T. 13 N., R. 26 E. Gravity line 132 (Fig. D-5) which passes near well 53-55 at the 700-m point did detect a low in the gravity values near the well. This low is interpreted as a depression in the basalt. The fifth, residual, aeromagnetic, contour map from the 750-m survey elevation shows a low in the residual magnetic field in the area of well 53-55. The residual aeromagnetic low displayed

an orientation to the northeast and is coincident with lows in the gravity data on line 132 (Fig. D-5). Well 55-60B to the northwest of well 53-55 is also located in a similar, residual, aeromagnetic depression which suggests that it is located in a bedrock depression of limited lateral extent. The interpreted extent of these depressions is plotted on Figure D-14.

SEISMIC ANOMALIES

Three zones of potential faulting were interpreted in this study area by Seismograph Service Corporation (SSC) (Appendix B) during their preliminary evaluation of SR profile 4 (Fig. D-13). Termination of reflective horizons near SP 980 and again near SP 1040 (Fig. D-13) were interpreted by SSC to represent fault zones with upthrown blocks to the north. However, in both cases, the seismic sections show no consistent offsetting of reflecting horizons in the lower layers with the same sense of displacement as the interpreted faults. Continuous reflective horizons may be traced across both of these zones, placing doubt on the existence of faults in this area. The termination of reflective horizons is assumed to represent the truncation of basalt layers and, possibly, the Ringold Formation due to erosion by floodwaters or by the ancestral Columbia River.

A nearly 150-m-wide zone of lost reflectors on the south side of the western Gable Mountain syncline is located near SP 920. This zone was interpreted by SSC as a fault. The lack of vertical offset across this zone makes the fault interpretation appear questionable. This anomaly has to date not been directly addressed by other ground geophysical survey methods.

GABLE GAP CONCLUSIONS

The overall geologic interpretation of the geophysical surveys in the Gable Gap area (Fig. D-14) involves the westward continuation of the structures observed on the western portion of Gable Mountain as mapped by Fecht (1978). This model requires the continuation of the southward asymmetrical fold on Gable Mountain (the western Gable Mountain anticline) to the north-west with decreasing asymmetry and an overall plunge to the west. The plunge of this feature may be related to the existence of a second-order synclinal feature (the western Gable Mountain syncline) to the south that may be equated roughly to the position of a northwest-trending paleochannel (as interpreted by Fecht, 1978; Myers, Price and others, 1979). The western Gable Mountain syncline is interpreted to be the result of structural processes with significant modification of the relief in the TOB by subsequent erosional processes.

The northwest orientation of most of the major structural features in the Gable Gap area does not suggest their continuation to the south into the Cold Creek syncline. The northeast-trending bedrock depressions interpreted around wells 53-55 and 55-60B are counter to this general northwest trend. However, based on aeromagnetic data, these features are interpreted to be of limited extent and not likely to continue into the Cold Creek syncline.

DB-10 AREA

A group of geophysical surveys was conducted by BWIP south of Gable Mountain and are referred to here as the DB-10 survey (Fig. D-1). The emphasis of the DB-10 survey was to examine the relationship between faulting interpreted south of Gable Mountain in DB-10 (Myers, Price and others, 1979) and faulting observed by Bingham and others (1970), Fecht (1978), and Myers, Price and others (1979) on the central portion of Gable Mountain (sec. 19, T. 13 N., R. 27 E.). Aeromagnetic, ground magnetics, gravity, and direct-current resistivity were the techniques used in this survey area.

Borehole data in the area indicated that DB-10 is located on a bedrock high. This bedrock high will be referred to as the DB-10 anticline. Interpreted trends from the geophysical data indicate that the DB-10 anticline is primarily oriented west to northwest, with a more northward orientation some 600 m west of the borehole. It is not certain whether these trends reflect simple reorientation of the DB-10 anticline or more complex structural complications, such as faulting or lower order folding. A connection between faults penetrated in DB-10 and faults observed on the central portion of Gable Mountain is not strongly indicated by the results of these surveys.

AEROMAGNETIC SURVEY

The faults mapped on the western and central segments of Gable Mountain (Myers, Price and others, 1979) are not displayed as solutions in the Werner deconvolution interpretive method, although some indication of the fault on central Gable Mountain is displayed in the total field and residual maps from the 760-m survey elevation (Appendix B). The southern face of the mountain displays a fault-like solution to the west, but the fault solution from the 990-m survey elevation terminates abruptly in the W1/2 sec. 19, T. 13 N., R. 27 E. The fault solution for the 760-m survey turns suddenly southeast in this location and continues to the north of DB-10 (sec. 29, T. 13 N., R. 27 E.; Fig. D-15). The presence of the Werner deconvolution solution in the location of DB-10 is not conclusive evidence for the continuation of the faulting on Gable Mountain to this borehole. Modeling of the aeromagnetic data in this area is planned to further evaluate this relationship.

GABLE MOUNTAIN SYNCLINE

Gravity data from the northern ends of lines 121, 122, and DB-10 north (Fig. D-9, D-10, and D-11) indicate an east-west-trending gravity low south of Gable Mountain. This low is interpreted to represent a continuation of the western Gable Mountain syncline across the area. A terrain-corrected gravity profile (DB-10 north; Fig. D-11) expresses a steeper gradient between 150 and 900 m than does line 122 (Fig. D-10). Gravity data are interpreted to represent a deepening of the Gable Mountain syncline to the east and places the syncline axis asymmetrically against the south side of Gable Mountain (Fig. D-15).

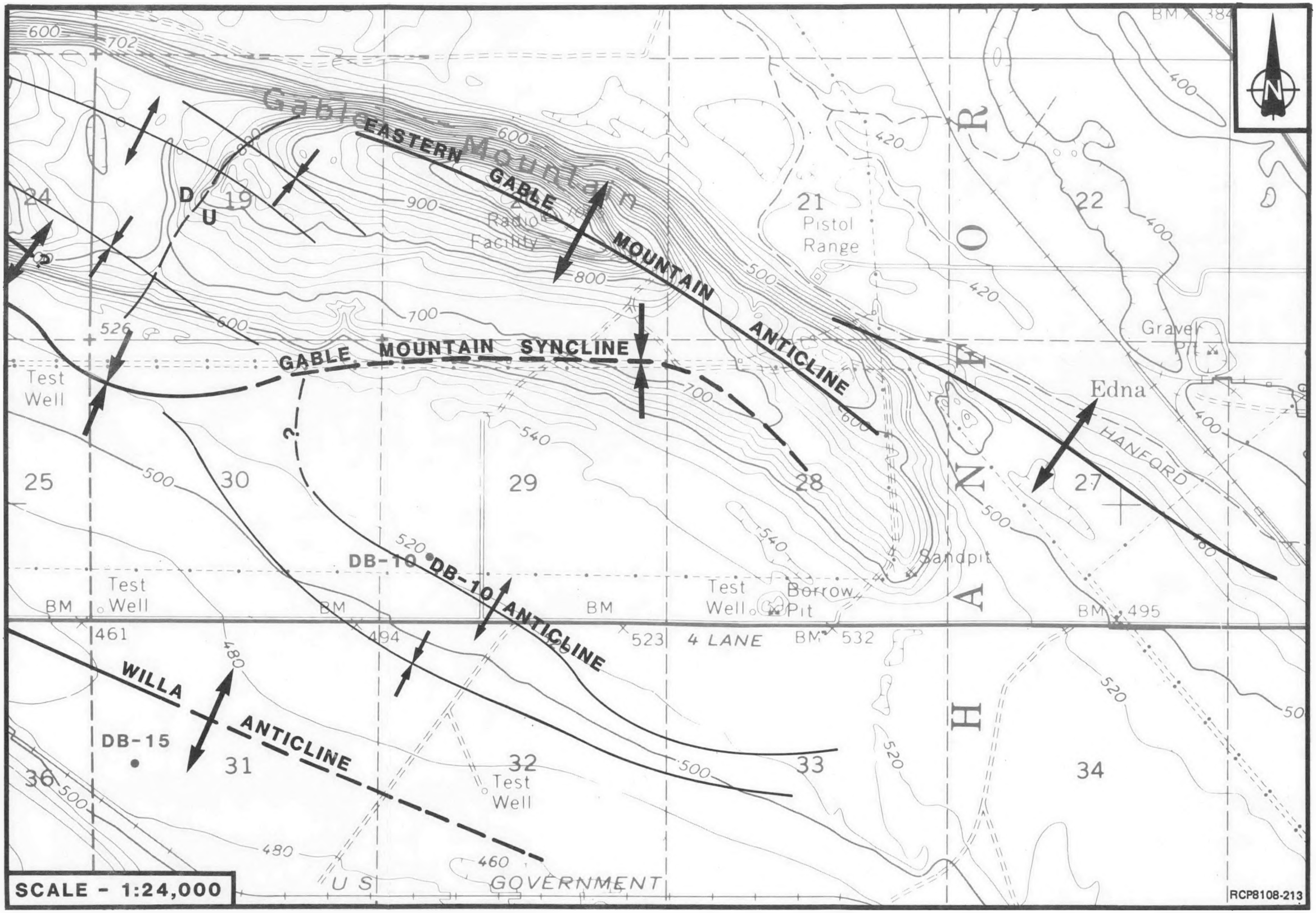

FIGURE D-15. DB-10 Area Interpretation Map (see Fig. D-14 for explanation).

Ground magnetics were used in the DB-10 survey area to interpret the continuation of the DB-10 anticline to the northwest from known control points near borehole DB-10. Magnetic profiles 206, 209, and 207 (Fig. D-8) show a subdued field up to the 1,300-m point where the signatures show a distinctive change. Magnetic lines to the east of this point (122, 125, 127, and 128; Fig. D-9, D-10, and D-11) exhibit similar anomalies. These magnetic anomalies are taken to represent a rise of the basalt to near the surface. This rise in the basalt is interpreted to represent a northern extension of the DB-10 anticline. This interpretation is supported by the presence of basalt outcrop at the 180-m point on line 122 (Fig. D-10), a coincident gravity high.

The trend of the magnetic anomalies in the vicinity of DB-10 are primarily west-northwest. The magnetic profiles to the west of line 122 (Fig. D-1), some 600 m west of borehole DB-10, show a reorientation of the magnetic anomalies to a north-northwest direction. The presence of anomalies near the 1,300-m point of line 209 demonstrates this general change of orientation. These magnetic data are interpreted to represent a northward reorientation of the bedrock high associated with the DB-10 anticline (see Fig. D-15).

The change of magnetic character between lines 126, 122, and 128, as opposed to lines 127, 206, and 209, suggests that there is a change of the configuration of the basalt subsurface and not simply a reorientation of the anticline. Interference from electrical transmission lines prevents the use of magnetic methods to trace this trend farther north. Other geophysical methods and further modeling studies will be required to examine the geometry of the bedrock surface and its northward continuation.

The continuation of the DB-10 anticline to a topographic high located on the east part of Gable Mountain indicates a possible genetic relationship between the DB-10 anticline and general structure on eastern Gable Mountain. However, this possible relationship does not necessarily imply the southward continuation of faulting observed on Gable Mountain. Preliminary gravity data from Weston Geophysical Research, Inc. (for Northwest Energy Services Company) are interpreted to indicate a trend for the DB-10 anticline well to the east of faulting mapped on the central portion of Gable Mountain.

GEOPHYSICAL CROSS SECTION, DB-10 ANTICLINE

Survey line 122 (Fig. D-10 and D-12) was run across the interpreted axis of the DB-10 anticline some 600 m to the west of borehole DB-10. Gravity, ground magnetics, and direct-current resistivity were conducted on this profile (Fig. D-1). A limited amount of preliminary gravity and magnetics modeling was conducted to test possible interpretations. The Elephant Mountain Member crops out near the 180-m position on this line, establishing a control point for the TOB in this area. The gravity data on line 122 (Fig. D-10 and D-12) show an increase of gravity values from a low point south of Gable Mountain to a high at the 240-m point, where

it drops again. The magnetic values show a gradual rise to the 390-m point on line 122, where the field varies considerably, probably due to the presence of basalts of varying polarity (reverse Pomona and transitional Elephant Mountain).

The dipole-dipole resistivity survey (Fig. D-12 [b]) yields a contoured pseudosection showing a central body of intermediate-apparent resistivity, most likely basalt, covered by a zone of high-apparent resistivities, most likely sediment cover. Contained within the intermediate-resistivity zone are two apparently north-dipping, low-resistivity zones which may represent saturated sedimentary interbeds. Gross averaging of the resistivity technique prevents direct literal interpretation of the pseudosection. Modeling of these resistivity data is necessary before further statements can be made about the actual dip of these resistivity zones.

Preliminary magnetic modeling indicates the existence of both folding and erosion of the units on the south flank of the anticline, although faulting has not been entirely ruled out. Gravity modeling based on the resistivity pseudosection yields the bedrock configuration shown on Figure D-12 (c). A comparison of the calculated and observed gravity values is shown in Figure D-12 (d) and, although a north-dipping sediment interbed is included in the model, it has little effect on the calculated values. This group of surveys indicates a southward, asymmetrical configuration of the TOB in the location of line 122 (Fig. D-10). It is not certain at this time whether this asymmetry is due to asymmetric folding of the DB-10 anticline, from erosion, or from faulting on the south side of the anticline.

DB-10 AREA CONCLUSIONS

Interpreted trends in geophysical data around borehole DB-10 are primarily west to northwest with a reorientation northward some 600 m west of the borehole. It is not certain whether these trends reflect simple reorientation of the anticline or more complex structural complications, such as faulting, complex folding, or erosion. Continuation of faults observed in borehole DB-10 to faults observed on the central portion of Gable Mountain is not strongly indicated by the results of these surveys. The presence of a Werner deconvolution solution between the DB-10 anticline and eastern Gable Mountain does indicate a possible structural relationship between these two features. Additional geophysical surveys and modeling studies will be necessary before further conclusions can be derived in this area. A geologic interpretation based on the current data set is shown in Figure D-15.

APPENDIX E - GEOPHYSICAL INVESTIGATIONS IN THE WEST GABLE BUTTE AREA

M. P. Cochran

INTRODUCTION

The west Gable Butte geophysical survey was designed to investigate the presence of potential bedrock faulting along the northern flank of Gable Butte (Fig. E-1). The possibility of faulting in this area was recognized on the basis of the preliminary interpretation of seismic-reflection (SR) data collected along line 5 (Route 6, Fig. E-1), which indicates a structural feature near the westernmost outcrops of Gable Butte (Appendix B). Attention was also given to the structural relationship between Umtanum Ridge and Gable Butte.

Basalt flows from the Umatilla, Esquatzel, Pomona, and Elephant Mountain Members of the Saddle Mountains Basalt are exposed on Gable Butte (Fig. E-1). These flows thin to the west over the Umtanum structure, which probably began growth in pre-Umatilla time (Goff, 1981). The Ringold Formation, glaciofluvial sands and gravels (Hanford formation), and a veneer of eolian loess cover parts of the flanks of Gable Butte and the surrounding plain (Lillie and others, 1978). See Chapters 2 and 3 for general details of the basalt stratigraphy and supra-basalt sediment stratigraphy.

The Gable Butte structure has been interpreted as parasitic folds situated within the closure of a larger anticline--the eastern Umtanum Ridge structure (Fecht, 1978). The major fold is asymmetrical, with a north flank that dips steeply into the Wahluke syncline and a south flank that dips gently into the Cold Creek syncline. The geomorphic expression of the Gable Butte area resulted from the complex folding and subsequent scouring by post-basalt fluvial systems (Fecht, 1978).

Jones and Deacon (1966) proposed a northeasterly trending, sinistral, strike-slip fault across the west end of Gable Butte. However, Fecht (1978) found no evidence for shearing in the bedrock at this location; he interpreted the exposures of bedrock structures at the western end of Gable Butte as west-northwest-trending, parasitic anticlines (Fig. E-1).

Previous ground geophysical studies in the vicinity of the west Gable Butte area utilized gravity, magnetic, and seismic-refraction techniques (Lillie and Richard, 1977; Raymond, 1958, 1968; Richard, 1976; Weston Geophysical Research, 1978a). The locations of the individual survey traverses from previous work are indicated on Figure E-1.

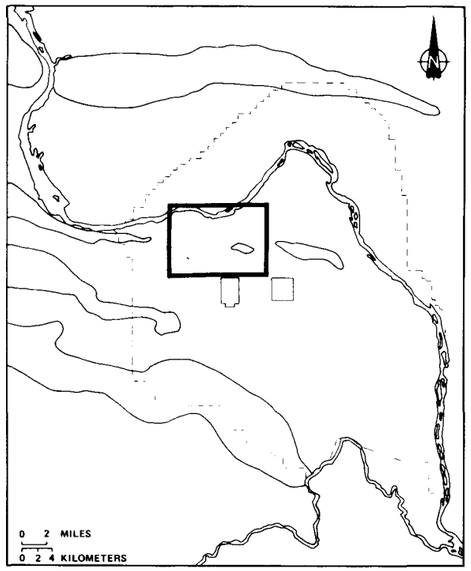

INDEX

GEOPHYSICAL TRAVERSE SYMBOLS

MAGNETIC SURVEY

GRAVITY SURVEY

SEISMIC SURVEY

REFLECTION SEISMIC ANOMALY

OVERLAPPING SURVEYS

MAGNETIC AND GRAVITY

MAGNETIC AND SEISMIC

GRAVITY AND SEISMIC

GRAVITY, MAGNETIC, AND SEISMIC

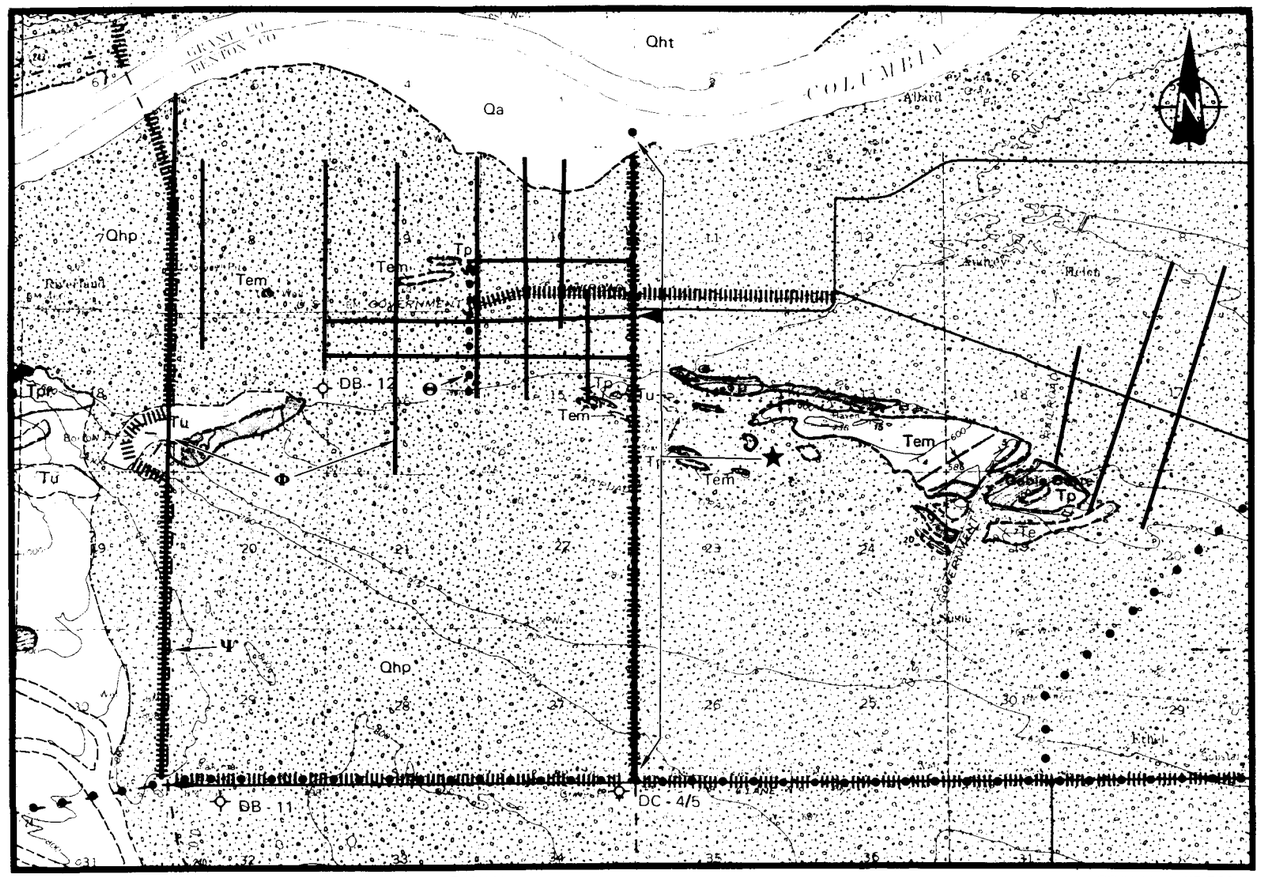

AEROMAGNETIC COVERAGE: (WPPSS, 1977; SWANSON AND OTHERS, 1979c; APPENDIX B)

Θ PACIFIC NORTHWEST LABORATORY SEISMIC REFRACTION LINE (RAYMOND, 1968)

★ ROUTE 6 INCLUDES THE FOLLOWING SURVEYS: GRAVITY (LILLIE AND RICHARD, 1977; WESTON GEOPHYSICAL, 1978a)
MAGNETICS (RAYMOND, 1958; WESTON GEOPHYSICAL, 1978a)
REFLECTION SEISMICS (APPENDIX B)

Φ MAGNETICS (RAYMOND, 1958)

Ψ INCLUDES THE FOLLOWING SURVEYS: GRAVITY (RICHARD, 1976; WESTON GEOPHYSICAL, 1978a)

RCP8108-214

FIGURE E-1. Location Map, Geophysical Surveys Conducted in West Gable Butte Area (see Table 3-1 for explanation).

Aeromagnetic surveys that included the west Gable Butte area have been flown at the following flight levels: (1) 150-m draped (Swanson and others, 1979c), (2) 305-m draped (WPPSS, 1977), and (3) 760-, 990-, 1,220-m constant level, with partial coverage over the southwestern half of the study area at 1,450- and 1,680-m levels (Appendix B).

SURVEY METHODS

Two geophysical methods were chosen for this study: (1) total field magnetics and (2) gravity. Data were collected along 10 magnetic traverses and 2 gravity traverses within the study area (Fig. E-2). Overlapping gravity and magnetic traverses were surveyed over the SR anomaly (traverse 7, Fig. E-2).

Total field magnetic intensity was sampled at 15-m station intervals with a GeoMetrics Model G 816 proton precession magnetometer. Station separation was established by pacing. Diurnal variations were monitored to within ±1 gamma, with a GeoMetrics Model G 826A base station magnetometer. Sensor elevation was kept at a constant 2.4 m above ground-surface elevation.

Gravity measurements were collected with a Worden gravimeter. Station separations on traverse 7 (Fig. E-2) varied from 61 m (from 0 to 244 and from 2,515 to 2,819 m) to 30.5 m (from 244 to 2,515 m). Intervals on traverse 9 (Fig. E-2) were established at a constant 100 m. Drift curves were established by the loop method, with individual bases reoccupied at intervals not exceeding 2 hr. Station elevations were surveyed to within ±0.03 m with a Zeiss Th 43 theodolite.

DATA PROCESSING

Data processing was minimal for the magnetic survey data. Diurnal variations were judged to be insignificant relative to anomaly amplitude; therefore, no drift corrections were applied to the data. Profile plots of total field magnetic intensity versus distance were utilized for qualitative interpretations (Fig. E-3 through E-7). Segments of magnetic data were omitted whenever sources of magnetic interference distorted the field (i.e., powerlines, pipes); these segments are queried on the profile plots.

Latitude, free-air, and Bouguer corrections were applied to the gravity data. A density of 2.67 g/cm^3 and mean sea-level datum were used for the Bouguer gravity calculations. Terrain corrections using Hammer's (1939) method (zones D through I) with a density of 2.67 g/cm^3 were applied to every fifth station along traverse 7. Corrections for intermediate stations were calculated by interpolation between these values. Bouguer gravity profiles are plotted on Figure E-8.

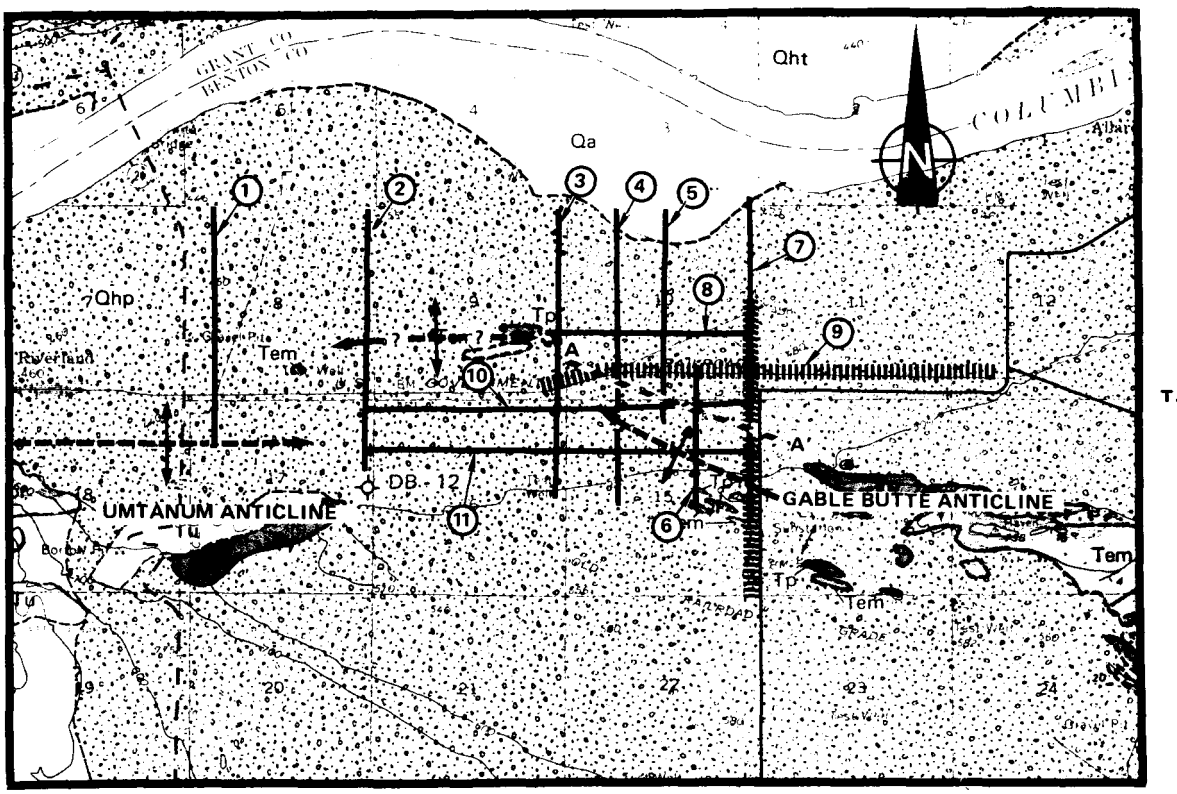

LEGEND

MAGNETIC TRAVERSE

GRAVITY TRAVERSE

TRAVERSE NUMBER (9)

INFERRED ANTICLINE

MAGNETIC LINEAR A — — — A'

REFER TO PREVIOUS FIGURE FOR INDEX LOCATION

RCP8108-215

FIGURE E-2. Basalt Waste Isolation Project Gravity and Magnetic Traverse Locations.

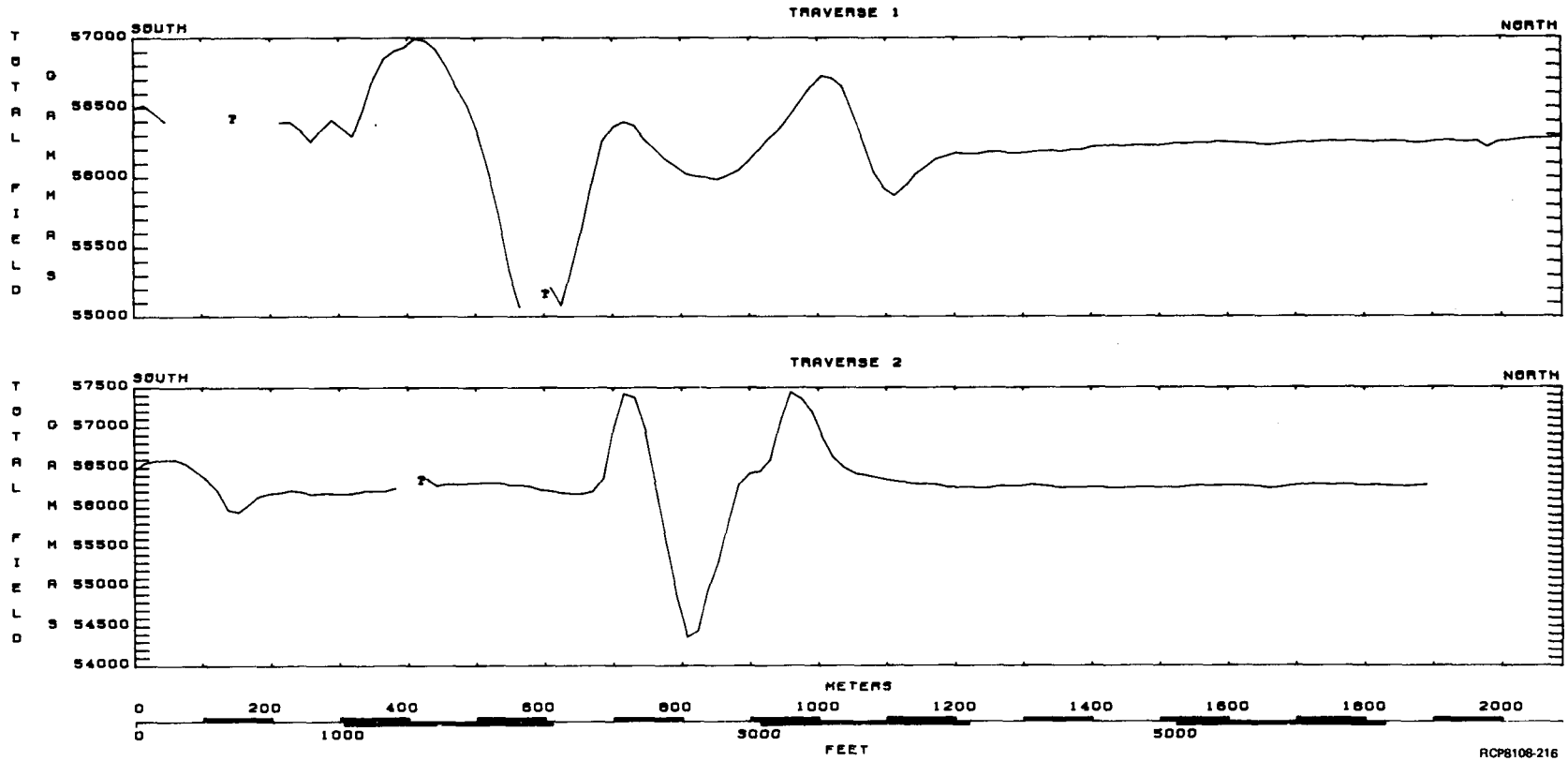

FIGURE E-3. West Gable Butte Magnetic Profiles for Traverses 1 and 2.

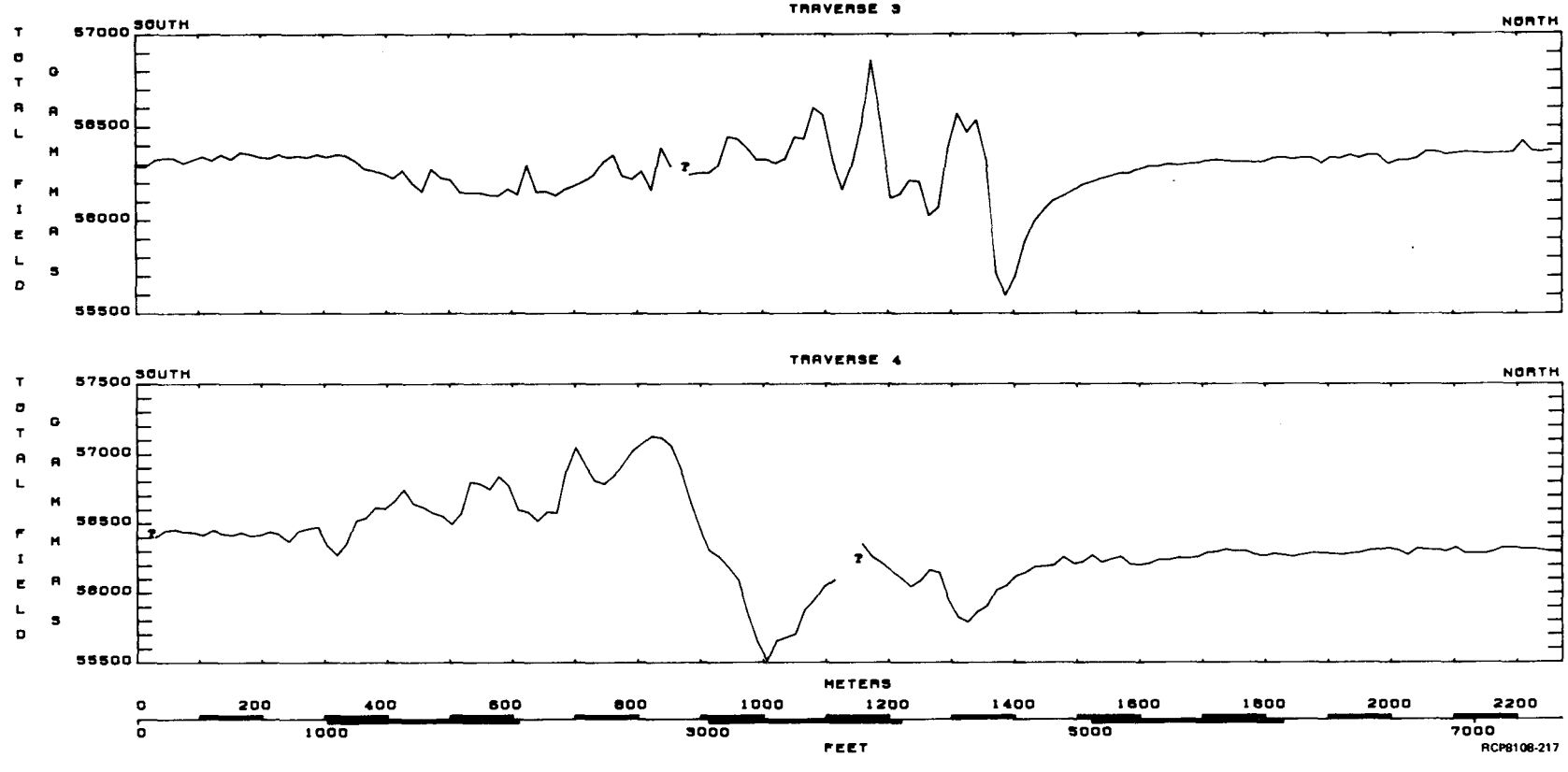

FIGURE E-4. West Gable Butte Magnetic Profiles for Traverses 3 and 4.

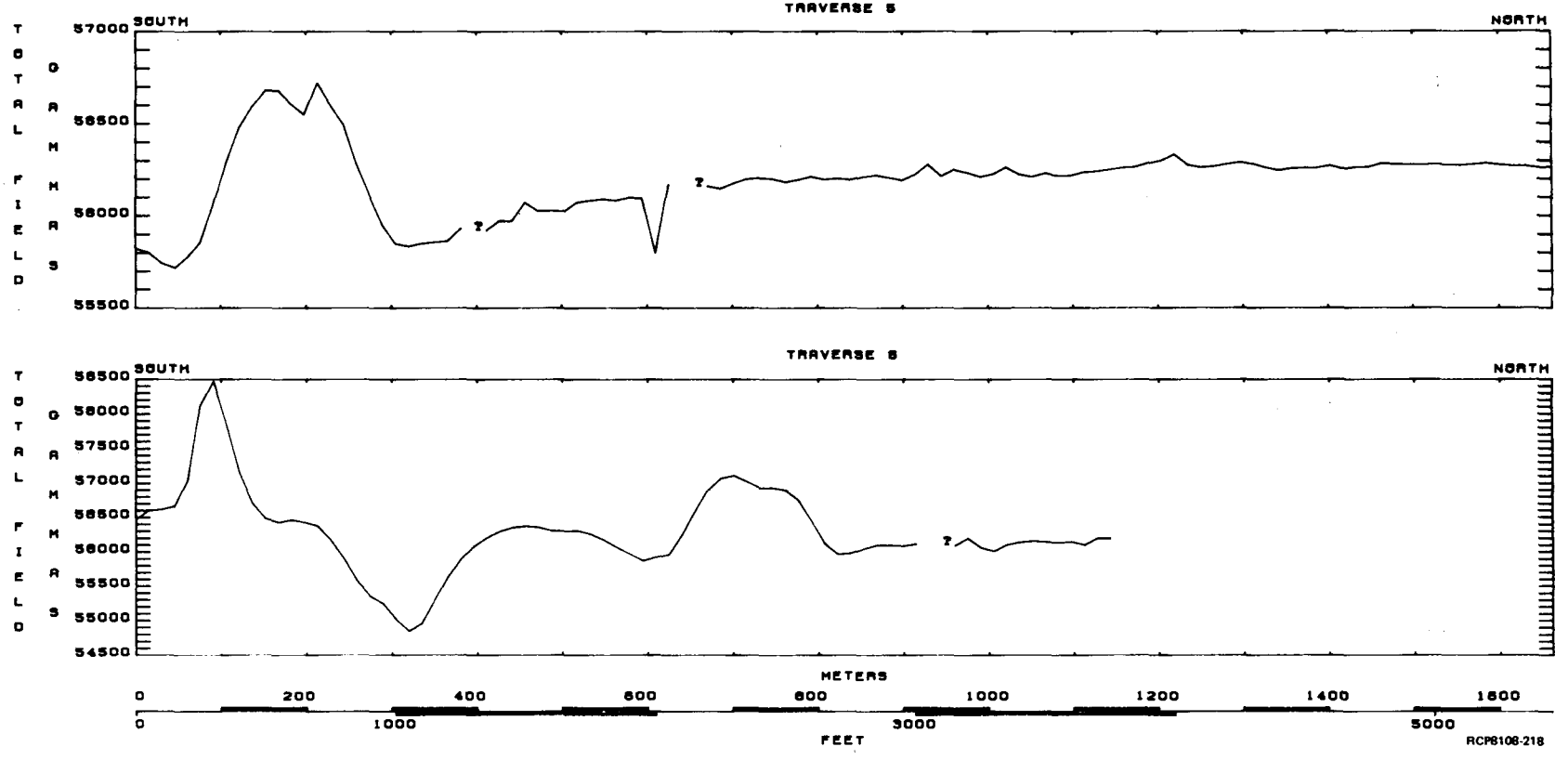

FIGURE E-5. West Gable Butte Magnetic Profiles for Traverses 5 and 6.

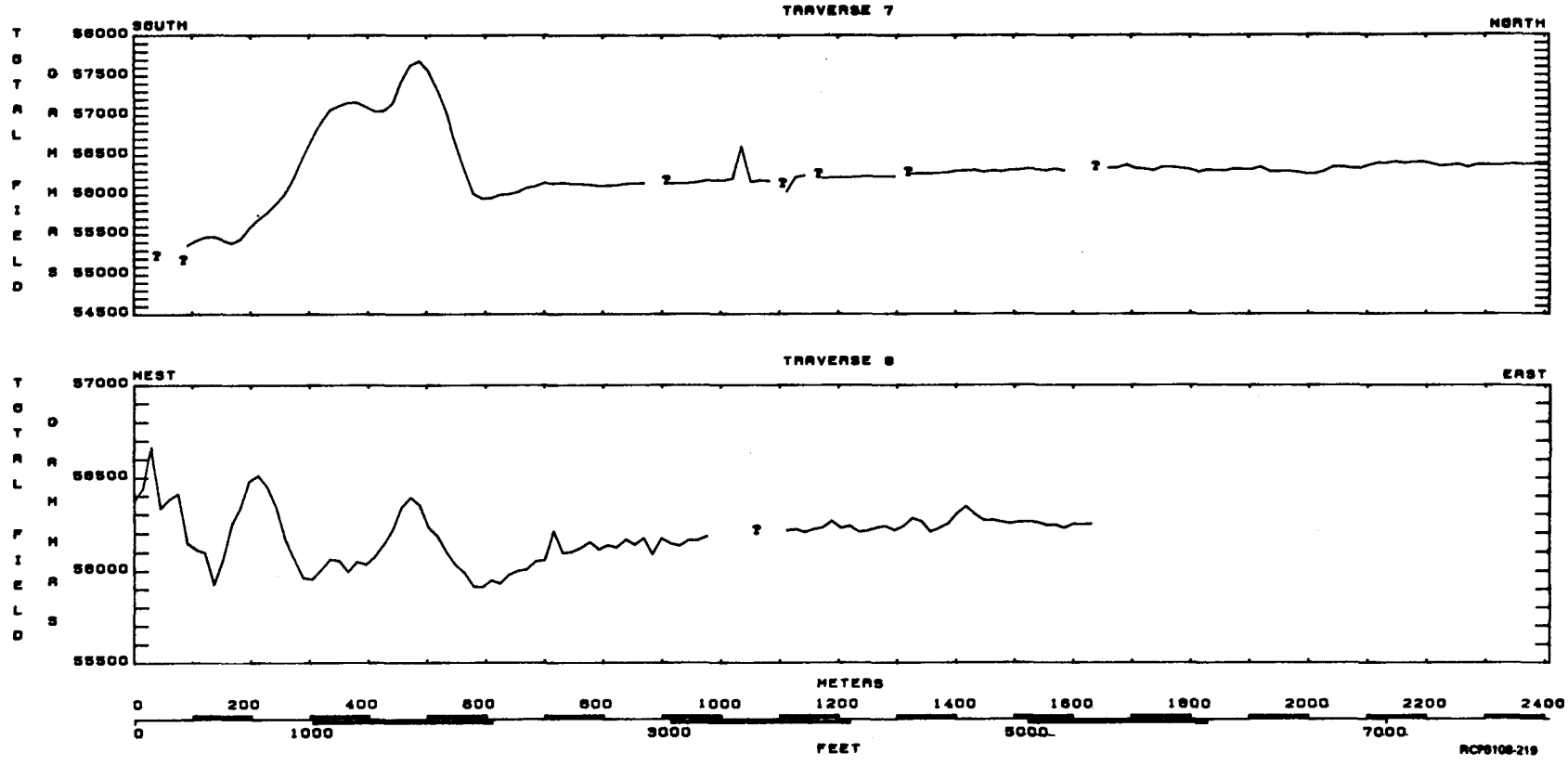

FIGURE E-6. West Gable Butte Magnetic Profiles for Traverses 7 and 8.

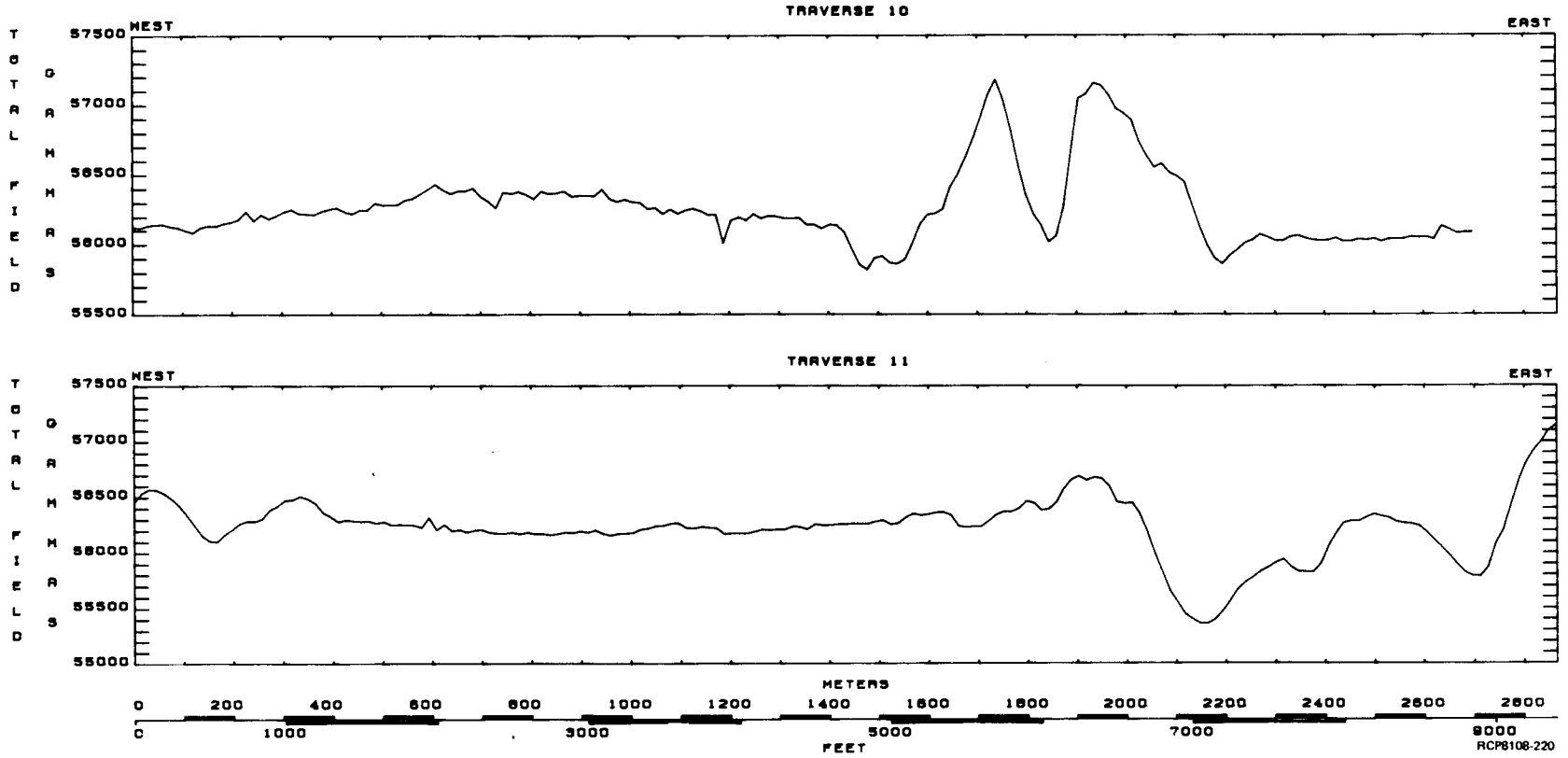

FIGURE E-7. West Gable Butte Magnetic Profiles for Traverses 10 and 11.

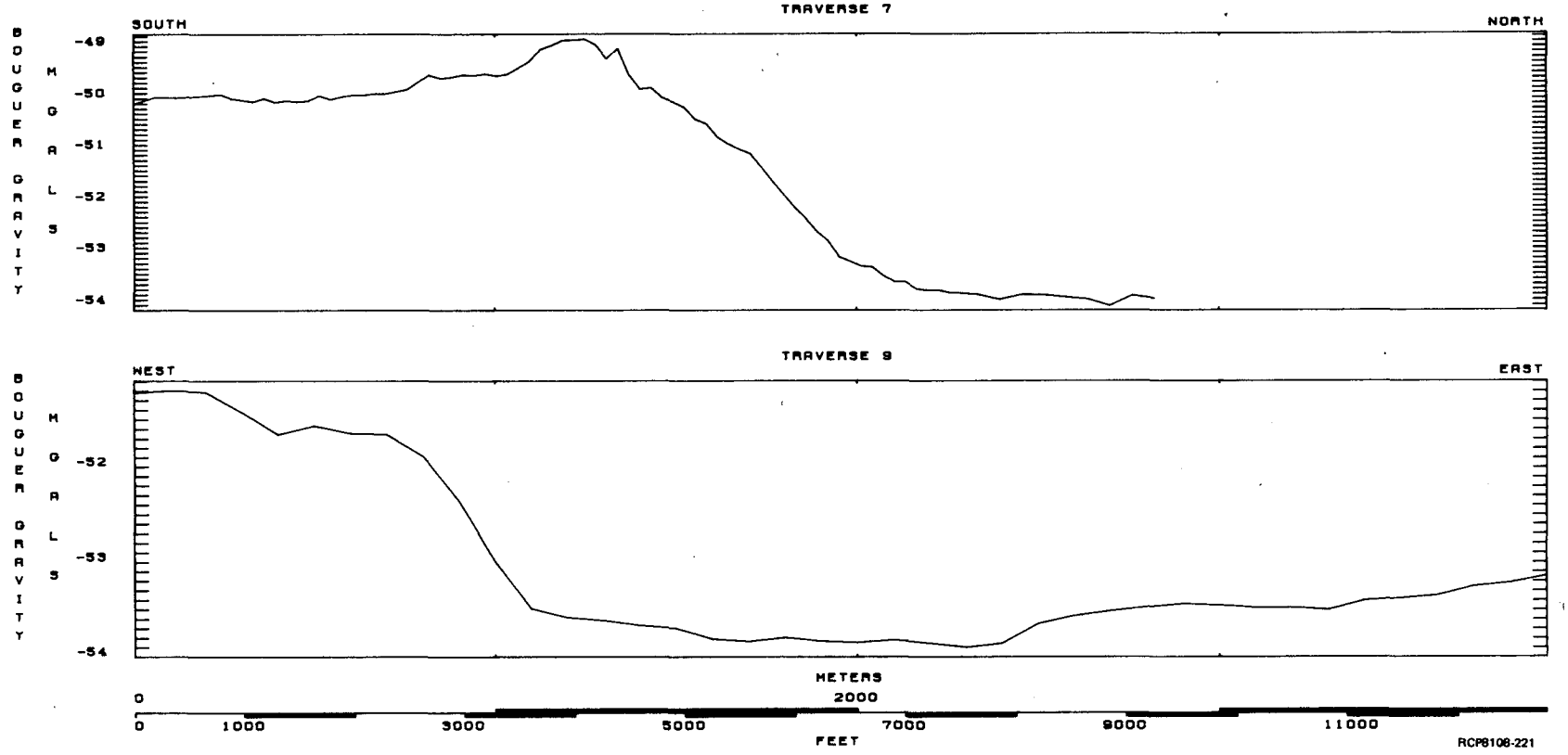

FIGURE E-8. West Gable Butte Bouguer Gravity Profiles for Traverses 7 and 9.

INTERPRETATION OF RESULTS

The gravity and magnetic traverses revealed trends and anomalies primarily related to effects originating from the shallow portion of the basalt bedrock.

The magnetic profiles show a complex set of anomalies that vary considerably between adjacent lines; however, some general relationships are evident. The positive magnetic anomalies centered at 200 m on traverse 5 (Fig. E-5), 700 m on traverse 6 (Fig. E-5), and 500 m on traverse 7 (Fig. E-6) have comparable wavelengths (200 to 250 m) and similar amplitudes (1,000 to 1,500 gammas). These features suggest a common source configuration, which may be a north-dipping basalt flow with positive natural remanent magnetism such as the Sillusi flow of the Umatilla Member. These anomalies align along a N70°W trend (A-A', Fig. E-2) which is approximately parallel to the strike of the Pomona and Umatilla outcrops on the north limb of the breached anticline exposed in the central part of sec. 14 due east of traverse 7. Traverse 4 revealed a similar positive anomaly where it intersects the projection of the N70°W trend (825 m, Fig. E-4), but is complicated by shorter wavelength anomalies to the north and south.

Magnetic anomalies on traverse 3 (Fig. E-4) do not correspond to the anomalies along the N70°W trend defined by the traverses to the east. Therefore, a structural or erosional boundary, or both, is interpreted to occur between the west Gable Butte structures and the bedrock exposures in sec. 9 between traverses 3 and 4.

Magnetic traverses 10 and 11 (Fig. E-7) both display high-amplitude anomalies on their eastern halves, but show relatively minor anomalies to the west. The symmetrical character of the anomalies on traverse 10, between 1,400 and 2,200 m, and on traverse 11, between 1,800 and 2,800 m, suggests a flow distribution that might be encountered along a traverse subperpendicular to the axis of a buried, breached anticline (Fig. E-2).

Gravity traverses 7 and 9 (Fig. E-8) both display significant anomalies related primarily to the density contrast between the basalts and overlying sediments. The abrupt increases in the Bouguer gravity, commencing at 2,000 m on traverse 7 and 1,100 m on traverse 9, are both attributed to an increase in the elevation of the top of basalt. Erosion of the Umtanum Ridge-Gable Mountain structure during the Pliocene and Pleistocene may have produced bedrock topography that does not necessarily follow structural trends. Therefore, it is speculative to interpret the Bouguer gravity anomalies on traverses 7 and 9 as being directly related to a common structural trend.

The positive magnetic anomaly (500 m, Fig. E-6) and the rise in Bouguer gravity (1,000 to 2,000 m, Fig. E-8) on traverse 7 are apparently indicating a common bedrock feature associated with the northern flank of the Gable Butte structure. The SR anomalies detected on Route 6 (Fig. E-1)

also correlate with this interval. It is not immediately apparent from the seismic section (Appendix B) what source configuration is responsible for these anomalies. However, both the gravity and magnetics indicate an abrupt, southerly rise in the surface of basalt at this location, which is interpreted as the north limb of the Gable Butte anticline (Fig. E-2). The gentle decrease in the Bouguer gravity to the south of the high on traverse 7 (1,300 m) probably reflects the gently dipping southern limb of the Umtanum-Gable Butte anticline.

Magnetic traverses 1 and 2 (Fig. E-3) display dissimilar anomalies, which are difficult to relate with anomalies on the traverses to the east. The magnetic anomaly on traverse 2 (Fig. E-3), located between 600 and 1,100 m, may be an expression of the structure exposed due east of the anomaly in the SE1/4 sec. 9 (Fig. E-2). Preliminary, two-dimensional, magnetic modeling suggests the source of this anomaly is a truncated sequence of southerly dipping Elephant Mountain and Pomona basalts similar to that exposed in sec. 9 (Fig. E-2). Alternatively, this anomaly may be related to the southern limb of an anticlinal structure; however, there is no geophysical evidence for the north-dipping limb on any of the current geophysical traverses in the northern halves of sec. 8 and 9 (Fig. E-2). Another possible explanation for this anomaly is that it represents the bedrock geometry associated with a southerly dipping thrust fault.

Magnetic anomalies located from 0 to 1,100 m on traverse 1 (Fig. E-3) do not appear directly related to the aforementioned anomaly on traverse 2. Rather, they appear to be an expression of the north limb of the Umtanum fold structure exposed in the S1/2 sec. 17 (Fig. E-2).

The magnetic anomalies between 0 and 150 m on traverse 2 (Fig. E-3) and between 0 and 400 m on traverse 11 (Fig. E-7) are probably related to the termination of the easterly plunging Umtanum anticline in sec. 17 (Fig. E-2).

CONCLUSIONS

The distribution and character of gravity and magnetic anomalies in the west Gable Butte area are interpreted as indicating three, main, buried, structural elements.

Magnetic anomalies on the southern half of traverse 1, the southern end of traverse 2, and the western end of traverse 11 are probably related to the eastern terminus of the Umtanum anticline (Fig. E-2).

The centrally located anomalies on traverses 2 and 3 are probably associated with either an east-west-trending, parasitic anticline, or a south-dipping, thrust fault. The buried bedrock structure producing these anomalies is most likely related to the exposures of bedrock in the SE1/4 sec. 9 (Fig. E-2).

The complex set of anomalies revealed by traverses 4 through 11 are most likely a product of the northwest-plunging Gable Butte anticline, located in sec. 14 and 15 (Fig. E-2). The structural relationship between this anticline and the inferred anticline or fault in sec. 9 is difficult to establish with the present data set. The high-frequency, variable, magnetic anomalies on traverses 3, 4, and 8 in the SW1/4 sec. 10 (Fig. E-2) are probably a function of the interference between these two structures, as well as scabland topography that developed from catastrophic flooding.

No conclusive evidence of faulting associated with the folding was recognizable in the survey area. The structural disturbance located by the SR survey along Route 6 (Fig. E-1) is probably associated with the steep, north-dipping limb of the Gable Butte anticline. It is difficult to say without additional drill hole information whether the northern limb of the structure has been disrupted by faulting. It appears, as Raymond (1958) concluded, that the Umtanum and Gable Butte folds are separate structures; however, they probably owe their evolution to similar regional stresses.

APPENDIX F - REFERENCES

Ames, L. L. 1980, Hanford basalt flow mineralogy: PNL-2847, Pacific Northwest Laboratory, Richland, Washington.

ARHCO, 1976, Preliminary feasibility study on storage of radioactive waste in Columbia River basalts: ARH-ST-137, Atlantic Richfield Hanford Company, Richland, Washington.

Baker, V. R., 1973, Paleohydrology and sedimentology of Lake Missoula flooding in Eastern Washington: Geological Society of America Special Paper 144.

Baker, V. R. and Nummedal, D., 1978, The channeled scabland: National Aeronautics and Space Administration field conference held on the Columbia Plateau, June 5-8, 1978.

Beck, M. E., Engebretson, D. C., and Plumley, P. W., Western Washington University, 1978, Magnetostratigraphy of the Grande Ronde sequence: RHO-BWI-C-18, Rockwell Hanford Operations, Richland, Washington.

Benson, L. V. and Teague, L. S., 1979, A study of rock-water-nuclear waste interactions in the Pasco Basin, Washington: LBL-9677, Lawerence Berkeley Laboratory, Berkeley, California.

Bentley, R. D., 1977, Stratigraphy of the Yakima Basalts and structural evolution of the Yakima Ridges in the Western Columbia Plateau: in Geology Excursions in the Pacific Northwest, Geological Society of America Annual Meeting, Seattle, Washington.

Bingham, J. W. and Grolier, M. J., 1966, The Yakima Basalt and Ellensburg Formation of south-central Washington: U.S. Geological Survey Bulletin 1224-G.

Bingham, J. W. and Walters, K. L., 1965, Stratigraphy of the upper part of the Yakima Basalt in Whitman and eastern Franklin Counties, Washington: U.S. Geological Survey Professional Paper 525-C, pp. C87-C90.

Bingham, J. W., Londquist, C. J., and Baltz, E. H., 1970, Geologic investigation of faulting in the Hanford region, Washington: with a section on the occurrence of microearthquakes by Pitt, A. M.: U.S. Geological Survey Open-File Report, 104 p.

Bjornstad, B. N., 1980, Sedimentology and depositional environment of the Touchet Beds, Walla Walla River Basin, Washington: RHO-BWI-SA-44, Rockwell Hanford Operations, Richland, Washington, 83 p.

Black, R. F., 1979, Clastic dikes of the Pasco Basin, southeastern Washington: RHO-BWI-C-64, Rockwell Hanford Operations, Richland, Washington, 65 p.

Blume, J. A. and Associates, 1971, Subsurface geologic investigations for the FFTF project in the Pasco Basin: JABE-WADCO-07, Westinghouse, Richland, Washington.

Bretz, J. H., 1923, The channeled scablands of the Columbia Plateau: Journal of Geology, v. 31, no. 8, pp. 617-649.

Bretz, J. H., 1925, The Spokane flood beyond the channeled scabland: Journal of Geology, v. 3, pp. 96-115.

Brooks, W. E., 1974, Stratigraphy and structures of the Columbia River basalt in the vicinity of Gable Mountain, Benton County, Washington: M.S. Thesis, University of Washington, Seattle, Washington.

Brown, D. J., 1959, Subsurface geology of the Hanford separation areas: HW-61780, General Electric Hanford Atomic Products Operation, Richland, Washington.

Brown, D. J. and Ledgerwood, R. K., 1973, Stratigraphy and structure of Yakima Basalt in the Pasco Basin, Washington: Geological Society of America Bulletin 77, Cordilleran Section Field Trip No. 6.

Brown, R. E., 1975, Ground-water and the basalts in the Pasco Basin: in Proceedings of the Thirteenth Engineering Geology and Soils Engineering Symposium, April 2, 3, 4, 1975, Moscow, Idaho.

Brown, R. E., 1981, A review of water well data from the unconfined aquifer in the eastern and southern parts of the Pasco Basin: RHO-BWI-C-56, Rockwell Hanford Operations, Richland, Washington.

Brown, R. E. and Raymond, J. R., 1964, Geophysical seismic evaluation study at Hanford: BNWL-47, Battelle, Pacific Northwest Laboratories, Richland, Washington.

BWIP Staff, 1980, Identificaton of candidate sites suitable for a geologic repository in basalt within Hanford: RHO-BWI-LD-24, Rockwell Hanford Operations, Richland, Washington.

Caggiano, J. A., Fecht, K. R., Price, S. M., Reidel, S. P., and Tallman, A. M., 1980, A preliminary assessment of the relative rate of deformation in the Pasco Basin, south-central Washington: Geological Society of America, Annual Meeting, Atlanta, Georgia; also RHO-BWI-SA-73A, Rockwell Hanford Operations, Richland, Washington.

Cain, J. C., Hendricks S., Daniels, W. E., and Jensen, D. C., 1968, revised by Cain, S. H., Computation of the main geomagnetic field from spherical harmonic expansions: NASA Technical Publication, Data Users Note NSSDC 68-11.

Camp, V. E., 1976, Petrochemical stratigraphy and structure of the Columbia River basalt, Lewiston Basin area, Idaho-Washington: Ph.D. Dissertation, Washington State University, Pullman, Washington.

Choinier, S. R. and Swanson, D. A., 1979, Magnetostratigraphy and correlation of Miocene basalts of the northern Oregon coast and Columbia Plateau, southeast Washington: American Journal of Science, v. 279, no. 7, pp. 755-777.

Clague, J. J., Armstrong, J. E., and Mathews, W. H., 1980, Advance of late Wisconsin Cordilleran ice sheet in southern British Columbia since 22,000 yr B.P.: Quaternary Research, v. 13, no. 3, pp. 322-326.

Cobbold, P. R., Cosgrove, J. W., and Summers, J. M., 1971, Development of internal structures in deformed anisotropic rocks: Tectonophysics, v. 12, pp. 23-53.

Coe, R. S., Bogue, S., University of California at Santa Cruz, and Myers, C. W., 1978, Paleomagnetism of the Grande Ronde (lower Yakima) Basalt exposed at Sentinel Gap: potential use for stratigraphic correlation: RHO-BWI-ST-2, Rockwell Hanford Operations, Richland, Washington.

Converse, Davis and Associates, 1969, Logs of exploratory trenches on Gable Mountain at the Hanford works of the U.S. Atomic Energy Commission, Richland, Washington: Pasadena, California.

Converse, Davis and Associates, 1971, Logs of exploratory trenches on Gable Mountain at the Hanford Works of the U.S. Atomic Energy Commission, Richland, Washington: Pasadena, California.

Deere, D. U., 1963, Technical description of rock cores for engineering purposes: Felsmechanik Und Ingenieurgeologie, v. 1, no. 1, pp. 16-22.

Deju, R. A. and Richard, B. H., 1975, A regional gravity investigation of the Hanford Reservation: ARH-C-8, Atlantic Richfield Hanford Company, Richland, Washington.

Diery, H., 1967, Stratigraphy and structure of Yakima canyon between Roza gap and Kittitas valley: Ph.D. Dissertation, University of Washington, Seattle, Washington.

DOE, 1980, Statement of position of the U.S. Department of Energy in the matter of proposed rulemaking on the storage and disposal of nuclear waste--waste confidence rulemaking: DOE/NE-0007, U.S. Department of Energy, Washington, D.C.

Donaldson, J. A., 1963, Seismic survey, Hanford Atomic Products Operation, Richland, Benton County, Washington: GEH-26275, General Electric Hanford Atomic Products Operation, Richland, Washington.

Fecht, K. R., 1978, Geology of Gable Mountain-Gable Butte area: RHO-BWI-LD-5, Rockwell Hanford Operations, Richland, Washington.

Fecht, K. R. and Lillie, J. T., in press, A catalog of borehole lithologic logs from the 600 Area, Hanford Site: RHO-LD-158, Rockwell Hanford Operations, Richland, Washington.

Fecht, K. R. and Tallman, A. M., 1978, Bergmounds along the western margin of the channeled scablands, south-central Washington: Geological Society of America, Abstracts with Programs, v. 10, no. 7; also, RHO-BWI-SA-11, Rockwell Hanford Operations, Richland, Washington.

Fenix and Scisson, 1977, Hole history, rotary hole DC-7, Hanford Washington: RHO-BWI-C-1, Rockwell Hanford Operations, Richland, Washington.

Fitzgerald, D. D., Theriot, J. C., and York, P. L., 1980, Obtaining valid dipmeter surveys in deviated wells: World Oil, p. 91.

Flint, R. F., 1938, Origin of the Cheney-Palouse scabland tract: Geological Society of America Bulletin, v. 49, p. 461.

Friedberg, J. L., 1975, Understanding and use of Werner deconvolution, Fourth Edition: Aero Service Corporation, Houston, Texas.

Fryxell, R., 1965, Mazama and Glacier Peak volcanic ash layers: relative ages: Science, v. 147, p. 1288.

Fuller, R. E., 1931, The aqueous chilling of basaltic lava on the Columbia River Plateau: American Journal Science, v. 21, pp. 281-300.

Gephart, R. E., Arnett, R. C., Baca, R. G., Leonhart, L. S., and Spane, F. A. Jr., 1979a, Hydrologic studies within the Columbia Plateau, Washington: an integration of current knowledge: RHO-BWI-ST-5, Rockwell Hanford Operations, Richland, Washington.

Gephart, R. E., Eddy, P. A., and Deju, R. A., 1979b, Geophysical logging and hydrologic testing of deep basalt flows in the Rattlesnake Hills Well Number One: RHO-BWI-ST-1, Rockwell Hanford Operations, Richland, Washington.

Ghosh, S. K., 1968, Experiments of buckling of multilayers which permit interlayer gliding: Tectonophysics, v. 6, no. 1, pp. 207-249.

Goff, F. E., 1981, Preliminary geology of eastern Umtanum Ridge, south-central Washington: RHO-BWI-C-21, Rockwell Hanford Operations, Richland, Washington.

Goff, F. E. and Myers, C. W., 1978, Structural evolution of eastern Umtanum and Yakima Ridges, south-central Washington: Geological Society of America, Abstracts with Program, v. 10, no. 7, p. 408.

Goles, G. G., 1977, Instrumental methods of neutron activation analysis: in Zussman et al., Editors: Determinative methods in physical mineralogy: John Wiley and Sons, pp. 343-369.

Grolier, M. J., 1965, Geology of part of the Big Bend area in the Columbia Plateau, Washington: Ph.D. Dissertation, The Johns Hopkins University, Baltimore, Maryland.

Grolier, M. J. and Bingham, J. W., 1971, Geologic map and sections of parts of Grant, Adams, and Franklin Counties, Washington: U.S. Geological Survey, Miscellaneous Geologic Investigations Map I-589.

Gustafson, E. P., 1973, The vertebrate fauna of the late Pliocene Ringold Formation, south-central Washington: M.S. Thesis, Washington State University, Pullman, Washington.

Gustafson, E. P., 1978, The vertebrate faunas of the Pliocene Ringold Formation, south-central Washington: Bulletin 25, Museum of Natural History, University of Oregon, Eugene, Oregon, 62 p.

Hammer, A. A., 1934, Rattlesnake Hills gas field, Benton County, Washington: Bulletin of the American Association of Petroleum Geologists, v. 18, no. 7, p. 847.

Hammer, S., 1939, Terrain corrections for gravimeter stations: Geophysics, v. 4, pp. 184-194.

Hart, D. H. and Frank, F. J., 1954, Aquifer evaluation test in the Gable Mountain area: U.S. Geological Survey Open-File Report.

Heineck, R. L. and Beggs, H. G., Seismograph Service Corporation, 1978, Evaluation of seismic reflection surveying on the Hanford Site, Benton County, Washington: RHO-BWI-C-20, Rockwell Hanford Operations, Richland, Washington.

Holden, G. S. and Hooper, P. R., 1976, Petrology and chemistry of a Columbia River basalt section, Rocky Canyon, west-central Idaho: Geological Society of America Bulletin, v. 87.

Holmgren, D. A., 1968, Origin of subhorizontal platy jointing in the Yakima Basalt: Northwest-Science, v. 42, no. 1, p. 35.

Hooper, P. R., Reidel, S. P., Brown, J. C., Bush, J. H., Holden, G. S., Kleck, W. D., Robinette, M., Sundstrom, C. E., and Taylor, R. L., 1976, Major element analyses of Columbia River basalt, part 1: Open-File Report, Basalt Research Group, Washington State University, Pullman, Washington.

Iddings, J. P., 1886, The Columbia structure in the igneous rock on Orange Mountain, New Jersey: American Journal of Science, v. 31, no. 185, pp. 321-331.

Jaeger, J. C., 1961, The cooling of irregularly shaped igneous bodies: American Journal of Science, v. 259, pp. 721-734.

James, A. V. G., 1920, Factors producing columnar structure in lavas and its occurrence near Melbourne, Australia: Journal of Geology, v. 27, pp. 458-469.

Jones, F. O. and Deacon, R. J., 1966, Geology and tectonic history of the Hanford area and its relation to the geology and tectonic history of the State of Washington and the active seismic zones of western Washington and western Montana: DUN-310, Douglas United Nuclear Industries, Inc., Richland, Washington.

Kienle, C. F. Jr., Bentley, R. D., and Anderson, J. L., 1978a, Geologic reconnaissance of the Cle Elum-Wallula lineament and related structures: in Preliminary safety analysis report, amendment 23, volume 2A, subappendix 2R-D: Washington Public Power Supply System, Inc., Richland, Washington.

Kienle, C. F. Jr., Sheriff, S. D., and Bentley, R. D., 1978b, Tectonic significance of the paleomagnetism of the Frenchman Springs basalt, Oregon and Washington: Geological Society of America, Abstracts with Programs, v. 10, no. 3, p. 111.

Konicek, D. L., 1975, Geophysical survey in south-central Washington: Northwest Science, v. 49, no. 2, pp. 106-117.

Laval, W. N., 1956, Stratigraphy and structural geology of portions of south-central Washington: Ph.D. Dissertation, University of Washington, Seattle, Washington.

Lillie, J. T. and Richard, B. H., 1977, An analysis of selected gravity profiles on the Hanford Reservation, Richland, Washington: RHO-BWI-C-6, Rockwell Hanford Operations, Richland, Washington.

Lillie, J. T., Tallman, A. M., and Caggiano, J. A., 1978, Preliminary geologic map of late Cenozoic sediments of the western half of the Pasco Basin: RHO-BWI-LD-8, Rockwell Hanford Operations, Richland, Washington.

Lindberg, J. W. and Brown, R. E., 1981, Pleistocene catastrophic flood deposits of the Pasco Basin, Washington and the role of the Snake River: Geological Society of America, Abstracts with Programs, v. 13, no. 2, p. 67.

Liverman, J. L., 1975, Final environmental statement - waste management operations - Hanford Reservation, Richland: ERDA-1538, U.S. Energy Research and Development Administration, Richland, Washington.

Lofgren, G., 1980, Experimental studies on the dynamic crystallization of silicate melts: in Hargraves, R. B., Editor, Physics of magmatic processes: Princeton University Press, Princeton, New Jersey.

Long, P. E., 1978, Characterization and recognition of intraflow structures, Grande Ronde Basalt: RHO-BWI-LD-10, Rockwell Hanford Operations, Richland, Washington.

Long, P. E., Ledgerwood, R. K., Myers, C. W., Reidel, S. P., Landon, R. D., Rockwell Hanford Operations, and Hooper, P. R., Washington State University, 1980, Chemical stratigraphy of Grande Ronde Basalt, Pasco Basin, south-central Washington: RHO-BWI-SA-32, Rockwell Hanford Operations, Richland, Washington.

Long, P. E., Landon, R. D., and Reidel, S. P., Rockwell Hanford Operations, and Goles, G. G., University of Oregon, 1981, Trace element composition of Grande Ronde Basalt, Pasco Basin, south-central Washington: EOS, Transactions of the American Geophysical Union, v. 62, no. 6.

Low, J. W., 1977, Subsurface maps and illustrations: in Subsurface geology--petroleum mining construction, LeRoy, L. W. and Raese, J. W., Editors: Colorado School of Mines, Golden, Colorado.

Mackin, J. H., 1961, A stratigraphic section in the Yakima Basalt and the Ellensburg Formation in South-Central Washington: Report of Investigations No. 19, Washington Division of Mines and Geology, Olympia, Washington.

Mallet, R., 1875, On the origin and mechanism of production of the prismatic (or columnar) structure of basalt: Philosophy, v. 4, pp. 122-135 and 201-226.

McKee, E. H., Swanson, D. A., and Wright, T. L., 1977, Duration and volume of Columbia River basalt volcanism; Washington, Oregon and Idaho: Geological Society of America, Abstracts with Program, v. 9, no. 4, p. 463.

Merriam, J. C. and Buwalda, J. P., 1917, Age of strata referred to the Ellensburg Formation in the White Bluffs of the Columbia River: Bulletin of Geology, University of California, v. 10, no. 15, p. 255.

Moak, D. J. and Wintczak, T. M., 1980, Near-Surface Test Facility, phase I, geologic site characterization report: RHO-BWI-ST-8, Rockwell Hanford Operations, Richland, Washington.

Mudd, R. D., Clearlock, D. B., and Reisenaur, A. E., 1970, Analysis of hydrologic factors influencing the Gable Mountain irrigation project: BNWL-1502, Battelle, Pacific Northwest Laboratories, Richland, Washington.

Mullineaux, D. R., Wilcox, R. E., Ebaugh, W. F., Fryxell, R., and Rubin, M., 1977, Age of the last major scabland flood of eastern Washington, as inferred from associated ash beds of Mt. St. Helens Set S: Geological Society of America, Abstracts with Program, v. 9, no. 7, p. 1105.

Myers, C. W., 1973, Yakima Basalt flows near Vantage, and from core holes in the Pasco Basin, Washington: Ph.D. Dissertation, University of California at Santa Cruz, Santa Cruz, California.

Myers, C. W. and Brown, D. J., 1973, Stratigraphy of the Yakima Basalt in the Pasco Basin, Washington: Geological Society of America, Abstracts with Program (Cordilleran Section), v. 5, no. 1, p. 80.

Myers, C. W., Price, S. M., Caggiano, J. A., Cochran, M. P., Czimer, W. J., Davidson, N. J., Edwards, R. C., Fecht, K. R., Holmes, G. E., Jones, M. G., Kunk, J. R., Landon, R. D., Ledgerwood, R. K., Lillie, J. T., Long, P. E., Mitchell, T. H., Price, E. H., Reidel, S. P., and Tallman, A. M., 1979, Geologic studies of the Columbia Plateau, a status report: RHO-BWI-ST-4, Rockwell Hanford Operations, Richland, Washington.

Newcomb, R. C., 1958, Ringold Formation of Pleistocene age in type locality, the White Bluffs, Washington: American Journal of Science, v. 256, pp. 328-340.

Newcomb, R. C. and Strand, J. R., 1953, Geology and groundwater characteristics of the Hanford Reservation of the Atomic Energy Commission, Washington: U.S. Geological Survey WP-8.

Newcomb, R. C., Strand, J. R., and Frank, F. J., 1972, Geology and ground-water characteristics of the Hanford Reservation of the U.S. Atomic Energy Commission, Washington: U.S. Geological Survey Professional Paper 717.

Noonan, A. F., Fredriksson, K., and Nelen, J., 1980, Phase chemistry of the Umtanum basalt, a reference repository host in the Columbia Plateau: RHO-BWI-SA-77, Rockwell Hanford Operations, Richland, Washington.

NRC, 1981a, Disposal of high-level radioactive wastes in geologic repositories; proposed licensing procedures: 10 CFR 60, Subparts A and B, U.S. Nuclear Regulatory Commission, Washington, D.C.

NRC, 1981b, Standard format and content of site characterization reports for high-level waste geologic repositories: Draft Regulatory Guide and Value/Impact Statement Task GS 027-4, U.S. Nuclear Regulatory Commission, Washington, D.C.

Obert, L. and Stephenson, D. E., 1965, Stress conditions under which core disking occurs: Society of Mining Engineers Transactions.

ONWI, 1981, NWTS program criteria for the geologic disposal of nuclear wastes: waste package functional criteria: ONWI-33(4) (Draft), Office of Nuclear Waste Isolation, Columbus, Ohio.

Packer, D. R. and Johnston, J. M., Woodward-Clyde Consultants, 1979, A preliminary investigation of the magnetostratigraphy of the Ringold Formation: RHO-BWI-C-42, Rockwell Hanford Operations, Richland, Washington.

Packer, D. R. and Petty, M. H., Woodward-Clyde Consultants, 1979, Magnetostratigraphy of the Grande Ronde Basalt, Pasco Basin, Washington: RHO-BWI-C-46, Rockwell Hanford Operations, Richland, Washington.

Pardee, J. T., 1942, Unusual currents in glacial Lake Missoula, Montana: Geological Society of America Bulletin, v. 53, pp. 1570-1599.

Patton, P. C. and Baker, V. R., 1978, New evidence for pre-Wisconsin flooding in the channeled scabland of eastern Washington: Geology, v. 6, p. 567.

Peck, D. L. and Minakami, T., 1968, The formation of columnar joints in the upper part of Kilauean Lava Lakes, Hawaii: Geological Society of America Bulletin, v. 79, pp. 1151-1166

Peterson, D. E., 1965, Variations in the Earth's gravity field at Hanford: BNWL-235, Battelle, Pacific Northwest Laboratories, Richland, Washington.

Peterson, D. E., 1966, Bouguer gravity anomalies on the Hanford Reservation: BNWL-481, Battelle, Pacific Northwest Laboratories, Richland, Washington.

Peterson, D. E. and Brown, R. E., 1966, Gravity anomalies and geologic structures of the central part of the Columbia River basalt plateau: BNWL-SA-812, Battelle, Pacific Northwest Laboratories, Richland, Washington.

Pierce, R. L., Obradovich, J. D., and Friedman, I., 1976, Obsidian hydration dating and correlation of Bull Lake and Pinedale glaciations near West Yellowstone, Montana: Geological Society of America Bulletin, v. 87, pp. 61-75.

Price, E. H., 1980, Strain distribution and model for formation of eastern Umtanum Ridge anticline, south-central Washington: Geological Society of America, Abstracts with Program, v. 12, no. 3, p. 148; also, RHO-BWI-SA-30, Rockwell Hanford Operations, Richland, Washington.

Price, E. H., in press, Structural geometry, strain distribution, and mechanical evolution of eastern Umtanum Ridge, and a comparison with other selected localities within Yakima fold structures, south-central Washington: RHO-BWI-SA-138, Rockwell Hanford Operations, Richland, Washington.

Price, S. M., 1977, An evaluation of dike-flow correlations indicated by geochemistry, Chief Joseph swarm, Columbia River basalt: Ph.D. Dissertation, University of Idaho, Moscow, Idaho.

Ramsay, J. G., 1967, Folding and fracturing of rock: McGraw-Hill, New York.

Raymond J. R., 1958, The magnetic method of geophysical exploration on the Hanford Project-interim report: HW-57309, General Electric Hanford Atomic Products Operation, Richland, Washington.

Raymond, J. R., 1968, Geophysical seismic exploration: BNWL-481-3, Battelle, Pacific Northwest Laboratories, Richland, Washington.

Raymond, J. R. and Ratcliffe, C. A., 1959, A test of the refraction seismic method of the Hanford Project: HW-61796, General Electric Hanford Atomic Products Operation, Richland, Washington.

Raymond, J. R. and McGhan, V. F., 1963, Results of an airborne magnetometer survey of the Hanford Project: HW-79824, General Electric Hanford Atomic Products Operation, Richland, Washington, 15 p.

Raymond, J. R. and Tillson, D. D., 1968, Evaluation of a thick basalt sequence in south-central Washington, geophysical and hydrological exploration of Rattlesnake Hills deep stratigraphic test well: BNWL-776, Battelle, Pacific Northwest Laboratories, Richland, Washington.

Reidel, S. P., 1978a, Geology of the Saddle Mountains between Sentinel Gap and 119° 31' longitude: RHO-BWI-LD-4, Rockwell Hanford Operations, Richland, Washington.

Reidel, S. P., 1978b, Stratigraphy and petrogenesis of the Grande Ronde Basalt in the lower Salmon and adjacent Snake River canyons: RHO-SA-62, Rockwell Hanford Operations, Richland, Washington.

Reidel, S. P., Ross, N. E., and Long, P. E., 1978, Orthopyroxene fractionation in the Grande Ronde Basalt, Columbia River group: EOS, Transactions of the American Geophysical Union, v. 59, no. 12, p. 123; also, RHO-BWI-SA-5A, Rockwell Hanford Operations, Richland, Washington.

Reidel, S. P. and Long, P. E., 1980, Discriminant analysis as a method of flow identification and correlation in layered basalt provinces: Geological Society of America, Abstracts with Program, v. 12, no. 7, p. 507; also, RHO-BWI-SA-69, Rockwell Hanford Operations, Richland, Washington.

Reidel, S. P., Ledgerwood, R. K., Myers, C. W., Jones, M. G., and Landon, R. D., 1980, Rate of deformation in the Pasco Basin during the Miocene as determined by distribution of Columbia River basalt flows: Geological Society of America, Abstracts with Program, v. 12, no. 3, p. 149; also, RHO-BWI-SA-29, Rockwell Hanford Operations, Richland, Washington.

Repenning, C. A., in press, Biochronology of the microtine rodents of the United States: in Cenozoic mammals; their temporal record, biostratigraphy, and biochronology: Woodburne, M. O., Editor: University of California Press, Berkeley, California.

Richard, B. H., 1976, Residual gravity analysis of selected cross sections of the Hanford Reservation: ARH-C-23, Atlantic Richfield Hanford Company, Richland, Washington.

Richard, B. H. and Deju, R. A., 1977, Three-dimensional gravity investigation of the Hanford Reservation: RHO-BWI-C-5, Rockwell Hanford Operations, Richland, Washington.

Richard, B. H. and Lillie, J. T., 1977, Gravity studies of the Hanford Reservation, Richland, Washington: RHO-BWI-C-4, Rockwell Hanford Operations, Richland, Washington.

Richard, B. H., Lillie, J. T., and Deju, R. A., 1977, Gravity studies of the Hanford Reservation, Richland, Washington: RHO-BWI-C-4, Rockwell Hanford Operations, Richland, Washington.

Richman, L. R., 1981, Sedimentary analysis of pre-Missoula gravels in the southeastern part of the Pasco Basin, Washington: M.S. Thesis, Washington State University, Pullman, Washington, 82 p.

Rietman, J. D., 1966, Remanent magnetization of the late Yakima Basalt, Washington State: Ph.D. Dissertation, Stanford University, Stanford, California.

Robbins, S. L., Burt, R. J., and Gregg, D. O., 1975, Gravity and aeromagnetic study of part of the Yakima River basin, Washington: U.S. Geological Survey Professional Paper 726-E.

Robbins, S. L., Martinez, R. J., and Smith, D. L., 1979, Principal facts for borehole gravity stations in wells DC-3, DC-5, DC-7 at the Hanford Site, Washington, and in well RSH #1 on Rattlesnake Hills, Washington: U.S. Geological Survey Open-File Report 79-849.

Ross, M. E., 1978, Stratigraphy, structure, and petrology of the Columbia River basalt in a portion of the Grande Ronde-Blue Mountains area of Oregon and Washington: RHO-SA-58, Rockwell Hanford Operations, Richland, Washington.

Routson, R. C. and Fecht, K. R., 1979, Soil (sediment) properties of twelve Hanford wells: RHO-LD-82, Rockwell Hanford Operations, Richland, Washington.

Routson, R. C., Price, W. H., Brown, D. J., and Fecht, K. R., 1979, High-level waste leakage from the 241-T-106 tank at Hanford: RHO-ST-14, Rockwell Hanford Operations, Richland, Washington.

Ryan, M. P. and Sammis, C. G., 1978, Cyclic fracture mechanisms in cooling basalt: Geological Society of America Bulletin, v. 89, pp. 1295-1308.

Schiffman, P., 1979, Phase relations and cooling histories of some Columbia River pillow basalts: EOS, Transactions of the American Geophysical Union, v. 60, no. 46.

Schmincke, H. U., 1964, Petrology, paleocurrents, and stratigraphy of the Ellensburg Formation and interbedded Yakima Basalt flows, south-central Washington: Ph.D. Dissertation, The Johns Hopkins University, Baltimore, Maryland; also in Geological Society of America Bulletin, v. 78, no. 3, p. 319.

Schmincke, H. U., 1967a, Flow directions in Columbia River basalt flows and paleocurrents of interbedded sedimentary rocks, south-central Washington: Geologische Rundschau, v. 56, p. 992.

Schmincke, H. U., 1967b, Stratigraphy and petrography of four upper Yakima Basalt flows in south-central Washington: Geological Society of America Bulletin, v. 78, pp. 1385-1422.

Shaw, H. P. and Swanson, D. A., 1969, Eruption and flow rates of flood basalts: in Gilmor, E. H. and Stradling, D., Editors, Proceedings of the second Columbia River basalt symposium, Cheney, Washington, March 1969: Eastern Washington State College Press, Cheney, Washington.

Sheriff, S. D. and Bentley, R. D., 1980, Anomalous paleomagnetic directions from the Miocene Wanapum Basalt, Washington and Oregon: EOS, Transactions of the American Geophysical Union, v. 1, no. 46, p. 949.

Siems, B. A., Bush, J. H., and Crosby, J. W., 1974, TiO_2 and geophysical logging criteria for Yakima Basalt correlation, Columbia Plateau: Geolocial Society of America Bulletin, v. 85, no. 7, pp. 1061-1068.

Smith, G. O., 1901, Geology water resources of a portion of Yakima County, Washington: U.S. Geological Survey Water-Supply Paper 55, p. 68.

Smith, G. O., 1903, Anticlinal mountain ridges in central Washington: Journal of Geology, v. 11, p. 166.

Smith, M. J., Anttonen, G. J., Barney, G. S., Coons, W. E. Hodges, F. N., Johnston, R. G., Kaser, J. D., Manabe, R. M., McCarel, S. C., Moore, E. L., Noonan, A. F., O'Rourke, J. E., Schulz, W. W., Taylor, C. L., Wood, B. J., and Wood, M. I., 1980, Engineered barrier development for a nuclear waste repository in basalt: an integration of current knowledge: RHO-BWI-ST-7, Rockwell Hanford Operations, Richland, Washington.

Smyth, J. R. and Caporuscio, F. A., 1981, Zeolite stability and radioactive waste isolation in volcanic rocks: EOS, Transactions of the American Geophysical Union, v. 62, no. 17.

Spry, A., 1962, The origin of columnar jointing particularly in basalt flows: Geological Society of Australia Journal, v. 8, pp. 191-216.

Stradling, P. F., Kiver, E. P., and Rigby, J. G., 1980, Late Pleistocene floods and landforms in the Spokane, Washington, area: RHO-BWI-SA-61A, Rockwell Hanford Operations, Richland, Washington.

Swanson, D. A., 1967, Yakima Basalt of the Tieton River area, south-central Washington: Geological Society of America Bulletin, v. 78, pp. 1077-1110.

Swanson, D. A. and Wright, T. L., 1976, Guide to field trip between Pasco and Pullman, Washington, emphasizing stratigraphy and vent areas and intracanyon flows of Yakima Basalt: in Proceedings, Geological Society of America, Cordilleran Section Meeting, Pullman, Washington, Field Guide 1., 33 p.

Swanson, D. A., Wright, T. L., and Helz, R. T., 1975, Linear vent systems and estimated rates of magma production and eruption for the Yakima Basalt on the Columbia Plateau: American Journal of Science, v. 275, pp. 877-905.

Swanson, D. A., Anderson, J. L., Bentley, R. D., Byerly, G. R., Camp, V. E., Gardner, J. N., and Wright, T. L., 1979a, Reconnaissance geologic map of the Columbia River Basalt Group in eastern Washington and northern Idaho: U.S. Geological Survey Open-File Map 79-1363, scale 1:250,000.

Swanson, D. A., Wright, T. L., Hooper, P. R., and Bentley, R. D., 1979b, Revisions in stratigraphic nomenclature of the Columbia River Basalt Group: U.S. Geological Survey Bulletin 1457-H.

Swanson, D. A., Wright, T. L., and Zietz, I., 1979c, Geologic aeromagnetic map and geologic interpretation of the west-central Columbia Plateau, Washington and adjacent Oregon: U.S. Geological Survey Geophysical Investigations Map GP-917.

Tallman, A. M., Lillie, J. T., and Caggiano, J. A., 1978, The late Cenozoic geology of the western Pasco Basin: in Basalt Waste Isolation Program annual report: RHO-BWI-78-100, Rockwell Hanford Operations, Richland, Washington, pp. 78-81.

Tallman, A. M., Fecht, K. R., Marratt, M. C., and Last, G. V., 1979, Geology of the separation areas, Hanford Site, south-central Washington: RHO-ST-23, Rockwell Hanford Operations, Richland, Washington.

Taubeneck, W. H., 1970, Dikes of Columbia River basalt in north-eastern Oregon, western Idaho, and southeastern Washington: in Gilmour, E. H. and Stradling, D., Editors, Proceedings of the second Columbia River basalt symposium, Cheney, Washington, March 1969: Eastern Washington State College Press, Cheney, Washington, pp. 73-96.

Taylor, T. L., 1976, The basalt stratigraphy and structure of the Saddle Mountains of south-central Washington: M.S. Thesis, Washington State University, Pullman, Washington.

Teague, L. S., 1980, Secondary minerals found in cores DC2-A1 and DC2-A2 taken from Grande Ronde Basalt Formation, Pasco Basin, Washington: LBL-10387, Lawerence Berkeley Laboratory, Berkeley, California.

Tomkeieff, S. I., 1940, Basalt lavas of the Giant's Causeway: Bulletin of Volcanology, v. 2, pp. 89-146.

Van Alstine, D. R. and Gillett, S. L., Sierra Geophysics, in press, Magnetostratigraphy of the Columbia River basalt, Pasco Basin and vicinity, Washington: RHO-BWI-C-110, Rockwell Hanford Operations, Richland, Washington.

Waitt, R. B. Jr., 1980, About forty last-glacial Lake Missoula jokulhlaups through southern Washington: Journal of Geology, v. 88, pp. 653-679.

Ward, A. W., 1976, Petrology and chemistry of the Huntzinger flow, Columbia River basalt, Washington: ARH-SA-272, Atlantic Richfield Hanford Company, Richland, Washington.

Waters, A. C., 1955, Geomorphology of south-central Washington, illustrated by the Yakima east quadrangle: Geological Society of America Bulletin, v. 66, pp. 663-684.

Waters, A. C., 1961, Stratigraphic and lithologic variations in the Columbia River basalt: American Journal of Science, v. 259, pp. 581-611.

Watkins, N. D. and Baksi, A. K., 1974, Magnetostratigraphy and oroclinal folding of the Columbia River, Steens and Owyhee basalts in Oregon, Washington and Idaho: American Journal of Science, v. 274, p. 148.

Webster, G. D., Pankratz-Kuhns, M. J., and Waggoner, G. L., in press, Late Cenozoic gravels in Hells Canyon and the Lewiston Basin: in Cenozoic geology of Idaho, Bonnicksen, B. and Breckenridge, R. M., Editors: Idaho Bureau of Mines and Geology, Moscow, Idaho.

Weston Geophysical Research, Inc., 1978a, Ground geophysical studies, Columbia Plateau and adjacent Cascade Mountains: prepared for Washington Public Power Supply System, Inc., Richland, Washington.

Weston Geophysical Research, Inc., 1978b, Qualitative aeromagnetic evaluation of structures in the Columbia Plateau and adjacent Cascade Mountains: prepared for Washington Public Power Supply System, Inc., Richland, Washington.

Woodward-Clyde Consultants, 1978, Paleomagnetic measurements of the Ringold Formation and loess units near Hanford, Washington and evaluation of age-dating potential of Quaternary deposits near Hanford, Washington: prepared for United Engineers and Constructors, Inc., 33 p.

Woodward-Clyde Consultants, in press, Site locality identification study: Hanford Site, v. 1: Methodology, Guidelines, and Screening, v. 2: Data Cataloging: RHO-BWI-C-107, Rockwell Hanford Operations, Richland, Washington.

WPPSS, 1974, Preliminary safety analysis report, amendment 9: Washington Public Power Supply System, Inc., Richland, Washington.

WPPSS, 1977, Preliminary safety analysis report, amendment 23, v. 1 and 2: Washington Public Power Supply System, Inc., Richland, Washington.

WPPSS, 1981, Final safety analysis report, amendment 14, no. 2 and 3: Washington Public Power Supply System, Inc., Richland, Washington.

Wright, T. L., Grolier, M. J., and Swanson, D. A., 1973, Chemical variation related to the stratigraphy of the Columbia River basalt: Geological Society of America Bulletin, v. 84, pp. 371-386.

Wright, T. L., Black, K. N., Swanson, D. A., and L'Hearn, T. O., 1980, Columbia River basalt: 1978-1979 sample data and chemical analyses: U.S. Geological Survey Open-File Report 80-921, 99 p.

Zietz, I., Hearn, B. C., Higgins, M. W., Robinson, G. D., and Swanson, D. A., 1971, Interpretation of an aeromagnetic strip across the northwestern United States: Geological Society of America Bulletin, v. 82, no. 12, pt. 3, pp. 3347-3372.